11-2014

Hydrolytically Stable Analogues of Sugar Phosphates and a Miniaturized in Situ Enzymatic Screen

Xiang Fei
University of Nebraska-Lincoln, xfei@huskers.unl.edu

Hydrolytically Stable Analogues of Sugar Phosphates and A Miniaturized In Situ Enzymatic Screen

by

Xiang Fei

A DISSERTATION

Presented to the Faculty of

The Graduate College at the University of Nebraska

In Partial Fulfillment of Requirements

For the Degree of Doctor of Philosophy

Major: Chemistry

Under the Supervision of Professor David B. Berkowitz

Lincoln, Nebraska

November, 2014

Hydrolytically Stable Analogues of Sugar Phosphates and A Miniaturized In Situ Enzymatic Screen

Xiang Fei, Ph.D.

University of Nebraska, 2014

Advisor: David. B. Berkowitz

The *glmS* riboswitch undergoes self-cleavage upon binding its metabolic product GlcN6P, thereby providing a negative feedback mechanism limiting translation of the *glmS* protein when GlcN6P is abundant. As a first step toward the development of novel antimicrobials, we have synthesized a series of GlcN6P analogues bearing phosphatase-inert surrogates in place of the natural phosphate ester functionality. The self-cleavage assay identified two such compounds that display significant riboswitch actuator activity; namely those bearing a 6-phosphonomethyl group or a 6-*O*-malonyl ether. These two analogues exhibit a 22-fold and a 27-fold higher catalytic efficiency, respectively, than does glucosamine. Docking experiments were conducted to provide insight into the structural basis for SAR (Structure/Activity Relationship) seen across this battery of GlcN6P analogues and directions for future design of such small molecule actuators.

M6P/IGF2R regulates intracellular sorting of lysosomal enzymes, as well as endocytosis of extracellular ligands. To explore the possibility of multivalent receptor-ligand interactions, we have utilized novel chemistries to synthesize “tailored” bivalent ligands. A “linker diversification” approach has been recently developed. It emanates from a monomer with a terminal azide. Five different chemistries were exploited to connect two monomers together, leading to five structurally and functionally distinct

linkages. The assay showed that when the angles between two linking bonds are acute rather than obtuse, the corresponding ligands present higher binding affinity, suggesting the three dimensional shape of the ligand is crucial for achieving multivalency.

The ISES technique has proven to be a useful technique for catalyst screening. In this procedure, an organic reaction product or byproduct diffuses into an aqueous layer, wherein an enzymatic transformation leads to signal that can be monitored by UV/vis spectroscopy. Herein, we describe proof of principle of a miniaturized ISES assay, in which volumes are significantly reduced by utilizing a quartz micromulticell. This miniaturized ISES platform is used to examine a 4 × 4 combinatorial library of salen ligands, that is derived from both oxa- and carbacyclic D-fructopyranosyl-1,2-diamines. The Co(III)-salen derived from 3',5'-diiodo-salicylaldehyde and β-D-carbafructopyranosyl-1,2-diamine shows the highest chiral bias. X-ray crystallographic analysis reveals important structural differences between the more selective carbofructopyranosyl-1,2-diamine-derived salens and their oxacyclic counterparts.

Acknowledgements

I am deeply grateful to my advisor, Professor David B. Berkowitz for his strong and enthusiastic mentorship. His constant encouragement and striving for excellence have helped me to grow as a scientist. I would like to thank other members of my committee: Professors Stephen G. DiMagno, Mark A. Griep, James M. Takacs and Richard G. MacDonald for their precious time and thoughtful suggestions, especially Professors Takacs and MacDonald for reading my thesis.

The work presented in this dissertation would have not been possible without the help and collaboration of the following friends: Dr. Kannan R. Karukurichi, Dr. Weijun Shen, Dr. Sangeeta Dey, Dr. Sylvain Broussy, Dr. Pulakesh Maity, David L. Nelson, Kaushik Panigrahi, Dr. Guillaume Malik, Professor Richard G. MacDonald, Dr. Christopher M. Connelly, Megan E. Zavorka, Professor Juliane K. Soukup and Thomas Holmes. I want to convey my gratitude to other members of the Berkowitz group for being wonderful colleagues.

I was very fortunate to have my family around during the time in Lincoln. I want to thank my wife Gonghua, for always being supportive and encouraging along the way. I want to acknowledge my parents, especially my mom for spending a great deal of time with us, and taking care of our sons Ben and Jerry. I also want to thank the boys for all the joys they have brought to the family.

List of Abbreviations

AA Amino Acid

Ac Acyl

ADH Alcohol Dehydrogenase

aq Aqueous

APPA 2-Amino-5-Phosphono-3-Pentenoic Acid

Ar Aryl

Bn Benzyl

Boc *tert*-Butyloxycarbonyl

Bu Butyl

Calcd. Calculated

CD-MPR Cation Dependent Mannose 6-Phosphate Receptor

CI-MPR Cation Independent Mannose 6-Phosphate Receptor

CM Cross Metathesis

cod Cyclooctadiene

Cy Cyclohexyl

DCE Dichloroethane

DCM Dichloromethane

de Diastereomeric excess

DMAP 4-N,N-Dimethylaminopyridine

DMF N,N-Dimethylformamide

DMSO Dimethyl Sulfoxide

DTBMP 2,6-Di-tert-butyl-4-methylpyridine

FPP Farnesyl Pyrophosphate

ee Enantiomeric Excess

ESI Electron Spray Ionization

Equiv. Equivalents

F6P Fructose 6-Phosphate

G6P Glucose 6-Phosphate

GlcN6P Glucosamine 6-Phosphate

GlcNAc N-Acetyl Glucosamine

GlmS Glucosamine 6-Phosphate Synthase

hGUS Human β-Glucuronidase

HMDS Hexamethyldisilazane

HMPA Hexamethylphosphoramide

HPLC High Performance Liquid Chromatography

HRMS High Resolution Mass Spectrometry

Hz Hertz

IDCP Iodonium Di-*sym*-Collidine Perchlorate

IGF Insulin Like Growth Factor

J Coupling Constant

KRED Ketoreductase

LDA Lithium diisopropylamide

M6P Mannose 6-Phosphate

M Molarity

MD Molecular Dynamics

Me Methyl

MeOH Methanol

min Minute

MRH Mannose 6-Phosphate Receptor Homology

MS Mass Spectrometry

N Normality

PEG Polyethylene Glycol

PMP Pentamannosyl Phosphate

Pyr Pyridine

rt Room Temperature

SES 2-Trimethylsilylethanesulfonyl

TBAF Tetrabutylammonium fluoride

Tf Trifluoromethanesulfonyl

TGN Trans Golgi Network

THF Tetrahydrofuran

TLC Thin Layer Chomatography

TBS *tert*-Butyldimethylsilyl

TBDPS *tert*-Butyldiphenylsilyl

TM Transition Metal

Ts 4-Toluenesulfonyl

Table of Contents

Table of Figures

Chapter 1

Chapter 2

Chapter 4

Table of Tables

Chapter 1

Overview of Phosphonates in Bioorganic Chemistry

Phosphonic acids, sometimes termed C-P compounds are a type of compound that contain the C-P(O)$(OH)_2$ moiety. The acid, salt and ester forms are generally referred to as phosphonates. Perhaps organic chemists encounter phosphonates more often when using them in the Horner–Wadsworth–Emmons reaction. However, this overview will focus on the phosphonates that are produced either in nature or in laboratories, to imitate biologically relevant phosphates or carboxylates.

I. Naturally Occurring Phosphonates

The first report of a phosphonate in a living system was in 1959, published in *Nature* by Horiguchi and Kandatsu.[1] While examining the amino acid composition of rumen protozoa from sheep, they observed a ninhydrin-positive substance which was later crystallized and determined to be 2-aminoethanephosphonic acid (AEP). This discovery opened a new chapter in the chemical biology of phosphorus metabolism. The unprecedented naturally-occurring C-P bond inspired biochemists in the years that followed to search for new phosphonates and novel enzymes in their biosynthetic pathways. After 55 years of exploration, a wealth of novel structures containing C-P bonds have been unveiled from various natural sources (Fig. 1.1).[2] Most of these compounds possess potent biological activities due to their structural similarities with the native carboxylates or phosphates. Herein, a few examples are elaborated to demonstrate the importance and the rising interest of these underexplored compounds in recent years.

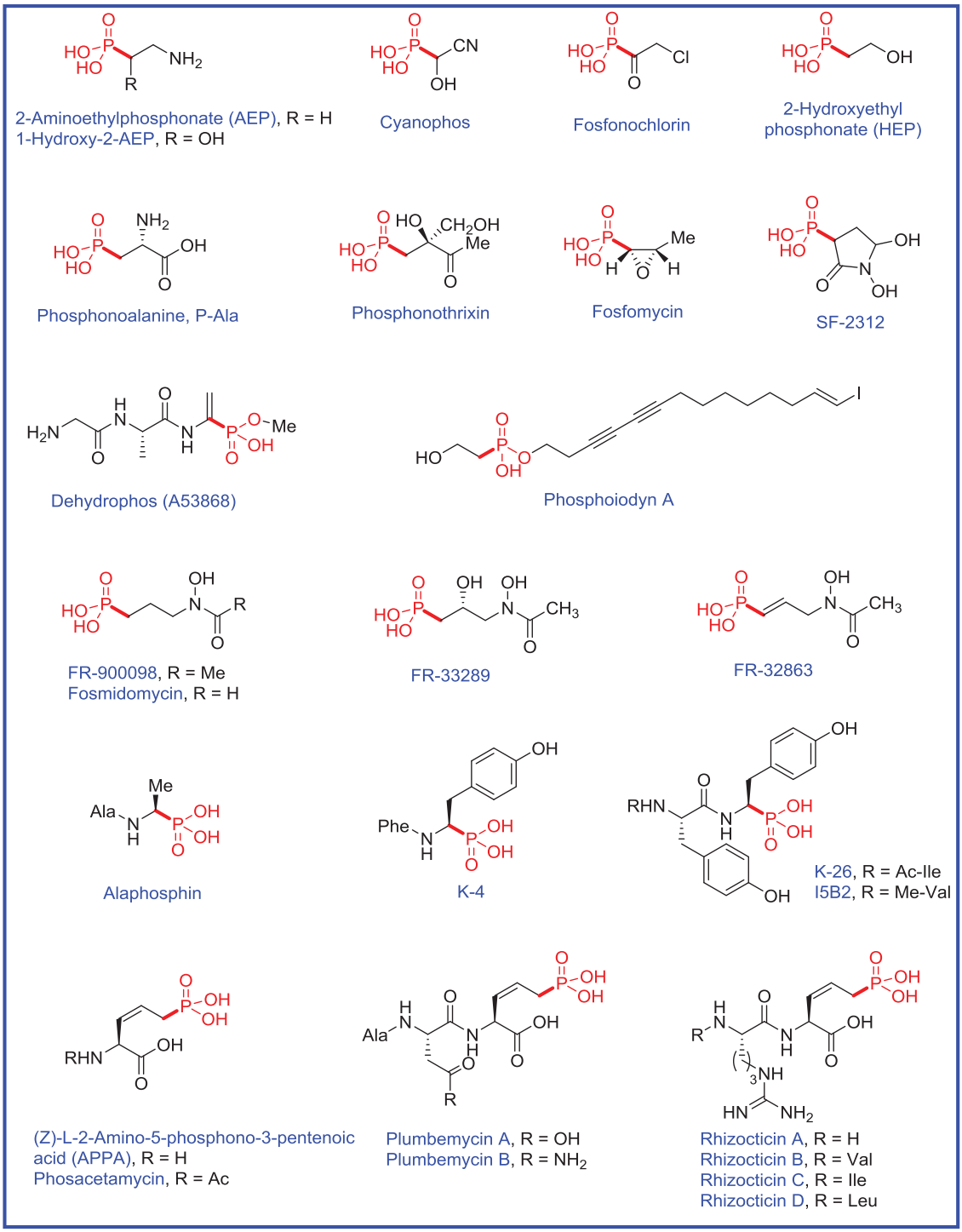

Figure 1.1: Structures of naturally-occurring phosphonates

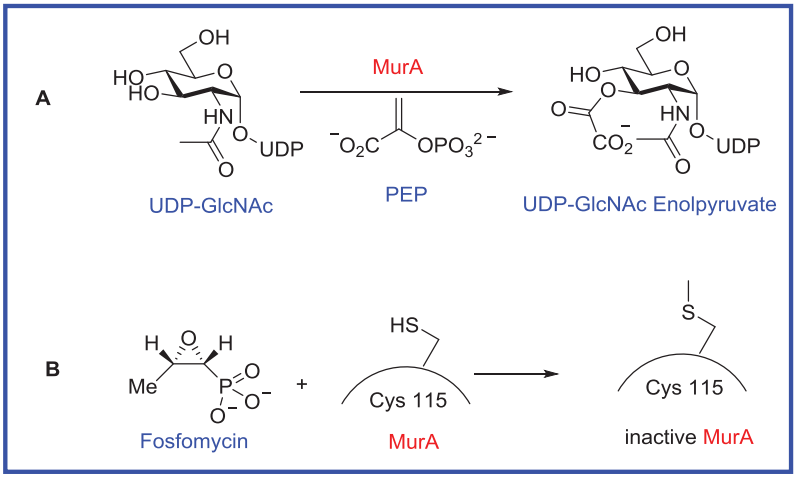

Figure 1.2: Irreversible inactivation of Fosfomycin on MurA

A. Fosfomycin/Fosphonomycin

The discovery of fosfomycin was announced in 1969 by Hendlin and colleagues, under its former name fosphonomycin.[3] This "new antibiotic" from strains of *Streptomyces* combines two unusual features: an epoxide ring and a carbon-phosphorus bond. In 1974, Kahan and colleagues studied the mechanism of action for its antimicrobial activities. They proposed that fosfomycin is an irreversible inhibitor of bacterial cell wall biogenesis.[4] More specifically, analogous to phosphoenolpyruvate (PEP), fosfomycin competes for binding to UDP-N-acetylglucosamine enolpyruvyl transferase (or MurA). MurA catalyzes the first committed step in peptidoglycan biosynthesis, ligating PEP to the 3'-hydroxy group of UDP-N-acetylglucosamine (Fig. 1.2).[5] An active site cysteine residue opens the epoxide ring of fosfomycin, resulting in the irreversible inactivation of the enzyme. Today, in the United States, fosfomycin tromethamine salt is used to treat urinary tract infections under the trade name Monurol®. Recently, the combination of fosfomycin and tobramycin was also used in clinical studies for treatment of cystic fibrosis.[6]

B. 2-Amino-5-Phosphono-3-Pentenoic Acid (APPA) and APPA-Containing Peptides: Plumbemycins and Rhizocticins

In 1977, Park, Hirota and Sakai isolated two peptide antibiotics from *Streptomyces plumbeus*: Plumbemycin A [(L)-Ala-(L)-Asp-(L,Z)-APPA] and Plumbemycin B [(L)-Ala-(L)-Asn-(L,Z)-APPA].[7] The non-proteinogenic amino acid (L, Z)-APPA[8] was later found at the C-terminus of the antifungal agents, Rhizocticins, as well.[9] It is believed that both plumbemycins and rhizocticins enter the cells through oligopeptide transport systems (Fig. 1.3).[10-11]

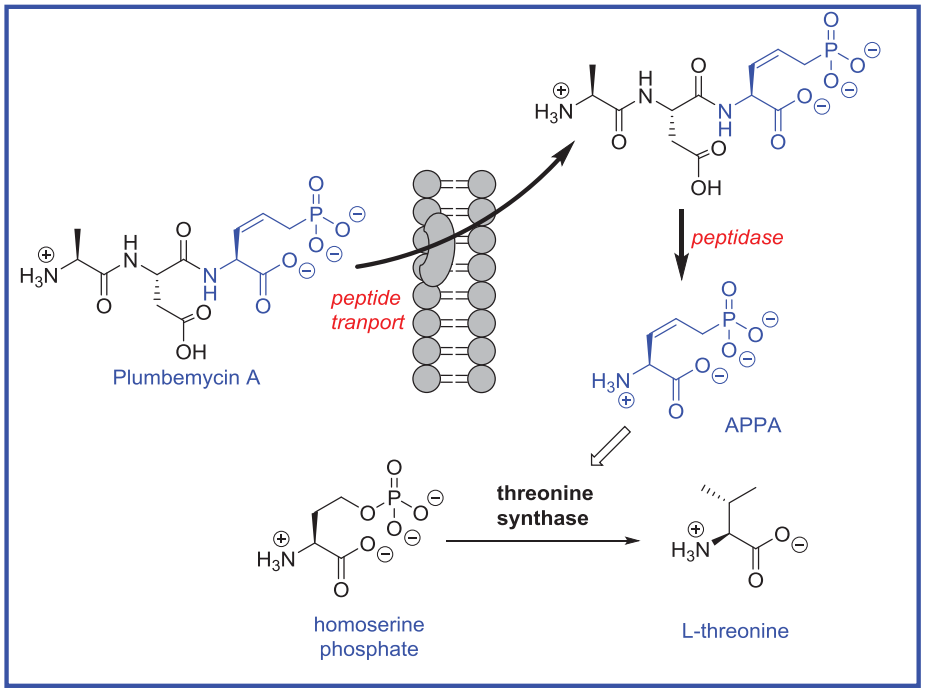

Figure 1.3: Mechanism of action for the APPA-Containing Peptides

Host oligopeptidases cleave the peptides, releasing the warhead (L,Z)-APPA which inhibits the pyridoxal 5'-phosphate dependent enzyme, threonine synthase (TS).[12] TS catalyzes the last step of threonine biosynthesis, which converts homoserine-*O*-phosphate to L-threonine. Structurally resembling the substrate homoserine-*O*-phosphate, (L,Z)-APPA competes for binding to TS, thereby interfering with the biosynthesis of

threonine, ultimately leading to the inhibition of cell growth.[13] It is noted that the selectivity of these antimicrobials is determined by the proteinogenic amino acids attached to the (L,Z)-APPA. The specific sequences of these peptides can be differentiated by oligopeptide transporters from varied organisms.[14] This is a nice prodrug strategy, demonstrated by Nature, that exploits a short peptide to deliver an active agent and selectively target a particular organism. In addition to the naturally-occurring Z-APPA, synthetic E-APPA has been studied, as well, mostly as a reversible inhibitor of cystathionine γ-synthase (synthesizes cystathionine from cysteine and homoserine phosphate).[15]

C. FR-900098 and Fosmidomycin

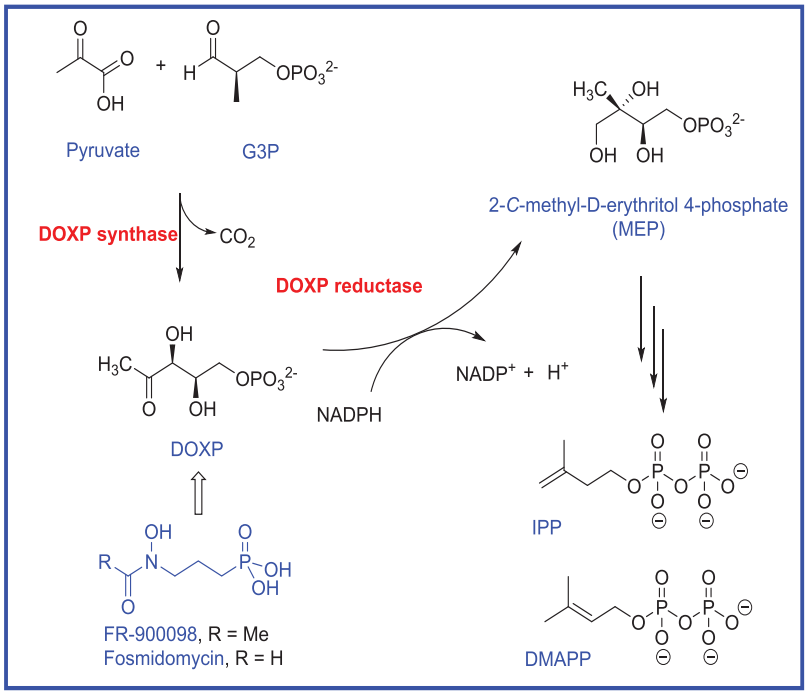

Figure 1.4: Inhibition of DOXP reductase by FR-900098 and fosmidomycin

FR-900098 and fosmidomycin were isolated from strains of *Streptomyces rubellomurinus* and *Streptomyces lavendulae,* respectively, by researchers at Fujisawa Pharmaceutical Co..[16-17] These compounds inhibit isoprenoid biosynthesis by blocking 1-deoxy-D-xylulose 5-phosphate (DOXP) reductoisomerase (Fig. 1.4).[18] This enzyme catalyzes the first committed step in the non-mevalonate pathway for biosynthesis of isopentenyl pyrophosphate (IPP) and dimethylallyl pyrophosphate (DMAPP), the fundamental building blocks for isoprenoid biosynthesis.[19-21] Probably because both IPP and DMAPP are biosynthesized via the mevalonate pathway in animals and humans, FR900098 and fosmidomycin displays limited toxicity for mammalian cells. In addition to their antibacterial activities, FR900098 and fosmidomycin also display potent antimalarial activity, owing to the unexpected presence of the non-mevalonate pathway in *Plasmodium falciparum*, the most common causative agent of malaria. Indeed, fosmidomycin and its clindamycin combination have already shown great promise in early human trials for treating malaria, including showing activity against drug-resistant strains.[22-24]

D. Latest Discoveries

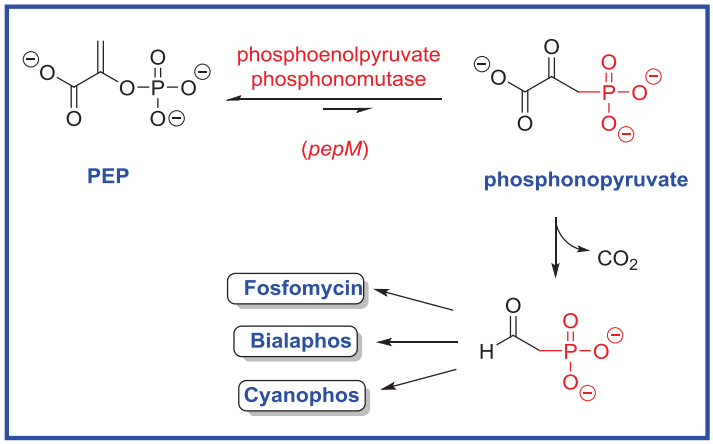

Figure 1.5. The essential enzyme *pepM* in phosphonate biosynthesis

The majority of phosphonate natural products were isolated in the 20th century. However, new phosphonates continue to be discovered thanks to newly developed detection technologies and recent advances in genome mining. In the last two years, a number of novel phosphonates have been uncovered from various organisms. Phosacetamycin is N-acetylated Z-APPA that inhibits growth of both bacteria and fungi.[25] Furthermore, Phosphoiodyn A bears a polyacetylene chain that is terminated with an unprecedented vinyl iodide.[26] Phosphoiodyn A exhibited significant agonistic activity toward human peroxisome proliferator-activated receptor delta (hPPARδ). It displayed an EC_{50} of 23.7 nM for hPPARδ activation and over 200-fold selectivity compared with other subtypes (hPPARα and hPPARγ).

Recently, Metcalf *et al* conducted a large-scale genome mining for the presence of *pepM*,[27] which encodes the essential enzyme phosphoenolpyruvate phosphonomutase found in most phosphonate biosynthetic pathways (Fig. 1.5). From one of the *pepM* positive strains, *Streptomyces regensis* strain WC-3744, a unique cyanohydrin-containing phosphonate, cyanophos, was isolated.[28] Considering the rarity of nitrile compounds in Nature,[29] the discovery of this phosphonate is particularly exciting, and it certainly expands the structural diversity of known naturally occurring phosphonates.

In summary, recent years have seen a renewed interest in the study of naturally occurring phosphonates. Nevertheless, natural C-P compounds remain understudied metabolites. The enzymes involved in their biosynthetic pathways represent even more intriguing subjects for biochemical studies. Given the great potential associated with these compounds, more effort and resources will be devoted to this topic.

II. Synthetic phosphonates

Synthetic phosphonates have played important roles in the pharmaceutical and agrochemical industries.[30] It is not an exaggeration to say that these molecules have changed our world. In this overview, three examples are discussed in detail to demonstrate the great impact that these compounds have brought to our lives.

A. Glyphosate/Roundup

Under the tradename "Roundup", glyphosate is a broad-spectrum herbicide that was discovered by Monsanto in the 1970s.[31] It kills weeds by blocking the shikimate pathway of aromatic amino acid biosynthesis.[32] Glyphosate targets 5-enolpyruvylshikimate 3-phosphate (EPSP) synthase (EC 2.5.1.19), which converts shikimate-3-phosphate (S3P) and phosphoenolpyruvate (PEP) into EPSP via a ternary enzyme-substrate complex.[33] Analogous to the transient PEP oxonium ion, glyphosate occupies the PEP binding site to form a more tightly bound ternary complex with S3P which slowly decrease the enzyme activity (Fig. 1.6). The formation of an EPSP synthase-S3P-glyphosate complex has been confirmed by X-ray crystallography.[34] In addition, kinetic studies have shown that glyphosate inhibits EPSP synthase in an uncompetitive manner.[35] Hence, glyphosate is a textbook example of uncompetitive inhibitors that bind not to the free enzyme, but rather, to the enzyme-substrate complex.

After its introduction to the market in 1974, glyphosate was quickly adopted by farmers due to its broad spectrum of activity and relatively low toxicity compared with other herbicides. It has grown even more popular since Monsanto induced genetically modified crops (termed "Roundup Ready System") that resist the herbicide. In 2007,

glyphosate became the most used herbicide in the United States agricultural industry, with 180 to 185 million pounds applied that year.[36] Nevertheless, recent years have seen rising concerns over the effect of glyphosate on the environment and human health. A 2014 article published in *Food Chemistry* implies that Roundup Ready soybeans have a high residual level of accumulated glyphosate, that could have "potential consequences for human and animal health".[37]

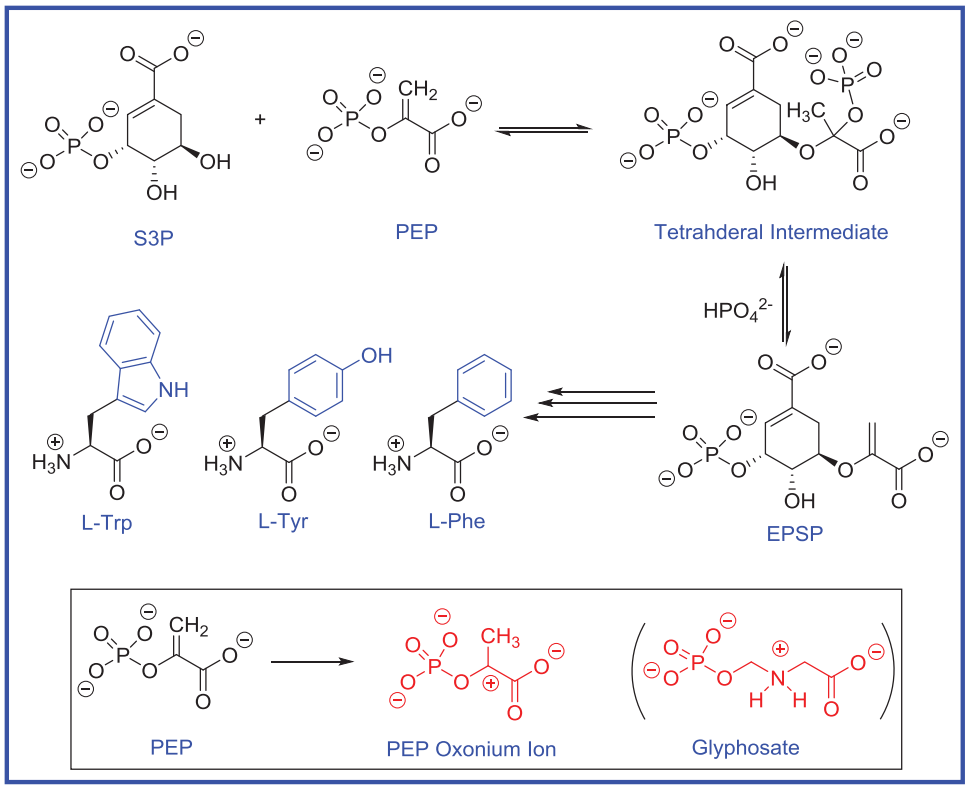

Figure 1.6: EPSP synthase and its inhibition by glyphosate

B. Bisphosphonates

Bisphosphonates are hydrolytically stable analogs of pyrophosphate (Fig. 1.7). The first reported synthesis of a bisphosphonate dates back to 1865 by German chemist Menschutkin.[38] However, in the following century, bisphosphonates were only developed

for industrial uses, mainly in the textile, fertilizer and oil industries.[39] In 1968, following the discovery that inorganic *pyrophosphate* inhibits both precipitation and dissolution of calcium phosphate,[40] analogous bisphosphonates were used in the studies of calcium metabolism.[41] This represents the first biological study of bisphosphonates. One year later, the collaboration between the Fleisch group (University of Berne, Davos, Switzerland) and David Francis (Procter & Gamble, Ohio, US) led to two seminal papers, published back to back in *Science*, which demonstrated for the first time that bisphosphonates are powerful inhibitors for both tissue calcification and bone resorption.[42-43] It is clear that, as is the case for the native pyrophosphate, bisphosphonates inhibit the formation of calcium phosphate crystals through calcium-chelating abilities, thereby preventing the calcification of soft tissues.[42] However, the mechanisms are more complicated for their use to prevent loss of bone mass.

The originally conceived theory that bisphosphonates inhibit dissolution of calcium phosphate appears unlikely *in vivo*.[39] Instead, most bisphosphonates are believed to decrease the numbers of osteoclasts (cells that break down bone tissue) by promoting their apoptosis.[44] Some non-N-containing bisphosphonates replace the terminal pyrophosphate of ATP through intracellular metabolism, leading to toxic ATP analogues which ultimately prompt osteoclasts apoptosis.[45] In contrast, most N-containing bisphosphonates bind to and inhibit farnesyl pyrophosphate synthase (FPPS) in the mevalonate pathway (Fig 1.8).[46-49] The disruption of FPP biosynthesis will block prenylation of proteins, including GTP-binding proteins, Ras, Rho and Rac.[49] Interfering with their cellular function could result in increased cellular death by apoptosis. Hence, by mechanism of action, bisphosphonates can be divided into two different classes.

Bisphosphonates have very high affinities for bone tissues and can be rapidly absorbed onto the bone surface. Thus, they are very specific for bone diseases. Currently there are about 9 bisphosphonates used worldwide to treat osteoporosis, osteitis deformans (Paget's disease), bone metastasis and other conditions that feature bone fragility.

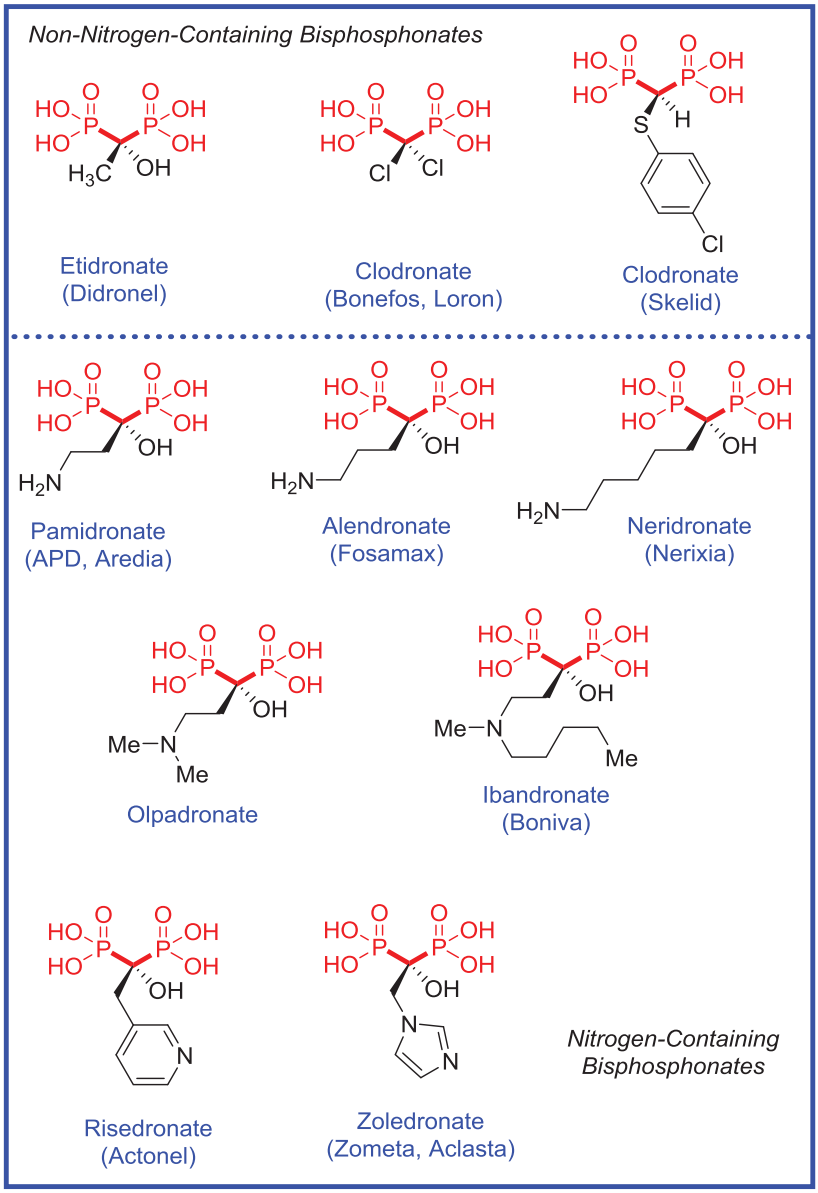

Figure 1.7: Structures of bisphosphonates

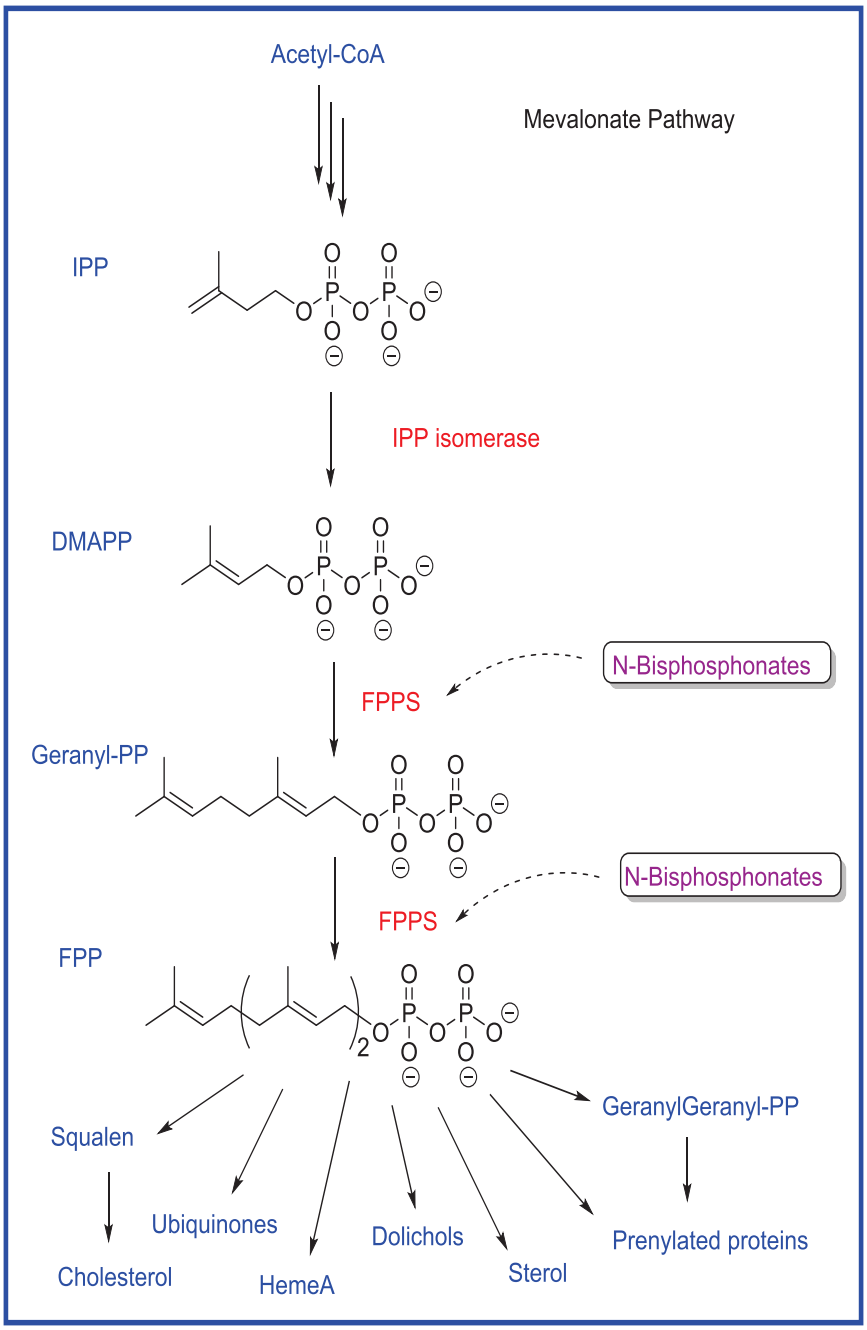

Figure 1.8. N-bisphosphonates inhibit the Mevalonate Pathway by targeting FPPS

C. Acyclic Nucleoside Phosphonates (ANPs)

Since its first clinic observation in 1981, human immunodeficiency virus infection/acquired immunodeficiency syndrome (HIV/AIDS) has caused an estimated 39

million deaths worldwide.[50] The retrovirus mainly infects the human immune system, reversely transcribing its RNA genome into double-stranded DNA in the host cells.[51]

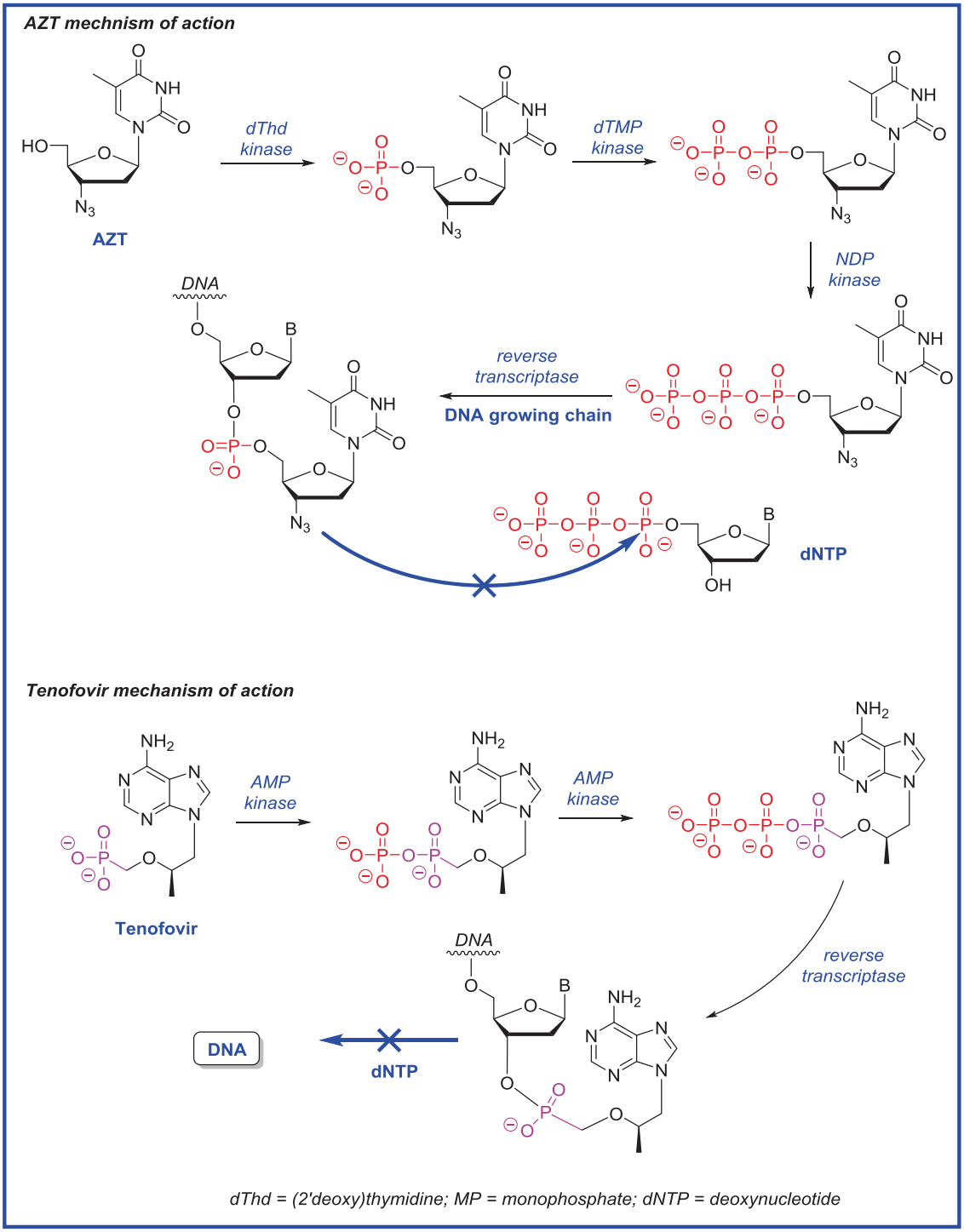

Figure 1.9: Inhibition of HIV-1 reverse transcriptase by AZT and tenofovir

Antiviral agents that target reverse transcriptases (RTs) have become crucial in management of the retroviral infections. 3′-Azido-3′-deoxythymidine (AZT, Zidovudine) was the first FDA-approved drug for HIV treatment.[52] AZT is a nucleoside analogue that needs to be converted to AZT- triphosphate (AZT-TP) that then acts as a chain terminator in RT-catalyzed DNA synthesis. The first phosphorylation of AZT, or other nucleoside analogues, has been identified as the bottleneck of the deactivation process. Addressing this, De Clercq and Holy have developed a number of acyclic nucleoside phosphonates (ANPs) that only need two phosphorylation steps to be activated to the chain-terminating metabolites (Fig. 1.9).[53-55] And then the ANP diphosphates are incorporated into the DAN chain, either by RNA reverse transcriptase or DNA polymerase. This mechanism is supported by a meticulous study with cidofovir diphosphate using gel electrophoresis.[56] Thus far, three of these nucleotide analogue/reverse transcriptase inhibitors (NtRTIs) have entered the pharmaceutical market. Tenofovir, in its oral prodrug form tenofovir disoproxil fumarate (TDF or PMPA), has been approved for treatment of HIV infection under the trade name Viread. Cidofovir (Vistide, which targets viral DNA polymerase) is administrated intravenously to treat CMV retinitis in AIDS patients. Adefovir has been approved in its prodrug form, adefovir dipivoxil (Hepsera), to treat chronic hepatitis B virus (HBV) infections.

In addition to these well-established classes, there are other phosphonates that have reached pre-clinical or clinical studies. For example, Perzinfotel (EAA-090), a potent NMDA antagonist, has been investigated for treatment of stroke; however, it was shown to lack an analgesic effect. Taken together, the phosphonate motif has been an

important group in modern drug discovery, and it will continue to serve as a non-hydrolyzable bioisotere for numerous phosphate and carboxylate metabolites.

III. Sugar Phosphonates in Bioorganic Chemistry

Carbohydrate phosphates play critical roles in cell survival and proliferation. As one of the most common metabolic intermediates, glucose 6-phosphate (G6P) lies in two major metabolic pathways, namely glycolysis and the pentose phosphate pathway.[57] The former converts G6P to pyruvate and releases free energy in the form of adenosine triphosphate (ATP). The latter converts G6P to ribose 5-phosphate (R5P) and erythrose 4-phosphate (E4P) which are utilized in biosynthesis of nucleic acids and aromatic amino acids, respectively. In addition, fructose 6-phosphate (F6P), mannose 6-phosphate (M6P), glucosamine 6-phosphate (GlcN6P) all emanate from G6P and are all essential intermediates in carbohydrate metabolism, influencing various cellular processes.

Like other phosphonates, replacing enzyme-lable O-P bonds with stable C-P bonds in carbohydrate scaffolds, generates sugar phosphonates. These compounds are resistant to phosphatase cleavage and, as such, exhibit a sort of "constitutive phosphorylation" phenotype and as such be able to block or articifially stimulate a metabolic pathway of interest, resulting in a desired cellular response. The first synthesis of sugar phosphonates dates back to the 1950s. Burger *et al.* synthesized a nonisosteric (one carbon unit shorter) phosphonate analogue of G6P via the Arbuzov reaction.[58] Later, the Syntex group claimed the synthesis of the isosteric phosphonate analogues of G6P, R5P, and M6P, exploiting a stabilized Wittig reagent.[59] However, these protocols had limited applications due to the inconvenient process and harsh conditions. Despite their

great potential in biosystems, sugar phosphonates have been incompletely investigated and underutilized in biochemical investigations.

In 1994, our group reported a direct displacement of sugar triflates with diethyl lithiomethylphosphonate, providing an expedient entry into valuable, sought after sugar phosphonates.[60] From the corresponding alcohols, the primary triflates can be easily synthesized, purified and stored under argon. At – 78 °C in THF, the triflates are rapidly displaced by the phosphonate anion in an SN_2 manner. Reactions are typically complete within 10 min following substrate addition. This reaction proved to be widely applicable toward various triflates, offering a general approach to the isosteric phosphonate analogues of sugar phosphates.

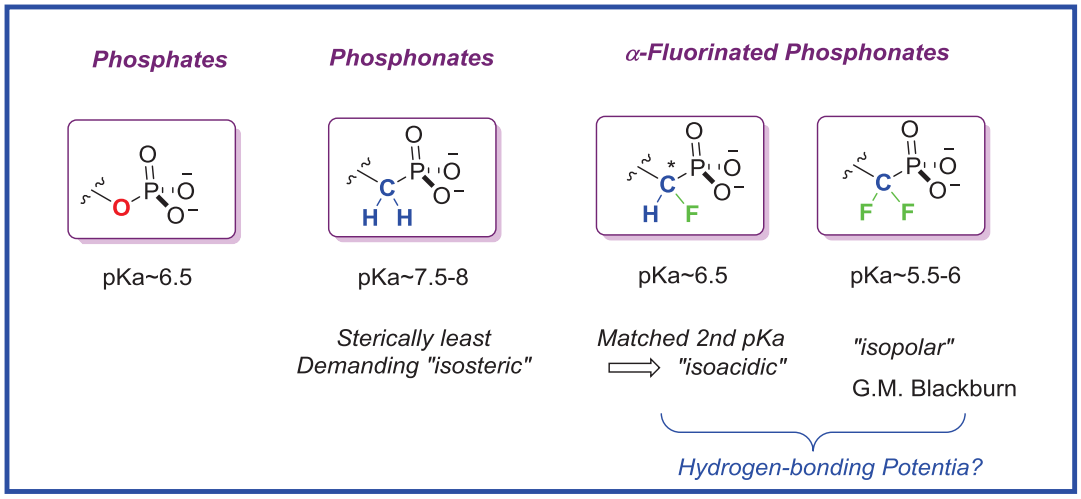

Figure 1.10. Three types of phosphonates vs native phosphates

Most importantly, this protocol is quite compatible with a variety of different C-nucleophiles, especially the α-fluorinated phosphonate anions.[60-65] As a matter of fact, the triflate displacement was originally applied with diethyl (α,α-difluoromethy)phosphonate anion, to give the acclaimed difluorinated phosphonate analogues of sugar phosphates.[61] In the 1980s, Blackburn pointed out that while

phosphonates sterically resemble phosphates, the replacement of an O-P bond with a C-P bond will largely change the polarity of the group.[66-68] This could be a crucial factor in the ability of phosphonates to bind to proteins as the deleted oxygen may have been involved in significant dipole-dipole interactions in the protein active site.[69-70] In such cases, α-halogenation, particularly α-fluorination, could potentially compensate for the removal of the oxygen eletronegative atom, and in this way provide a more effective surrogates for the native phosphate (Fig. 1.10).[71]

Mostly promoted by Blackburn and McKenna, the -CF_2- moiety has been employed as an isopolar replacement of the bridging oxygen. Indeed, in a number of notable cases, α, α-difluorinated phosphonates have been observed to be superior analogues to their non-fluorinated counterparts.[72-81] Perhaps the most impressive case was a series of hexapeptides, developed by Burke and coworkers, utilizing non-hydrolyzable analogues of phosphotyrosine to inhibit protein phosphotyrosine phosphatase PTP1B. The Burke group chose to use a hexapeptide (Ac-Asp-Ala-Asp-Glu-pTyr-Leu-C(O)NH2) that represents the sequence at the EGFR (epidermal growth factor receptor) phosphorylation site, an excellent substrate for rat PTP1. The peptide

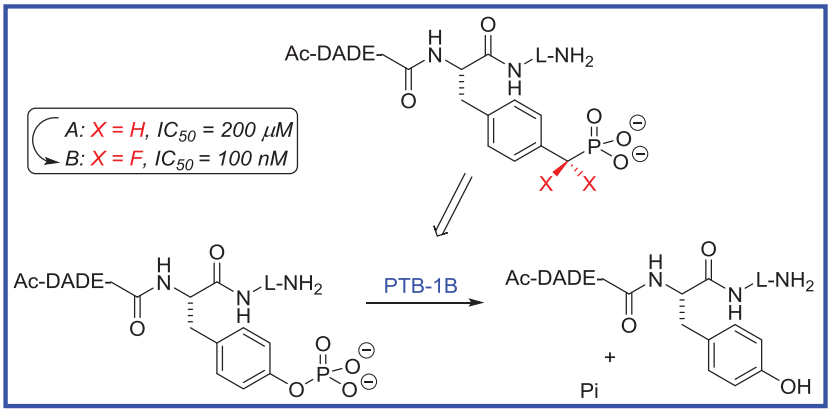

Figure 1.11: Peptides containing non- and difluorophosphonate analogues of phosphotyrosine are PTP1B inhibitors

containing the difluorophosphonotyrosine in place of pTyr exhibited 2000-fold greater inhibition than the non-fluorinated congener (Fig. 1.11).[82]

Nonetheless, an extensive SAR study from our group showed that the -CH_2- analogue of G6P is a better substrate for G6P dehydrogenase (G6PDH) than the difluorinated counterpart.[83] More importantly, the two diastereomeric α-monofluorinated phosphonates have also been synthesized through the addition of a phosphite anion to the appropriate aldehyde, followed by deoxyfluorination. Interestingly, out of the four synthetic substrates examined, (7*S*)-glucose-CHF-phosphonate displayed the best substrate activity with k_{cat}/K_m = 922 $mM^{-1}S^{-1}$, 11-fold higher than its (7*R*)-diastereomer (Fig. 1.12). Together with other cases,[74, 77] this study suggests that any of the non-, mono- and difluoro-phosphonates could have the best fit for an active site. The activity of these analogues is determined by assaying binding to the targeted macromolecule. And, as can be seen from the discussion above, this is clearly an experimental science, i.e. for a given

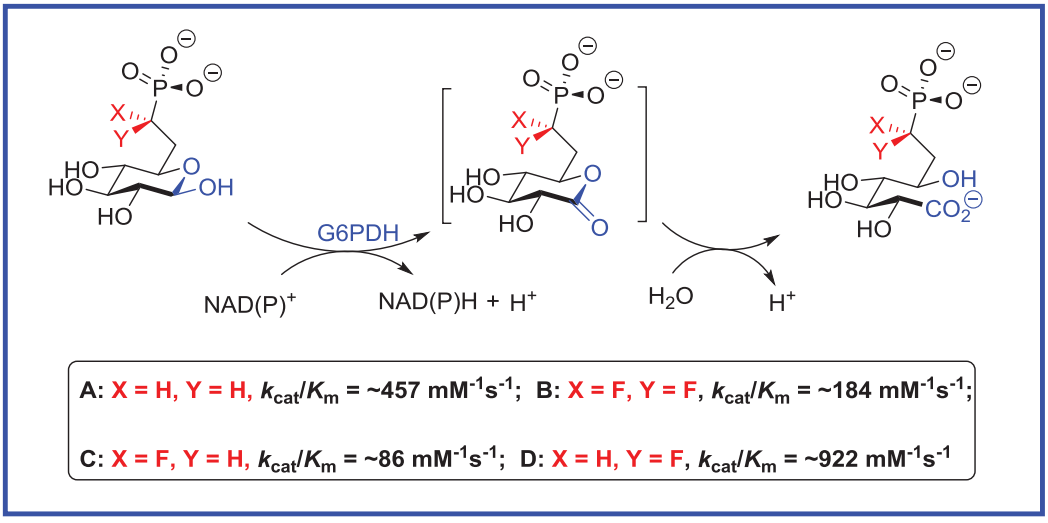

Figure 1.12: Phosphonate analogues are examined as pseudosubstrates for Glc6P dehydrogenase

active site, it is generally best to synthesize all phosphonate analogues and examine these for binding to the target macromolecule.

A year after our 2000 *JOC* article describing the importance of monofluorinated phosphonates based upon their tunability for binding to G6PDH, our group reported a triflate displacement approach to the monofluorinated phosphonates.[84] This is realized by using a McCarthy reagent as the nucleophile, followed by reductive removal of the phenylsulfonyl group. Emanating from a common precursor, one can thus access all three types of phosphonate in a divergent, late stage value-added manner (Fig. 1.13). This feature renders the triflate displacement one of the more useful methods for the synthesis of biologically relevant phosphonates. Applying this strategy, we have carried out several case studies and discovered a variety of interesting phosphonates, mostly as analogues of sugar phosphates. For instance, the nonfluorinated phosphonate analogue of M6P is shown to be excellent monodentate ligand for the M6P receptor, while the difluorinated congener showed significantly lower binding affinity.[85] The α,α-difluorinated phosphonate analogue of fructofuranose 6-phosphate has been seen to be a slow-binding inhibitor of glucosamine 6-phosphate synthase.[86] Furthermore, the Berkowitz group was the first to synthesize the α,α-difluorophosphonate analogues of serine-*O*-phosphate and threonine-*O*-phosphate.[64] The former has since been extensively utilized in chemical biology to understand the role of protein phosphorylation at specific loci.[87]

Chapters two and three of this thesis will discuss the use of the triflate displacement chemistry to probe two distinct biological systems, targeting both a protein (M6P/IGF2R) and an RNA target (the *glmS* riboswitch). In these sections, detailed

syntheses of the relevant phosphonate analogues are presented and their corresponding biochemical characterization is also described.

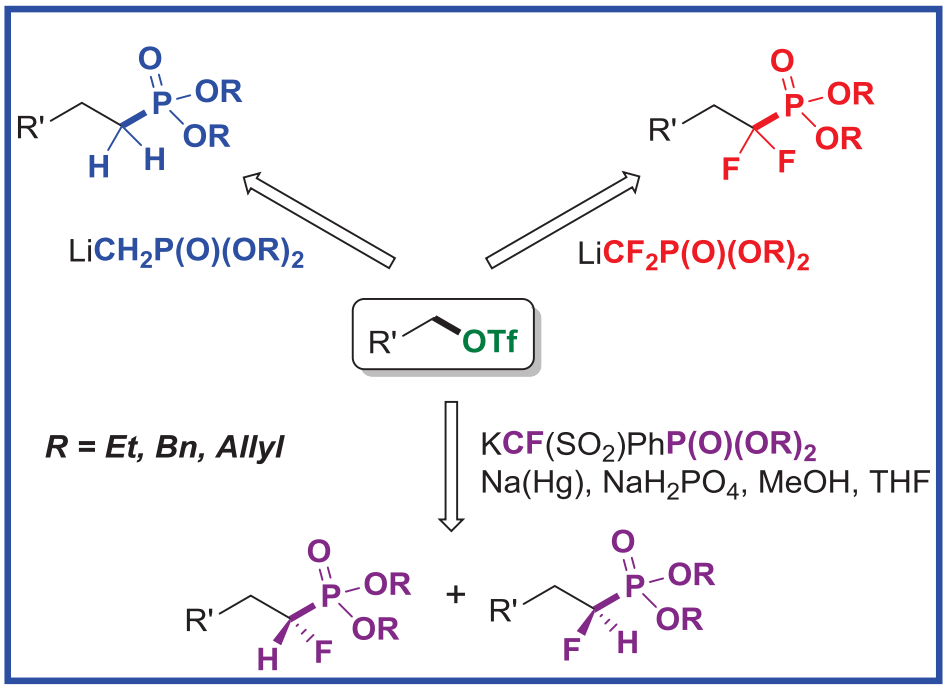

Figure 1.13: A divergent approach to three types of phosphonates

IV. References

1. Horiguchi, M.; Kandatsu, M., Isolation of 2-aminoethane phosphonic acid from rumen protozoa. *Nature* **1959,** *184(Suppl 12)*, 901-2.
2. Metcalf, W. W.; van der Donk, W. A., Biosynthesis of phosphonic and phosphinic acid natural products. *Annu. Rev. Biochem.* **2009,** *78*, 65-94.
3. Hendlin, D.; Stapley, E. O.; Jackson, M.; Wallick, H.; Miller, A. K.; Wolf, F. J.; Miller, T. W.; Chaiet, L.; Kahan, F. M.; Foltz, E. L.; Woodruff, H. B.; Mata, J. M.; Hernandez, S.; Mochales, S., Phosphonomycin, a new antibiotic produced by strains of streptomyces. *Science* **1969,** *166* (3901), 122-3.
4. Kahan, F. M.; Kahan, J. S.; Cassidy, P. J.; Kropp, H., The mechanism of action of fosfomycin (phosphonomycin). *Ann. N. Y. Acad. Sci.* **1974,** *235* (0), 364-86.
5. Brown, E. D.; Vivas, E. I.; Walsh, C. T.; Kolter, R., MurA (MurZ), the enzyme that catalyzes the first committed step in peptidoglycan biosynthesis, is essential in Escherichia coli. *J. Bacteriol.* **1995,** *177* (14), 4194-7.
6. Trapnell, B. C.; McColley, S. A.; Kissner, D. G.; Rolfe, M. W.; Rosen, J. M.; McKevitt, M.; Moorehead, L.; Montgomery, A. B.; Geller, D. E., Fosfomycin/tobramycin for inhalation in patients with cystic fibrosis with pseudomonas airway infection. *Am. J. Respir. Crit. Care. Med.* **2012,** *185* (2), 171-8.

7. Park, B. K.; Hirota, A.; Sakai, H., Studies on new antimetabolite produced by microorganism. Part III. Structure of plumbemycin A and B, antagonists of L-threonine from Streptomyces plumbeus. *Agricultural and Biological Chemistry* **1977,** *41* (3), 573-9.

8. Park, B. K.; Hirota, A.; Sakai, H., Studies on new antimetabolite produced by microorganism. Part II. 2-Amino-5-phosphono-3-pentenoic acid, a new amino acid from N-1409 substance, an antagonist of threonine. *Agricultural and Biological Chemistry* **1976,** *40* (9), 1905-6.

9. Rapp, C.; Jung, G.; Kugler, M.; Loeffler, W., Rhizocticins - new phosphono-oligopeptides with antifungal activity. *Liebigs. Annalen. der. Chemie.* **1988,** (7), 655-61.

10. Diddens, H.; Dorgerloh, M.; Zoehner, H., Metabolic products of microorganisms. 176. On the transport of small peptide antibiotics in bacteria. *Journal of Antibiotics* **1979,** *32* (1), 87-90.

11. Kugler, M.; Loeffler, W.; Rapp, C.; Kern, A.; Jung, G., Rhizocticin A, an antifungal phosphono-oligopeptide of Bacillus subtilis ATCC 6633: biological properties. *Archives of Microbiology* **1990,** *153* (3), 276-81.

12. Laber, B.; Gerbling, K. P.; Harde, C.; Neff, K. H.; Nordhoff, E.; Pohlenz, H. D., Mechanisms of interaction of Escherichia coli threonine synthase with substrates and inhibitors. *Biochemistry* **1994,** *33* (11), 3413-23.

13. Laber, B.; Lindell, S. D.; Pohlenz, H. D., Inactivation of Escherichia coli threonine synthase by DL-Z-2-amino-5-phosphono-3-pentenoic acid. *Arch. Microbiol.* **1994,** *161* (5), 400-3.

14. Borisova, S. A.; Circello, B. T.; Zhang, J. K.; van der Donk, W. A.; Metcalf, W. W., Biosynthesis of rhizocticins, antifungal phosphonate oligopeptides produced by Bacillus subtilis ATCC6633. *Chem. Biol.* **2010,** *17* (1), 28-37.

15. Steegborn, C.; Laber, B.; Messerschmidt, A.; Huber, R.; Clausen, T., Crystal structures of cystathionine gamma-synthase inhibitor complexes rationalize the increased affinity of a novel inhibitor. *J. Mol. Biol.* **2001,** *311* (4), 789-801.

16. Okuhara, M.; Kuroda, Y.; Goto, T.; Okamoto, M.; Terano, H.; Kohsaka, M.; Aoki, H.; Imanaka, H., Studies on new phosphonic acid antibiotics. I. FR-900098, isolation and characterization. *J. Antibiot. (Tokyo)* **1980,** *33* (1), 13-7.

17. Okuhara, M.; Kuroda, Y.; Goto, T.; Okamoto, M.; Terano, H.; Kohsaka, M.; Aoki, H.; Imanaka, H., Studies on new phosphonic acid antibiotics. III. Isolation and characterization of FR-31564, FR-32863 and FR-33289. *J. Antibiot. (Tokyo)* **1980,** *33* (1), 24-8.

18. Shigi, Y., Inhibition of bacterial isoprenoid synthesis by fosmidomycin, a phosphonic acid-containing antibiotic. *J. Antimicrob. Chemother.* **1989,** *24* (2), 131-45.

19. Eisenreich, W.; Bacher, A.; Arigoni, D.; Rohdich, F., Biosynthesis of isoprenoids via the non-mevalonate pathway. *Cell. Mol. Life Sci.* **2004,** *61* (12), 1401-26.

20. Hunter, W. N., The non-mevalonate pathway of isoprenoid precursor biosynthesis. *J. Biol. Chem.* **2007,** *282* (30), 21573-7.

21. Rohmer, M., The discovery of a mevalonate-independent pathway for isoprenoid biosynthesis in bacteria, algae and higher plants. *Nat. Prod. Rep.* **1999,** *16* (5), 565-74.

22. Borrmann, S.; Lundgren, I.; Oyakhirome, S.; Impouma, B.; Matsiegui, P. B.; Adegnika, A. A.; Issifou, S.; Kun, J. F.; Hutchinson, D.; Wiesner, J.; Jomaa, H.; Kremsner, P. G., Fosmidomycin plus clindamycin for treatment of pediatric patients aged 1 to 14 years with Plasmodium falciparum malaria. *Antimicrob. Agents. Chemother.* **2006,** *50* (8), 2713-8.

23. Missinou, M. A.; Borrmann, S.; Schindler, A.; Issifou, S.; Adegnika, A. A.; Matsiegui, P. B.; Binder, R.; Lell, B.; Wiesner, J.; Baranek, T.; Jomaa, H.; Kremsner, P. G., Fosmidomycin for malaria. *Lancet* **2002,** *360* (9349), 1941-2.

24. Na-Bangchang, K.; Ruengweerayut, R.; Karbwang, J.; Chauemung, A.; Hutchinson, D., Pharmacokinetics and pharmacodynamics of fosmidomycin monotherapy and combination therapy with clindamycin in the treatment of multidrug resistant falciparum malaria. *Malar. J.* **2007,** *6*, 70.

25. Evans, B. S.; Zhao, C.; Gao, J.; Evans, C. M.; Ju, K. S.; Doroghazi, J. R.; van der Donk, W. A.; Kelleher, N. L.; Metcalf, W. W., Discovery of the antibiotic phosacetamycin via a new mass spectrometry-based method for phosphonic acid detection. *ACS Chem. Biol.* **2013,** *8* (5), 908-13.

26. Kim, H.; Chin, J.; Choi, H.; Baek, K.; Lee, T. G.; Park, S. E.; Wang, W.; Hahn, D.; Yang, I.; Lee, J.; Mun, B.; Ekins, M.; Nam, S. J.; Kang, H., Phosphoiodyns A and B, unique phosphorus-containing iodinated polyacetylenes from a Korean sponge Placospongia sp. *Org. Lett.* **2013,** *15* (1), 100-3.

27. Ju, K. S.; Doroghazi, J. R.; Metcalf, W. W., Genomics-enabled discovery of phosphonate natural products and their biosynthetic pathways. *J. Ind. Microbiol. Biotechnol.* **2014,** *41* (2), 345-56.

28. Cioni, J. P.; Doroghazi, J. R.; Ju, K. S.; Yu, X.; Evans, B. S.; Lee, J.; Metcalf, W. W., Cyanohydrin phosphonate natural product from Streptomyces regensis. *J. Nat. Prod.* **2014,** *77* (2), 243-9.

29. Fleming, F. F., Nitrile-containing natural products. *Natural Product Reports* **1999,** *16* (5), 597-606.

30. Engel, R., Phosphonates as analogs of natural phosphates. *Chemical Reviews (Washington, DC, United States)* **1977,** *77* (3), 349-67.

31. Franz, J. E. N-Organo-N-phosphonomethylglycine-N-oxides and phytotoxicant compositions containing them. 1977-836338 4131448, 19770926., 1978.

32. Bentley, R., The shikimate pathway--a metabolic tree with many branches. *Crit. Rev. Biochem. Mol. Biol.* **1990,** *25* (5), 307-84.

33. Steinruecken, H. C.; Amrhein, N., The herbicide glyphosate is a potent inhibitor of 5-enolpyruvylshikimic acid 3-phosphate synthase.

Biochemical and Biophysical Research Communications **1980,** *94* (4), 1207-12.

34. Schonbrunn, E.; Eschenburg, S.; Shuttleworth, W. A.; Schloss, J. V.; Amrhein, N.; Evans, J. N.; Kabsch, W., Interaction of the herbicide glyphosate with its target enzyme 5-enolpyruvylshikimate 3-phosphate synthase in atomic detail. *Proc. Natl. Acad. Sci. U S A* **2001,** *98* (4), 1376-80.

35. Sammons, R. D.; Gruys, K. J.; Anderson, K. S.; Johnson, K. A.; Sikorski, J. A., Reevaluating Glyphosate as a Transition-State Inhibitor of EPSP Synthase: Identification of an EPSP Synthase·EPSP·Glyphosate Ternary Complex. *Biochemistry* **1995,** *34* (19), 6433-40.

36. United States EPA 2007 Pesticide Market Estimates Agriculture.

37. Bohn, T.; Cuhra, M.; Traavik, T.; Sanden, M.; Fagan, J.; Primicerio, R., Compositional differences in soybeans on the market: glyphosate accumulates in Roundup Ready GM soybeans. *Food Chem.* **2014,** *153*, 207-15.

38. Menschutkin, v. N., Ueber die Einwirkung des Chloracetyls auf phosphorige Säure. *Justus. Liebigs. Annalen. der. Chemie.* **1865,** *133* (3), 317-320.

39. Fleisch, H., Development of bisphosphonates. *Breast Cancer Res.* **2002,** *4* (1), 30-4.

40. Fleisch, H.; Russell, R. G.; Straumann, F., Effect of pyrophosphate on hydroxyapatite and its implications in calcium homeostasis. *Nature* **1966,** *212* (5065), 901-3.

41. Fleisch, H.; Russell, R. G.; Bisaz, S.; Casey, P. A.; Muhlbauer, R. C., The influence of pyrophosphate analogues (diphosphonates) on the precipitation and dissolution. *Calcif. Tissue. Res.* **1968**, Suppl:10-10a.

42. Fleisch, H.; Russell, R. G.; Francis, M. D., Diphosphonates inhibit hydroxyapatite dissolution in vitro and bone resorption in tissue culture and in vivo. *Science* **1969,** *165* (3899), 1262-4.

43. Francis, M. D.; Russell, R. G.; Fleisch, H., Diphosphonates inhibit formation of calcium phosphate crystals in vitro and pathological calcification in vivo. *Science* **1969,** *165* (3899), 1264-6.

44. Hughes, D. E.; Wright, K. R.; Uy, H. L.; Sasaki, A.; Yoneda, T.; Roodman, G. D.; Mundy, G. R.; Boyce, B. F., Bisphosphonates promote apoptosis in murine osteoclasts in vitro and in vivo. *J. Bone Miner Res.* **1995,** *10* (10), 1478-87.

45. Rogers, M. J.; Brown, R. J.; Hodkin, V.; Blackburn, G. M.; Russell, R. G. G.; Watts, D. J., Bisphosphonates are incorporated into adenine nucleotides by human aminoacyl-tRNA synthetase enzymes. *Biochemical and Biophysical Research Communications* **1996,** *224* (3), 863-869.

46. Luckman, S. P.; Coxon, F. P.; Ebetino, F. H.; Russell, R. G.; Rogers, M. J., Heterocycle-containing bisphosphonates cause apoptosis and inhibit bone resorption by preventing protein prenylation: evidence from structure-

activity relationships in J774 macrophages. *J. Bone. Miner. Res.* **1998,** *13* (11), 1668-78.

47. van Beek, E.; Pieterman, E.; Cohen, L.; Lowik, C.; Papapoulos, S., Farnesyl Pyrophosphate Synthase Is the Molecular Target of Nitrogen-Containing Bisphosphonates. *Biochemical and Biophysical Research Communications* **1999,** *264* (1), 108-111.

48. Bergstrom, J. D.; Bostedor, R. G.; Masarachia, P. J.; Reszka, A. A.; Rodan, G., Alendronate Is a Specific, Nanomolar Inhibitor of Farnesyl Diphosphate Synthase. *Archives of Biochemistry and Biophysics* **2000,** *373* (1), 231-241.

49. Oades, G. M.; Senaratne, S. G.; Clarke, I. A.; Kirby, R. S.; Colston, K. W., Nitrogen containing bisphosphonates induce apoptosis and inhibit the mevalonate pathway, impairing Ras membrane localization in prostate cancer cells. *J. Urol.* **2003,** *170* (1), 246-52.

50. World Health Organization, HIV/AIDS.

51. Weiss, R. A., How does HIV cause AIDS? *Science* **1993,** *260* (5112), 1273-9.

52. Mitsuya, H.; Weinhold, K. J.; Furman, P. A.; St Clair, M. H.; Lehrman, S. N.; Gallo, R. C.; Bolognesi, D.; Barry, D. W.; Broder, S., 3'-Azido-3'-deoxythymidine (BW A509U): an antiviral agent that inhibits the infectivity and cytopathic effect of human T-lymphotropic virus type III/lymphadenopathy-associated virus in vitro. *Proc. Natl. Acad. Sci. U S A* **1985,** *82* (20), 7096-100.

53. Cihlar, T.; Chen, M. S., Identification of enzymes catalyzing two-step phosphorylation of cidofovir and the effect of cytomegalovirus infection on their activities in host cells. *Mol. Pharmacol.* **1996,** *50* (6), 1502-10.

54. De Clercq, E.; Holy, A., Acyclic nucleoside phosphonates: a key class of antiviral drugs. *Nat. Rev. Drug Discov.* **2005,** *4* (11), 928-40.

55. Robbins, B. L.; Greenhaw, J.; Connelly, M. C.; Fridland, A., Metabolic pathways for activation of the antiviral agent 9-(2-phosphonylmethoxyethyl)adenine in human lymphoid cells. *Antimicrob. Agents Chemother.* **1995,** *39* (10), 2304-8.

56. Magee, W. C.; Hostetler, K. Y.; Evans, D. H., Mechanism of inhibition of vaccinia virus DNA polymerase by cidofovir diphosphate. *Antimicrob. Agents Chemother.* **2005,** *49* (8), 3153-62.

57. Rose, I. A.; O'Connell, E. L., The Role of Glucose 6-Phosphate in the Regulation of Glucose Metabolism in Human Erythrocytes. *J. Biol. Chem.* **1964,** *239*, 12-7.

58. Griffin, B. S.; Burger, A., D-Glucopyranose 6- deoxy- 6- phosphonic acid. *Journal of the American Chemical Society* **1956,** *78*, 2336-8.

59. J. G. Moffattand, G. H. J., Patent 3524846 (18 Aug 1970);. **1970**.

60. Shen, Q.; Sloss, D. G.; Berkowitz, D. B., Displacement of sugar triflates with C-nucleophiles: D-glucopyranose and D-ribofuranose chain extension and functionalization. *Synthetic Communications* **1994,** *24* (11), 1519-30.

61. Berkowitz, D. B.; Eggen, M.; Shen, Q.; Sloss, D. G., Synthesis of (α,α-difluoroalkyl)phosphonates by displacement of primary triflates. *Journal of Organic Chemistry* **1993,** *58* (23), 6174-6.

62. Berkowitz, D. B.; Shen, Q.; Maeng, J.-H., Synthesis of the (α,α-difluoroalkyl)phosphonate analog of phosphoserine. *Tetrahedron Letters* **1994,** *35* (35), 6445-8.

63. Berkowitz, D. B.; Sloss, D. G., Diallyl (Lithiodifluoromethyl)phosphonate: A New Reagent for the Introduction of the (Difluoromethylene)phosphonate Functionality. *Journal of Organic Chemistry* **1995,** *60* (21), 7047-50.

64. Berkowitz, D. B.; Eggen, M.; Shen, Q.; Shoemaker, R. K., Ready Access to Fluorinated Phosphonate Mimics of Secondary Phosphates. Synthesis of the (α,α-Difluoroalkyl)phosphonate Analogs of L-Phosphoserine, L-Phosphoallothreonine, and L-Phosphothreonine. *Journal of Organic Chemistry* **1996,** *61* (14), 4666-4675.

65. Berkowitz, D. B.; Bhuniya, D.; Peris, G., Facile installation of the phosphonate and (α,α-difluoromethyl)phosphonate functionalities equipped with benzyl protection. *Tetrahedron Letters* **1999,** *40* (10), 1869-1872.

66. Blackburn, G. M.; Brown, D.; Martin, S. J., A novel synthesis of fluorinated phosphonoacetic acids. *Journal of Chemical Research, Synopses* **1985,** (3), 92-3.

67. Blackburn, G. M.; Kent, D. E., Synthesis of α- and γ-fluoroalkylphosphonates. *Journal of the Chemical Society, Perkin Transactions 1: Organic and Bio-Organic Chemistry (1972-1999)* **1986,** (6), 913-17.

68. Blackburn, G. M.; Brown, D.; Martin, S. J.; Parratt, M. J., Studies on selected transformations of some fluoromethanephosphonate esters. *Journal of the Chemical Society, Perkin Transactions 1: Organic and Bio-Organic Chemistry (1972-1999)* **1987,** (1), 181-6.

69. McKenna, C. E.; Khawli, L. A.; Bapat, A.; Harutunian, V.; Cheng, Y. C., Inhibition of herpesvirus and human DNA polymerases by alpha-halogenated phosphonoacetates. *Biochem. Pharmacol.* **1987,** *36* (19), 3103-6.

70. McKenna, C. E.; Pham, P. T.; Rassier, M. E.; Dousa, T. P., Alpha-halo [(phenylphosphinyl)methyl]phosphonates as specific inhibitors of Na(+)-gradient-dependent Na(+)-phosphate cotransport across renal brush border membrane. *J. Med. Chem.* **1992,** *35* (26), 4885-92.

71. Romanenko, V. D.; Kukhar, V. P., Fluorinated phosphonates: synthesis and biomedical application. *Chem. Rev.* **2006,** *106* (9), 3868-935.

72. Chambers, R. D.; Jaouhari, R.; O'Hagan, D., Synthesis of a difluoromethylenephosphonate analog of glycerol-3-phosphate. A substrate for NADH linked glycerol-3-phosphate dehydrogenase. *Journal of the Chemical Society, Chemical Communications* **1988,** (17), 1169-70.

73. Diab, S. A.; De Schutter, C.; Muzard, M.; Plantier-Royon, R.; Pfund, E.; Lequeux, T., Fluorophosphonylated Nucleoside Derivatives as New Series of Thymidine Phosphorylase Multi-Substrate Inhibitors. *Journal of Medicinal Chemistry* **2012,** *55* (6), 2758-2768.

74. Forget, S. M.; Bhattasali, D.; Hart, V. C.; Cameron, T. S.; Syvitski, R. T.; Jakeman, D. L., Synthesis and enzymatic evaluation of ketose phosphonates: the interplay between mutarotation, monofluorination, and acidity. *Chemical Science* **2012,** *3* (6), 1866-1878.

75. Halazy, S.; Ehrhard, A.; Danzin, C., 9-(Difluorophosphonoalkyl)guanines as a new class of multisubstrate analog inhibitors of purine nucleoside phosphorylase. *Journal of the American Chemical Society* **1991,** *113* (1), 315-17.

76. Hikishima, S.; Hashimoto, M.; Magnowska, L.; Bzowska, A.; Yokomatsu, T., Synthesis and biological evaluation of 9-deazaguanine derivatives connected by a linker to difluoromethylene phosphonic acid as multi-substrate analogue inhibitors of PNP. *Bioorganic & Medicinal Chemistry Letters* **2007,** *17* (15), 4173-4177.

77. Nieschalk, J.; O'Hagan, D., Monofluorophosphonates as phosphate mimics in bioorganic chemistry: a comparative study of CH2-, CHF- and CF2-phosphonate analogs of sn-glycerol-3-phosphate as substrates for sn-glycerol-3-phosphate dehydrogenase. *Journal of the Chemical Society, Chemical Communications* **1995,** (7), 719-20.

78. Phillion, D. P.; Cleary, D. G., Disodium salt of 2-[(dihydroxyphosphinyl)difluoromethyl]propenoic acid: an isopolar and isosteric analog of phosphoenolpyruvate. *Journal of Organic Chemistry* **1992,** *57* (9), 2763-4.

79. Surya Prakash, G. K.; Zibinsky, M.; Upton Thomas, G.; Kashemirov Boris, A.; McKenna Charles, E.; Oertell, K.; Goodman Myron, F.; Batra Vinod, K.; Pedersen Lars, C.; Beard William, A.; Shock David, D.; Wilson Samuel, H.; Olah George, A., Synthesis and biological evaluation of fluorinated deoxynucleotide analogs based on bis-(difluoromethylene)triphosphoric acid. *Proc. Natl. Acad. Sci. U S A* **2010,** *107* (36), 15693-8.

80. Vinod, T. K.; Griffith, O. H.; Keana, J. F. W., Synthesis of isosteric and isopolar phosphonate substrate analogs designed as inhibitors for phosphatidylinositol-specific phospholipase C from Bacillus cereus. *Tetrahedron Letters* **1994,** *35* (39), 7193-6.

81. Walker, S. R.; Cumming, H.; Parker, E. J., Substrate and reaction intermediate mimics as inhibitors of 3-deoxy-d-arabino-heptulosonate 7-phosphate synthase. *Organic & Biomolecular Chemistry* **2009,** *7* (15), 3031-3035.

82. Burke, T. R., Jr.; Kole, H. K.; Roller, P. P., Potent inhibition of insulin receptor dephosphorylation by a hexamer peptide containing the phosphotyrosyl mimetic F2Pmp. *Biochemical and Biophysical Research Communications* **1994,** *204* (1), 129-34.

83. Berkowitz, D. B.; Bose, M.; Pfannenstiel, T. J.; Doukov, T., alpha-fluorinated phosphonates as substrate mimics for glucose 6-phosphate dehydrogenase: the CHF stereochemistry matters. *J. Org. Chem.* **2000,** *65* (15), 4498-508.

84. Berkowitz, D. B.; Bose, M.; Asher, N. G., A convergent triflate displacement approach to (alpha-monofluoroalkyl)phosphonates. *Org. Lett.* **2001,** *3* (13), 2009-12.

85. Berkowitz, D. B.; Maiti, G.; Charette, B. D.; Dreis, C. D.; MacDonald, R. G., Mono- and bivalent ligands bearing mannose 6-phosphate (M6P) surrogates: targeting the M6P/insulin-like growth factor II receptor. *Org. Lett.* **2004,** *6* (26), 4921-4.

86. unpublished results.

87. Panigrahi, K.; Eggen, M.; Maeng, J. H.; Shen, Q.; Berkowitz, D. B., The alpha,alpha-difluorinated phosphonate L-pSer-analogue: an accessible chemical tool for studying kinase-dependent signal transduction. *Chem. Biol.* **2009,** *16* (9), 928-36.

Chapter 2

Phosphatase-Inert Actuators for the *glmS* Riboswitch

I. Introduction

A. Background of Riboswitches

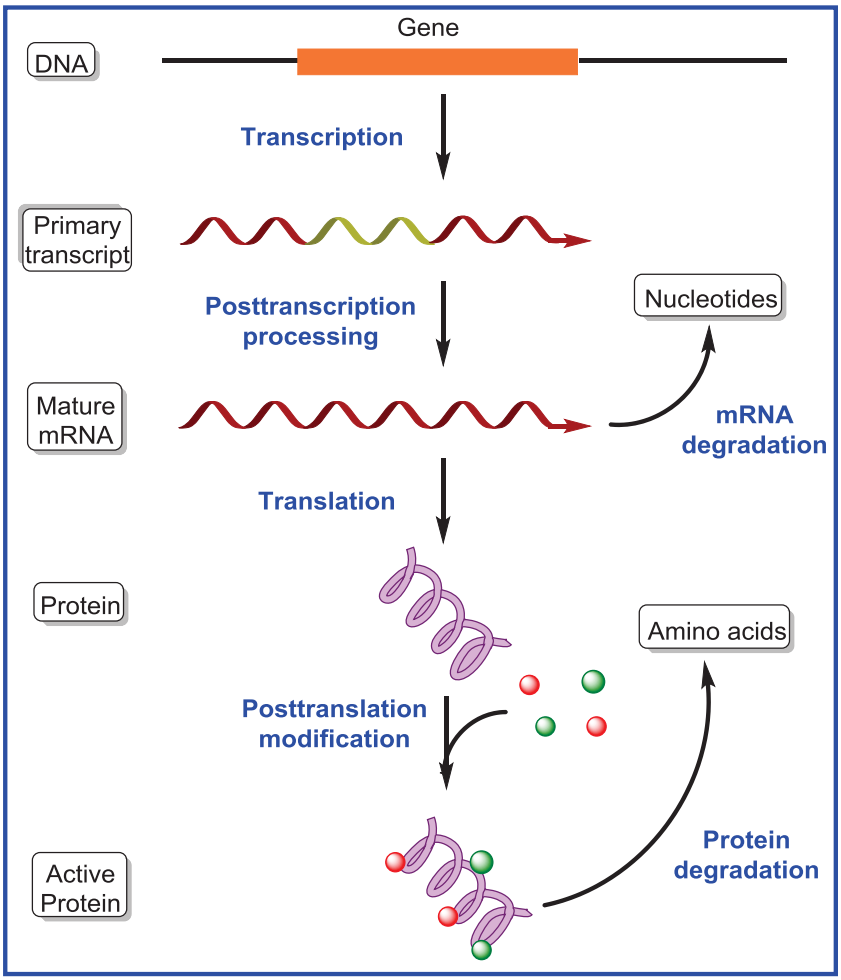

Figure 2.1: Regulation of gene expression could occur in any step of its process

At any given time, a typical human or bacterial cell only expresses a fraction of its genes (~3% to 5%). "The fundamental problem of chemical physiology and of embryology is to understand why tissues cells do not all express, all the time, all the

potentialities in their genome," commented Jacob and Monod.[1] Indeed, gene expression is controlled by an extremely sophisticated system that coordinates numerous tasks to respond to developmental needs and environmental stimuli.[2] Essentially, any step of the expression process can be recruited to modulate levels of gene products in a cell (Fig. 2.1). The most well-characterized mechanism is the protein-based modulation of transcription initiation.[3] Numerous transcription factors have been uncovered since the initial discovery of the lactose repressor (LacI), which interacts with the *lac* operon to ultimately control the production levels of lactose-metabolism enzymes.[4] In addition to their interactions with DNA, protein factors can bind to mRNA to regulate either transcription termination (e.g. the PyrR protein[5]) or translation (e.g., TRAP protein[6] and CUGBP1[7]). Because proteins can adopt different conformations to respond to cellular and environmental cues, they can carry out a variety of regulatory activities. In contrast, nucleic acids were considered to be merely responsible for storing and transferring genetic information.[2]

Discoveries made in recent decades have proven that RNA plays a far more sophisticated role than originally believed. Notable examples include the discoveries of small interfering RNA (siRNA) and micro RNA (miRNA) which are central to RNA interference (RNAi).[8-9] These small non-coding RNAs exert posttranscriptional gene control, either through protein-associated RNA cleavage (siRNA)[10] or sequence specific RNA binding (miRNA)[11-12]. RNAi mechanism has been found in many eukaryotic cells including plants and animals. In 2006, the Nobel Prize in Physiology or Medicine was awarded to Fire and Mello for their discovery of RNA interference.[13]

Within the last 12 years, a new gene-control mechanism has emerged in which mRNA self-regulates its own translation, with no obligate needs for protein factors.[14-20] Termed riboswitches, these 5'-untranslated regions (UTRs) sense specific secondary metabolites. Upon binding RNA,these small molecules typically induce allosteric changes in the conserved structures, which ultimately leads to the termination of gene expression.[21] Prior to the discovery of the existence of riboswitches in nature, the regulation of some essential genes in bacterial metabolism remained enigmatic. For example, thiamin (Vitamin B1) is a crucial coenzyme for bacterial cell growth. However, when bacteria are in thiamin-adequate media, they will exploit exogenous thiamin rather than produce their own. Therefore, there must be a regulatory factor that senses the concentration of the product and controls the expression of the biosynthetic genes. This led to the postulate that a thiamin pyrophosphate (TPP) sensing protein was involved in the modulation of thiamin biosynthetic genes.[22] However, such a regulatory protein has not been discovered in nature thus far.

Alternatively, in 2001, Miranda-Rios and Soberon disclosed that the conserved structure (*thi* box) of the mRNAs encoding thiamin biosynthetic enzymes is indispensable for *thi* gene expression, implying the presence of a RNA-dependent gene regulating system.[23] In 2002, Breaker *et al*. confirmed that the mRNAs (*thiM* and *thiC*) indeed regulate *thi* gene expression via an allosteric mechanism.[24] Namely, the 5'-UTRs of *thiM* and *thiC* bind thiamin or its pyrophosphate derivative, ultimately leading to the reduction of gene expression. The resultant/resulting complex is shown to take on a conformation than is distinct from that of the unbound RNA structure, which is proposed

Table 2.1: Known riboswitches in the nature and their cognate ligands

Riboswitch	Functional System	Cognate ligand	K_d	Discovery
TPP riboswitch (THI-box)	Thiamin biosynthesis; transport of thiamin and related compounds	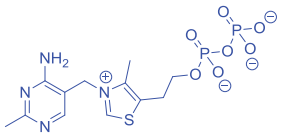	8-600 nM	**2002**
FMN riboswitch (RFN-element)	Riboflavin biosynthesis and transport	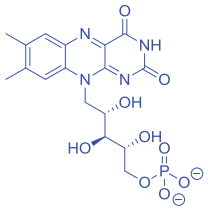	~5 nM	**2002**
SAM riboswitches (S-box)	Methionine biosynthesis and transport; SAM metabolism	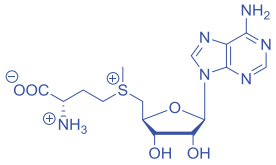	4 nM	*SAM-I:* **2003** *SAM-II:* **2005** *SAM-III:* **2006** *SAM-IV*: **2007** *SAM-V*: **2007**
SAH riboswitch	SAH recycling system for SAM biosynthesis	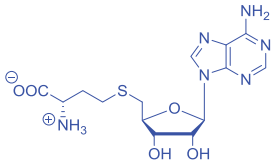	~ 20 nM	**2008**
Purine riboswitch (G-box or XptR regulon)	Purine metabolism and transport	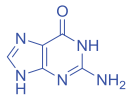	~5 nM	**2003**
			0.47 μM	
PreQ1 riboswitches	Pre-queuosine metabolism and transport	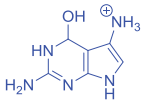	~2.5 nM	**2007**
ATP riboswitch (ydaO leader)	ATP metabolism and transport	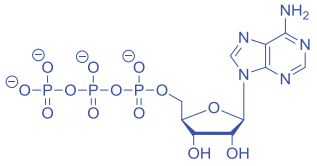	0.6 mM	**2012**

Table 2.1 (Continued).

cyclic di-GMP riboswitches	c-di-GMP involved singal transduction	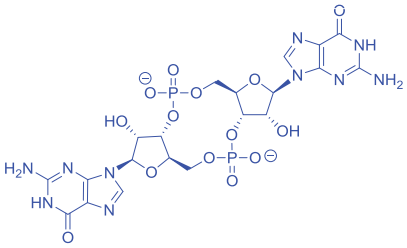	Class I: 16 nM Class II: 2.2 nM	**2008**
Lysine riboswitch (L-box or LYS-element)	Lysine biosynthesis, transport and catabolism	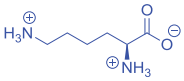	1 μM	**2003**
Glycine riboswitch	Glycine metabolism	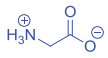	5 nM- 30 μM	**2004**
Glutamine riboswitch	Glutamine and nitrogen metabolism	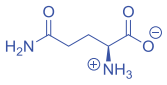	150-575 μM	**2011**
glmS riboswitch	GlcN6P metabolism	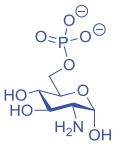	k_{cat}/K_m: 1.1-100 min^{-1}	**2004**
THF riboswitch	tetrahydrofolate metabolism and transport	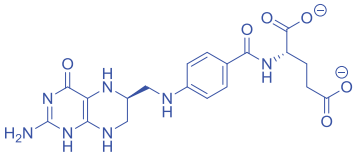	~8 μM	**2010**
Cobalamin riboswitch (B_{12} element)	Cobalamin biosynthesis; transport of cobalamin and related compounds; cobalt transport; cobalaminindependent isozymes of cobalamin-dependent enzymes	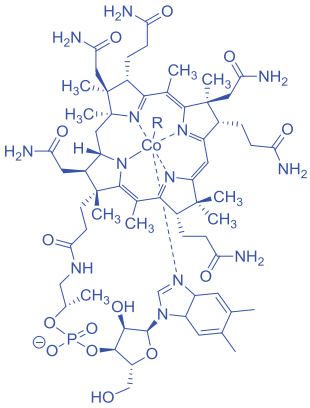	300 nM	**2002**

as the mechanism underlying the translation inhibition.[25] In the same year, the Breaker group unveiled two more riboswitches that sense flavin mononucleotide (FMN, Vitamin B_2)[26] and cobalamin (Vitamin B_{12}),[27] respectively. Since then, this mRNA self-regulating mechanism has been found be widely used in prokaryotic cells (Table 2.1).[18] To date, there are approximately two dozen riboswitches that have been experimentally validated to sense 17 different metabolites, one secondary messenger (cyclic di-GMP) and one divalent cation (Mg^{2+}).[28]

B. Background of the *glmS* riboswitch

In 2004, a unique riboswitch was disclosed by the Breaker group by exploiting bioinformatics in bacterial genomes. Riboswitches have conserved sequence and secondary structures, typically located in the noncoding or intergenic regions (IGRs). Using the database known as the Breaker Laboratory Intergenic Sequence Server (BLISS), they examined the IGRs of 91 microbial genomes, that led to a variety of conserved RNA motifs.[29] The *glmS* element was found to be highly conserved in 18 gram-positive bacteria (Fig 2.2). It resides upstream of the *glmS* gene which codes for the enzyme glucosamine 6-phosphate synthase or synthetase (glmS). GlmS lies at the beginning of the cell wall biosynthesis. It converts fructose 6-phosphate to glucosamine 6-phosphate, exploiting glutamine as the amine source. Along the biochemical pathway, several metabolites could serve as the signaling molecule for the putative *glmS* riboswitch.

To identify effective ligands for riboswitches, an “in line probing” assay was previously developed.[27] This assay relies on the structure-dependent RNA self-cleavage. Single strand RNA is relatively unstable and can be cleaved spontaneously over time.

The rate of the cleavage is found to be closely related to the secondary and tertiary structure. The spontaneous cleavage only occurs at a substantial rate when the

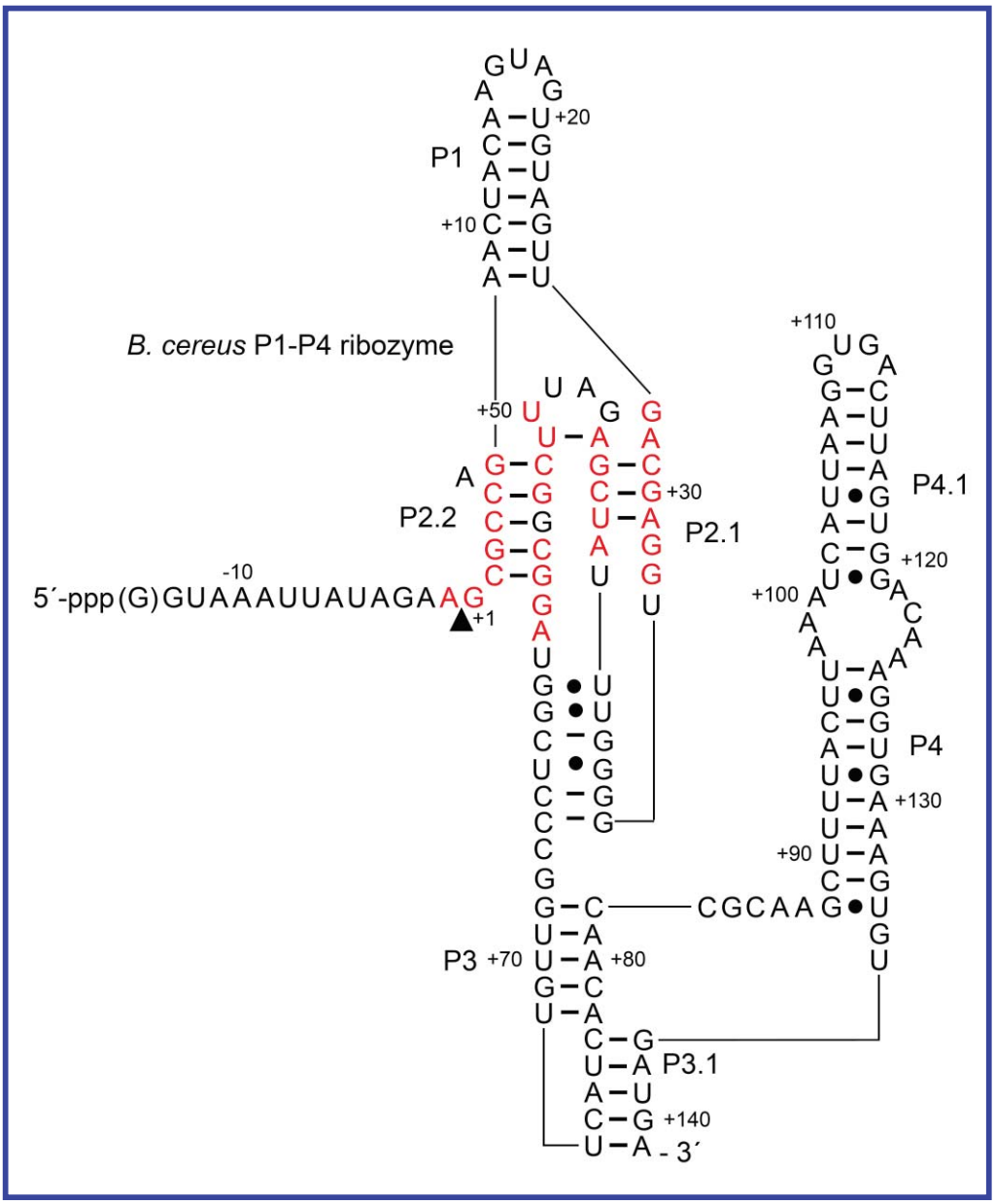

Figure 2.2: Secondary structure of the *Bacillus cereus glmS* riboswitch/ribozyme. The highly conserved core sequence of the *glmS* ribozyme is shown in red (P2.1 and P2.2), while requisite structural elements (P1 and P2) and peripheral structural elements (P3-P4) are also displayed with nucleotide detail. The arrowhead denotes the site of self-cleavage.

nucleophilic 2'-oxygen, phosphorus, and the leaving 5'-oxygen are in the proper position. Thus, regions with stable base-paired structures rarely undergo cleavage, while the nucleotides in some tertiary structures are particularly vulnerable to adjacent nucleophilic attack. Therefore, by incubating a messenger RNA in the presence or absence of potential ligands and examining the change in cleavage patterns, one can identify small molecule effectors as well as their binding regions on the RNA.

Prior to the discovery of GlcN6P as a riboswitch ligand, the "in line probing" assay had successfully recognized cobalamin[27], thiamin[24], FMN[26], SAM[30], glycine[31] and lysine[32] for binding their corresponding riboswitches. Consequently, Breaker *et al.* subjected a 246-nucleotide *glmS* mRNA from *Bacillus subtilis* to the assay with various metabolite candidates. Gel electrophoresis revealed that the mRNA was mostly cleaved within 1 min in the presence of 200 μM GlcN6P, while the same cleavage fragment in the absence of GlcN6P was almost negligible. Such an observation experimentally confirms the existence of the *glmS* riboswitch in bacteria, and divulges that GlcN6P serves as a handle, exerting a genetic switch to regulate *glmS* gene expression.[33]

More interestingly, single-site cleavage is 1000-fold faster than the spontaneous cleavage of a typical unconstrained RNA linkage, and 10-fold faster than any known constrained RNA structure that favors the phosphodiester transesterification.[34] This made Breaker and others wonder whether this "spontaneous cleavage" is really spontaneous or actually catalytic. The extensive kinetic characterization and x-ray crystal structures have now led to the conclusion that the *glmS* RNA is indeed a novel class of ribozyme.[35] In the presence of GlcN6P, it accelerates its self-cleavage by $10^{6\text{-}8}$ fold.[33, 36-37] This feature makes the *glmS* riboswitch/ribozyme unique in both categories. As a riboswitch, it

undergoes a self-cleavage rather than a conformational change to regulate gene expression. As a catalytic RNA, it is the first known natural ribozyme that requires a small molecule cofactor for the catalysis.[35] Together with the other 13 classes of naturally-occurring ribozymes, the *glmS* ribozyme supports the "RNA world" theory which hypothesizes that life begins from self-replicating RNA, rather than the DNA-RNA-protein system in current biology.[38]

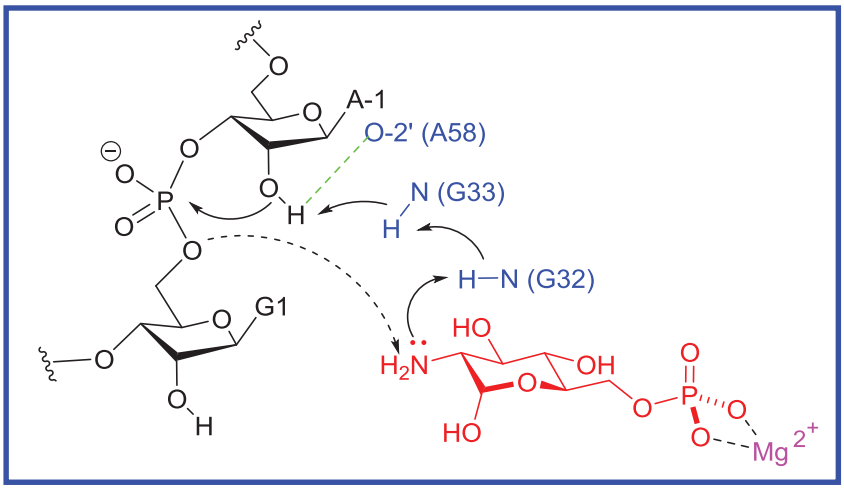

Figure 2.3: Plausible mechanism for the GlcN6P activated RNA cleavage

There has been debate about the role of GlcN6P in the mechanism of *glmS* self-cleavage. Previously, it was proposed that GlcN6P only acts as a general acid which protonates the leaving oxygen of the phosphate group. This was supported by the crystal structure that shows a nearby guanine (G33) posed to deprotonate the 2'-OH of the attacking nucleotide A-1.[39-40] Furthermore, a G33A mutation deactivates the *glmS* self-cleavage, which validates that the guanine is essential for the catalysis.[40] However, in 2011, Fedor *et al.* conducted a pH-fluorescence profiling using a fluorescent guanosine analogue, 8-azaguanosine. The microscopic p*K*a of the active site guanine was measured

to be around 8.9, which suggests the guanine (N1) should be protonated under the assay pH (~7.3).[41]

Furthermore , it has been demonstrated that the cleavage rate has a dependence on the pK_a of the amino group of GlcN6P.[37] The Brønsted β-value for GlcN6P was recently determined to be 0.7 in Fedor's group, suggesting a general base role in the catalysis.[36] GlcN6P analogues that lack the base function of the 2-amino group also failed to catalyze the cleavage.[42] Therefore, the mechanistic most consistent with all available data appears to be on in which GlcN6P serves as a general base and a general acid in the activation of the *glmS* self-cleavage. As shown in Fig. 2.3, in this view, the GlcN6P-2-amino group deprotonates the 2'-OH of A-1 through a proton hopping mechanism. The 2'-oxygen attacks the phosphodiester linkage, forming the 2'-3' cyclic phosphodiester. The 2-amino group protonates the leaving oxygen of G1, facilitating the cleavage. This proposed mechanism is supported by Raman difference crystallography studies[43] and computational simulations[44]. These studies suggest that the *glmS* active site tunes down the GlcN6P ($-NH_2$) pK_a to align with the optimal reaction pH.

C. *GlmS* riboswitch as an antimicrobial target

In addition to being a great study subject, the *glmS* riboswitch also represents a potential new target for antimicrobial drug development. Bacterial resistance is emerging at an alarming rate. A 2014 WHO report reveals that "this serious threat is no longer a prediction for the future, it is happening right now in every region of the world and has the potential to affect anyone, of any age, in any country."[45] However, most academic groups and companies are working on known scaffolds and known targets.[46] To

sustainably battle bacterial pathogens, especially the multidrug-resistant "superbugs", new targets in the bacterial life cycle are in great demand. Riboswitches have emerged as attractive alternatives for the development of new antibiotics.[47-48] These metabolite-sensing RNAs regulate expression of genes that are essential in bacterial metabolism. In addition, most riboswitches are present in prokaryotic cells. No natural riboswitch has been detected in mammalian cells to date. This reduces the potential toxicity issues that are affecting many antibiotic candidates.

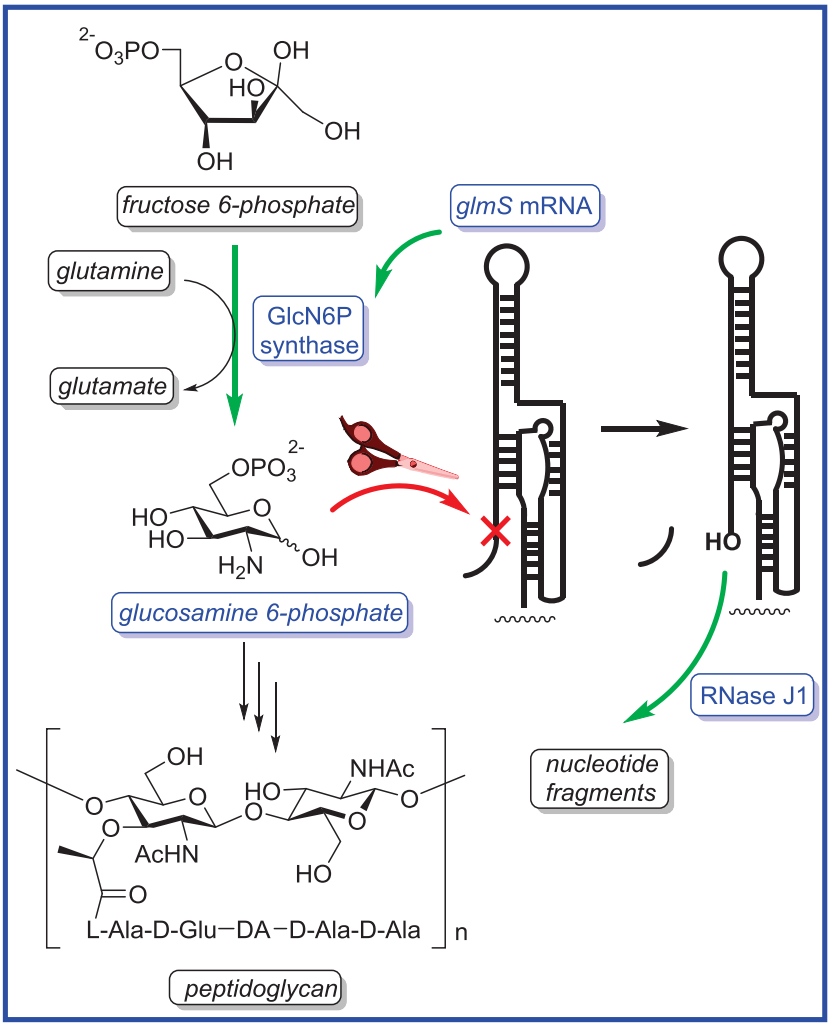

Figure 2.4: A negative feedback mechanism exerted by the *glmS* riboswitch to regulate *glmS* gene expression

In addition, the *glmS* riboswitch is found in a number of pathogenic bacteria, including high profile ones such as *S. aureus*, *Clostridium difficile*, and *B. anthracis.*[49] In the life cycle of these bacteria, proper control of *glmS* gene expression is critical for the production of GlcN6P, an essential metabolic precursor for bacterial cell wall synthesis.[50] As GlcN6P accumulates in the cell, it facilitates the self-cleavage of *glmS* RNA, unleashing a new 5'-end as a marker for Ribonuclease J1 (RNase J1).[51] Further degradation destroys the coding region of *glmS* RNA, decreasing the production of GlcN6P synthase and therefore the product of GlcN6P in the cell. Thus, a small molecule that artificially actuates the *glmS* riboswitch could lead to significant reduction of *glmS* gene expression, consequently disrupting the cell wall biosynthesis (Fig. 2.4). This idea has prompted several efforts to develop artificial actuators for the *glmS* riboswitch.

In a 2004 *Nature* paper, the Breaker group demonstrated that the *glmS* RNA strongly favors GlcN6P against even closely related analogues.[33] This was later reinforced by several other SAR characterizations from Breaker and other groups.[36-37, 42] From these studies, along with x-ray crystal structures, a series of key molecular components were proposed for GlcN6P-actuator activity: i) the 6-phosphate is the anchoring element that binds one of two Mg^{2+} ions in the active site; ii) the 4-hydroxyl group is considered as an indispensable hydrogen-bond donor for the binding; iii) the fact that *glmS* RNA binds only the α-anomer GlcN6P suggests that the anomeric -OH is also involved in molecular recognition; iv) the free 2-amino group has proven to be essential for the actuation, and in the Soukup model, this amino group serves the role of a general base and a general acid (in the ammonium form) for the catalytic RNA-cleavage.

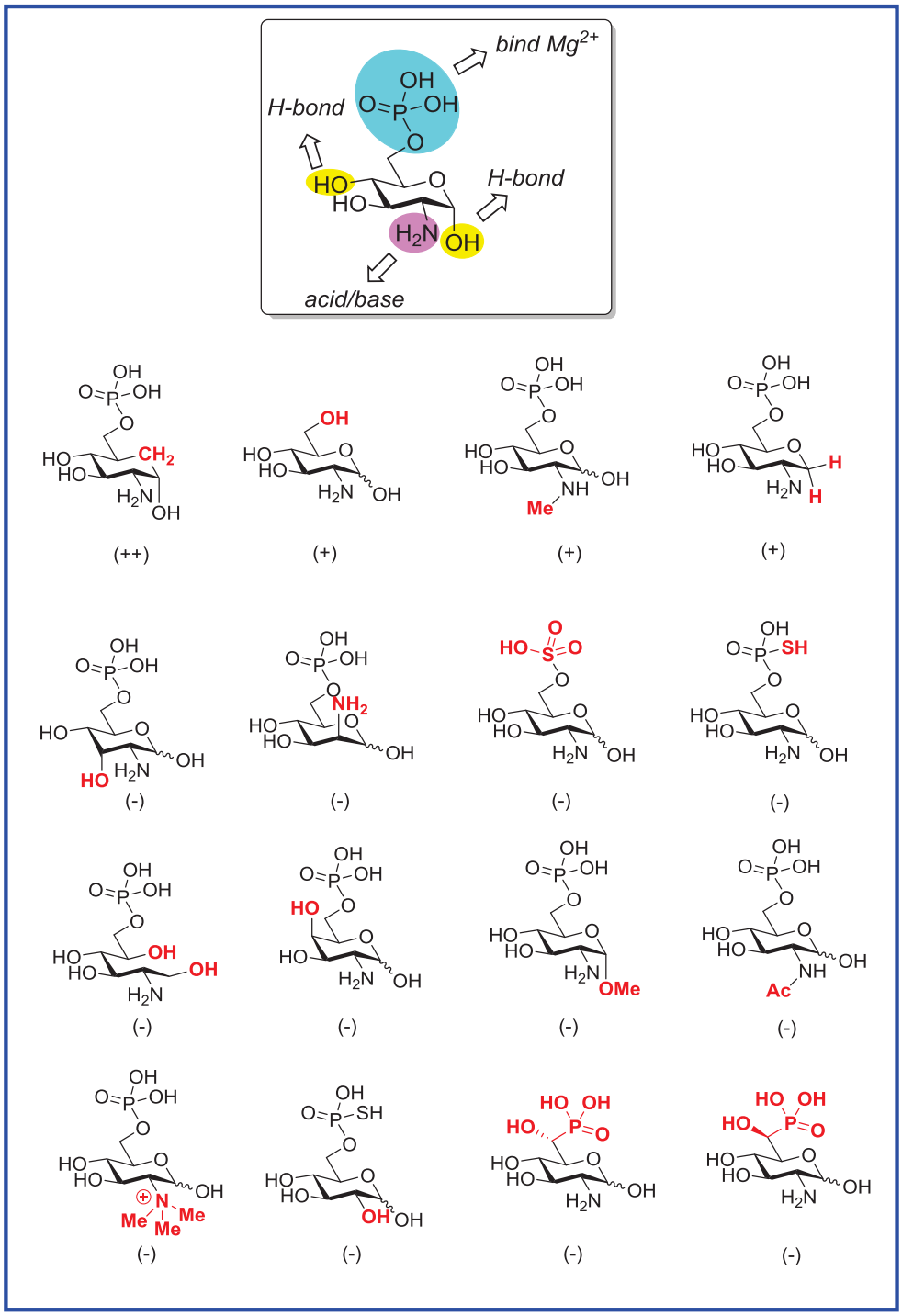

Figure 2.5: Ligand characterization for the *glmS* riboswitch

In 2006, Mayer and Famulok developed a "high throughput compatible" assay to identify artificial actuators of the *glmS* riboswitch.[52] They derivatized the 5'-end of an 81-nucleotide *glmS* RNA with a fluorescent label. Utilizing fluorescence polarization (FP),

they were able to estimate binding affinity between the nucleic acid and the small molecules. The modified RNA responded well to GlcN6P, as the intensity of FP showed strict dependence on GlcN6P's concentration. However, to their disappointment, the screening of an initial 88-membered library, and later over 5000 compounds[53] did not yield any compounds that could actuate the *glmS* riboswitch.

In 2011, Mayer *et al.* went back to the structure-based approach. They synthesized and tested 9 analogues of GlcN6P.[53] Interestingly, the replacement of the ring oxygen with -CH_2- only resulted in a modest loss of activity. At a concentration of 200 μM, the carba-GlcN6P promotes the RNA self-cleavage with a reported rate constant of 0.153 min^{-1}, comparable to that of 0.177 min^{-1} from the natural metabolite. Other modifications of the sugar phosphate, however, were much less tolerated in the *glmS*-riboswitch active site. It is noted that this carbocyclic glucosamine 6-phosphate was later included in another SAR characterization. In this study, a different group also synthesized a pair of nonisosteric α-hydroxyl phosphonate analogues.[54] Nonetheless, these shortened phosphonate analogues showed no activity for the cleavage assay. Recently, Posakony and Ferré-D'Amaré synthesized a series of GlcN6P and GlcN analogues as well; however, the activities of these were not disclosed in the report.[55]

II. Results and Discussion

A. Synthesis of GlcN6P Analogues

As a group that excels in synthesizing phosphonate analogues, we embarked on the *glmS* project in collaboration with Prof. Julianne Soukup from Creighton University. Perhaps, the most obvious such analogue to target was the isosteric phosphonate

surrogate for GlcN6P. However, phosphonate analogues of aminosugar 6-phosphates had not been reported prior to this work. A synthetic strategy remained to be established. To adopt our triflate displacement methodology, we needed to design and synthesize a viable glucosamine 6-*O*-triflate. And one significant challenge was to find a proper protecting group, that would be compatible for both the triflate installation step and the displacement step. The initial effort using an acetyl group met with little success in the triflate installation stage, while the trifluoroacetyl group proved to be incompatible with the displacement conditions. One the other hand, sulfonyl protecting groups were well tolerated under such conditions, with the (2-trimethylsilyl)ethanesulfonyl (SES) group being optimal.

The key step in our synthetic route involves an iodonium-mediated sulfonamidoglycosylation of glycals. This chemistry was discovered in 1990s by Griffith and Danishefsky, and has been broadly employed to assemble glucosamine-containing oligosaccharides.[56-57] This particular iodonium salt, iodonium di(*sym*-collidine) perchlorate (IDCP) was shown to be critical for the success of the initial alkene iodination reaction. Therefore, staring from the glucal **1**, we first introduced the sulfonylamino functionality to the 1-position using freshly prepared IDCP. Upon treatment with an alcohol, in the presence of a silver salt and base, the amino group "rolls over" to the 2-position of the sugar, via a presumed N-sulfonyl aziridine intermediate, that is opened on the anomeric side by the alkoxide present. Following the successful application of this N-rollover reaction with benzyloxy-anion opening of the putative sulfonyl aziridine intermediate, the sulfonyl nitrogen was further protected via N-benzylation. Fluoride deprotection of the TBDPS group then gave the free alcohol **3**

which proved to be a convenient stage at which to store significant quantities of material, as a key intermediate.

. The reaction between **3** and triflic anhydride provided the glucosamine 6-*O*-triflate in over 90% yield. This triflate intermediate displayed only modest stability under argon. Its DCM solution (concentration < 1 g/L) was stored in a -40 °C freezer for 3 days, with no significant degradation using NMR analysis. However, when being dried under vacuum, the compound turned to a brown color within 1 h at rt. A TLC analysis showed that multiple degradation products were generated from the triflate. Consequently, compound **4** was normally freshly prepared and immediately subjected to the displacement reaction. The displacement of 6-*O*-triflate with excess di-*O*-benzyl phosphonomethyl lithium gave the phosphonate product **5** in up to 62% yield. Additives such as HMPA were explored in effort to increase the reaction yield, however, no appreciable improvement was observed. Following the SES deprotection with CsF, the global deprotection of six benzyl groups proceeded smoothly in 86% yield. The fully

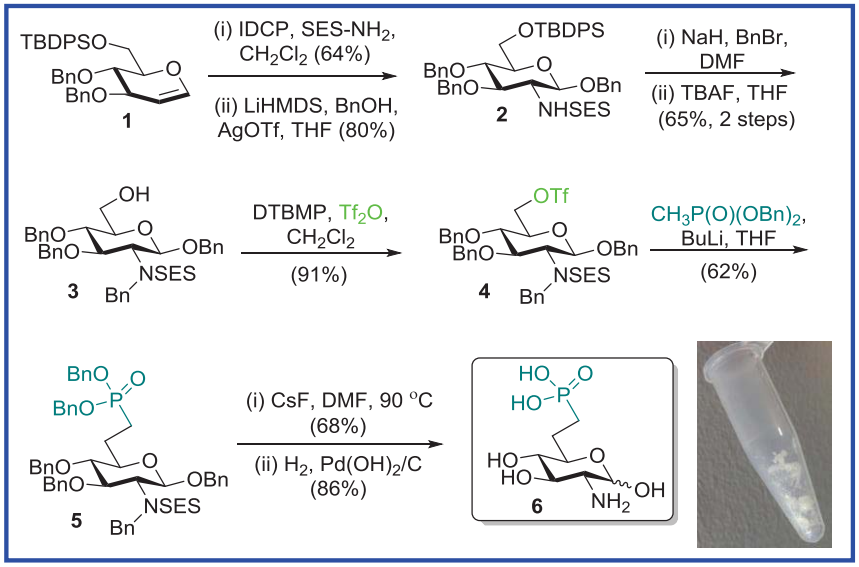

Figure 2.6: Synthesis of phosphonate 6 via triflate

deprotected phosphonate was then purified by trituration with methanol, to a purity of over 95% (estimated from NMR analysis). Lyophilization finally afforded the desired phosphonate surrogate of GlcN6P **6** as a white foam (Fig. 2.6).

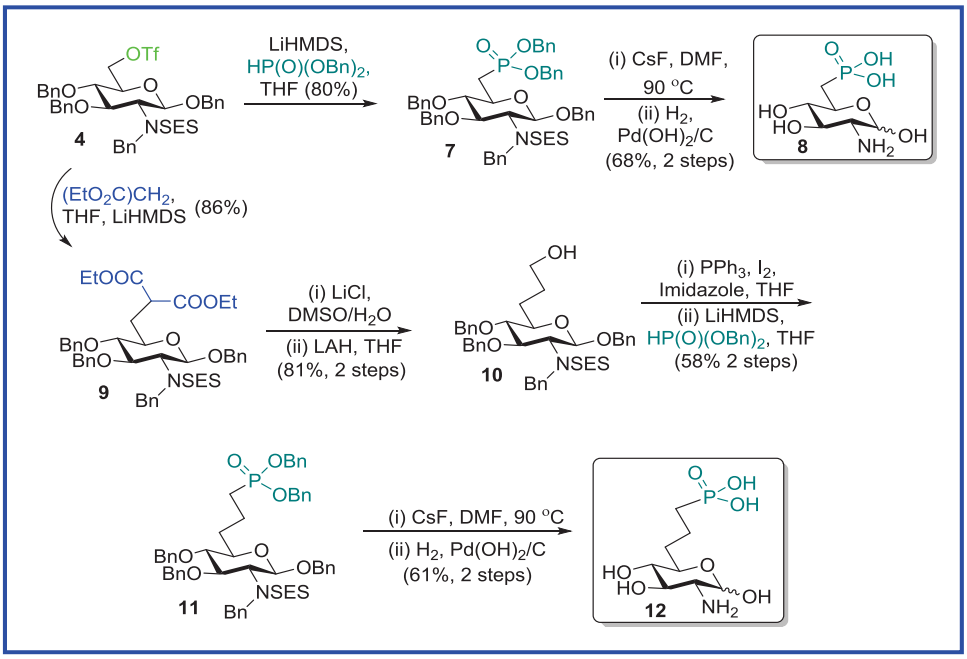

Figure 2.7: Synthesis of the "truncated" (8) and "elongated" phosphonate (12) analogues

Motivated by this synthetic achievement, we set out to exploit this route for synthesis of a series of GlcN6P analogues. First, we decided to explore tether length in the phosphonate-based analogues. Phosphite anions are known as better nucleophiles than phosphonoalkyl anions.[58] The C-P bond can be constructed via substituting a variety of electrophiles with phosphite anions. Herein, we reacted the key triflate intermediate **4** with dibenzyl phosphite anion to provide the one-carbon "truncated" phosphonate **7** in 80% yield. Standard deprotection procedures were then followed to give analogue **8**. This strategy was subsequently adopted to synthesize the "elongated" phosphonate analogue. The requisite alcohol **10** was prepared from the displacement of **4** with a malonate anion,

followed by a mono-decarboxylation/reduction sequence. Nevertheless, the extended triflate, built on the alcohol **10,** was highly unstable even at low temperature (- 40 °C). Therefore, the corresponding iodide was employed as an alternative electrophile for the displacement reaction with dibenzyl phosphite anion. After removal of SES and benzyl groups, the phosphonate compound **12** was obtained as an "elongated" phosphonate analogue.

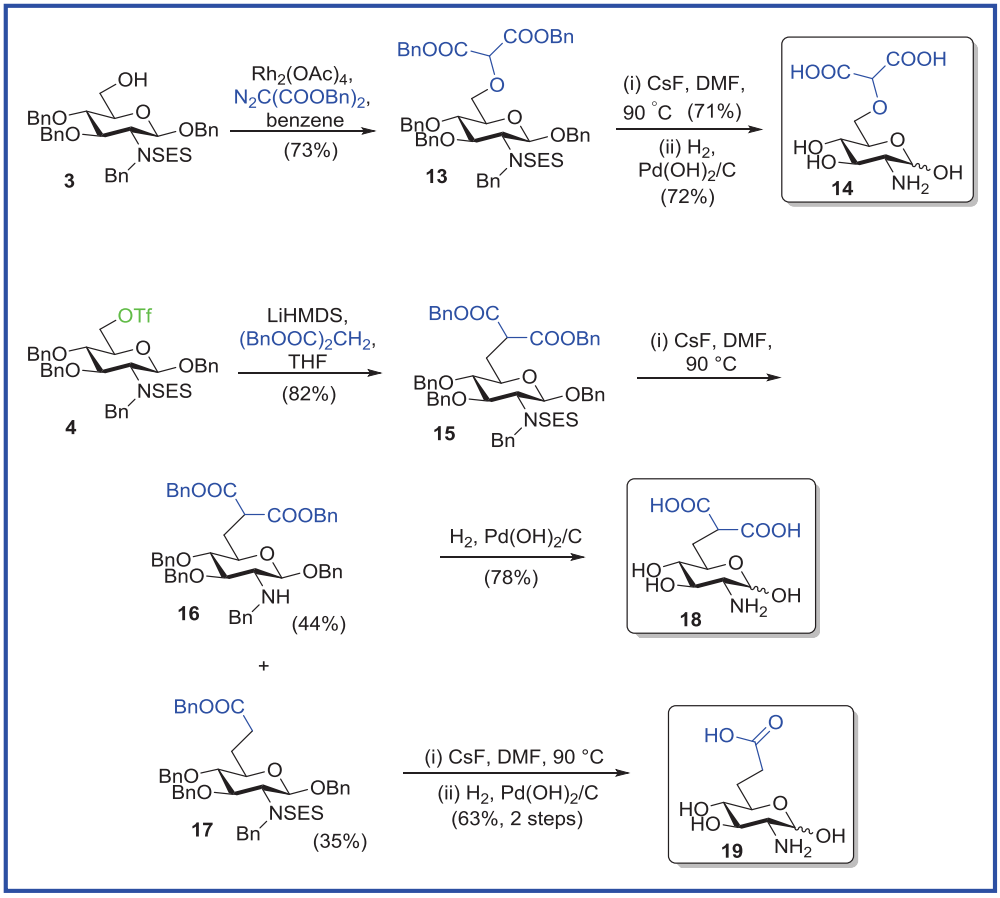

Figure 2.8: Synthesis of the malonyl ether, malonate and carboxylate analogues

Additionally, we set out to explore other phosphate isosteres that have been used in bioorganic chemistry. In particular, we were inspired by the use of the malonate motif in phosphate mimics. For instance, the Frost group had synthesized a set of 3-deoxy-D-

arabino-heptulosonic acid 7-phosphate (DAHP) analogues that competitively inhibit 3-dehydroquinate (DHQ) synthase.[59] Malonate, α-hydroxyl malonate and malonyl ether functional groups were utilized to replace the phosphate in binding to that enzyme. These carbocyclic inhibitors displayed excellent inhibition, with *K*i = 0.7, 0.3, 7 μM respectively, compared with a *K*m = 3.6 μM for DAHP. Recently, a malonate analogue of mannose 6-phosphate, which was first synthesized in our group for the M6P receptor[60], was found to be a strong inhibitor of *S. cerevisiae* M6P isomerase (IC_{50} = 18.1 μM, *K*i = 10.5 μM).[61]

Hence, malonate and malonyl ether analogues of GlcN6P were considered reasonable candidates for *glmS* riboswitch binding/self-cleavage . The malonate functionality was installed by displacement of the triflate **4** with dibenzyl malonate anion, in 82% yield. However, in the SES deprotection step , a major byproduct was obtained, namely the moncarboxylate resulting from Krapcho de-alkoxycarboxylation.[62] Subsequently, both products were further deprotected to afford malonate analogue **18** and carboxylate analogue **19**. In the meantime, the malonyl ether analogue **14** was also synthesized via a Rh(II)-mediated insertion into the O-H bond at the 6-position of the sugar by the Rh(II)-carbenoid species derived from dibenzyl diazomalonate. Standard deprotection procedures were employed for all three carboxylate-based phosphate mimics (Fig 2.8).

Next, the phosphoramide analogue was targeted as a novel mimic for GlcN6P. The triflate **4** was again employed in a S_N2 reaction with $TMSN_3$. Sequential SES-removal and Staudinger reduction then resulted in the 2,6-diamino-2-deoxy glucoside **21**.

This diamine was then subjected to the reaction with dibenzyl chlorophosphate. Pleasingly, the *N*-phosphorylation exclusively proceeded on the primary amino group. Finally, the global Bn-deprotection gave the sought-after glucosamine 6-phosphoramide **23** (Fig. 2.9).

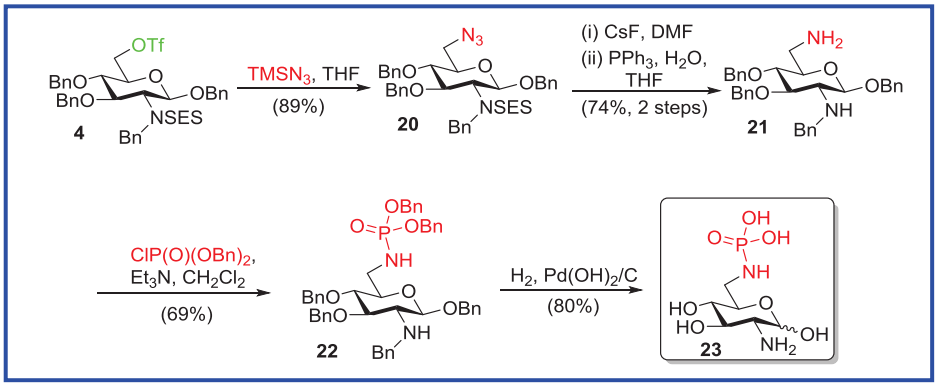

Figure 2.9: Synthesis of phosphoramide analogue 23

The 2-amino group plays a significant role in catalysis. Modulation of its pK_a and spatial hindrance are expected to potentially influence the RNA self-cleavage reaction, potentially also providing insight into the mechanism of this reaction. Consistent with this picture, the *N*-acetyl GlcN6P had already been shown to be inactive toward *glmS* riboswitch actuation. *N,N,N*-trimethylation also completely deactivates the cofactor. In contrast, *N*-methylation of GlcN6P only led to a 16-fold loss of activity in terms of observed rate constant (k_{obs}).[42] This is consistent with the postulate that the 2-amino group serves as a general base in catalyzing the self-cleavage reaction.. In this case, we slightly modify the synthetic route to analogue **6**, and synthesized two *N*-methylated phosphonate analogues of GlcN6P. After the "roll-over" reaction, the silyl ether **2** was methylated using MeI and NaH in DMF, followed by the TBDPS deprotection. The alcohol intermediate was then conveniently transformed into the phosphonate **25,** following standard triflate displacement procedures. Interestingly, a significant

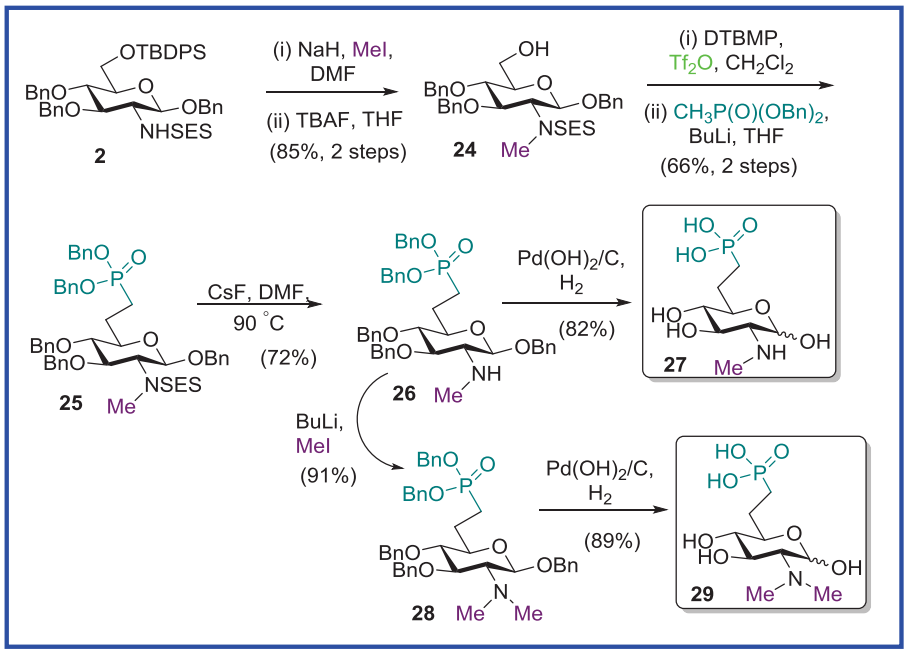

Figure 2.10: Synthesis of the *N*-methyl (27) and *N,N*-dimethyl (29) phosphonate analogues

improvement of yield was observed for the displacement of the N-methyl glucosamine 6-*O*-triflate (75%), compared with the N-benzyl glucosamine 6-*O*-triflate (62%). This is probably because the N-methyl intermediate is more stable than the N-benzyl compound. As a result, the former is less likely to undergo side reactions such as hydrolysis or elimination reactions. Following SES removal, compound **26** was either hydrogenated to give the *N*-mono-methylated phosphonate **27**, or methylated again to yield the *N,N*-dimethyl analogue **29**, after debenzylation (Fig. 2.10).

In summary, nine analogues of GlcN6P have been synthesized (Fig 2.11). All but one of the syntheses proceed through displacement of a protected amino sugar triflate intermediate, attesting to the value of this synthetic strategy.

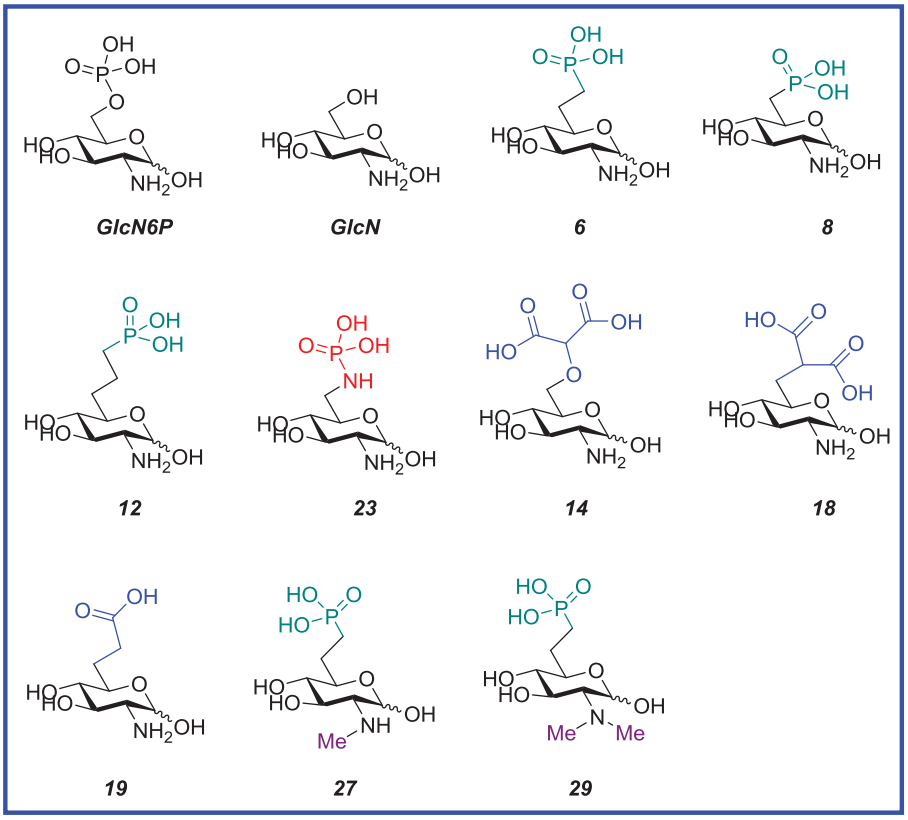

Figure 2.11: Structures of all the nine GlcN6P analogues

B. Self-Cleavage Assays with the *glmS* Riboswitch

The self-cleavage assay was conducted in the Soukup Laboratory at Creighton University. A 154-nucleotide *Bacillus cereus glmS* riboswitch was utilized in the assay. The RNA was prepared through *in vitro* transcription from the amplified *glmS* DNA using T7 RNA polymerase. ^{32}P-Labelled UTP (the α phosphate) was utilized in this process to radiolabel the RNA, which was then purified by polyacrylamide gel electrophoresis.[37] During this research, I was able to participate by conducting some of the self-cleavage assays. The *glmS* RNA was incubated with different analogues, and aliquots were taken to measure the intensity of the cleaved and the uncleaved fragments. From the percentage of the cleaved fragments, apparent rate constants could be determined. All nine analogues were tested for their ability to support *glmS* self-cleavage.

Compounds **12** and **19** were tested at 1 mM owing to their limited quantities, while the remaining seven compounds were assayed at 10 mM concentration. Glucosamine (GlcN) was chosen as the control in these assays, as it was shown to facilitate the *glmS* riboswitch self-cleavage at rates that can be readily measured under such conditions.[37] Although GlcN6P is the native cofactor for the *glmS* ribozyme and should be the direct compound of reference here, it is very difficult to measure its cleavage rate accurately. It is claimed that the reactions are extremely fast, even in the presence of low GlcN6P concentration. The reactions need to be quenched within seconds after initiation. Currently, there is ambiguity in the literature as to the value of k_{obs} for GlcN6P, with reported values ranging from 1.1 to 100 min^{-1}.[33, 36-37]

Time-point cleavage gels are presented in Figure 2.12 and Figure 2.13. Experimentally determined pseudo-first-order rate constants are presented in Table 2.2. Of the nine GlcN6P analogues synthesized, five displayed substantial cleavage rates; namely the isosteric phosphonate **6**, its *N*-methyl **27**, and *N,N*-dimethyl **29** congeners, as well as malonyl ether analogue **14** and the phosphoramide **23** (Fig. 2.12). In contrast**,** the two nonisosteric phosphonate analogues, **8** and **12,** showed very modest activation of *glmS* riboswitch self-cleavage, suggesting that the position of the phosphonate or phosphate in the RNA-active site is crucial for binding and catalysis. Deletion or insertion of one methylene ($-CH_2-$) unit alters the distance between the phosphonate- presumed to coordinate to an active site Mg^{2+} ion- and the catalytically important amine functionality, thereby greatly decreasing actuator activity. As mentioned above, Ye *et al*. also reported on studies of two truncated α-hydroxyl phosphonate analogues of GlcN6P in 2010. These two compounds structurally resemble analogue **8**, and α-hydroxylation

failed to increase their potencies. Additionally, the mono-anionic carboxylate analogue **19** is nearly inactive in the cleavage assay. This supports the proposal that di-carboxylate functionalities are superior to mono-carboxylates for Mg-binding. Perhaps related to this observation, it was also previously shown that glucosamine 6-sulfate is not an actuator for this ribozyme. To our surprise, the malonate analogue **18** exhibited a weak *glmS* actuation, similar to that of compound **19**. Compared with malonyl ether analogue **14**, the deletion of the 6-oxygen significantly reduces activity in the self-cleavage assay (Fig. 2.13). Subsequently, the five active analogues and **18** were further characterized to determine their apparent second-order rate constants (k_{cat}/K_m).

In these kinetic studies, the apparent pseudo-first order rate constants (k_{obs}) were calculated by fitting the percentage cleavage versus time to equation (1):

$$\frac{f_{cleav}-f_0}{f_{total}} = k_{obs}t \qquad (1)$$

Note that k_{obs} values were measured at different concentrations for each analogues. Under the presumed "k_{cat}/K_m conditions", the k_{obs} should have a linear relationship with the concentration. Commonly observed as the linear part of a Michaelis-Menten plot, the empirical "k_{cat}/K_m region" represents a range where the substrate concentration is < 20% K_m. However, in this case, K_m is not determined for these analogues. Nonetheless, within the assay concentration range (up to 100 mM), the plot of k_{obs} vs concentration remained fairly linear for most analogues. Therefore, the second order rate constants were derived from the following equation (2):

$$k_{obs} = \frac{k_{cat}}{K_m}[\text{cofactor}] \qquad (2)$$

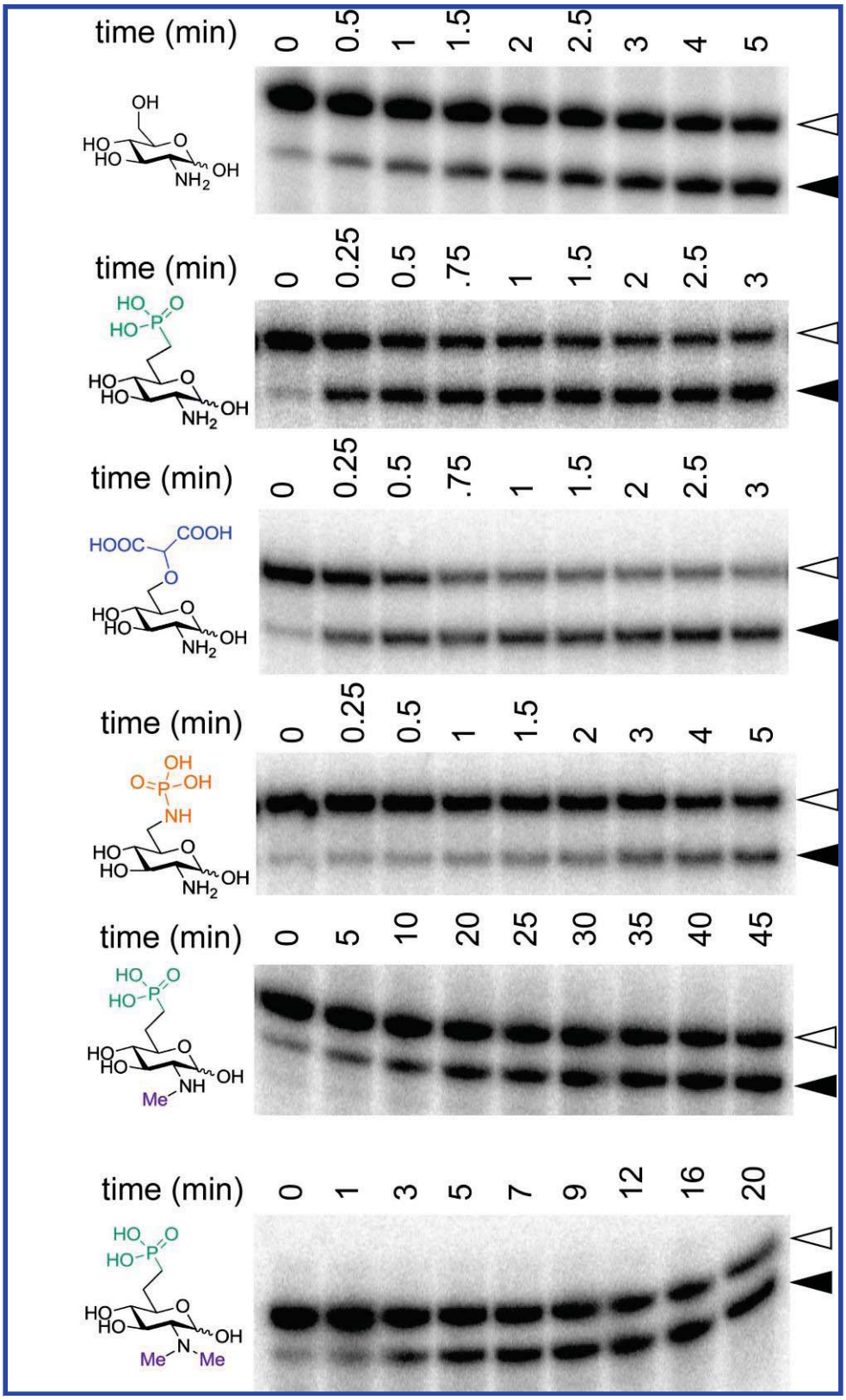

Figure 2.12: Cleavage gels of the five most active analogues

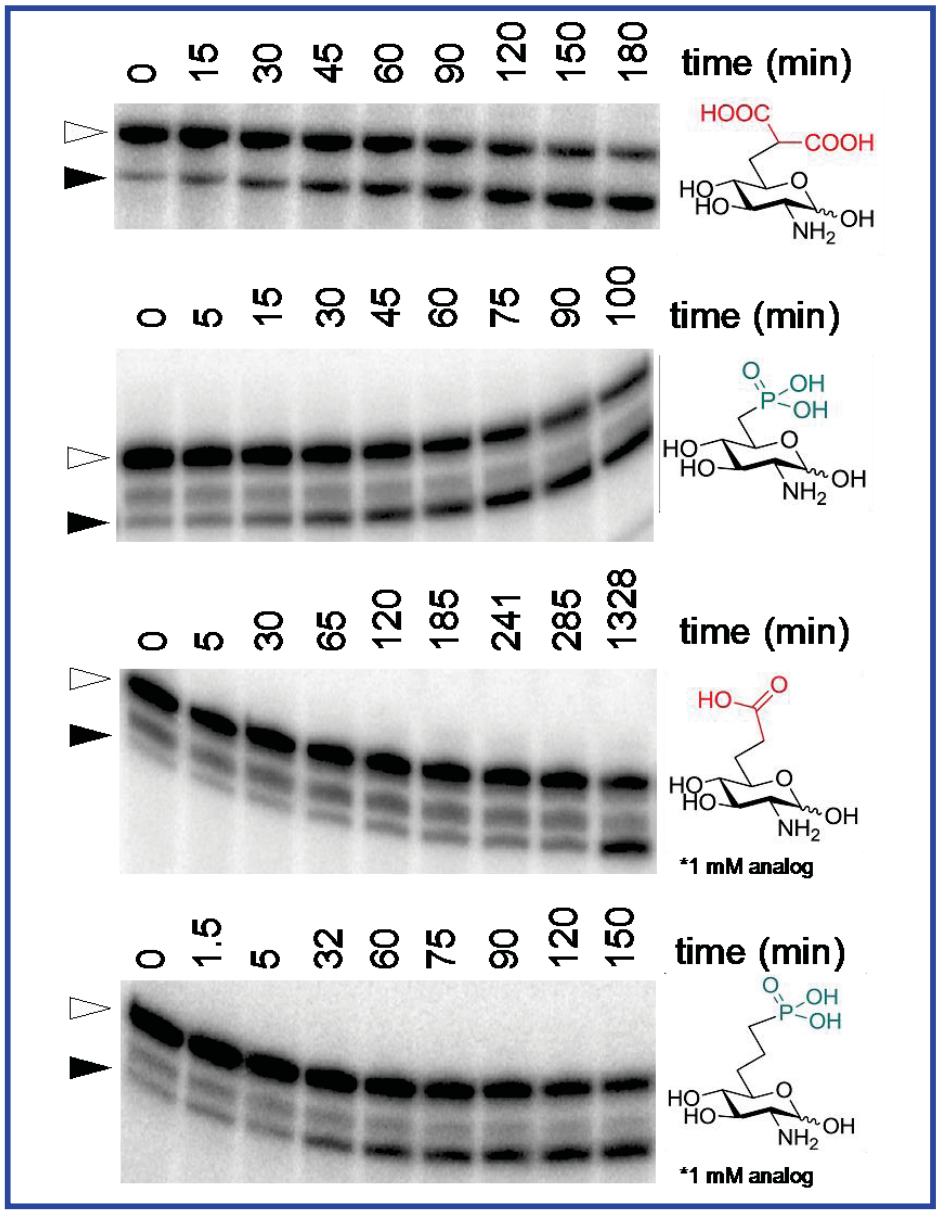

Figure 1.13: Cleavage gels of the less active analogues

Pleasingly, the phosphonate analogue **6** and the malonyl ether **14** proved to be excellent actuators for the *glmS* riboswitch. Compared with GlcN, **6** and **14** displayed a 22-fold and 27-fold greater catalytic efficiency, respectively. The previously promising phosphoramide **23**, however, trailed in the second order kinetic analysis, with a k_{cat}/K_m of 0.01 $mM^{-1}min^{-1}$. It has been reported that the P-N bond of phosphoramide is susceptible

to hydrolysis.[63] Nonetheless, a stability test of **22** showed no apparent degradation in D_2O at rt for days. Although it is possible that the presence of RNA or Mg^{2+} phosphoramide cleavage may underlie some of the perceived decrease in riboswitch actuation,[64] the phosphoramide functionality may simply be a poor surrogate in this case study. As for the *N*-methylated phosphonates **27** and **29**, neither is as effective as analogue **6** in *glmS* activation, suggesting limited steric tolerance in this RNA active site. However, it should

Table 2.2: Kinetic characterization and pK_as of GlcN6P analogues for *glmS* self-cleavage

`	k_{obs} (min^{-1})[a]	k_{cat}/K_m ($mM^{-1}min^{-1}$)[b]	RCE[c]	pK_a1 (-OH)	pK_a2 (-NH)
GlcN	0.174 ±0.025	0.0178	1.00	-	-
6	0.924 ±0.10	0.394	22.1	7.3	7.9
14	1.006 ± 0.21	0.488	27.4	3.9	8.1
23	0.101±0.013	0.0101	0.567		
27	0.027 ± 0.011	0.0035	0.197	7.6	8.2
29	0.0423 ± 0.010	0.0100	0.562	7.5	7.8
GlcN6P	1.1-100 (refs 33,36,37)	-	-	6.2[37]	8.2[37]

[a] 10 mM actuator, pH 7.3, 25 ˚C; rates are indicated ± standard deviation
[b] 1.0-0.01 mM actuator, pH 7.3, 25 ˚C
[c] Relative Catalytic Efficiency (RCE) = k_{cat}/K_m relative to GlcN.

be noted that the dimethyl phosphonate **29** is 2-3 times more active than the less sterically hindered **27**. In our hands, titration studies, yield pK_a values of 8.2 and 7.8 for these two analogues, respectively (Table 2.2). As seen in Table 2.2 and Fig. 2.17, each titration curve has two inflection points, indicating two pK_a values, corresponding to the second pK_a of the diacid functionalities and the amine group. We presume that the first one is

induced by phosphate surrogates and the second one is by the amino group. This suggests that it is optimal if the pK_a of the 2-amino group is close to the pH of the cleavage assay (~7.3), so that this amino group can serve as both a general acid and a general base catalyst for RNA cleavage, as postulated above.

C. Molecular Modeling and pK_a Determination by Titration

Although compound **6** represents one of best analogues to date, it is still ~1/7 as active as GlcN6P. For future ligand design, we set out to assess the interactions between the phosphonate and the *glmS* riboswitch. Currently, there are 18 x-ray crystal structures of the *glmS* riboswitch from two different organisms: *Thermoanaerobacter tengcongensis* and *Bacillus anthracis*.[65-69] Six structures are in the pre-cleavage stage with GlcN6P bound (2Z74; 2Z75; 3B4B; 3B4C; 3G8T ; 2NZ4). All of these riboswitches are mutated in the active site. Hence they can form a stable complex with bound actuator and are unable to undergo self-cleavage.

One riboswitch structure from *B.anthracis* with pdb code 2NZ4[66] was utilized in the molecular docking experiments. This RNA construct displays 98% identity with the *B. cereus* riboswitch employed in the self-cleavage assays here. As seen in Fig. 2.14, the active site adenosine (A-1) was modified by methylation of the 2'-hydroxyl group. Therefore, this RNA structure is inert toward GlcN6P-actuated self-cleavage. The coordinates of GlcN6P were removed from the complex structure, and the dianionic form of phosphonate analogue **6** was docked (Autodock 4). Compareing with the GlcN6P co-crystal structure, compound **5** fits well in the active site in our best docked structure. Namely, the phosphonate binds strongly with one Mg^{2+} atom and the 2-amino group is

appropriately positioned in the catalytic pocket. In the native 3D structure, we did not observe any significant interactions between the bridging oxygen and the RNA, nor did we notice any deleterious effect from substituting methylene for this oxygen.

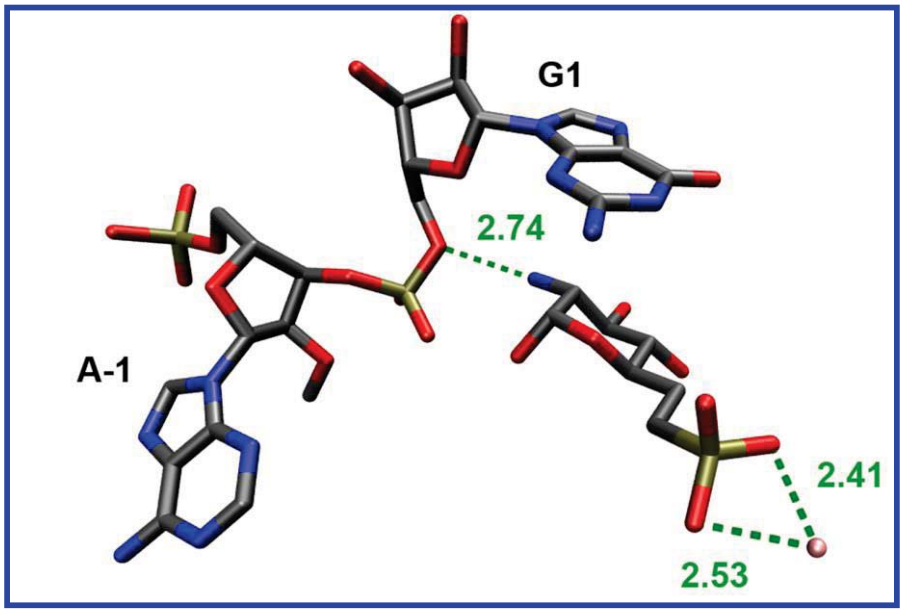

Figure 2.14: Projected structure of phosphonate analogue 6 in the active site of *glmS* riboswitch 2NZ4 (*Bacillus anthracis*)

As discussed above, although phosphonates are generally isosteric to phosphates, they are not considered to be isoacidic analogues. The second pK_a of a phosphonate monoester is usually around 7.5, which is one unit higher than that of a phosphate. This effect could result in a different distribution of phosphonate ionic species, compared with that of phosphates. Therefore, to better assess the ionization state of these analogues, the most interesting analogues were titrated to give an estimated pKa for the second proton dissociation. Indeed, the second pK_a of phosphonate analogue **6** was determined to be ~7.4 from titration curves. Therefore, at the assay pH (~7.3), only ~50% of the phosphonate is in di-anionic form. On the other hand, the second pK_a of GlcN6P is

reported to be ~6.2, which means >90% of the phosphate will be fully deprotonated at the same pH. From the assay results of the carboxylate and sulfate analogues, we believe that only dianions can bind to the RNA efficiently through magnesium ion chelation. Therefore, the diminished activity of **5**, relative to the native GlcN6, may be in part due to its elevated pK_a.

Interestingly, malonyl ether analogue **14** is ~300-fold more active than the malonate analogue **18**. Titration of these bis-carboxylates revealed that the second pK_a of **14** is ~3.9 and that of **18** is ~5.3. Theoretically, the difference between their ionization states is not significant at pH 6.2. The dianionic form is likely to be dominant for both phosphate-surrogate functionalities under the assay conditions. Thus, each compound is docked into the x-ray crystal structures as a dianion and the results are very interestingly (Fig.2.15). The malonyl ether analogue is properly placed in the active site. However, contrasting with to the natural metabolite GlcN6P or the phosphonate analogue **6**, the di-anionic bis-carboxylate appears well-suited to chelate both magnesium ions in the catalytic site. The malonate analogue **18** showed a similar bis-chelation pattern in the docking experiment. However, the docking result suggests that the 2-amino group is unable to reach the pocket where the cleavage occurs. Instead, the amino group sticks to the nearby P2.1 region, strongly interacting with the A42-U43 linkage. As a result, analogue **18** may well bind to the riboswitch, but lacks the ability to actuate the self-cleavage. On the other hand, due to its extended length, malonyl ether **14** binds to the anchoring Mg^{2+}s, while still able to deploy the amino group into the active site. Of course, these models can, in principle, be tested by obtaining x-ray structures of the analogue-bound riboswitches.

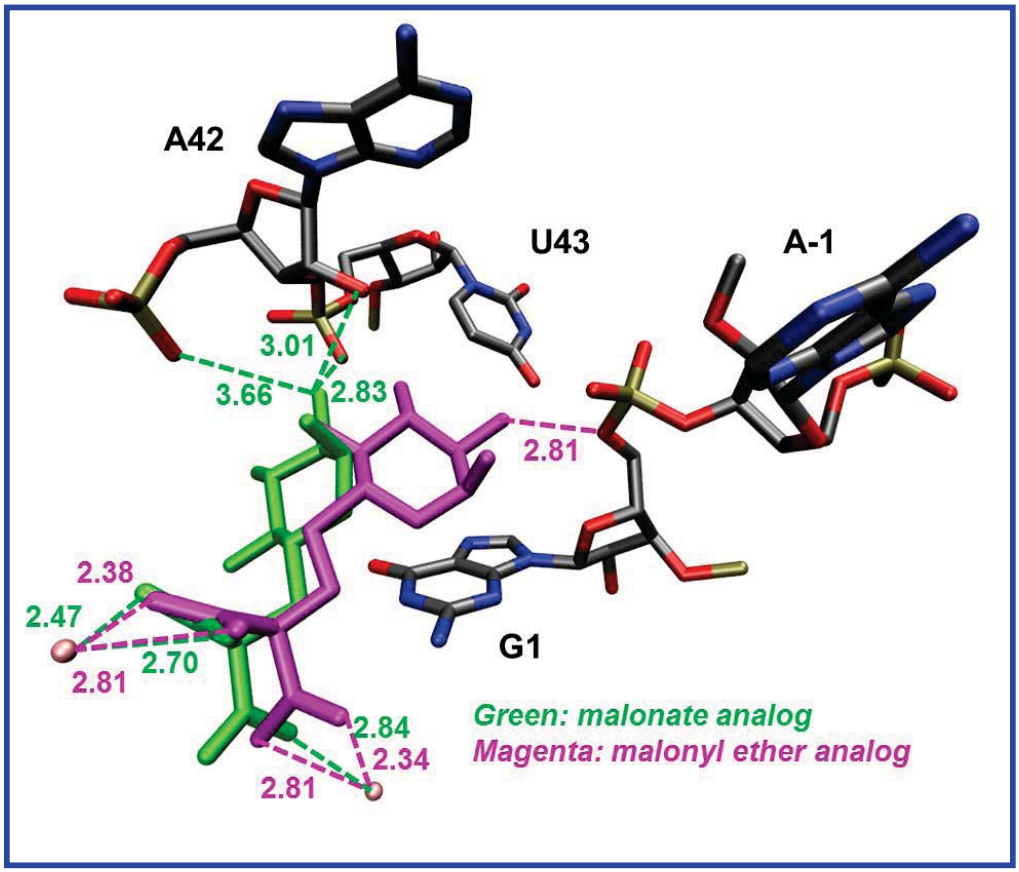

Figure 2.15: Overlay of docked structures of malonate and malonyl ether analogues in the active site. Green represents malonate analogue; Magenta represents malonyl ether analogue. Both bis-carboxylates bind tightly with two Mg^{2+} ions. However, malonyl ether analogue poses the amino group to protonate the leaving oxygen, while for the malonate analog, the amino group docks near the A42-U43 phosphodiester, instead of the scissile A-1-G1 phosphodiester, consistent with its weak actuator activity.

III. Future directions

The *glmS* riboswitch represents an exciting subject for bioorganic chemistry. The fluorinated analogues are intriguing compounds for future SAR studies. The best actuator could then, in principal, be made into a prodrug form to improve its cell permeability (Fig

2.16). Disoproxil (bis-isoproxycarbonyloxymethyl ester) is an esterase-sensitive functional group and has been used in the prodrug form of tenofovir (Viread®).[70] Additionally, acyl imidazolides represent a novel group that were proposed in prodrugging non-steroidal anti-inflammatory drugs (NSAIDs), though the hydrolytic stability of such analogues need to be addressed for cellular studies.[71] These and/or other prodrug forms could be prepared for the best analogues and tested for anti-bacterial activities.

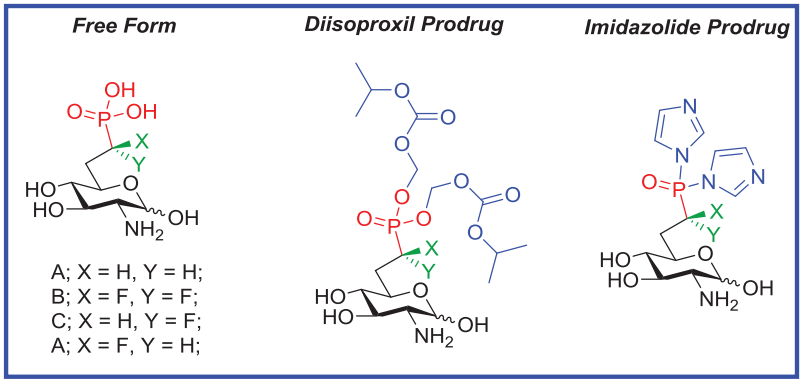

Figure 2.16: Two potential prodrug approaches

IV. Experimental Section

A. Organic Synthesis

General Methods

Reactions were conducted under argon atmosphere using oven-dried glassware. Methylene chloride was distilled from CaH_2. THF was distilled from sodium benzophenone ketyl. MeOH was distilled from magnesium-iodide. Other reagents were obtained from commercial sources and used without further purification. TLC was

carried out on Silica Gel 60 F_{254} (Merck, layer thickness 0.2 mm). Flash chromatography was performed using Merck silica gel 60 (230-400 mesh). ^{1}H NMR spectra were recorded on a Bruker-DRX-Avance- 500 MHz, 400 MHz and 300 MHz instrument with chemical shifts reported relative to residual $CHCl_3$ (7.25 ppm). Proton-decoupled ^{13}C NMR spectra were acquired on a Bruker-DRX-Avance 400 MHz and 600 MHz instrument with chemical shifts reported relative to $CDCl_3$ (77.0 ppm). ^{31}P NMR spectra were obtained on the 400 MHz instrument with chemical shifts reported relative to 85% phosphoric acid (0 ppm). Mass spectra were acquired at the Nebraska Center for Mass Spectrometry (University of Nebraska-Lincoln).

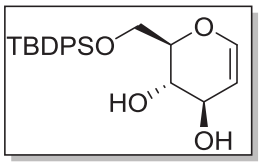

6-*O*-(tert-Butyldiphenylsilyl)-D-glucal (45). To a solution of D-glucal (5 g, 34.2 mmol), imidazole (2.56 g, 37.6 mmol) in DMF (300 mL), was added *tert*-butyl(chloro)diphenylsilane (9.78 mL, 37.6 mmol) dropwise through syringe. The reaction mixture was stirred at room temperature for 24h, and then quenched by addition of saturated $NaHCO_3$. The mixture was extracted with DCM (3 x 50 mL). The organic phase was combined, dried over Na_2SO_4, filtered and concentrated *in vacuo.* The crude product was purified by flash column chromatography (20% EtOAc -hexanes) to yield **45** (12.9 g, 98%) as a colorless oil: ^{1}H NMR (400 MHz, $CDCl_3$) δ 7.71 – 7.73 (m, 4 H), 7.40 – 7.49 (m, 6 H), 6.34 (dd, J = 1.6, 6 Hz, 1 H), 4.74 (dd, J = 2.4, 6 Hz, 1 H), 4.30 (br s, 1 H), 4.03 (dd, J = 4, 11.6 Hz, 1 H), 3.99 (dd, J = 4, 11.2 Hz, 1 H), 3.92 (ddd, J = 2.4, 6.8, 9.6 Hz, 1 H), 3.84 (td, J = 4, 9.6 Hz, 1 H), 3.09 (d, J = 2.8 Hz, 1 H), 2.55 (d, J = 4 Hz, 1 H), 1.10 (s, 9 H); ^{13}C NMR (100 MHz, $CDCl_3$) δ 144.4, 135.7, 135.6, 132.9, 132.7, 129.99, 129.95, 127.89, 127.83,

102.4, 71.7, 69.7, 63.8, 26.8, 19.3; HRMS (FAB *m/z*) calcd for $C_{22}H_{28}O_4SiLi$ ($M+Li^+$) 391.1917, obsd 391.1906.

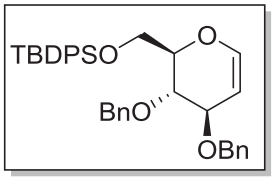

3,4-Di-O-benzyl-6-*O*-(tert-Butyldiphenylsilyl)-D-glucal (1). To a solution of **45** (6.3 g, 16.1 mmol) in DMF (100 mL) was added NaH (708 mg, 17.7 mmol) portionwise at 0 °C. After stirring for 30 min, BnBr (2.1 mL, 17.7 mmol) was added through syringe. The reaction mixture was slowly raised to room temperature and stirred overnight. Saturated NH_4Cl solution was added to quench the reaction. The mixture was extracted with DCM (3 x 50 mL). The organic phases were combined and sequentially washed with NH_4Cl, water, brine. The organic layers were dried over Na_2SO_4, filtered and concentrated *in vacuo.* The residue was purified by flash column chromatography (10% Et_2O -hexanes) to yield **1** (7.6 g, 80%) as a colorless oil: ^{1}H NMR (400 MHz, $CDCl_3$) δ 7.72 – 7.75 (m, 4 H), 7.27 – 7.50 (m, 14 H), 7.22 – 7.28 (m, 2 H), 6.29 (d, J = 6.4 Hz, 1 H), 4.73 (d, J = 11.6 Hz, 1 H), 4.65 (s, 2 H), 4.56 (d, J = 11.2 Hz, 1H), 4.50 (dd, J = 4.4, 6.4 Hz, 1 H), 4.42 (t, J = 4.4 Hz, 1 H), 4.20 (dt, J = 2.8, 6 Hz, 1 H), 3.97 (dd, J = 6, 10.4 Hz, 1 H), 3.81 (dd, J = 5.2, 6.4 Hz, 1 H), 3.79 (dd, J = 2.8, 10.8 Hz, 1 H), 1.11 (s, 9 H); ^{13}C NMR (100 MHz, $CDCl_3$) δ 143.3, 138.1, 138.0, 136.0, 135.9, 134.1, 133.5, 129.8, 128.44, 128.38, 127.9, 127.79, 127.74, 127.71, 127.66, 102.5, 76.3, 73.5, 73.2, 68.6, 67.8, 27.0, 19.2; HRMS (ESI *m/z*) calcd for $C_{36}H_{40}O_4SiNa$ ($M+Na^+$) 587.2594, obsd 587.2585.

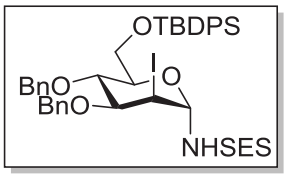

3,4-Di-*O*-benzyl-6-*O*-(*tert*-butyldiphenylsilyl)-2-deoxy-2-iodo-α-D-mannopyranosyl-2-(trimethylsilyl)ethanesulfonamide (46). To a suspension of glucal **1** (3.68 g, 6.54 mmol), 2-

(trimethylsilyl)ethanesulfonamide (4.74 g, 26.2 mmol) and powdered 4 Å molecular sieves (4 g) in CH_2Cl_2 (30 mL) at 0 °C was added I(*sym*-collidine)$_2ClO_4$ (12.3 g, 26.2 mmol) in CH_2Cl_2 (10 mL). Following stirring for 30 min, the mixture was filtered and diluted with CH_2Cl_2 (100 mL). The organic layers were sequentially washed with $Na_2S_2O_3$ (30 mL), saturated $CuSO_4$ (5 x 20 mL), $Na_2S_2O_3$ (20 mL), and saturated NaCl (30 mL), dried over $MgSO_4$, and concentrated *in vacuo.* The residue was purified by flash column chromatography (10% EtOAc -hexanes) to yield **46** (3.6 g, 64%) as a white foam: ^{1}H NMR (400 MHz, $CDCl_3$) δ 7.67 – 7.71 (m, 4 H), 7.24 – 7.46 (m, 16 H), 5.62 (d, J = 8.4 Hz, 1 H), 5.50 (dd, J = 4.8, 8.8 Hz, 1 H), 4.80 (d, J = 11.2 Hz, 1 H), 4.69 (d, J = 11.6 Hz, 1 H), 4.63 (d, 11.2 Hz, 1 H), 4.59 (t, J = 4.4 Hz, 1 H), 4.57 (d, J = 11.6 Hz, 1 H), 4.13 (t, J = 6.4 Hz, 1 H), 4.02 (dd, J = 4, 10.8 Hz, 1 H), 3.86 (dd, J = 4.4, 11.2 Hz, 1 H), 3.82 (td, J = 4, 6 Hz, 1 H), 3.36 (dd, J = 3.6, 6.8 Hz, 1 H), 2.83 – 2.97 (m, 2 H), 1.10 (s, 9 H), 0.84 – 1.01 (m, 2 H), -0.12 (s, 9 H); ^{13}C NMR (100 MHz, $CDCl_3$) δ 137.8, 137.1, 135.8, 135.6, 133.3, 132.8, 129.79, 129.75, 128.52, 128.50, 128.2, 128.02, 127.97, 127.8, 127.7, 82.2, 77.7, 77.2, 75.2, 74.2, 73.8, 71.9, 61.8, 51.1, 30.9, 26.9, 19.3, 10.1, -2.1; HRMS (ESI *m/z*) calcd for $C_{41}H_{54}O_6NSSi_2INa$(M+Na$^+$) 894.2153, obsd 894.2149.

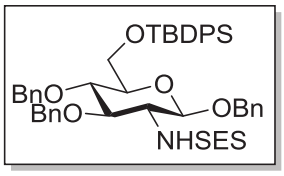

Benzyl 3,4-bis-*O*-benzyl-6-*O*-(*tert*-butyldiphenylsilyl)-2-dexoy-2-trimethylsilylethylsulfonyl-amino-β-D-glucopyranoside (2). To a solution of iodosulfonamide **46** (2.1 g, 2.35 mmol) and benzyl alcohol (365 μL, 3.5 mmol) in THF (20 mL) at -78 °C was added LiHMDS (5.2 mL, 1M in THF, 5.2 mmol) dropwise. After stirring for 10 min, a solution of AgOTf (900mg, 3.5 mmol) in THF (5 mL) was added to the reaction mixture. The

reaction flask was covered with foil and allowed to warm to room temperature. The mixture was then stirred overnight followed by addition of solid NH_4Cl (several equivalents). The mixture was stirred for 10 minutes and filtered through a pad of Celite. The filtrate was concentrated and further purified by flash column chromatography (20% EtOAc -hexanes) to afford **2** (1.6 g, 80%) as a white solid: ^{1}H NMR (400 MHz, $CDCl_3$) δ 7.68 – 7.75 (m, 4 H), 7.17 – 7.44 (m, 21 H), 4.92 (d, J = 12 Hz, 1 H), 4.91 (d, J = 10.8 Hz, 1 H), 4.86 (d, J = 9.6 Hz, 2 H), 4.70 (d, J = 10.8 Hz, 1 H), 4.61 (d, J = 11.6 Hz, 1 H), 4.33 (d, J = 7.6 Hz, 1 H), 4.18 (d, J = 7.6 Hz, 1 H), 3.94 (d, J = 2.8 Hz, 2 H), 3.87 (t, J = 8.8 Hz, 1 H), 3.46 – 3.60 (m, 2 H), 3.35 (td, J = 3.2, 9.2 Hz, 1 H), 2.90 – 3.09 (m, 2 H), 1.08 (s, 9 H), 0.96 – 1.05 (m, 2 H), -0.11 (s, 9 H); ^{13}C NMR (100 MHz, $CDCl_3$) δ 137.9, 137.7, 136.7, 135.9, 135.6, 133.5, 132.9, 129.72, 129.71, 128.61, 128.58, 128.50, 128.12, 128.06, 127.99, 127.8, 127.8, 127.6, 99.8, 82.0, 77.9, 76.1, 74.86, 74.78, 69.9, 62.6, 58.8, 50.8, 26.8, 19.3, 10.2, -2.17; HRMS (FAB *m/z*) calcd for $C_{48}H_{62}O_7NSSi_2$ ($M+H^+$) 852.3786, obsd. 852.3770.

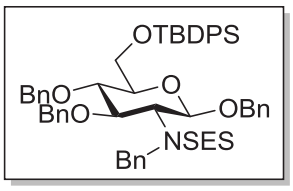

N-benzyl-2-(trimethylsilyl)-N-((2R,3R,4R,5S,6R)-2,4,5-tris(benzyloxy)-6-(((tert-butyldiphenylsilyl)oxy)methyl)tetrahydro-2H-pyran-3-yl)ethanesulfonamide (47). To a solution of **2** (1.2 g, 1.41 mmol) and BnBr (168 μL, 1.41 mmol) in DMF (20 mL) was added NaH (62 mg, 60% suspension in mineral oil) at 0 °C. The reaction was allowed to rise to room temperature slowly. After stirring overnight, the reaction was diluted by CH_2Cl_2 and quench with saturated NH_4Cl. The organic layers were sequentially washed with water and brine, then dried over $MgSO_4$,

filtered and evaporated. The crude product was purified by flash column chromatography (10% EtOAc -hexanes) to afford **47** (1.13 g, 86%) as a colorless oil: ^{1}H NMR (400 MHz, DMSO-d6, 90 °C) δ 7.65-7.71 (m, 4 H), 7.22-7.48 (m, 24 H), 7.13-7.19 (m, 2 H), 4.84 (d, J = 8.4 Hz, 1 H), 4.83 (d, J = 11.6 Hz, 1 H), 4.77 (s, 2 H), 4.71 (d, J = 11.2 Hz. 1H), 4.61 (d, J = 11.2 Hz, 1 H), 4.53 (d, J = 15.6 Hz, 1 H), 4.50 (d, J = 11.6 Hz, 1 H), 4.46 (d, J = 11.6 Hz, 1 H), 3.91-4.08 (m, 3 H), 3.75 (t, J = 8.8 Hz, 1 H), 3.67 (t, J = 9.6 Hz, 1 H), 3.54 (ddd, J = 2.0, 4.8, 9.6 Hz, 1 H), 2.65-2.83 (m, 2 H), 1.06 (s, 9 H), 0.821-0.945 (m, 2 H), -0.169 (s, 9 H); ^{13}C NMR (100 MHz, C_6D_6, 75 °C) δ 139.2, 138.7, 137.9, 137.6, 135.9, 135.7, 134.9, 134.1, 133.7, 129.6, 129.3, 128.4, 128.3, 128.2, 127.8, 127.6, 127.5, 127.3, 127.2, 100.0, 80.3, 76.5, 74.5, 70.2, 63.6, 52.8, 51.3, 26.9, 26.5, 19.3, 10.1, -2.49; HRMS (FAB *m/z*) calcd for $C_{55}H_{68}NO_7SSi_2$ ($M+H^+$) 942.4177, obsd. 942.4298.

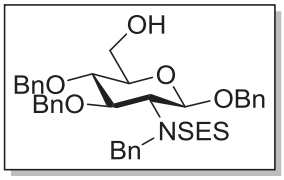

N-benzyl-2-(trimethylsilyl)-N-((2R,3R,4R,5S,6R)-2,4,5-tris(benzyloxy)-6-(hydroxymethyl)tetrahydro-2H-pyran-3-yl)ethanesulfonamide (3). To a solution of **47** (629 mg, 0.67 mmol) in THF (7 mL) was added TBAF (0.67 mL, 1 M solution in THF) dropwise at 0 °C. The mixture was stirred at 0 °C for 16 h. Saturated NH_4Cl was added to quench the reaction. The aqueous layer was extracted with Et_2O (3 x 10 mL). The organic layer was dried over $MgSO_4$, filtered, evaporated. The residue was purified by flash column chromatography (20% EtOAc -hexanes) to afford **3** (358 mg, 76%) as a colorless oil: ^{1}H NMR (400 MHz, DMSO-d6, 90 °C) δ 7.42-7.48 (m, 2 H), 7.22-7.41 (m, 18 H), 4.86 (d, J = 11.6 Hz, 1 H), 4.71-4.82 (m, 3 H), 4.67 (s, 2 H), 4.47 (d, J = 6.8 Hz, 1 H), 4.45 (d, J = 12 Hz, 1 H), 4.41 (t, J = 5.2 Hz, 1 H), 3.99 (t, J = 9.2 Hz, 1 H), 3.73-3.80 (m, 1 H), 3.71

(d, *J* = 8.8 Hz, 1 H), 3.65 (t, *J* = 5.2 Hz, 1 H), 3.60 (t, *J* = 8.4 Hz, 1 H), 3.39 (ddd, *J* = 2.4, 4.8, 9.6 Hz, 1 H), 2.67-2.83 (m, 2 H), 0.857-0.900 (m, 2 H), -0.165 (m, 9 H); ^{13}C NMR (100 MHz, DMSO-d6, 90 °C) δ 139.1, 138.9, 137.91, 137.88, 129.7, 128.65, 128.59, 128.5, 128.4, 128.3, 128.1, 128.0, 127.9, 127.85, 127.78, 127.6, 99.4, 80.2, 76.3, 73.9, 73.5, 70.2, 61.1, 50.2, 10.2, -1.74; HRMS (FAB *m/z*) calcd for $C_{39}H_{49}NO_7SSi_2Na$ ($M+Na^+$) 726.2897, obsd. 726.2902.

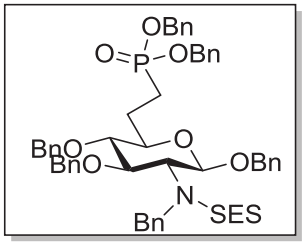

Dibenzyl (2-((2R,3R,4R,5R,6R)-5-(N-benzyl-2--trimethylsilyl)ethylsulfonamido)-3,4,6-tris(benzyloxy)tetrahydro-2H-pyran-2-yl)ethyl)phosphonate (5). To a solution of **3** (112 mg, 0.16 mmol) and 2,6-di-*tert*-butyl-4-methylpyridine (98 mg, 0.48 mmol) in CH_2Cl_2 (2 mL), was slowly added trifluoromethanesulfonic anhydride (54 μL, 0.32 mmol) at -40 °C and stirring continued for 0.5 h at that temperature. The reaction mixture was then concentrated *in vacuo* and directly applied to column chromatography (8% EtOAc - hexanes) to afford the triflate **4** (120 mg, 90%) as a pale yellow oil: HRMS (ESI *m/z*) calcd for $C_{40}H_{48}O_9NF_3S2SiNa$ ($M+Na^+$) 858.2390, obsd. 858.2386.

Then the triflate **4** (120 mg, 0.144 mmol) was dissolved in THF (2 mL) with dibenzyl methylphosphonate (151 mg, 0.576 mmol) and cooled to -78 °C. To the solution was added slowly *n*-BuLi (0.36 mL, 1.6 M solution in hexanes). After stirring for 10 min at -78 °C, the reaction was quenched with saturated aqueous NH_4Cl. Then Et_2O (20 mL) was added to dilute the solution. The organic layers were sequentially washed with NH_4Cl, water and brine, and then dried over $MgSO_4$. Filtration and evaporation gave crude

product, which was purified by flash column chromatography (20-40% EtOAc-hexanes) to afford **5** (85 mg, 62%) as a colorless oil: ^{1}H NMR (400 MHz, DMSO-d6, 90 °C) δ 7.41-7.46 (m, 2 H), 7.17-7.40 (m, 28 H), 5.04 (d, J = 12.4 Hz, 1 H), 5.01 (d, J = 12.8 Hz, 1 H), 4.98 (d, J = 12.8 Hz, 1 H), 4.96 (d, J = 12 Hz, 1 H), 4.72-4.83 (m, 4 H), 4.69 (d, J = 11.2 Hz, 1 H), 4.57 (d, J = 4.57 Hz, 1 H), 4.50 (d, J = 15.6 Hz, 1 H), 4.44 (d, J = 12 Hz, 1 H), 4.43 (d, J = 15.2 Hz, 1 H), 3.95 (t, J = 8.8 Hz, 1 H), 3.68 (t, J = 8.8 Hz, 1 H), 3.41 (dt, J = 2.8, 9.2 Hz, 1 H), 3.33 (t, J = 12.8 Hz, 1 H), 2.63-2.84 (m, 2 H), 2.02-2.16 (m, 1 H), 1.81-2.02 (m, 2 H), 1.66-1.82 (m, 1 H), 0.839-0.948 (m, 2 H), -0.169 (s, 9 H); ^{13}C NMR (100 MHz, DMSO-d6, 90 °C) δ 139.0, 138.6, 137.9, 137.8, 137.3 (d, *Jcp* = 6 Hz), 129.7, 128.8, 128.6, 128.6, 128.49, 128.46, 128.1, 128.0, 127.9, 127.8, 127.7, 99.6, 83.3, 74.1, 74.0 (d, *Jcp* = 15 Hz), 73.4, 70.6, 67.0 (d, *Jcp* = 7.5 Hz), 66.97 (d, *Jcp* = 7.5 Hz), 50.3, 25.1 (d, *Jcp* = 5 Hz), 21.6 (d, *Jcp* = 139.5 Hz), 10.2, -1.75; ^{31}P NMR (162 MHz, DMSO-d6, 90 °C) δ 32.60; HRMS (ESI *m/z*) calcd for $C_{54}H_{64}NO_9PSSi_2Na$ ($M+Na^+$) 984.3706, obsd. 984.3746.

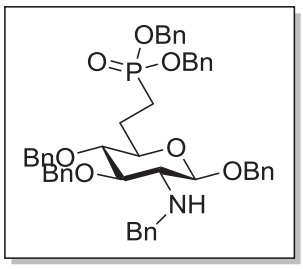

Dibenzyl (2-((2R,3R,4R,5R,6R)-5-(benzylamino)-3,4,6-tris(benzyloxy)tetrahydro-2H-pyran-2-yl)ethyl)phosphonate (48). To a solution of **5** (162 mg, 0.168 mmol) in DMF (3 mL) was added CsF (179 mg, 1.18 mmol) in one portion. The mixture was heated to 90 °C and stirred for 16 h. Saturated aqueous NH_4Cl was added to quench the reaction. The mixture was extracted with ethyl acetate. The organic layers were dried over $MgSO_4$, filtered and concentrated in vacuum. The crude product was purified by flash column chromatography (30-50% EtOAc-hexanes) to

give **48** (90 mg, 68%) as a white solid: ^{1}H NMR (400 MHz, $CDCl_3$) δ 7.22-7.39 (m, 28 H), 7.16-7.19 (m, 2 H), 5.08 (d, J = 12 Hz, 1 H), 5.06 (d, J = 12 Hz, 1 H), 5.00 (d, J = 11.6 Hz, 1 H), 4.98 (d, J = 12 Hz, 1 H), 4.90 (d, J = 11.6 Hz, 1 H), 4.86 (d, J = 12 Hz, 1 H), 4.81 (d, J = 10.8 Hz, 1 H), 4.69 (d, J = 11.2 Hz, 1 H), 4.59 (t, J = 10.8 Hz, 2 H), 4.33 (d, J = 8 Hz, 1 H), 4.01 (d, J = 13.2, Hz ,1 H), 3.82 (d, J = 13.2 Hz, 1 H), 3.44 (t, J = 8.4 Hz, 1 H), 3.22-3.34 (m, 2 H), 2.72 (dd, J = 8, 10 Hz, 1 H), 2.15-2.29 (m, 1 H), 1.98-2.14 (m, 1 H), 1.71-1.92 (m, 2 H); ^{13}C NMR (100 MHz, $CDCl_3$) δ 140.6, 138.0, 137.7, 137.4, 136.44 (d, *Jcp* = 6 Hz), 136.43 (d, *Jcp* = 6 Hz), 128.6, 128.5, 128.45, 128.40, 128.35, 128.27, 128.0, 127.9, 127.8, 126.8, 103.8, 83.5, 82.5, 75.1, 74.4 (d, *Jcp* = 16 Hz), 71.2, 67.14 (d, *Jcp* = 6 Hz), 67.11 (d, *Jcp* = 6 Hz), 62.8, 53.7, 24.8 (d, *Jcp* = 4 Hz), 22.1 (d, *Jcp* = 142 Hz); ^{31}P NMR (162 MHz, $CDCl_3$) δ 33.27; HRMS (ESI *m/z*) calcd for $C_{49}H_{52}NO_7PNa$ ($M+Na^+$) 820.3379, obsd 820.3378.

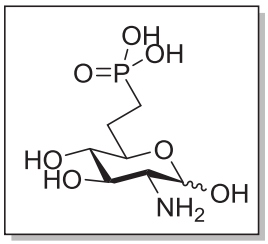

Glucosamine 6-phosphonate (6). A solution of **48** (46 mg, 0.058 mmol) in MeOH (2 mL) was stirred in the presence of 40% $Pd(OH)_2/C$ (18 mg) and trace amount of TFA (1 drop), under balloon pressure of hydrogen, for 24 h at room temperature. Filtrate the mixture through a pad of Celite and wash the filter cake with 2 mL MeOH. Suspend the filter cake in 2 mL H_2O and stir for 5 min, and then filtrate again through a pad of Celite. Concentrate the aqueous solution and dry over high vacuum to yield **6** (12 mg, 87%) as a colorless foam: ^{1}H NMR (400 MHz, D_2O) δ 5.30 (d, J = 3.6 Hz, 0.5 H), 4.77 (d, J = 8.4 Hz, 0.5 H), 3.70-3.80 (m, 1 H), 3.50 (dd, J = 1.6, 8.8 Hz, 0.5 H), 3.35 (dt, J = 2.4, 10 Hz, 0.5 H), 3.23 (t, J = 9.2 Hz, 1 H), 3.17 (dd, J = 4, 10.8 Hz, 0.5 H), 2.85 (dd,

J = 2, 8.4 Hz, 0.5 H), 1.96-2.00 (m, 1 H), 1.52-1.72 (m, 2 H), 1.37-1.46 (m, 1 H); ^{13}C NMR (100 MHz, D_2O) δ 99.2, 89.2, 75.9 (d, *Jcp* = 16 Hz), 73.04, 73.05, 72.4, 71.4 (d, *Jcp* = 17 Hz), 69.8, 57.0, 54.5, 25.1 (d, *Jcp* = 4 Hz), 24.9 (d, *Jcp* = 3 Hz), 23.5 (d, *Jcp* = 133 Hz), 23.6 (d, *Jcp* = 135 Hz); ^{31}P NMR (162 MHz, D_2O) δ 24.91, 24.77; HRMS (ESI *m/z*) calcd for $C_7H_{16}NO_7PNa$ ($M+Na^+$) 280.0562, obsd 280.0567.

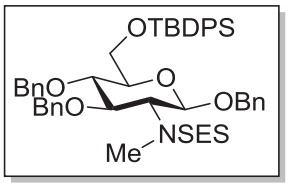

N-methyl-2-(trimethylsilyl)-N-((2R,3R,4R,5S,6R)-2,4,5-tris(benzyloxy)-6-(((tert-butyldiphenylsilyl)oxy)methyl)tetrahydro-2H-pyran-3-yl)ethanesulfonamide (49). To a solution of **2** (200 mg, 0.212 mmol) in DMF (2 mL) was added NaH (10 mg, 60% suspension in mineral oil, 0.233 mmol) at 0 °C. The mixture was stirred for 0.5 h at 0 °C. Then MeI (15 μL, 0.233 mmol) was added to the solution. The reaction was allowed to rise to room temperature slowly. After stirring overnight, the reaction was diluted by CH_2Cl_2 and quench with saturated NH_4Cl. The organic layers were sequentially washed with water and brine, then dried over $MgSO_4$, filtered and evaporated. The crude product was purified by flash column chromatography (30% EtOAc-hexanes) to afford **49** (168 mg, 92%) as a colorless oil: ^{1}H NMR (400 MHz, DMSO-d6, 90 °C) δ 7.13-7.81 (m, 25 H), 4.85 (d, *J* = 11.6 Hz, 2 H), 4.78 (d, *J* = 8.8 Hz, 1 H), 4.78 (d, *J* = 10.8 Hz, 1 H), 4.74 (d, *J* = 11.2 Hz, 1 H), 4.68 (d, *J* = 12 Hz, 1 H), 4.62 (d, *J* = 11.6 Hz, 1 H), 4.01 (dd, *J* = 2, 11.6 Hz, 1 H), 3.90-3.97 (m, 2 H), 3.72 (dd, *J* = 8.4, 10 Hz, 1 H), 3.67 (dd, *J* = 8.4, 9.6 Hz, 1 H), 3.58 (ddd, *J* = 1.2, 4.4, 9.6 Hz, 1 H), 3.05 (s, 3 H), 2.89-2.96 (m, 2 H), 1.07 (s, 9 H), 0.85-0.99 (m, 2 H), -0.09 (s, 9 H); ^{13}C NMR (100 MHz, DMSO-d6, 90 °C) δ 139.0, 138.8, 137.7, 135.7, 135.5, 135.0, 133.9, 133.7, 130.1,

128.8, 128.6, 128.5, 128.3, 128.21, 128.15, 128.07, 1277.9, 127.8, 127.7, 98.1, 79.3, 79.0, 75.9, 74.3, 73.9, 70.2, 63.7, 62.4, 30.3, 19.4, 10.2, -1.7; HRMS (ESI *m/z*) calcd for $C_{49}H_{63}NO_7Si_2SNa$ ($M+Na^+$) 888.3762, obsd 888.3748.

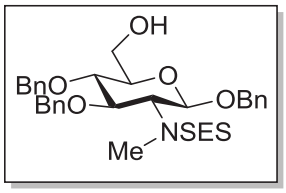

N-methyl-2-(trimethylsilyl)-N-((2R,3R,4R,5S,6R)-2,4,5-tris(benzyloxy)-6-(hydroxymethyl) tetrahydro-2H-pyran-3-yl)ethanesulfonamide (24). TBAF (0.19 mL, 1 M solution in THF) was added to a solution of **49** (168 mg, 0.194 mmol) in THF (2 mL) at 0 °C. The mixture was raised to room temperature and stirred for 12 h. Then saturated NH_4Cl was added and the mixture was extracted with Et_2O. The combined organic layers were dried over $MgSO_4$, filtered and concentrated in vacuum. The crude product was purified by flash column chromatography (40% EtOAc-hexanes) to yield **24** (113 mg, 93%) as a white solid: ^{1}H NMR (400 MHz, DMSO-d6, 90 °C) δ 7.22-7.42 (m, 15 H), 4.86 (d, J = 9.6 Hz, 1 H), 4.83 (d, J = 8.4 Hz, 1 H), 4.66-4.76 (m, 5 H), 4.39 (t, J = 5.2 Hz, 1 H), 3.88 (dd, J = 8.4, 10.4 Hz, 1 H), 3.78 (ddd, J = 1.2, 4.0, 12.0 Hz, 1 H), 3.67 (dd, J = 8.4, 10.4 Hz, 1 H), 3.64 (t, J = 6.4 Hz, 1 H), 3.59 (t, J = 8.4 Hz, 1 H), 3.42 (ddd, J = 2, 4.8, 9.2 Hz, 1 H), 2.86-2.92 (m, 2 H), 2.97 (br s, 1 H), 2.82 (s, 3 H), 0.841-0.956 (m, 2 H), -0.095 (s, 9 H); ^{13}C NMR (100 MHz, DMSO-d6, 90 °C) δ 139.1, 137.8, 128.7, 128.6, 128.5, 128.4, 128.2, 128.1, 127.9, 127.8, 127.7, 98.3, 79.5, 79.1, 76.4, 74.1, 73.7, 70.5, 62.3, 61.2, 47.5, 31.1, 30.3, 10.2, -1.65; HRMS (ESI *m/z*) calcd for $C_{33}H_{45}NO_7SSiNa$ ($M+Na^+$) 650.2584, obsd. 650.2587.

Dibenzyl (2-((2R,3R,4R,5R,6R)-3,4,6-tris(benzyloxy)-5-(N-methyl-2-(trimethylsilyl)ethyl

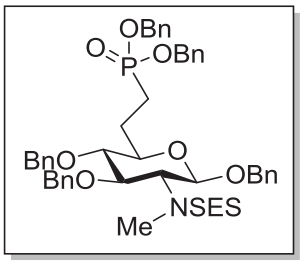

sulfonamido)tetrahydro-2H-pyran-2-yl)ethyl)phosphonate (25). To a solution of **24** (188 mg, 0.3 mmol) and 2,6-di-*tert*-butyl-4-methylpyridine (184 mg, 0.9 mmol) in CH_2Cl_2 (3 mL), was slowly added trifluoromethanesulfonic anhydride (101 μL, 0.6 mmol) at -40 °C and stirring continued for 0.5 h at that temperature. The reaction mixture was then concentrated *in vacuo* and directly applied to column chromatography (10-20% EtOAc -hexanes) to afford the corresponding triflate (186 mg, 82%) as a pale yellow oil: HRMS (ESI *m/z*) calcd for $C_{34}H_{44}O_9NF_3S2SiNa$ ($M+Na^+$) 759.2179, obsd. 782.2056.

Then the triflate (186 mg, 0.246 mmol) was dissolved in THF (3 mL) with dibenzyl methylphosphonate (258 mg, 0.984 mmol) and cooled to -78 °C. To the solution was added slowly *n*-BuLi (0.62 mL, 1.6 M solution in hexanes, 0.984 mmol). After stirring for 15 min at -78 °C, the reaction was quenched with saturated aqueous NH_4Cl. Then Et_2O (50 mL) was added to dilute the solution. The organic layers were sequentially washed with NH_4Cl, water and brine, and then dried over $MgSO_4$, filtered and concentrated in vacuum to give crude product, which was purified by flash column chromatography (30-40% EtOAc-hexanes) to afford **25** as a colorless oil: ^1H NMR (400 MHz, DMSO-d6, 90 °C) δ 7.15-7.65 (m, 25 H), 5.06 (dd, J = 1.6, 8.4 Hz, 1 H), 5.03 (dd, J = 2, 8.4 Hz, 1 H), 5.00 (dd, J = 2.4, 8 Hz, 1 H), 4.97 (dd, J = 2.4, 8 Hz, 1 H), 4.84 (d, J = 11.2 Hz, 1 H), 4.78 (d, J = 7.2 Hz, 1 H), 4.75 (d, J = 6.8 Hz, 1 H), 4.71 (d, J = 10.8 Hz,

1 H), 4.65 (d, *J* = 8.4 Hz, 1 H), 4.62 (d, *J* = 9.6 Hz, 1 H), 4.60 (d, *J* = 9.2 Hz, 1 H), 3.82 (dd, *J* = 8.4, 10.4 Hz, 1 H), 3.68 (dd, *J* = 8.4, 10 Hz, 1 H), 3.43 (dt, *J* = 2.8, 9.2 Hz, 1 H), 3.35 (dd, *J* = 8.4, 9.2 Hz, 1 H), 2.85-2.94 (m, 2 H), 2.81 (s, 3 H), 1.66-2.21 (m, 4 H), 0.83- 1.02 (m, 2 H), -0.09 (s, 9 H); ^{13}C NMR (100 MHz, DMSO-d6, 90 °C) δ 138.9, 138.7, 137.8, 137.3 (d, *Jcp* = 6 Hz), 128.8, 128.7, 128.6, 128.5, 128.4, 128.2, 128.05, 128.02, 127.93, 127.86, 127.7, 98.6, 82.7, 79.0, 74.3, 74.0 (d, *Jcp* = 15 Hz), 73.7, 70.8, 67.0 (d, *Jcp* = 6 Hz), 66.96 (d, *Jcp* = 6 Hz), 47.6, 30.4, 25.1 (*Jcp* = 4 Hz), 21.6 (*Jcp* = 139 Hz), 10.2, -1.7; ^{31}P NMR (162 MHz, $CDCl_3$) δ 32.62; HRMS (ESI *m/z*) calcd for $C_{43}H_{48}NO_7PNa$ ($M+Na^+$) 908.3393, obsd 908.3367.

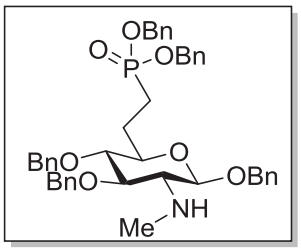

Dibenzyl (2-((2R,3R,4R,5R,6R)-3,4,6-tris(benzyloxy)-5-(methylamino)tetrahydro-2H-pyran-2-yl)ethyl)phosphonate (26). To a solution of **25** (107 mg, 0.12 mmol) in DMF (2 mL) was added CsF (127 mg, 0.84 mmol) in one portion. The mixture was heated to 90 °C and stirred for 12 h. Saturated aqueous NH_4Cl was added to quench the reaction. The mixture was extracted with ethyl acetate. The combined organic layers were dried over $MgSO_4$, filtered and concentrated in vacuum. The crude product was purified by flash column chromatography (50% EtOAc-hexanes) to give **26** (62 mg, 72%) as a pale yellow solid: ^{1}H NMR (400 MHz, $CDCl_3$) δ 7.23-7.42 (m, 25 H), 5.08 (d, *J* = 11.6 Hz, 1 H), 5.05 (d, *J* = 11.6 Hz, 1 H), 5.00 (d, *J* = 12 Hz, 1 H), 4.98 (d, *J* = 11.6 Hz, 1 H), 4.94 (d, *J* = 11.6 Hz, 1 H), 4.84 (d, *J* = 7.2 Hz, 1 H), 4.81 (d, *J* = 6.4 Hz, 1 H), 4.70 (d, *J* = 11.6 Hz, 1 H), 4.62 (d, *J* = 10.8 Hz, 1 H), 4.56 (d, *J* = 11.6 Hz, 1 H), 4.26 (d, *J* = 8.0 Hz, 1 H), 3.41 (dd, *J* = 8.4, 10 Hz, 1 H), 3.31 (t, *J* = 9.2 Hz, 1 H), 3.25 (dt, *J* = 2.8,

9.2 Hz, 1 H), 2.51 (dd, *J* = 8, 10 Hz, 1 H), 2.42 (s, 3 H), 2.15-2.27 (m, 1 H), 1.94-2.11 (m, 1 H), 1.70-1.99 (m, 2 H), 1.65 (s, 1 H); ^{13}C NMR (100 MHz, $CDCl_3$) δ 138.2, 137.7, 137.4, 136.43 (d, *Jcp* = 6 Hz), 136.42 (d, *Jcp* = 6 Hz), 128.6, 128.5, 128.42, 128.40, 128.00, 127.98, 127.94, 127.84, 127.81, 103.3, 83.3, 82.5, 77.3, 75.1, 74.9, 74.3 (d, *Jcp* = 16 Hz), 71.1, 67.14 (d, *Jcp* = 7 Hz), 67.11 (d, *Jcp* = 7 Hz), 65.1, 24.8 (d, *Jcp* = 4 Hz), 22.1 (d, *Jcp* = 141 Hz); ^{31}P NMR (162 MHz, $CDCl_3$) δ 33.11; HRMS (ESI *m/z*) calcd for $C_{43}H_{48}NO_7PNa$ ($M+Na^+$) 744.3066, obsd 744.3081.

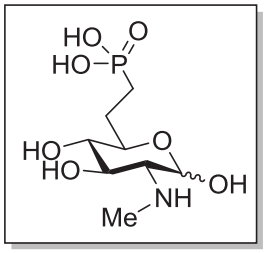

N-Methyl glucosamine 6-phosphonate (27). A solution of **26** (36 mg, 0.05 mmol) in MeOH (2 mL) was stirred in the presence of 40% $Pd(OH)_2/C$ (15 mg) and trace amount of TFA (1 drop), under balloon pressure of hydrogen, for 24 h at room temperature. Filtrate the mixture through a pad of Celite and wash the filter cake with 2 mL MeOH. Suspend the filter cake in 2 mL H_2O and stir for 5 min, and then filtrate again through a pad of Celite. Concentrate the aqueous solution and dry over high vacuum to yield **27** (11 mg, 82%) as a colorless foam: ^{1}H NMR (400 MHz, D_2O) δ 5.45 (d, *J* = 3.2 Hz, 0.7 H), 4.94 (d, *J* = 8.4 Hz, 0.3 H), 3.62-3.84 (m, 1.7 H), 3.36 (t, *J* = 7.6 Hz, 0.3 H), 3.20-3.27 (m, 1 H), 3.15 (dd, *J* = 3.2, 10.4 Hz, 0.7 H), 2.72-2.94 (m, 0.3 H), 2.76 (s, 0.9 H), 2.72 (s, 2.1 H), 1.90-2.09 (m, 1 H), 1.48-1.77 (m, 3 H); ^{13}C NMR (100 MHz, D_2O) δ 91.8, 87.4, 75.5 (d, *Jcp* = 16 Hz), 73.4, 73.1, 70.8 (d, *Jcp* = 17 Hz), 70.3, 69.5, 63.0, 61.3, 30.95, 30.86, 24.7 (d, *Jcp* = 3 Hz), 24.5 (d, *Jcp* = 3 Hz), 22.90 (d, *Jcp* = 134 Hz), 22.89 (d, *Jcp* = 134 Hz); ^{31}P NMR (162 MHz, D_2O) δ 25.25, 25.06; HRMS (ESI *m/z*) calcd for $C_8H_{19}NO_7P$ ($M+H^+$) 272.0899, obsd 272.0891.

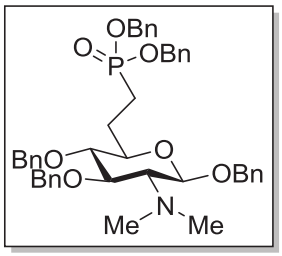

Dibenzyl (2-((2R,3R,4R,5R,6R)-3,4,6-tris(benzyloxy)-5-(dimethylamino)tetrahydro-2H-pyran-2-yl)ethyl)phosphonate (28). To a solution of **26** (75 mg, 0.1 mmol) in THF (1 mL) was added n-BuLi (71 μL, 1.6 M solution in hexanes, 0.11 mmol) dropwise at -78 °C. The mixture was stirred at that temperature for 30 min, followed by addition of MeI (7 μL, 0.11 mmol). The solution was then raised to 0 °C and stirred for 3 h when TLC indicated the completion of the reaction. The reaction was quenched with saturated NH_4Cl and extracted with Et_2O. The combined organic layers were dried over $MgSO_4$, filtered and concentrated in vacuum. The crude product was purified by flash column chromatography (30% EtOAc-hexanes) to give **28** (68 mg, 93%) as a pale yellow solid: ^{1}H NMR (400 MHz, $CDCl_3$) δ 7.24-7.42 (m, 25 H), 5.09 (dd, J = 3.2, 9.2 Hz, 1 H), 5.06 (dd, J = 2.8, 8.8 Hz, 1 H), 5.01 (dd, J = 1.2, 8 Hz, 1 H), 4.98 (dd, J = 1.2, 8.4 Hz, 1 H), 4.97 (d, J = 11.2 Hz, 1 H), 4.87 (d, J = 10.8 Hz, 1 H), 4.84 (d, J = 11.6 Hz, 1 H), 4.75 (d, J = 10.4 Hz, 1 H), 4.59 (d, J = 10.8 Hz, 1 H), 4.54 (d, J = 11.6 Hz, 1 H), 4.43 (d, J = 8.8 Hz, 1 H), 3.54 (dd, J = 8, 10 Hz, 1 H), 3.16-3.25 (m, 2 H), 2.67 (dd, J = 8.4, 10 Hz, 1 H), 2.46 (s, 6 H), 2.15-2.28 (m, 1 H), 1.98-2.11 (m, 1 H), 1.82-1.92 (m, 1 H), 1.66-1.81 (m, 1 H); ^{13}C NMR (100 MHz, $CDCl_3$) δ 138.9, 138.2, 137.3, 136.45 (d, *Jcp* = 6 Hz), 136.43 (d, *Jcp* = 6 Hz), 128.6, 128.42, 128.40, 128.35, 128.32, 128.2, 128.1, 128.01, 127.97, 127.94, 127.8, 127.7, 127.5, 100.1, 82.3, 80.7, 77.3, 75.1, 75.0, 73.9 (d, *Jcp* = 15 Hz), 70.5, 69.4, 67.1 (d, *Jcp* = 6 Hz), 41.7, 25.1 (d, *Jcp* = 4 Hz), 22.0 (d, *Jcp* = 141 Hz); ^{31}P NMR (162 MHz, $CDCl_3$) δ 33.32; HRMS (ESI *m/z*) calcd for $C_{44}H_{50}NO_7PNa$ ($M+Na^+$) 758.3223, obsd 758.3226.

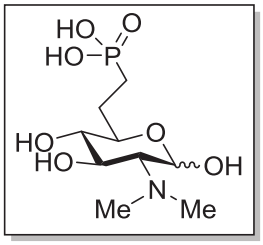

N, N-Dimethyl glucosamine 6-phosphonate (29). A solution of **28** (62 mg, 0.084 mmol) in MeOH (3 mL) was stirred in the presence of 40% $Pd(OH)_2/C$ (25 mg) and trace amount of TFA (1 drop), under balloon pressure of hydrogen, for 24 h at room temperature. Filtrate the mixture through a pad of Celite and evaporate the solvent to yield **29** (21 mg, 89%) as a colorless foam: ^{1}H NMR (400 MHz, D_2O) δ 5.50 (d, J = 2.8 Hz, 0.4 H), 5.02 (d, J = 8.4 Hz), 3.97 (t, J = 9.2 Hz, 0.4 H), 3.73-3.82 (m, 1 H), 3.22-2.39 (m, 2 H), 3.04 (dd, J = 1.6, 8.8 Hz, 0.6 H), 2.95 (s, 2.4 H), 2.93 (s, 3.6 H), 1.97-2.04 (m, 1 H), 1.42-1.79 (m, 3 H); ^{13}C NMR (100 MHz, D_2O) δ 91.2, 88.3, 75.6 (d, *Jcp* = 16 Hz), 73.9, 73.8, 70.9 (d, *Jcp* = 17 Hz), 69.4, 68.8, 67.5, 65.8, 42.2 (br), 41.2 (br), 40.6 (br), 24.9 (d, *Jcp* = 3 Hz), 24.7 (d, *Jcp* = 3 Hz), 23.2 (d, *Jcp* = 134 Hz), 22.7 (d, *Jcp* = 133 Hz); ^{31}P NMR (162 MHz, D_2O) δ 25.60, 25.40; HRMS (ESI *m/z*) calcd for $C_9H_{21}NO_7P$ ($M+H^+$) 286.1056, obsd 286.1061.

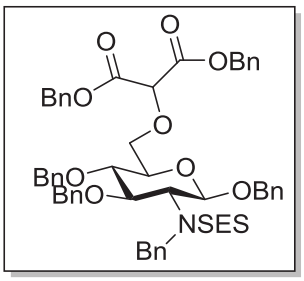

Dibenzyl 2-(((2R,3S,4R,5R,6R)-5-(N-benzyl-2-(trimethylsilyl)ethylsulfonamido)-3,4,6-tris(benzyloxy)tetrahydro-2H-pyran-2-yl)methoxy)malonate (13). To a stirred solution of **3** (100 mg, 0.14 mmol) and rhodium acetate dimer (6 mg, 0.014 mmol) in benzene (1 mL), under reflux, was added, dropwise, a solution of dibenzyl diazomalonate (44 mg, 0.14 mmol) in benzene (1 mL). After complete addition, the reaction mixture was refluxed for 16 h. Volatiles were removed under reduced pressure and the crude residue purified by flash

chromatography (20% EtOAc-hexane) to give **13 (**102 mg, 73%) as a white solid: ^{1}H NMR (400 MHz, DMSO-d6, 90 °C) δ 7.20-7.55 (m, 30 H), 5.23 (d, J = 12.8 Hz, 1 H), 5.21 (d, J = 12.4 Hz, 1 H), 5.17 (d, J = 12.4 Hz, 1 H), 5.16 (d, J = 12.4 Hz, 1 H), 4.96 (s, 1 H), 4.76-4.87 (m, 4 H), 4.64 (s, 2 H), 4.42-4.56 (m, 3 H), 4.00 (t, 8.8 Hz, 1 H), 3.93 (d, J = 3.2 Hz, 2 H), 3.72 (t, J = 8.4 Hz, 1 H), 3.68 (t, J = 9.6 Hz, 1 H), 3.59 (td, J = 3.2, 10 Hz, 1 H), 2.64-2.83 (m, 2 H), 0.84-0.94 (m, 2 H), -0.17 (m, 9 H); ^{13}C NMR (100 MHz, DMSO-d6, 90 °C) δ 166.6, 166.5, 139.0, 138.7, 137.9, 137.7, 135.82, 135.76, 129.7, 128.8, 128.65, 128.61, 128.58, 128.50, 128.23, 128.20, 128.05, 128.00, 127.96, 127.89, 127.81, 127.7, 99.4, 80.0, 79.8, 74.8, 74.0, 73.6, 70.5, 70.4, 67.3, 67.2, 50.3, 10.2, -1.75; HRMS (ESI *m/z*) calcd for $C_{56}H_{63}NO_{11}SSiNa$ ($M+Na^{+}$) 1008.3789, obsd 1008.3747.

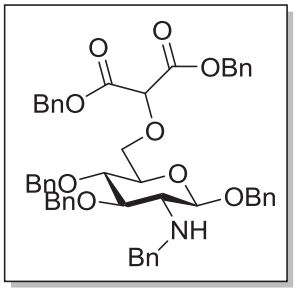

Dibenzyl 2-(((2R,3S,4R,5R,6R)-5-(benzylamino)-3,4,6-tris(benzyloxy)tetrahydro-2H-pyran-2-yl)methoxy)malonate (50). A suspension of **13** (162 mg, 0.16 mmol) and CsF (125 mg, 0.82 mmol) in DMF (2 mL) was heated at 90 °C for 16 h. The reaction was then cooled down and quenched with aqueous NH_4Cl. The mixture was extracted with EtOAc. The combined organic phase was dried, filtered and concentrated in vacuum. The crude product was purified by flash column chromatography (20-40% EtOAc-hexanes) to give **50** (93 mg, 71%) as a white solid: ^{1}H NMR (400 MHz, $CDCl_3$) δ 7.13 – 7.15 (m, 2 H), 7.21 – 7.32 (m, 28 H), 5.20 (d, J = 12 Hz, 1 H), 5.17 (s, 2 H), 5.11 (d, J = 12 Hz, 1 H), 4.87 (d, J = 11.6 Hz, 1 H), 4.86 (s, 1 H), 4.82 (d, J = 11.6 Hz, 1 H), 4.77 (d, J = 10.8 Hz, 1 H), 4.69 (d, J = 10.8 Hz, 1 H), 4.65 (d, J = 11.6 Hz, 1 H), 4.55 (d, J = 12 Hz, 1 H), 4.35 (d, J = 7.6 Hz, 1 H), 3.99 (t, J = 2.8 Hz,

1 H), 3.97 (t, *J* = 2 Hz, 1 H), 3.91 (dd, *J* = 1.6, 12.4 Hz, 1 H), 3.79 (d, *J* = 12.8 Hz, 1 H), 3.74 (d, *J* = 9.2 Hz, 1 H), 3.47 (ddd, *J* = 1.6, 4.4, 9.2 Hz, 1 H), 3.45 (t, *J* = 9.2 Hz, 1 H), 2.70 (dd, *J* = 7.6, 10 Hz, 1 H); ^{13}C NMR (100 MHz, $CDCl_3$) δ 166.5, 166.4, 140.5, 138.1, 138.0, 137.4, 135.0, 134.9, 128.59, 128.57, 128.48, 128.40, 128.36, 128.30, 128.1, 127.95, 127.90, 127.84, 127.76, 126.8, 103.9, 88.3, 80.1, 78.2, 75.4, 74.8, 74.7, 71.1, 70.3, 67.56, 67.49, 62.3, 53.48, 53.45; HRMS (FAB *m/z*) calcd for $C_{51}H_{52}O_9N$ ($M+H^+$) 822.3642, obsd 822.3640.

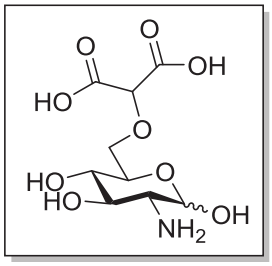

Glucosamine 6-malonyl ether (14). A suspension of **50** (56 mg, 0.068 mmol) in MeOH (2 mL) was stirred in the presence of 40% $Pd(OH)_2/C$ (23 mg) and trace amount of TFA (1 drop), under balloon pressure of hydrogen, for 24 h at room temperature. Filtrate the mixture through a pad of Celite and wash the filter cake with 2 mL MeOH. Suspend the filter cake in 2 mL H_2O and stir for 5 min, and then filtrate again through a pad of Celite. Concentrate the aqueous solution and dry over high vacuum to yield **14** (13 mg, 72%) as a colorless foam: ^{1}H NMR (500 MHz, D_2O) δ 5.42 (d, *J* = 2.8 Hz, 0.6 H), 4.92 (d, *J* = 6.8 Hz, 0.4 H), 4.65 (s, 0.4 H), 4.64 (s, 0.6 H), 4.04 (td, *J* = 2.4, 8 Hz, 0.6 H), 3.95 (dd, *J* = 1.2, 9.2 Hz, 0.4 H), 3.86-3.91 (m, 2 H), 3.82 (dd, *J* = 4.8, 9.2 Hz, 0.4 H), 3.62-3.69 (m, 0.6 H), 3.60 (t, *J* = 7.6 Hz, 0.6 H), 3.55 (t, *J* = 7.6 Hz, 0.4 H), 3.29 (dd, *J* = 2.8, 8.4 Hz, 0.6 H), 3.01 (dd, *J* = 6.8, 8.4 Hz, 0.4 H); ^{13}C NMR (100 MHz, D_2O) δ 171.4, 171.3, 92.8, 89.1, 75.1, 71.8, 70.7, 69.6, 69.4, 69.3, 56.6, 54.2; HRMS (ESI *m/z*) calcd for $C_9H_{15}NO_9Na$ ($M+Na^+$) 304.0645, obsd 304.0658.

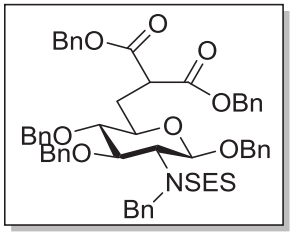

Dibenzyl 2-(((2R,3R,4R,5R,6R)-5-(N-benzyl-2-(trimethylsilyl)ethylsulfonamido)-3,4,6-tris(benzyloxy)tetrahydro-2H-pyran-2-yl)methyl)malonate (15). To a solution of the triflate **4** (122 mg, 0.156 mmol) and dibenzyl malonate (177 mg, 0.624 mmol) in THF (2 mL) was added LiHMDS (0.624 mL, 1 M solution in THF, 0.624 mmol) at -78 °C. The solution was then slowly warmed to room temperature and stirred overnight. Aqueous NH_4Cl was added to quench the reaction. The mixture was extracted with Et_2O (2 x 20 mL). The combined organic layers were dried over $MgSO_4$, filtered and concentrated in vacuum. The residue was purified by flash column chromatography (20% EtOAc-hexanes) to afford **15** (124 mg, 82%) as a colorless oil: ^{1}H NMR (400 MHz, DMSO-d6, 90 °C) δ 7.21-7.48 (m, 30 H), 5.16 (s, 2 H), 5.16 (d, J = 12.4 Hz, 1 H), 5.08 (d, J = 12.4 Hz, 1 H), 4.68-4.79 (m, 5 H), 4.63 (d, J = 11.2, 1 H), 4.50 (d, J = 15.6 Hz, 1 H), 4.43 (d, J = 15.6 Hz, 1 H), 4.33 (d, J = 11.6 Hz, 1 H), 3.97 (br, 1 H), 3.79 (dd, J = 5.2, 9.2 Hz, 1 H), 3.70 (br, 1 H), 3.39-3.47 (m, 2 H), 2.61-2.79 (m, 2 H), 2.47 (dd, J = 2.4, 9.2 Hz, 1 H), 2.05-2.13 (m, 2 H), -0.19 (s, 9 H), ^{13}C NMR (100 MHz, DMSO-d6, 90 °C) δ 168.9, 168.8, 139.0, 138.5, 137.8, 136.10, 136.08, 129.7, 128.82, 128.78, 128.64, 128.62, 128.60, 128.5, 128.4, 128.3, 128.08, 128.05, 127.95, 127.93, 127.8, 127.7, 99.6, 83.5, 74.1, 73.5, 72.5, 70.4, 67.1, 67.0, 50.3, 48.8, 31.2, 10.2, -1.77; HRMS (ESI *m/z*) calcd for $C_{56}H_{63}O_{10}NSSiNa$ ($M+Na^+$) 992.3840, obsd 992.3856.

Dibenzyl 2-(((2R,3R,4R,5R,6R)-5-(benzylamino)-3,4,6-tris(benzyloxy)tetrahydro-2H-pyran-2-yl)methyl)malonate (**16**) To a solution of **15** (224 mg, 0.23 mmol) in DMF

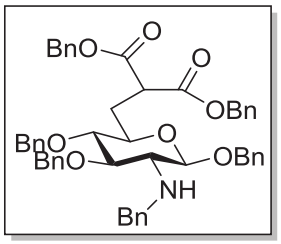

(3 mL) was added CsF (175 mg, 1.15 mmol) in one portion. The suspension was heated to 90 °C and stirred at that temperature for 16 h. Then the reaction was quenched with aqueous ammonium chloride and extracted with ethyl acetate. The combined organic phase was dried over $MgSO_4$, filtered and concentrated in vacuum. The crude product was purified by flash column chromatography (20-30% EtOAc-hexanes) to give **16** (80 mg, 44%) as a white solid: ^{1}H NMR (400 MHz, $CDCl_3$) δ 6.95 – 7.33 (m, 30 H), 5.16 (s, 2 H), 5.16 (d, J = 12.4 Hz, 1 H), 5.11 (d, J = 12.4 Hz, 1 H), 4.87 (d, J = 11.2 Hz, 1 H), 4.83 (d, J = 10.8 Hz, 1 H), 4.81 (d, J = 12 Hz, 1 H), 4.68 (d, J = 10.8 Hz, 1 H), 4.67 (d, J = 11.2 Hz, 1 H), 4.49 (d, J = 12 Hz, 1 H), 4.23 (d, J = 8 Hz, 1 H), 3.98 (d, J = 12.8 Hz, 1 H), 3.79 (d, J = 12.8 Hz, 1 H), 3.77 (dd, J = 5.2, 10 Hz, 1 H), 3.40 (t, J = 8.4 Hz, 1 H), 3.34 (t, J = 8.8 Hz, 1 H), 3.28 (dt, J = 2.4, 10 Hz, 1 H), 2.70 (dd, J = 8, 9.2 Hz, 1 H), 2.61 (ddd, J = 2.4, 10, 14 Hz, 1 H), 2.05 – 2.14 (m, 1 H); ^{13}C NMR (100 MHz, $CDCl_3$) δ 169.0, 168.8, 140.6, 138.0, 137.7, 137.5, 135.3, 128.63, 128.57, 128.54, 128.45, 128.40, 128.37, 128.29, 128.2, 128.01, 127.99, 127.94, 127.91, 127.7, 126.9, 103.8, 83.3, 82.7, 75.1, 72.4, 71.0, 67.2, 62.6, 53.4, 48.6, 31.1; HRMS (FAB *m/z*) calcd for $C_{51}H_{52}O_8N$ ($M+H^+$) 806.3693, obsd 806.3713.

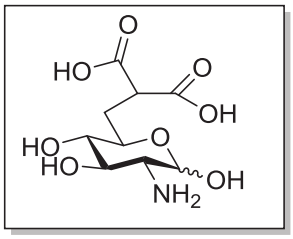

Glucosamine 6-malonate (18). A suspension of **16** (39 mg, 0.048 mmol) in MeOH (2 mL) was stirred in the presence of 40% $Pd(OH)_2$/C (15 mg) and trace amount of TFA (1 drop), under balloon pressure of hydrogen, for 24 h at room temperature. Filtrate the mixture through a pad of Celite and wash the filter cake with 2 mL MeOH.

Suspend the filter cake in 2 mL H_2O and stir for 5 min, and then filtrate again through a pad of Celite. Concentrate the aqueous solution and dry over high vacuum to yield **18** (10 mg, 78%) as a colorless foam: ^{1}H NMR (400 MHz, D_2O) δ 5.27 (d, J = 3.6 Hz, 0.45 H), 4.76 (d, J = 8.4 Hz, 0.55 H), 3.66-3.76 (m, 1 H), 3.57 (dd, J = 8.4, 10.4 Hz, 0.45 H), 3.15-3.30 (m, 2.1 H), 2.89 (dd, J = 8.4, 10.4 Hz, 0.45 H), 2.20-2.37 (m, 1 H), 1.68-1.84 (m, 1 H); ^{13}C NMR (100 MHz, D_2O) δ 178.4, 178.2, 92.8, 88.9, 74.3, 73.75, 73.73, 71.9, 69.6, 69.5, 56.9, 54.4, 31.8, 31.7, 31.6, 31.5; HRMS (ESI *m/z*) calcd for $C_9H_{16}NO_8$ (M M+H^+) 266.0876, obsd 266.0978.

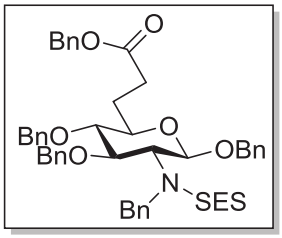

Benzyl 3-((2R,3R,4R,5R,6R)-5-(N-benzyl-2-(trimethylsilyl)ethylsulfonamido)-3,4,6-tris(benzyloxy)tetrahydro-2H-pyran-2-yl)propanoate (17). Further elution (40-50% EtOAc-hexanes) to give **17** (67 mg, 35%) as a white solid: ^{1}H NMR (400 MHz, DMSO-d6, 90 °C) δ 7.22-7.46 (m, 25 H), 5.12 (d, J = 12.4 Hz, 1 H), 5.08 (d, J = 12.8 Hz, 1 H), 4.70- 4.77 (m, 5 H), 4.62 (d, J = 11.6 Hz, 1 H), 4.51 (d, J = 15.2 Hz, 1 H), 4.44 (d, J = 7.6 Hz, 1 H), 4.41 (d, J = 3.6 Hz, 1 H), 3.96 (t, J = 8.8 Hz, 1 H), 3.69 (t, J = 8.8 Hz, 1 H), 3.35-3.43 (m, 2 H), 2.63-2.85 (m, 2 H), 2.48 (dd, J = 2.8, 10 Hz, 2 H), 2.11-2.20 (m, 1 H), 1.73-1.82 (m, 1 H), 0.82-0.96 (m, 2 H), -0.17 (s, 9 H), ^{13}C NMR (100 MHz, DMSO-d6, 90 °C) δ 172.8, 139.1, 138.7, 137.89, 137.84, 136.9, 129.7, 128.8, 128.64, 128.60, 128.5, 128.3, 128.2, 128.07, 128.04, 127.94, 127.91, 127.8, 127.6, 99.6, 83.6, 74.1, 73.7, 73.5, 70.5, 65.9, 50.3, 30.2, 27.3, 10.2, -1.75; HRMS (ESI *m/z*) calcd for $C_{48}H_{57}O_8NSSiNa$ (M+Na^+) 858.3472, obsd 858.3477.

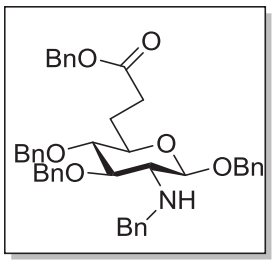

Benzyl 3-((2R,3R,4R,5R,6R)-5-(benzylamino)-3,4,6-tris(benzyloxy)tetrahydro-2H-pyran-2-yl)propanoate (51). To a solution of **17** (41 mg, 0.05 mmol) in DMF (1 mL) was added CsF (53 mg, 0.35 mmol) in one portion. The suspension was heated to 90 °C and stirred overnight. Then the reaction was quenched with aqueous ammonium chloride and extracted with ethyl acetate. The combined organic phase was dried over $MgSO_4$, filtered and concentrated in vacuum. The crude product was purified by flash column chromatography (50% EtOAc-hexanes) to give **51** (26 mg, 78%), as a white solid: ^{1}H NMR (400 MHz, $CDCl_3$) δ 7.13-7.42 (m, 25 H), 5.17 (d, J = 12.4 Hz, 1 H), 5.14 (d, J = 12.4 Hz, 1 H), 4.92 (d, J = 10 Hz, 1 H), 4.90 (d, J = 7.2 Hz, 1 H), 4.87 (d, J = 7.2 Hz, 1 H), 4.72 (d, J = 4 Hz, 1 H), 4.69 (d, J = 3.6 Hz, 1 H), 4.61 (d, J = 15.6 Hz, 1 H), 4.36 (d, J = 8 Hz, 1 H), 4.03 (d, J = 13.2 Hz, 1 H), 3.84 (d, J = 12.8 Hz, 1 H), 3.48 (t, J = 8.8 Hz, 1 H), 3.37 (t, J = 9.2 Hz, 1 H), 3.32 (td, J = 2.4, 9.2 Hz, 1 H), 2.75 (dd, J = 8, 9.6 Hz, 1 H), 2.46-2.63 (m, 2 H), 2.27-2.37 (m, 1 H), 1.80-1.89 (m, 1 H), 1.66 (br, 1 H), ^{13}C NMR (100 MHz, $CDCl_3$) δ 173.1, 140.5, 138.0, 137.8, 137.4, 136.0, 128.64, 128.61, 128.56, 128.5, 128.4, 128.33, 128.27, 128.0, 127.8, 126.9, 103.8, 83.5, 82.8, 75.1, 73.9, 71.1, 66.3, 62.7, 53.5, 30.4, 27.1; HRMS (ESI *m/z*) calcd for $C_{43}H_{46}O_6N$ ($M+H^+$) 672.3325, obsd 672.3319.

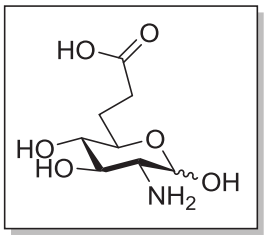

Glucosamine 6-carboxylate (19). A solution of **51** (26 mg, 0.038 mmol) in MeOH (2 mL) was stirred in the presence of 40% $Pd(OH)_2$/C (10 mg) and trace amount of TFA (1 drop), under

balloon pressure of hydrogen, for 24 h at room temperature. Filtrate the mixture through a pad of Celite and evaporate the solvent to yield **19** (5 mg, 63%) as a colorless foam: ^{1}H NMR (400 MHz, D_2O) δ 5.22 (d, J = 4 Hz, 0.45 H), 4.66 (d, J = 8.4 Hz, 0.55 H), 3.61-3.75 (m, 1 H), 3.41 (dd, J = 9.2, 10 Hz, 0.45 H), 3.24 (dt, J = 2, 9.6 Hz, 0.55 H), 3.14 (t, J = 9.2 Hz, 1 H), 3.08 (dd, J = 3.6, 10.4 Hz, 0.55 H), 2.75 (dd, J = 8.8, 10.2 Hz, 0.45 H), 2.07-2.28 (m, 2 H), 1.92-2.06 (m, 1 H), 1.47-1.61 (m, 1 H); HRMS (ESI *m/z*) calcd for $C_9H_{16}NO_8$ (M M+Na^+) 266.0876, obsd 266.0978.; HRMS (EI *m/z*) calcd for $C_8H_{15}NO_6Na$ (M+Na^+) 244.0797, obsd 266.0802.

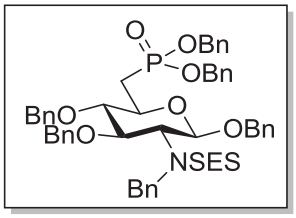

Dibenzyl (((2S,3S,4R,5R,6R)-5-(N-benzyl-2-(trimethylsilyl)ethylsulfonamido)-3,4,6-tris(benzyloxy)tetrahydro-2H-pyran-2-yl)methyl)phosphonate (7). To a solution of the triflate **4** (219 mg, 0.28 mmol) and dibenzyl phosphite (187 μL, 0.84 mmol) in THF (3 mL) was added LiHMDS (0.84 mL, 1 M solution in THF, 0.84 mmol) at -78 °C. The solution was then slowly warmed to room temperature and stirred overnight. Aqueous NH_4Cl was added to quench the reaction. The mixture was extracted with Et_2O (2 x 20 mL). The combined organic layers were dried over $MgSO_4$, filtered and concentrated in vacuum. The residue was purified by flash column chromatography (20-30% EtOAc-hexanes) to afford **7** (212 mg, 80%) as a colorless oil: ^{1}H NMR (400 MHz, DMSO-d6, 90 °C) δ 7.18-7.58 (m, 30 H), 4.95-5.08 (m, 4 H), 4.71-4.83 (m, 5 H), 4.64 (d, J = 11.7 Hz, 1 H), 4.52 (d, J = 15.5 Hz, 1 H), 4.42 (d, J = 15.5 Hz, 1 H), 4.29 (d, J = 11.7 Hz, 1 H), 3.99 (t, J = 9.6 Hz, 1 H), 3.68-3.82 (m, 2 H), 3.51 (t, J = 8.8 Hz, 1 H), 2.60-2.82 (m, 2 H), 2.12-2.38 (m, 2 H),

0.80-0.96 (m, 2 H), -0.19 (s, 9 H); ^{13}C NMR (100 MHz, DMSO-d6, 90 °C) δ 138.9, 138.6, 137.8, 137.5, 137.2, 137.11 (d, *Jcp* = 7 Hz), 137.10 (d, *Jcp* = 7 Hz), 129.7, 128.8, 128.7, 128.6, 128.5, 128.4, 128.10, 128.06, 127.97, 127.91, 127.8, 127.7, 99.2, 83.6 (d, *J* = 14 Hz), 74.2, 73.5, 70.58, 70.52, 70.2, 67.02 (d, *Jcp* = 6 Hz), 66.97 (d, *Jcp* = 5 Hz), 50.3, 28.7 (d, *J* = 140 Hz), 10.2, -1.77; ^{31}P NMR (162 MHz, DMSO-d6, 90 °C) δ 28.88; HRMS (ESI *m/z*) calcd for $C_{53}H_{62}O_9NSiPSNa$ ($M+Na^+$) 970.3550, obsd 970.3526

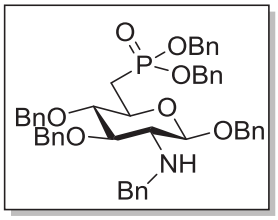

Dibenzyl (((2S,3S,4R,5R,6R)-5-(benzylamino)-3,4,6-tris(benzyloxy)tetrahydro-2H-pyran-2-yl)methyl)phosphonate (52). To a solution of **7** (78 mg, 0.082 mmol) in DMF (1 mL) was added CsF (87 mg, 0.57 mmol) in one portion. The reaction was heated to 90 °C and stirred at that temperature for 16 h. Then aqueous ammonium chloride was added and the mixture was extracted with ethyl acetate. The organic phase was combined, dried over $MgSO_4$, filtered and concentrated in vacuum. The crude product was purified by flash column chromatography (40-50% EtOAc/hexanes) to give **52** (49 mg, 77%) as a white solid: ^{1}H NMR (400 MHz, $CDCl_3$) δ 7.14–7.35 (m, 30 H), 4.99 – 5.08 (m, 4 H), 4.87 (d, *J* = 11.6 Hz, 1 H), 4.78 (d, *J* = 11.6 Hz, 1 H), 4.70 (d, *J* = 11.6 Hz, 1 H), 4.62 (d, *J* = 11.2 Hz, 1 H), 4.49 (d, *J* = 11.6 Hz, 1 H), 4.38 (d, *J* = 8 Hz, 1 H), 3.99 (d, *J* = 12.8 Hz, 1 H), 3.80 (d, *J* = 12.8 Hz, 1 H), 3.67-3.77 (m, 1 H), 3.46 (t, *J* = 8.8 Hz, 1 H), 3.41 (dd, *J* = 8.8, 16.4 Hz, 1 H), 2.77 (dd, *J* = 8, 9.6 Hz, 1 H), 2.36 (ddd, *J* = 2, 15.2, 19.6 Hz, 1 H), 2.01 (app dt, *J* = 10, 15.6 Hz, 1 H), 1.68 (br, 1 H); ^{13}C NMR (100 MHz, $CDCl_3$) δ 140.6, 137.9, 137.7, 137.3, 136.39 (d, *Jcp* = 6 Hz), 136.33 (d, *Jcp* = 6 Hz), 128.61, 128.58, 128.4, 128.3, 128.03, 127.99, 127.92, 127.7,

126.8, 103.5, 83.54 (d, *Jcp* = 2 Hz), 82.5 (d, *Jcp* = 14 Hz), 75.1, 74.9, 70.8, 70.5 (d, *Jcp* = 7 Hz), 67.24 (d, *Jcp* = 6 Hz), 67.08 (d, *Jcp* = 6 Hz), 62.7, 53.4, 28.7 (d, *Jcp* = 142 Hz); ^{31}P NMR (162 MHz, $CDCl_3$) δ 29.60; HRMS (ESI *m/z*) calcd for $C_{48}H_{50}O_7NPNa$ ($M+Na^+$) 806.3223, obsd 806.3243.

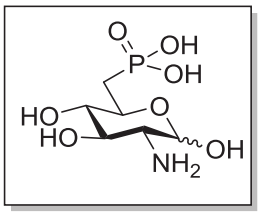

Glucosamine 5-phosphonate (8). A solution of **52** (42 mg, 0.054 mmol) in MeOH (2 mL) was stirred in the presence of 40% $Pd(OH)_2/C$ (12 mg) and trace amount of TFA (1 drop), under balloon pressure of hydrogen, for 24 h at room temperature. Filtrate the mixture through a pad of Celite and wash the filter cake with 2 mL MeOH. Suspend the filter cake in 2 mL H_2O and stir for 5 min, and then filtrate again through a pad of Celite. Concentrate the aqueous solution and dry over high vacuum to yield **8** (12 mg, 88%) as a colorless foam: ^{1}H NMR (400 MHz, D_2O) δ 5.34 (d, *J* = 3.2 Hz, 0.5 H), 4.86 (d, *J* = 8 Hz, 0.5 H), 4.06 (ddt, *J* = 3.6, 9.6, 9.6 Hz, 0.5 H), 3.82 (dd, *J* = 9.2, 10.4 Hz, 0.5 H), 3.56-3.65 (m, 1 H), 3.26 (t, *J* = 8.8 Hz, 0.5 H), 3.24 (t, *J* = 9.2 Hz, 1 H), 3.23 (dd, *J* = 3.2, 9.6 Hz, 0.5 H), 2.94 (dd, *J* = 8.8, 10.8 Hz, 0.5 H), 2.02-2.16 (m, 1 H), 1.69-1.81 (m, 1 H); ^{13}C NMR (100 MHz, D_2O) δ 92.8, 89.0, 74.6 (d, *Jcp* = 12 Hz), 74.5 (d, *Jcp* = 11 Hz), 72.7 (d, *Jcp* = 4 Hz), 71.9, 69.5, 67.9 (d, *Jcp* = 5 Hz), 56.7, 54.3, 31.2 (d, *Jcp* = 133 Hz), 30.8 (d, *Jcp* = 133 Hz); ^{31}P NMR (162 MHz, D_2O) δ 20.7, 20.0; HRMS (EI *m/z*) calcd for $C_6H_{14}O_7NPNa$ ($M+Na^+$) 266.0406, obsd 266.0414.

Diethyl 2-(((2R,3R,4R,5R,6R)-5-(N-benzyl-2-(trimethylsilyl)ethylsulfonamido)-3,4,6-tris(benzyloxy)tetrahydro-2H-pyran-2-yl)methyl)malonate (9): To a solution of the

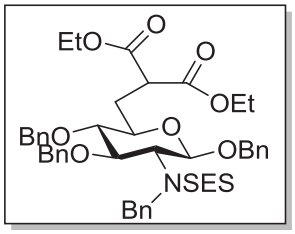

triflate **4** (205 mg, 0.25 mmol) and diethyl malonate (152 μL, 1 mmol) in THF (2 mL) was added LiHMDS (1 mL, 1 M solution in THF, 1 mmol) at -78 °C. The solution was then slowly warmed to room temperature and stirred overnight. Aqueous NH_4Cl was added to quench the reaction. The mixture was extracted with Et_2O (2 x 20 mL). The combined organic layers were dried over $MgSO_4$, filtered and concentrated in vacuum. The residue was purified by flash column chromatography (20% EtOAc-hexanes) to afford **9** (194 mg, 92%) as a colorless oil: ^{1}H NMR (400 MHz, DMSO-d6, 90 °C) δ 7.22-7.65 (m, 20 H), 4.73-4.82 (m, 5 H), 4.66 (d, J = 11.6 Hz, 1 H), 4.53 (d, J = 15.6 Hz, 1 H), 4.47 (d, J = 16.4 Hz, 1 H), 4.43 (d, J = 12 Hz, 1 H), 4.06-4.24 (m, 4 H), 4.02 (br, 1 H), 3.74 (t, J = 8 Hz, 1 H), 3.64 (dd, J = 5.2, 8.8 Hz, 1 H), 3.44 (dd, J = 2, 5.2 Hz, 2 H), 2.67-2.84 (m, 2 H), 2.46 (ddd, J = 1.6, 9.2, 14 Hz, 1 H), 2.01-2.09 (m, 1 H), 1.21 (td, J = 7.2, 10.4 Hz, 6 H), 0.86-0.96 (m, 2 H), -0.16 (s, 9 H); ^{13}C NMR (100 MHz, DMSO-d6, 90 °C) δ 169.2, 169.0, 139.0, 138.6, 137.85, 137.81, 129.7, 128.7, 128.6, 128.5, 128.0, 127.9, 127.8, 127.7, 99.6, 83.6, 74.2, 73.5, 72.6, 70.4, 61.33, 61.31, 50.3, 48.8, 31.2, 14.3, 14.2, 10.2, -1.79; HRMS (ESI *m/z*) calcd for $C_{46}H_{59}O_{10}NSSiNa$ ($M+Na^+$) 868.3527, obsd 868.3514.

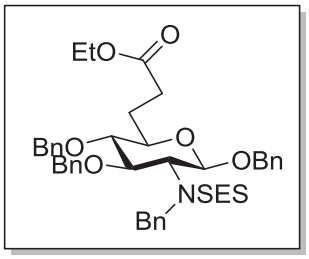

Ethyl 3-((2R,3R,4R,5R,6R)-5-(N-benzyl-2-(trimethylsilyl)ethylsulfonamido)-3,4,6-tris(benzyloxy)tetrahydro-2H-pyran-2-yl)propanoate (53). To a solution of **9** (135 mg, 0.16 mmol) in DMSO (2 mL) was added LiCl (51 mg, 1.2 mmol) in one potion. The suspension was refluxed at 200 °C for

8 h. Then the reaction was cooled down to room temperature and quenched with aqueous NH_4Cl. The mixture was extracted with Et_2O (3 x 10 mL). The combined organic layers were dried over $MgSO_4$, filtered and concentrated in vacuum. The residue was purified by flash column chromatography (10% EtOAc-hexanes) to afford **53** (118 mg, 96%) as a colorless oil: ^{1}H NMR (400 MHz, DMSO-d6, 90 °C) δ 7.23-7.52 (m, 20 H), 4.72-4.80 (m, 5 H), 4.63 (d, J = 11.6 Hz, 1 H), 4.52 (d, J = 15.6 Hz, 1 H), 4.45 (10.8 Hz, 1 H), 4.44 (d, 16 Hz, 1 H), 4.04-4.12 (m, 2 H), 3.97 (t, J = 8.8 Hz, 1 H), 3.70 (t, J = 8.8 Hz, 1 H), 3.34-3.42 (m, 2 H), 2.65-2.82 (m, 2 H), 2.42 (t, 8.4 Hz, 1 H), 2.09-2.18 (m, 1 H), 1.70-1.79 (m, 1 H), 1.19 (t, J = 7.2 Hz, 1 H), 0.85-0.92 (m, 2 H), -0.17 (9 H); ^{13}C NMR (100 MHz, DMSO-d6, 90 °C) δ 172.9, 139.1, 138.7, 137.89, 137.87, 129.7, 128.7, 128.6, 128.5, 128.1, 128.04, 128.00, 127.95, 127.94, 127.8, 127.7, 99.5, 83.6, 74.1, 73.7, 73.4, 70.4, 60.1, 50.3, 30.3, 27.3, 14.5, 10.2, -1.75; HRMS (ESI *m/z*) calcd for $C_{43}H_{55}O_8NSSiNa$ ($M+Na^+$) 796.3315, obsd 796.3320.

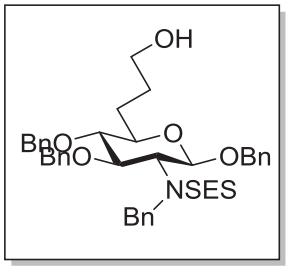

N-benzyl-2-(trimethylsilyl)-N-((2R,3R,4R,5R,6R)-2,4,5-tris(benzyloxy)-6-(3-hydroxypropyl)tetrahydro-2H-pyran-3-yl)ethanesulfonamide (10). To a stirred suspension of $LiAlH_4$ (17 mg, 0.44 mmol) in dry THF (2 mL) was added dropwise a solution of **53** (173 mg, 0.22 mmol) in dry THF at 0 °C under nitrogen. The reaction mixture was warmed to room temperature and stirred for 2 h. After successively adding water, 15% NaOH and water at 0 °C, the mixture was diluted with EtOAc. The aqueous layer was extracted by EtOAc. The organic layers were combined, dried over $MgSO_4$, filtered and concentrated. Purification by flash column chromatography (30% EtOAc-

hexanes) gave **10** (153 mg, 95%) as a colorless oil: ^{1}H NMR (400 MHz, DMSO-d6, 90 °C) δ 7.23-7.52 (m, 20 H), 4.82 (d, J = 11.6 Hz, 1 H), 4.77 (d, J = 12.8 Hz, 1 H), 4.76 (s, 2 H), 4.72 (d, J = 11.6 Hz, 1 H), 4.65 (d, J = 11.6 Hz, 1 H), 4.53 (d, J = 15.2 Hz, 1 H), 4.49 (d, J = 8.8 Hz, 1 H), 4.45 (d, J = 12.8 Hz, 1 H), 3.97 (t, J = 8.8 Hz, 1 H), 3.71 (t, J = 8.8 Hz, 1 H), 3.48 (t, J = 6.4 Hz, 2 H), 3.39 (dt, J = 2.8, 9.2 Hz, 1 H), 3.35 (t, J = 9.2 Hz, 1 H), 2.67-2.83 (m, 2 H), 1.87-1.96 (m, 1 H), 1.67-1.75 (m, 1 H), 1.49-1.63 (m, 2 H), 0.83-0.95 (m, 2 H), -0.16 (s, 9 H); ^{13}C NMR (100 MHz, DMSO-d6, 90 °C) δ 139.1, 138.8, 137.9, 129.7, 128.67, 128.59, 128.58, 128.46, 128.1, 128.03, 127.99, 127.93, 127.86, 127.80, 127.6, 99.4, 84.0, 74.7, 74.1, 73.5, 70.4, 61.4, 50.3, 28.9, 28.4, 10.2, 10.1, -1.75; HRMS (ESI *m/z*) calcd for $C_{41}H_{53}O_7NSSiNa$ ($M+Na^+$) 754.3210, obsd 754.3212.

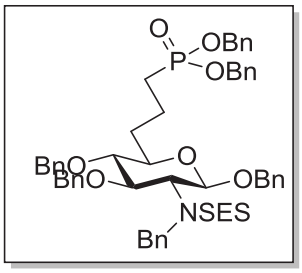

Dibenzyl (3-((2R,3R,4R,5R,6R)-5-(N-benzyl-2-(trimethylsilyl)ethylsulfonamido)-3,4,6-tris(benzyloxy)tetrahydro-2H-pyran-2-yl)propyl)phosphonate (11). To a solution of **10** (75 mg, 0.1 mmol) in THF (1 mL) was added triphenylphosphine (53 mg, 0.2 mmol), imidazole (15 mg, 0.223 mmol), and idodine (51 mg, 0.2 mmol). The mixture was stirred at room temperature overnight and then diluted with Et_2O. The organic layer was sequentially washed with saturated $Na_2S_2O_3$, water and brine, followed by drying and concentration in vacuum. The residue was purified by flash column chromatography (10% EtOAc-hexanes) to afford the iodide (72 mg, 85%) as a colorless oil: ^{1}H NMR (300 MHz, DMSO-d6, 90 °C) δ 7.21-7.62 (m, 20 H), 4.68-4.91 (m, 5 H), 4.6 2 (d, J = 9 Hz, 1 H), 4.41-4.55 (m, 3 H), 3.95 (t, J = 9 Hz, 1 H), 3.69 (t, J = 9 Hz), 3.37 (t, J = 9 Hz, 2 H), 3.29

(t, *J* = 6 Hz, 1 Hz), 3.06 (br, 1 H), 2.63-2.84 (m, 2 H), 1.80-2.04 (m, 3 H), 1.47-1.65 (m, 1 H), 0.86 (t, *J* = 6 Hz, 2 Hz), -0.18 (s, 9 Hz); ^{13}C NMR (300 MHz, DMSO-d6, 90 °C) δ 139.1, 138.7, 137.87, 137.86, 129.8, 128.7, 128.6, 128.5, 128.10, 128.06, 128.00, 127.9, 127.8, 127.6, 99.5, 83.6, 74.2, 73.7, 73.4, 70.5, 50.3, 32.5, 29.6, 10.2, 8.6, -1.7; HRMS (ESI *m/z*) calcd for $C_{41}H_{52}O_6NSSiINa$ ($M+Na^+$) 864.2227, obsd 864.2224.

To a solution of the iodide (72 mg, 0.08 mmol) and dibenzyl phosphite (56 μL, 0.25 mmol) was added LiHMDS (0.25 mL, 1 M in THF, 0.25 mmol) dropwise at -78 °C, the solution was allowed to warm to room temperature and stirred for 1 h before quenched with aqueous NH_4Cl. The aqueous layer was separated and extracted with Et_2O. Combined organic layers were dried, filtered and concentrated. The phosphonate product **11** was purified by flash column chromatography (30%-% EtOAc-hexanes) as a colorless oil (56 mg, 68%): ^{1}H NMR (400 MHz, DMSO-d6, 90 °C) δ 7.21-7.48 (m, 30 H), 5.04 (d, *J* = 8.8 Hz, 1 H), 5.01 (d, *J* = 8.4 Hz, 1 H), 4.98 (dd, *J* = 2, 8 Hz, 1 H), 4.95 (dd, *J* = 2, 8 Hz, 1 H), 4.79 (d, *J* = 8.4 Hz. 1 H), 4.76 (d, *J* = 12 Hz, 1 H), 4.73 (br, 2 H) 4.67 (d, *J* = 11.6 Hz, 1 H), 4.58 (d, *J* = 11.2 Hz, 1 H), 4.51 (d, *J* = 15.2 Hz, 1 H), 4.43 (dd, *J* = 1.6, 12 Hz, 2 H), 3.94 (t, *J* = 9.2 Hz, 1 H), 3.68 (t, *J* = 9.2 Hz, 1 H), 3.35 (dt, *J* = 2.8, 9.6 Hz, 1 H), 3.30 (t, *J* = 9.2 Hz, 1 H), 2.63-2.83 (m, 2 H), 1.28-1.92 (m, 6 H), 0.85-0.91 (m, 2 H), -0.17 (s, 9 H); ^{13}C NMR (100 MHz, DMSO-d6, 90 °C) δ 139.1, 138.7, 137.9, 137.8, 137.3 (d, *Jcp* = 6 Hz), 129.7, 128.8, 128.66, 128.59, 128.57, 128.46, 128.42, 128.1, 128.03, 127.98, 127.95, 127.88, 127.78, 127.6, 99.4, 83.7, 74.1 (d, *Jcp* = 5 Hz), 73.4, 70.4, 66.87 (d, *Jcp* = 6 Hz), 66.88 (*Jcp* = 6 Hz), 50.3, 32.2 (d, *Jcp* = 15 Hz), 25.5 (*Jcp* = 137 Hz),

18.6 (d, *Jcp* = 5 Hz), 10.2, -1.76; ^{31}P NMR (162 MHz, DMSO-d6, 90 °C) δ 32.65; HRMS (ESI *m/z*) calcd for $C_{55}H_{66}O_9NPSSiNa$ ($M+Na^+$) 998.3846, obsd 998.3835.

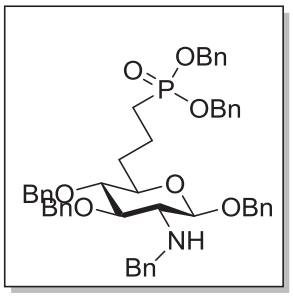

Dibenzyl (3-((2R,3R,4R,5R,6R)-5-(benzylamino)-3,4,6-tris(benzyloxy)tetrahydro-2H-pyran-2-yl)propyl)phosphonate (54). To solution of **11** (98 mg, 0.1 mmol) in DMF (1 mL) was added CsF (107 mg, 0.7 mmol) in one portion. The reaction was heated at 90 °C for 16 h, followed by addition of aqueous ammonium chloride. The mixture was extracted by ethyl acetate and the combined organic layers were dried, filtered and concentrated in vacuum. The crude product was purified by flash column chromatography (50% EtOAc/hexanes) to give **54** (59 mg, 72%) as a white solid: ^{1}H NMR (400 MHz, $CDCl_3$) δ 7.147.34 (m, 30 H), 5.06 (dd, *J* = 1.6, 8.8 Hz, 1 H), 5.03 (dd, *J* = 1.2, 8.8 Hz, 1 H), 4.97 (dd, *J* = 4, 8 Hz, 1 H), 4.94 (dd, *J* = 4, 7.6 Hz, 1 H), 4.67 (d, *J* = 11.2, 1 H), 4.56 (app t, *J* = 9.6 Hz, 2 H), 4.33 (d, *J* = 8 Hz, 1 H), 4.00 (d, *J* = 12.8 Hz, 1 H), 3.81 (d, *J* = 12.8 Hz, 1 H), 3.44 (t, *J* = 9.2 Hz, 1 H), 3.28 (t, *J* = 9.2 Hz, 1 H), 3.21 (t, *J* = 8.8 Hz, 1 H), 2.70 (dd, *J* = 8, 10 Hz, 1 H), 1.64–1.88 (m, 5 H), 1.48–1.57 (m, 1 H); ^{13}C NMR (100 MHz, $CDCl_3$) δ 138.0, 137.8, 137.3, 136.4 (d, *Jcp* = 6 Hz), 128.63, 128.61, 128.5, 128.45, 128.39, 128.34, 128.05, 127.99, 127.94, 127.91, 127.88, 127.82, 126.9, 103.5, 83.6, 82.8, 75.1 (d, *Jcp* = 1 Hz), 74.4, 71.0, 67.1 (d, *Jcp* = 6 Hz), 62.7, 53.5, 32.3 (d, *Jcp* = 17 Hz), 26.1 (d, *Jcp* = 140 Hz), 18.8 (d, *Jcp* = 5 Hz); ^{31}P NMR (162 MHz, $CDCl_3$) δ 33.17; HRMS (ESI *m/z*) calcd for $C_{50}H_{54}O_7NPNa$ ($M+Na^+$) 834.3536, obsd 834.3524.

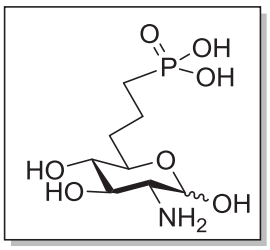

Glucosamine 7-phosphonate (12). A solution of **54** (33 mg, 0.04 mmol) in MeOH (2 mL) was stirred in the presence of 40% $Pd(OH)_2/C$ (12 mg) and trace amount of TFA (1 drop), under balloon pressure of hydrogen, for 24 h at room temperature. Filtrate the mixture through a pad of Celite and wash the filter cake with 2 mL MeOH. Suspend the filter cake in 2 mL H_2O and stir for 5 min, and then filtrate again through a pad of Celite. Concentrate the aqueous solution and dry over high vacuum to yield **12** (9 mg, 85%) as a colorless foam: ^{1}H NMR (400 MHz, D_2O) δ 5.34 (d, J = 3.6 Hz, 0.4 H), 4.83 (d, J = 8.4 Hz, 0.6 H), 3.79 (dt, J = 3.2, 9.2 Hz, 0.6 H), 3.76 (t, J = 10.4 Hz, 0.4 H), 3.54 (dd, J = 9.2, 10.4 Hz, 0.4 H), 3.38 (t, J = 9.2 Hz, 0.6 H), 3.18-3.33 (m, 1.6 H), 2.90 (dd, J = 8.4, 10.4 Hz, 0.4 H), 1.80-1.94 (m, 1 H), 1.42-1.77 (m, 5 H); ^{13}C NMR (100 MHz, D_2O) δ 93.0, 89.0, 75.2, 73.30, 73.29, 72.3, 70.3, 69.8, 56.9, 54.4, 31.7 (d, *Jcp* = 17 Hz), 31.2 (d, *Jcp* = 17 Hz), 27.4 (d, *Jcp* = 133 Hz), 27.5 (d, *Jcp* = 133 Hz), 18.9 (br); ^{31}P NMR (162 MHz, D_2O) δ 25.7 (br); HRMS (ESI *m/z*) calcd for $C_8H_{19}O_7NP$ ($M+H^+$) 272.0899, obsd 272.0904.

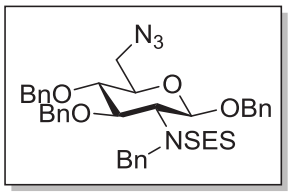

N-((2R,3R,4R,5R,6R)-6-(azidomethyl)-2,4,5-tris(benzyloxy)tetrahydro-2H-pyran-3-yl)-N-benzyl-2-(trimethylsilyl)ethanesulfonamide (20). To a solution of the triflate **4** (247 mg, 0.32 mmol) in THF was added $TMSN_3$ (131 μL, 1 mmol) dropwise at room temperature. The solution was stirred for 12h then quenched with aqueous NH_4Cl. The mixture was extracted with ether. Then combined organic layers were dried, filtered and concentrated in vacuum. The crude product was purified by flash column chromatography (10% EtOAc/hexanes) to give **20** (208 mg, 89%) as a colorless oil: ^{1}H

NMR (400 MHz, DMSO-d6, 90 °C) δ 7.23-7.52 (m, 20 H), 4.91 (d, J = 8.4 Hz, 1 H), 4.85 (d, J = 11.6 Hz, 1 H), 4.79 (d, J = 11.2 Hz, 1 H), 4.76 (s, 1 H), 4.72 (d, J = 11.6 Hz, 1 H), 4.60 (d, J = 11.2 Hz, 1 H), 4.53 (d, J = 15.6 Hz, 1 H), 4.49 (d, J = 11.6 Hz, 1 H), 4.47 (d, J = 15.6 Hz, 1 H), 4.05 (t, J = 9.2 Hz, 1 H), 3.75 (t, J = 9.2 Hz, 1 H), 3.65-3.70 (m, 1 H), 3.56 (d, J = 8.4 Hz, 1 H), 3.45-3.54 (m, 2 H), 2.64-2.81 (m, 2 H), 0.82-0.94 (m, 2 H), -0.17 (m, 9 H); ^{13}C NMR (100 MHz, DMSO-d6, 90 °C) δ 138.9, 138.5, 137.8, 137.6, 129.8, 128.70, 128.65, 128.63, 128.5, 128.2, 128.1, 128.0, 127.8, 127.7, 99.4, 80.9, 74.5, 74.2, 73.6, 70.5, 63.9, 51.8, 50.4, 10.2, -1.76; HRMS (ESI *m/z*) calcd for $C_{50}H_{54}O_7NPNa$ ($M+Na^+$) 751.2962, obsd 751.2948.

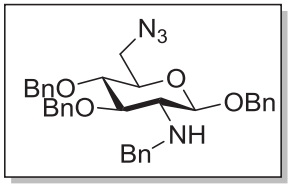

(2R,3R,4R,5R,6R)-6-(azidomethyl)-N-benzyl-2,4,5-tris(benzyloxy)tetrahydro-2H-pyran-3-amine (55). A mixture of **20** (322 mg, 0.44 mmol) and CsF (471 mg, 3.1 mmol) in DMF (5 mL) was stirred for 16 h at 90 °C. The reaction was quenched by adding aqueous NH_4Cl. The mixture was extracted by DCM. The combined organic layers were dried, filtered and concentrated in vacuum. The residue was purified by flash column chromatography (30% EtOAc/hexanes) to give **55** (198 mg, 80%) as a white solid: ^{1}H NMR (400 MHz, $CDCl_3$) δ; ^{13}C NMR (100 MHz, $CDCl_3$) δ 7.13-7.41 (m, 20 H), 4.96 (d, J = 11.6 Hz, 1 H), 4.91 (d, J = 11.6 Hz, 1 H), 4.87 (d, J = 11.2 Hz, 1 H), 4.71 (d, J = 11.2 Hz, 1 H), 4.65 (d, J = 11.6 Hz, 1 H), 4.60 (d, J = 11.2 Hz, 1 H), 4.45 (d, J = 8 Hz, 1 H), 4.02 (d, J = 12.8 Hz, 1 H), 3.83 (d, J = 12.8 Hz, 1 H), 3.46-3.57 (m, 3 H), 3.34-3.43 (m, 2 H), 2.78 (t, J = 8.8 Hz, 1 H), 1.69 (br, 1 H); ^{13}C NMR (100 MHz, $CDCl_3$) δ 140.5, 137.8, 137.5, 137.2, 128.66, 128.69, 128.5, 128.4, 128.3, 128.2, 128.04, 128.00, 127.9, 126.9,

103.6, 83.5, 79.6, 75.1, 75.04, 75.03, 71.1, 62.6, 53.5, 51.4; HRMS (ESI *m/z*) calcd for $C_{34}H_{36}O_4N_4Na$ ($M+Na^+$) 587.2634, obsd 587.2639.

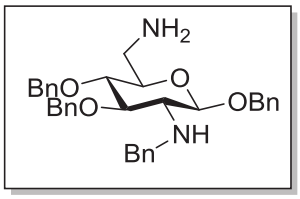

(2R,3R,4R,5R,6R)-6-(aminomethyl)-N-benzyl-2,4,5-tris(benzyloxy)tetrahydro-2H-pyran-3-amine (21). To a solution of **55** (127 mg, 0.22 mmol) and triphenylphosphine (174 mg, 0.66 mmol) in THF (2 mL) was added H_2O (20 μL, 1.1 mmol). The mixture was stirred at room temperature for 12 h when TLC indicated the completion of reaction. The solution was concentrated under vacuum and the residue was purified by flash column chromatography (30/70/10: EtOAc/hexanes/Et_3N) to give **21** (110 mg, 93%) as a white solid: ^{1}H NMR (400 MHz, $CDCl_3$) δ 7.14-7.42 (m, 20 H), 4.94 (d, J = 13.2 Hz, 1 H), 4.93 (d, J = 11.6 Hz, 1 H), 4.87 (d, J = 11.2 Hz, 1 H), 4.73 (d, J = 12 Hz, 1 H), 4.68 (s, 1 H), 4.67 (d, J = 10.8 Hz, 1 H), 4.47 (d, J = 8 Hz, 1 H), 4.04 (d, J = 12.8 Hz, 1 H), 3.86 (d, J = 12.8 Hz, 1 H), 3.48-3.56 (m, 1 H), 3.33 (t, J = 6.8 Hz, 1 H), 3.11 (d, J = 12 Hz, 1 H), 2.78-2.89 (m, 1 H), 2.76 (dd, J = 8, 9.2 Hz, 1 H), 1.50 (br, 2 H); ^{13}C NMR (100 MHz, $CDCl_3$) δ 140.6, 138.1, 137.8, 137.5, 128.62, 128.58, 128.46, 128.37, 128.30, 128.1, 128.0, 127.9, 126.8, 104.1, 83.7, 80.0, 75.1, 74.9, 71.4, 62.8, 53.6; HRMS (ESI *m/z*) calcd for $C_{34}H_{38}O_4N_2Na$ ($M+Na^+$) 561.2729, obsd 561.2721.

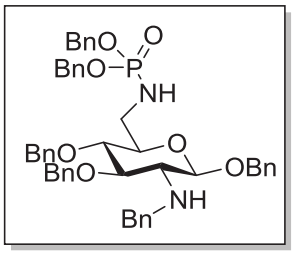

Dibenzyl (((2R,3R,4R,5R,6R)-5-(benzylamino)-3,4,6-tris(benzyloxy)tetrahydro-2H-pyran-2-yl)methyl)phosphoramidate (22). To a solution of **21** (65 mg, 0.12 mmol) in DCM (1 mL) was added slowly

dibenzylphosphoryl chloride (0.72 mL, 0.5 mol in toluene (freshly prepared from NCS and dibenzyl phosphite), 0.36 mmol). Then Et_3N (167 μL, 1.2 mmol) was added through syringe. The reaction was stirred for 6 h at room temperature and then quenched by aqueous NH_4Cl. The mixture was extracted with DCM and the organic layers were dried, filtered and concentrated in vacuum. The residue was purified by flash column chromatography (40/60/5: EtOAc/hexanes/Et_3N) to give **22** (66 mg, 69%) as a white solid: ^{1}H NMR (400 MHz, $CDCl_3$) δ 7.11-7.38 (m, 30 H), 5.01-5.06 (m, 4 H), 4.87 (d, J = 11.6 Hz, 1 H), 4.83 (d, J = 11.6 Hz, 1 H), 4.74 (d, J = 10.8 Hz, 1 H), 4.65 (d, J = 11.2 Hz, 1 H), 4.4.59 (d, J = 10. 4 Hz, 1 H), 4.59 (d, J = 12.4 Hz, 1 H), 4.34 (d, J = 8 Hz, 1 H), 3.98 (d, J = 12.8 Hz, 1 H), 3.79 (d, J = 12.8 Hz, 1 H), 3.36-3.45 (m, 2 H), 3.21-3.32 (m, 2 H), 2.97-3.35 (m, 2 H), 2.62- 2.68 (m, 1 H), 1.66 (br, 1 H); ^{13}C NMR (100 MHz, $CDCl_3$) δ 140.5, 137.9, 137.7, 137.3, 136.3 (d, *Jcp* = 8 Hz), 128.63, 128.60, 128.56, 128.54, 128.50, 128.39, 128.34, 128.29, 128.1, 128.01, 127.97, 127.92, 127.87, 127.85, 126.9, 104.1, 83.3, 79.4, 75.0, 74.8, 74.51 (d, *Jcp* = 7 Hz), 71.5, 68.14 (d, *Jcp* = 5 Hz), 68.10 (d, *Jcp* = 5 Hz), 62.5, 53.5, 42.2; ^{31}P NMR (162 MHz, $CDCl_3$) δ 9.53; HRMS (ESI *m/z*) calcd for $C_{48}H_{51}O_7N_2PNa$ $(M+Na)^+$ 821.3332, obsd 821.3348.

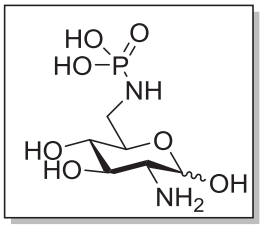

Glucosamine 6-phosphoramide (23). A solution of **22** (44 mg, 0.055 mmol) in MeOH (2 mL) was stirred in the presence of 40% $Pd(OH)_2/C$ (17 mg) and trace amount of TFA (1 drop), under balloon pressure of hydrogen, for 24 h at room temperature. Filtrate the mixture through a pad of Celite and wash the filter cake with 2 mL MeOH. Suspend the filter cake in 2 mL H_2O and stir for 5 min, and then filtrate again through a

pad of Celite. Concentrate the aqueous solution and dry over high vacuum to yield **23** (11 mg, 80%) as a colorless foam: ^{1}H NMR (400 MHz, D_2O) δ 5.37 (d, J = 3.2 Hz, 0.7 H), 4.87 (d, J = 8.4 Hz, 0.3 H), 3.98 (dt, J = 2, 9.2 Hz, 0.7 H), 3.80 (t, J = 9.6 Hz, 0.7 H), 3.50-3.71 (m, 1.3 H), 3.26-3.45 (m, 2.3 H), 3.24 (dd, J = 3.2, 10.4 Hz, 0.7 H), 2.95 (t, J = 8.8 Hz, 0.3 H); ^{31}P NMR (162 MHz, D_2O) δ 1.44 (br); HRMS (ESI *m/z*) calcd for $C_6H_{15}O_7N_2PNa$ $(M+Na)^+$ 281.0514, obsd 281.0517.

B. Self-Cleavage Assay

Preparation of RNA. Templates for transcription were prepared by primer extension and PCR amplification using synthetic DNA corresponding to ribozyme sequence. Ribozymes were prepared by *in vitro* transcription using T7 RNA polymerase and ^{32}P-labeled by incorporation of [^{32}P]-UTP. Transcription products were separated by denaturing 10% polyacrylamide gel electrophoresis (PAGE) and ribozymes were eluted in solution containing 50 mM HEPES (pH 7.3 at 22˚C) and 200 mM NaCl, precipitated with ethanol, and redissolved in water.

Self-Cleavage Assay. Ribozyme reactions were performed as previously described.[37] Briefly, reactions contained ligand analog as indicated and were performed under standard conditions consisting of incubation at 22˚C in solution containing 50 mM HEPES pH 7.3. A saturating concentration of $MgCl_2$ was used in order to avoid a slow folding step and to allow for formation of native *glmS* RNA structure.[69] The [^{32}P]-UTP-labeled *glmS* ribozyme (<250 nM) was prefolded in 50 mM HEPES pH 7.5, 0.1 mM EDTA, and 50 mM $MgCl_2$ at 22 ˚C. Reactions were started by adding coenzyme at

varying concentration (10 mM – 10 μM final concentration) in 50 mM HEPES pH 7.3 buffer. Reactions were terminated by the addition of a gel loading dye containing 10 M urea, 50 mM EDTA, 0.1% bromophenol blue, 0.1% xylene cyanol. Products were separated by denaturing 10% PAGE and analyzed using a PhosphorImager and IMAGEQUANT software (Molecular Dynamics). k_{obs} values for self-cleavage were derived by plotting the natural logarithm of the fraction of uncleaved ribozyme versus time and establishing the negative slope of the resulting line. Stated values represent the average of at least three replicate assays. First-order cleavage rates were obtained at different concentrations of coenzyme in the linear range of a Michaelis−Menten plot (coenzyme concentration ~20% of apparent K_m value) and were fit by linear regression to obtain apparent second-order rate constants k_{cat}/K_m.[36]

C. pK_a Titration Experiments

Each analogue was prepared in 1 mM (**6**, **27**, **29**) or 3 mM (**18**, **22**) solution and titrated with 100 mM NaOH solution. pH was recorded after each addition of 0.1 equivalent of NaOH solution (blue curve). The reciprocal of the change of pH (1/ΔpH) was plotted to aid identification of the inflection points (Fig. 2.17, red curve).

D. Molecular Docking

The crystal structure of glucosamine-6-phosphate bound to the (2'-OMe)A-1 *glmS* riboswitch was obtained from the Brookhaven Protein Data Bank (http://www.rcsb.org/pdb) (PDB ID:2NZ4). This *glmS* riboswitch is obtained from

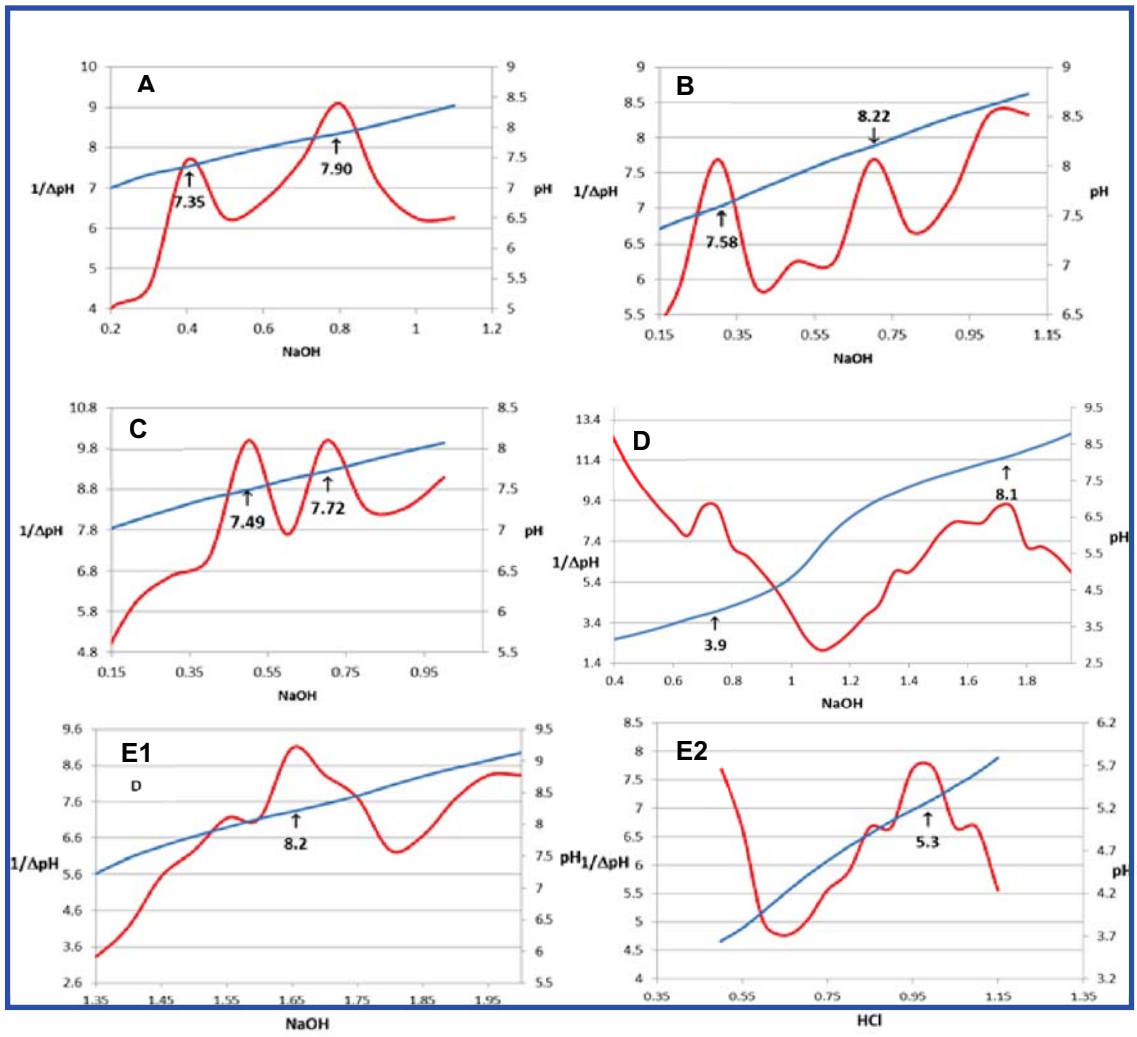

Figure 2.17: Titration curves for GlcN6P analogues. (A) **6**; (B) **27**; (C) **29**. (D) **14**; (E1) **18** with 100 mM NaOH; (E2) **18** with 100 mM HCl.

Bacillus anthracis which is the same source of the riboswitch in our cleavage assay. Ligands were prepared with Spartan 08 with phosphate-mimicking groups fully deprotonated. Virtual docking experiments were performed using Autodock 4. Each trial was run in a grid map with X x Y x Z dimensions = 40 x 40 x 20 Å centered at C-5 of GlcN6P from the reference structure. The Lamarckian Genetic Algorithm was used as the search method. Each trials consisted of 100 runs, with a maximum of 2,500,000 energy

evaluations. Images were generated in VMD with conformations in the lowest energy cluster.

The Mg-O distances were slightly adjusted to represent typical binding distances in crystal structures. In this crystal structure (2NZ4), the phosphate is ~4 Å away from each magnesium ion. However a typical binding distance between oxygen and magnesium is ~ 2.5 – 3.0 Å, as observed in 2H0Z (2.44 Å, 3.30 Å); 2Z74 (2.56 Å, 2.63 Å); 2Z75 (2.55 Å, 2.88 Å).Therefore, the structure is subsequently adjusted using Spartan 2008.

V. References

1. Jacob, F.; Monod, J., Genetic regulatory mechanisms in the synthesis of proteins. *J Mol Biol* **1961,** *3*, 318-56.
2. Ptashne, M.; Gann, A., *Genes and Signals*. Cold Spring Harbor Laboratory Press: Cold Spring Harbor, New York, 2002.
3. Browning, D. F.; Busby, S. J., The regulation of bacterial transcription initiation. *Nat Rev Microbiol* **2004,** *2* (1), 57-65.
4. Matthews, K. S.; Nichols, J. C., Lactose repressor protein: functional properties and structure. *Prog Nucleic Acid Res Mol Biol* **1998,** *58*, 127-64.
5. Switzer, R. L.; Turner, R. J.; Lu, Y., Regulation of the Bacillus subtilis pyrimidine biosynthetic operon by transcriptional attenuation: control of gene expression by an mRNA-binding protein. *Prog Nucleic Acid Res Mol Biol* **1999,** *62*, 329-67.
6. Babitzke, P.; Yanofsky, C., Reconstitution of Bacillus subtilis trp attenuation in vitro with TRAP, the trp RNA-binding attenuation protein. *Proc Natl Acad Sci U S A* **1993,** *90* (1), 133-7.
7. Timchenko, N. A.; Welm, A. L.; Lu, X.; Timchenko, L. T., CUG repeat binding protein (CUGBP1) interacts with the 5' region of C/EBPbeta mRNA and regulates translation of C/EBPbeta isoforms. *Nucleic Acids Res* **1999,** *27* (22), 4517-25.
8. Hannon, G. J., RNA interference. *Nature* **2002,** *418* (6894), 244-51.
9. Agrawal, N.; Dasaradhi, P. V.; Mohmmed, A.; Malhotra, P.; Bhatnagar, R. K.; Mukherjee, S. K., RNA interference: biology, mechanism, and applications. *Microbiol Mol Biol Rev* **2003,** *67* (4), 657-85.

10. Hamilton, A. J.; Baulcombe, D. C., A species of small antisense RNA in posttranscriptional gene silencing in plants. *Science* **1999,** *286* (5441), 950-2.

11. Ambros, V., The functions of animal microRNAs. *Nature* **2004,** *431* (7006), 350-5.

12. Bartel, D. P., MicroRNAs: genomics, biogenesis, mechanism, and function. *Cell* **2004,** *116* (2), 281-97.

13. Razskazovskii, Y.; Roginskaya, M.; Sevilla, M. D., Modification of the reductive pathway in gamma-irradiated DNA by electron scavengers: targeting the sugar-phosphate backbone. *Radiat Res* **1998,** *149* (5), 422-32.

14. Brantl, S., Bacterial gene regulation: from transcription attenuation to riboswitches and ribozymes. *Trends Microbiol* **2004,** *12* (11), 473-5.

15. Garst, A. D.; Batey, R. T., A switch in time: detailing the life of a riboswitch. *Biochim Biophys Acta* **2009,** *1789* (9-10), 584-91.

16. Mandal, M.; Boese, B.; Barrick, J. E.; Winkler, W. C.; Breaker, R. R., Riboswitches control fundamental biochemical pathways in Bacillus subtilis and other bacteria. *Cell* **2003,** *113* (5), 577-86.

17. Mandal, M.; Breaker, R. R., Gene regulation by riboswitches. *Nat Rev Mol Cell Biol* **2004,** *5* (6), 451-63.

18. Serganov, A.; Nudler, E., A decade of riboswitches. *Cell* **2013,** *152* (1-2), 17-24.

19. Serganov, A.; Patel, D. J., Ribozymes, riboswitches and beyond: regulation of gene expression without proteins. *Nat Rev Genet* **2007,** *8* (10), 776-90.

20. Winkler, W. C.; Breaker, R. R., Regulation of bacterial gene expression by riboswitches. *Annu Rev Microbiol* **2005,** *59*, 487-517.

21. Wakeman, C. A.; Winkler, W. C.; Dann, C. E., 3rd, Structural features of metabolite-sensing riboswitches. *Trends Biochem Sci* **2007,** *32* (9), 415-24.

22. Webb, E.; Downs, D., Characterization of thiL, encoding thiamin-monophosphate kinase, in Salmonella typhimurium. *J Biol Chem* **1997,** *272* (25), 15702-7.

23. Miranda-Rios, J.; Navarro, M.; Soberon, M., A conserved RNA structure (thi box) is involved in regulation of thiamin biosynthetic gene expression in bacteria. *Proc Natl Acad Sci U S A* **2001,** *98* (17), 9736-41.

24. Winkler, W.; Nahvi, A.; Breaker, R. R., Thiamine derivatives bind messenger RNAs directly to regulate bacterial gene expression. *Nature* **2002,** *419* (6910), 952-6.

25. Serganov, A.; Polonskaia, A.; Phan, A. T.; Breaker, R. R.; Patel, D. J., Structural basis for gene regulation by a thiamine pyrophosphate-sensing riboswitch. *Nature* **2006,** *441* (7097), 1167-71.

26. Winkler, W. C.; Cohen-Chalamish, S.; Breaker, R. R., An mRNA structure that controls gene expression by binding FMN. *Proc Natl Acad Sci U S A* **2002,** *99* (25), 15908-13.

27. Nahvi, A.; Sudarsan, N.; Ebert, M. S.; Zou, X.; Brown, K. L.; Breaker, R. R., Genetic control by a metabolite binding mRNA. *Chem Biol* **2002,** *9* (9), 1043.

28. Deigan, K. E.; Ferre-D'Amare, A. R., Riboswitches: discovery of drugs that target bacterial gene-regulatory RNAs. *Acc Chem Res* **2011,** *44* (12), 1329-38.

29. Barrick, J. E.; Corbino, K. A.; Winkler, W. C.; Nahvi, A.; Mandal, M.; Collins, J.; Lee, M.; Roth, A.; Sudarsan, N.; Jona, I.; Wickiser, J. K.; Breaker, R. R., New

RNA motifs suggest an expanded scope for riboswitches in bacterial genetic control. *Proc. Natl. Acad. Sci. U. S. A.* **2004,** *101* (17), 6421-6426.

30. Winkler, W. C.; Nahvi, A.; Sudarsan, N.; Barrick, J. E.; Breaker, R. R., An mRNA structure that controls gene expression by binding S-adenosylmethionine. *Nat Struct Biol* **2003,** *10* (9), 701-7.

31. Mandal, M.; Lee, M.; Barrick, J. E.; Weinberg, Z.; Emilsson, G. M.; Ruzzo, W. L.; Breaker, R. R., A glycine-dependent riboswitch that uses cooperative binding to control gene expression. *Science* **2004,** *306* (5694), 275-9.

32. Sudarsan, N.; Wickiser, J. K.; Nakamura, S.; Ebert, M. S.; Breaker, R. R., An mRNA structure in bacteria that controls gene expression by binding lysine. *Genes Dev* **2003,** *17* (21), 2688-97.

33. Winkler, W. C.; Nahvi, A.; Roth, A.; Collins, J. A.; Breaker, R. R., Control of gene expression by a natural metabolite-responsive ribozyme. *Nature* **2004,** *428* (6980), 281-286.

34. Li, Y.; Breaker, R. R., Kinetics of RNA Degradation by Specific Base Catalysis of Transesterification Involving the 2'-Hydroxyl Group. *Journal of the American Chemical Society* **1999,** *121* (23), 5364-5372.

35. Ferre-D'Amare, A. R., The glmS ribozyme: use of a small molecule coenzyme by a gene-regulatory RNA. *Quarterly Reviews of Biophysics* **2010,** *43* (4), 423-447.

36. Viladoms, J.; Fedor, M. J., The glmS Ribozyme Cofactor is a General Acid-Base Catalyst. *Journal of the American Chemical Society* **2012,** *134* (46), 19043-19049.

37. McCarthy, T. J.; Plog, M. A.; Floy, S. A.; Jansen, J. A.; Soukup, J. K.; Soukup, G. A., Ligand requirements for glmS ribozyme self-cleavage. *Chem. Biol.* **2005,** *12* (11), 1221-1226.

38. Gilbert, W., Origin of life: The RNA world. *Nature* **1986,** *319* (6055), 618-618.

39. Klein, D. J.; Ferre-D'Amare, A. R., Structural basis of glmS ribozyme activation by glucosamine-6-phosphate. *Science* **2006,** *313* (5794), 1752-1756.

40. Klein, D. J.; Been, M. D.; Ferre-D'Amare, A. R., Essential role of an active-site guanine in glmS ribozyme catalysis. *Journal of the American Chemical Society* **2007,** *129* (48), 14858-+.

41. Viladoms, J.; Scott, L. G.; Fedor, M. J., An active-site guanine participates in glmS ribozyme catalysis in its protonated state. *J Am Chem Soc* **2011,** *133* (45), 18388-96.

42. Lim, J.; Grove, B. C.; Roth, A.; Breaker, R. R., Characteristics of ligand recognition by a glmS self-cleaving ribozyme. *Angew Chem Int Ed Engl* **2006,** *45* (40), 6689-93.

43. Gong, B.; Klein, D. J.; Ferre-D'Amare, A. R.; Carey, P. R., The glmS ribozyme tunes the catalytically critical pK(a) of its coenzyme glucosamine-6-phosphate. *J Am Chem Soc* **2011,** *133* (36), 14188-91.

44. Xin, Y.; Hamelberg, D., Deciphering the role of glucosamine-6-phosphate in the riboswitch action of glmS ribozyme. *RNA* **2010,** *16* (12), 2455-63.

45. WHO, Antimicrobial resistance: global report on surveillance 2014. 2014.

46. Walsh, C. T.; Wencewicz, T. A., Prospects for new antibiotics: a molecule-centered perspective. *J Antibiot (Tokyo)* **2014,** *67* (1), 7-22.

47. Lee, E. R.; Blount, K. F.; Breaker, R. R., Metabolite-sensing riboswitches as antibacterial drug targets. *Emerging Trends in Antibacterial Discovery* **2011**, 107-130.

48. Blount, K. F.; Breaker, R. R., Riboswitches as antibacterial drug targets. *Nature Biotechnology* **2006,** *24* (12), 1558-1564.

49. McCown, P. J.; Winkler, W. C.; Breaker, R. R., Mechanism and distribution of glmS ribozymes. *Methods Mol Biol* **2012,** *848*, 113-29.

50. Milewski, S., Glucosamine-6-phosphate synthase--the multi-facets enzyme. *Biochim Biophys Acta* **2002,** *1597* (2), 173-92.

51. Collins, J. A.; Irnov, I.; Baker, S.; Winkler, W. C., Mechanism of mRNA destabilization by the glmS ribozyme. *Genes Dev* **2007,** *21* (24), 3356-68.

52. Mayer, G.; Famulok, M., High-throughput-compatible assay for glmS riboswitch metabolite dependence. *ChemBioChem* **2006,** *7* (4), 602-604.

53. Lunse, C. E.; Schmidt, M. S.; Wittmann, V.; Mayer, G., Carba-sugars Activate the glmS-Riboswitch of Staphylococcus aureus. *ACS Chem. Biol.* **2011,** *6* (7), 675-678.

54. Wang, G. N.; Lau, P. S.; Li, Y. F.; Ye, X. S., Synthesis and evaluation of glucosamine-6-phosphate analogues as activators of glmS riboswitch. *Tetrahedron* **2012,** *68* (46), 9405-9412.

55. Posakony, J. J.; Ferre-D'Amare, A. R., Glucosamine and Glucosamine-6-phosphate Derivatives: Catalytic Cofactor Analogues for the glmS Ribozyme. *Journal of Organic Chemistry* **2013,** *78* (10), 4730-4743.

56. Griffith, D. A.; Danishefsky, S. J., Sulfonamidoglycosylation of glycals. A route to oligosaccharides with 2-aminohexose subunits. *Journal of the American Chemical Society* **1990,** *112* (15), 5811-19.

57. Griffith, D. A.; Danishefsky, S. J., Total synthesis of allosamidin: an application of the sulfonamidoglycosylation of glycals. *Journal of the American Chemical Society* **1991,** *113* (15), 5863-4.

58. Engel, R., Phosphorus addition at sp2 Carbon. *Organic Reactions (Hoboken, NJ, United States)* **1988,** *36*, No pp given.

59. Tian, F.; Montchamp, J. L.; Frost, J. W., Inhibitor Ionization as a Determinant of Binding to 3-Dehydroquinate Synthase. *J Org Chem* **1996,** *61* (21), 7373-7381.

60. Berkowitz, D. B.; Maiti, G.; Charette, B. D.; Dreis, C. D.; MacDonald, R. G., Mono- and bivalent ligands bearing mannose 6-phosphate (M6P) surrogates: targeting the M6P/insulin-like growth factor II receptor. *Org Lett* **2004,** *6* (26), 4921-4.

61. Foret, J.; de Courcy, B.; Gresh, N.; Piquemal, J. P.; Salmon, L., Synthesis and evaluation of non-hydrolyzable D-mannose 6-phosphate surrogates reveal 6-deoxy-6-dicarboxymethyl-D-mannose as a new strong inhibitor of phosphomannose isomerases. *Bioorg Med Chem* **2009,** *17* (20), 7100-7.

62. Krapcho, A. P.; Weimaster, J. F.; Eldridge, J. M.; Jahngen, E. G. E., Jr.; Lovey, A. J.; Stephens, W. P., Synthetic applications and mechanism studies of the decarbalkoxylations of geminal diesters and related systems effected in dimethyl sulfoxide by water and/or by water with added salts. *Journal of Organic Chemistry* **1978,** *43* (1), 138-47.

63. Durka, M.; Tikad, A.; Perion, R.; Bosco, M.; Andaloussi, M.; Floquet, S.; Malacain, E.; Moreau, F.; Oxoby, M.; Gerusz, V.; Vincent, S. P., Systematic synthesis of inhibitors of the two first enzymes of the bacterial heptose biosynthetic pathway: towards antivirulence molecules targeting lipopolysaccharide biosynthesis. *Chemistry* **2011,** *17* (40), 11305-13.

64. Sem, D. S.; Cleland, W. W., Phosphorylated aminosugars: synthesis, properties, and reactivity in enzymatic reactions. *Biochemistry* **1991,** *30* (20), 4978-84.

65. Klein, D. J.; Ferre-D'Amare, A. R., Structural basis of glmS ribozyme activation by glucosamine-6-phosphate. *Science* **2006,** *313* (5794), 1752-6.

66. Cochrane, J. C.; Lipchock, S. V.; Strobel, S. A., Structural investigation of the GlmS ribozyme bound to Its catalytic cofactor. *Chem Biol* **2007,** *14* (1), 97-105.

67. Klein, D. J.; Been, M. D.; Ferre-D'Amare, A. R., Essential role of an active-site guanine in glmS ribozyme catalysis. *J Am Chem Soc* **2007,** *129* (48), 14858-9.

68. Klein, D. J.; Wilkinson, S. R.; Been, M. D.; Ferre-D'Amare, A. R., Requirement of helix P2.2 and nucleotide G1 for positioning the cleavage site and cofactor of the glmS ribozyme. *J Mol Biol* **2007,** *373* (1), 178-89.

69. Cochrane, J. C.; Lipchock, S. V.; Smith, K. D.; Strobel, S. A., Structural and chemical basis for glucosamine 6-phosphate binding and activation of the glmS ribozyme. *Biochemistry* **2009,** *48* (15), 3239-46.

70. Van Gelder, J.; Deferme, S.; Annaert, P.; Naesens, L.; De Clercq, E.; Van den Mooter, G.; Kinget, R.; Augustijns, P., Increased absorption of the antiviral ester prodrug tenofovir disoproxil in rat ileum by inhibiting its intestinal metabolism. *Drug Metab Dispos* **2000,** *28* (12), 1394-6.

71. Wu, Y.-Q.; Hamilton, G. S.; Belyakov, S.; Waldon, D. Preparation of enhanced tissue penetration prodrugs of carboxy-containing drugs. 2006-US22671 2006138187, 20060609., 2006.

VI. NMR Spectra

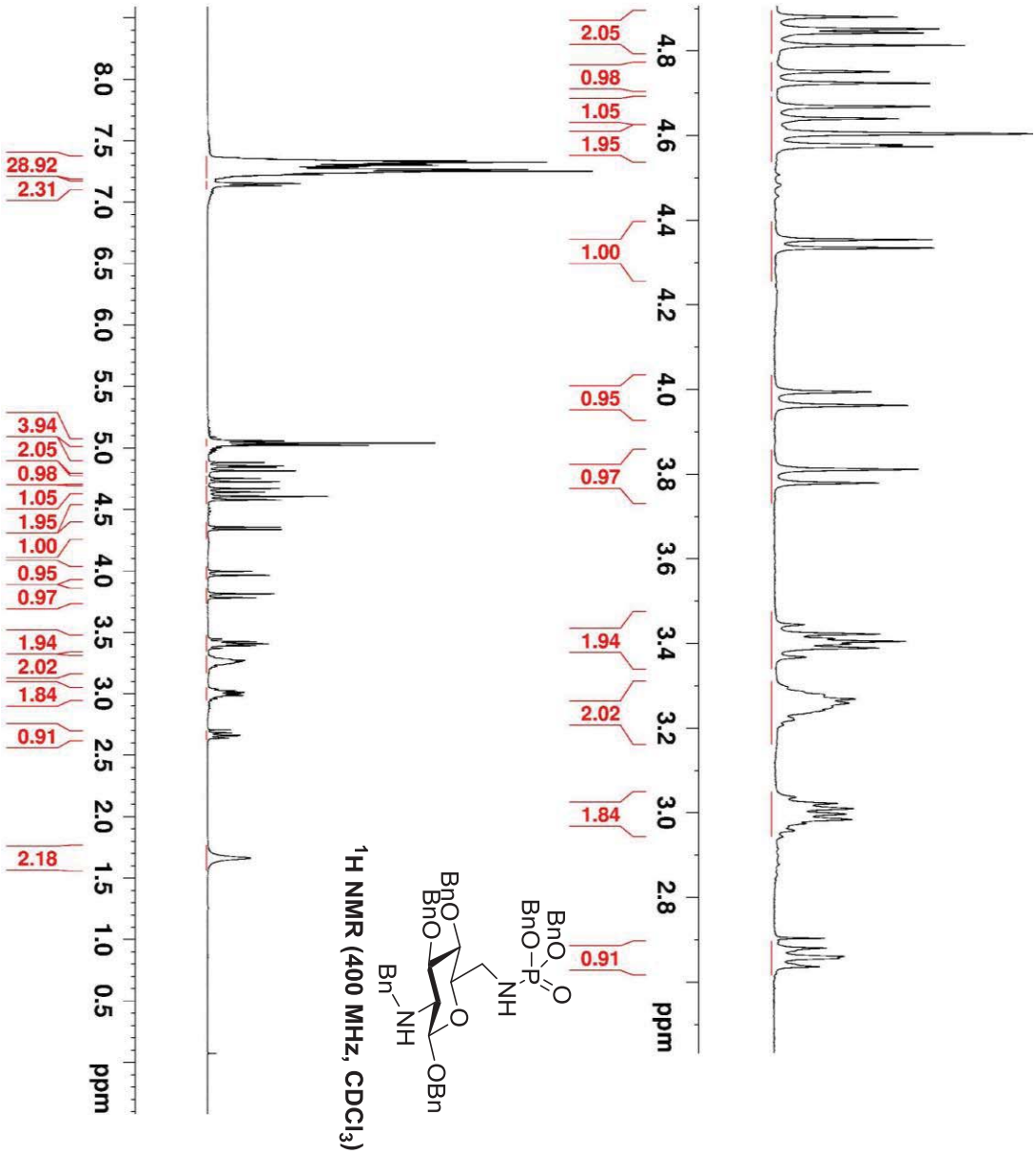

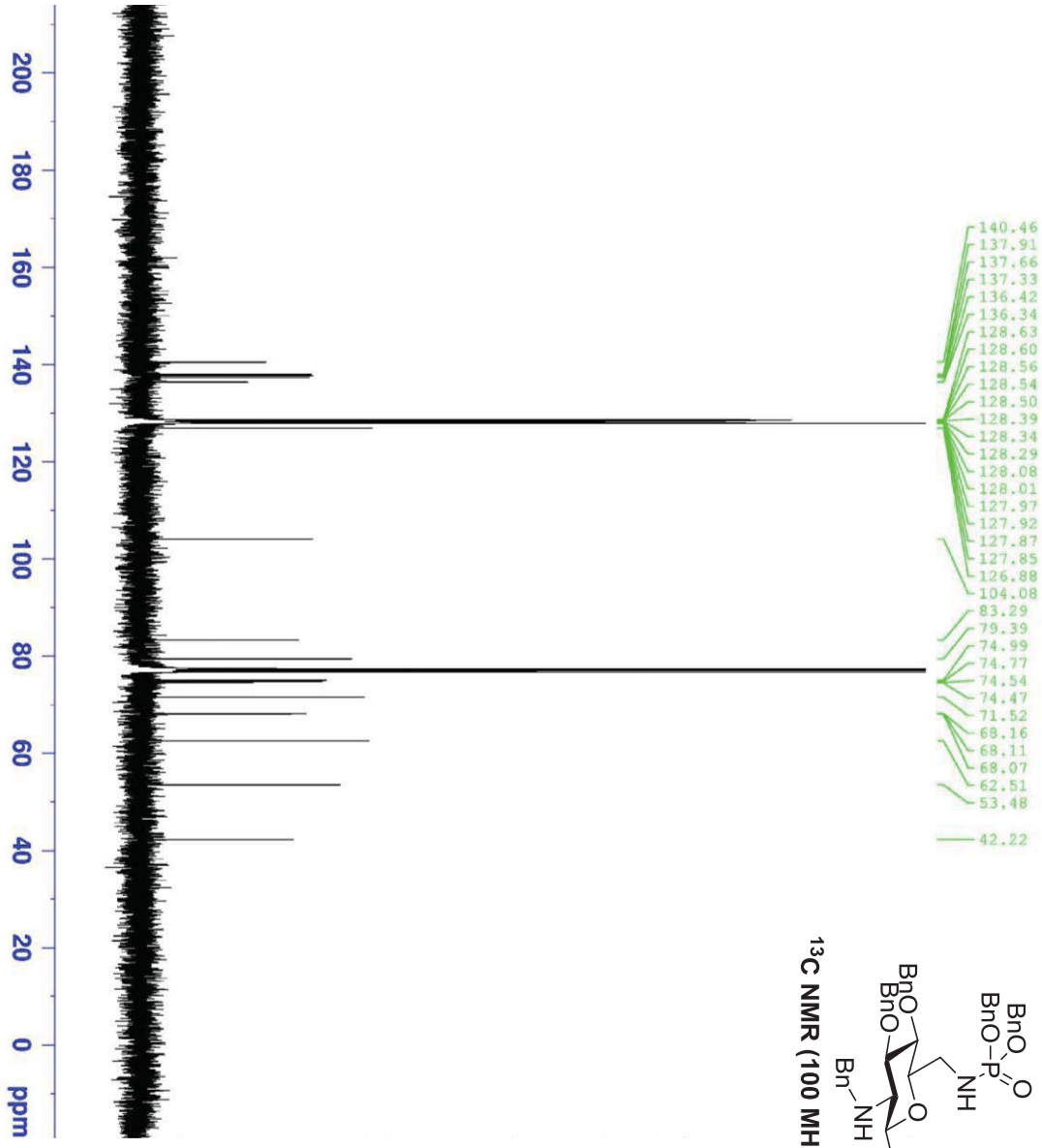

^{13}C NMR (100 MHz, $CDCl_3$)

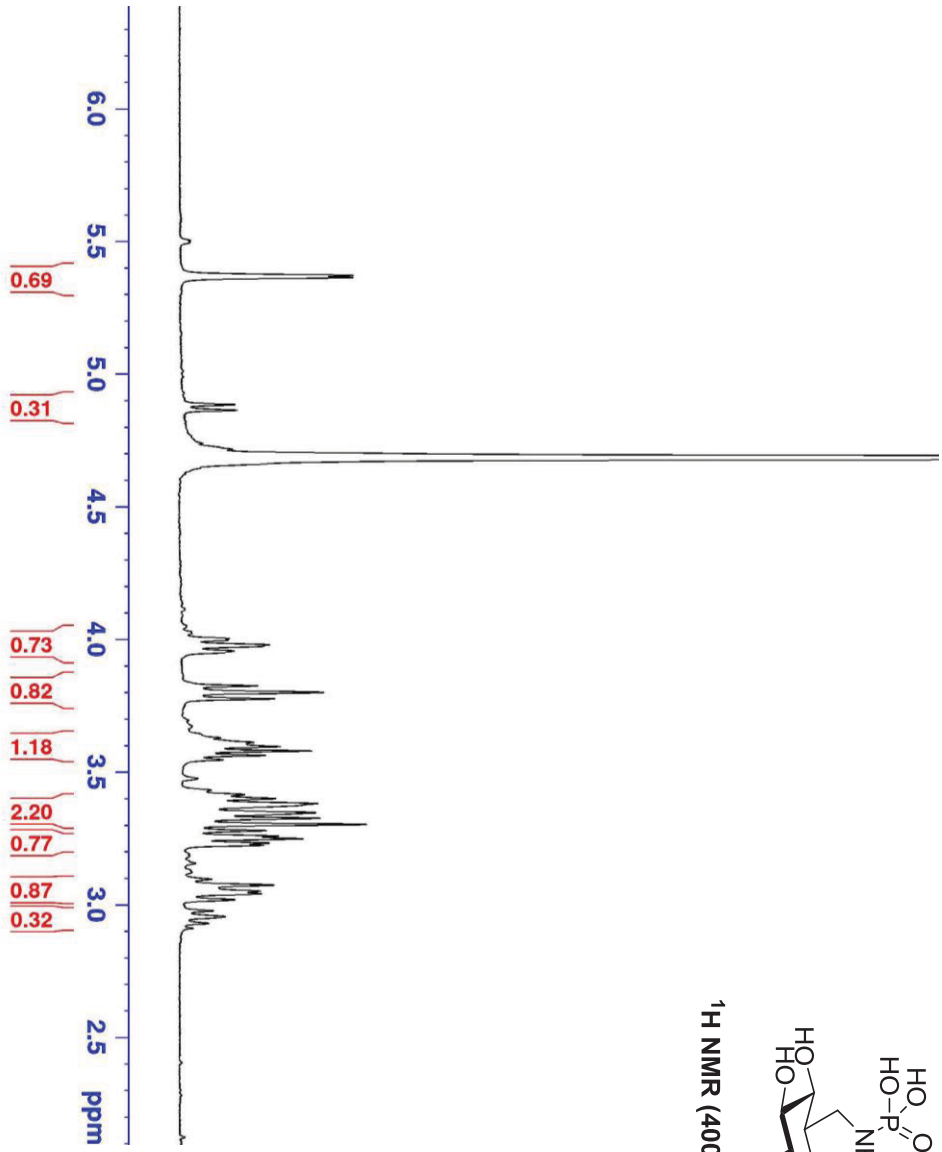

^{1}H NMR (400 MHz, D_2O)

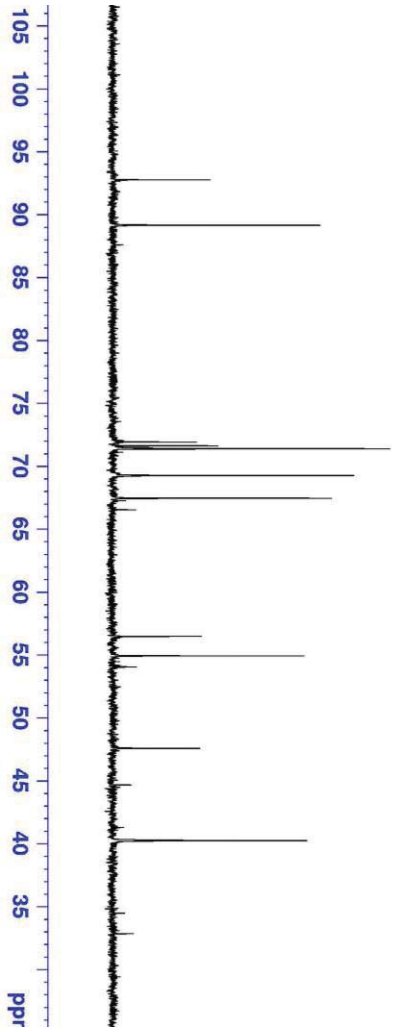

92.76
89.16
71.92
71.61
71.40
71.37
69.27
67.45
56.48
54.93
40.30
40.24

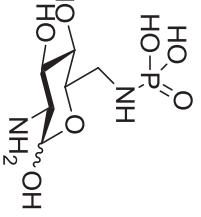

^{13}C NMR (100 MHz, D_2O)

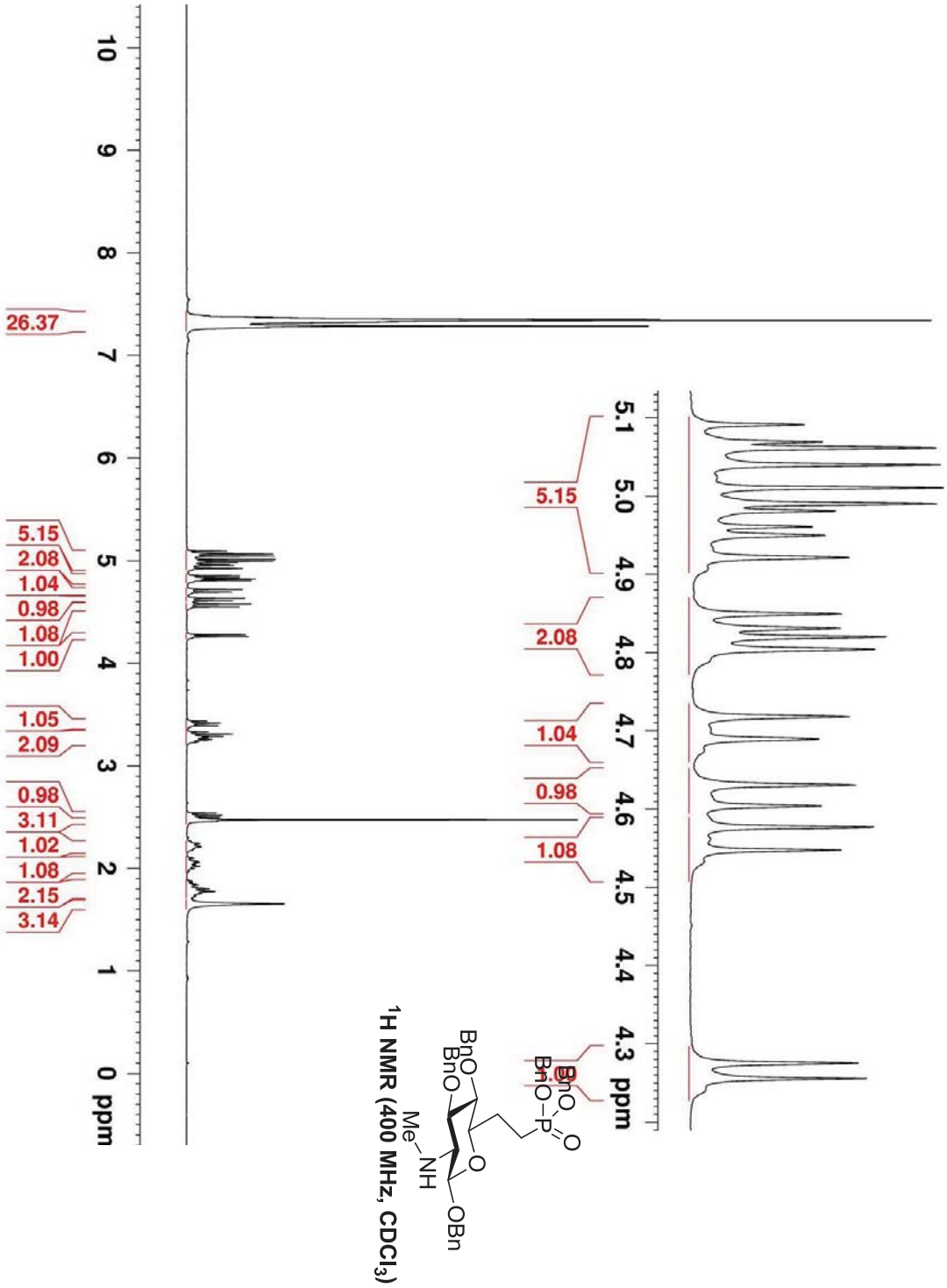
26.37
5.15
2.08
1.04
0.98
1.08
1.00
1.05
2.09
0.98
3.11
1.02
1.08
2.15
3.14
10 9 8 7 6 5 4 3 2 1 0 ppm
5.15
2.08
1.04
0.98
1.08
5.1 5.0 4.9 4.8 4.7 4.6 4.5 4.4 4.3 ppm
BnO
BnO
BnO
O
P
O
BnO
O
OBn
Me
NH
¹H NMR (400 MHz, CDCl₃)

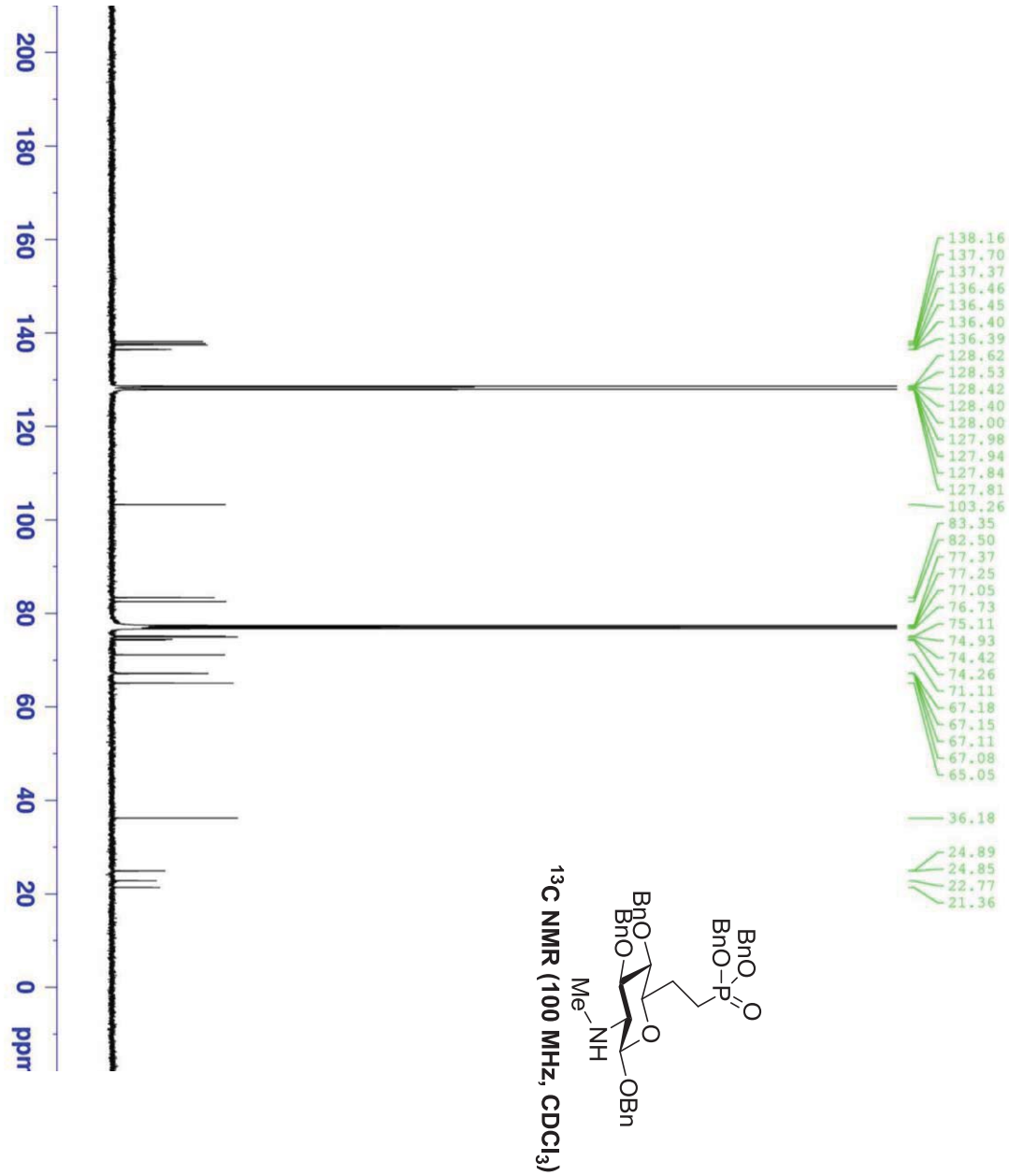

^{13}C NMR (100 MHz, $CDCl_3$)

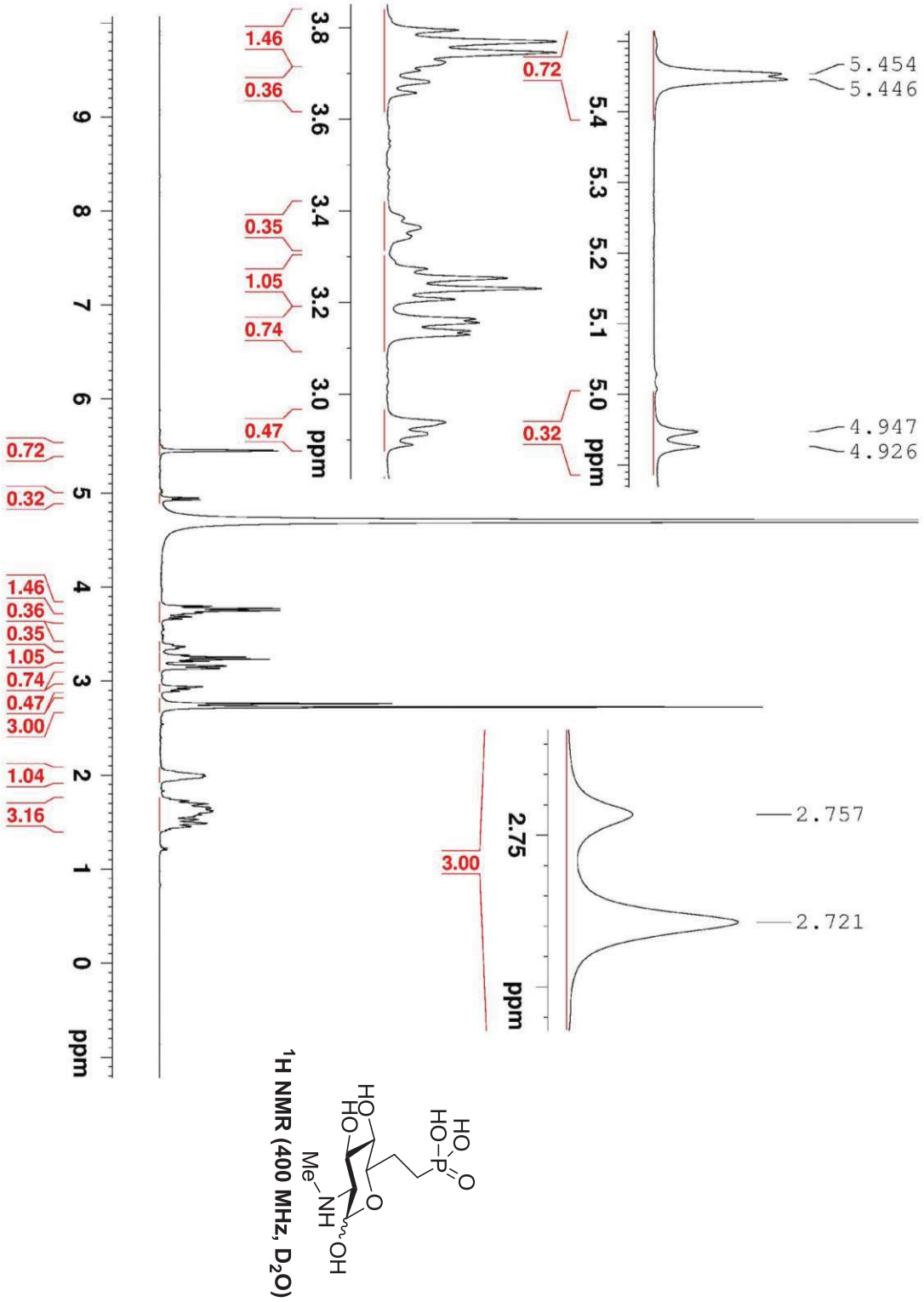

^{1}H NMR (400 MHz, D_2O)

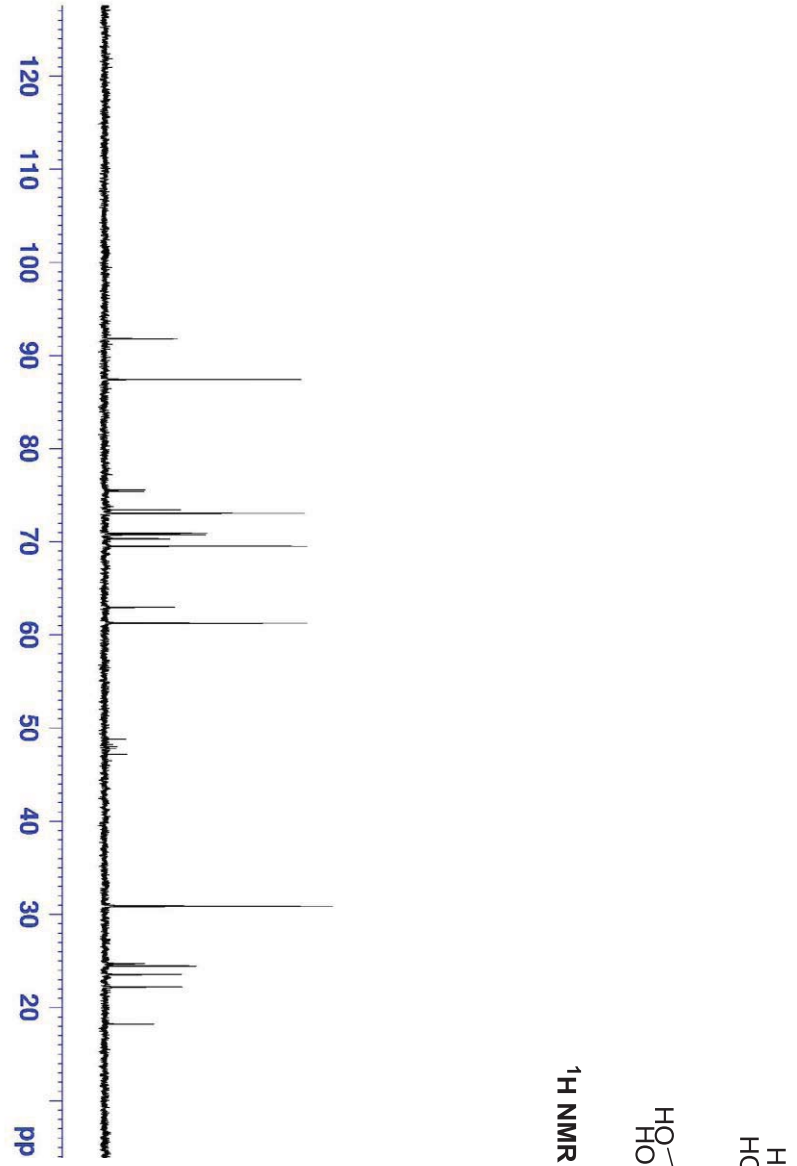

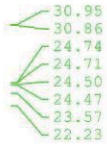

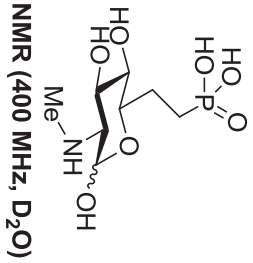

^{1}H NMR (400 MHz, D_2O)

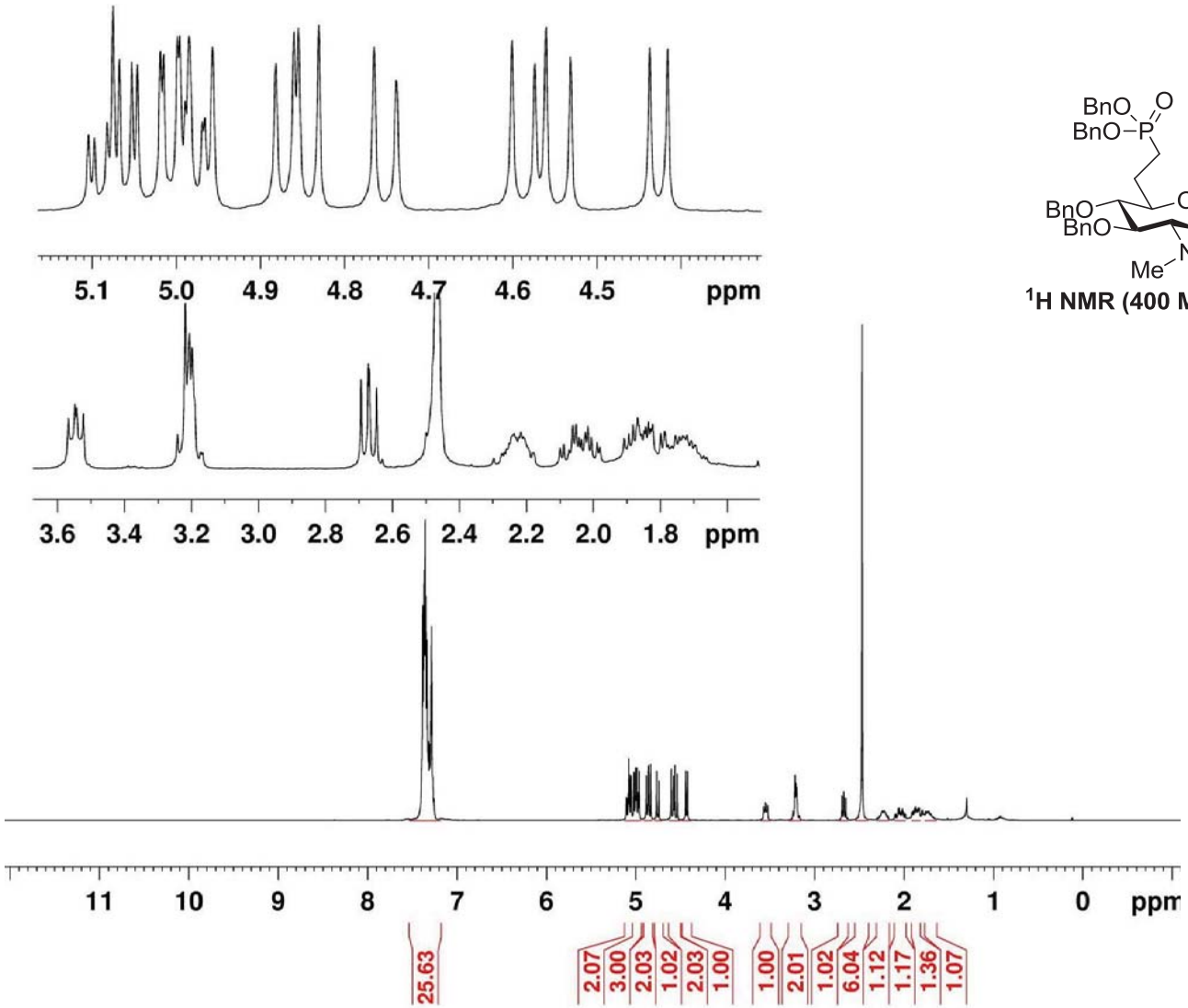

^{1}H NMR (400 MHz, $CDCl_3$)

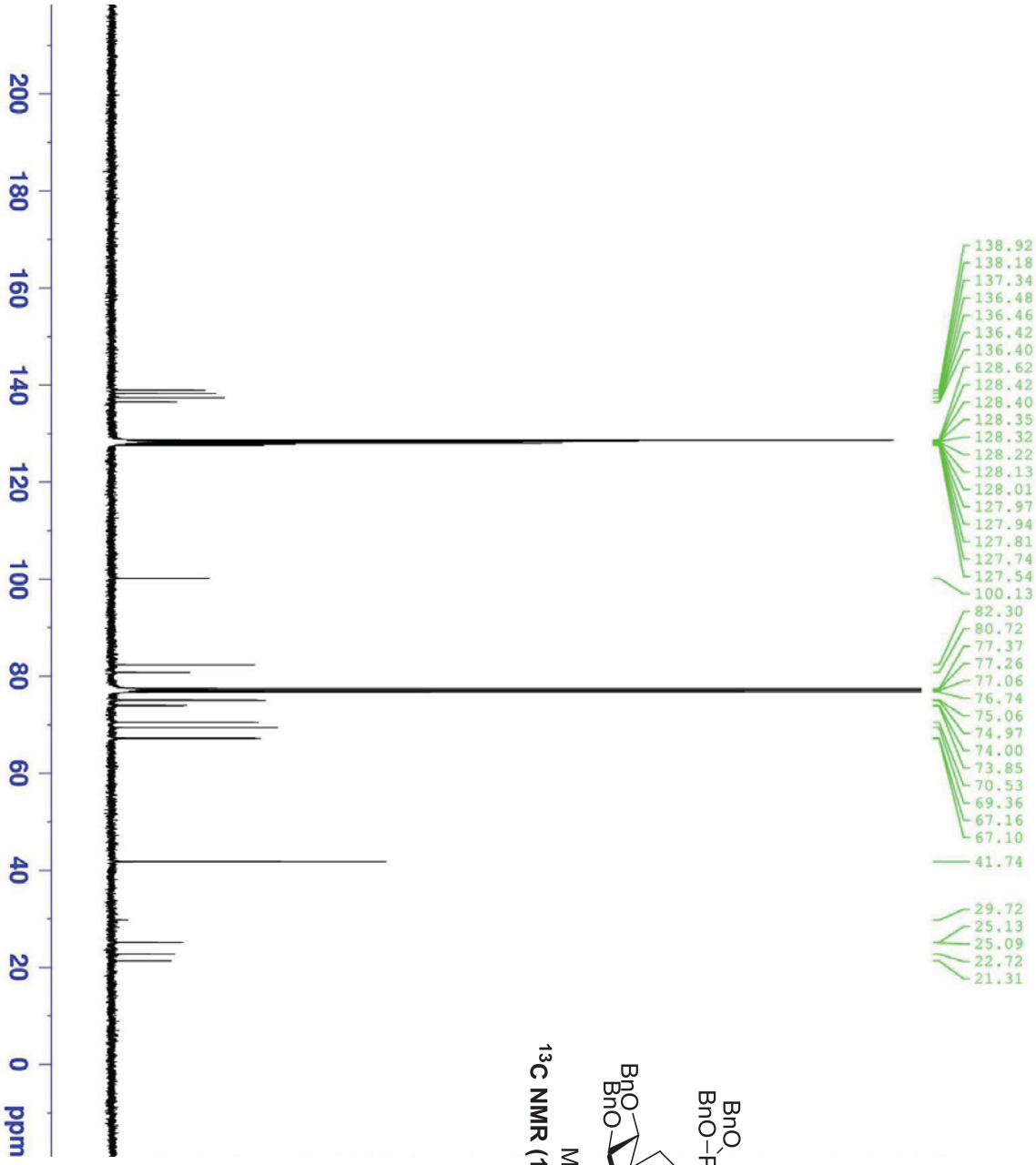

^{13}C NMR (100 MHz, $CDCl_3$)

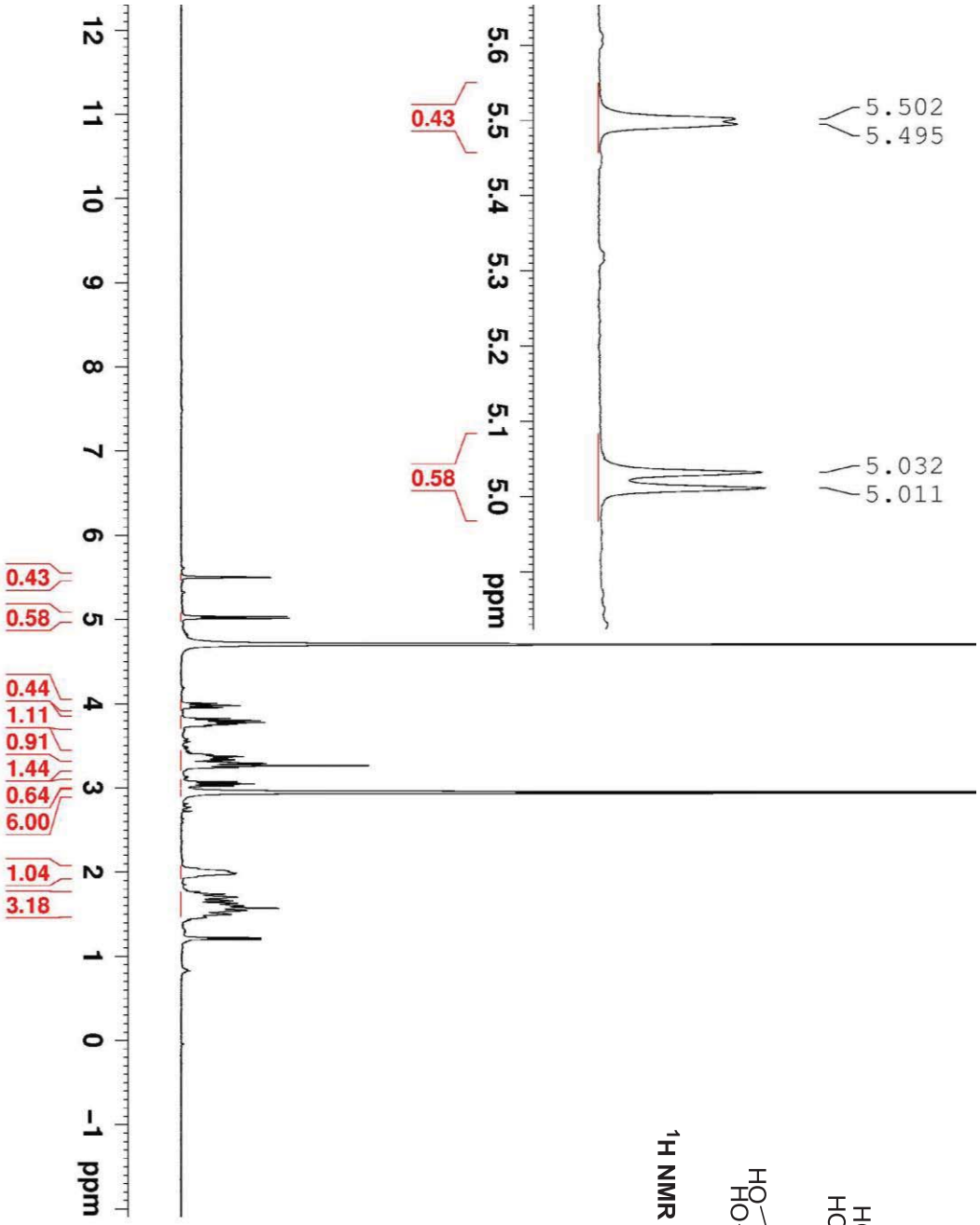

^{1}H NMR (400 MHz, D_2O)

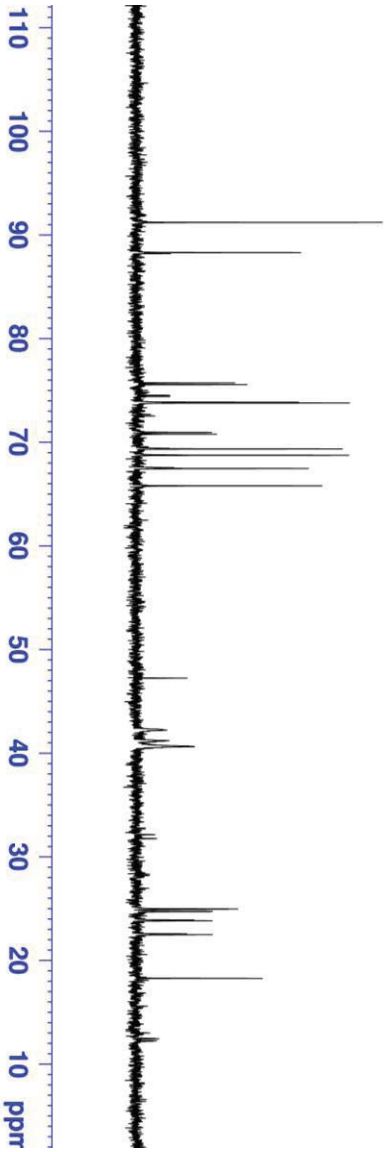

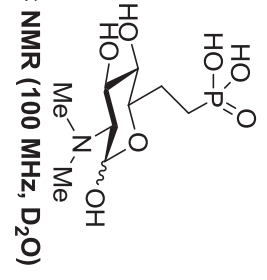

^{13}C NMR (100 MHz, D_2O)

Chapter 3

Hydrolytically-Stable Bivalent Ligands for CI-MPR

I. Introduction

A. Background of M6P/IGF2R

Lectins are carbohydrate-binding proteins.[1-5] Different from carbohydrate-specific enzymes and antibodies, they do not possess any enzymatic activities and are not generated from the immune system.[6] The first lectin was discovered in plants; Stillmark reported the isolation of ricin from castor beans in 1888.[3] Since then, numerous lectins have been found in all six kingdoms of life.[4] Through protein-carbohydrate interactions, they regulate many cellular processes such as microbial adhesion, cell-cell recognition and protein sorting. As the interpreters of the sugar code, lectins have drawn growing interest from the biochemical and biophysical research community in the post-genomic era. For example, in 2003, Fisher reported that during the window of receptivity, human fetal trophoblasts express L-selectin while uterine epithelial cells up-regulates sialyl-Lewis^X (sLe^X) based ligands.[7] This selectin-sLe^X recognition was proposed to be critical for pregnancy establishment. Recently, from ultrasensitive mass spectrometric analyses, human sperm-egg binding was also suggested to be mediated through sLe^X ligands.[8] However, while human oocytes (zona pellucida) were shown to be coated with sLe^X sequences, human spermatozoa are known to lack the expression of selectins.[9] Therefore, the sLe^X-binding lectin that crucially controls human fertilization remains mysterious; this represents one of many important lectins that need to be identified.

In the early 1980s, two distinct lectins were recognized as mannose 6-phosphate (M6P) binding proteins. Designated as "P-type" lectins, cation-dependent M6P receptor (CD-MPR) and cation-independent M6P receptor (CI-MPR) bind phosphorylated high-mannose N-glycans (Fig. 3.1).[10] By then, these M6P-bearing carbohydrates had been known to mediate the intracellular trafficking of newly synthesized lysosomal enzymes.[11] Also called as "acid hydrolases" (owing to the acidic environment of lysosome), these hydrolytic enzymes play an essential role in catabolism of various cellular macromolecules. The deficiency of these enzymes in lysosomes results in the macromolecule accumulation, causing a variety of lysosomal storage diseases, such as I-cell disease (mucolipidosis type II).[12-14]

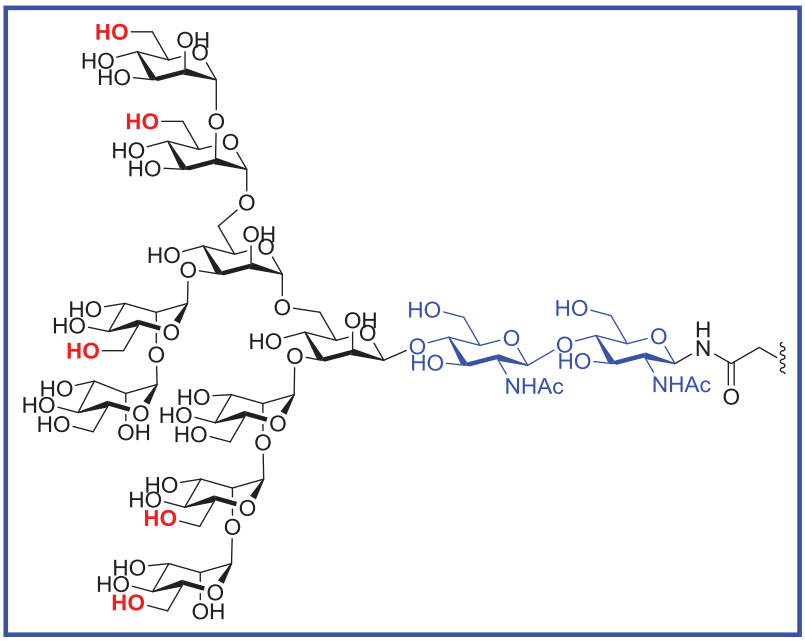

Figure 3.1: Structure of the full-size, high-mannose N-glycan (red hydroxyl groups= possible phosphorylation sites)

Lysosomal enzymes are assembled by the ribosomes that are bound to rough endoplasmic reticulum (RER). To be successfully delivered to the lysosome, the nascent

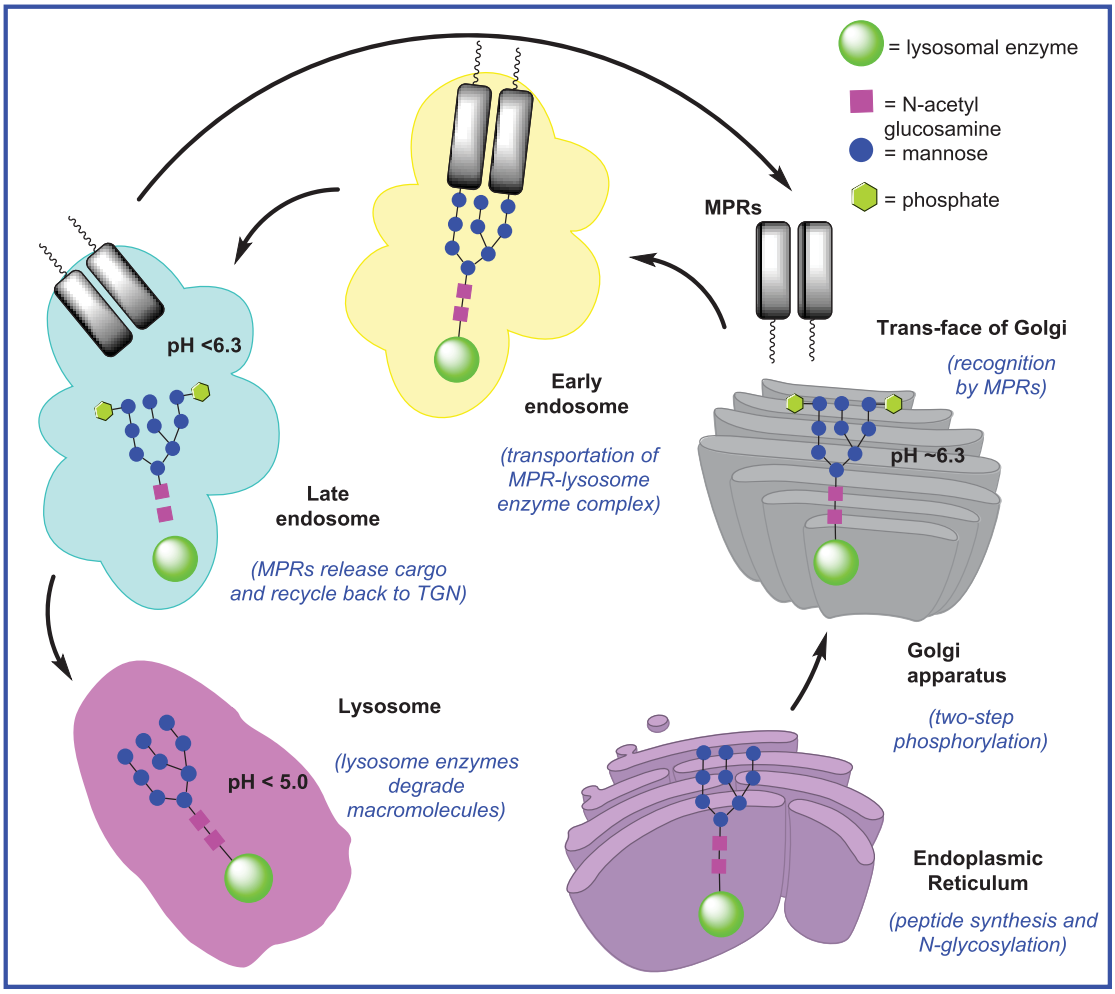

Figure 3.2: MPR pathway for intracellular lysosomal enzyme trafficking

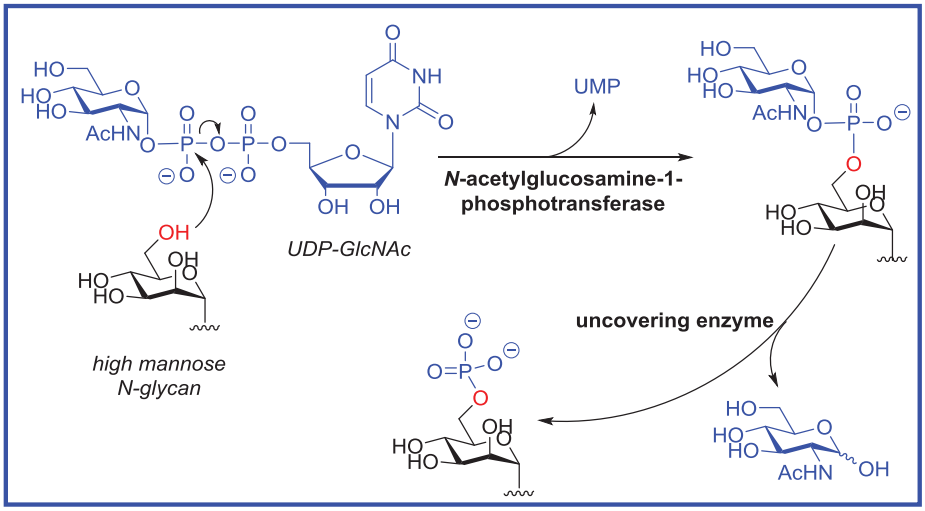

Figure 3.3: The two-step phosphorylation of N-glycans in mammalian cells

proteins need to be labeled with a M6P marker for recognition by MPRs.[15] Selected asparagine residues are co-translationally glycosylated with the high-mannose glycan ($GlcNAc_2Man_9Glc_3$),[16-17] followed by sequential removal of terminal glucoses.[18] The oligosaccharide is then trimmed down for glycoprotein folding and maturation (Fig. 3.2).[15, 18] Phosphorylation of the exposed mannose is a two-step enzymatic process, utilizing UDP-*N*-acetylglucosamine (UDP-GlcNAc) as the phosphate source (Fig. 3.3). First, *N*-acetylglucosamine-1-phosphotransferase transfers GlcNAc-1-P to the 6-hydroxyl group of mannose, forming a phosphodiester bond.[19] Then *N*-acetylglucosamine-1-phosphodiester α-*N*-acetylglucosaminidase, commonly known as "uncovering enzyme" [20-21], removes the GlcNAc, unmasking the terminal M6P residue. Subsequently, these phosphorylated glycoproteins will strongly bind to MPRs in the trans-Golgi network (TGN) at a pH of ~6.3. Then the cargo-bound MPRs travel to the late endosome, where pH drops below 6.3. Consequently, MPRs release the acid hydrolases which are ultimately transported to the lysosome for their functions (Fig. 3.3).[22-24] In the meantime, MPRs do not enter the lysosomes. Instead, they are recycled back to the cell surface or TGN for the next delivery.[25-26] MPR pathway is conserved in vertebrates,[27] and has been discovered in several invertebrates. [28-29]

P-lectins are characterized by the presence of one or more mannose 6-phosphate receptor homology (MRH) domains.[30] MRH domains share a similar fold and size. They use four key residues (Gln, Arg, Glu and Tyr) to bind the mannose. Three disulfide bonds are also conserved through MRH domains.[31-32] Other MRH-containing proteins have been discovered in ER and Golgi compartments, such as human glucosidase II β-subunit[33-34], GlcNAc-phosphotransferase γ-subunit[35-36], ortholog of fungi Yos9p (OS-9)[37-

[38] and XTP3-B (Erlectin)[39-40]. They bind non-phosphorylated high mannose N-glycans to assess the glycoprotein folding or traffic them through different compartments.[30]

Thus far, three-dimensional structures have been reported for 11 MRH domains.[30, 41] CD-MPR is a 46 kDa type-I transmembrane protein, composed of four functional domains.[10] Its single MRH domain is embedded in its 159-residue extracytoplasmic region. Several crystal structures of ligand-free[42], M6P-bound[43] or pentamannosyl phosphate (PMP)-bound[44] CD-MPR have been solved. The crystal structures show that the receptor exists as a dimer. Three disulfide bonds are critical for generating the ligand binding conformation. Furthermore, four key residues (Q66, R111, E133, and Y143) are shown to have extensive contacts with the 2-, 3-, and 4-hydroxyl groups of the phosphorylated mannose (Fig. 3.4).[44-45] This is consistent with the observation that glucose 6-phosphate (2-epimer of M6P) has ~10,000 fold less affinity to CD-MPR, compared with M6P. Another active site residue, Asp103, coordinates the divalent cations to enhance its binding affinity.

In contrast to CD-MPR, CI-MPR is a ~300 kDa transmembrane glycoprotein, with 15 homologous domains in its extracytoplasmic region. Each domain has ~147 amino acids that share a 15-40% identity with CD-MPR.[46] Two high-affinity binding sites for M6P are located in domain 1-3 and domain 9.[28, 47-48] The three-dimensional structures for 8 out of the 15 MRH domains (domains 1, 2, 3, 5, 11, 12, 13, 14) have been solved.[49-53] A structure-based sequence alignment shows that domain 1-3 uses the same key residues to bind M6P as does the CD-MPR, however, it lacks the aspartate residue for cation chelation (Fig. 3.5).[52] Recently, a low-affinity M6P binding site was identified in domain 5, which exhibited a preference to the GlcNAc-P-Man phosphodiester.[54]

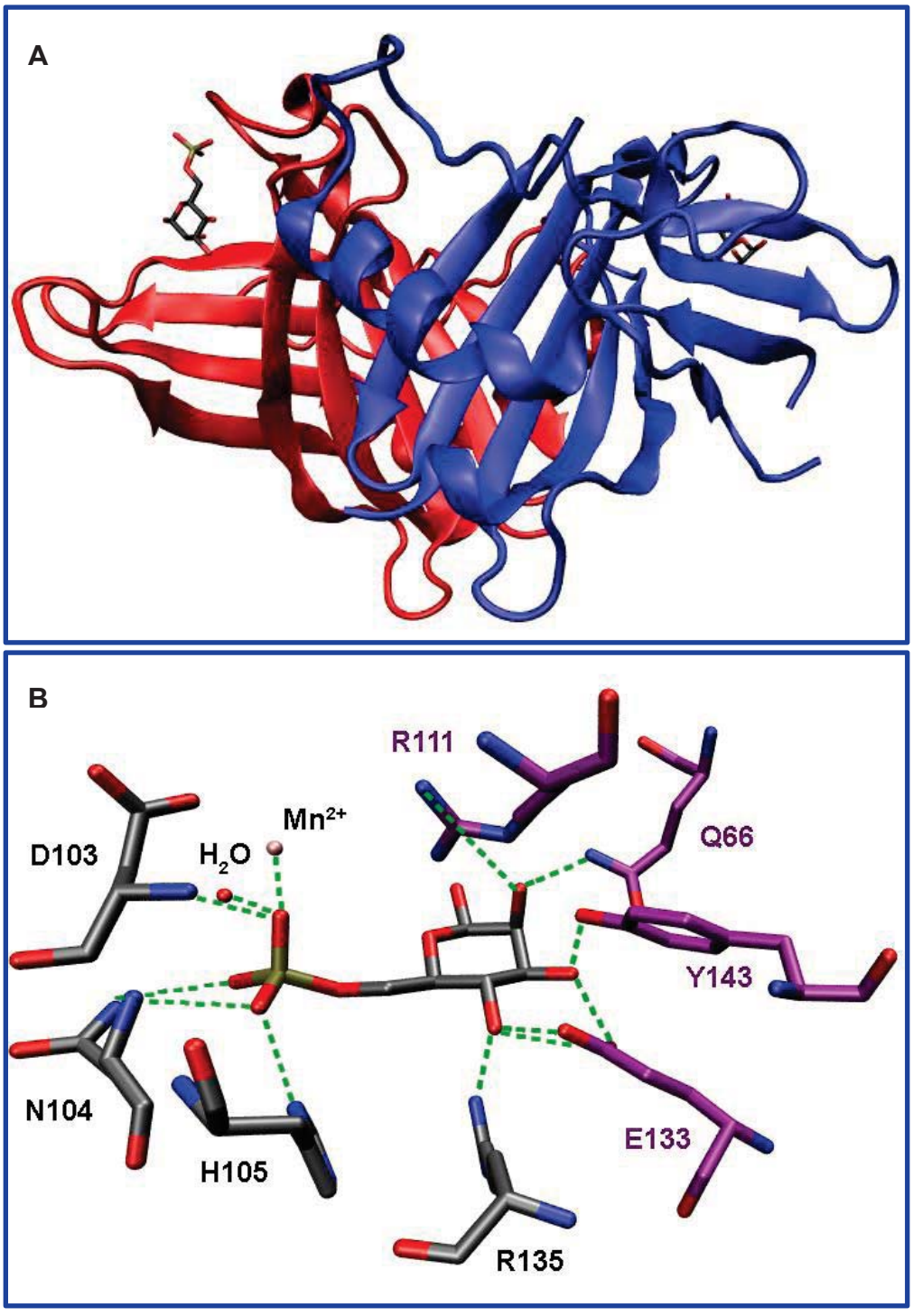

Figure 3.4: A. Crystal structure of bovine CD-MPR with M6P bound (2RL8); B. Active site residues (MRH-conserved residues marked in purple)

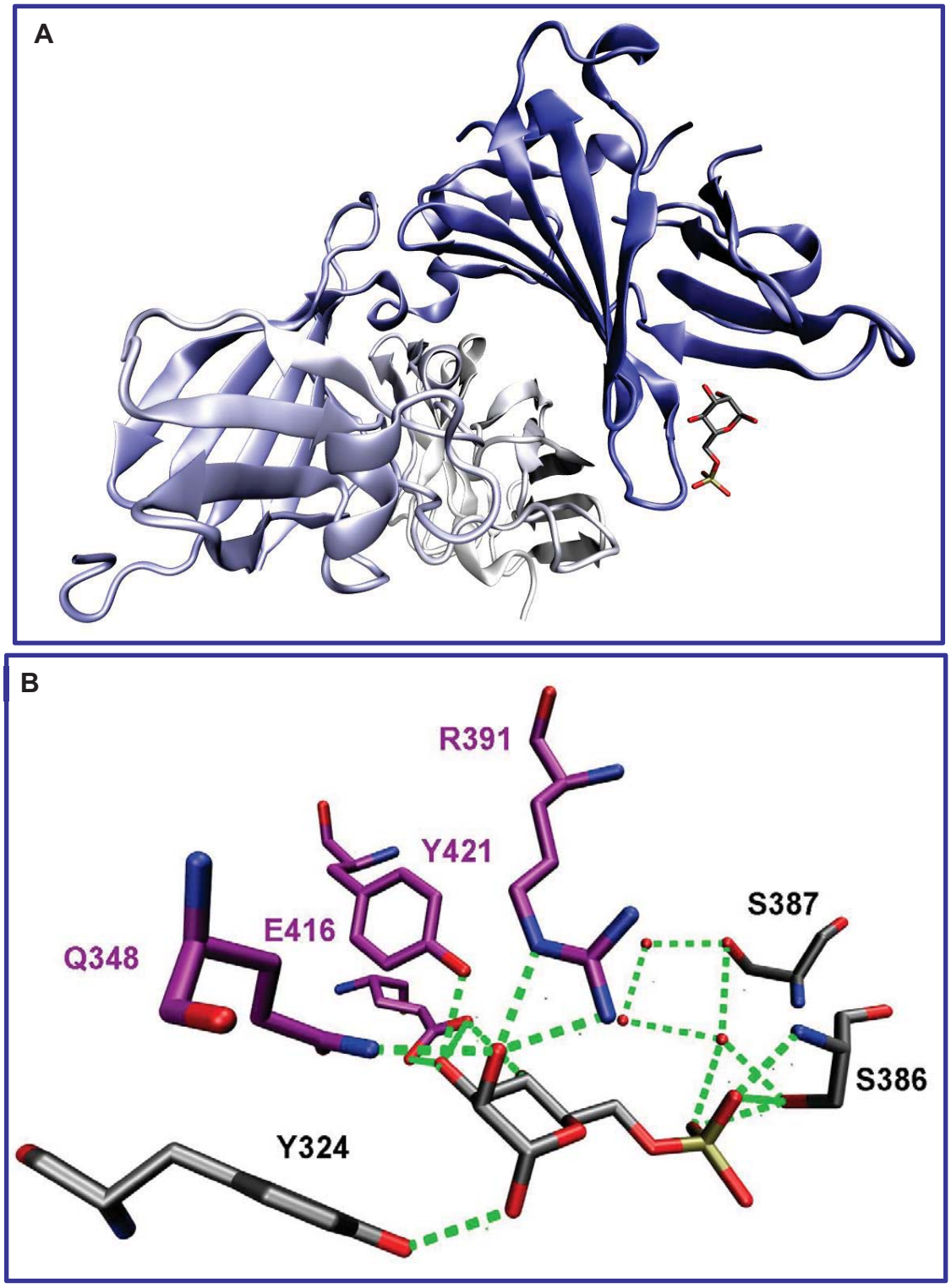

Figure 3.5 : A. Crystal structure of Domain 1-3 of bovine CI-MPR with M6P bound (1SYO); B. Active site residues (MRH-reserved residues marked in purple)

In addition to its role in intracellular protein sorting and trafficking, CI-MPR also plays an important role in the endocytic pathway. A small percentage (~ 10%) of the CI-MPR is distributed in the cell surface.[55-57] The cell-surface receptors can bind M6P-containing ligands and deliver them to the endosome via the "secretion-recapture" pathway.[58] For example, some acid hydrolases are secreted into the medium even though they carry a M6P marker. This is particularly significant for some activated macrophages under inflammatory conditions. Surface CI-MPR can bind and internalize these enzymes, to ultimately transport them to lysosome.[59]

Moreover, harnessing its versatile MRH domains, CI-MPR can bind a variety of non-M6P-containing ligands for their endocytosis and degradation in lysosome.[60] Perhaps, most importantly, CI-MPR was found to bind insulin-like growth factor II (IGF-II) via domain 11 in the extracellular region (Fig. 3.6).[61-63] The IGF system is involved in various signaling pathways that are critical for cell proliferation and malignant transformation.[64] The IGF axis comprises two growth factors (IGF-I and IGF-II), three types of receptor (IGF1R, CI-MPR/IGF2R and IR-A) and a family of IGF binding proteins (IGFBPs).[65] IGF-II promotes cell growth, survival and differentiation, mainly through interactions with IGF1R.[66] It can also stimulate cell mitosis via binding to insulin receptor isoform A (IR-A), which is predominantly expressed in the fetus and cancer cells.[67] Another high-affinity receptor for IGF-II is CI-MPR, which mostly targets IGF-II for degradation, thereby controlling the bioavailability of IGF-II in bloodstream.[68-70] As a result, CI-MPR is also referred to as M6P/IGF2R or simply IGF2R. CI-MPR exploits its hydrophobic sites in domain 11 to interact with IGF-II, distinct from the binding pattern for M6P. In humans, site-directed studies have shown that F48, R49, S50, A54 and L55

are the key binding residues.[70] It is also known that the residues in repeat domain 13 contribute significantly to the high-affinity binding (~ 0.1 nM) (Fig. 3.6).[71-72]

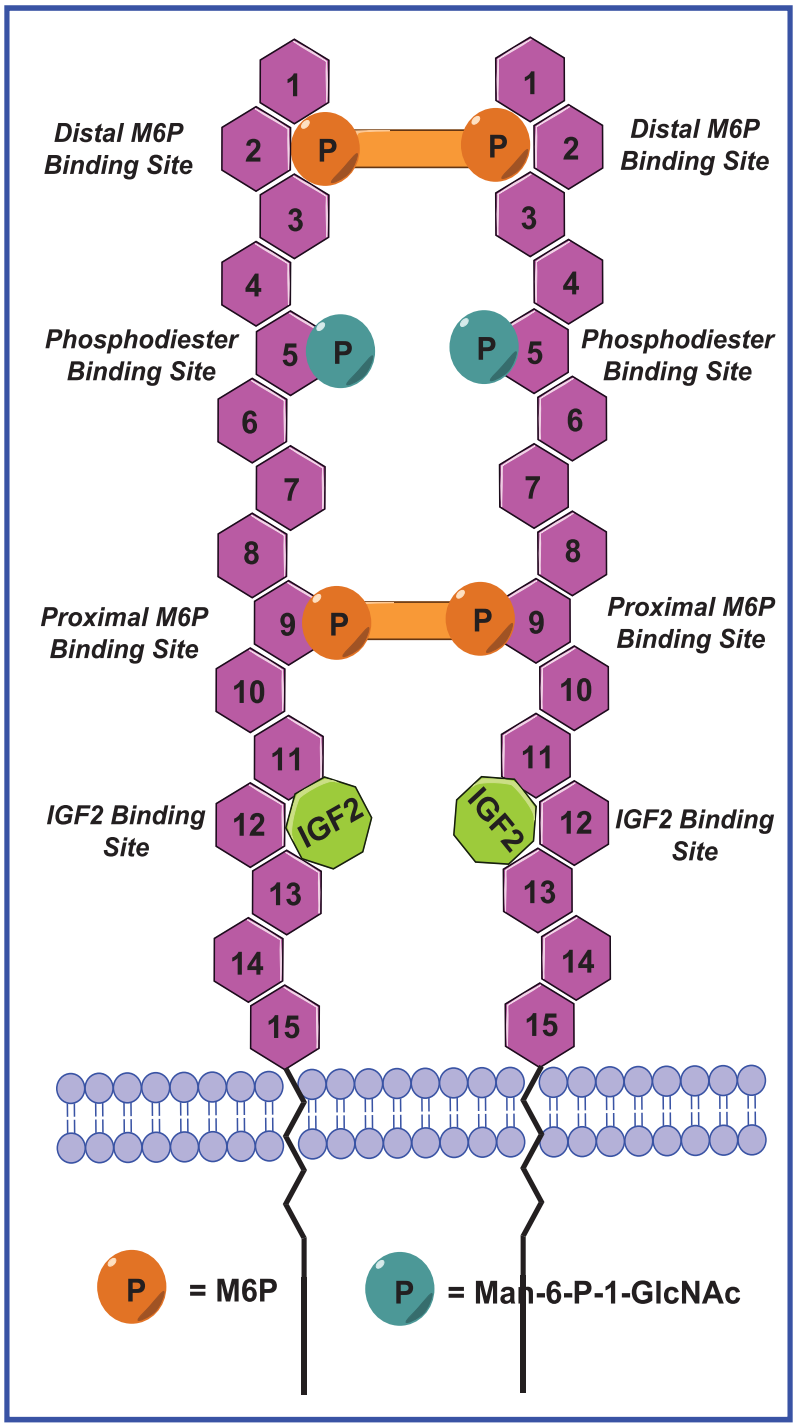

Figure 3.6: Schematic structure of the CI-MPR dimer with a postulated bivalent interaction with M6P-containing ligands

Although M6P binds unrelated domains, the presence of a M6P-containing acid hydrolase seems to stimulate the receptor-mediated endocytosis of IGF-II. In 1998, York *et al.* have shown that in the presence of excess (10 nM) human β-glucuronidase (hGUS), the internalization rate of a iodine-125-labeled IGF-II was accelerated by 3-4 fold.[73] On the other hand, this cooperative effect was not observed for M6P, even at a saturation concentration (10 mM). This leads to the postulation that the multivalent hGUS promotes the oligomerization, most likely dimerization, of the receptor.[74-75] The consequent conformational change will be transduced to the endoplasmic region, resulting in an accelerated endocytosis of the ligand-receptor complex. Therefore, in a similar fashion a synthetic ligand that cross-bridges two monomeric receptors, could potentially stimulate the endocytosis of circulating IGF-II. The limited bioavailability of IGF-II would ultimately inhibit growth and survival of cancer cells that are dependent on IGF-II signaling.[76] Thus, the *igf2r* gene has been acclaimed as a potential anti-cancer gene, particularly for suppressing breast tumor.[77-78] Thus, we set out to develop such bivalent ligands for the receptor.

B. Previous Work on Multivalent Ligands for M6P/IGF2R

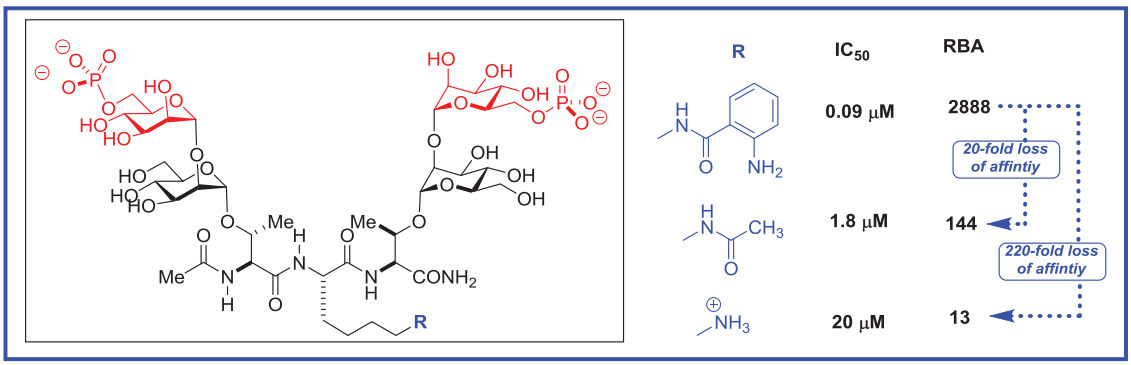

Figure 3.7: Bock's synthetic glycopeptides as bivalent ligands for IGF2R

Multivalency has been observed throughout many cellular processes, particularly frequent in lectin-carbohydrate recognition.[79-80] Monovalent interactions between a carbohydrate and a protein are usually weak. Hence, to achieved a specific cellular response, multivalent oligosaccharide ligands are regularly employed to interact with lectins.[81-83] By occupying multiple binding sites, these ligands usually possess exponentially high affinities to the receptors. Nonetheless, it is important to distinguish a high-affinity ligand from an "effector." In addition to its apparent high affinity, an effector also has the desired functions such as clustering receptors.[84-86] For instance, Bock *et al.* have synthesized a series of phosphorylated glycopeptides for CI-MPR.[87-88] One of these bivalent ligands displayed three orders of magnitude higher binding affinity than M6P, leading to the assumption that this is the first small molecule that spans two M6P-binding sites. However, in the 1998 study, this ligand failed to increase the IGF-II endocytosis rate.[73] Indeed, the protecting groups of these peptides seem to have a major influence on the binding affinities. Specifically, when the central lysine residue was not protected instead of being protected with an anthranoyl group, the binding affinity of the peptide decreased by ~220-fold (Fig. 3.7).[88] This implies that the exhibited high affinity is a result from the strong interaction with non-M6P binding sites. The ligand did not really fulfill the true "bivalency".

In addition to the glycopeptide-based approach, some groups have constructed various oligosaccharide-tethered ligands. Hindsgaul *et al.* synthesized the pentamannosyl core found in the N-glycans.[89] And they demonstrated that the bis-phosphorylated ligand exhibited ~10-fold higher affinity than the mono-phosphorylated pentasaccharide. It is also noted that mono-phosphorylated pentamannose exhibited 12-fold higher affinity than

M6P, suggesting that the high mannose scaffold may be important to the receptor binding (Fig. 3.8).

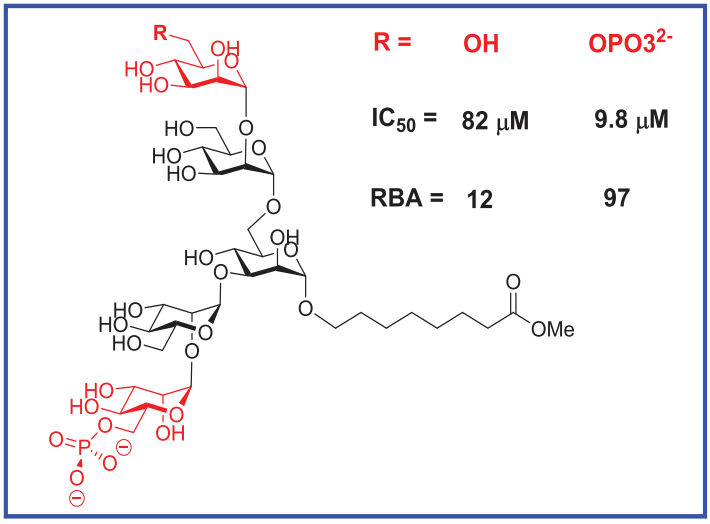

Figure 3.8: Hindsgaul's synthetic biantennary oligosaccharide

More recently, Chen and co-workers made a triantennary $GlcNAc_2Man_5P_2$ ligand. Subsequent modification allows this ligand to be covalently attached to human carbonic anhydrase II (HCAII) via a cysteine residue. After labeling with a fluorescent tag, the neoglycoprotein was subjected to IGF2R-mediated cellular uptake, and demonstrated much faster internalization rate compared with the apoprotein.[90] Additionally, a series of mono- and bis-phosphorylated N-glycans were enzymatically prepared from digestion of bovine ribonuclease B (RNase B) and soybean agglutinin. Derivatized with a fluorescent label/tether, they were printed on glass slides and measured for binding to IGF2R.[91] Despite the success of this biomimetic approach, the preparation of these phosphorylated carbohydrates is usually tedious. The enzymatic synthesis sometimes cannot provide defined glycan structures.[91] Thus, our group set out to explore novel synthetic strategies to rapidly assemble bivalent ligands that contain M6P mimics. And we seek ligands that have three orders of magnitude higher binding affinity than M6P exhibited by hGUS.

II. Results and Discussion

A. Monovalent ligands and cross-metathesis approach

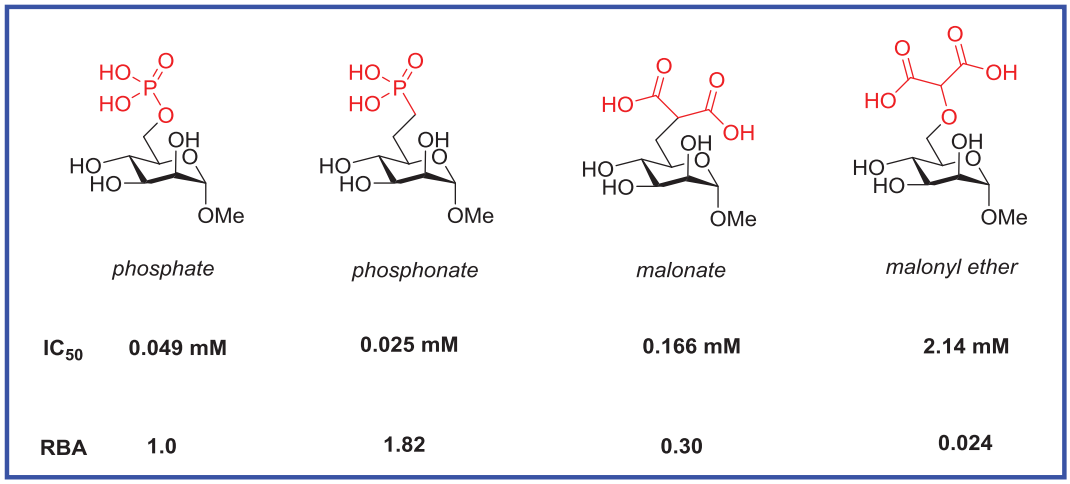

Figure 3.9: Monovalent ligands synthesized and tested in Berkowitz-MacDonald collaboration

Previously, both Montero and our group have synthesized phosphonate analogues of M6P.[92] In addition, our group has synthesized a panel of other hydrolytically stable analogues, and tested them for binding affinities.[93] Pleasingly, the replacement of the bridging oxygen with carbon did not have a deleterious effect on the receptor binding. Phosphonate analogue displayed an IC_{50} of ~25 μM to the receptor, which is similar to that of M6P (Fig. 3.9). Moreover, the second best ligand, malonate analogue, showed only a 3-fold weaker binding to IGF2R. Subsequently, these two analogues were utilized tobuild bivalent ligands by cross metathesis chemistry. The allyl mannoside was easily prepared from methyl α-D-mannopyranoside. By triflate displacement chemistry, manolate functionality was installed smoothly. The Ru(II)-mediated cross metathesis, followed by hydrogenation, efficiently tethered two surrogates together through a carbon chain (Fig. 3.10). For the synthesis of ligand **7**, the alcohol **2** was subjected to cross

metathesis to yield the diol **6** in 84% yield (E/Z = 4/1). The bis-triflate was then cleanly prepared and displaced by two equivalents of dibenzyl lithiomethylphosphonate in 75% yield. The product was subsequently hydrogenated, to afford the first bivalent ligand that

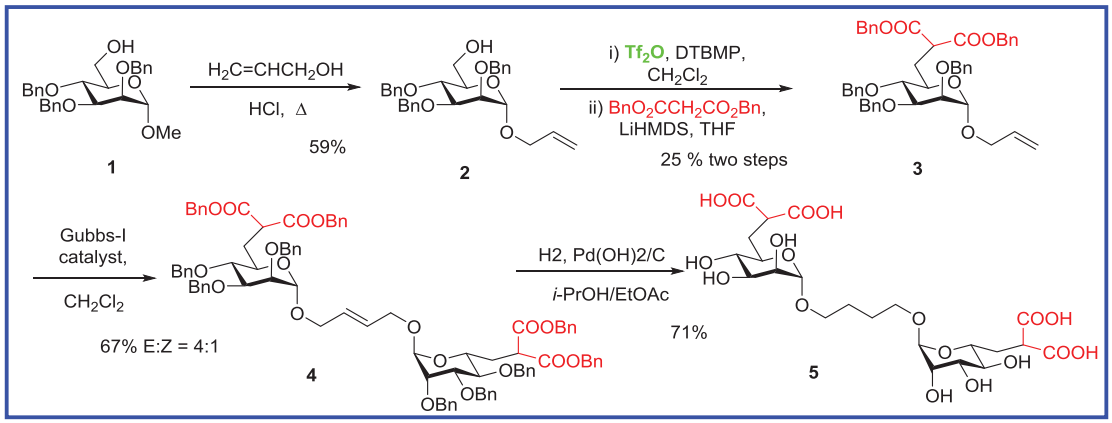

Figure 3.10: Synthesis of bis-malonate analogue of M6P

bears two phosphonate analogues (Fig. 3.11). However, both ligands **5** and **7** demonstrated little effect of sought-after bivalency. A quick molecular modeling using Merck Molecular Force Field (MMFF) estimated the distance between two phosphorus atoms to be around 12 Å. This is likely too short to intermolecularly span two M6P

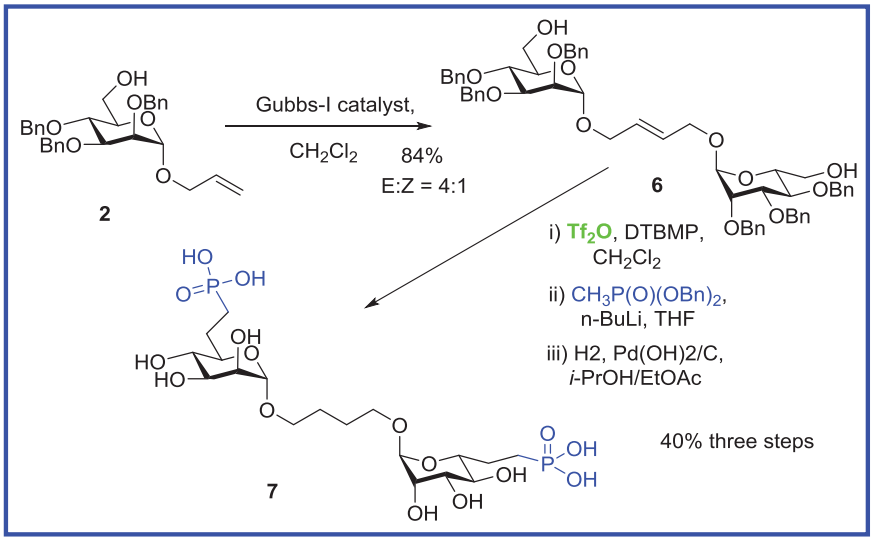

Figure 3.11: Synthesis of bis-phosphonate analogue of M6P

binding sites. In 2004, Olson *et al.* constructed a homology model of the whole receptor, based on the crystal structures of domain 1-3, using topographical information from amino acid sequence of each domain. They estimated that the distance between the M6P-binding sites domain 3 and domain 9 on a single receptor is ~ 45 Å for a "bent" model.[53] And few studies have shed light on the length required for a ligand to bind two sites intermolecularly. Therefore, we decided to make a set of bivalent ligands with longer tethers.[94]

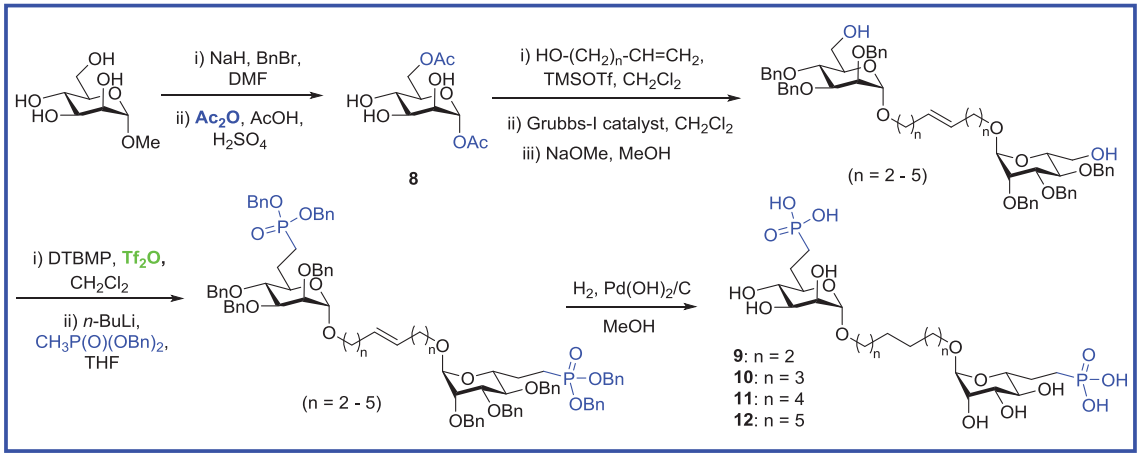

Figure 3.12: Synthesis of a set of phosphatase-inert "molecular rulers"

Benzylation of α-D-mannopyranoside, followed by treatment with acetic anhydride yielded the di-acetate compound **8**. A Vorbrüggen-type glycosylation[95] using TMSOTf afforded a set of alkene terminated mannosides. Then Grubbs-I catalyst was utilized in the alkene cross metathesis[96] to generate the bis-mannosides. Following the removal of acetate groups, triflate displacement chemistry was efficiently applied to each of the diol substrates. The final alkene hydrogenation/global debenzylation step rendered four bis-phosphonate ligands (**9** – **12**) with incrementally increased lengths (Fig. 3.12). These compounds represents the first set of "molecular rulers" that has been developed to

probe the bivalent interactions with the receptor. The IC_{50} values and relative binding affinities (RBAs) are summarized in Table 3.1, as well as the estimated P-P distances. Statistically, all these compounds exhibited a similar binding affinity to M6P, suggesting they still bind in a monovalent manner. Although compound **12** has about twice the length of the original ligand **7**, its RBA showed little improvement. Furthermore, the 12-carbon tether starts to have a detrimental effect on the solubility of these bis-phosphonate ligands in water. Thus, we need to build the bivalent ligands with longer and more hydrophilic tethers. More importantly, we seek diverse structural features in the new generation of ligands, to acquire more information about the bivalent contact between the receptor and the native ligands.

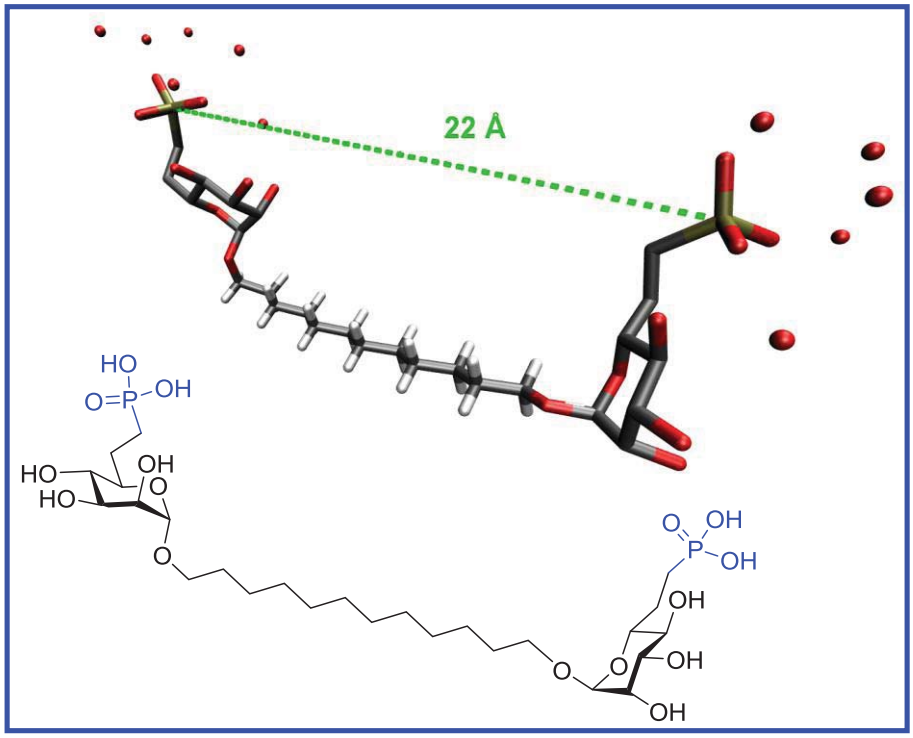

Figure 3.13: One of the low-energy conformers of the 12-C tethered ligands found by a MMFF minimization

Table 3.1. Relative CI-MPR binding affinities

Ligand	IC_{50}(n) (μM)[a]	RBA[b]	M_r	Length[c]
M6P	11.5 ± 2.51 (4)	1.0	340	NA
G6P	>10 (4)	NA	282	NA
9 (6C)	4.76 ± 2.50 (4)	2.63 ± 0.74	666	18.5Å
10 (8C)	5.03 ± 1.34 (4)	2.39 ± 0.83	694	19.5Å
11 (10C)	4.44 ± 1.40 (4)	2.65 ± 0.52	722	21.8Å
12 (12C)	3.65 ± 0.54 (4)	3.13 ± 0.52	750	24.7Å

[a]IC_{50}s for competitive displacement of radiolabeled PMP-BSA from the receptor (n = no. of trials); [b]RBA = relative binding affinity, normalized to free M6P; [c]Length = P-P distance, as estimated by molecular mechanics minimization (MMFF)

B. Ligand Diversification at the Linking Stage

Synthetic ligands have been regularly employed to probe multivalent interactions.[81, 83-84] This is because the natural ligands are commonly too complex to apprehend. For instance, hGUS is a homotetrameric glycoprotein. In each monomer, four Asn residues could potentially be glycosylated with a variety of high-mannose N-glycans, ranging from $Man_5GlcNAc_2$ to $Man_9GlcNAc_2$.[97] Therefore, it is extremely difficult to interpret how hGUS achieves multivalency through interactions with IGF2R. In contrast, small-molecule ligands have defined structures, such as valency and distance. And they are relatively easy to modify for extensive SAR studies. Hence, these "tailored ligands" are important tools to probe multivalent interactions with macromolecules.[98] Furthermore, synthetic ligands can block the binding of the natural ligands, thereby inducing desired cellular response.[99] In this particular case, however, the goal is to have a synthetic ligand

that activates the IGF2R-mediated endocytosis, leading to the inhibition of IGF-II dependent tumor growth. And with our phosphonate analogue as the binding motif, such a bivalent ligand would become a novel anti-cancer drug candidate instantly.

Pioneering studies from Kiessling group have demonstrated the great influence of tethers or valency on the ligand-receptor binding.[84, 98, 100-101] However, few groups have looked over the effect of linkages despite a growing list of conjugation chemistries. It appears many multivalent ligands are linked through 1,4-triazoles, utilizing the copper(I)-

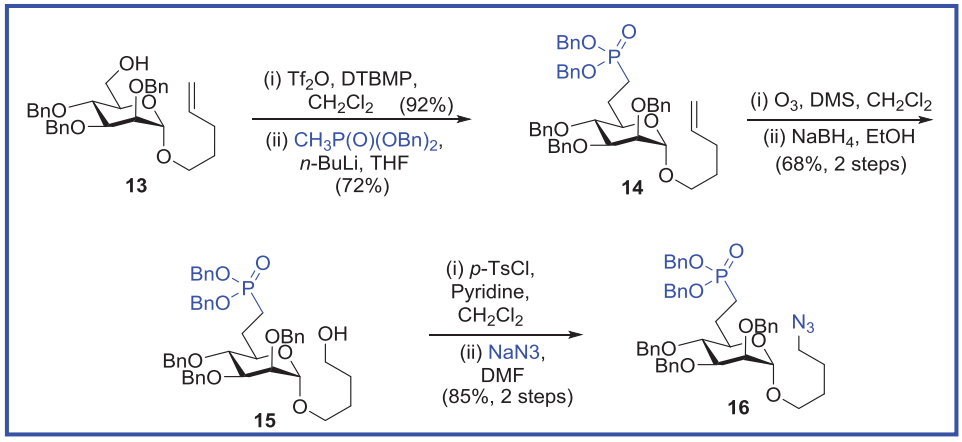

Figure 3.14: Synthesis of an azide-terminated mannosyl phosphonate

catalyzed azide-alkyne cycloaddition (CuAAC).[102] Indeed, this transformation has become so popular that this chemistry has become synonymous with the term "click chemistry". Although CuAAC is highly efficient, the myopic focus on this chemistry is truly a missed opportunity.[103] Namely, with the azide functionality, one can rapidly diversify the linkage with an array of conjugation chemistries.[104] In this manner, one can introduce diversity to the important molecular features, such as size, shape and lipophilicity. Therefore, we decided to demonstrate this linker-diversification strategy, by building a new generation of bivalent ligands for IGF2R.

The synthesis of the new set of ligands emanates from *n*-pentenyl 2,3,4-tri-O-benzyl-α-D-mannopyranoside **13**. Triflate displacement chemistry was successfully applied, with 66% yield over the two steps, that installed the phosphonate moiety. The terminal double bond was then subjected to ozonolysis, followed by treatment with dimethyl sulfide. Further reduction of the aldehyde yielded the intermediate **15**. Tosylation of the terminal -OH, followed by NaN_3 displacement afford the key azido precursor **16**, set for a series of conjugation chemistries.

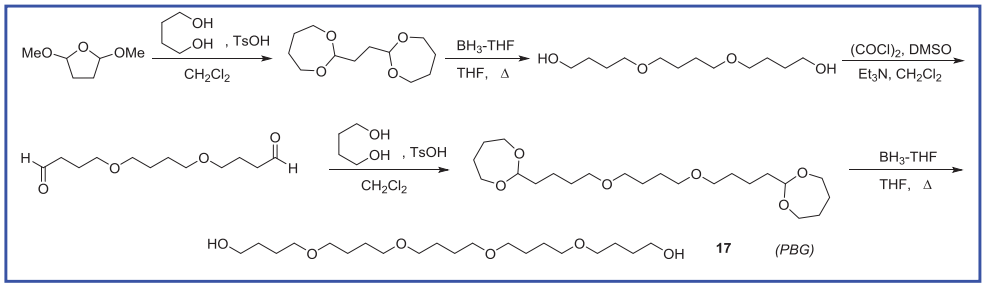

Figure 3.15: Gin's iterative procedure for synthesis of pentabutylene glycol

In the meantime, we have selected pentabutylene glycol (PBG) as the tethering part. It represents the type of tethers with ideal length, flexibility and hydrophilicity for our system. PBG was synthesized in gram scale following Gin's iterative process (Fig.

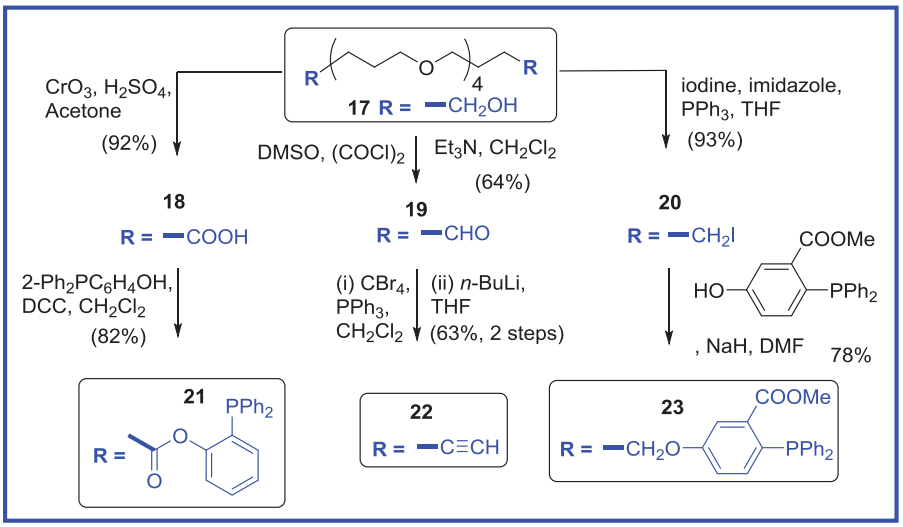

Figure 3.16: Synthesis of three types of tethers

3.15).[105] 2,5-Dimethoxy tetrahydrofuran was treated with 1,4-butanediol and catalytic *p*-toluenesulfonic acid (TsOH) to generate the diacetal in 75% yield. Reductive opening of the seven-membered ring resulted in tributylene glycol quantitatively. Swern oxidation efficiently converted the terminal alcohols to aldehydes, which were reacted with 1,4-butanediol and TsOH to give the extended diacetal. Further treatment with borane-THF rendered PBG in 91% yield. PBG was further modified to install functional groups that are ready to couple with azides (Fig. 3.16). First the terminal hydroxyl groups were oxidized to carboxylic acids, of which DCC-promoted esterification yielded the phosphine-ester **21** expeditiously. PBG was also converted to the dialdehyde **19**, followed by Corey-Fuchs reaction to afford diacetylene **22**. Finally, Appel reaction transformed the diol to diiodide **20** in 93% yield. Methyl 2-(diphenylphosphino)-5-hydroxybenzoate was used to displace the iodide, providing a different phosphino-ester, compound **23**.

With both coupling components in hand, we set out to examine a set of five conjugation reactions, as a novel strategy to introduce diversity to the ligands. First, the phosphino-esters **21** and **23** were reacted with the azide precursor respectively, to provide two distinct amide linkages. This Staudinger-type conjugation was first developed by the Bertozzi group.[106-107] Azides can be efficiently reduced by phosphines to afford aza-ylide intermediates. Hydrolysis of these ylides gives amines and phosphine oxide. By cleverly using an adjacent ester, Bertozzi *et al.* were able to trap the aza-ylide to form a phosphonium amide. Upon hydrolysis[108], the phosphonium amide broke down to phosphine oxide and an amide bond, which serves as the linkage to a variety of bioconjugates.[109]

Herein, for the "traceless" coupling between **21** and **16**, the formed phosphine oxide was released from the reaction to yield the simple amide linked compound **24**. On the other hand, for the ligation of **23** and **16**, hydrolysis expelled MeOH as the byproduct, while phosphine oxide was conserved as a part of a novel linkage. The latter strategy was successfully utilized to engineer cell surfaces.[106, 110] Thus it is intriguing to employ this underused linking functionality in our system. Both Staudinger-type ligation proceeded efficiently with over 82% yield (>90% for each coupling). Alternatively, compound **24** could be accessed by Williams ligation which uses thio carboxylic acids to react with azides.[111] However, we found the azide **16** to be a challenging substrate for this type of transformation. The reaction between **16** and the bis-thio carboxylic acid rendered the desired product in <20% yield, with a notable decomposition of the azide.

Next, we set out to explore two types of azide-alkyne chemistries. CuAAC has been widely applied in bioorganic chemistry, ranging from ligand assembly to target

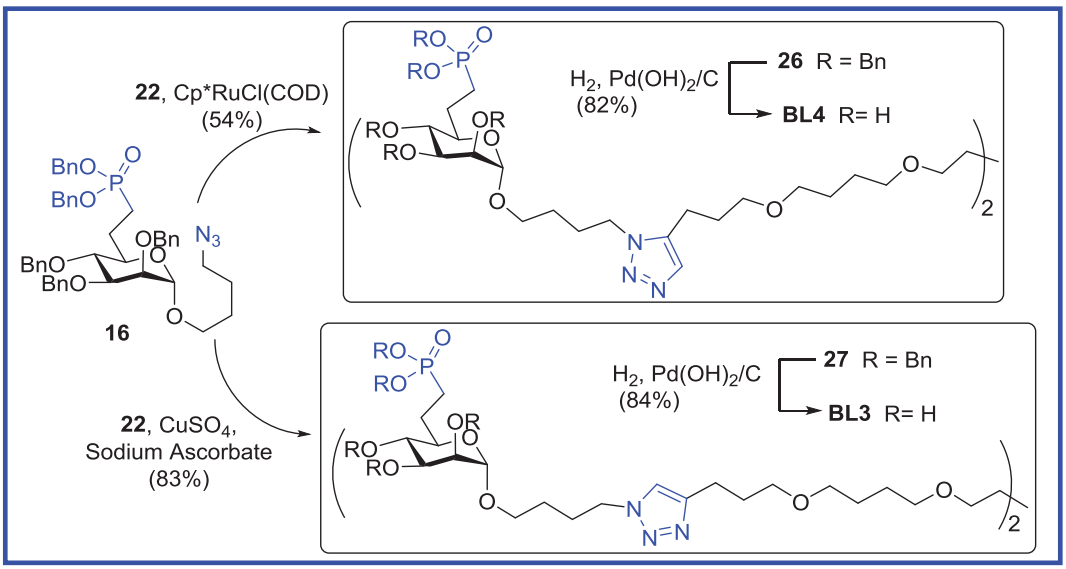

Figure 3.20: Ru(II)- and Cu(I)-catalyzed azide-alkyne Huisgen cycloaddition

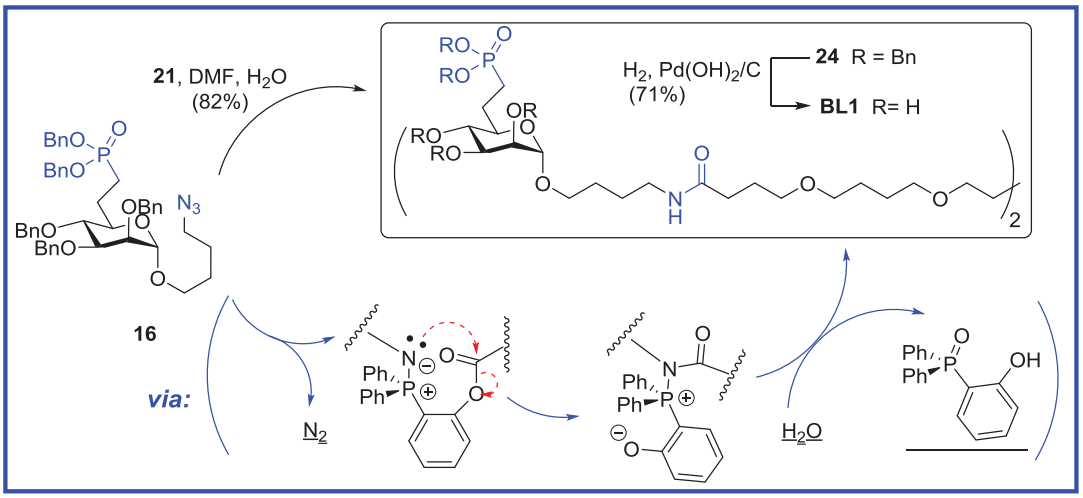

Figure 3.17: "Traceless" Staudinger ligation to make the simple amide linkage

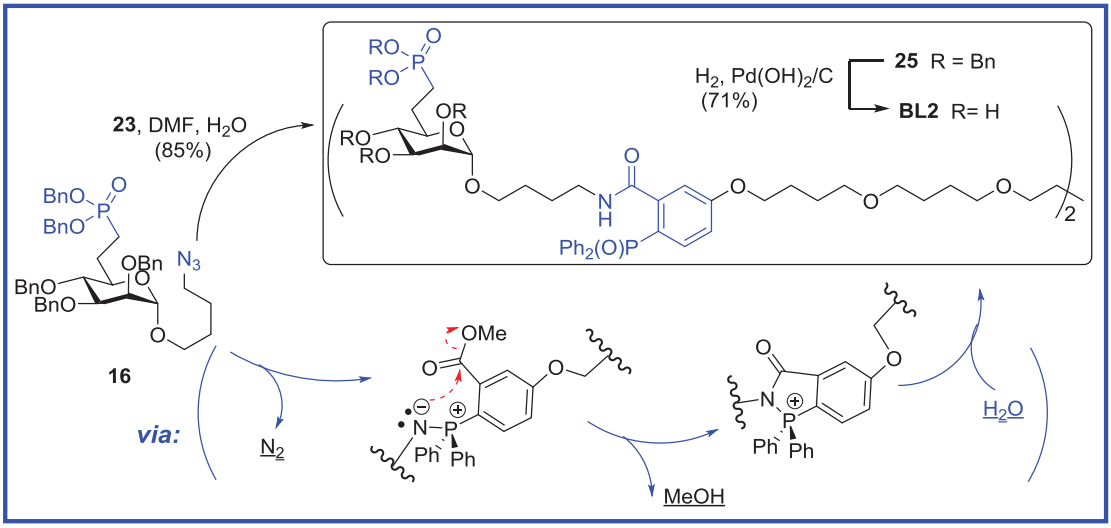

Figure 3.18: Staudinger ligation to make the triphenylphosphine oxide-amide linkage

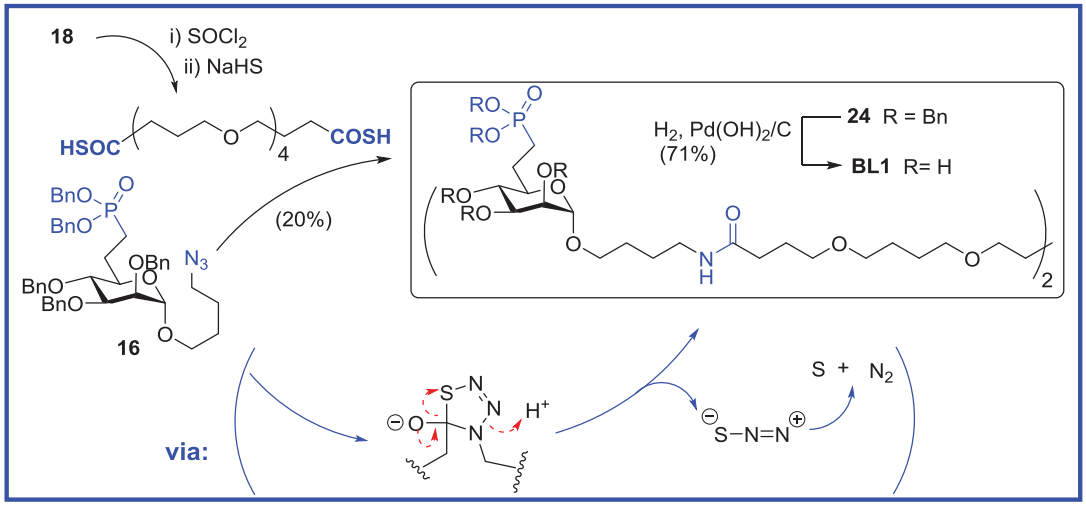

Figure 3.19: Williams thioacid-azide ligation to make simple amide linkage

labeling.[112] There are numerous bioconjugates and small-molecule conjugates that bear the 1,4-triazole linkage. Recently, Ru(II)-catalyzed azide-alkyne cycloaddition (RuAAC) has emerged as an exciting alternative.[113-114] Although this reaction is not as efficient as CuAAC, it provides an interesting 1,5-triazole linking functionality. This regioisomeric linkage could, in principle, forge the molecule in a different trajectory. For example, Liskamp *et al*. have utilized the triazole group to replace the E-ring of vancomycin, aiming to synthesize the constrained mimics of the antimicrobial agent.[115] The successful execution of the CuAAC and RuAAC reactions lead to two macrocyclic peptides with distinct structural features. However, the synthesis of these vancomycin analogues was not completed and no biochemical studies were presented. Herein, the Huisgen cycloaddition reactions were conducted with both the copper and ruthenium catalysts, to yield the 1,4-triazole linked compound **27** and the 1,5-triazole linked **26**, respectively (Fig 3.20). After the global debenzylation., two bivalent phosphonate ligands were afforded. And a direct comparison of the binding affinities of the 1,4- and 1,5-triazole linked ligands is prominent.

Finally, we set out to explore an even less exploited ligation chemistry, namely the 1,3-dipolar cycloaddition reactions of azides and sulfonyl cyanide. Subsequent nucleophilic aromatic substitution (S_NAr) of the sulfonyl tetrazoles could ligate various nucleophiles to the tetrazole components. This transformation was first discovered under thermal conditions by Demko and Sharpless.[116] Tosyl cyanide (TsCN)[117], owing to its relative stability and commercial accessibility, is the only sulfonyl cyanide that has been explored in this reaction. A wide range of aliphatic azides gave quantitative yields; however, aromatic azides are generally poor substrates for the cycloaddition. In 2007,

Vilarrasa *et al*. examined an array of metal catalysts and found $Cu_2(OTf)_2$ is particularly effective in promoting the reactions.[118] Hence, we initially attempted to fulfill the cycloaddition of azide **16** and tosyl cyanide using this catalyst. As seen in Table 3.2, the tetrazole **28** was synthesized in poor to moderate yields under catalysis, with $Cu_2(OTf)_2 \bullet C_7H_8$ complex giving the best result (48% yield). Perhaps more disappointingly, the Cu(I)-catalyzed cycloaddition reactions afforded mediocre selectivities. The 1,4- and 1,5-tetrazole linkages were generated in a ratio of ~ 3:7. And these two regioisomers proved to be difficult to separate. Other metals also failed to give satisfactory results. Notably, Fokin's Ru(II) catalyst[113] failed to produce any detectable product after 48 h (Table 3.2, entry 5). Hence, we set to examine this reaction under thermal conditions.

Table 3.2: Optimization of the azide-sulfonyl cyanide 1,3-dipolar cycloaddition

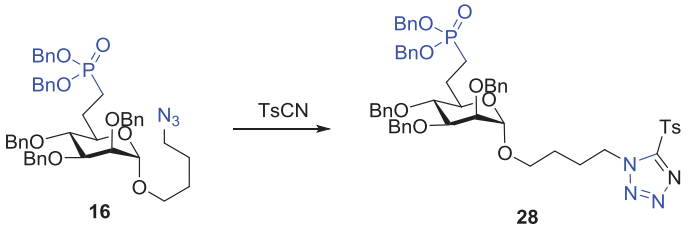

16 28

entry	catalyst	solvent	temp (°C)	time, h	yield (%)	sel.[a]
1	$Cu_2(OTf)_2 \bullet C_6H_6$	CH_2Cl_2	23	22	31	75/25
2	$Cu_2(OTf)_2 \bullet C_7H_8$	CH_2Cl_2	23	22	48	70/30
3	$Cu(OTf)_2$	CH_2Cl_2	23	22	13	71/29
4	$ZnCl_2$	CH_2Cl_2	23	22	15	93/7
5	$Cp^*(COD)RuCl$	CH_2Cl_2	23	48	0	NA
6	none	none	95	20	72	>99/1
7	none	none	95[b]	1	70	>99/1

[a.] Selectivity of the cycloaddition reaction with ratios of 1,5-tetrazole over 1,4-tetrazole. [b.] This reaction temperature was achieved by microwave irradiation.

To our satisfaction, the functionally dense azide **16** reacted efficiently with TsCN at 95 °C without any solvent. The desired sulfonyl 1,5-tetrazole was synthesized in 72% yield as the only detected isomer (Table 3.2, entry 6). Next, we utilized microwave to promote this thermal reaction to a greater efficiency. Vilarrasa *et al.* have used microwave irradiation to facilitate the 1,3-dipolar cycloaddition reactions between azides and acetyl cyanides.[118] However, prior to this work, no one has reported the use of microwave to accelerate the cycloaddition of an azide and tosyl cyanide. A synthesizer demo was kindly provided by CEM at that time. The reaction was then heated at 95 °C under microwave irradiation. TLC analysis indicated the completion of the reaction within 1 h. Further purification afforded only the 1,5-tetrazole compound **28** in 70% yield (Table 3.2, entry 7). This represents a significant improvement of the reaction efficiency, compared with the one using the conventional heating source. The sulfonyl tetrazole **28** was then reacted with the nucleophilic PBG alkoxide, providing the 1,5-tetrazole-linked compound **29** in 79% yield (89% for each displacement, Fig. 3.21).

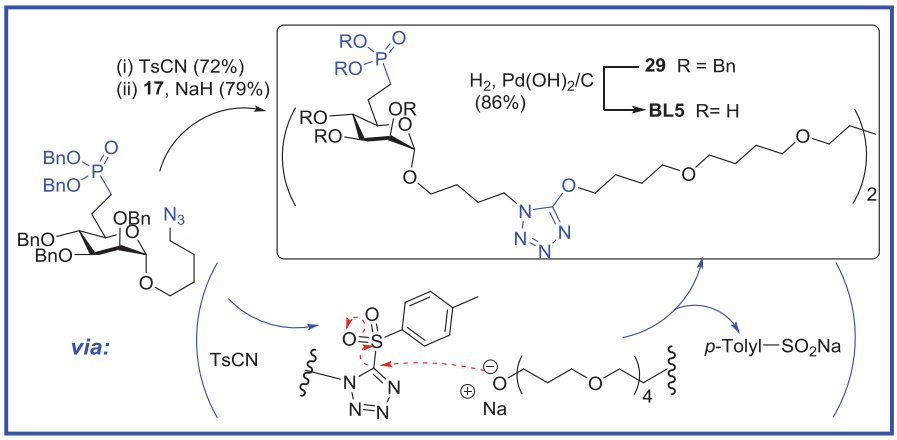

Figure 3.21: Demko-Sharpless azide-nitrile cycloaddition/S_NAr sequence

C. Binding Affinity Assay

All the protected bis-phosphonate compounds (**24**, **25**, **26**, **27**, **29**) were subjected to the final global deprotection step, to afford the active ligands (**BL1** – **BL5**) for the binding affinity assay. The assay was conducted in Prof. MacDonald's lab at the University of Nebraska Medical Center (UNMC). Thanks to Prof. MacDonald and graduate student Megan Zavorka's patient guidance, I had the opportunity to have a hands-on experience of this displacement assay.

IGF2R was previously prepared and immobilized on the cyanogen bromide-activated Sepharose resin. I^{125}-PMP-BSA, a radiolabelled high-affinity ligand, was utilized to competitively bind to the receptor. Thus, aliquots of receptor resins were incubated with I^{125}-PMP-BSA, in the presence of increasing concentrations of synthetic ligands. The mixture was agitated at 4 °C for 16 h, followed by repetitive washing with buffer. The I^{125}-PMP-BSA-bound resins were then quantified in a Perkin-Elmer WIZARD Automatic Gamma Counter. The data were converted to percent binding values by comparing with the test ligand-free controls. Then these values were plotted against the concentrations of test ligands in semi-log graphs. Nonlinear regression analysis (Prism GraphPad) was applied to estimate the best-fit curve and IC_{50} for each ligand. Relative binding affinities (RBAs) were also calculated for each compound by comparing to the IC_{50} of M6P. Each value in Table 3.3 represents the mean of at least three replicate experiments.

In addition to the binding affinities, a few molecular features of these linking functionalities are also listed in the table, particularly the ones related to the Lipinski's

rule of five[119]; namely, (i) number of hydrogen bond donors, (ii) number of hydrogen bond acceptors, (iii) molecular weight, (iv) calculated logP (of the molecules with methyl groups on each side)and (v) angle types of the two linkage bonds.

Table 3.3: Molecular features of the linkages and RBAs of the bivalent ligands

ligand	**BL1**	**BL2**	**BL3**	**BL4**	**BL5**
linkage	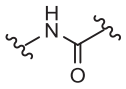	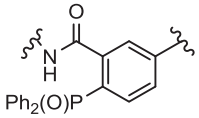	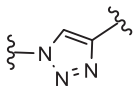	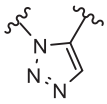	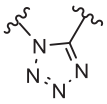
functional group	amide	amide & triphenyl phosphine oxide	1,4-triazole	1,5-triazole	1,5-tetrazole
RBA[a]	2.1	0.67	1.3	3.9	2.4
H-bond donor	1	1	0	0	0
H-bond acceptor	1	2	2	2	3
M.W.	43	319	67	67	68
clogP	-1.078	1.319	-0.261	-0.261	-0.238
angle	*linear*	*obtuse*	*obtuse*	*acute*	*acute*

[a.] Relative binding affinity was calculated by dividing the IC_{50} value for each compound by that of M6P

As seen in Table 3.3, the linkage shapes seem to have the most prominent effect on the receptor binding. 1,5-Triazole-linked **BL4** exhibited a 3-fold higher RBA than the 1,4-triazole linked **BL3**. Moreover, 1,5-tetrazole linked ligand **BL5** displayed the second strongest binding in this series. These two linkages represent the "bent" trajectory that might support the desired conformation for receptor binding. On the other hand, the amide linkage is linear and the amide linked **BL1** displayed a mediocre RBA (2.1). For the ligand **BL2**, the steric hindrance seems paramount for the receptor. While this linking functionality served well in the purpose of cell-surface engineering, the

triphenylphosphine oxide-amide linkage trailed other ligands here, exhibiting the lowest binding affinity (RBA = 0.67). It should be noted that even the best ligand **BL4** did not provide the sought-after 3 orders of magnitude higher RBA than M6P. Instead, **BL4** only showed a statistically 2-fold higher binding affinity than M6P. This implies that these bidentate ligands fail to concurrently bind two binding sites. There are many possible reasons for this result and a few of them are discussed in detail later.

D. PEG Based Bivalent Ligands

Table 3..4: Optimization of the displacement reaction of the sulfonyl tetrazole

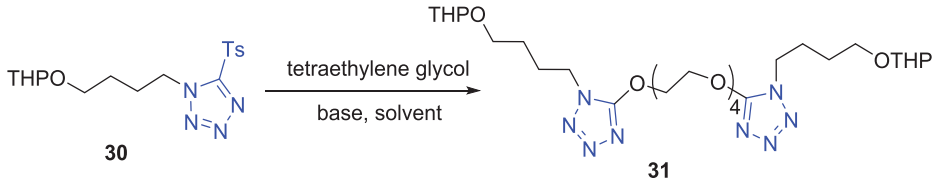

entry	base	solvent	additive	yield (%)
1	NaH	DMF	none	45
2	Ag_2O	DMF	none	0
3	PS-TBD	DMF	none	0
4	PS-BEMP	DMF	none	0
5	KHMDS	THF	none	31[a]
6	NaHMDS	toluene	none	77[a]
7	NaHMDS	toluene	crown ether	72[a]
8	KHMDS	toluene	none	87[a]

[a.] The reaction was carried out using the following procedure: To a solution of tetraethylene glycol (1 equiv.) in toluene (0.2 mmol) was added KHMDS (0.5 M in toluene, 2.1 equiv.) and additive (2.1 equiv.). After stirring at r.t. for 0.5 h, the mixture was cooled to -78°C and added to a solution of **30** (2.1 equiv) in toluene. The reaction was slowly warmed to r.t. and stirred for 8-10 h. After aqueous workup, column chromatographic purification (5% MeOH-EtOAc) yielded compound **31** as a colorless oil.

Out of this study, the newly-improved azide-cyanide cycloaddition/S_NAr ligation chemistry is one of the most interesting results. To further demonstrate the potential of this method in chemical biology, we employed it to synthesize a second generation of ligands with incrementally increasing lengths . Commercially available polyethylene glycols (PEGs) were utilized as proof of principle. Therefore, the tetrazole compound **28** was prepared in large scale under microwave conditions. The substitution reactions proceeded efficiently for the sodium alkoxides with 6,8,10 and 12 PEG units.

However, PEG-4 reacted poorly with **28** using NaH in DMF (45% yield). To improve the yield, we explored the S_NAr under various conditions. The tetrazole compound **30** was utilized as a model substrate and can be accessed readily. Then we tried an array of bases with diverse structures (Table 3.4). Ag_2O and two polystyrene-immobilized bases (PS-TBD, PS-BEMP) met with little success in facilitating the substitution. On the other hand, NaHMDS proved to be an efficient base in this reaction. The tetrazole compound **31** was produced in 77% yield in toluene (Table 3.4, entry 6). However, the yield decreases dramatically in more polar solvents such as THF or diethyl ether. This suggests that the poor solvation of the anion markedly increases its nucleophilicity, thereby accelerating this S_NAr reaction. Additionally, using KHMDS, we were able to improve the yield to 87% (Table 2.4, entry 8), which means >93% yield for each coupling. Subsequently, the optimized conditions were applied to the reaction between PEG-4 and **28**, which proceeded very efficiently as well. The tetrazoles linked, PEG-4 tethered bis-phosphonate **29** was made in 78% yield. Further deprotection of these compounds afforded a new set of ligands that could potentially measure the spatial distance between two M6P binding sites.

Nonetheless, the binding affinity assay demonstrated little to no difference among these PEG-tether ligands (Table 3.5). These results indicate that even the closest distance between two binding sites is beyond these ligands' reach. One reason is that PEGs tend to take folded conformations in aqueous medium. This phenomenon was even quantified in the recent review by Gambhir *et al*.[120] In water, the length of a PEG polymer (PEG-n) can be described in terms of the Flory radius (F), which can be calculated using equation (1).

$$F = \alpha n^{\frac{3}{5}} \qquad (1)$$

This equation proved to be practical for larger PEGs (n = 10^3 - 10^4). Herein, we applied the equation to have a rough idea of the lengths of these shorter PEG tethers. The F of PEG-12 is calculated to be around 15 Å, which falls short of the predicted distance between two binding sites (~ 30 – 50 Å).[49] Therefore, the marriage between PEG tethers and the cycloaddition/S_NAr sequence may be more useful in probing shorter distances.

Overall, ten bivalent ligands were synthesized in this study. Although they did not exhibit the sought-after binding affinities, we did gain some insights on the ligand-receptor interactions. For example, the receptor showed a notable preference for the cis-linked ligands, suggesting the rigid conformation of the native ligand is crucial for high affinity binding. Moreover, the triphenylphosphine oxide moiety was not well tolerated in the protein interactions. This indicates steric hindrance does play a role in binding this receptor, even for the monovalent interactions. The reason(s) why these ligands failed to cross-bridge IGF2R is not yet clear. In addition to their shorter lengths, there are a couple of other plausible factors. 1) These ligands are still too flexible compared with naturally-occurring oligosaccharides. The conformational dynamics of the receptor requires the ligands to be orientated in a specific way to chelate. Although we introduced heterocycles

or amide bonds as the rigid linker, the ligand can still take numerous conformations thanks to the PBG or PEG tether. Thus, the entropy penalty could simply be too high for these ligands to concomitantly bind two receptors. 2) The α-1,2-linked mannose disaccharide could be critical for high-affinity binding. As we analyze previous ligands for this receptor, it seems the oligosaccharide motif is preserved through high-binding-affinity ligands. More importantly, as seen in the crystal structure of the bovine CD-MPR (PMP-bound), the residues (D43, Y45) inside the M6P binding pocket have significant interactions with the penultimate mannoside (Fig. 3.22).[44] Therefore, to achieve high binding affinities and induce receptor dimerization, it may be important to add the second mannose to our ligand design.

Table 3.5: Synthesis of PEG-tethered ligands as spatial probes

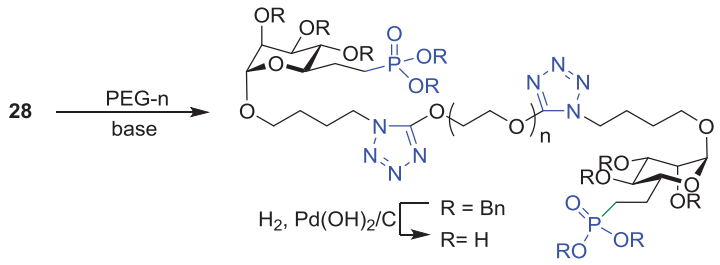

entry	Ligand	n	S_NAr (%)[a]	debenzylation yield (%)	Flory radius (Å)[b]
1	**BL6**	4	78	91	9.2
2	**BL7**	6	79	89	10.2
3	**BL8**	8	84	90	12.2
4	**BL9**	10	78	92	13.9
5	**BL10**	12	64	92	15.5

[a.] For n = 4, the yield is from the reaction in toluene using KHMDS. All other yields are from reactions in DMF with NaH. [b.] Flory radius is calculated from the equation $F = \alpha n^{3/5}$ (α = 3.5 Å for PEG).

In conclusion, we have demonstrated a way to generate diversity at the linking stage, even with the functionally dense sugar-phosphonate. One can quickly assemble a library of diverse ligands, by harnessing the versatility of an azido terminus. This is particularly useful in synthesizing peptidomimetic libraries, as all five linkages have amide or amide-mimicking character. Moreover, for the first time, the Sharpless-Demko cycloaddition/S_NAr sequence has been applied in probing the distance between two binding sites. Given the popularity of PEG spacers in multivalent ligand assembly, we believe that this strategy will find broad application in chemical biology.

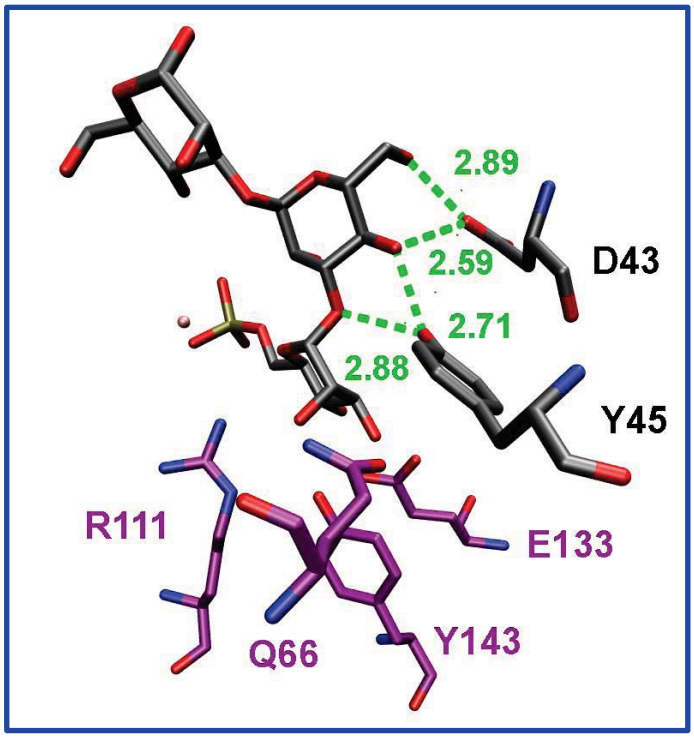

Figure 3.22: Crystal structure of bovine CD-MPR with phosphoryl pentamannoside bound. The image was rendered from IC39. Three of the pentamannose were found in the active site. The MRH domain-preserved residues interact with the terminal M6P (purple color). The penultimate mannose interacts with D43 and Y45. The antepenultimate mannose weakly interacts with Q68 (not shown here).

In the future, we can increase the rigidity of our ligands which may decrease the entropy penalty for the binding event. Oligopeptide and oligosaccharide tethers are confined structures that could be utilized in the ligand assembly. By screening a series of short peptides, we may find a ligand that takes the optimal conformation for binding. Furthermore, we should make the α-1,2-linked mannose disaccharide that is armed with phosphonate functionality and use it as the monomeric precursor to build bivalent or multivalent ligands.

III. Experimental Section

A. Organic Synthesis

Reactions were conducted under argon atmosphere using oven-dried glassware. Methylene chloride was distilled from CaH_2. THF was distilled from sodium benzophenone ketyl. MeOH was distilled from magnesium-iodide. Other reagents were obtained from commercial sources and used without further purification. Flash chromatography was performed using Merck silica gel 60 (230-400 mesh). ^{1}H NMR spectra were recorded on a Bruker-DRX-Avance 500 MHz and 400 MHz instrument with chemical shifts reported relative to residual $CHCl_3$ (7.25 ppm). Proton-decoupled ^{13}C NMR spectra were acquired on a Bruker-DRX-Avance 400 MHz and 600 MHz instrument with chemical shifts reported relative to $CDCl_3$ (77.0 ppm). ^{31}P NMR spectra were obtained on the 400 MHz instrument with chemical shifts reported relative to 85% phosphoric acid (0 ppm). Mass spectra were acquired at the Nebraska Center for Mass Spectrometry (University of Nebraska-Lincoln).

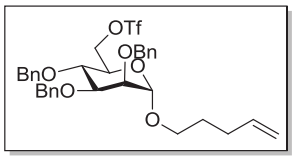

***n*-Pentenyl 2,3,4-tri-*O*-benzyl-6-*O*-trifluoromethanesulfonyl-α-D-mannopyranoside (32).** To a solution of *n*-pentenyl 2,3,4-tri-*O*-benzyl-α-D-mannopyranoside (820mg, 1.58 mmol) and 2,6-di-*tert*-butyl-4-methylpyridine (1.3g, 6.32 mmol) in CH_2Cl_2 (16 mL), was slowly added trifluoromethanesulfonic anhydride (794 μL, 4.74mmol) at -40 °C and stirring continued for 0.5 h at that temperature. The reaction mixture was then concentrated *in vacuo* and directly applied to column chromatography (8% EtOAc -

hexanes) to afford **32** (942 mg, 92%) as pale yellow oil: ^{1}H NMR (400 MHz, $CDCl_3$) δ 7.36-7.51 (m, 15H), 5.82-5.94 (m, 1H), 5.13 (dd, J = 1.6, 3.2 Hz, 1H), 5.05-5.11 (m, 1H), 4.91 (d, J = 1.6 Hz, 1H), 4.85 (d, J = 12.4 Hz, 1H), 4.78 (d, J = 12.4 Hz, 1H), 4.74 (d, J = 10.4 Hz, 1H), 4.74 (s, 2H), 4.70 (d, J = 11.2 Hz, 1H), 4.65 (dd, J =1.2, 5.2 Hz, 1H), 4.01-4.08 (m, 1H), 3.94-4.02 (m, 2H), 3.87 (dd, J = 2.4, 2.8 Hz, 1H), 3.74 (td, J = 6.8, 9.6, 1H), 3.46 (td, J = 6.4, 9.6 Hz, 1H), 2.12-2.21 (m, 2H), 1,73 (quint, J = 6.8 Hz, 2H); ^{13}C NMR (100 MHz, $CDCl_3$) δ 138.21, 138.19, 137.90, 137.87, 130.6, 129.0, 128.8, 128.6, 128.54, 128.50, 128.4, 128.3, 128.13, 128.07, 127.85, 127.84, 126.2, 126.1, 120.3 (t, $J_{C\text{-}F}$ = 318 Hz, 1C), 115.1, 113.9, 97.9, 80.1, 75.7, 75.2, 74.6, 73.7, 72.8, 72.2, 70.0, 67.3, 30.3, 28.6; ^{19}F NMR (376 MHz, $CDCl_3$) δ -74.5 (s, 3F).

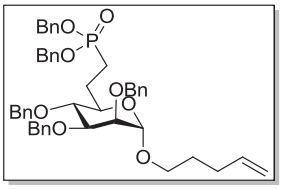

***n*-Pentenyl 6-deoxy-6-(dibenzyl)phosphonomethyl-2,3,4-tri-*O*-benzyl-α-D-mannopyranoside (14).** To a solution of triflate **32 (**942 mg, 1.45mmol) and dibenzyl methylphosphonate (1.6 g, 5.8 mmol) in THF (15 mL) at -78 °C was added slowly *n*-BuLi (3.62 mL of a 1.6 M solution in hexane, 5.8 mmol). After stirring for 20 min at -78 °C, the reaction was quenched with saturated aqueous NH_4Cl. Et_2O (100 mL) was added to dilute the solution. The organic layer was sequentially washed with NH_4Cl, water and brine, and then dried over $MgSO_4$. Filtration and evaporation gave crude product, which was purified by flash column chromatography (30-40% EtOAc-hexanes) to afford **14** (810 mg, 72%) as a colorless oil: ^{1}H NMR (400 MHz, $CDCl_3$) δ 7.26-7.43 (m, 25H), 5.75-5.85 (m, 1H), 5.09 (d, J = 8.8 Hz, 1H), 5.06 (d, J = 8 Hz, 1H), 4.97-5.04

(m, 4H), 4.95 (d, *J* = 10.8 Hz, 1H), 4.80 (d, *J* = 12.4 Hz, 1H), 4.76 (d, *J* = 1.6 Hz, 1H), 4.74 (d, *J* = 12.8 Hz, 1H), 4.66 (s, 2H), 4.62 (d, *J* = 10.8 Hz, 1H), 3.89 (dd, *J* = 2.8 Hz, 9.6 Hz, 1H), 3.79 (dd, *J* = 2 Hz, 2.8 Hz, 1H), 3.68 (t, *J* = 9.6 Hz, 1H), 3.50-3.59 (m, 2H), 3.31 (td, *J* = 6.4 Hz, 9.6 Hz, 1H), 2.11-2.30 (m, 2H), 2.00-2.11 (m, 2H), 1.70-1.92 (m, 2H), 1.62 (quint, *J* = 6.8 Hz, 2H); ^{13}C NMR (100 MHz, $CDCl_3$) δ 138.5, 138.4, 138.0, 136.5 (d, *J* = 6 Hz), 128.6, 128.5, 128.4, 128.2, 127.98, 127.95, 127.76, 127.74, 127.67, 115.1, 97.9, 80.3, 78.3, 75.4, 74.9, 72.9, 72.2, 71.4 (d, 18 Hz), 67.16, 67.09, 66.7, 30.3, 28.5, 24.7 (d, *J* = 4 Hz), 22.3 (d, *J* = 141 Hz); ^{31}P NMR (162 MHz, $CDCl_3$) δ 33.79; HRMS (ESI *m/z*) calcd for $C_{47}H_{53}O_8PNa$ ($M+Na^+$) 799.3376, obsd 799.3401.

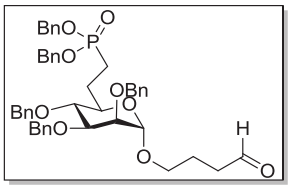

3-Formylpropyl 6-deoxy-6-(dibenzyl)phosphonomethyl 2,3,4-tri-*O*-benzyl--D-mannopyranoside (33). 14 (2.6 g, 3.35 mmol) was dissolved in 30 mL CH_2Cl_2. The solution was then cooled to -78 °C. A stream of O_3/O_2 was bubbled into the reaction mixture until the solution turned pale blue. Excess ozone was discharged by bubbling with N_2. The reaction was stirred at room temperature for 48h following addition of dimethyl sulfide (~30 equiv.). The residue obtained upon concentration was purified by flash column chromatography (20% EtOAc-hexanes) to afford **33 (**2.2 g, 85%) as a colorless oil: ^{1}H NMR (400 MHz, $CDCl_3$) δ 9.69 (t, *J* = 1.6 Hz, 1H), 7.24-7.39 (m, 25H), 5.058 (dd, *J* = 1.2 Hz, 8.8 Hz, 1H), 5.03 (dd, *J* = 1.2 Hz, 8.4 Hz, 1H), 4.99 (dd, *J* = 1.6 Hz, 8 Hz, 1H), 4.96 (dd, *J* = 1.2 Hz, 8.4 Hz, 1H), 4.92 (d, *J* = 10.8 Hz, 1H), 4.77 (d, *J* = 12.4 Hz, 1H), 4.70 (s, 1H), 4.69 (d, *J* = 12.4 Hz, 1H), 4.63 (s, 2H), 4.59 (d, *J* = 10.8 Hz, 1H), 3.80 (dd, *J* = 2.8 Hz, 8.8 Hz, 1H), 3.72 (dd, *J* = 2 Hz, 3.2 Hz, 1H), 3.64 (t, *J* = 9.6

Hz, 1H), 3.56 (td, J = 6.4 Hz, 9.6 Hz, 1H), 3.46 (dt, J = 2.4 Hz, 8.8 Hz, 1H), 3.29 (td, J = 6.4 Hz, 9.6 Hz, 1H), 2.44 (ddt, J = 1.6 Hz, 17.4 Hz, 7.2 Hz, 1H), 2.37 (ddt, J = 1.6 Hz, 17.6 Hz, 7.2 Hz, 1H), 2.11-2.24 (m, 2H), 1.68-1.88 (m, 4H); ^{13}C NMR (100 MHz, $CDCl_3$) δ 201.7, 138.4, 138.3, 136.5 (d, J = 6 Hz), 128.6, 128.4, 128.3, 128.2, 127.94, 127.91, 127.89, 127.75, 127.73, 127.6, 97.9, 80.1, 78.2, 75.4, 74.8, 75.4, 74.8, 72.9, 72.2, 71.5 (d, J = 17 Hz), 67.1, 67.0, 66.3, 40.9, 24.7 (d, J = 4 Hz), 22.2 (d, J = 141 Hz), 22.1; ^{31}P NMR (162 MHz, $CDCl_3$) δ 33.58; HRMS (ESI *m/z*) calcd for $C_{46}H_{51}O_9PNa$ ($M+Na^+$) 801.3168, obsd 801.3164.

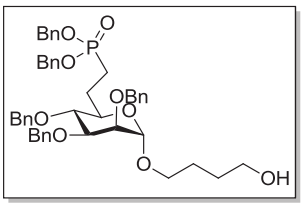

4-Hydroxybutyl 6-deoxy-6-(dibenzyl)phosphonomethyl 2,3,4-tri-*O*-benzyl--D-mannopyranoside (15). 33 (1.34 g, 1.72 mmol) was dissolved in 20 mL MeOH. $NaBH_4$ (72 mg, 1.91 mmol) was added at room temperature in one portion. The mixture was stirred for another 30 min followed by addition of saturated aqueous NH_4Cl. The solution was extracted with CH_2Cl_2 (3 × 25 mL). The organic layer was then dried over $MgSO_4$, filtered and concentrated *in vacuo*. The residue was purified by flash column chromatography (40-60% EtOAc-hexanes) to afford **15** (1.28 g, 96%) as a colorless oil: ^{1}H NMR (400 MHz, $CDCl_3$) δ 7.23-7.38 (m, 25H), 4.93-5.06 (m, 4H), 4.91 (d, J = 10.8 Hz, 1H), 4.77 (d, J = 12.4 Hz, 1H), 4.74 (d, J = 1.6 Hz, 1H), 4.70 (d, J = 12.4 Hz, 1H), 4.63 (s, 2H), 4.58 (d, J = 10.8 Hz, 1H), 3.85 (dd, J = 2.8 Hz, 8.8 Hz, 1H), 3.76 (dd, J = 2 Hz, 2.8 Hz, 1H), 3.64 (t, J = 9.2 Hz, 1H), 3.56-3.63 (m, 3H), 3.54 (dt, J = 2.4 Hz, 9.2 Hz, 1H), 3.30 (td, J = 6 Hz, 9.6 Hz, 1H), 1.98-2.25 (m, 2H), 1.71-1.88 (m, 2H), 1.51-1.67 (m, 4H); ^{13}C NMR (100 MHz, $CDCl_3$) δ 138.5, 138.3, 136.5 (d, J = 6 Hz),

128.6, 128.4, 128.3, 128.1, 127.94, 127.91, 127.89, 127.7, 127.6, 97.9, 80.3, 78.4, 75.3, 74.9, 72.9, 72.2, 71.3 (d, 16 Hz), 67.3, 67.2, 67.1, 67.0, 62.3, 29.5, 25.8, 24.8 (d, J = 5 Hz), 22.2 (d, J = 142 Hz); ^{31}P NMR (162 MHz, $CDCl_3$) δ 33.59; HRMS (ESI *m/z*) calcd for $C_{46}H_{53}O_9PNa$ ($M+Na^+$) 803.3325, obsd 803.3312.

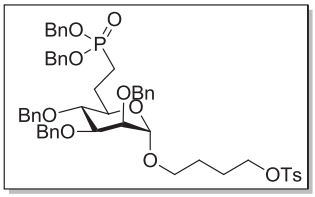

4-Tosyloxybutyl 6-deoxy-6-(dibenzyl)phosphonomethyl 2,3,4-tri-*O*-benzyl--D-mannopyranoside (34). To a solution of **15** (414 mg, 0.54 mmol) and anhydrous pyridine (172 μL, 2.2 mmol) in distilled dichloromethane (5 mL) under argon, was added *p*-toluenesulfonyl chloride (418 mg, 2.2 mmol) in one portion. The solution was stirred at room temperature overnight. Then the reaction was diluted with CH_2Cl_2 (15 mL) and sequentially washed with $NaHCO_3$, water and brine. The organic layer was dried over $MgSO_4$, filtered and concentrated. The crude product was purified by flash column chromatography (10-30% EtOAc-hexanes) to afford **34** (474 mg, 94%) as a colorless oil: ^{1}H NMR (400 MHz, $CDCl_3$) δ 7.78 (d, J = 8 Hz, 2H), 7.23-7.38 (m, 27H), 5.04 (dd, J = 0.8 Hz, 8.8 Hz, 1H), 5.01 (dd, J = 1.2 Hz, 8.8 Hz, 1H), 4.97 (d, J = 8 Hz, 1H), 4.94 (d, J = 8 Hz, 1H), 4.89 (d, J = 10.4 Hz, 1H), 4.75 (d, J = 12.4 Hz, 1H), 4.66 (d, J = 1.6 Hz, 1H), 4.67 (d, J = 12.4 Hz, 1H), 4.61 (s, 2H), 4.56 (d, J = 10.4 Hz, 1H), 3.99 (t, J = 6.4 Hz, 2H), 3.78 (dd, J = 2.8 Hz, 9.2 Hz, 1H), 3.71 (t, J = 2 Hz, 1H), 3.61 (t, J = 9.2 Hz, 1H), 3.47 (td, J = 6 Hz, 9.6 Hz, 1H), 3.40 (dt, J = 2.4 Hz, 9.2 Hz, 1H), 3.21 (td, J = 6 Hz, 9.6 Hz, 1H), 2.41 (s, 3H), 2.10-2.23 (m, 1H), 1.99-2.10 (m, 1H), 1.73-1.85 (m, 2H), 1.58-1.72 (m, 2H), 1.46-1.58 (m, 2H); ^{13}C NMR (100 MHz, $CDCl_3$) δ 144.8,

138.4, 138.3, 136.5 (d, J = 6 Hz), 133.1, 129.9, 128.6, 128.4, 128.3, 128.2, 127.93, 127.91, 127.89, 127.73, 127.69, 127.63, 97.8, 80.2, 78.2, 75.4, 74.8, 72.9, 72.2, 71.4 (d, 18 Hz), 70.2, 67.11, 67.05, 66.4, 25.9, 25.4, 24.7 (d, J = 4 Hz), 22.4 (d, J = 141 Hz), 21.7; ^{31}P NMR (162 MHz, $CDCl_3$) δ 33.59; HRMS (ESI *m/z*) calcd for $C_{53}H_{59}O_{11}PNa$ ($M+Na^+$) 957.3413, obsd 957.3403.

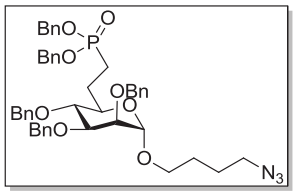

4-Azidobutyl 6-deoxy-6-(dibenzyl)phosphonomethyl 2,3,4-tri-*O*-benzyl--D-mannopyranoside (16). NaN_3 (200 mg, 3 mmol) was added to a solution of **34** (411 mg, 0.44 mmol) in DMF (5 mL) in one portion. After stirring for 12 h at room temperature, dichloromethane (40 mL) was added. The mixture was sequentially washed with saturated aqueous NH_4Cl, water and brine. The organic layer was dried over $MgSO_4$, filtered and concentrated *in vacuo.* The residue was purified by flash column chromatography (20-30% EtOAc-hexanes) to afford **16** (321 mg, 91%) as a colorless oil: ^{1}H NMR (400 MHz, $CDCl_3$) δ 7.23-7.38 (m, 25H), 5.04 (dd, J = 0.8 Hz, 9.6 Hz, 1H), 5.01 (dd, J = 0.8 Hz, 8.4 Hz, 1H), 4.98 (d, J = 8 Hz, 1H), 4.95 (d, J = 8 Hz, 1H), 4.90 (d, J = 10.8 Hz, 1H), 4.76 (d, J = 12.4 Hz, 1H), 4.70 (s, 1H), 4.69 (d, J = 12 Hz, 1H), 4.62 (s, 2H), 4.57 (d, J = 10.8 Hz, 1H), 3.82 (dd, J = 2.8 Hz, 9.2 Hz, 1H), 3.73 (t, J = 2 Hz, 1H), 3.63 (t, J = 9.2 Hz, 1H), 3.53 (td, J = 6 Hz, 9.6 Hz, 1H), 3.45 (dt, J = 2 Hz, 9.2 Hz, 1H), 3.28 (td, J = 6.4 Hz, 9.6 Hz, 1H), 3.23 (br t, J = 6.4, 2H), 2.02-2.23 (m, 2H), 1.64-1.87 (m, 2H), 1.49-1.64 (m, 4H); ^{13}C NMR (100 MHz, $CDCl_3$) δ 138.4, 138.28, 138.25, 136.5 (d, J = 6 Hz), 128.6, 128.42, 128.40, 128.3, 128.2, 127.93, 127.89, 127.73, 127.70, 127.6, 97.9, 80.2, 78.2, 75.4, 74.8, 72.9, 72.2, 71.4 (d, J = 18 Hz), 67.10, 67.04, 66.7, 51.2, 26.6, 25.9, 24.7 (d, J = 4 Hz),

22.4, 22.2 (d, J = 142 Hz); ^{31}P NMR (162 MHz, $CDCl_3$) δ 33.59; HRMS (ESI *m/z*) calcd for $C_{46}H_{52}N_3O_8PNa$ ($M+Na^+$) 828.3390, obsd 828.3395.

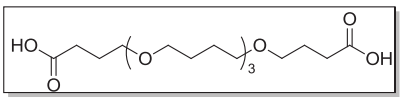

5,10,15,20-Tetraoxatetracosane-1,24-dioic acid (18). To a solution of pentabutylene glycol **17**[12] (266 mg, 0.71 mmol) in acetone (3 mL) at room temperature, Jones Reagent was added dropwise until the solution color persisted orange. After stirring for 0.5 h, the reaction was quenched with isopropanol. Water (10 mL) was added and the solution was extracted with CH_2Cl_2 (5 × 10 mL). The combined organic layer was dried over $MgSO_4$, filtered and concentrated *in vacuo.* The residue was purified by column chromatography (10% MeOH-EtOAc) to afford **18** (204 mg, 71%) as a colorless oil: ^{1}H NMR (400 MHz, $CDCl_3$) δ 8.85 (br, 2H), 3.43 (t, J = 5.6 Hz, 4H), 3.40 (br s, 12H), 2.41 (t, J = 7.2 Hz, 4H), 1.86 (app quin, J = 6.4 Hz, 4H), 1.59 (br s, 12 H); ^{13}C NMR (100 MHz, $CDCl_3$) 70.7, 70.6, 70.5, 69.5, 26.37, 26.34, 26.31, 24.8; HRMS (ESI *m/z*) calcd for $C_{20}H_{38}O_8Na$ ($M+Na^+$) 429.2464, obsd 429.2447.

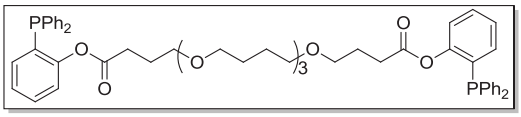

Bis(2-(diphenylphosphino)phenyl)- 5, 10,15,20-tetraoxatetracosane-1,24-dioate (21). To a solution of 2-(diphenylphosphino)phenol (178 mg, 0.53 mmol), dicarboxylic acid **18** (107 mg, 0.26 mmol) and DMAP (8 mg, 0.065 mmol) in dry CH_2Cl_2 (3 mL) was added a solution of DCC (156 mg, 0.76 mmol) in CH_2Cl_2 (1 mL) at room temperature. After stirring for 12 h, the mixture was filtered through Celite and concentrated *in vacuo.* The residue was purified by flash column chromatography (50%

EtOAc-hexanes) to afford **21** (210 mg, 87%) as a colorless oil: ^{1}H NMR (400 MHz, $CDCl_3$) δ 7.28-7.43 (m, 22H), 7.06-7.14 (m, 4H), 6.78-6.82 (m, 2H), 3.35-3.42 (m, 12H), 3.34 (t, J = 6.4 Hz, 4H), 2.33 (t, J = 7.2 Hz, 4H), 1.75 (app quin, J = 6.8 Hz, 4H), 1.59-1.63 (m, 12H); ^{13}C NMR (100 MHz, $CDCl_3$) δ 171.4, 152.8 (d, J = 17 Hz), 135.6 (d, J = 11 Hz), 134.1, 133.9, 133.7 (d, J = 2 Hz), 130.3 (d, J = 14 Hz), 129.9, 129.0, 128.62, 128.55, 126.1, 122.6 (d, J = 2 Hz), 70.64, 70.62, 70.60, 69.4, 30.8, 26.53, 26.50, 24.7; ^{31}P NMR (162 MHz, $CDCl_3$) δ -16.03; HRMS (ESI *m/z*) calcd for $C_{56}H_{64}O_8P_2Na$ ($M+Na^+$) 949.3974, obsd 949.3989.

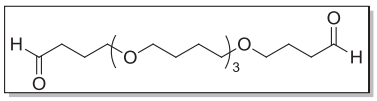

5,10,15,20-Tetraoxatetracosane-1,24-dial (19). To a solution of oxalyl chloride (582 μL, 6.67 mmol) in CH_2Cl_2 (20 mL) at -40 °C, DMSO (472 μL, 6.67 mmol) was added dropwise. Then a solution of pentabutylene glycol (1 g, 2.67 mmol) in CH_2Cl_2 (10 mL) was added slowly within 10 min. After stirring for 1 h at -40 °C, triethylamine (9.3 mL, 67 mmol) was added, followed by stirring for another 30 min. Upon completion, the reaction mixture was warmed to room temperature and poured into water (30 mL). The aqueous phase was extracted with CH_2Cl_2 (2 × 25 mL). The organic layer was dried, filtered and concentrated *in vacuo*. The residue was purified by flash column chromatography (40% EtOAc-hexanes) to afford **19** (818 mg, 82%) as a colorless oil: ^{1}H NMR (400 MHz, $CDCl_3$) δ 9.74 (t, J = 1.6 Hz, 2H), 3.40 (t, J = 6 Hz, 4H), 3.37-3.39 (m, 12H), 2.49 (dt, J = 1.6 Hz, 6.8 Hz, 4H), 1.83-1.90 (m, 4H), 1.53-1.59 (m, 12H); ^{13}C NMR (100 MHz, $CDCl_3$) δ 202.4, 70.7, 70.6, 70.5, 69.6, 41.0, 26.5, 26.4, 22.6; HRMS (ESI *m/z*) calcd for $C_{20}H_{38}O_6Na$ ($M+Na^+$) 397.2566, obsd 397.2561.

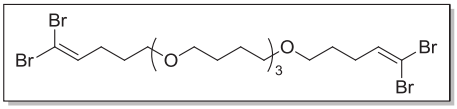

1,1,26,26-Tetrabromo-6,11,16,21-tetra-oxahexacosa-1,25-diene (35). To a solution of triphenylphosphine (1.55 g, 5.93 mmol) and tetrabromomethane (983 mg, 2.96 mmol) in CH_2Cl_2 (5 mL) at 0 °C, was added a solution of dialdehyde **19** (277 mg, 0.74 mmol) in CH_2Cl_2 (4 mL). The mixture was stirred at 0 °C for 1h followed by evaporation of the solvent. The residue was purified by flash column chromatography (10-30% EtOAc-hexanes) to afford the bis-dibromoalkene **35 (**436 mg, 86%) as a colorless oil: ^{1}H NMR (400 MHz, $CDCl_3$) δ 6.39 (t, J = 8 Hz, 2H), 3.37-3.40 (m, 16H), 2.16 (app q, J = 7.2 Hz, 4H), 1.66 (app quin, J = 6.8, 4H), 1.58-1.62 (m, 12H); ^{13}C NMR (100 MHz, $CDCl_3$) δ 138.3, 88.9, 70.8, 70.63, 70.59, 69.7, 30.0, 27.9, 26.5; HRMS (ESI *m/z*) calcd for $C_{22}H_{38}O_4Br_4Na$ ($M+Na^+$) 704.9401, obsd 704.9417.

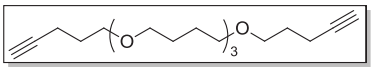

6,11,16,21-Tetraoxahexacosa-1,25-diyne (22). **35** (436 mg, 0.64 mmol) was dissolved in THF (7 mL) under argon. Then *n*-BuLi (2 mL of a 1.6 M solution in hexane, 3.2 mmol) was added at -78 °C over 2 min. After stirring for 2 h, the reaction was quenched with saturated aqueous NH_4Cl. The aqueous layer was extracted with Et_2O (2 × 15 mL). The combined organic layers were dried over MgSO4, filtered and concentrated *in vacuo.* The residue was purified by flash column chromatography (20% EtOAc-hexanes) to afford **22** (205 mg, 84%) as a colorless oil: ^{1}H NMR (400 MHz, $CDCl_3$) δ 3.48 (t, J = 6.4 Hz, 4H), 3.37-3.45 (m, 12H), 2.26 (dt, J = 2.4 Hz, 7.2 Hz, 4H), 1.92 (t, J = 2.4, 2H), 1.76 (app quin, J =

6.4 Hz, 4H), 1.57-1.67 (m, 12H); ^{13}C NMR (100 MHz, $CDCl_3$) δ 84.1, 70.7, 70.62, 70.59, 69.0, 68.4, 28.6, 26.50, 26.47, 15.3; HRMS (ESI *m/z*) calcd for $C_{22}H_{38}O_4Na$ ($M+Na^+$) 389.2668, obsd 389.2685.

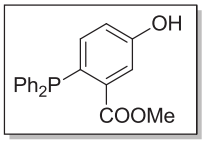

Methyl 2-(diphenylphosphino)-5-hydroxybenzoate (36). To a solution of methyl 5-hydroxy-2-iodobenzoate (5.13g, 18.4 mmol) in anhydrous degassed CH_3CN, anhydrous triethylamine (2.56 mL, 18.4 mmol), palladium(II) acetate (166 mg, 0.74 mmol) and 1,4-bis(diphenylphosphino)butane (315 mg, 0.74 mmol) were added at room temperature. Diphenylphosphine (3.2 mL, 18.4 mmol) was added to the mixture slowly via syringe upon which the solution turned deep red. The solution was heated at reflux for 4 h, after which the reaction was complete as indicated by TLC. The solution was concentrated under vacuum and the residue was purified by flash column chromarography (10% EtOAc-hexanes) to afford **36** as a white solid: ^{1}H NMR (400 MHz, $CDCl_3$) δ 7.56 (t, J = 2.8 Hz, 1H), 7.27-7.37 (m, 10H), 6.88 (dd, J = 2.8 Hz, 8.4 Hz, 1H), 6.83 (dd, J = 3.6 Hz, 8.4 Hz, 1H), 5.37 (s, 1H), 3.76 (s, 3H); ^{13}C NMR (100 MHz, $CDCl_3$) δ 167.1 (d, J = 2 Hz), 155.9, 138.2 (d, J = 11 Hz), 136.2, 135.9 (d, J = 21 Hz), 133.7 (d, J = 20 Hz), 130.8 (d, J = 23 Hz), 128.50 (d, J = 14 Hz), 128.49, 119.3, 117.7 (d, J = 3 Hz), 52.2; ^{31}P NMR (162 MHz, $CDCl_3$) δ -6.23; HRMS (ESI *m/z*) calcd for $C_{20}H_{17}O_3PNa$ ($M+Na^+$) 359.0813, obsd 359.0817.

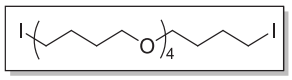

1,24-Diiodo-5,10,15,20-tetraoxatetracosane (20). To a

solution of pentabutylene glycol (580 mg, 1.5 mmol) in dry THF (10 mL), imidazole (462 mg, 6.8 mmol), triphenyl phosphine (1.60 g, 6.1 mmol) and iodine (1.56 g, 6.1 mmol) were added at room temperature. The mixture was stirred for 24 h. Then the reaction was diluted with Et_2O (50 mL) and sequentially washed with saturated $Na_2S_2O_3$ (2 × 20 mL), water (20 mL) and brine (20 mL). The organic layer was dried over $MgSO_4$, filtered and concentrated *in vacuo*. The crude product was purified by flash column chromatography (20% EtOAc-hexanes) to afford **20** (823 mg, 90%) as colorless oil: ^{1}H NMR (400 MHz, $CDCl_3$) δ 3.14-3.38 (m, 16H), 3.16 (t, J = 6.8 Hz, 4H), 1.86 (quin, J = 6.8 Hz, 4H), 1.56-1.64 (m, 16H); ^{13}C NMR (100 MHz, $CDCl_3$) δ 70.7, 70.56, 70.51, 69.4, 30.6, 30.4, 26.5, 7.0; HRMS (ESI *m/z*) calcd for $C_{20}H_{40}O_4I_2Na$ ($M+Na^+$) 621.0914, obsd 621.0892.

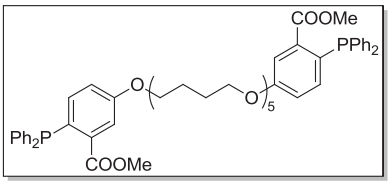

Dimethyl 5,5'-(5,10,15,20-tetraoxatetracosane-1,24-diylbis(oxy))bis(2-(diphenylphosphino)-benzoate) (23). NaH (16 mg, 0.39 mmol) was added to a solution of methyl 2-(diphenylphosphino)-5-hydroxybenzoate (120 mg, 0.36 mmol) in DMF (0.4 mL) at 0 °C. The mixture was allowed to warm to room temperature and stirred for 0.5 h, then a solution of diiodide **20** (96 mg, 0.16 mmol) in DMF (0.4 mL) was added to the reaction mixture. After stirring for 12 h, the reaction was diluted with DCM (10 mL) and quenched with saturated NH_4Cl. The organic layer was sequentially washed with saturated NH_4Cl (5 mL), water (3 × 5 mL) and brine (5 mL). The organic layer was dried over $MgSO_4$, filtered and concentrated *in vacuo*. The residue was purified by flash column chromatography (30% EtOAc-Hexanes) to afford **23** (112 mg, 69%) as a

colorless oil: ^{1}H NMR (400 MHz, $CDCl_3$) δ 7.58 (t, J = 3.2 Hz, 2H), 7.25-7.39 (m, 20H), 9.93 (dd, 2.8 Hz, 8.4 Hz, 2H), 6.85 (dd, 3.6 Hz, 8.4 Hz, 2H), 4.03 (t, 6.4 Hz, 4H), 3.77 (s, 6H), 3.49 (t, J = 6.4 Hz, 4H), 3.42-3.47 (m, 12H), 1.85-1.92 (m, 4H), 1.74-1.79 (m, 4H), 1.62-1.66 (m, 12H); ^{13}C NMR (100 MHz, $CDCl_3$) δ 167.1 (d, J = 2 Hz), 159.1, 138.4 (d, J = 12 Hz), 135.9, 135.8 (d, J = 21 Hz), 133.7 (d, J = 20 Hz), 130.6 (d, J = 22 Hz), 128.45, 128.43 (d, J = 10 Hz), 118,5, 116.3 (d, J = 4 Hz), 70.7, 70.64. 70.61, 70.3, 67.9, 52.1, 26.5, 26.3, 26.1; ^{31}P NMR (162 MHz, $CDCl_3$) δ -6.44; HRMS (ESI *m/z*) calcd for $C_{60}H_{73}O_{10}P_2$ ($M+H^+$) 1015.4679, obsd 1015.4673.

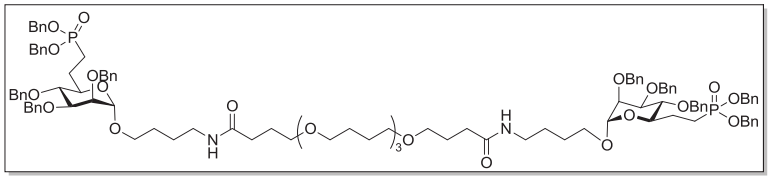

(24). Azide **16** (111mg, 0.14 mmol) and phosphine **21** (60 mg, 0.065 mmol) were dissolved in DMF/H_2O (1.4 mL, v/v = 6:1). The mixture was heated at 70 °C for 18h. The volatiles were removed under vacuum. The residue was purified by flash column chromatography (0-10% MeOH-EtOAc) to afford **24** (108 mg, 86%) as a colorless oil: ^{1}H NMR (400 MHz, $CDCl_3$) δ 7.25-7.39 (m, 50H), 5.95 (t, J = 5.2 Hz, 2H), 4.90-5.07 (m, 8H), 4.89 (d, J = 10.8 Hz, 2H), 4.75 (d, J = 12.4 Hz, 2H), 4.70 (d, J = 2 Hz, 2H), 4.69 (d, J = 12.4 Hz, 2H), 4.61 (s, 4H), 4.56 (d, J = 10.4 Hz, 2H), 3.82 (dd, J = 2.8 Hz, 9.2 Hz, 2H), 3.75 (br s, 2H), 3.62 (t, J = 9.2 Hz, 2H), 3.46-3.55 (m, 4H), 3.34-3.46 (m, 14H), 3.22-3.30 (m, 2H), 3.14-3.22 (m, 4H), 2.24 (t, J = 8.8 Hz, 4H), 2.11-2.23 (m, 6H), 1.88 (app quin, J = 7.2 Hz, 4H), 1.69-1.84 (m, 4H), 1.54-1.67 (m, 12H), 1.41-1.54 (m, 8H); ^{13}C NMR (100 MHz, $CDCl_3$) δ 172.8, 138.4, 138.31, 138.29, 136.4 (d, J = 6

Hz), 128.6, 128.38, 128.34, 128.2, 127.88, 127.86, 127.7, 127.63, 127.59, 97.9, 80.3, 78.3, 75.4, 74.8, 72.9, 72.2, 71.2 (d, J = 16 Hz), 70.7, 70.6, 69.9, 67.14, 67.10, 67.08, 67.04, 67.00, 39.1, 33.5, 26.7, 26.5, 25.8, 24.7 (d, J = 4 Hz), 22.6 (d, J = 141 Hz); ^{31}P NMR (162 MHz, $CDCl_3$) δ 33.58; HRMS (ESI m/z) calcd for $C_{114}H_{143}N_2O_{22}P_2$ ($M+H^+$) 1929.9607, obsd 1929.9567.

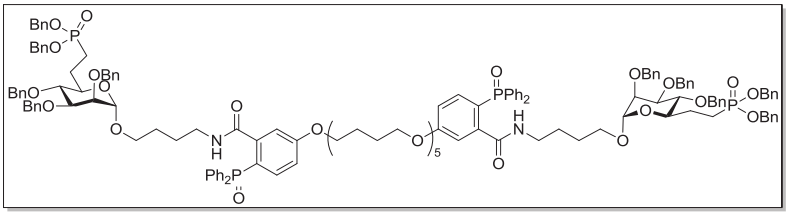

(25). A solution of the azide **16** (183 mg, 0.23 mmol) and **23** (115 mg, 0.11 mmol) in DMF/H_2O (2.1 mL, v/v = 6:1) was stirred at room temperature overnight. The reaction was concentrated and directly purified by flash column chromatography (5-10% MeOH-EtOAc) to afford **25** (183 mg, 71%) as a light yellow oil: ^{1}H NMR (400 MHz, $CDCl_3$) δ 8.84 (br s, 2H), 7.64-7.68 (m, 8H), 7.53-7.56 (m, 6H), 7.43-7.49 (m, 8H), 7.24-7.42 (m, 50H), 6.94-6.99 (m, 2H), 6.72-6.78 (m, 2H), 5.06 (d, J = 9.2 Hz, 2H), 5.03 (d, J = 8.8 Hz, 2H), 5.00 (d, J = 8.4 Hz, 2H), 4.97 (d, J = 10.8 Hz, 2H), 4.92 (d, J = 10.8 Hz, 2H), 4.77 (d, J = 12.4 Hz, 2H), 4.72 (s, 2H), 4.70 (d, J = 12.4 Hz, 2H), 4.64 (s, 4H), 4.59 (d, J = 10.8 Hz, 2H), 4.07 (t, J = 6 Hz, 4H), 3.86 (dd, J = 2.8 Hz, 9.2 Hz, 2H), 3.77 (br s, 2H), 3.64 (t, J = 9.2 Hz, 2H), 3.43-3.49 (m, 20H), 3.20 (td, J = 6 Hz, 9.6 Hz, 2H), 2.90-2.91 (m, 4H), 2.06-2.17 (m, 2H), 2.17-2.28 (m, 2H), 1.82-1.93 (m, 6H), 1.68-1.81 (m, 6H), 1.65 (br s, 12H), 1.38-1.44 (m, 8H); ^{13}C NMR (100 MHz, $CDCl_3$) δ 167.2 (d, J = 5 Hz), 162.3 (d, J = 4 Hz), 143.3 (d, J = 9 Hz), 138.5, 138.4, 136.5 (d, J = 6 Hz), 135.5 (d, J = 7 Hz), 132.2, 131.8, 131.7, 131.1, 128.8, 128.6, 128.5, 128.4, 128.3, 128.1, 127.90, 127.85,

127.65, 127.61, 127.53,120.6, 119.5, 117.3 (d, J = 10 Hz), 116.1 (d, J = 13 Hz), 97.7, 80.3, 78.2, 75.3, 74.9, 72.8, 72.1, 71.3 (d, J = 18 Hz), 70.7, 70.64, 70.61, 70.2, 68.1, 67.09, 67.0, 66.8, 39.9, 26.9, 26.5, 26.3, 25.9, 25.4, 24.7 (d, J = 4 Hz), 22.2 (d, J = 142 Hz); ^{31}P NMR (162 MHz, $CDCl_3$) δ 34.75, 33.70; HRMS (ESI *m/z*) calcd for $C_{150}H_{172}N_2O_{26}P_4Na_2$ ($M+2Na^+$) 1293.5466, obsd 1293.5475.

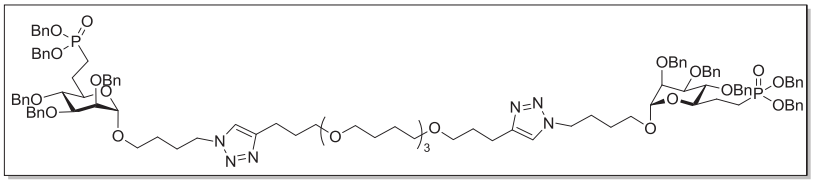

(27). To a mixture of **16** (130 mg, 0.162 mmol) and bisalkyne **22** (30 mg, 0.078 mmol) in THF/H_2O/*t*-BuOH (1 mL, v/v/v = 1:1:1) was added copper sulfate (0.2 M solution in H_2O, 155 μL, 0.031 mmol), followed by sodium ascorbate (freshly prepared 1 M solution in H_2O, 62 μL, 0.062 mmol). The reaction mixture was stirred vigorously overnight at room temperature. After completion, the volatiles were removed under vacuum and the residue was purified by flash column chromatography (0-10% MeOH-EtOAc) to afford **27** (135 mg, 88%) as a colorless oil: ^{1}H NMR (400 MHz, $CDCl_3$) δ 7.25-7.39 (m, 52H), 5.06 (dd, J = 1.2 Hz, 8.8 Hz, 2H), 5.03 (dd, J = 1.2 Hz, 8.8 Hz, 2H), 4.99 (d, J = 7.6 Hz, 2H), 4.96 (d, J = 8.8 Hz, 2H), 4.92 (d, J = 10.4 Hz, 2H), 4.78 (d, J = 12.4 Hz, 2H), 4.71 (s, 2H), 4.70 (d, J = 12.4 Hz, 2H), 4.64 (s, 4H), 4.59 (d, J = 10.4 Hz, 2H), 4.28 (t, J = 6.8 Hz, 4H), 3.82 (dd, J = 2.8 Hz, 8.8 Hz, 2H), 3.74 (t, J = 1.6 Hz, 2H), 3.64 (t, J = 9.6 Hz, 2H), 3.56 (td, J = 6 Hz, 9.6 Hz, 2H), 3.48 (t, J = 6.4 Hz, 4H), 3.43-3.50 (m, 14H), 3.27 (td, J = 6 Hz, 9.6 Hz, 2H), 2.80 (t, J = 7.2 Hz, 4H), 2.13-2.24 (m, 2H), 2.02-2.13 (m, 2H), 1.96 (app quin, J = 6.4 Hz, 4H), 1.69-1.88 (m, 8H), 1.64-1.65 (m, 12H), 1.50-1.58 (m, 4H); ^{13}C NMR (100 MHz, $CDCl_3$) δ 147.8, 138.4, 138.24, 138.22, 136.4 (d, J = 5 Hz), 128.6, 128.40, 128.38, 128.37, 128.33, 128.2, 127.90,

127.87, 127.72, 127.66, 127.62, 120.7, 97.9, 80.1, 78.2, 75.4, 74.8, 72.9, 72.2, 71.4 (d, *J* = 17 Hz), 70.69, 70.64, 70.61, 69.9, 67.12, 67.06, 66.5, 49.9, 29.5, 27.4, 26.5, 26.4, 24.7 (d, *J* = 4 Hz), 22.4, 22.2 (d, *J* = 142 Hz); ^{31}P NMR (162 MHz, $CDCl_3$) δ 33.52; HRMS (ESI m/z) calcd for $C_{114}H_{142}N_6O_{20}P_2Na$ ($M+Na^+$) 1999.9652, obsd 1999.9602.

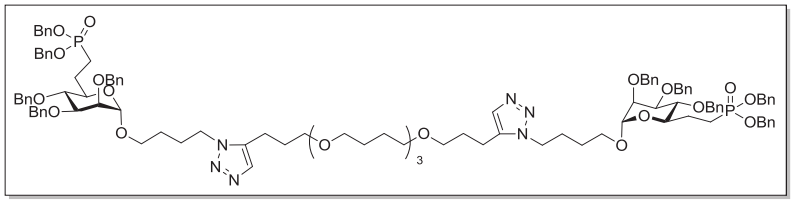

(26). A mixture of **16** (194 mg, 0.24 mmol), bisalkyne **22** (40 mg, 0.11 mmol) and Cp*RuCl(COD) (8 mg, 0.022 mmol) in THF (1 mL) was stirred at room temperature under argon for 24 h. The reaction was concentrated under vacuum and the residue was purified by flash column chromatography (0-10% MeOH-EtOAc) to afford **26** (112 mg, 52%) as a greenish oil: ^{1}H NMR (400 MHz, $CDCl_3$) δ 7.47 (s, 2H) 7.27-7.39 (m, 50H), 5.06 (d, *J* = 7.6 Hz, 2H), 5.03 (dd, *J* = 8.4 Hz, 2H), 5.00 (d, *J* = 8 Hz, 2H), 4.97 (d, *J* = 8.8 Hz, 2H), 4.92 (d, *J* = 10.4 Hz, 2H), 4.78 (d, *J* = 12.4 Hz, 2H), 4.72 (s, 2H), 4.71 (d, *J* = 12.4 Hz, 2H), 4.64 (s, 4H), 4.59 (d, *J* = 10.8 Hz, 2H), 4.22 (t, *J* = 6.8 Hz, 4H), 3.83 (dd, *J* = 2.4 Hz, 9.2 Hz, 2H), 3.76 (br s, 2H), 3.65 (t, *J* = 9.2 Hz, 2H), 3.57 (td, *J* = 6 Hz, 9.6 Hz, 2H), 3.43-3.50 (m, 18H), 3.29 (td, *J* = 6 Hz, 9.6 Hz, 2H), 2.71 (t, *J* = 7.2 Hz, 4H), 2.14-2.22 (m, 2H), 2.07-2.14 (m, 2H), 1.87-1.95 (m, 8H), 1.70-1.85 (m, 4H), 1.64 (br s, 12H), 1.50-1.58 (m, 4H); ^{13}C NMR (100 MHz, $CDCl_3$) δ 138.4, 138.3, 136.5 (d, *J* = 6 Hz), 136.4, 132.1 128.6, 128.39, 128.38, 128.33, 128.16, 127.91, 127.89, 127.86, 127.7, 127.65, 127.61, 97. 9, 80.2, 78.1, 75.4, 74.8, 72.9, 72.2, 71.4 (d, *J* = 18 Hz), 70.9, 70.7, 70.6, 69.0, 67.11, 67.05, 66.5, 47.3, 28.4, 27.0, 26.54, 26.51, 24.7 (d, *J* = 4 Hz), 22.2 (d, *J*

= 142 Hz), 19.8; ^{31}P NMR (162 MHz, $CDCl_3$) δ 33.57; HRMS (ESI *m/z*) calcd for $C_{114}H_{142}N_6O_{20}P_2Na$ ($M+Na^+$) 1999.9652, obsd 1999.9569.

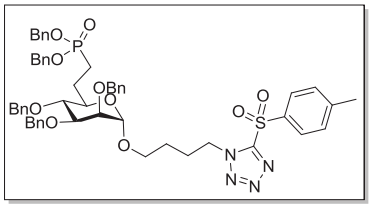

Dibenzyl (2-((2R,3S,4S,5S,6S)-3,4,5-tris(benzyloxy)-6 (4-(5-tosyl-1H-tetrazol-1-yl)butoxy)tetrahydro-2H-pyran-2-yl)ethyl)phosphonate (28). (i) Procedure with metal catalysts: Metal catalyst (20 mol%) was added to a solution of **16** (30 mg, 0.04 mmol) and *p*-toluenesulfonyl cyanide (7.4 mg, 0.04 mmol) in DCM. The mixture was kept at ~ 1 M concentration and stirred for 20 h or 48 h. Then the solvent was removed under vacuum. The crude product was purified by flash column chromatography (60% EtOAc-hexanes). The yield was given as a mixture of 1,4- and 1,5-regioisomers with the ratio determined by ^{1}H NMR. **(ii) Procedure using oil bath heating**: A vial was charged with a stir bar, *p*-toluenesulfonyl cyanide (109 mg, 0.6 mmol) and **S6** (442 mg, 0.55 mmol), and tightly capped. The reaction mixture was stirred neat at 95 °C for 20 h. The crude product was then purified as indicated above (60% EtOAc-hexanes) to afford **28** (391 mg, 72%) as the only product. **(iii) Procedure under microwave irradiation: 16** (50 mg, 0.06 mmol), *p*-toluenesulfonyl cyanide (12 mg, 0.06 mmol) and a stir bar were placed at the bottom of a CEM 10 mL vial. The vial was filled with N_2, sealed and irradiated at 95 °C using a CEM Discover® SP synthesizer. After 1 h, the vial was cooled down and the crude product was purified as indicated above to yield **28** (43 mg, 70%) as a pale yellow oil: ^{1}H NMR (400 MHz, $CDCl_3$) δ 7.99 (d, J = 8.4 Hz, 2H), 7.44 (d, J = 8 Hz, 2H), 7.22-7.41 (m, 25H), 5.06 (dd, J = 2 Hz, 9.2 Hz, 1H), 5.04 (dd, J = 1.6 Hz, 8.8 Hz, 1H), 5.00 (dd, J = 1.2 Hz, 8.8 Hz,

1H), 4.97 (dd, J = 1.6 Hz, 7.6 Hz, 1H), 4.93 (d, J = 10.8 Hz, 1H), 4.79 (d, J = 12.4 Hz, 1H), 4.68-4.76 (m, 4H), 4.66 (s, 2H), 4.60 (d, J = 10.8 Hz, 1H), 3.85 (dd, J = 2.8 Hz, 9.2 Hz, 1H), 3.80 (t, J = 2 Hz, 1H), 3.59-3.66 (m, 1H), 3.60 (t, J = 8.4 Hz, 1H), 3.50 (dt, J = 2.4 Hz, 8.8 Hz, 1H), 3.32 (td, J = 6.4 Hz, 9.6 Hz, 1H), 2.50 (s, 3H), 2.17-2.28 (m, 1H), 1.97- 2.17 (m, 3H), 1.70-1.92 (m, 2H), 1.52-1.66 (m, 2H); ^{13}C NMR (100 MHz, $CDCl_3$) δ 155.0, 147.6, 138.4, 138.3, 136.5 (d, J = 6 Hz), 134.1, 130.4, 129.3, 128.9, 128.6, 128.40, 128.39, 128.36, 128.32, 128.1, 127.91, 127.89, 127.72, 127.70, 127.6, 98.0, 80.0, 78.2, 75.3, 74.9, 72.9, 72.1, 71.5 (d, J = 17 Hz), 67.1, 67.0, 66.3, 49.7, 27.2, 26.0, 24.7 (d, J = 4 Hz), 22.2 (d, J =141 Hz), 21.9; ^{31}P NMR (162 MHz, $CDCl_3$) δ 33.53; HRMS (ESI *m/z*) calcd for $C_{54}H_{59}N_4O_{10}PSNa$ ($M+Na^+$) 1009.3587, obsd 1009.3611.

General procedure A for displacement of the sulfonyl tetrazole 28. To a stirred solution of pentabutylene glycol or polyethylene glycol (1 equiv.) in DMF (0.2 mmol) was added NaH (2.1 equiv.) in one portion. The mixture was stirred at room temperature for 30 min, and then a solution of **28** (2.1 equiv.) in DMF (0.2 mmol) was added. The resulting solution was stirred at room temperature for 12 h. Then the reaction was quenched with saturated aqueous NH_4Cl. The aqueous layer was extracted with EtOAc. The combined organic phases were dried over $MgSO_4$, filtered and concentrated under vacuum. The crude product was then purified by flash column chromatography to afford 1,5-tetrazole-linked ligands.

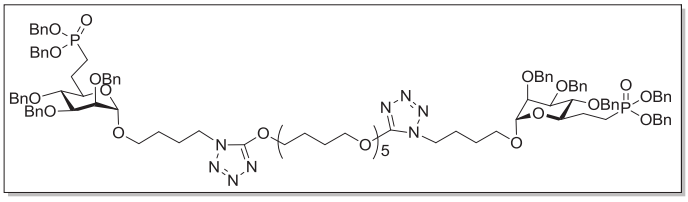

(29): Following general procedure A, with pentabutylene

glycol (22 mg, 0.057 mmol) and **28** (113 mg, 0.11 mmol), with column chromatographic purification (10% MeOH-EtOAc), was obtained compound **29** (92 mg, 79%) as a colorless oil ^{1}H NMR (400 MHz, $CDCl_3$) δ 7.24-7.41 (m, 50H), 5.06 (d, J = 8 Hz, 2H), 5.03 (d, J = 8.4 Hz, 2H), 4.99 (d, J = 8 Hz, 2H), 4.96 (d, J = 8 Hz, 2H), 4.91 (d, J = 10.8 Hz, 2H), 4.78 (d, J = 12.4 Hz, 2H), 4.71 (s, 2H), 4.70 (d, J = 11.6 Hz, 2H), 4.64 (s, 4H), 4.53-4.61 (m, 6H), 4.04 (t, J = 7.2 Hz, 4H), 3.82 (dd, J = 3.2 Hz, 9.2 Hz, 2H), 3.74 (t, J = 2.4 Hz, 2H), 3.65 (t, J = 9.6 Hz, 2H), 3.56 (td, J = 6 Hz, 9.6 Hz, 2H), 3.37-3.48 (m, 18H), 3.28 (td, J = 6 Hz, 9.6 Hz, 2H), 2.14-2.26 (m, 2H), 2.02-2.14 (m, 2H), 1.94 (quint, J = 7.2 Hz, 4H), 1.68-1.88 (m, 12H), 1.61-1.68 (m, 12H), 1.47-1.57 (m, 4H); ^{13}C NMR (100 MHz, $CDCl_3$) δ 161.1, 138.4, 138.25, 138.22, 136.5 (d, J = 6 Hz), 128.6, 128.40, 128.38, 128.37, 128.32, 128.2, 127.90, 127.87, 127.85, 127.71, 127.66, 127.61, 97.9, 80.1, 78.1, 75.4, 74.8, 73.3, 72.9, 72.2, 71.4 (d, J = 17 Hz), 70.8, 70.66, 70.59, 69.9, 67.1, 67.0, 66.3, 45.2, 26.5, 26.2, 25.90, 25.87, 27.6 (d, J = 4 Hz), 22.2 (d, J = 141 Hz); ^{31}P NMR (162 MHz, $CDCl_3$) δ 33.48; HRMS (ESI *m/z*) calcd for $C_{114}H_{144}N_8O_{22}P_2Na$ ($M+Na^+$) 2061.9768, obsd 2061.9839.

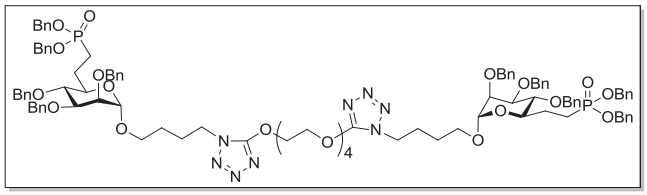

(**37**). Follow the general procedure A, with tetraethylene glycol (22 mg, 0.11 mmol) and **28** (214 mg, 0.22 mmol), with column chromatographic purification (5% MeOH-EtOAc) was obtained compound **37** (91 mg, 45%) as a colorless oil: ^{1}H NMR (600 MHz, $CDCl_3$) δ 7.41-7.20 (m, 50H), 5.04 (dd, J = 8.8, 1.9 Hz, 2H), 5.02 (dd, J = 8.7, 1.9 Hz, 2H), 4.97

(d, J = 7.8 Hz, 2H), 4.95 (d, J = 7.8 Hz, 2H), 4.90 (d, J = 10.5 Hz, 2H), 4.76 (d, J = 12.1 Hz, 2H), 4.70-4.68 (m, 3H), 4.67 (br s, 1H), 4.66-4.64 (m, 4H), 4.63 (br s, 3H), 4,62-4.69 (m, 1H), 4.57 (s, J = 10.5 Hz, 2H), 4.04 (t, J = 7.2 Hz, 4H), 3.85-3.82 (m, 4H), 3.80 (dd, J = 9.5, 3.0 Hz, 2H), 3.74-3.72 (m, 2H), 3.65-3.59 (m, 6H), 3.59-3.51 (m, 6H), 3.45 (td, J = 9.2 , 2.5Hz, 2H), 3.30-3.23 (m, 2H), 2.23-2.13 (m, 2H), 2.12-2.00 (m, 2H), 1.90-1.66 (m, 8H), 1.56-1.42 (m, 4H); ^{13}C NMR (125 MHz, $CDCl_3$) δ 161.1, 138.4, 138.29, 138.26, 136.5 (d, J = 6.6 Hz), 128.6, 128.50, 128.44, 128.42, 128.40, 128.36, 128.2, 127.94, 127.91, 127.88, 127.74, 127.70, 127.67, 127.64, 98.0, 80.1, 78.2, 75.4, 74.9, 73.0, 72.21, 72.17, 71.47 (d, J = 17.6 Hz), 70.56, 70.54. 70.52, 70.49, 68.8, 67.13, 67.09, 66.4, 45.3, 26.2, 25.9, 24.7 (d, J = 4.0 Hz), 22.2 (d, J = 142.5 Hz); ^{31}P NMR (202 MHz, $CDCl_3$) δ 34.23; HRMS (ESI *m/z*) calcd for $C_{102}H_{120}N_8O_{21}P_2Na$ $(M+Na)^+$ 1877.7741, obsd 1877.7943.

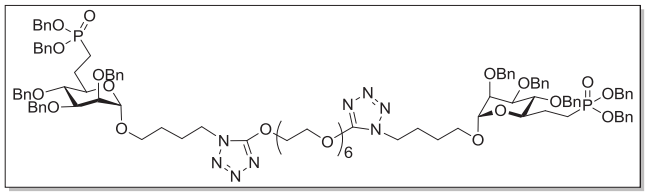

(**38**). Following general procedure A, with hexaethylene glycol (18 mg, 0.061 mmol) and **28** (122 mg, 0.12 mmol), and thin-layer chromatographic purification (10% MeOH-EtOAc), was obtained compound **38** (93 mg, 79%) as a colorless oil: ^{1}H NMR (600 MHz, $CDCl_3$) δ 7.41-7.20 (m, 50H), 5.04 (dd, J = 8.6, 1.5 Hz, 2H), 5.02 (dd, J = 8.6, 1.5 Hz, 2H), 4.98 (d, J = 7.9 Hz, 2H), 4.95 (d, J = 7.9 Hz, 2H), 4.90 (d, J = 10.5 Hz, 2H), 4.76 (d, J = 12.4 Hz, 2H), 4.71-4.67 (m, 4H), 4.68-4.64 (m, 4H), 4.63 (br s, 3H), 4.61-4.58 (m, 1H), 4.57 (s, J = 10.7 Hz, 2H), 4.05 (t, J = 7.2 Hz, 4H), 3.87-3.83 (m, 4H), 3.80 (dd, J = 9.2, 3.0 Hz, 2H), 3.74-3.71 (m, 2H), 3.66-3.57 (m, 18H), 3.57-3.51 (m, 2H), 3.44 (td, J = 9.0 , 2.7Hz,

2H), 3.30-3.23 (m, 2H), 2.22-2.13 (m, 2H), 2.12-2.01 (m, 2H), 1.90-1.66 (m, 8H), 1.57-1.43 (m, 4H); ^{13}C NMR (125 MHz, $CDCl_3$) δ 161.0, 138.3, 138.17, 138.14, 136.4 (d, J = 7.0 Hz), 128.6, 128.43, 128.41, 128.39, 128.35, 128.2, 127.93, 127.90, 127.77, 127.75, 127.66, 127.64, 97.8, 80.1, 78.1, 75.4, 74.6, 72.9, 72.15, 72.13, 71.37 (d, J = 17.8 Hz), 70.56, 70.54. 70.52, 70.49, 68.8, 67.09, 67.04, 66.3, 45.3, 26.2, 25.9, 24.6 (d, J = 4.6 Hz), 22.2 (d, J = 141.8 Hz); ^{31}P NMR (202 MHz, $CDCl_3$) δ 34.23; HRMS (ESI *m/z*) calcd for $C_{106}H_{128}N_8O_{23}P_2$2Na $(M+2Na)^{2+}$ 994.4181, obsd 994.4166.

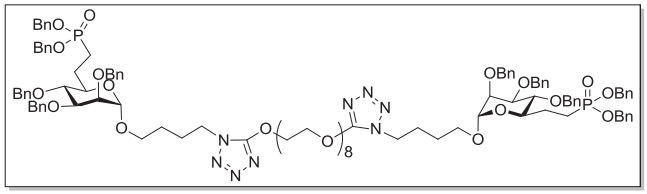

(**39**). Following general procedure A, with octaethylene glycol (22 mg, 0.06 mmol) and **28** (128 mg, 0.13 mmol), and thin layer chromatographic purification (10% MeOH-EtOAc), was obtained compound **39** (101 mg, 84%) as a colorless oil: ^{1}H NMR (400 MHz, $CDCl_3$) δ 7.24-7.43 (m, 50H), 5.06 (d, J = 12 Hz, 2H), 5.03 (d, J = 8.8 Hz, 2H), 4.99 (d, J = 8 Hz, 2H), 4.97 (d, J = 8 Hz, 2H), 4.92 (d, J = 10.8 Hz, 2H), 4.78 (d, J = 12.4 Hz, 2H), 4.56-4.74 (m, 12H), 4.59 (d, J = 10.4 Hz, 2H), 4.07 (t, J = 7.2 Hz, 4H), 3.87 (t, J = 4.4 Hz, 4H), 3.82 (dd, J = 2.8, 9.2 Hz, 2H), 3.75 (br s, 2H), 3.61-3.71 (m, 26H), 3.56 (td, J = 6, 9.6 Hz, 2H), 3.46 (t, J = 8.8 Hz, 2H), 3.29 (td, J = 6, 9.6 Hz, 2H), 2.02-2.24 (m, 4H), 1.73-1.94 (m, 8H), 1.46-1.59 (m, 4H); ^{13}C NMR (100 MHz, $CDCl_3$) δ 161.1, 138.4, 138.26, 138.23, 136.5 (d, J = 6 Hz), 128.6, 128.40, 128.39, 128.37, 128.32, 128.2, 127.91, 127.88, 127.85, 127.71, 127.67, 127.6, 97.9, 80.1, 78.1, 75.4, 74.8, 72.9, 72.21, 72.17, 71.4 (d, J = 18 Hz), 70.60. 70.58, 70.55, 69.8, 67.1, 67.0, 66.3, 45.3, 26.2, 25.9, 24.7 (d, J = 4 Hz), 22.2 (d, J

= 141 Hz); ^{31}P NMR (202 MHz, $CDCl_3$) δ 33.49; HRMS (ESI *m/z*) calcd for $C_{110}H_{137}N_8O_{25}P_2$ ($M+H^+$) 2031.9170, obsd 2031.9114.

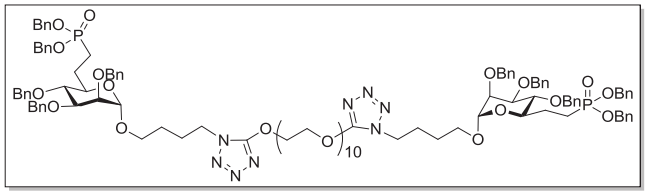

(**40**). Following general procedure A, with decaethylene glycol (28 mg, 0.061 mmol) and **28** (123 mg, 0.12 mmol), and thin-layer chromatographic purification (15% MeOH-EtOAc), was obtained compound **40** (100 mg, 78%) as a colorless oil: ^{1}H NMR (600 MHz, $CDCl_3$) δ 7.41-7.20 (m, 50H), 5.04 (dd, *J* = 8.7, 1.6 Hz, 2H), 5.02 (dd, *J* = 8.7, 1.6 Hz, 2H), 4.97 (d, *J* = 7.9 Hz, 2H), 4.95 (d, *J* = 7.9 Hz, 2H), 4.90 (d, *J* = 10.6 Hz, 2H), 4.76 (d, *J* = 12.2 Hz, 2H), 4.69 (br s, 4H), 4.68-4.65 (m, 4H), 4.63 (s, 3H), 4.62-4.58 (m, 1H), 4.57 (s, *J* = 10.9 Hz, 2H), 4.05 (t, *J* = 7.1 Hz, 4H), 3.89-3.84 (m, 4H), 3.80 (dd, *J* = 9.2, 3.1 Hz, 2H), 3.74-3.71 (m, 2H), 3.70-3.58 (m, 34H), 3.58-3.52 (m, 2H), 3.45 (td, *J* = 9.1 , 2.3Hz, 2H), 3.30-3.25 (m, 2H), 2.22-2.13 (m, 2H), 2.12-2.01 (m, 2H), 1.90-1.76 (m, 8H), 1.55-1.44 (m, 4H); ^{13}C NMR (125 MHz, $CDCl_3$) δ 161.1, 138.4, 138.28, 138.26, 136.5 (d, *J* = 6.1 Hz), 128.6, 128.41, 128.40, 128.38, 128.33, 128.2, 127.92, 127.89, 127.86, 127.72, 127.68, 127.62, 97.9, 80.1, 78.2, 75.4, 74.9, 72.9, 72.23, 72.19, 71.45 (d, *J* = 17.6 Hz), 70.63, 70.60. 70.58, 68.8, 67.10, 67.06, 66.4, 45.3, 26.2, 25.9, 24.7 (d, *J* = 4 Hz), 22.2 (d, *J* = 143 Hz); ^{31}P NMR (202 MHz, $CDCl_3$) δ 34.26; HRMS (ESI *m/z*) calcd for $C_{114}H_{144}N_8O_{27}P_23Na$ $(M+3Na)^{3+}$ 729.3103, obsd 729.3098.

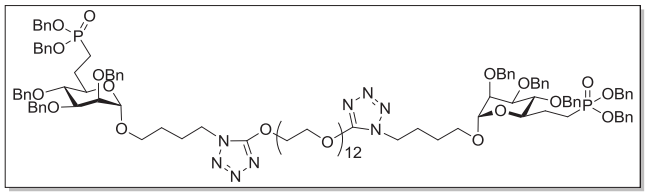

(**41**). Following general procedure A, with dodecaethylene glycol (34 mg, 0.061 mmol) and **28** (120 mg, 0.12 mmol), and thin-layer chromatographic purification (15% MeOH-EtOAc), was obtained compound **41** (85 mg, 64%) as a colorless oil: ^{1}H NMR (400 MHz, $CDCl_3$) δ 7.41-7.11 (m, 50H), 5.04 (dd, J = 9 Hz, 1.5 Hz, 2H), 5.01 (d, J = 8.8 Hz, 1.0 Hz, 2H), 4.98 (d, J = 7.9 Hz, 2H), 4.95 (d, J = 8.2 Hz, 2H), 4.90 (d, J = 10.6 Hz, 2H), 4.76 (d, J = 12.2 Hz, 2H), 4.72-4.51 (m, 14H), 4.05 (t, J = 7.3 Hz, 4H), 3.89-3.82 (m, 4H), 3.80 (dd, J = 9.1, 3.0 Hz, 2H), 3.74-3.70 (m, 2H), 3.68-3.51 (m, 42H), 3.58-3.52 (m, 2H), 3.44 (td, J = 8.8 , 2.2Hz, 2H), 3.31-3.23 (m, 2H), 2.22-1.96 (m, 4H), 1.90-1.67 (m, 8H), 1.58-1.42 (m, 4H); ^{13}C NMR (100 MHz, $CDCl_3$) δ 161.1, 138.4, 138.25, 138.23, 136.5 (d, J = 5.8 Hz), 128.6, 128.39, 128.36, 128.32, 128.2, 127.91, 127.88, 127.86, 127.7, 127.67, 127.61, 97.9, 80.1, 78.1, 75.4, 74.8, 72.9, 72.21, 72.17, 71.4 (d, J = 17.5 Hz), 70.55, 68.8, 67.1, 67.04, 66.3, 45.3, 26.2, 25.9, 24.7, 22.1 (d, J = 142Hz); ^{31}P NMR (202 MHz, $CDCl_3$) δ 34.25; HRMS (ESI *m/z*) calcd for $C_{118}H_{152}N_8O_{29}P_23Na$ $(M+3Na)^{3+}$ 758.6611, obsd 758.6596.

General procedure B for deprotection of benzyl groups: A solution of protected bis-phosphonate (~0.015 mmol) in distilled MeOH (2 mL) was stirred in the presence of 40% $Pd(OH)_2/C$ and trace amount of TFA, under balloon pressure of hydrogen, for 24 h, at room temperature. Filtration through Celite, then removal of solvent under vacuum afforded bivalent ligands **BL1 - BL10**.

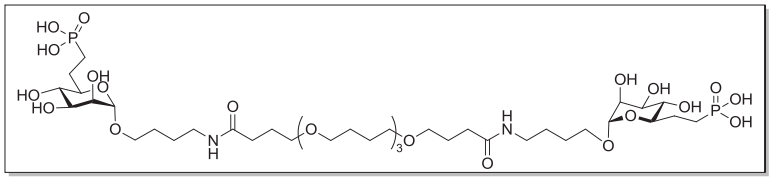

BL1: Following general procedure B, from **24** (27 mg, 0.015 mmol), bivalent ligand **BL1** (12 mg, 86%) was obtained as a colorless oil: ^{1}H NMR (400 MHz, MeOD) δ 4.71 (d, J = 1.2 Hz, 2H), 3.80 (dd, J = 1.6 Hz, 2.8 Hz, 2H), 3.71 (dt, J = 10 Hz, 6 Hz, 2H), 3.66 (dd, J = 3.2 Hz, 8.8 Hz, 2H), 3.42-3.51(m, 22H), 3.21 (t, J = 6 Hz, 4H), 2.28 (t, J = 8 Hz, 4H), 2.13-2.21 (m, 2H), 1.90-2.03 (m, 2H), 1.87 (quint, J = 6.8 Hz, 4H), 1.74-1.83 (m, 2H), 1.55-1.70 (m, 22H); ^{13}C NMR (100 MHz, MeOD) δ 174.3, 100.1, 72.4 (d, J = 12 Hz), 71.2, 70.9, 70.6, 70.31, 70.26, 69.6, 66.6, 38.8, 32.5, 26.6, 26.1 (d, J = 2 Hz), 25.9 (d, J = 133 Hz), 25.3; ^{31}P NMR (162 MHz, MeOD) δ 26.57; HRMS (ESI m/z) calcd for $C_{42}H_{82}N_2O_{22}P_2Na$ ($M+Na^+$) 1051.4732, obsd 1051.474.

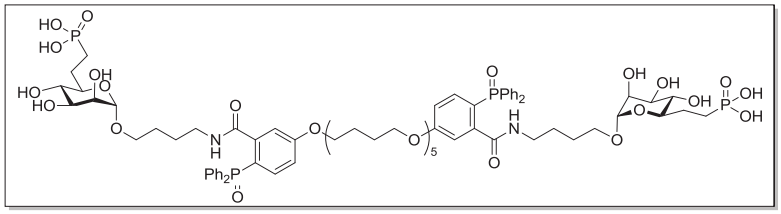

BL2: Following general procedure B, from **25** (42 mg, 0.016 mmol), bivalent ligand **BL2** (24 mg, 89%) was obtained as a colorless oil: ^{1}H NMR (400 MHz, MeOD) δ 7.61-7.73 (m, 12H), 7.48-7.59 (m, 8H), 7.38-7.49 (m, 2H), 7.23-7.31 (m, 2H), 7.11-7.17 (m, 2H), 4,47 (br s, 2H), 4.14 (t, J = 5.6 Hz, 4H), 3.81 (br, 2H), 3.61-3.71 (m, 4H), 3.51 (t, J = 6.4 Hz, 4H), 3.41-3.49 (m, 16H), 3.37 (br s, 2H), 2.87 (t, J = 6.4 Hz, 4H), 2.16-2.25 (m, 2H), 1.97-2.11 (m, 2H), 1.83-1.95 (m, 4H), 1.73-1.82 (m, 8H), 1.61-1.68 (m, 12H), 1.45-1.56 (m, 4H), 1.32-1.45 (m, 4H); ^{13}C NMR (100 MHz, MeOD) δ 169.0, 162.3, 142.0, 136.9 (d, J = 8 Hz), 132.6, 132.2, 132.1, 131.6, 131.1, 130.4, 129.3, 128.54, 128.46, 128.38, 128.26, 128.20, 128.05, 127.95, 127.92, 100.1, 72.2 (d, J = 12 Hz), 72.0,

71.3, 70.8, 70.7, 70.3, 70.25, 70.22, 69.9, 68.3, 68.2, 66.4, 66.1, 39.4, 39.2, 29.0, 26.4, 26.24, 26.16, 25.94, 25.87, 25.7, 24.8 (d, J = 3 Hz), 22.8 (d, J = 138 Hz); ^{31}P NMR (162 MHz, MeOD) δ 35.06, 30.58; HRMS (ESI m/z) calcd for $C_{80}H_{113}N_2O_{26}P4Na$ ($M+H^+$) 1641.6532, obsd 1641.6533.

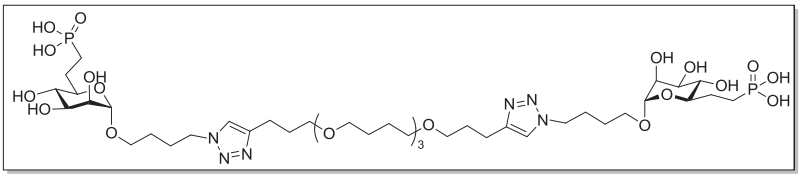

BL3: Following general procedure B, from **27** (25 mg, 0.013 mmol), bivalent ligand **BL3** (13 mg, 96%) was obtained as a colorless oil: ^{1}H NMR (400 MHz, MeOD) δ 7.73 (s, 2H), 4.53 (br, 2H), 4.28 (t, J = 6.8 Hz, 4H), 3.62 (br, 2H), 3.55 (dt, J = 9.6 Hz, 6.8 Hz, 2H), 3.42-3.50 (m, 2H), 3.22-3.33 (m, 16H), 3.14 (br, 6H), 2.64 (t, J = 7.6 Hz, 4H), 1.98-2.03 (m, 2H), 1.72-1.88 (m, 8H), 1.50-1.62 (m, 4H), 1.45 (br, 18H); ^{13}C NMR (100 MHz, MeOD) δ 122.3, 100.2, 72.1, 71.9, 71.2, 70.8, 70.6, 70.32, 70.26, 69.4, 66.4, 53.4, 50.0, 29.0, 26.9, 26.15, 26,13, 24.8 (d, J = 4 Hz), 22.2 (d, J = 128 Hz), 17.9; ^{31}P NMR (162 MHz, $CDCl_3$) δ 29.42; HRMS (ESI m/z) calcd for $C_{44}H_{82}N_6O_{20}P_2Na$ ($M+Na^+$) 1099.4957, obsd 1099.4971.

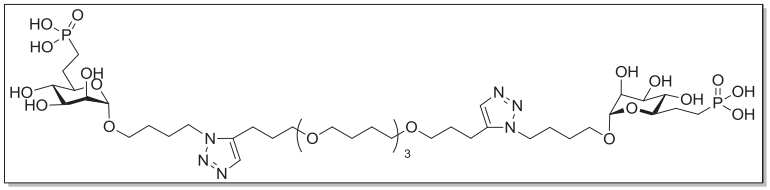

BL4: Following general procedure B, from **26** (22 mg, 0.011 mmol), bivalent ligand **BL4** (11 mg, 93%) was obtained as a colorless oil: ^{1}H NMR (400 MHz, MeOD) δ 7.41 (s, 2H), 4.56 (d, J = 1.6 Hz, 2H), 4.23 (t, J = 6.8 Hz, 4H), 3.65 (dd, J = 1.6 Hz, 3.2 Hz, 2H), 3.58 (dt, J = 10 Hz, 6 Hz, 2H), 3.49 (dd, J = 3.6 Hz, 9.2 Hz, 2H), 3.30-3.36 (m,

16H), 3.21 (br s, 2H), 3.17 (quint, J = 1.6 Hz, 4H), 2.68 (t, J = 7.6 Hz, 4H), 1,99-2.06 (m, 2H), 1.77-1.90 (m, 8H), 1.57-1.66 (m, 4H), 1.48-1.49 (m, 18H); ^{13}C NMR (100 MHz, MeOD) δ 137.7, 131.3, 100.2, 72.1, 71.9, 71.2, 70.1, 70.8, 70.6, 70.4, 70.28, 70.27, 68.8, 66.4, 28.1, 26.6, 26.20, 26.16, 24.7 (d, J = 4 Hz), 22.8 (d, J = 135 Hz), 19.2; ^{31}P NMR (162 MHz, MeOD) δ 33.57; HRMS (ESI m/z) calcd for $C_{44}H_{82}N_6O_{20}P_2Na$ ($M+Na^+$) 1099.4957, obsd 1099.4963.

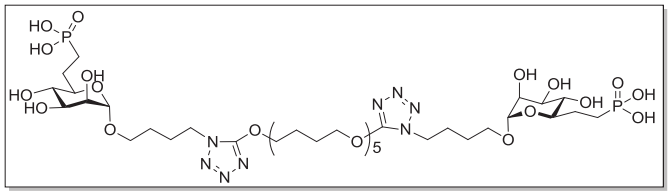

BL5: Following general procedure B, from **29** (27 mg, 0.013 mmol), bivalent ligand **BL5** (13 mg, 88%) was obtained as a colorless oil:^{1}H NMR (400 MHz, MeOD) δ 4.72 (d, J = 1.2 Hz, 2H), 4.58 (t, J = 6.5 Hz, 4H), 4.22 (t, J = 7.2 Hz, 4H), 3.79-3.82 (m, 2H), 3.74 (dt, J = 10 Hz, 6 Hz, 2H), 3.63-3.67 (m, 2H), 3.52 (t, J = 6 Hz, 4H), 3.41-3.49 (m, 18H), 2.14-2.27 (m, 4H), 1.92-2.02 (m, 8H), 1.71-1.81 (m, 8H), 1.51-1.66 (m, 16H); ^{13}C NMR (150 MHz, MeOD) δ 161.2, 100.2, 73.3, 72.0 (d, J = 17 Hz), 71.2, 70.8, 70.5, 70.34, 70.25, 69.8, 66.2, 45.1, 29.0, 26.1, 26.0, 25.6, 25.5, 24.7 (d, J = 3 Hz), 22.8 (d, J = 140 Hz); ^{31}P NMR (162 MHz, MeOD) δ 30.36; HRMS (ESI m/z) calcd for $C_{44}H_{85}N_8O_{22}P_2$ ($M+H^+$) 1139.5253, obsd 1139.5271.

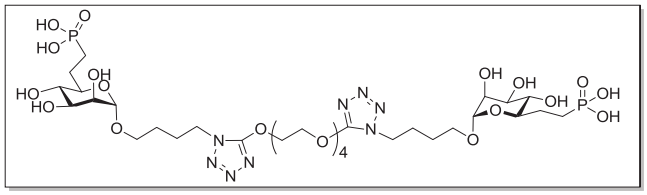

BL6: Following general procedure B, from **37** (38 mg, 0.02 mmol), bivalent ligand **BL6** (18 mg, 95%) was obtained as a colorless oil: ^{1}H NMR (600 MHz, MeOD) ; 4.71 (br, 2H), 4.69 (m, 4H),

4.22 (t, *J* = 6.8 Hz, 4H), 3.91-3.86 (m, 4H), 3.80 (br, 2H), 3.76-3.70 (m, 2H), 3.69-3.57 (m, 10H), 3.50-3.38 (m, 6H), 2.22-2.12 (m, 2H), 2.08-1.89 (m, 6H), 1.81-1.66 (m, 4H), 1.67-1.55 (m, 4H) ; ^{13}C NMR (150 MHz, MeOD) δ 162.7, 101.6, 73.8, 72.8 (d, *J* = 16.9); 72.6, 72.1, 72.0, 71.6, 69.9, 67.6, 46.5, 30.4, 27.3, 26.8, 26.3, 22.9 (d, *J* = 142.2 Hz), ^{31}P NMR (202 MHz, MeOD) δ 30.5; HRMS (ESI *m/z*) calcd for $C_{32}H_{60}N_8O_{21}P_2Na$ ($M+Na^+$) 977.3246, obsd 977.3214.

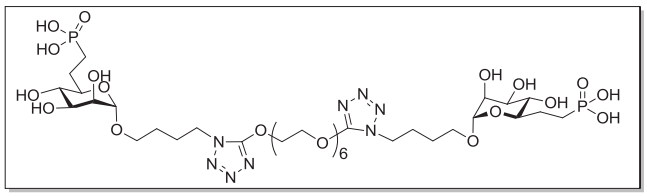

BL7: Following general procedure B, from **38** (30 mg, 0.015 mmol), bivalent ligand **BL7** (17 mg, quantitative) was obtained as a colorless oil: ^{1}H NMR (400 MHz, MeOD) 4.73-4.62 (m, 6H), 4.22 (t, *J* = 6.6 Hz, 4H), 3.93-3.86 (m, 4H), 3.79 (br s, 2H), 3.76-3.53 (m, 20H), 3.50-3.38 (m, 6H), 2.22-2.10 (m, 2H), 2.06-1.89 (m, 6H), 1.83-1.68 (m, 4H), 1.68-1.52 (m, 4H); ^{13}C NMR (150 MHz, MeOD) δ 162.7, 101.6, 73.8, 73.4 (d, *J* = 15.4 Hz), 72,6, 72.2, 71,9, 71.62, 71.56, 71.52, 69.9, 67.6, 46.5, 30.4, 27.4, 26.9, 26.2, 24.25 (d, *J* = 142.1 Hz); ^{31}P NMR (202 MHz, MeOD) δ 30.8; HRMS (ESI *m/z*) calcd for $C_{36}H_{68}N_8O_{23}P_2Na$ ($M+Na^+$) 1065.3770, obsd 1065.3770.

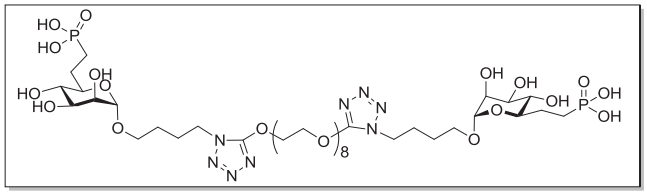

BL8: Following general procedure B, from **39** (28 mg, 0.013 mmol), bivalent ligand **BL8** (13 mg, 88%) was obtained as a colorless oil: ^{1}H NMR (400 MHz, MeOD) .72 (d, *J* = 1.2 Hz, 2H), 4.68-4.71 (m, 4H), 4.24 (t, *J* = 6.8 Hz, 4H), 3.88-3.94 (m, 4H), 3.81-3.84 (dd, *J* =

1.6 Hz, 3.2 Hz, 2H), 3.58-3.77 (m, 28H), 3.42-3.52 (m, 6H), 2.13-2.26 (m, 2H), 1.92-2.06 (m, 6H), 1.71-1.85 (m, 4H), 1.61-1.69 (m, 4H); ^{13}C NMR (100 MHz, MeOD) δ 161.3, 100.2, 72.4, 72.5 (d, J = 17.7 Hz), 71.2, 70.8, 70.5, 70.21, 70.17, 70.16, 70.11, 68.5, 66.2, 45.1, 29.0, 26.0, 25.5, 24.7 (d, J = 3.7 Hz), 22.8 (d, J = 138 Hz), 17.9; ^{31}P NMR (162 MHz, MeOD) δ 30.32; HRMS (ESI *m/z*) calcd for $C_{40}H_{77}N_8O_{25}P_2$ ($M+H^+$) 1131.4475, obsd 1131.4435.

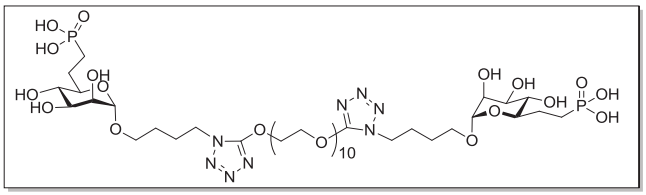

BL9: Following general procedure B, from **40** (30 mg, 0.014 mmol), bivalent ligand **BL9** (18 mg, quantitative) was obtained as a colorless oil: ^{1}H NMR (600 MHz, MeOD) 4.71 (br s, 2H), 4.70-4.66 (m, 4H), 4.22 (t, J = 6.9 Hz, 4H), 3.92-3.86 (m, 4H), 3.80 (br s, 2H), 3.76-3.53 (m, 40H), 3.48-3.40 (m, 6H), 2.22-2.12 (m, 2H), 2.06-1.83 (m, 6H), 1.83-1.68 (m, 4H), 1.68-1.58 (m, 4H); ^{13}C NMR (100 MHz, MeOD) δ 162.7, 101.6, 73.8, 73.4 (d, J = 17.7 Hz), 72.6, 72.2, 71.9, 71.61, 71.56, 71.53, 71.47, 69.9, 67.6, 46.5, 30.4, 27.4, 26.9, 26.2 (d, J = 3.7 Hz), 24.2 (d, J = 139.9) ; ^{31}P NMR (202 MHz, MeOD) δ 30.77; HRMS (ESI *m/z*) calcd for $C_{44}H_{84}N_8O_{27}P_2Na$ ($M+Na^+$) 1241.4819, obsd 1241.4832.

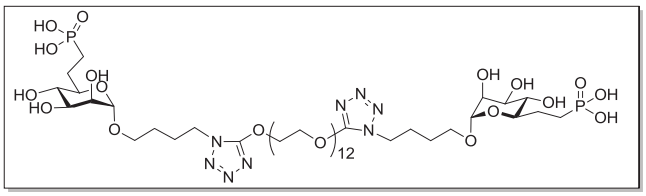

BL10: Following general procedure B, from **41** (30 mg, 0.014 mmol), bivalent ligand **BL10** (18 mg, 97%) was obtained as a colorless oil: ^{1}H NMR (400 MHz, MeOD) 4.71 (br s, 2H), 4.70-4.66 (m, 4H), 4.22 (t, J = 6.9 Hz, 4H), 3.92-3.86 (m, 4H), 3.80 (br s, 2H), 3.76-3.53 (m, 44H),

3.48-3.40 (m, 6H), 2.22-2.12 (m, 2H), 2.06-1.83 (m, 6H), 1.83-1.55 (m, 8H); ^{13}C NMR (100 MHz, MeOD) δ 162.7, 101.6, 73.8, 73.4 (d, J = 16.7), 72.6, 72.1, 71.9, 71.6, 71.5, 71.49, 71.43, 71.4, 71.36, 71.33, 69.9, 67.6, 46.5, 30.4, 27.3, 26.9, 26.2, 24.2 (d, J = 140.3) ; ^{31}P NMR (202 MHz, MeOD) δ 30.17; HRMS (ESI *m/z*) calcd for $C_{48}H_{92}N_8O_{29}P_2Na$ ($M+Na^+$) 1329.5343, obsd 1329.5331.

B. Binding Affinity Assay

Soluble bovine M6P/IGF2R was purified from fetal bovine serum (Life Technologies) according to the procedure of Byrd *et al.*[121]. The collected fractions were dialyzed to remove M6P, lyophilized to concentrate the receptor, and stored at -20°C. The purified and re-dissolved receptor was coupled to CNBr-activated Sepharose 4B resin, according to the manufacturer's instructions.

A M6P/IGF2R-Sepharose 4B resin-based radioligand displacement assay was used to evaluate the ability of each of the M6P-based ligands to bind the receptor. Aliquots (20 µL) of receptor resin (50% slurry) were incubated with 1.5 nM ^{125}I-PMP-BSA in the presence of increasing concentrations of M6P-based ligands (0.1 µM to 1 mM) in assay buffer (50 mM HEPES, pH 7.4, 0.15 M NaCl, 0.05% Triton X-100) in a volume of 0.2 ml tube, for 16 h at 4°C on an end-over-end clinical mixer. As positive and negative controls, parallel assays were done that had increasing concentrations of M6P (0.1 µM to 10 mM) or G6P (1 to 10 mM), respectively. The resin pellets were collected by centrifugation for 1 min at 9,000 x g at 4°C, and were washed with 2 x 1 mL of ice-cold buffer. The tips of the tubes with the resin pellets were cut and quantified in a WIZARD 1470 Automatic Gamma Counter (Perkin Elmer). The data were converted into

percent binding values based on comparison with the test ligand-free controls (designated as 100% radioligand binding). The competitive binding data were graphed as semi-log plots of percent binding vs. concentration of M6P, G6P, or the M6P-based ligands. Best-fit curves were generated by nonlinear regression analysis using Prism GraphPad software (San Diego, CA), which also estimated the IC_{50} values (the test ligand concentration that displaces 50% of radioligand binding). Values for relative binding affinity (RBA) for the M6P-based ligands were normalized to M6P for a given experim

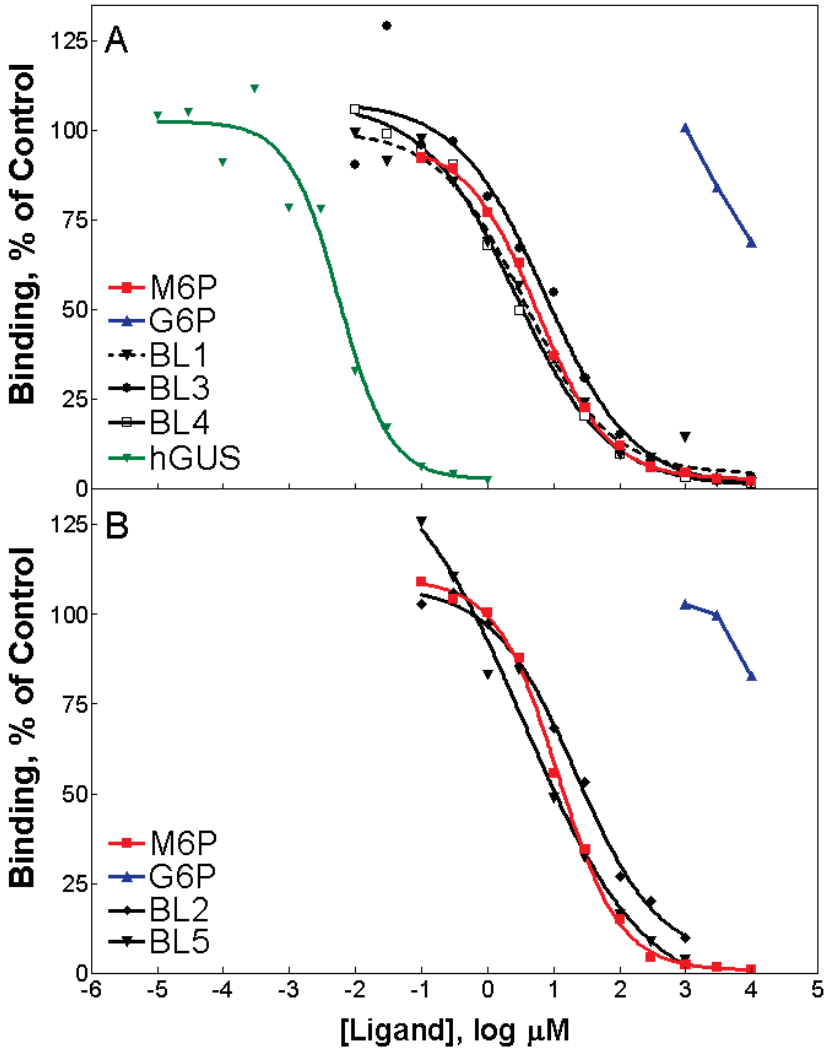

Figure 3.23 Competitive binding analysis for bivalent ligands BL1 – BL5

IV. References

1. Gabius, H.-J.; Siebert, H.-C.; Andre, S.; Jimenez-Barbero, J.; Ruediger, H., Chemical biology of the sugar code. *ChemBioChem* **2004,** *5* (6), 740-764.
2. Lis, H.; Sharon, N., Lectins as molecules and as tools. *Annual Review of Biochemistry* **1986,** *55*, 35-67.
3. Lis, H.; Sharon, N., Lectins: Carbohydrate-Specific Proteins that Mediate Cellular Recognition. *Chemical Reviews (Washington, D. C.)* **1998,** *98* (2), 637-674.
4. Nilsson Carol, L., Lectins: proteins that interpret the sugar code. *Analytical chemistry* **2003,** *75* (15), 348A-353A.
5. Sharon, N.; Lis, H., Lectins as cell recognition molecules. *Science (Washington, DC, United States)* **1989,** *246* (4927), 227-34.
6. Lee, Y. C.; Lee, R. T., Carbohydrate-Protein Interactions: Basis of Glycobiology. *Accounts of Chemical Research* **1995,** *28* (8), 321-7.
7. Genbacev, O. D.; Prakobphol, A.; Foulk, R. A.; Krtolica, A. R.; Ilic, D.; Singer, M. S.; Yang, Z.-Q.; Kiessling, L. L.; Rosen, S. D.; Fisher, S. J., Trophoblast L-Selectin-Mediated Adhesion at the Maternal-Fetal Interface. *Science (Washington, DC, U. S.)* **2003,** *299* (5605), 405-408.
8. Pang, P.-C.; Chiu, P. C. N.; Lee, C.-L.; Chang, L.-Y.; Panico, M.; Morris, H. R.; Haslam, S. M.; Khoo, K.-H.; Clark, G. F.; Yeung, W. S. B.; Dell, A., Human Sperm Binding Is Mediated by the Sialyl-Lewisx Oligosaccharide on the Zona Pellucida. *Science (Washington, DC, U. S.)* **2011,** *333* (6050), 1761-1764.

9. Clark, G. F.; Patankar, M. S.; Hinsch, K. D.; Oehninger, S., New concepts in human sperm-zona pellucida interaction. *Human reproduction (Oxford, England)* **1995,** *10 Suppl 1*, 31-7.

10. Dahms, N. M.; Hancock, M. K., P-type lectins. *Biochimica et Biophysica Acta, General Subjects* **2002,** *1572* (2-3), 317-340.

11. Helenius, A.; Aebi, M., Intracellular functions of N-linked glycans. *Science* **2001,** *291* (5512), 2364-9.

12. Dwek, R. A.; Butters, T. D.; Platt, F. M.; Zitzmann, N., Targeting glycosylation as a therapeutic approach. *Nature Reviews Drug Discovery* **2002,** *1* (1), 65-75.

13. Futerman, A. H.; van Meer, G., The cell biology of lysosomal storage disorders. *Nature Reviews Molecular Cell Biology* **2004,** *5* (7), 554-565.

14. Neufeld, E. F., Lysosomal storage diseases. *Annual Review of Biochemistry* **1991,** *60*, 257-80.

15. Kornfeld, R.; Kornfeld, S., Assembly of asparagine-linked oligosaccharides. *Annu Rev Biochem* **1985,** *54*, 631-64.

16. Rothman, J. E.; Lodish, H. F., Synchronized transmembrane insertion and glycosylation of a nascent membrane protein. *Nature (London, United Kingdom)* **1977,** *269* (5631), 775-80.

17. Chen, W.; Helenius, J.; Braakman, I.; Helenius, A., Cotranslational folding and calnexin binding during glycoprotein synthesis. *Proc Natl Acad Sci U S A* **1995,** *92* (14), 6229-33.

18. Moremen, K. W.; Trimble, R. B.; Herscovics, A., Glycosidases of the asparagine-linked oligosaccharide processing pathway. *Glycobiology* **1994,** *4* (2), 113-25.

19. Reitman, M. L.; Kornfeld, S., UDP-N-acetylglucosamine:glycoprotein N-acetylglucosamine-1-phosphotransferase. Proposed enzyme for the phosphorylation of the high mannose oligosaccharide units of lysosomal enzymes. *J Biol Chem* **1981,** *256* (9), 4275-81.

20. Mullis, K. G.; Ketcham, C. M., The synthesis of substrates and two assays for the detection of N-acetylglucosamine-1-phosphodiester alpha-N-acetylglucosaminidase (uncovering enzyme). *Anal Biochem* **1992,** *205* (2), 200-7.

21. Mullis, K. G.; Huynh, M.; Kornfeld, R. H., Purification and kinetic parameters of bovine liver N-acetylglucosamine-1-phosphodiester alpha-N-acetylglucosaminidase. *J Biol Chem* **1994,** *269* (3), 1718-26.

22. Tong, P. Y.; Kornfeld, S., Ligand interactions of the cation-dependent mannose 6-phosphate receptor. Comparison with the cation-independent mannose 6-phosphate receptor. *J Biol Chem* **1989,** *264* (14), 7970-5.

23. Watanabe, H.; Grubb, J. H.; Sly, W. S., The overexpressed human 46-kDa mannose 6-phosphate receptor mediates endocytosis and sorting of beta-glucuronidase. *Proc Natl Acad Sci U S A* **1990,** *87* (20), 8036-40.

24. Ludwig, T.; Griffiths, G.; Hoflack, B., Distribution of newly synthesized lysosomal enzymes in the endocytic pathway of normal rat kidney cells. *J Cell Biol* **1991,** *115* (6), 1561-72.

25. Storrie, B.; Desjardins, M., The biogenesis of lysosomes: is it a kiss and run, continuous fusion and fission process? *Bioessays* **1996,** *18* (11), 895-903.

26. Schweizer, A.; Kornfeld, S.; Rohrer, J., Proper sorting of the cation-dependent mannose 6-phosphate receptor in endosomes depends on a pair of aromatic amino acids in its cytoplasmic tail. *Proc Natl Acad Sci U S A* **1997,** *94* (26), 14471-6.

27. Nolan, C. M.; McCarthy, K.; Eivers, E.; Jirtle, R. L.; Byrnes, L., Mannose 6-phosphate receptors in an ancient vertebrate, zebrafish. *Dev Genes Evol* **2006,** *216* (3), 144-51.

28. Marron-Terada, P. G.; Hancock, M. K.; Haskins, D. J.; Dahms, N. M., Recognition of Dictyostelium discoideum lysosomal enzymes is conferred by the amino-terminal carbohydrate binding site of the insulin-like growth factor II/mannose 6-phosphate receptor. *Biochemistry* **2000,** *39* (9), 2243-53.

29. Nadimpalli, S. K.; Amancha, P. K., Evolution of mannose 6-phosphate receptors (MPR300 and 46): lysosomal enzyme sorting proteins. *Curr Protein Pept Sci* **2010,** *11* (1), 68-90.

30. Castonguay, A. C.; Olson, L. J.; Dahms, N. M., Mannose 6-phosphate receptor homology (MRH) domain-containing lectins in the secretory pathway. *Biochimica et Biophysica Acta, General Subjects* **2011,** *1810* (9), 815-826.

31. Satoh, T., Molecular and structural basis for sugar recognition by mannose 6-phosphate receptor homology domain-containing lectins and proteins. *Trends in Glycoscience and Glycotechnology* **2012,** *24* (139), 193-202.

32. Kim Jung-Ja, P.; Olson Linda, J.; Dahms Nancy, M., Carbohydrate recognition by the mannose-6-phosphate receptors. *Current opinion in structural biology* **2009,** *19* (5), 534-42.

33. Hu, D.; Kamiya, Y.; Totani, K.; Kamiya, D.; Kawasaki, N.; Yamaguchi, D.; Matsuo, I.; Matsumoto, N.; Ito, Y.; Kato, K.; Yamamoto, K., Sugar-binding activity of the MRH domain in the ER alpha-glucosidase II beta subunit is important for efficient glucose trimming. *Glycobiology* **2009,** *19* (10), 1127-35.

34. D'Alessio, C.; Caramelo, J. J.; Parodi, A. J., UDP-GlC:glycoprotein glucosyltransferase-glucosidase II, the ying-yang of the ER quality control. *Seminars in Cell & Developmental Biology* **2010,** *21* (5), 491-499.

35. Qian, Y.; Lee, I.; Lee, W. S.; Qian, M.; Kudo, M.; Canfield, W. M.; Lobel, P.; Kornfeld, S., Functions of the alpha, beta, and gamma subunits of UDP-GlcNAc:lysosomal enzyme N-acetylglucosamine-1-phosphotransferase. *J Biol Chem* **2010,** *285* (5), 3360-70.

36. Lee, W. S.; Payne, B. J.; Gelfman, C. M.; Vogel, P.; Kornfeld, S., Murine UDP-GlcNAc:lysosomal enzyme N-acetylglucosamine-1-phosphotransferase lacking the gamma-subunit retains substantial activity toward acid hydrolases. *J Biol Chem* **2007,** *282* (37), 27198-203.

37. Mikami, K.; Yamaguchi, D.; Tateno, H.; Hu, D.; Qin, S. Y.; Kawasaki, N.; Yamada, M.; Matsumoto, N.; Hirabayashi, J.; Ito, Y.; Yamamoto, K., The sugar-binding ability of human OS-9 and its involvement in ER-associated degradation. *Glycobiology* **2010,** *20* (3), 310-21.

38. Hosokawa, N.; Kamiya, Y.; Kamiya, D.; Kato, K.; Nagata, K., Human OS-9, a lectin required for glycoprotein endoplasmic reticulum-associated degradation, recognizes mannose-trimmed N-glycans. *J Biol Chem* **2009,** *284* (25), 17061-8.

39. Yamaguchi, D.; Hu, D.; Matsumoto, N.; Yamamoto, K., Human XTP3-B binds to alpha1-antitrypsin variant null(Hong Kong) via the C-terminal MRH domain in a glycan-dependent manner. *Glycobiology* **2010,** *20* (3), 348-55.

40. Hosokawa, N.; Wada, I.; Nagasawa, K.; Moriyama, T.; Okawa, K.; Nagata, K., Human XTP3-B forms an endoplasmic reticulum quality control scaffold with the HRD1-SEL1L ubiquitin ligase complex and BiP. *J Biol Chem* **2008,** *283* (30), 20914-24.

41. Olson, L. J.; Orsi, R.; Alculumbre, S. G.; Peterson, F. C.; Stigliano, I. D.; Parodi, A. J.; D'Alessio, C.; Dahms, N. M., Structure of the lectin mannose 6-phosphate receptor homology (MRH) domain of glucosidase II, an enzyme that regulates glycoprotein folding quality control in the endoplasmic reticulum. *J Biol Chem* **2013,** *288* (23), 16460-75.

42. Olson, L. J.; Zhang, J.; Dahms, N. M.; Kim, J. J., Twists and turns of the cation-dependent mannose 6-phosphate receptor. Ligand-bound versus ligand-free receptor. *J Biol Chem* **2002,** *277* (12), 10156-61.

43. Roberts, D. L.; Weix, D. J.; Dahms, N. M.; Kim, J. J., Molecular basis of lysosomal enzyme recognition: three-dimensional structure of the cation-dependent mannose 6-phosphate receptor. *Cell* **1998,** *93* (4), 639-48.

44. Olson, L. J.; Zhang, J.; Lee, Y. C.; Dahms, N. M.; Kim, J. J., Structural basis for recognition of phosphorylated high mannose oligosaccharides by the cation-dependent mannose 6-phosphate receptor. *J Biol Chem* **1999,** *274* (42), 29889-96.

45. Sun, G.; Zhao, H.; Kalyanaraman, B.; Dahms, N. M., Identification of residues essential for carbohydrate recognition and cation dependence of the 46-kDa mannose 6-phosphate receptor. *Glycobiology* **2005,** *15* (11), 1136-49.

46. Lobel, P.; Dahms, N. M.; Kornfeld, S., Cloning and sequence analysis of the cation-independent mannose 6-phosphate receptor. *J Biol Chem* **1988,** *263* (5), 2563-70.

47. Hancock, M. K.; Haskins, D. J.; Sun, G.; Dahms, N. M., Identification of residues essential for carbohydrate recognition by the insulin-like growth factor II/mannose 6-phosphate receptor. *J Biol Chem* **2002,** *277* (13), 11255-64.

48. Hancock, M. K.; Yammani, R. D.; Dahms, N. M., Localization of the carbohydrate recognition sites of the insulin-like growth factor II/mannose 6-phosphate receptor to domains 3 and 9 of the extracytoplasmic region. *J Biol Chem* **2002,** *277* (49), 47205-12.

49. Brown, J.; Delaine, C.; Zaccheo, O. J.; Siebold, C.; Gilbert, R. J.; van Boxel, G.; Denley, A.; Wallace, J. C.; Hassan, A. B.; Forbes, B. E.; Jones, E. Y., Structure and functional analysis of the IGF-II/IGF2R interaction. *EMBO J* **2008,** *27* (1), 265-76.

50. Brown, J.; Esnouf, R. M.; Jones, M. A.; Linnell, J.; Harlos, K.; Hassan, A. B.; Jones, E. Y., Structure of a functional IGF2R fragment determined from the anomalous scattering of sulfur. *EMBO J* **2002,** *21* (5), 1054-62.

51. Olson, L. J.; Dahms, N. M.; Kim, J. J., The N-terminal carbohydrate recognition site of the cation-independent mannose 6-phosphate receptor. *J Biol Chem* **2004,** *279* (32), 34000-9.

52. Olson, L. J.; Peterson, F. C.; Castonguay, A.; Bohnsack, R. N.; Kudo, M.; Gotschall, R. R.; Canfield, W. M.; Volkman, B. F.; Dahms, N. M., Structural basis for recognition of phosphodiester-containing lysosomal enzymes by the cation-independent mannose 6-phosphate receptor. *Proc Natl Acad Sci U S A* **2010,** *107* (28), 12493-8.

53. Olson, L. J.; Yammani, R. D.; Dahms, N. M.; Kim, J. J., Structure of uPAR, plasminogen, and sugar-binding sites of the 300 kDa mannose 6-phosphate receptor. *EMBO J* **2004,** *23* (10), 2019-28.

54. Reddy, S. T.; Chai, W.; Childs, R. A.; Page, J. D.; Feizi, T.; Dahms, N. M., Identification of a low affinity mannose 6-phosphate-binding site in domain 5 of the cation-independent mannose 6-phosphate receptor. *J Biol Chem* **2004,** *279* (37), 38658-67.

55. Bleekemolen, J. E.; Stein, M.; von Figura, K.; Slot, J. W.; Geuze, H. J., The two mannose 6-phosphate receptors have almost identical subcellular distributions in U937 monocytes. *Eur J Cell Biol* **1988,** *47* (2), 366-72.

56. Scheel, G.; Herzog, V., Mannose 6-phosphate receptor in porcine thyroid follicle cells. Localization and possible implications for the intracellular transport of thyroglobulin. *Eur J Cell Biol* **1989,** *49* (1), 140-8.

57. Klumperman, J.; Hille, A.; Veenendaal, T.; Oorschot, V.; Stoorvogel, W.; von Figura, K.; Geuze, H. J., Differences in the endosomal distributions of the two mannose 6-phosphate receptors. *J Cell Biol* **1993,** *121* (5), 997-1010.

58. Neufeld, E. F.; Sando, G. N.; Garvin, A. J.; Rome, L. H., The transport of lysosomal enzymes. *J Supramol Struct* **1977,** *6* (1), 95-101.

59. Varki, A.; Kornfeld, S., P-type Lectins. **2009**.

60. Ghosh, P.; Dahms, N. M.; Kornfeld, S., Mannose 6-phosphate receptors: new twists in the tale. *Nat Rev Mol Cell Biol* **2003,** *4* (3), 202-12.

61. Dahms, N. M.; Wick, D. A.; Brzycki-Wessell, M. A., The bovine mannose 6-phosphate/insulin-like growth factor II receptor. Localization of the insulin-like growth factor II binding site to domains 5-11. *J Biol Chem* **1994,** *269* (5), 3802-9.

62. Garmroudi, F.; Devi, G.; Slentz, D. H.; Schaffer, B. S.; MacDonald, R. G., Truncated forms of the insulin-like growth factor II (IGF-II)/mannose 6-phosphate receptor encompassing the IGF-II binding site: characterization of a point mutation that abolishes IGF-II binding. *Mol Endocrinol* **1996,** *10* (6), 642-51.

63. MacDonald, R. G.; Pfeffer, S. R.; Coussens, L.; Tepper, M. A.; Brocklebank, C. M.; Mole, J. E.; Anderson, J. K.; Chen, E.; Czech, M. P.; Ullrich, A., A single receptor binds both insulin-like growth factor II and mannose-6-phosphate. *Science* **1988,** *239* (4844), 1134-7.

64. Zumkeller, W., IGFs and IGFBPs: surrogate markers for diagnosis and surveillance of tumour growth? *Mol Pathol* **2001,** *54* (5), 285-8.

65. Jones, J. I.; Clemmons, D. R., Insulin-like growth factors and their binding proteins: biological actions. *Endocr Rev* **1995,** *16* (1), 3-34.

66. Chao, W.; D'Amore, P. A., IGF2: epigenetic regulation and role in development and disease. *Cytokine Growth Factor Rev* **2008,** *19* (2), 111-20.

67. Denley, A.; Wallace, J. C.; Cosgrove, L. J.; Forbes, B. E., The insulin receptor isoform exon 11- (IR-A) in cancer and other diseases: a review. *Horm Metab Res* **2003,** *35* (11-12), 778-85.

68. Brown, J.; Jones, E. Y.; Forbes, B. E., Interactions of IGF-II with the IGF2R/cation-independent mannose-6-phosphate receptor mechanism and biological outcomes. *Vitam Horm* **2009,** *80*, 699-719.

69. Scott, C. D.; Firth, S. M., The role of the M6P/IGF-II receptor in cancer: tumor suppression or garbage disposal? *Horm Metab Res* **2004,** *36* (5), 261-71.

70. Martin-Kleiner, I.; Gall Troselj, K., Mannose-6-phosphate/insulin-like growth factor 2 receptor (M6P/IGF2R) in carcinogenesis. *Cancer Lett* **2010,** *289* (1), 11-22.

71. Devi, G. R.; Byrd, J. C.; Slentz, D. H.; MacDonald, R. G., An insulin-like growth factor II (IGF-II) affinity-enhancing domain localized within extracytoplasmic repeat 13 of the IGF-II/mannose 6-phosphate receptor. *Mol Endocrinol* **1998,** *12* (11), 1661-72.

72. Linnell, J.; Groeger, G.; Hassan, A. B., Real time kinetics of insulin-like growth factor II (IGF-II) interaction with the IGF-II/mannose 6-phosphate receptor: the effects of domain 13 and pH. *J Biol Chem* **2001,** *276* (26), 23986-91.

73. York, S. J.; Arneson, L. S.; Gregory, W. T.; Dahms, N. M.; Kornfeld, S., The rate of internalization of the mannose 6-phosphate/insulin-like growth factor II receptor is enhanced by multivalent ligand binding. *J Biol Chem* **1999,** *274* (2), 1164-71.

74. Byrd, J. C.; MacDonald, R. G., Mechanisms for high affinity mannose 6-phosphate ligand binding to the insulin-like growth factor II/mannose 6-phosphate receptor. *J Biol Chem* **2000,** *275* (25), 18638-46.

75. Byrd, J. C.; Park, J. H.; Schaffer, B. S.; Garmroudi, F.; MacDonald, R. G., Dimerization of the insulin-like growth factor II/mannose 6-phosphate receptor. *J Biol Chem* **2000,** *275* (25), 18647-56.

76. Brown, J.; Jones, E. Y.; Forbes, B. E., Keeping IGF-II under control: lessons from the IGF-II-IGF2R crystal structure. *Trends Biochem Sci* **2009,** *34* (12), 612-9.

77. Macdonald, R. G.; Byrd, J. C., The insulin-like growth factor II/mannose 6-phosphate receptor: implications for IGF action in breast cancer. *Breast Dis* **2003,** *17*, 61-72.

78. Oates, A. J.; Schumaker, L. M.; Jenkins, S. B.; Pearce, A. A.; DaCosta, S. A.; Arun, B.; Ellis, M. J., The mannose 6-phosphate/insulin-like growth factor 2 receptor (M6P/IGF2R), a putative breast tumor suppressor gene. *Breast Cancer Res Treat* **1998,** *47* (3), 269-81.

79. Mammen, M.; Choi, S.-K.; Whitesides, G. M., Polyvalent Interactions in Biological Systems: Implications for Design and Use of Multivalent Ligands and Inhibitors. *Angewandte Chemie International Edition* **1998,** *37* (20), 2754-2794.

80. Whitty, A., Cooperativity and biological complexity. *Nat Chem Biol* **2008,** *4* (8), 435-9.

81. Kiessling, L. L.; Grim, J. C., Glycopolymer probes of signal transduction. *Chemical Society Reviews* **2013,** *42* (10), 4476-4491.

82. Lahmann, M., Architectures of multivalent glycomimetics for probing carbohydrate-lectin interactions. *Top Curr Chem* **2009,** *288*, 183-65.

83. Pieters, R. J., Maximising multivalency effects in protein-carbohydrate interactions. *Org Biomol Chem* **2009,** *7* (10), 2013-25.

84. Kiessling, L. L.; Gestwicki, J. E.; Strong, L. E., Synthetic multivalent ligands in the exploration of cell-surface interactions. *Curr Opin Chem Biol* **2000,** *4* (6), 696-703.

85. Bertozzi, C. R.; Kiessling, L. L., Chemical glycobiology. *Science* **2001,** *291* (5512), 2357-64.

86. Clemons, P. A., Design and discovery of protein dimerizers. *Curr Opin Chem Biol* **1999,** *3* (1), 112-5.

87. Christensen, M. K.; Meldal, M.; Bock, K.; Cordes, H.; Mouritsen, S.; Elsner, H., Synthesis of Glycosylated Peptide Templates Containing 6'-O-Phosphorylated Mannose Disaccharides and Their Binding to the Cation-Independent Mannose 6-Phosphate Receptor. *Journal of the Chemical Society-Perkin Transactions 1* **1994,** (10), 1299-1310.

88. Franzyk, H.; Christensen, M. K.; Joergensen, R. M.; Meldal, M.; Cordes, H.; Mouritsen, S.; Bock, K., Constrained glycopeptide ligands for MPRs. Limitations of unprotected phosphorylated building blocks. *Bioorganic & Medicinal Chemistry* **1997,** *5* (1), 21-40.

89. Distler, J. J.; Guo, J.; Jourdian, G. W.; Srivastava, O. P.; Hindsgaul, O., The binding specificity of high and low molecular weight phosphomannosyl receptors from bovine testes. Inhibition studies with chemically synthesized 6-O-

phosphorylated oligomannosides. *Journal of Biological Chemistry* **1991,** *266* (32), 21687-92.

90. Liu, Y. P.; Chan, Y. M.; Wu, J. H.; Chen, C.; Benesi, A.; Hu, J.; Wang, Y. M.; Chen, G., Chemical Synthesis of a Bisphosphorylated Mannose-6-Phosphate N-Glycan and its Facile Monoconjugation with Human Carbonic Anhydrase II for in vivo Fluorescence Imaging. *Chembiochem* **2011,** *12* (5), 685-690.

91. Song, X. Z.; Lasanajak, Y.; Olson, L. J.; Boonen, M.; Dahms, N. M.; Kornfeld, S.; Cummings, R. D.; Smith, D. F., Glycan Microarray Analysis of P-type Lectins Reveals Distinct Phosphomannose Glycan Recognition. *Journal of Biological Chemistry* **2009,** *284* (50), 35201-35214.

92. Vidil, C.; Morere, A.; Garcia, M.; Barragan, V.; Hamdaoui, B.; Rochefort, H.; Montero, J. L., Synthesis and biological activity of phosphonate analogs of mannose 6-phosphate (M6P). *European Journal of Organic Chemistry* **1999,** (2), 447-450.

93. Berkowitz, D. B.; Maiti, G.; Charette, B. D.; Dreis, C. D.; MacDonald, R. G., Mono- and bivalent ligands bearing mannose 6-phosphate (M6P) surrogates: Targeting the M6P/insulin-like growth factor II receptor. *Organic Letters* **2004,** *6* (26), 4921-4924.

94. Fei, X.; Connelly, C. M.; MacDonald, R. G.; Berkowitz, D. B., A set of phosphatase-inert "molecular rulers" to probe for bivalent mannose 6-phosphate ligand-receptor interactions. *Bioorganic & Medicinal Chemistry Letters* **2008,** *18* (10), 3085-3089.

95. Niedballa, U.; Vorbrüggen, H., A General Synthesis of Pyrimidine Nucleosides. *Angewandte Chemie International Edition in English* **1970,** *9* (6), 461-462.

96. Chatterjee, A. K.; Choi, T. L.; Sanders, D. P.; Grubbs, R. H., A general model for selectivity in olefin cross metathesis. *J Am Chem Soc* **2003,** *125* (37), 11360-70.

97. LeBowitz, J. H.; Grubb, J. H.; Maga, J. A.; Schmiel, D. H.; Vogler, C.; Sly, W. S., Glycosylation-independent targeting enhances enzyme delivery to lysosomes and decreases storage in mucopolysaccharidosis type VII mice. *Proc Natl Acad Sci U S A* **2004,** *101* (9), 3083-8.

98. Gestwicki, J. E.; Cairo, C. W.; Strong, L. E.; Oetjen, K. A.; Kiessling, L. L., Influencing receptor-ligand binding mechanisms with multivalent ligand architecture. *J Am Chem Soc* **2002,** *124* (50), 14922-33.

99. Fasting, C.; Schalley, C. A.; Weber, M.; Seitz, O.; Hecht, S.; Koksch, B.; Dernedde, J.; Graf, C.; Knapp, E. W.; Haag, R., Multivalency as a Chemical Organization and Action Principle. *Angewandte Chemie-International Edition* **2012,** *51* (42), 10472-10498.

100. Kiessling, L. L.; Pohl, N. L., Strength in numbers: non-natural polyvalent carbohydrate derivatives. *Chem Biol* **1996,** *3* (2), 71-7.

101. Cairo, C. W.; Gestwicki, J. E.; Kanai, M.; Kiessling, L. L., Control of multivalent interactions by binding epitope density. *J Am Chem Soc* **2002,** *124* (8), 1615-9.

102. Kolb, H. C.; Sharpless, K. B., The growing impact of click chemistry on drug discovery. *Drug Discov Today* **2003,** *8* (24), 1128-37.

103. Kalia, J.; Raines, R. T., Advances in Bioconjugation. *Current Organic Chemistry* **2010,** *14* (2), 138-147.

104. Braese, S.; Friedrich, A.; Gartner, M.; Schroeder, T., Cycloaddition reactions of azides including bioconjugation. *Top. Heterocycl. Chem.* **2008,** *12* (Synthesis of Heterocycles via Cycloadditions I), 45-115.

105. Knuf, E. C.; Jiang, J. K.; Gin, M. S., Preparation of discrete oligoethers: Synthesis of pentabutylene glycol and hexapropylene glycol by two complementary methods. *Journal of Organic Chemistry* **2003,** *68* (23), 9166-9169.

106. Saxon, E.; Bertozzi, C. R., Cell surface engineering by a modified Staudinger reaction. *Science* **2000,** *287* (5460), 2007-2010.

107. Saxon, E.; Armstrong, J. I.; Bertozzi, C. R., A "traceless" Staudinger ligation for the chemoselective synthesis of amide bonds. *Org Lett* **2000,** *2* (14), 2141-3.

108. Lin, F. L.; Hoyt, H. M.; van Halbeek, H.; Bergman, R. G.; Bertozzi, C. R., Mechanistic investigation of the staudinger ligation. *J Am Chem Soc* **2005,** *127* (8), 2686-95.

109. Laughlin, S. T.; Bertozzi, C. R., Metabolic labeling of glycans with azido sugars and subsequent glycan-profiling and visualization via Staudinger ligation. *Nat Protoc* **2007,** *2* (11), 2930-44.

110. Kiick, K. L.; Saxon, E.; Tirrell, D. A.; Bertozzi, C. R., Incorporation of azides into recombinant proteins for chemoselective modification by the Staudinger ligation. *Proc Natl Acad Sci U S A* **2002,** *99* (1), 19-24.

111. Shangguan, N.; Katukojvala, S.; Greenberg, R.; Williams, L. J., The reaction of thio acids with azides: a new mechanism and new synthetic applications. *J Am Chem Soc* **2003,** *125* (26), 7754-5.

112. Moses, J. E.; Moorhouse, A. D., The growing applications of click chemistry. *Chem Soc Rev* **2007,** *36* (8), 1249-62.

113. Zhang, L.; Chen, X. G.; Xue, P.; Sun, H. H. Y.; Williams, I. D.; Sharpless, K. B.; Fokin, V. V.; Jia, G. C., Ruthenium-catalyzed cycloaddition of alkynes and organic azides. *Journal of the American Chemical Society* **2005,** *127* (46), 15998-15999.

114. Boren, B. C.; Narayan, S.; Rasmussen, L. K.; Zhang, L.; Zhao, H.; Lin, Z.; Jia, G.; Fokin, V. V., Ruthenium-catalyzed azide-alkyne cycloaddition: scope and mechanism. *J Am Chem Soc* **2008,** *130* (28), 8923-30.

115. Zhang, J.; Kemmink, J.; Rijkers, D. T.; Liskamp, R. M., Cu(I)- and Ru(II)-mediated "click" cyclization of tripeptides toward vancomycin-inspired mimics. *Org Lett* **2011,** *13* (13), 3438-41.

116. Demko, Z. P.; Sharpless, K. B., A click chemistry approach to tetrazoles by Huisgen 1,3-dipolar cycloaddition: Synthesis of 5-sulfonyl tetrazoles from azides and sulfonyl cyanides. *Angewandte Chemie-International Edition* **2002,** *41* (12), 2110-2113.

117. Fei, X., Toluenesulfonyl Cyanide (TsCN). *Synlett* **2013,** *24* (15), 2021-2022.

118. Bosch, L.; Vilarrasa, J., Cu-2(OTf)(2)-catalyzed and microwave-controlled preparation of tetrazoles from nitriles and organic azides under mild, safe conditions. *Angewandte Chemie-International Edition* **2007,** *46* (21), 3926-3930.

119. Lipinski, C. A., Lead- and drug-like compounds: the rule-of-five revolution. *Drug Discovery Today: Technologies* **2004,** *1* (4), 337-341.

120. Jokerst, J. V.; Lobovkina, T.; Zare, R. N.; Gambhir, S. S., Nanoparticle PEGylation for imaging and therapy. *Nanomedicine* **2011,** *6* (4), 715-28.

121. Byrd, J. C.; MacDonald, R. G., Mechanisms for high affinity mannose 6-phosphate ligand binding to the insulin-like growth factor II/mannose 6-phosphate receptor - Negative cooperactivity and receptor oligomerization. *Journal of Biological Chemistry* **2000,** *275* (25), 18638-18646.

V. NMR Spectra

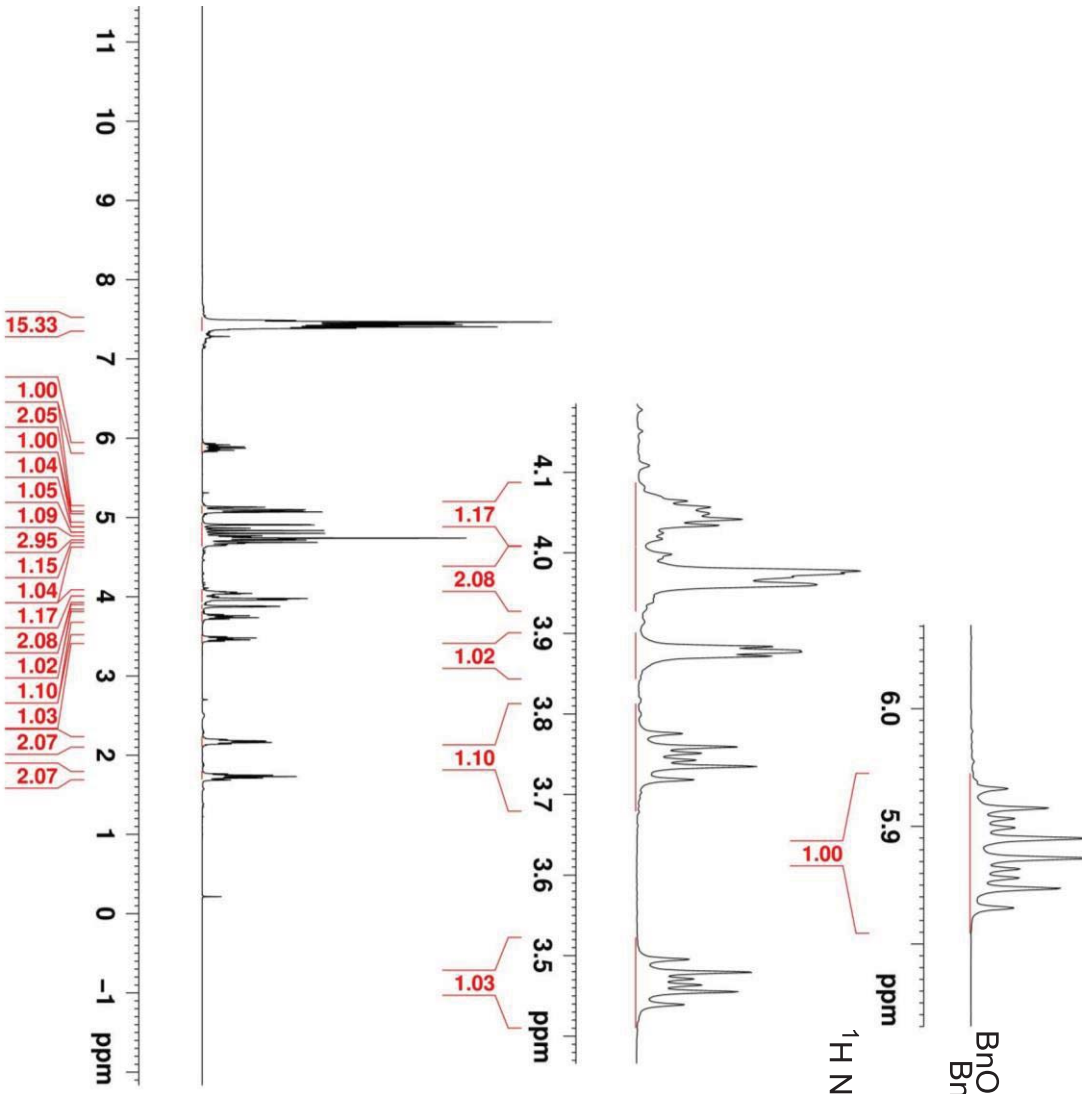

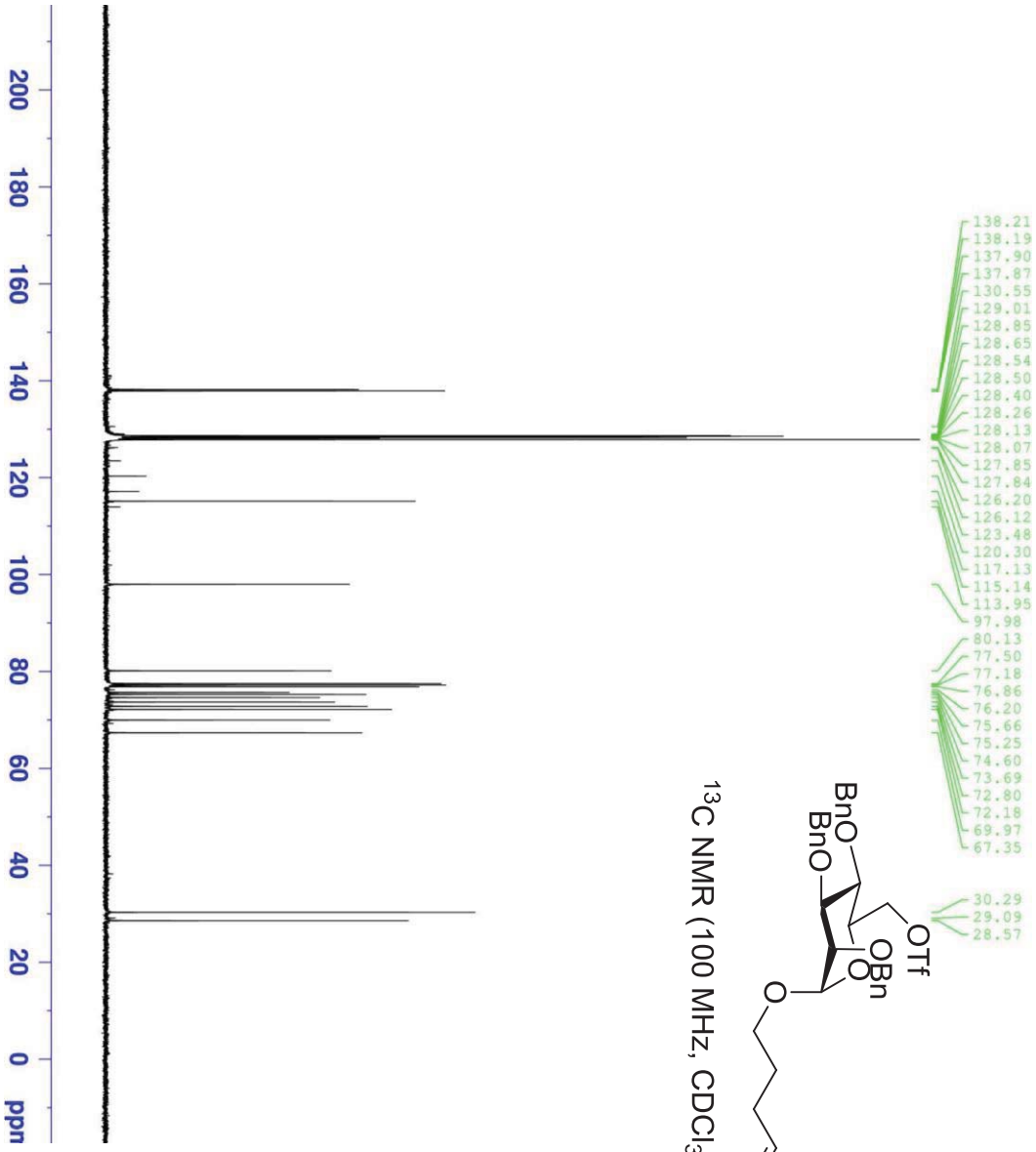

^{13}C NMR (100 MHz, $CDCl_3$)

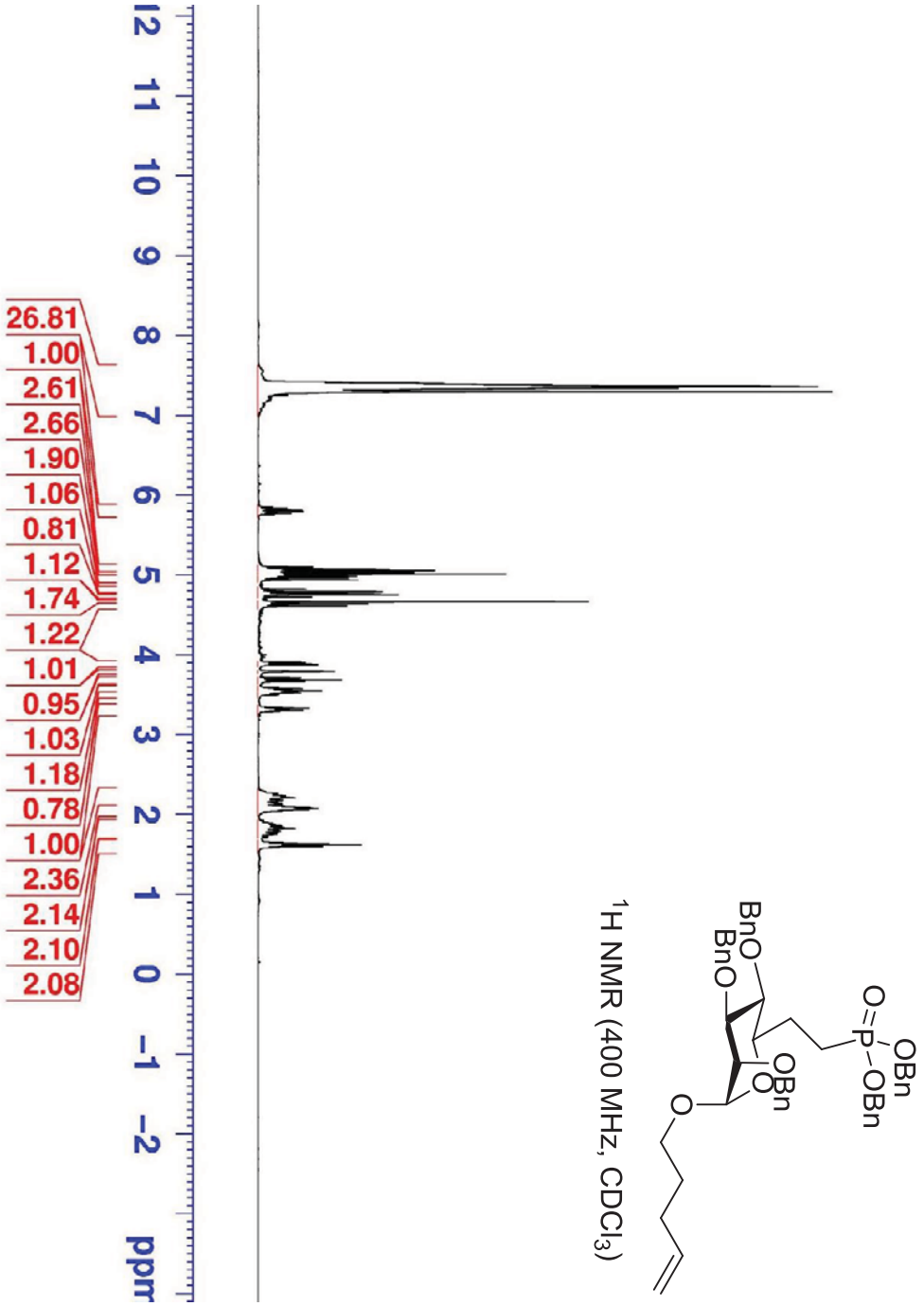

^{1}H NMR (400 MHz, $CDCl_3$)

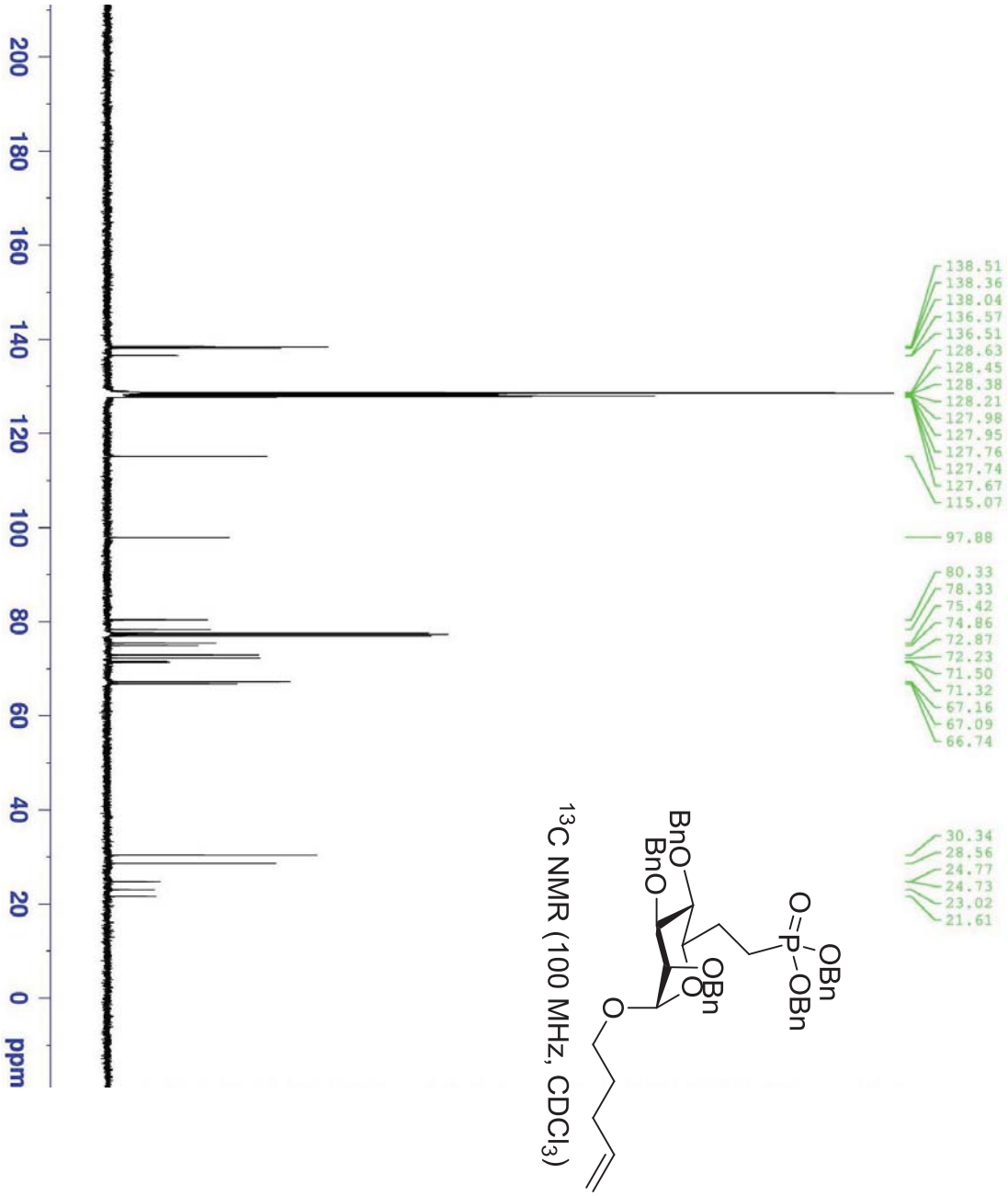

^{13}C NMR (100 MHz, $CDCl_3$)

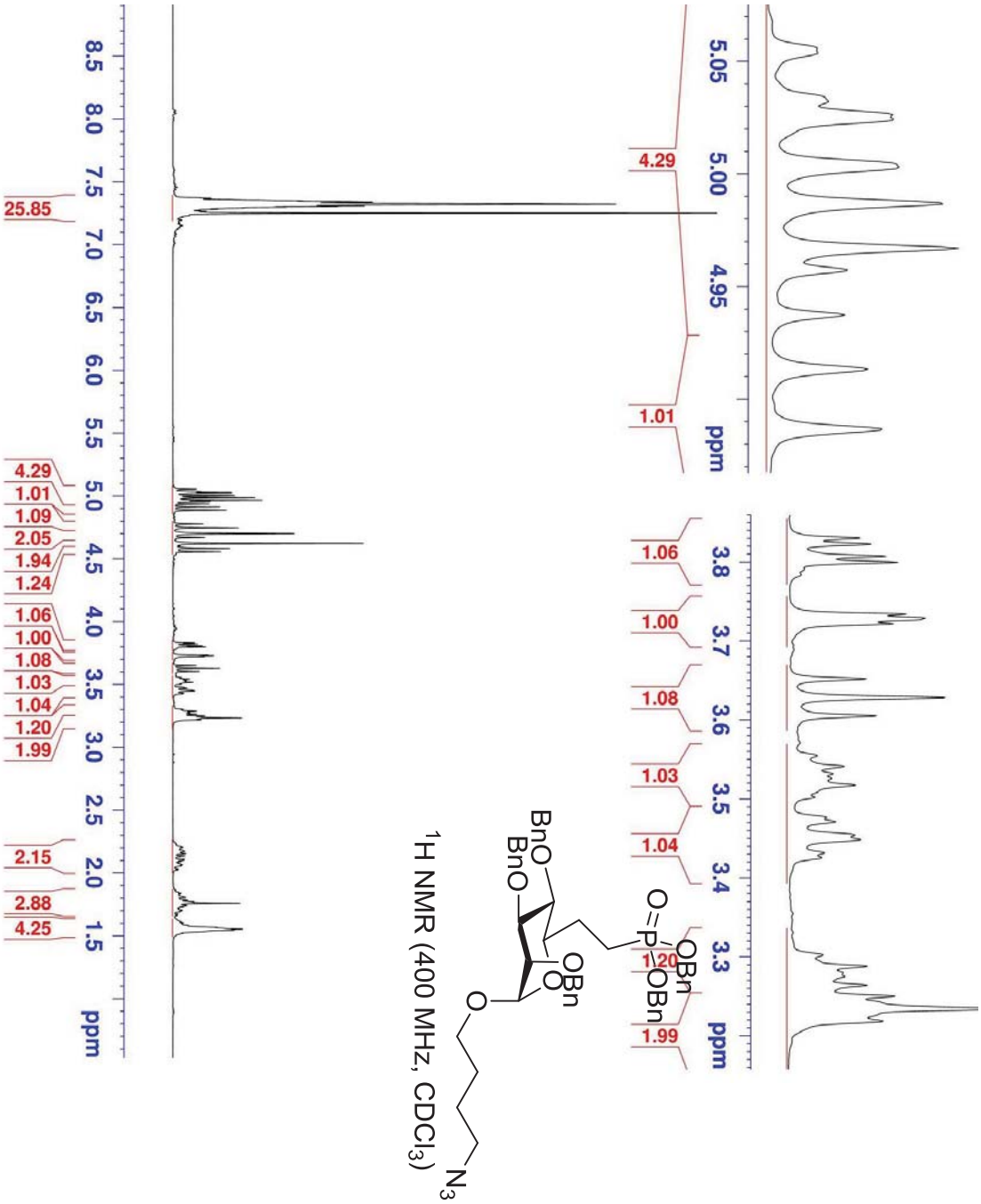
BnO
BnO
OBn
O
O=P
OBn
OBn
O
N3
1H NMR (400 MHz, CDCl3)
ppm

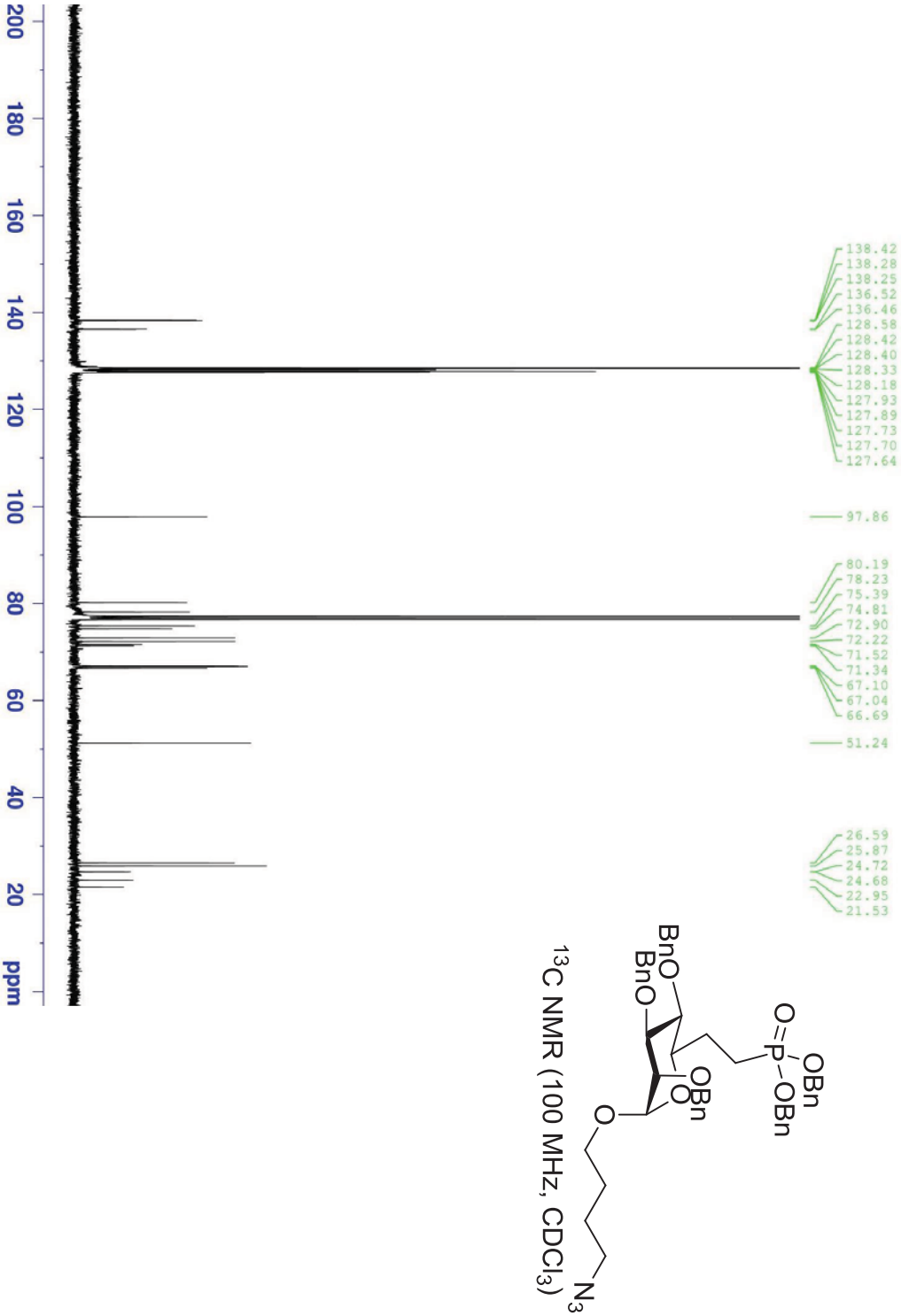

^{13}C NMR (100 MHz, $CDCl_3$)

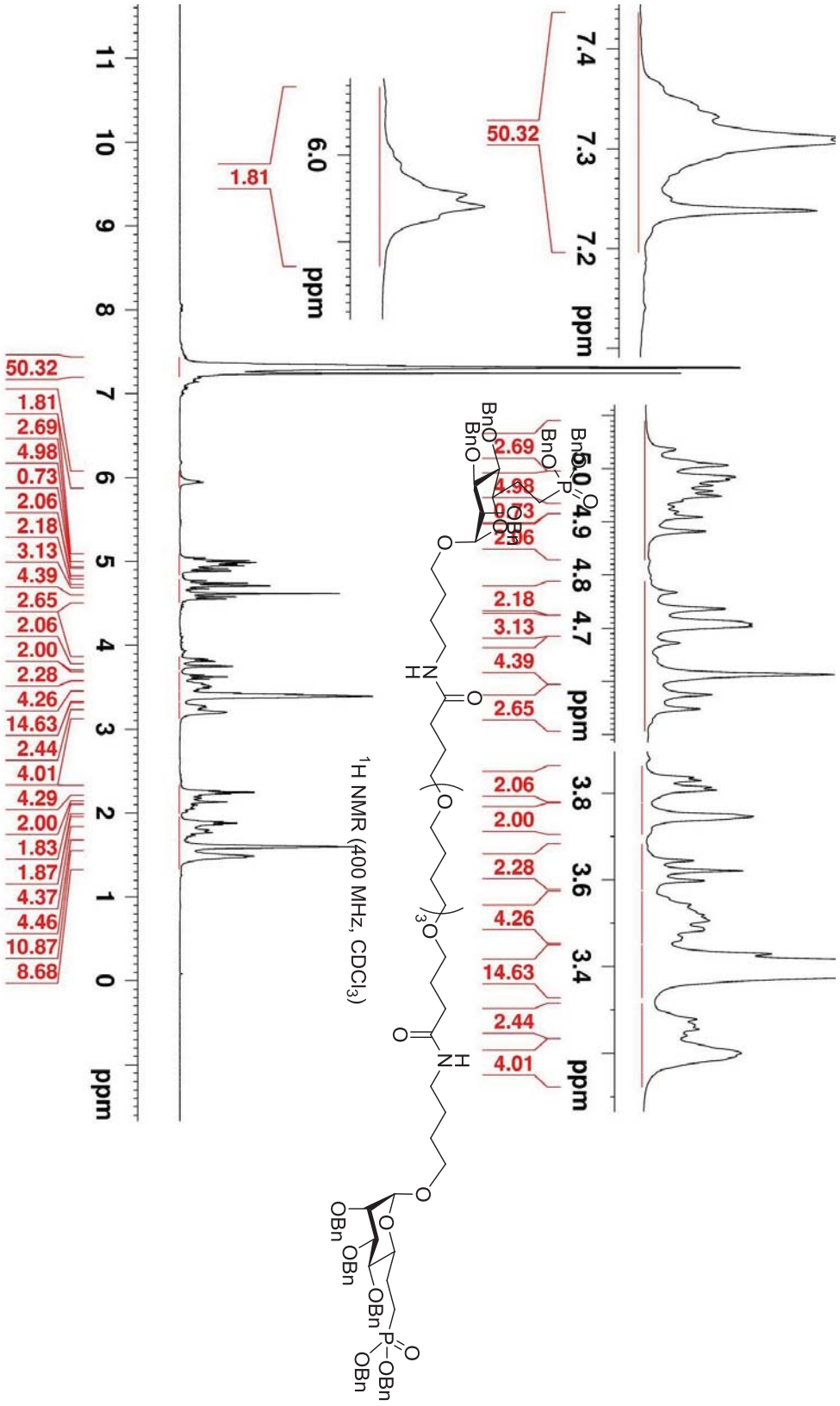
50.32
1.81
2.69
4.98
0.73
2.06
2.18
3.13
4.39
2.65
2.06
2.00
2.28
4.26
14.63
2.44
4.01
4.29
2.00
1.83
1.87
4.37
4.46
10.87
8.68
ppm
^{1}H NMR (400 MHz, CDCl$_3$)

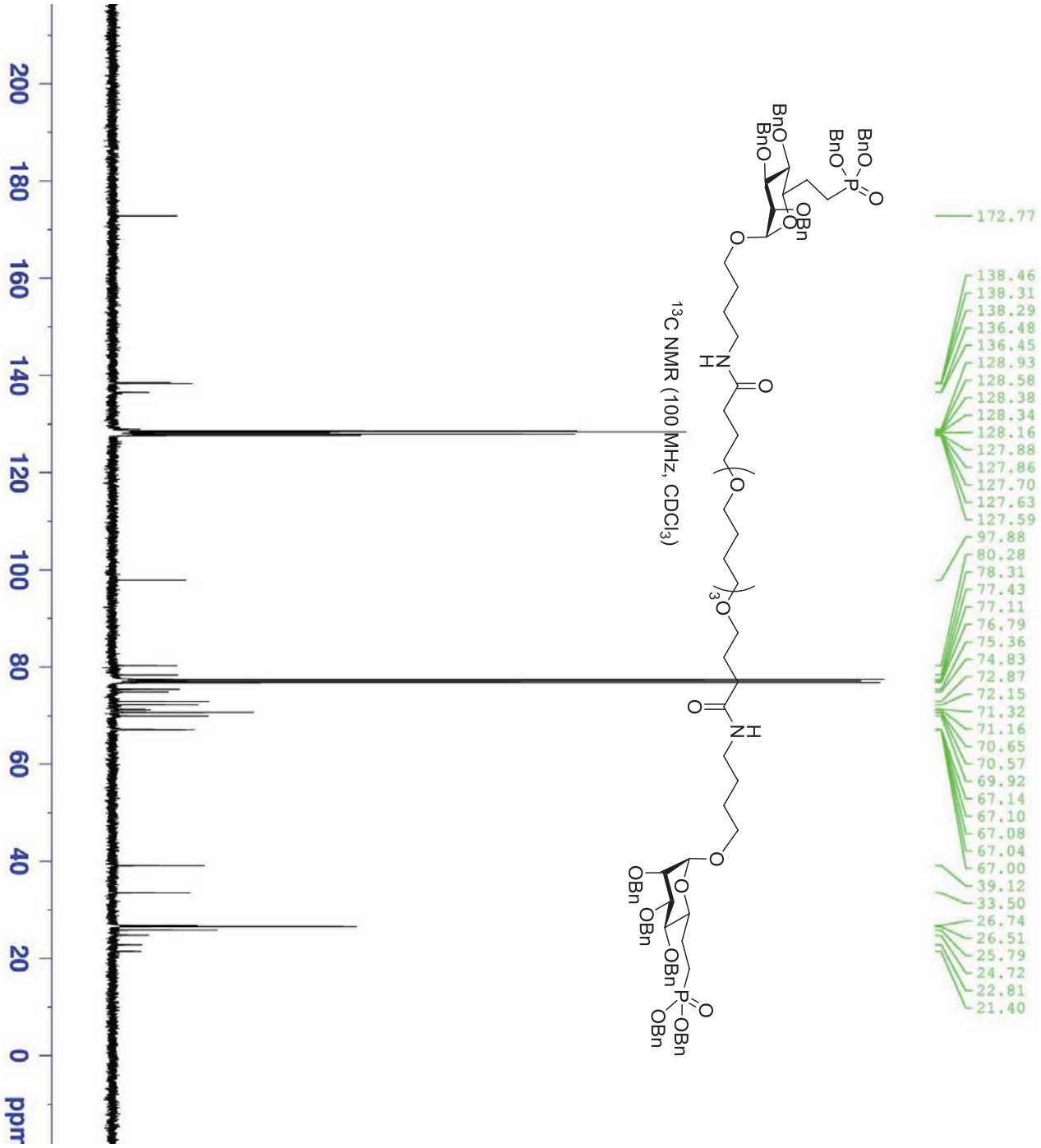
^{13}C NMR (100 MHz, $CDCl_3$)
172.77
138.46
138.31
138.29
136.48
136.45
128.93
128.58
128.38
128.34
128.16
127.88
127.86
127.70
127.63
127.59
97.88
80.28
78.31
77.43
77.11
76.79
75.36
74.83
72.87
72.15
71.32
71.16
70.65
70.57
69.92
67.14
67.10
67.08
67.04
67.00
39.12
33.50
26.74
26.51
25.79
24.72
22.81
21.40
200
180
160
140
120
100
80
60
40
20
0
ppm

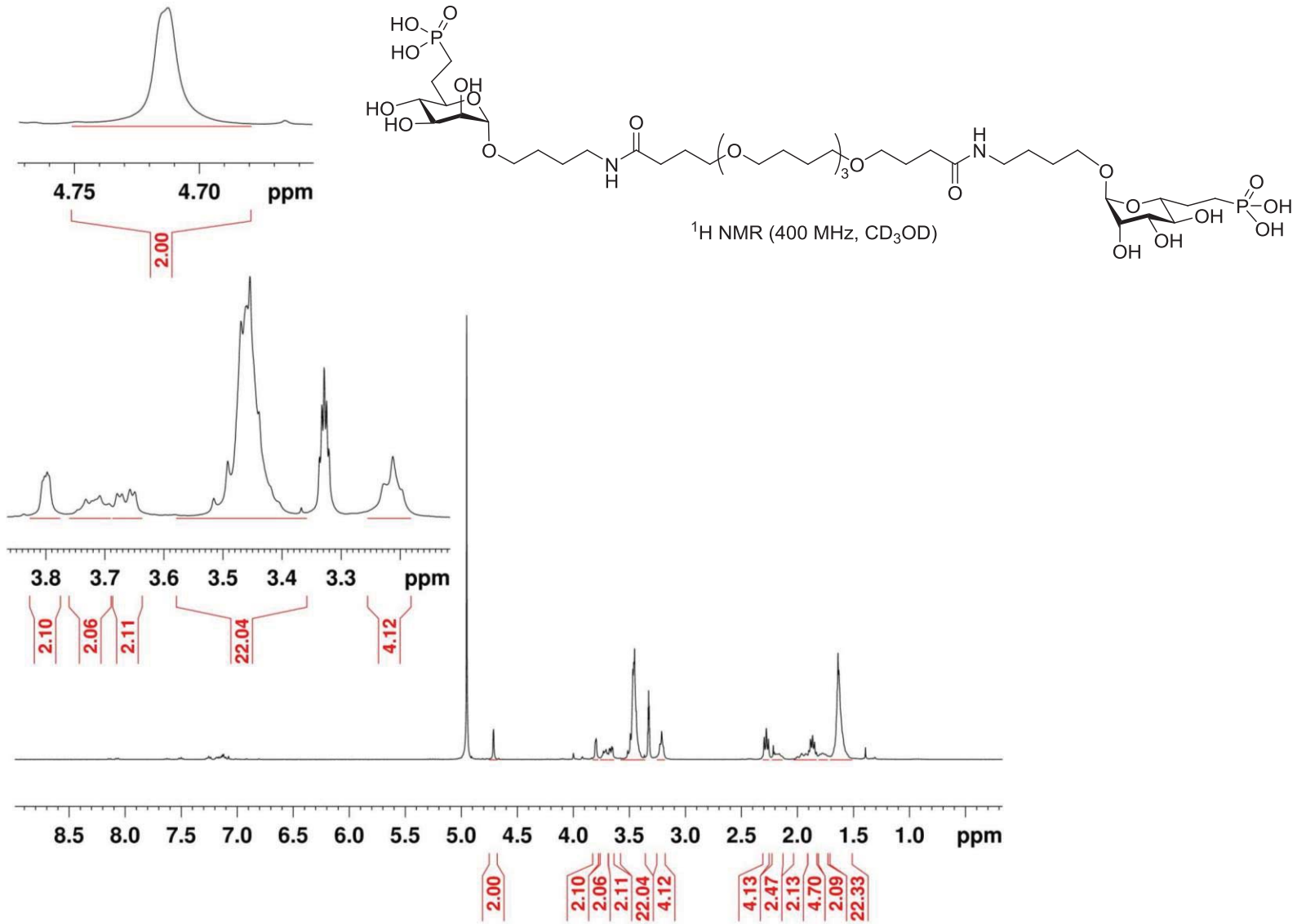

^{1}H NMR (400 MHz, CD_3OD)

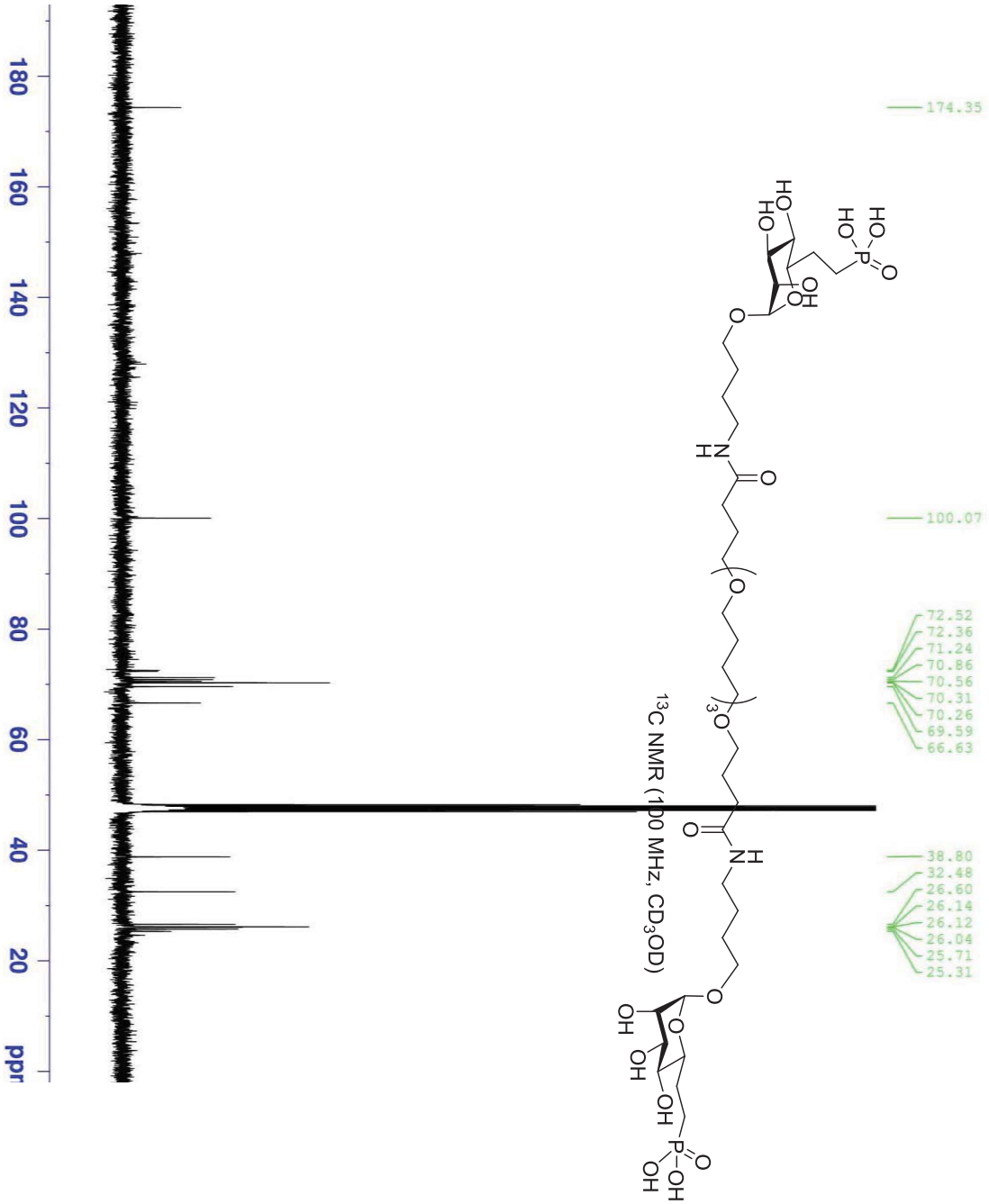
174.35
100.07
72.52
72.36
71.24
70.86
70.56
70.31
70.26
69.59
66.63
38.80
32.48
26.60
26.14
26.12
26.04
25.71
25.31
^{13}C NMR (100 MHz, CD_3OD)
180
160
140
120
100
80
60
40
20
ppm

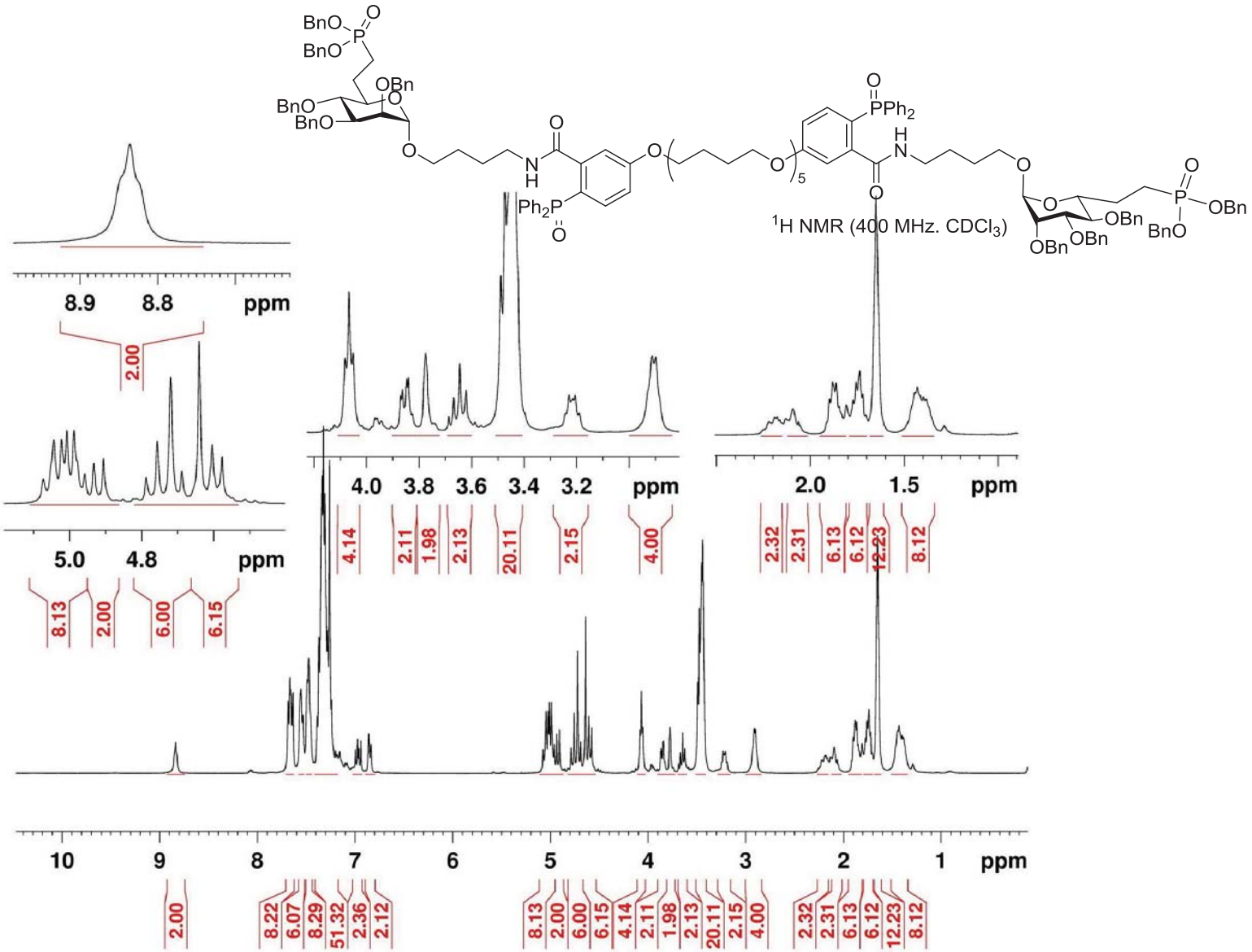
^{1}H NMR (400 MHz. $CDCl_3$)
ppm

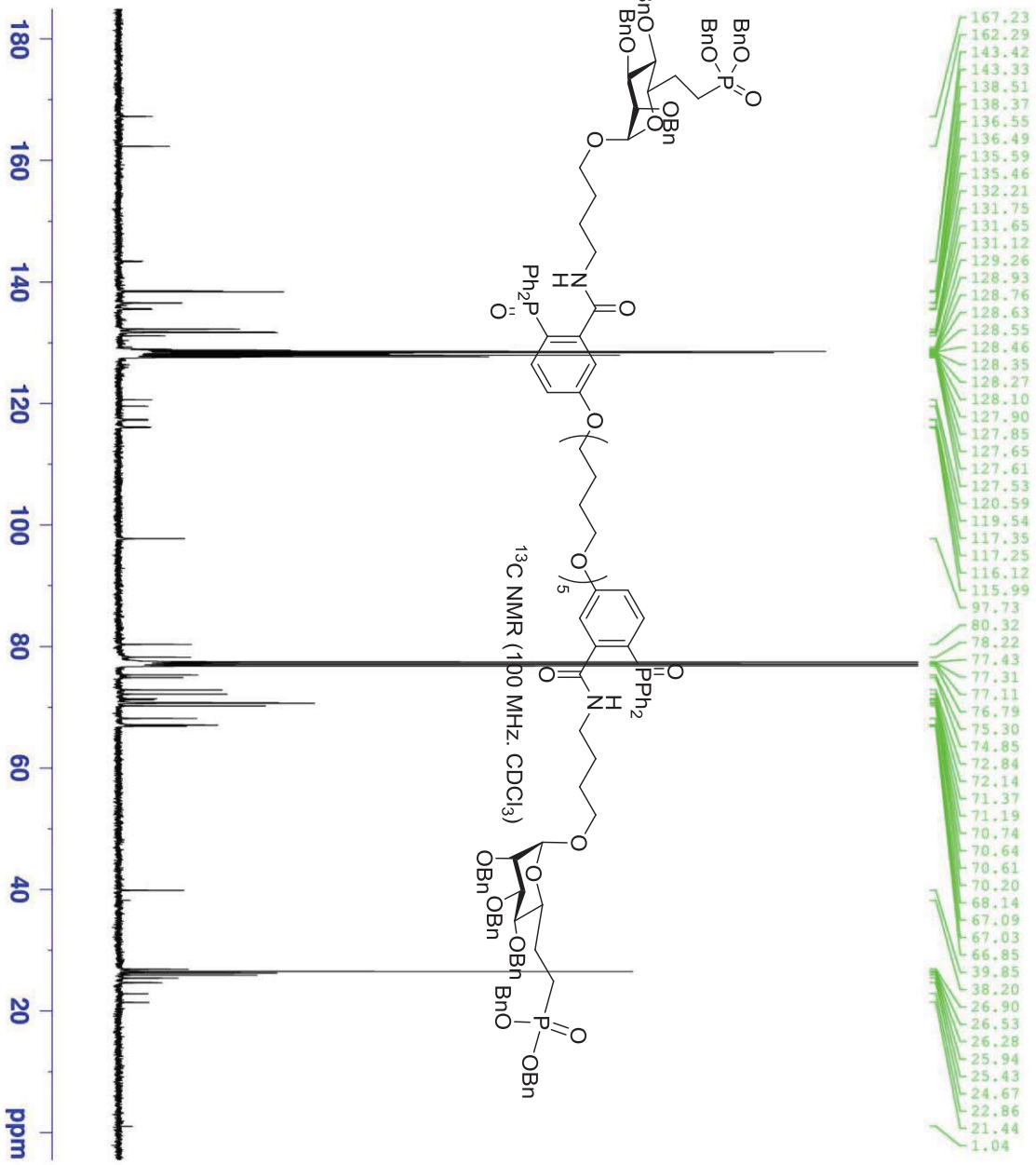
^{13}C NMR (100 MHz. $CDCl_3$)
ppm
180
160
140
120
100
80
60
40
20
167.23
162.29
143.42
143.33
138.51
138.37
136.55
136.49
135.59
135.46
132.21
131.75
131.65
131.12
129.26
128.93
128.76
128.63
128.55
128.46
128.35
128.27
128.10
127.90
127.85
127.65
127.61
127.53
120.59
119.54
117.35
117.25
116.12
115.99
97.73
80.32
78.22
77.43
77.31
77.11
76.79
75.30
74.85
72.84
72.14
71.37
71.19
70.74
70.64
70.61
70.20
68.14
67.09
67.03
66.85
39.85
38.20
26.90
26.53
26.28
25.94
25.43
24.67
22.86
21.44
1.04

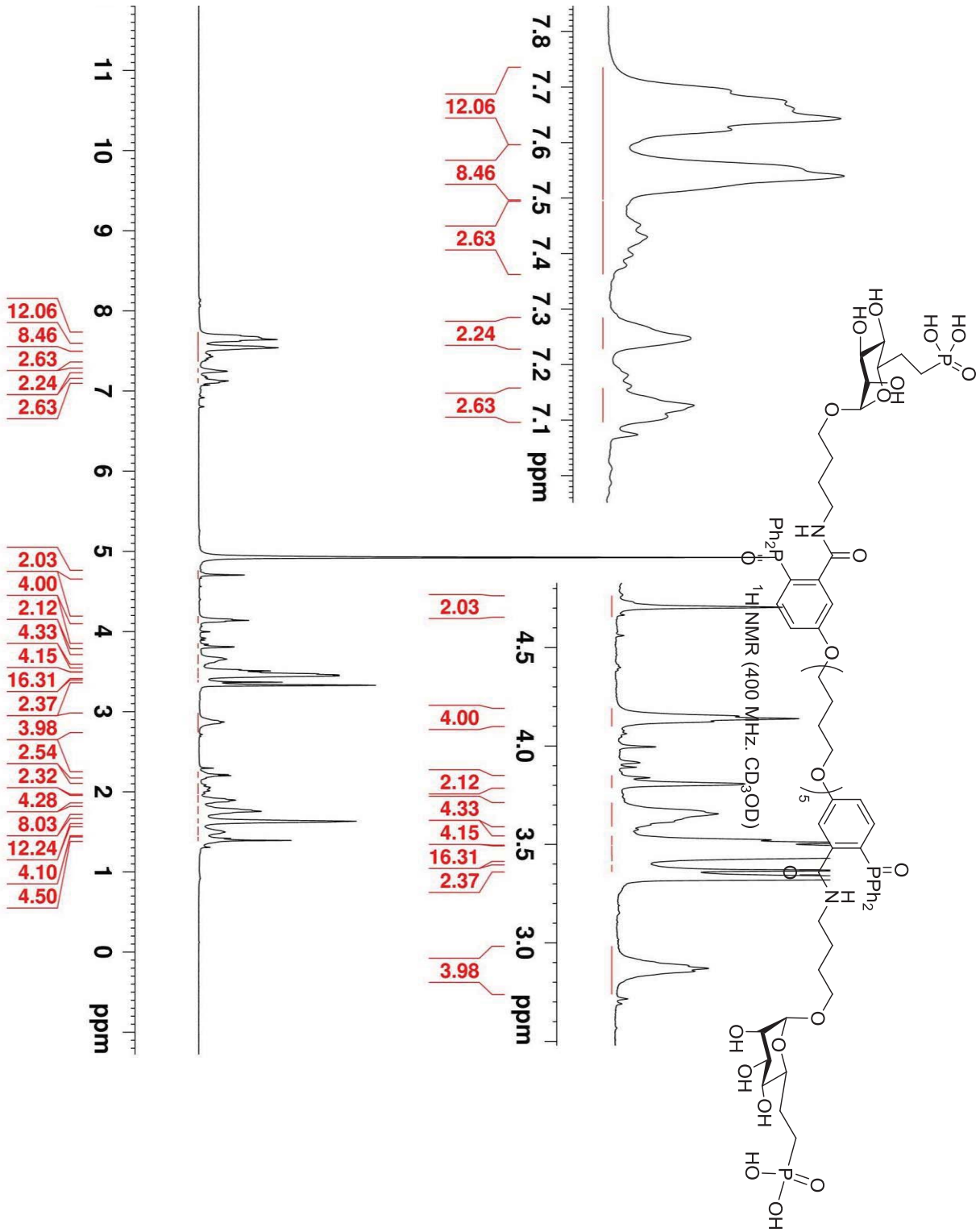
12.06
8.46
2.63
2.24
2.63
2.03
4.00
2.12
4.33
4.15
16.31
2.37
3.98
2.54
2.32
4.28
8.03
12.24
4.10
4.50
ppm
^{1}H NMR (400 MHz. CD_3OD)

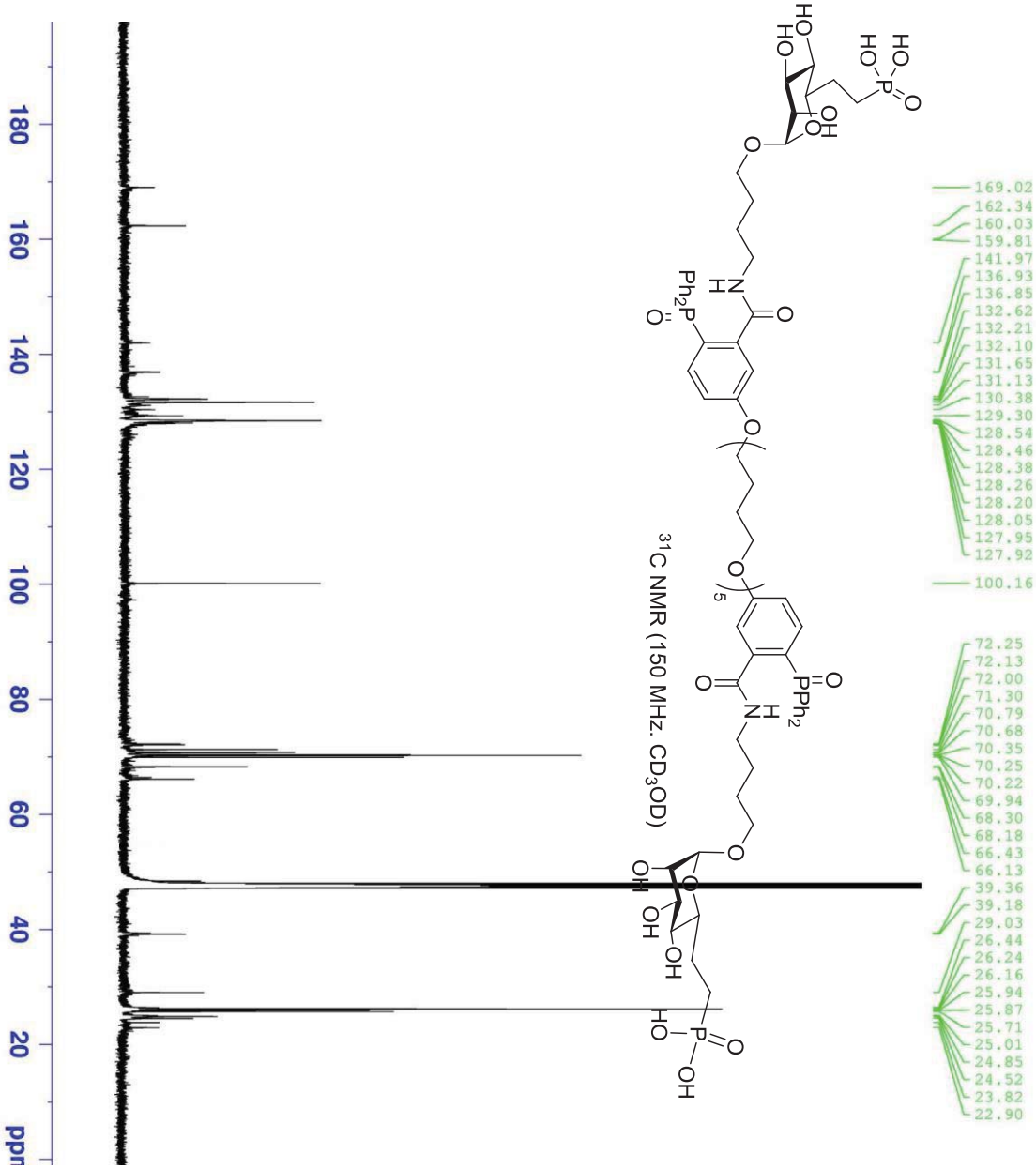
169.02
162.34
160.03
159.81
141.97
136.93
136.85
132.62
132.21
132.10
131.65
131.13
130.38
129.30
128.54
128.46
128.38
128.26
128.20
128.05
127.95
127.92
100.16
72.25
72.13
72.00
71.30
70.79
70.68
70.35
70.25
70.22
69.94
68.30
68.18
66.43
66.13
39.36
39.18
29.03
26.44
26.24
26.16
25.94
25.87
25.71
25.01
24.85
24.52
23.82
22.90
180
160
140
120
100
80
60
40
20
ppm
^{31}C NMR (150 MHz. CD_3OD)

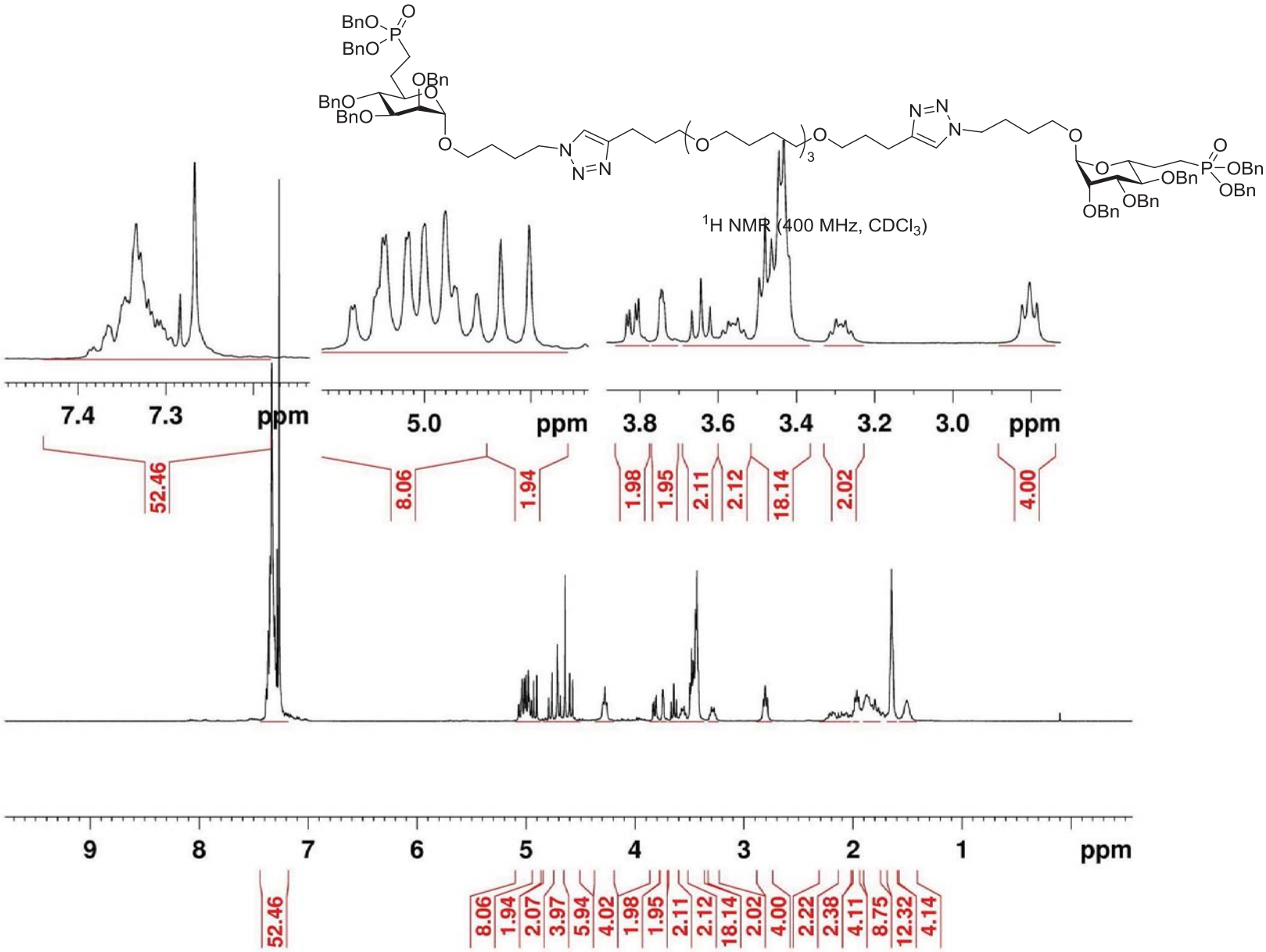
BnO
BnO
P
O
OBn
BnO
BnO
O
O
N
N=N
O
3
O
N=N
N
O
O
OBn
OBn
OBn
P
O
OBn
OBn
1H NMR (400 MHz, CDCl3)
7.4
7.3
ppm
5.0
ppm
3.8
3.6
3.4
3.2
3.0
ppm
52.46
8.06
1.94
1.98
1.95
2.11
2.12
18.14
2.02
4.00
9
8
7
6
5
4
3
2
1
ppm
52.46
8.06
1.94
2.07
3.97
5.94
4.02
1.98
1.95
2.11
2.12
18.14
2.02
4.00
2.22
2.38
4.11
8.75
12.32
4.14

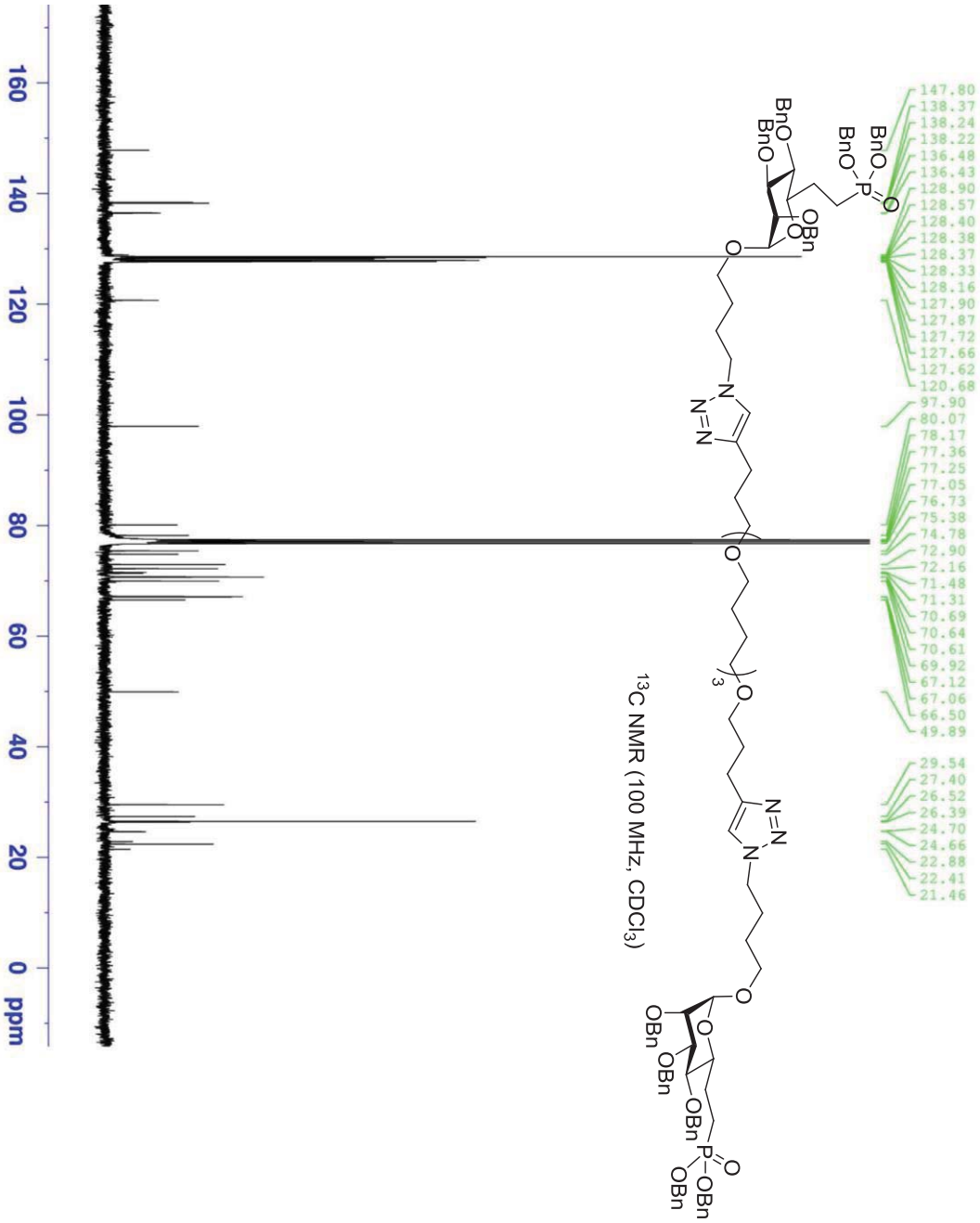

^{13}C NMR (100 MHz, $CDCl_3$)

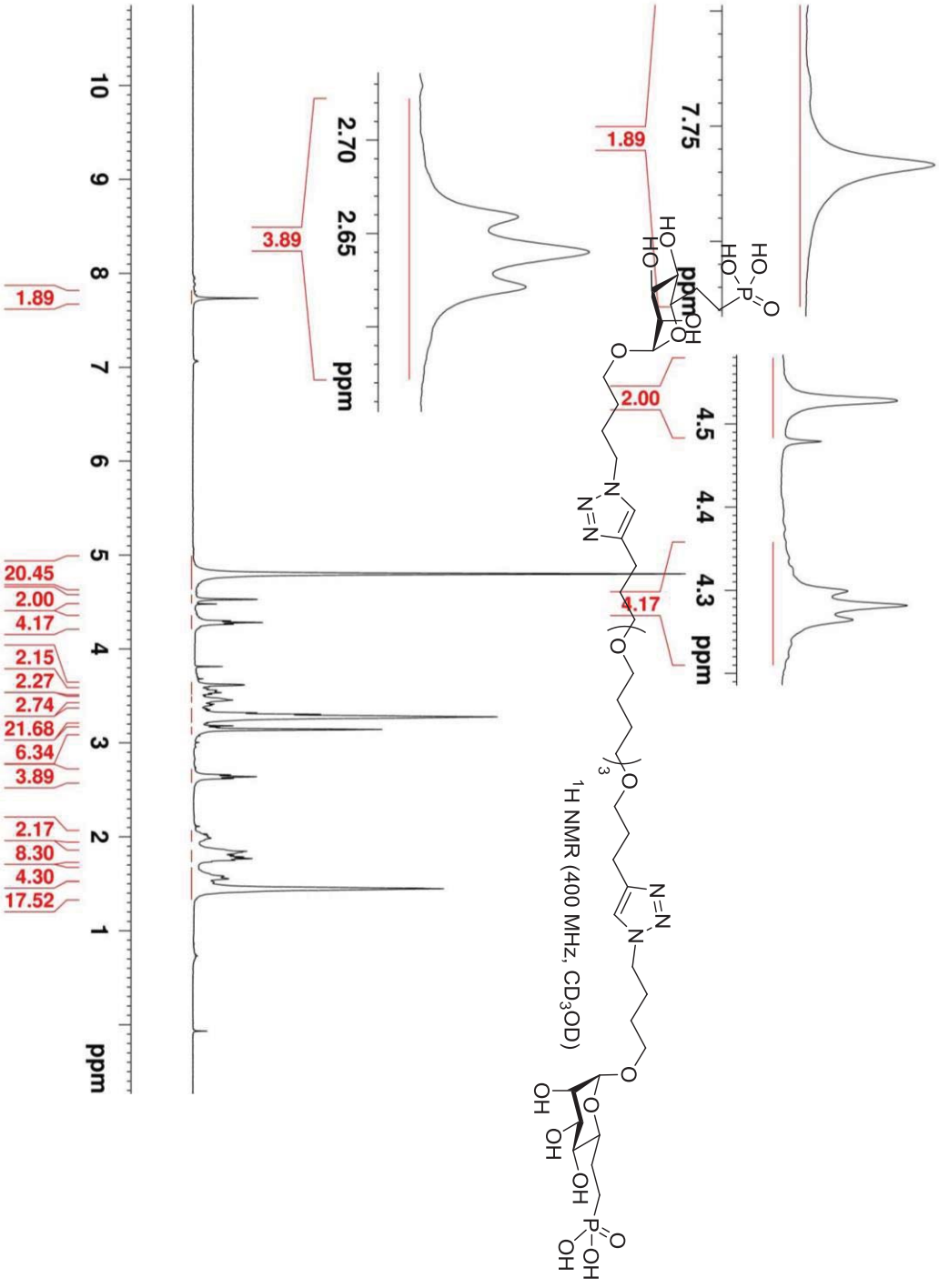
1.89
20.45
2.00
4.17
2.15
2.27
2.74
21.68
6.34
3.89
2.17
8.30
4.30
17.52
ppm
3.89
2.70
2.65
ppm
1.89
7.75
ppm
2.00
4.5
4.4
4.3
ppm
4.17
^{1}H NMR (400 MHz, CD_3OD)

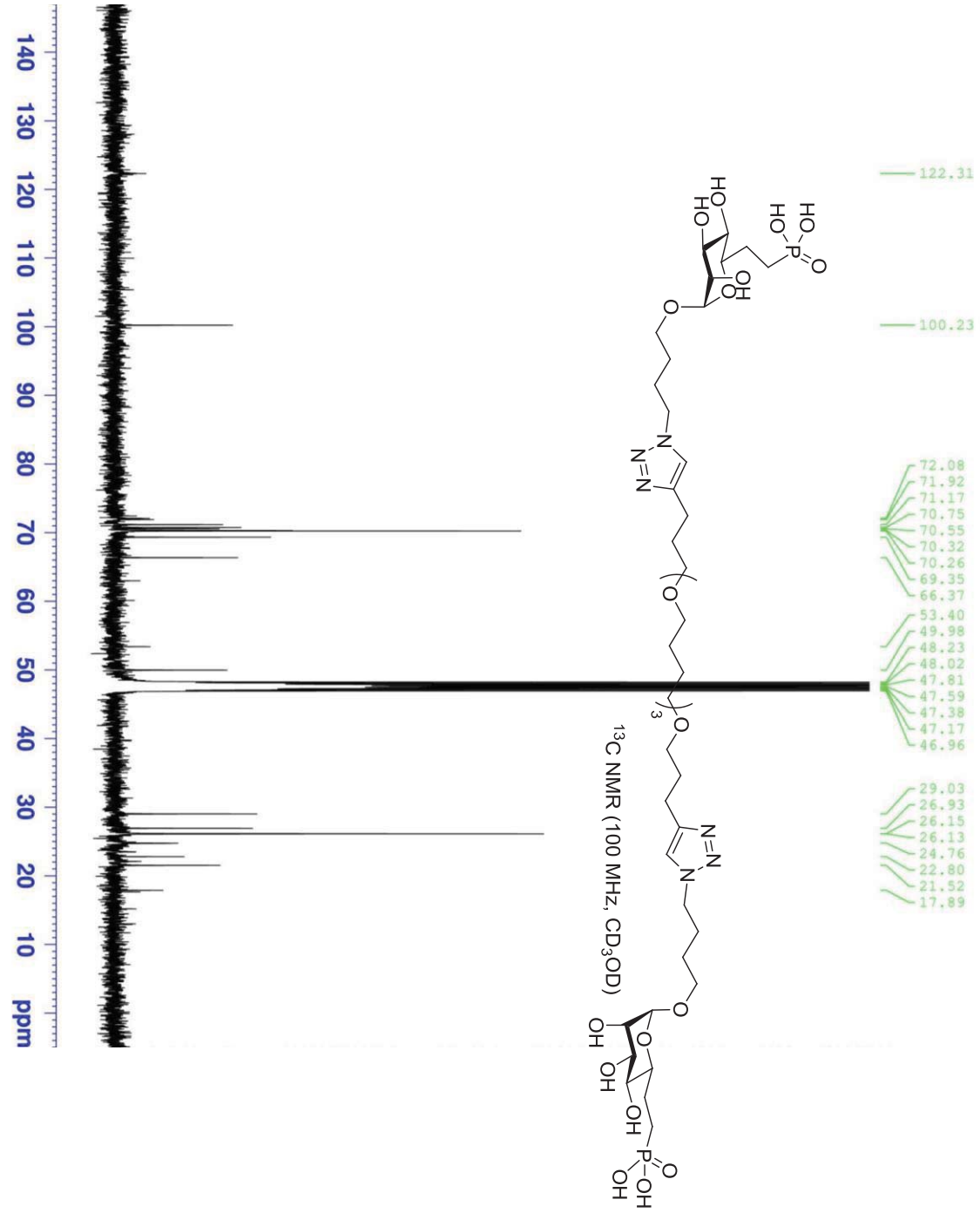
140
130
120
110
100
90
80
70
60
50
40
30
20
10
ppm
122.31
100.23
72.08
71.92
71.17
70.75
70.55
70.32
70.26
69.35
66.37
53.40
49.98
48.23
48.02
47.81
47.59
47.38
47.17
46.96
29.03
26.93
26.15
26.13
24.76
22.80
21.52
17.89
^{13}C NMR (100 MHz, CD_3OD)

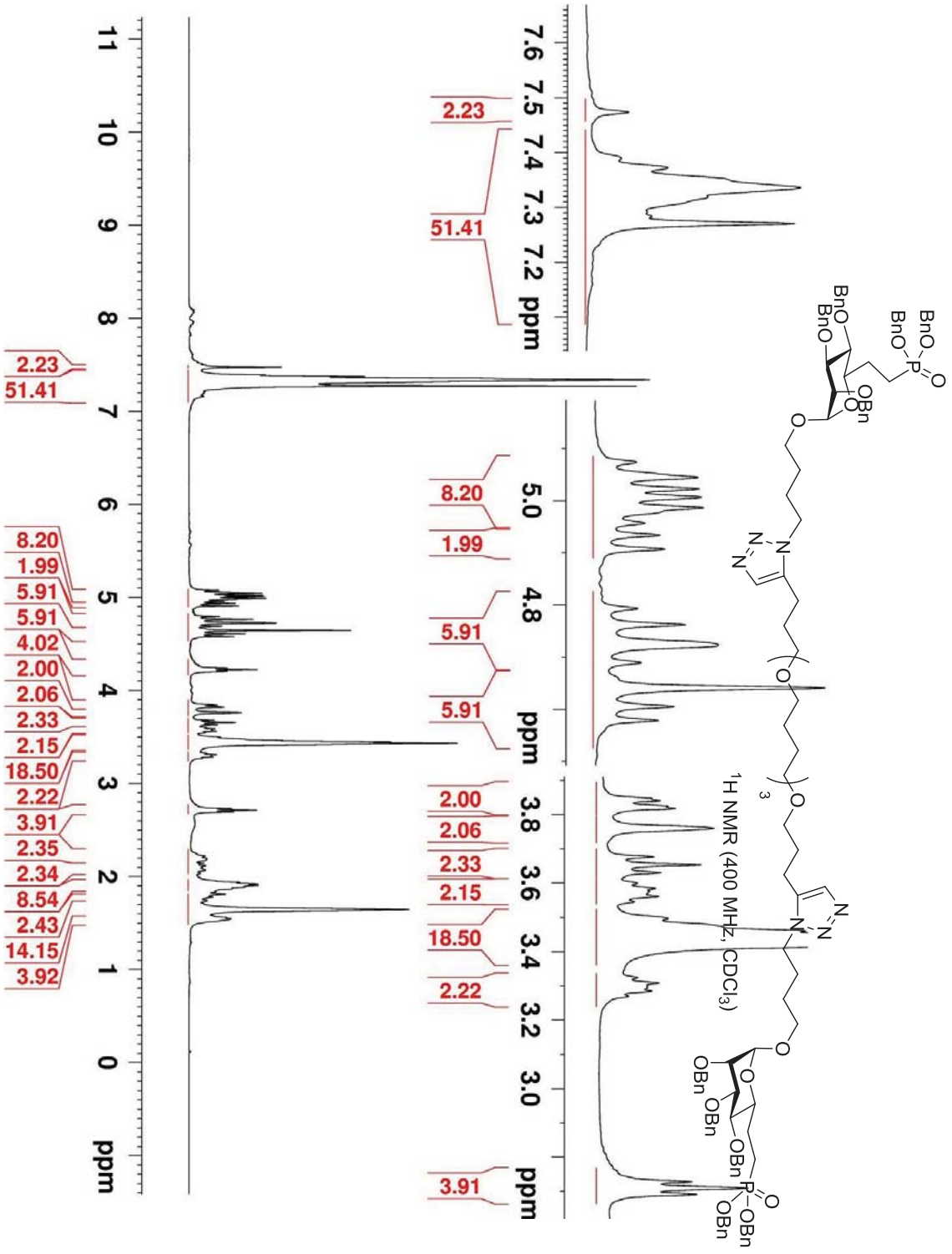
^{1}H NMR (400 MHz, $CDCl_3$)
2.23
51.41
8.20
1.99
5.91
5.91
2.00
2.06
2.33
2.15
18.50
2.22
3.91
ppm

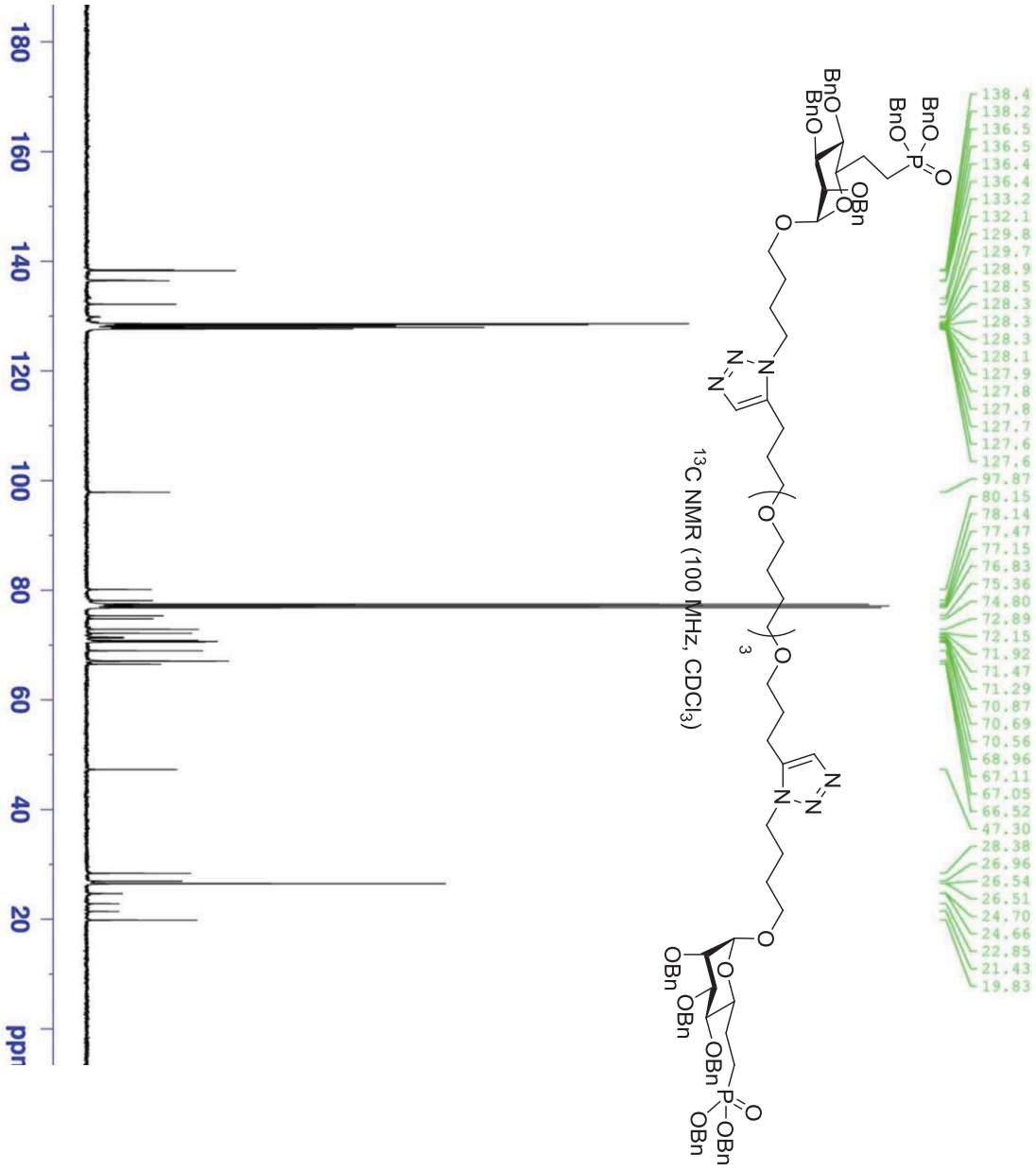
^{13}C NMR (100 MHz, $CDCl_3$)
138.4
138.2
136.5
136.5
136.4
136.4
133.2
132.1
129.8
129.7
128.9
128.5
128.3
128.3
128.3
128.1
127.9
127.8
127.8
127.7
127.6
127.6
97.87
80.15
78.14
77.47
77.15
76.83
75.36
74.80
72.89
72.15
71.92
71.47
71.29
70.87
70.69
70.56
68.96
67.11
67.05
66.52
47.30
28.38
26.96
26.54
26.51
24.70
24.66
22.85
21.43
19.83
180
160
140
120
100
80
60
40
20
ppm

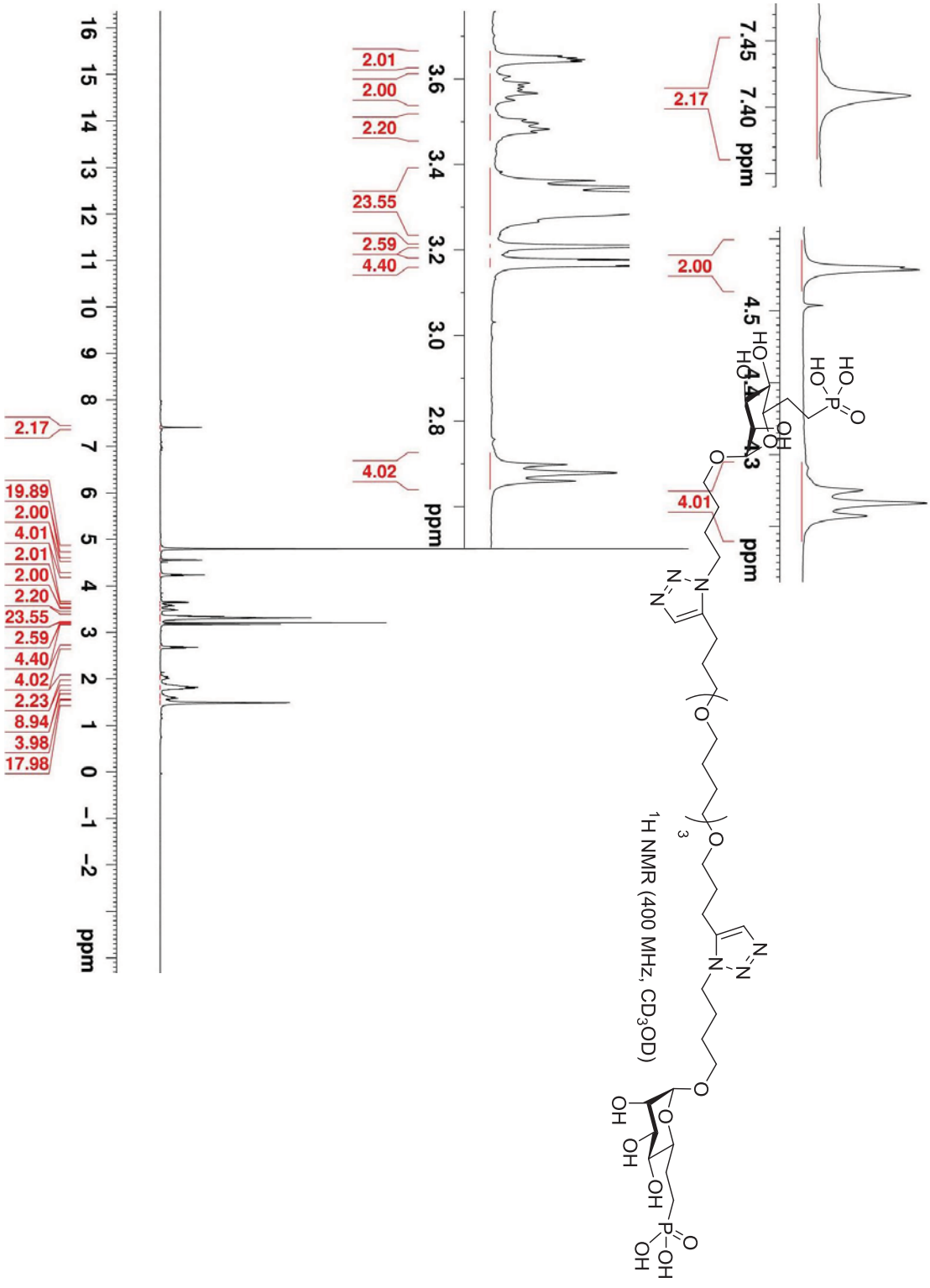
2.17
19.89
2.00
4.01
2.01
2.00
2.20
23.55
2.59
4.40
4.02
2.23
8.94
3.98
17.98
2.01
2.00
2.20
23.55
2.59
4.40
4.02
2.17
2.00
4.01
ppm
^{1}H NMR (400 MHz, CD_3OD)

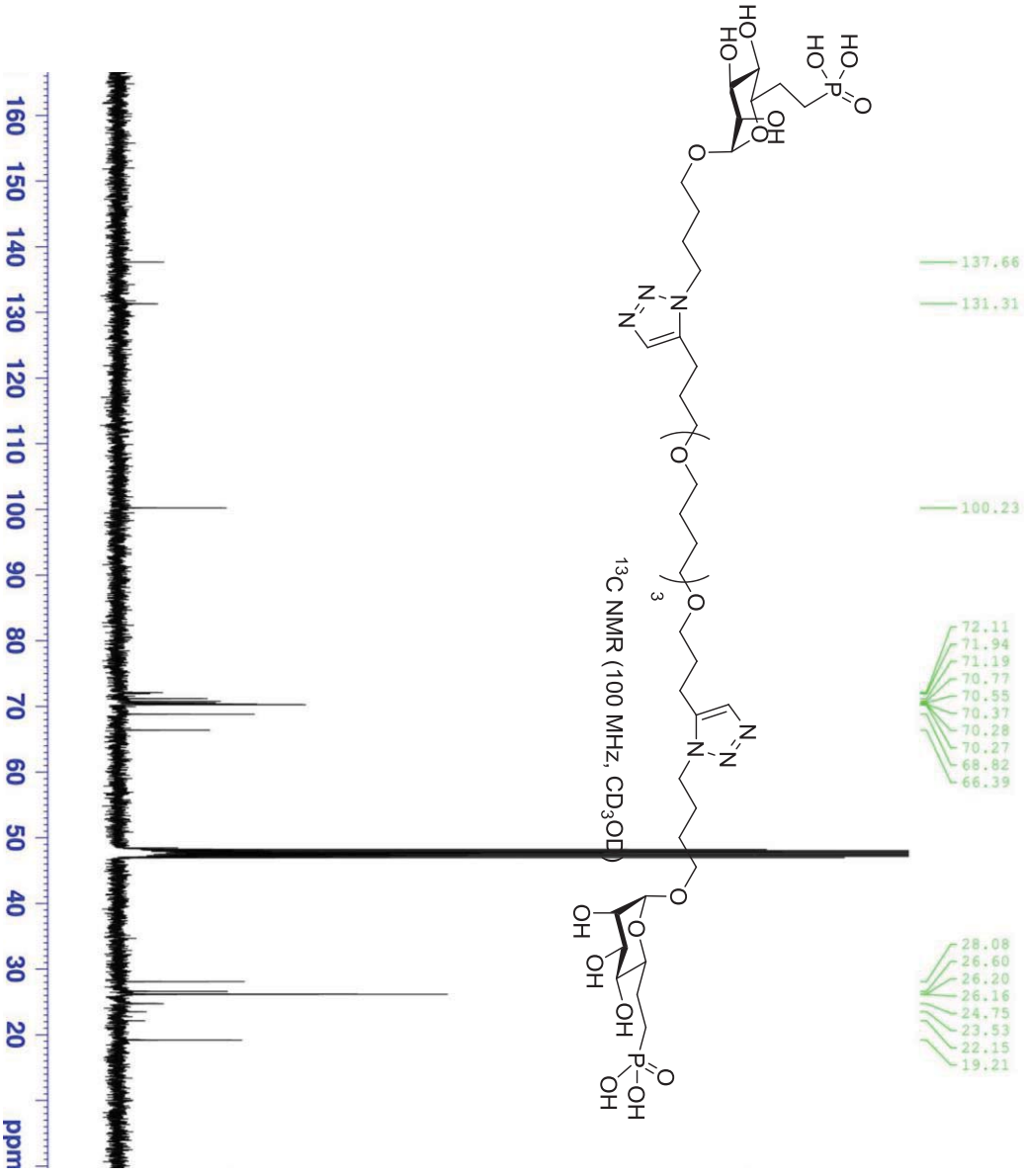
137.66
131.31
100.23
72.11
71.94
71.19
70.77
70.55
70.37
70.28
70.27
68.82
66.39
28.08
26.60
26.20
26.16
24.75
23.53
22.15
19.21
^{13}C NMR (100 MHz, CD_3OD)
160 150 140 130 120 110 100 90 80 70 60 50 40 30 20 ppm

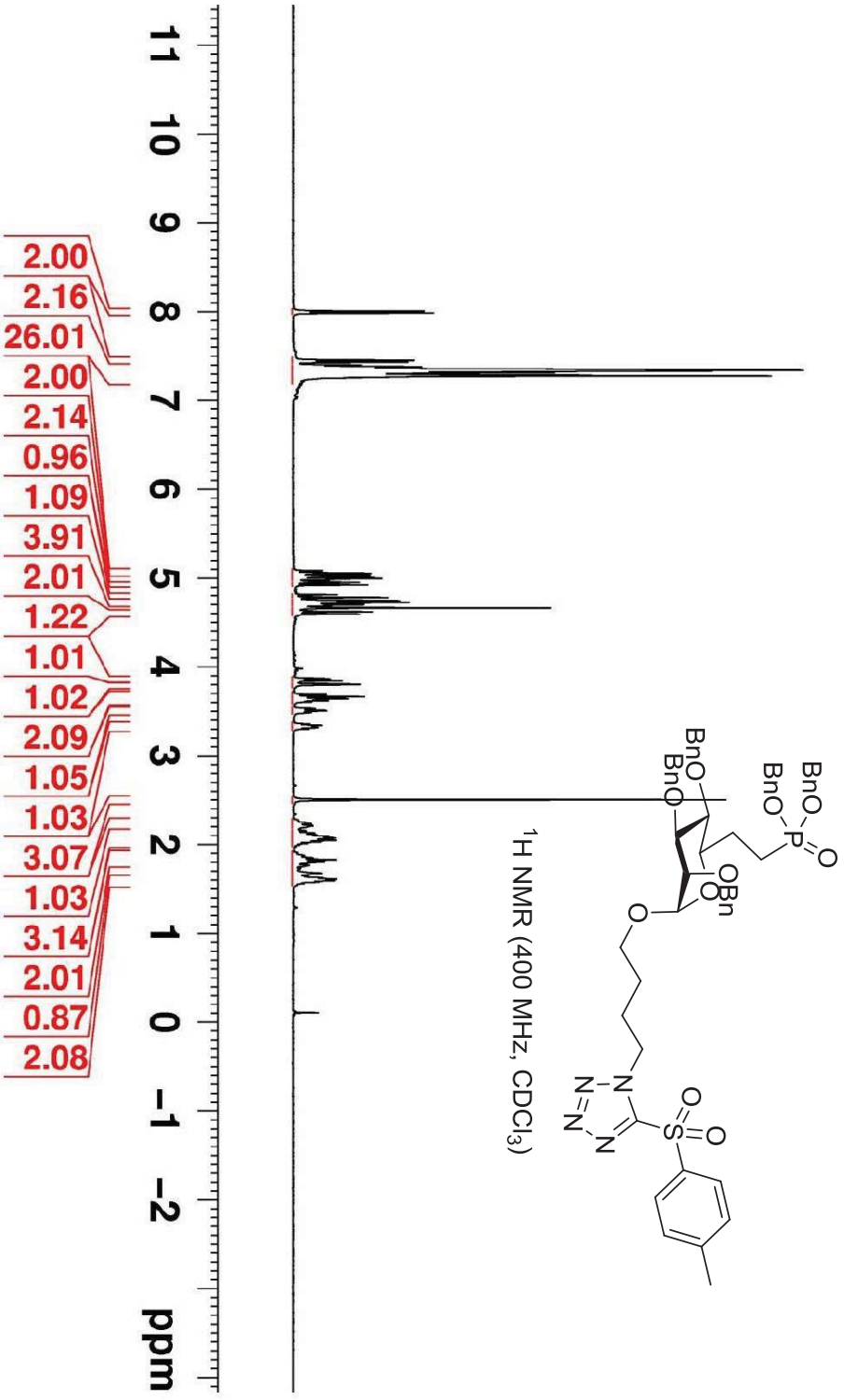
2.00
2.16
26.01
2.00
2.14
0.96
1.09
3.91
2.01
1.22
1.01
1.02
2.09
1.05
1.03
3.07
1.03
3.14
2.01
0.87
2.08
11 10 9 8 7 6 5 4 3 2 1 0 −1 −2 ppm
^{1}H NMR (400 MHz, CDCl$_3$)

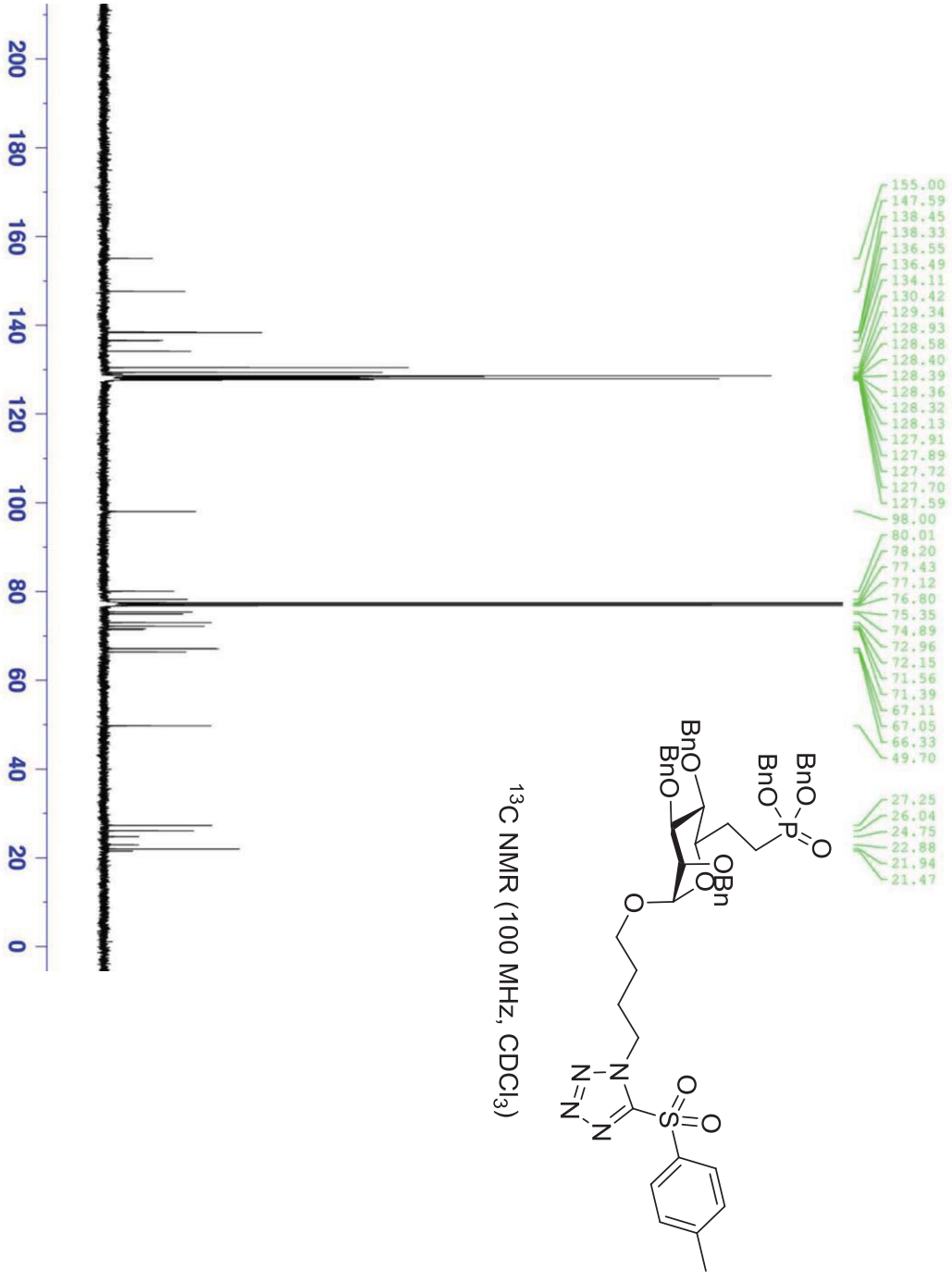

^{13}C NMR (100 MHz, $CDCl_3$)

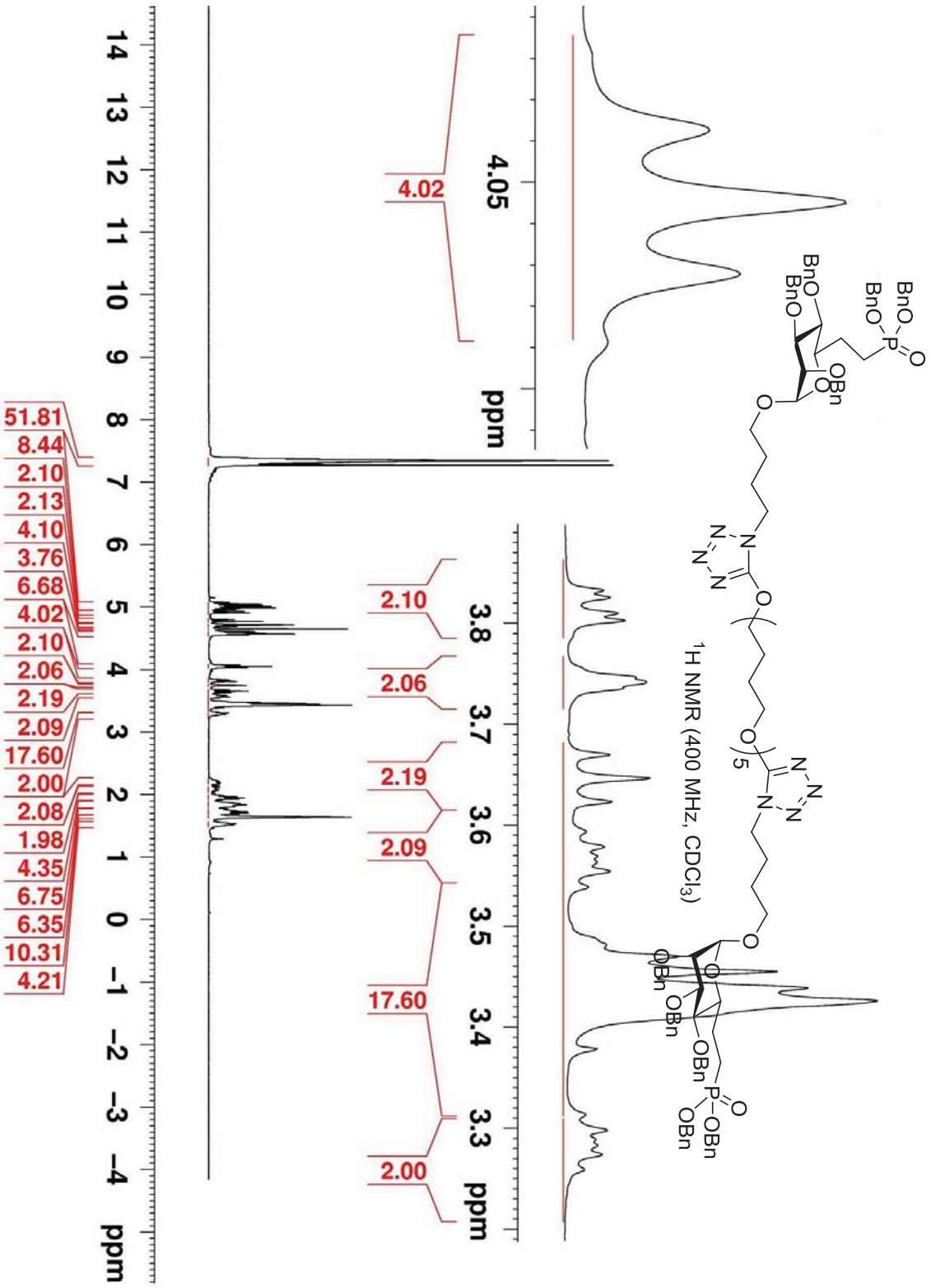
^{1}H NMR (400 MHz, CDCl$_3$)
4.02
4.05
ppm
2.10
2.06
2.19
2.09
17.60
2.00
3.8
3.7
3.6
3.5
3.4
3.3
ppm
51.81
8.44
2.10
2.13
4.10
3.76
6.68
4.02
2.10
2.06
2.19
2.09
17.60
2.00
2.08
1.98
4.35
6.75
6.35
10.31
4.21
14 13 12 11 10 9 8 7 6 5 4 3 2 1 0 −1 −2 −3 −4 ppm

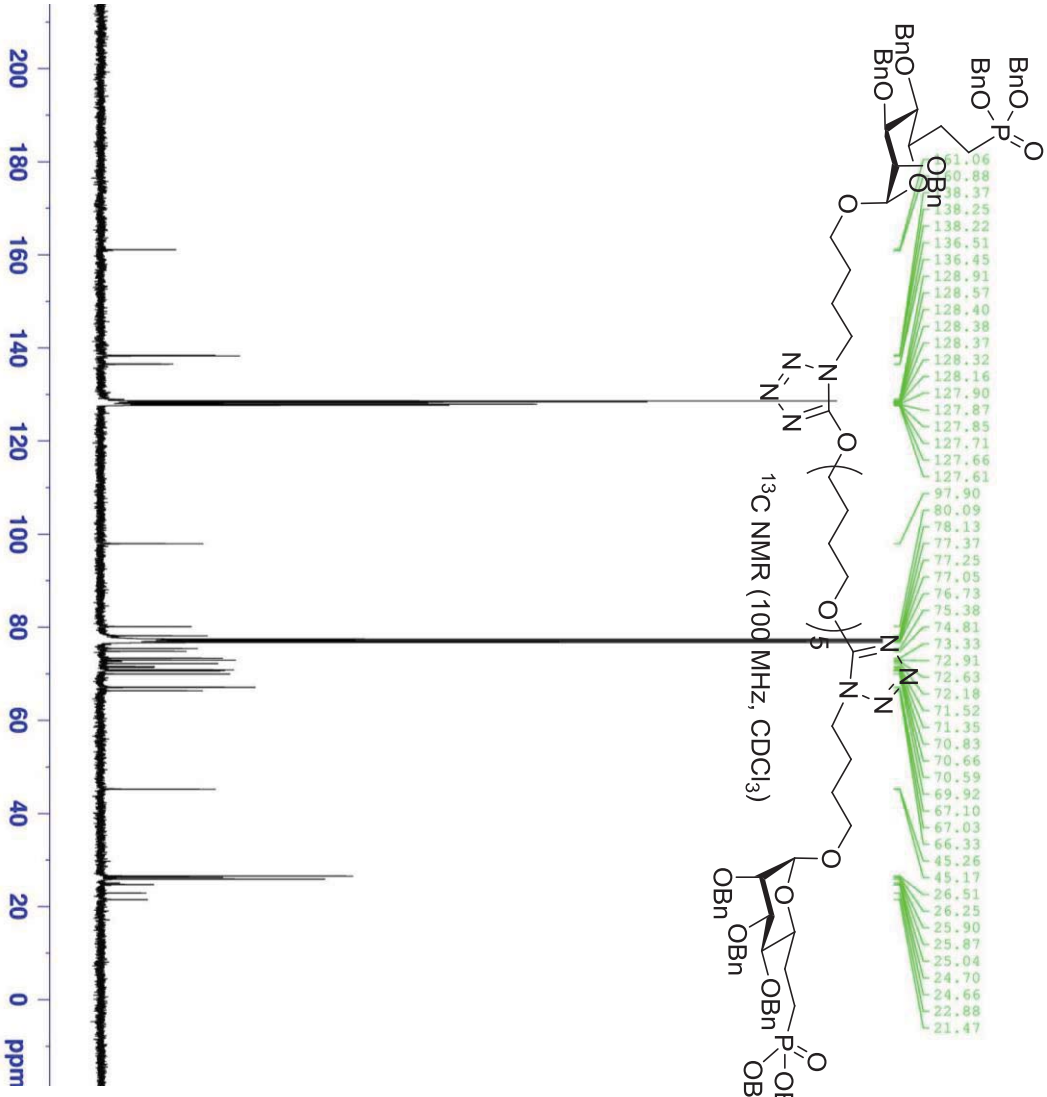
^{13}C NMR (100 MHz, CDCl$_3$)
200
180
160
140
120
100
80
60
40
20
0
ppm

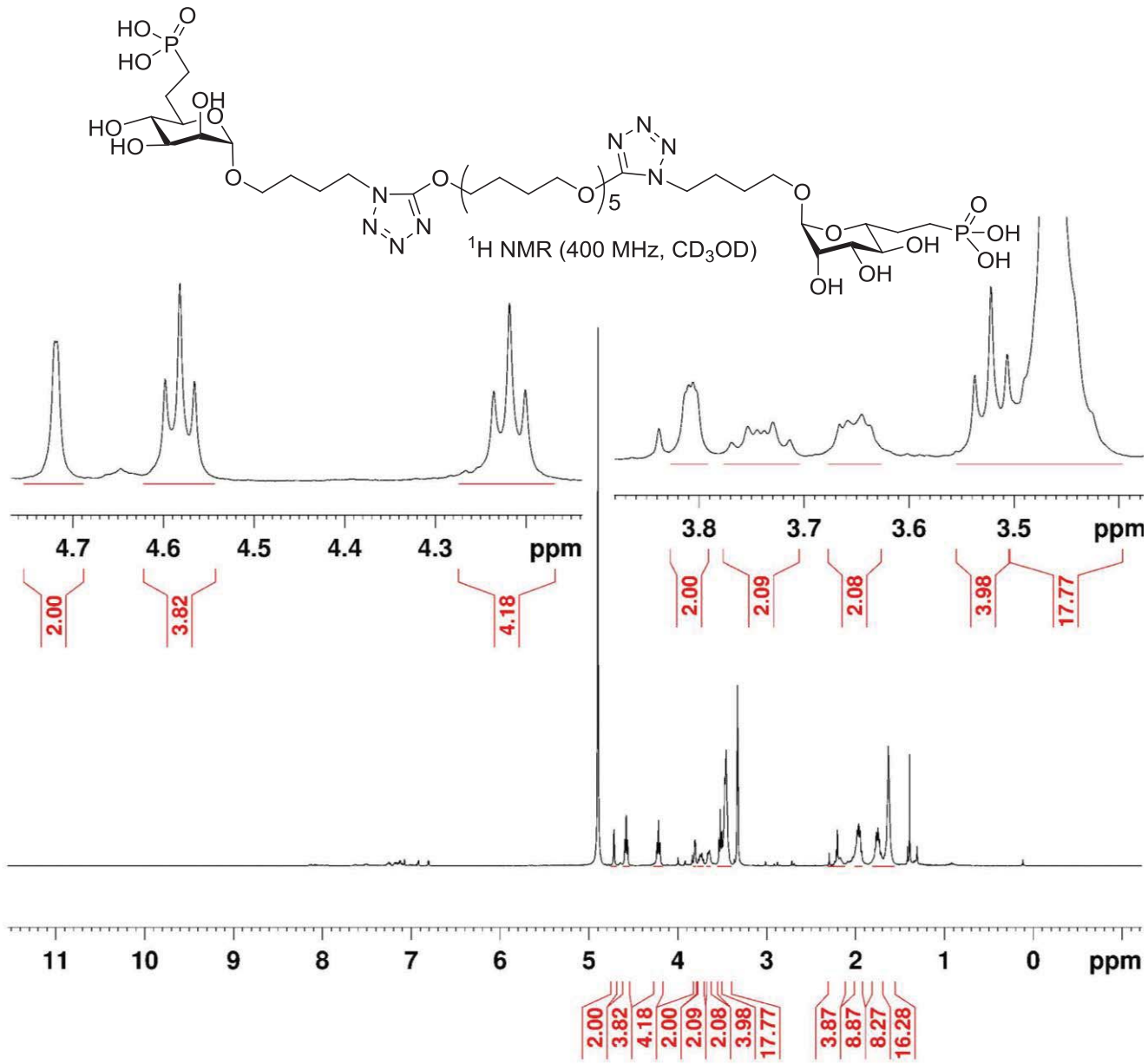
^{1}H NMR (400 MHz, CD_3OD)
4.7
4.6
4.5
4.4
4.3
ppm
2.00
3.82
4.18
3.8
3.7
3.6
3.5
ppm
2.00
2.09
2.08
3.98
17.77
11
10
9
8
7
6
5
4
3
2
1
0
ppm
2.00
3.82
4.18
2.00
2.09
2.08
3.98
17.77
3.87
8.87
8.27
16.28

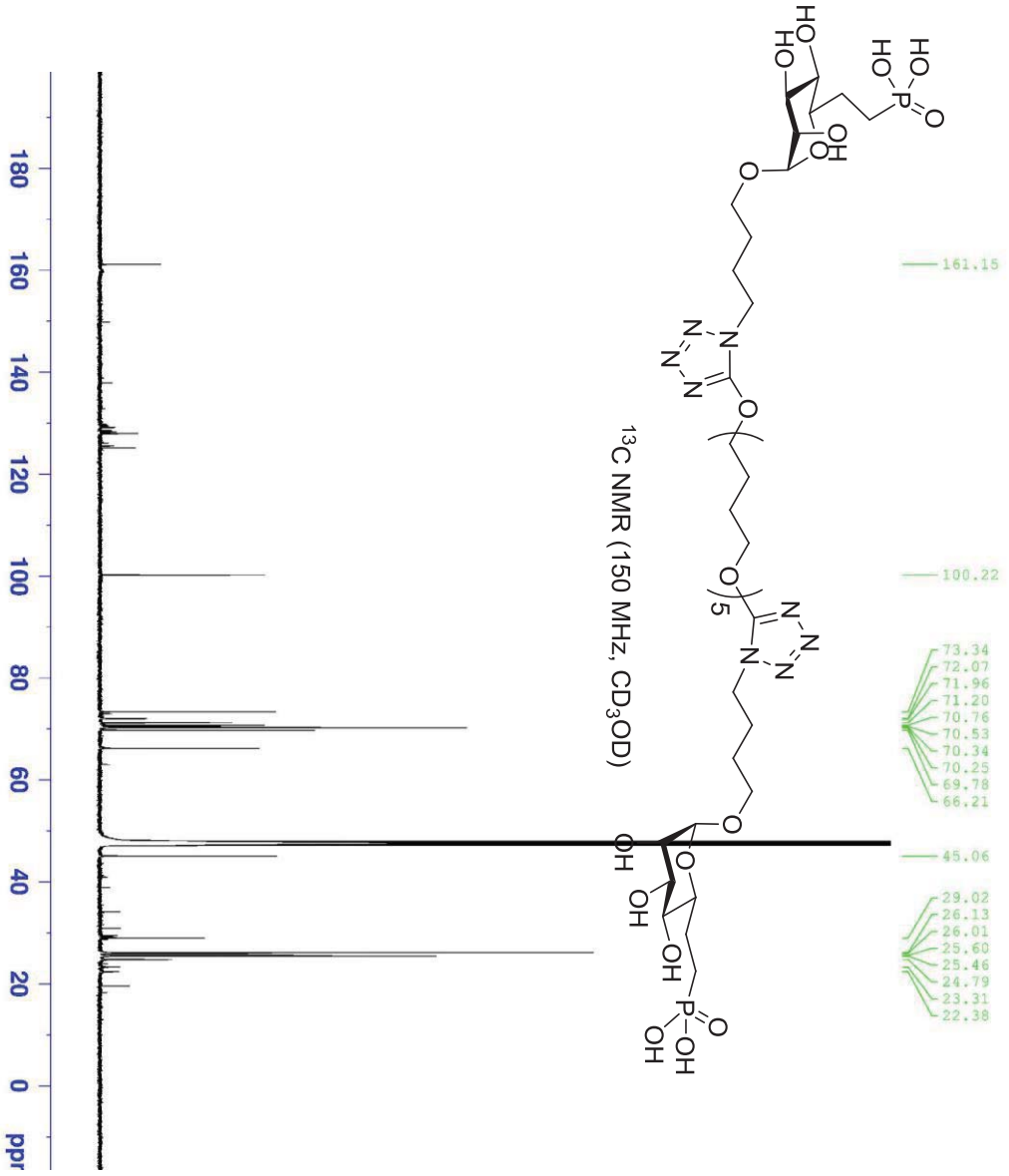
^{13}C NMR (150 MHz, CD_3OD)
161.15
100.22
73.34
72.07
71.96
71.20
70.76
70.53
70.34
70.25
69.78
66.21
45.06
29.02
26.13
26.01
25.60
25.46
24.79
23.31
22.38
180
160
140
120
100
80
60
40
20
0
ppm

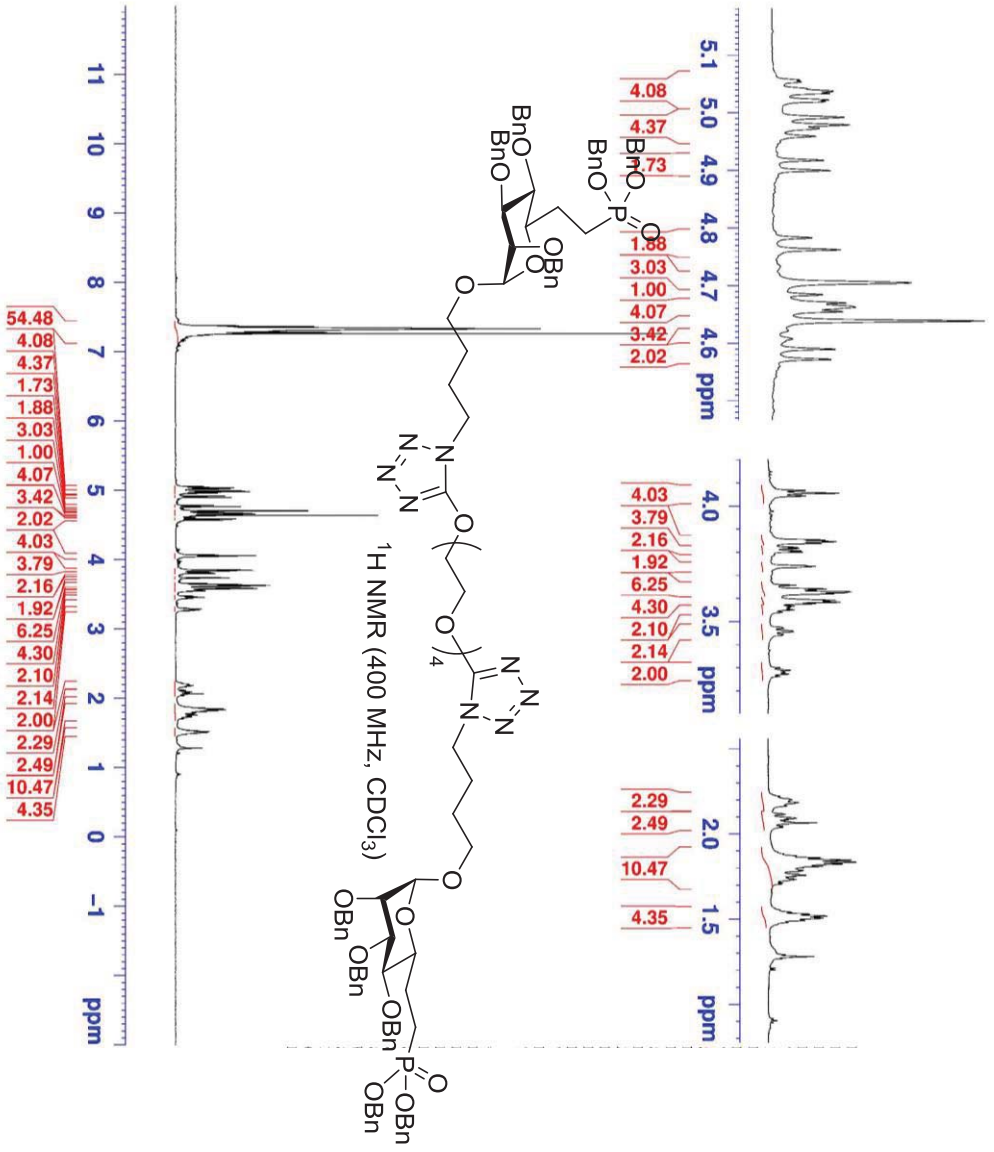
^{1}H NMR (400 MHz, $CDCl_3$)
ppm

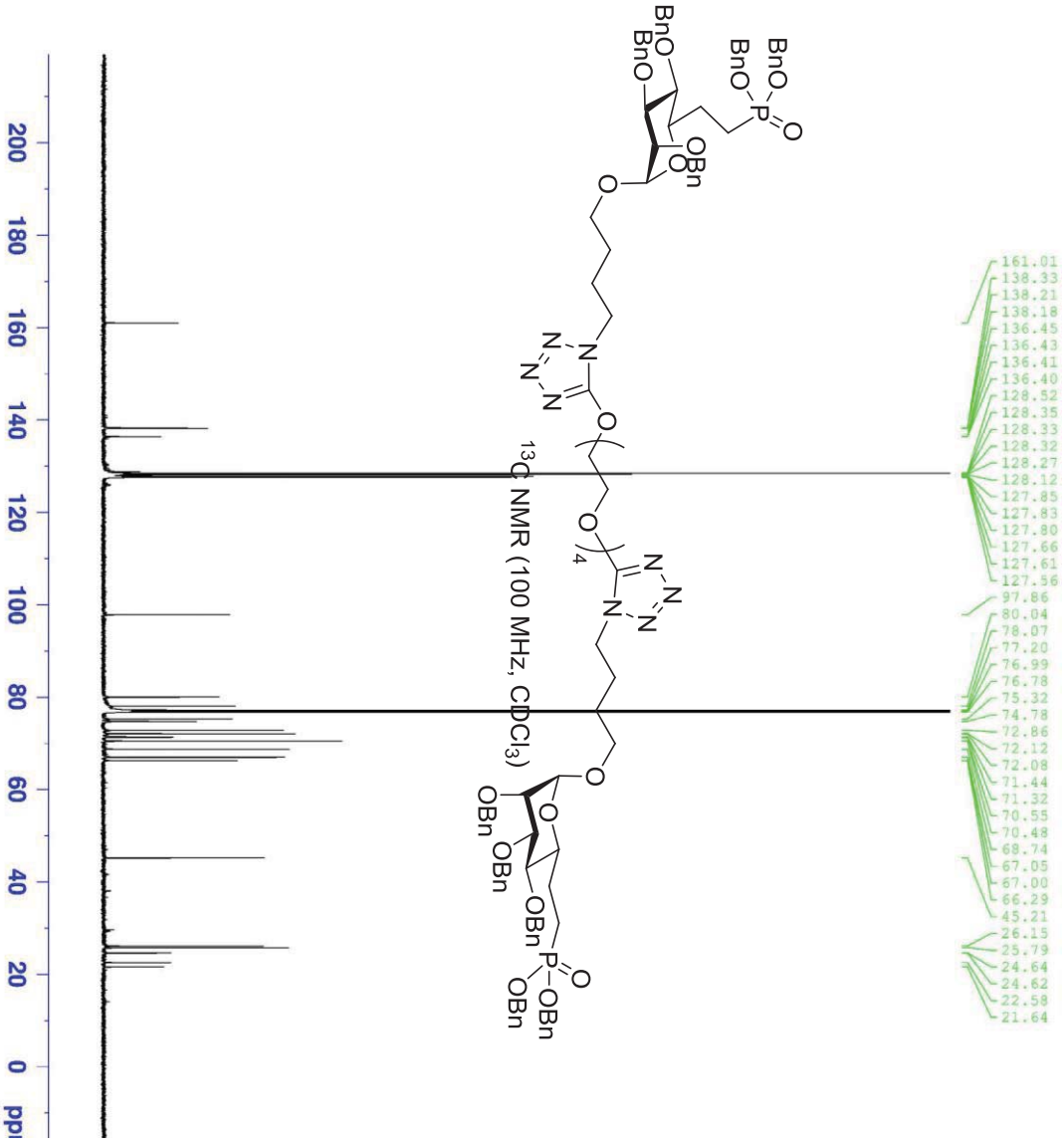
^{13}C NMR (100 MHz, CDCl$_3$)
161.01
138.33
138.21
138.18
136.45
136.43
136.41
136.40
128.52
128.35
128.33
128.32
128.27
128.12
127.85
127.83
127.80
127.66
127.61
127.56
97.86
80.04
78.07
77.20
76.99
76.78
75.32
74.78
72.86
72.12
72.08
71.44
71.32
70.55
70.48
68.74
67.05
67.00
66.29
45.21
26.15
25.79
24.64
24.62
22.58
21.64
200
180
160
140
120
100
80
60
40
20
0
ppm

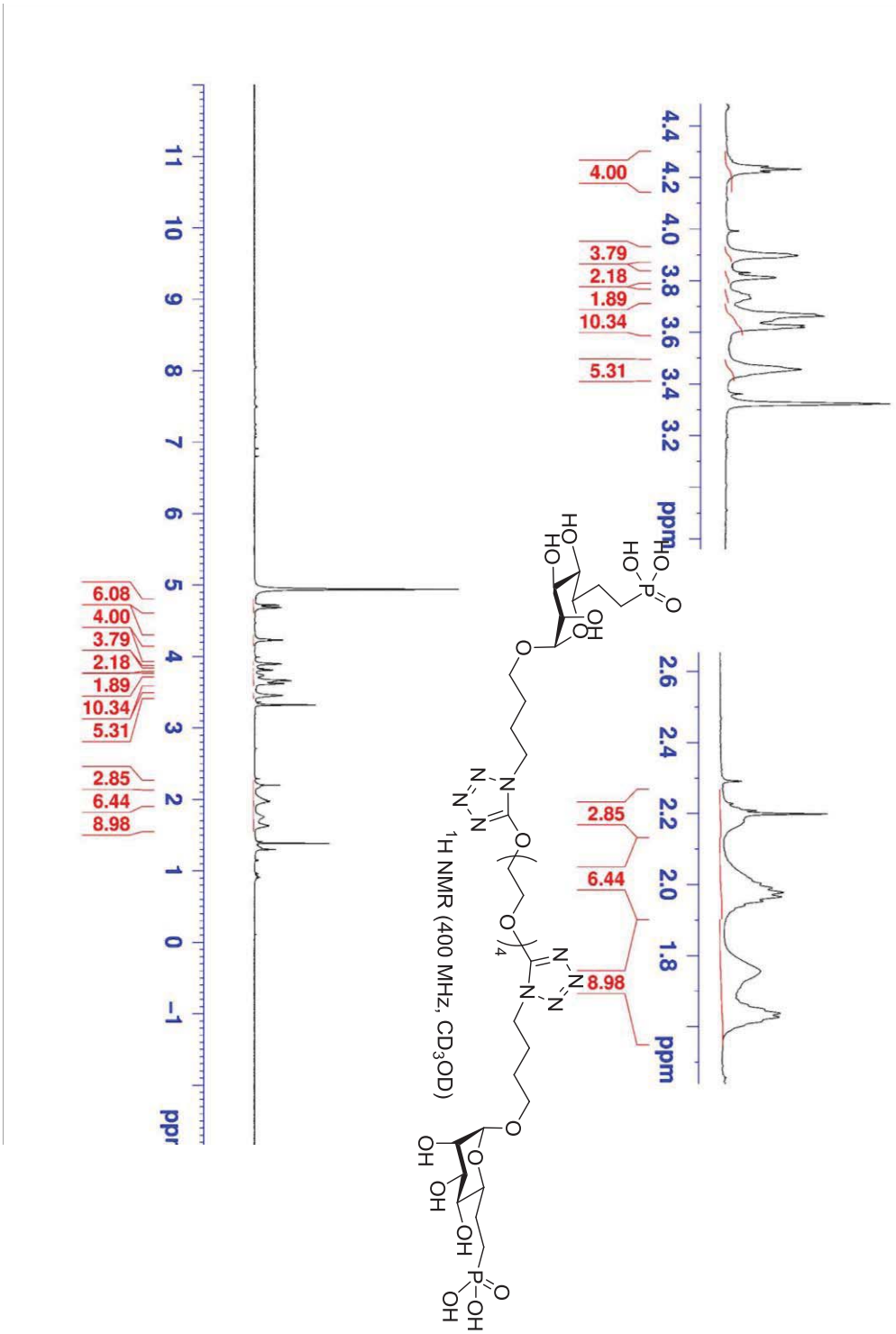
4.4 4.2 4.0 3.8 3.6 3.4 3.2 ppm
4.00
3.79
2.18
1.89
10.34
5.31
2.6 2.4 2.2 2.0 1.8 ppm
2.85
6.44
8.98
11 10 9 8 7 6 5 4 3 2 1 0 −1 ppm
6.08
4.00
3.79
2.18
1.89
10.34
5.31
2.85
6.44
8.98
^{1}H NMR (400 MHz, CD_3OD)

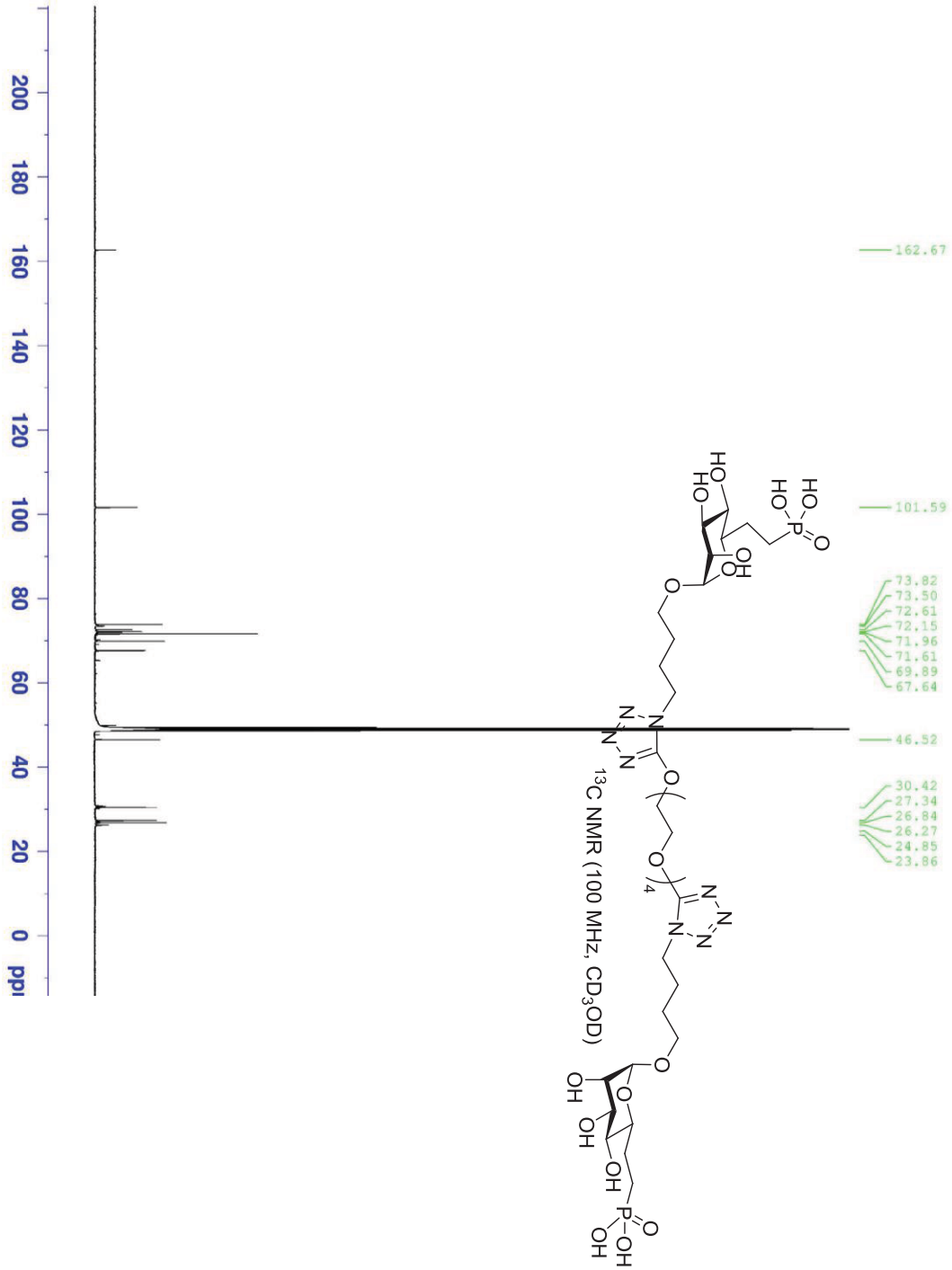
200
180
160
140
120
100
80
60
40
20
0 ppm
162.67
101.59
73.82
73.50
72.61
72.15
71.96
71.61
69.89
67.64
46.52
30.42
27.34
26.84
26.27
24.85
23.86
^{13}C NMR (100 MHz, CD_3OD)

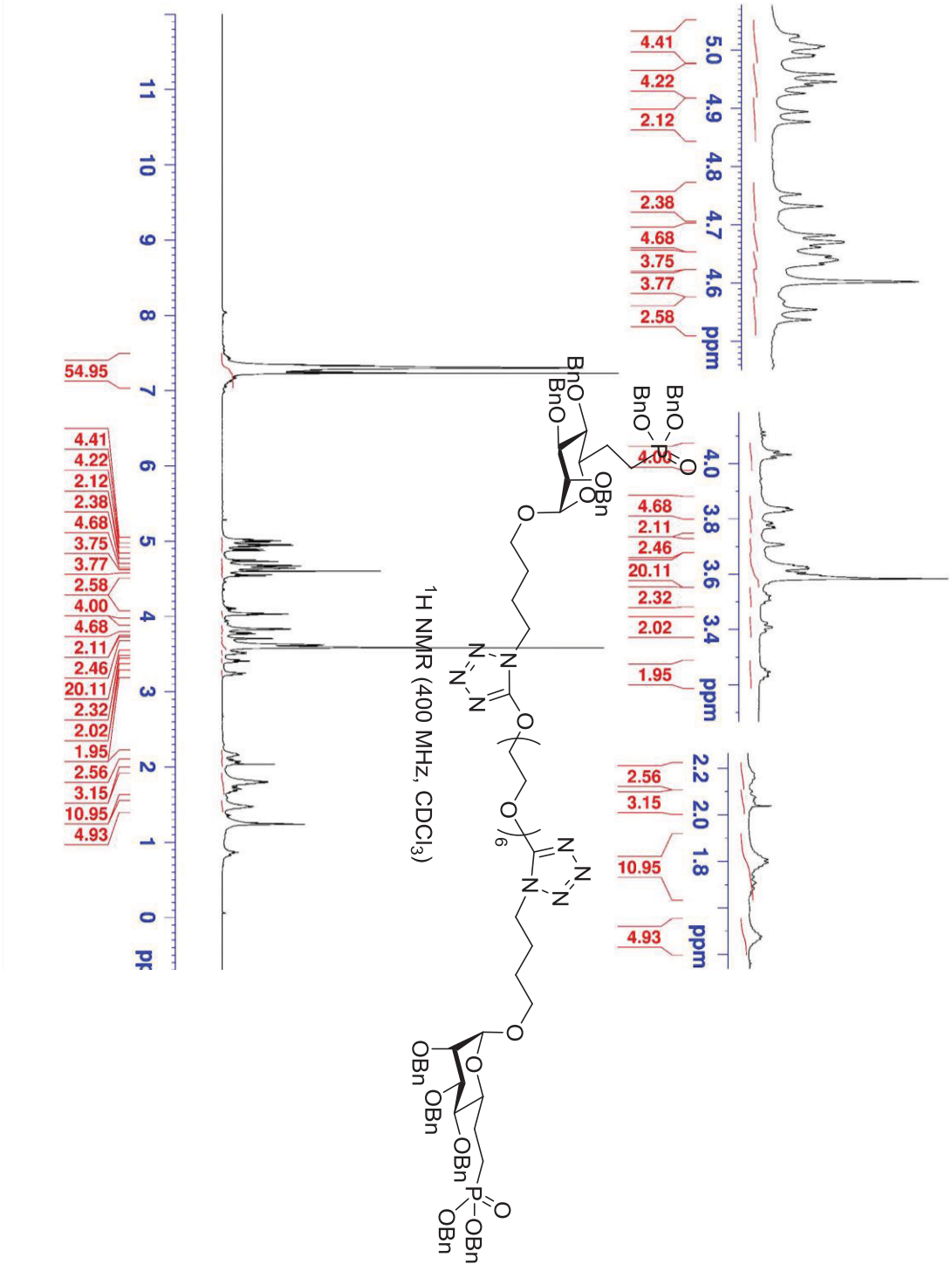
^{1}H NMR (400 MHz, CDCl$_3$)

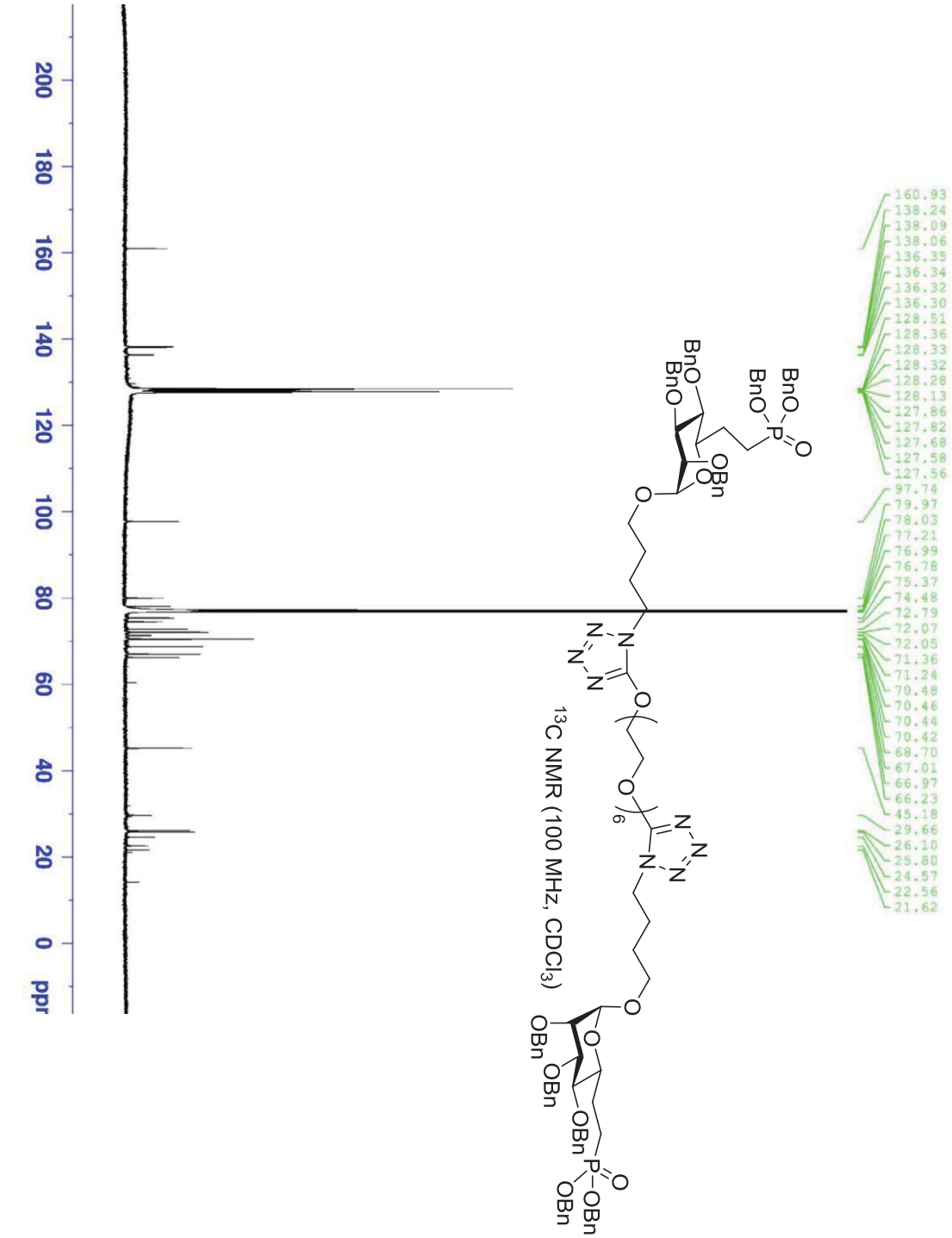
160.93
138.24
138.09
138.06
136.35
136.34
136.32
136.30
128.51
128.36
128.33
128.32
128.28
128.13
127.86
127.82
127.68
127.58
127.56
97.74
79.97
78.03
77.21
76.99
76.78
75.37
74.48
72.79
72.07
72.05
71.36
71.24
70.48
70.46
70.44
70.42
68.70
67.01
66.97
66.23
45.18
29.66
26.10
25.80
24.57
22.56
21.62
^{13}C NMR (100 MHz, CDCl$_3$)
200
180
160
140
120
100
80
60
40
20
0
ppm

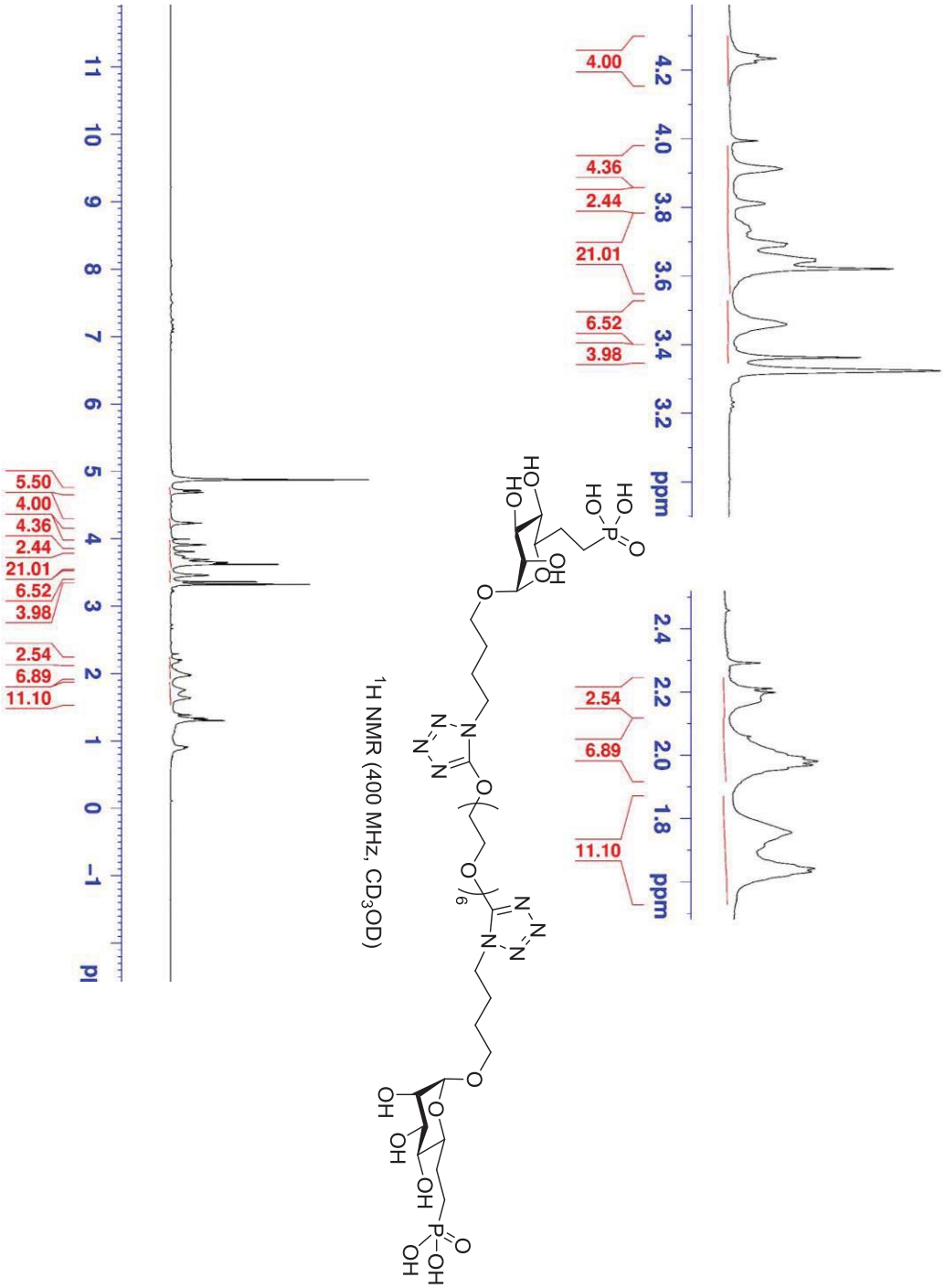
4.00
4.36
2.44
21.01
6.52
3.98
2.54
6.89
11.10
5.50
4.00
4.36
2.44
21.01
6.52
3.98
2.54
6.89
11.10
ppm
ppm
pp
^{1}H NMR (400 MHz, CD$_3$OD)

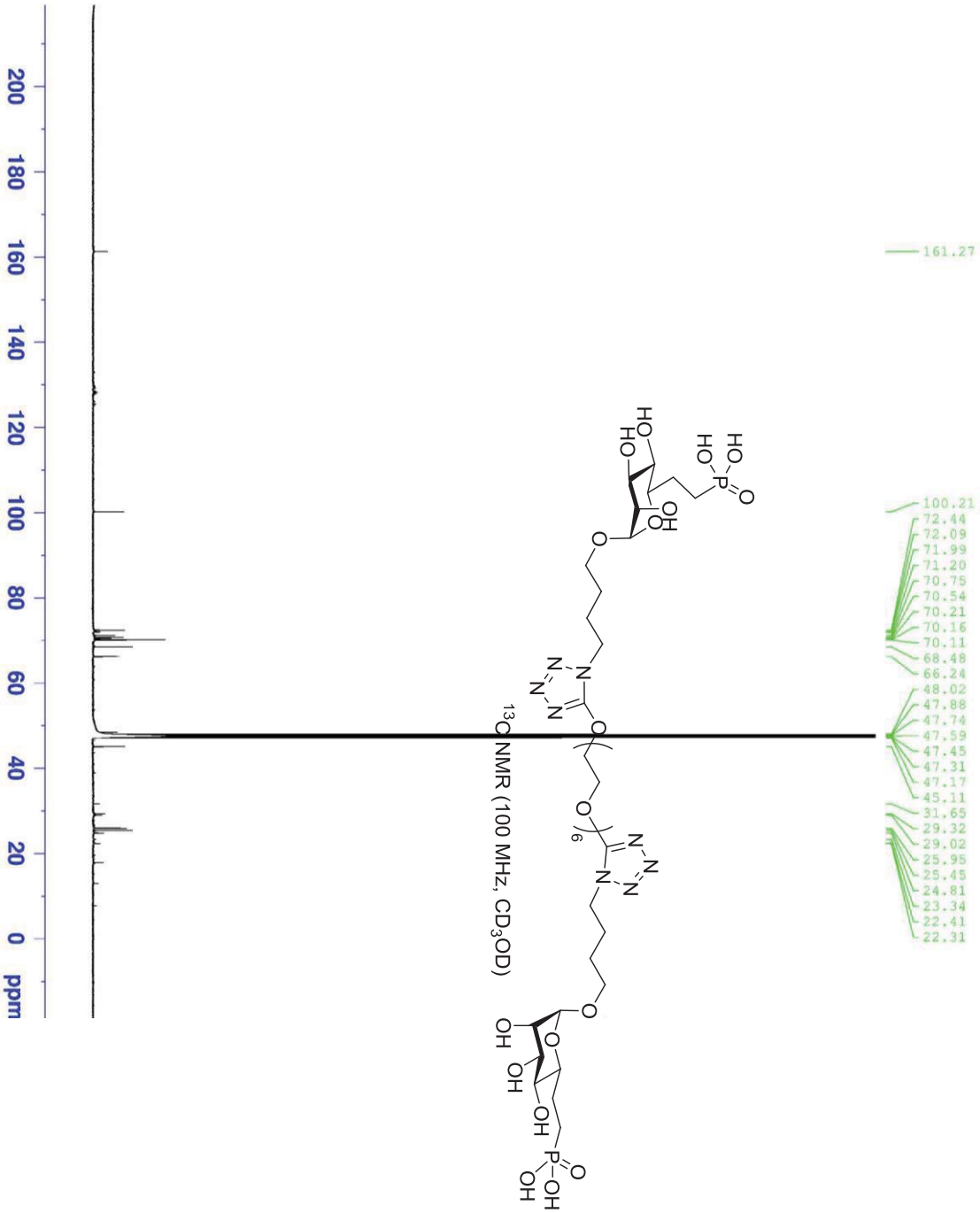

^{13}C NMR (100 MHz, CD_3OD)

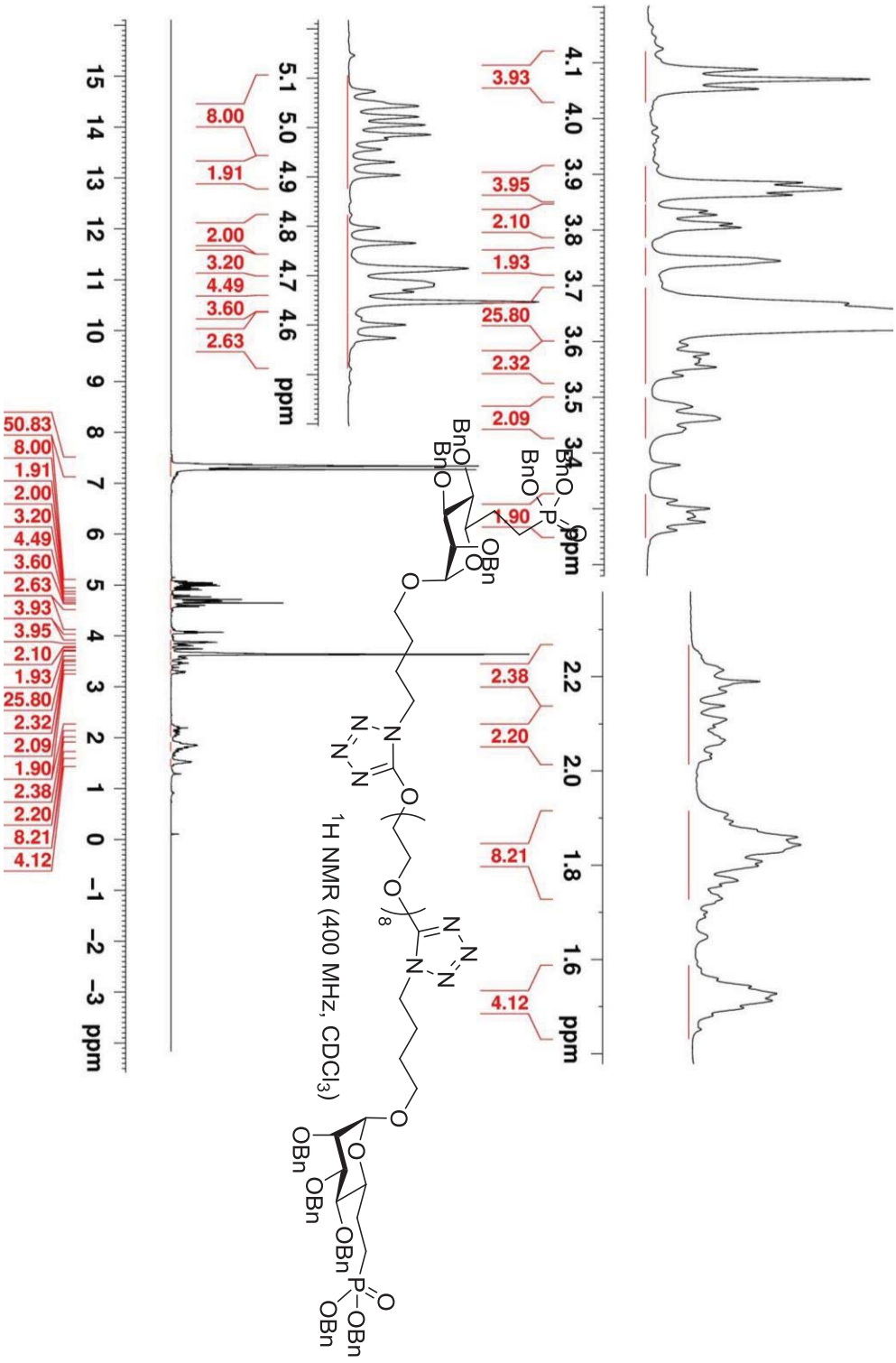
^{1}H NMR (400 MHz, CDCl$_3$)
50.83
8.00
1.91
2.00
3.20
4.49
3.60
2.63
3.93
3.95
2.10
1.93
25.80
2.32
2.09
1.90
2.38
2.20
8.21
4.12
ppm

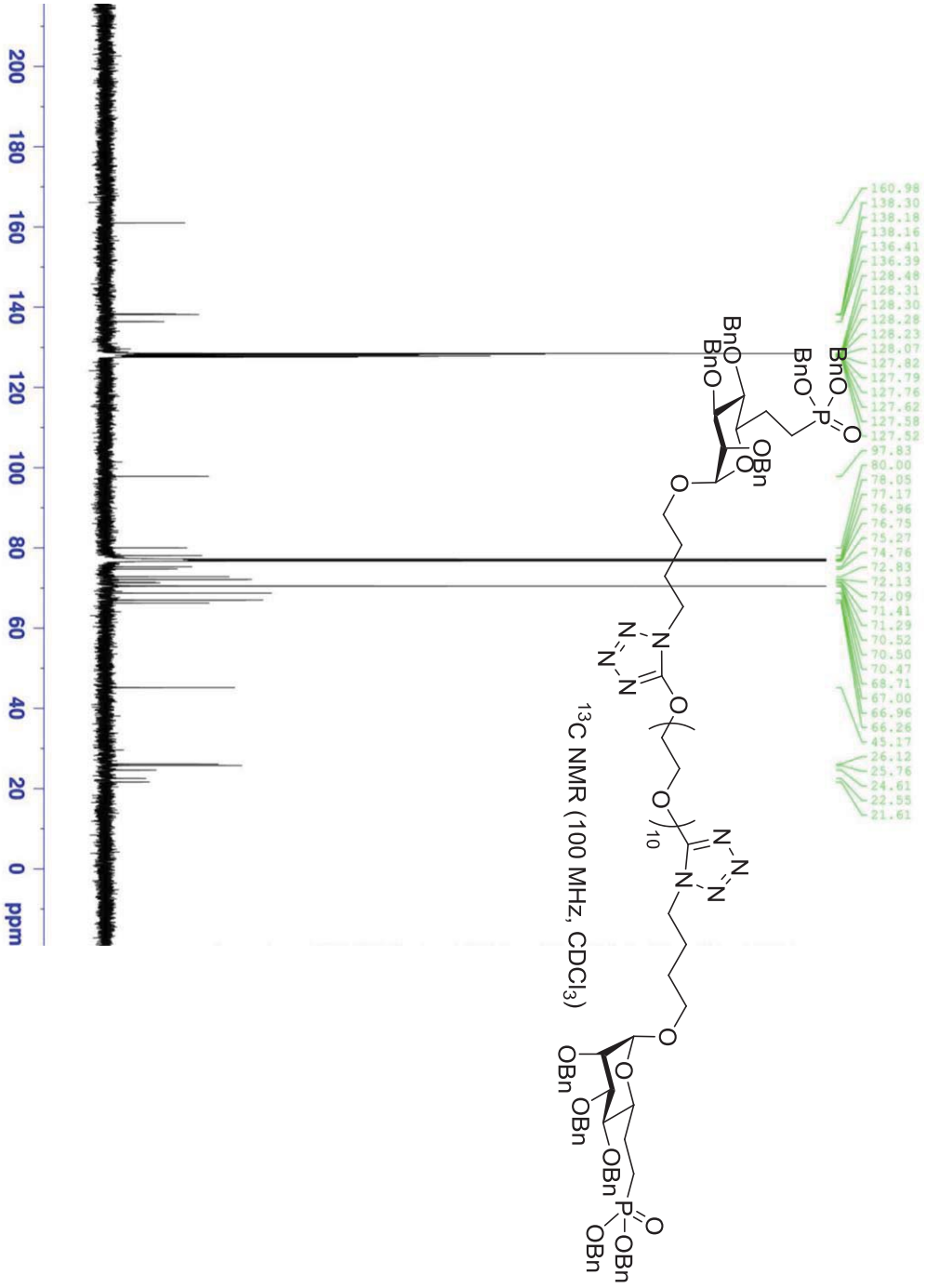
^{13}C NMR (100 MHz, $CDCl_3$)
200
180
160
140
120
100
80
60
40
20
0
ppm

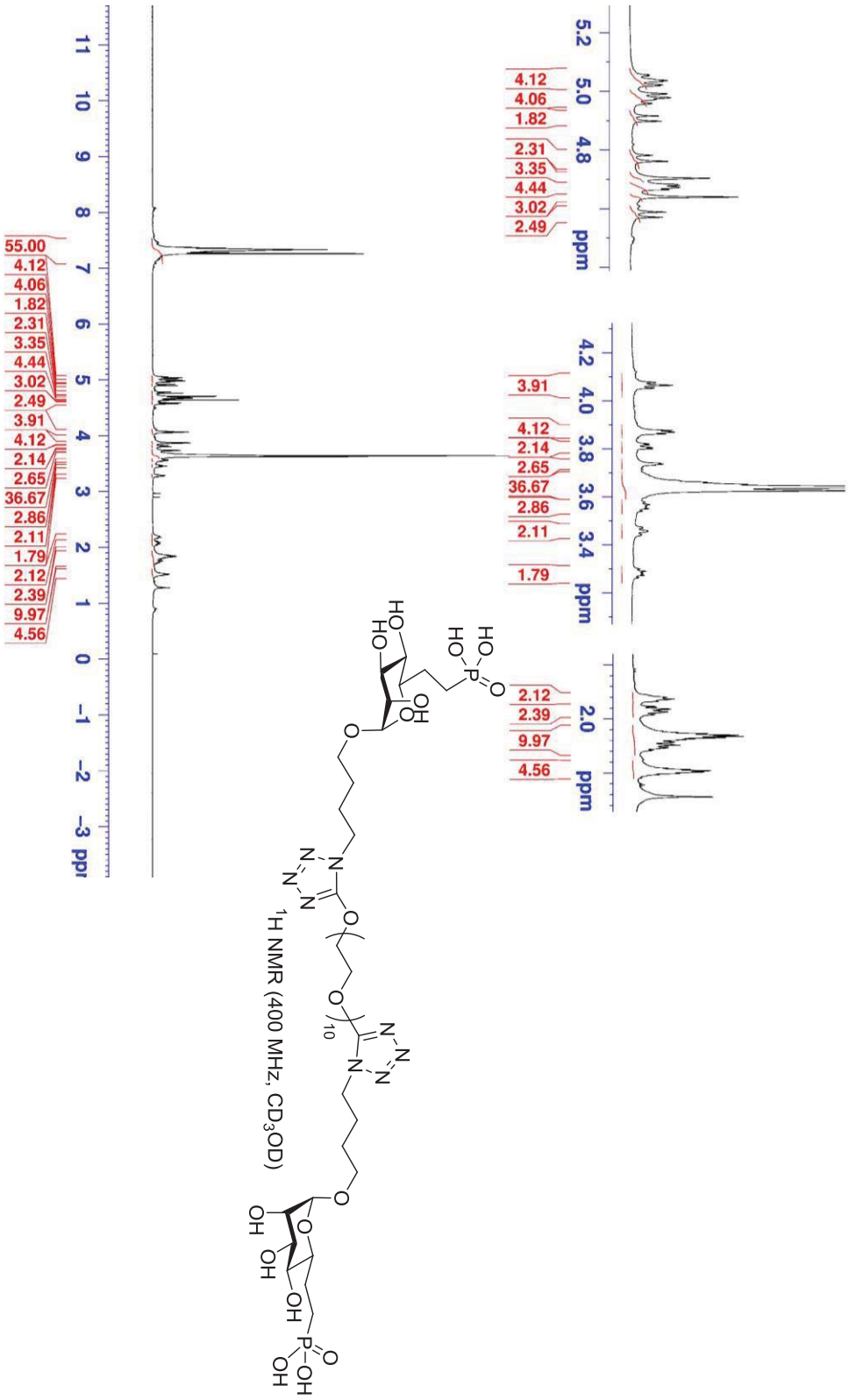
55.00
4.12
4.06
1.82
2.31
3.35
4.44
3.02
2.49
3.91
4.12
2.14
2.65
36.67
2.86
2.11
1.79
2.12
2.39
9.97
4.56
ppm
^{1}H NMR (400 MHz, CD$_3$OD)

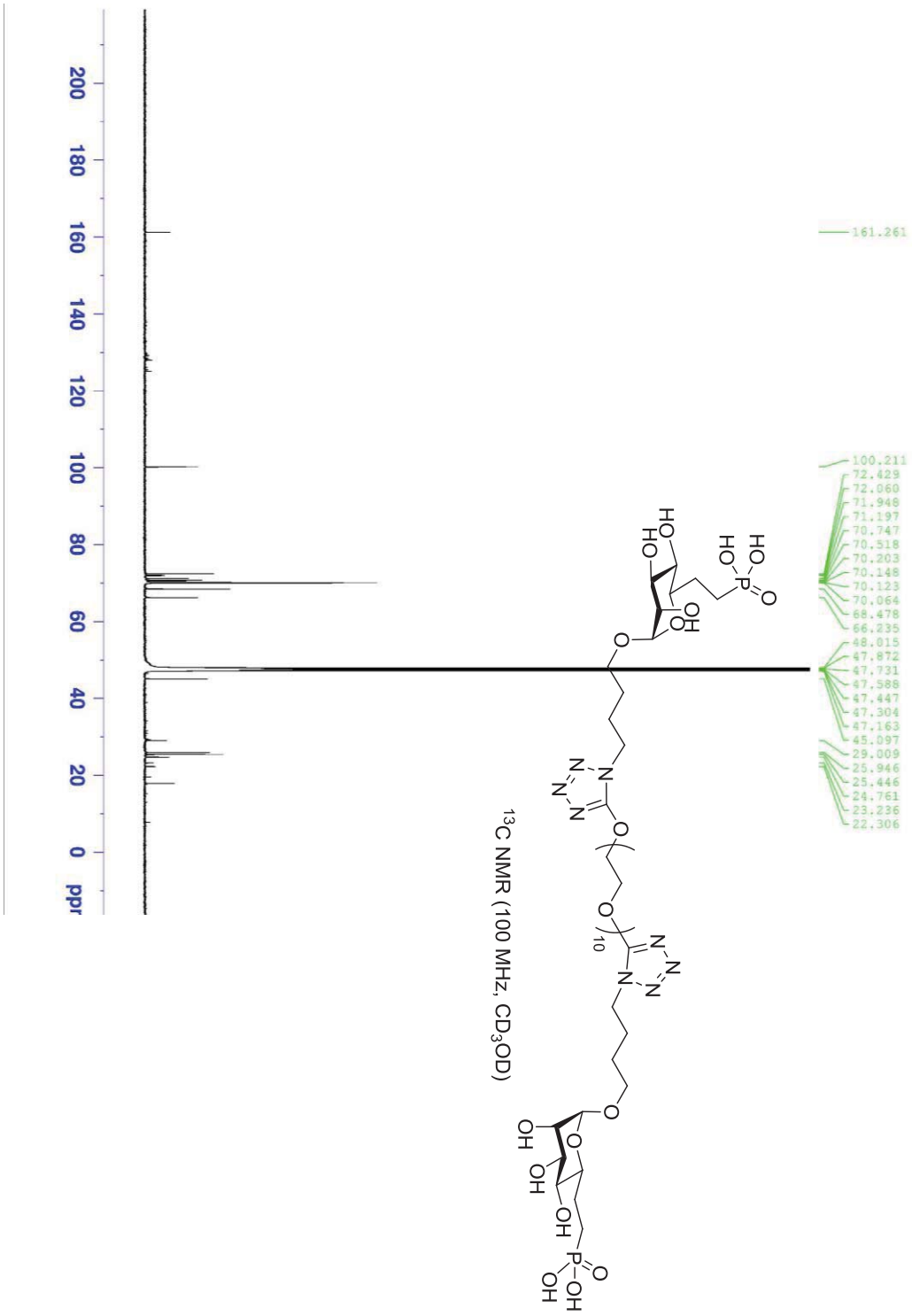

^{13}C NMR (100 MHz, CD_3OD)

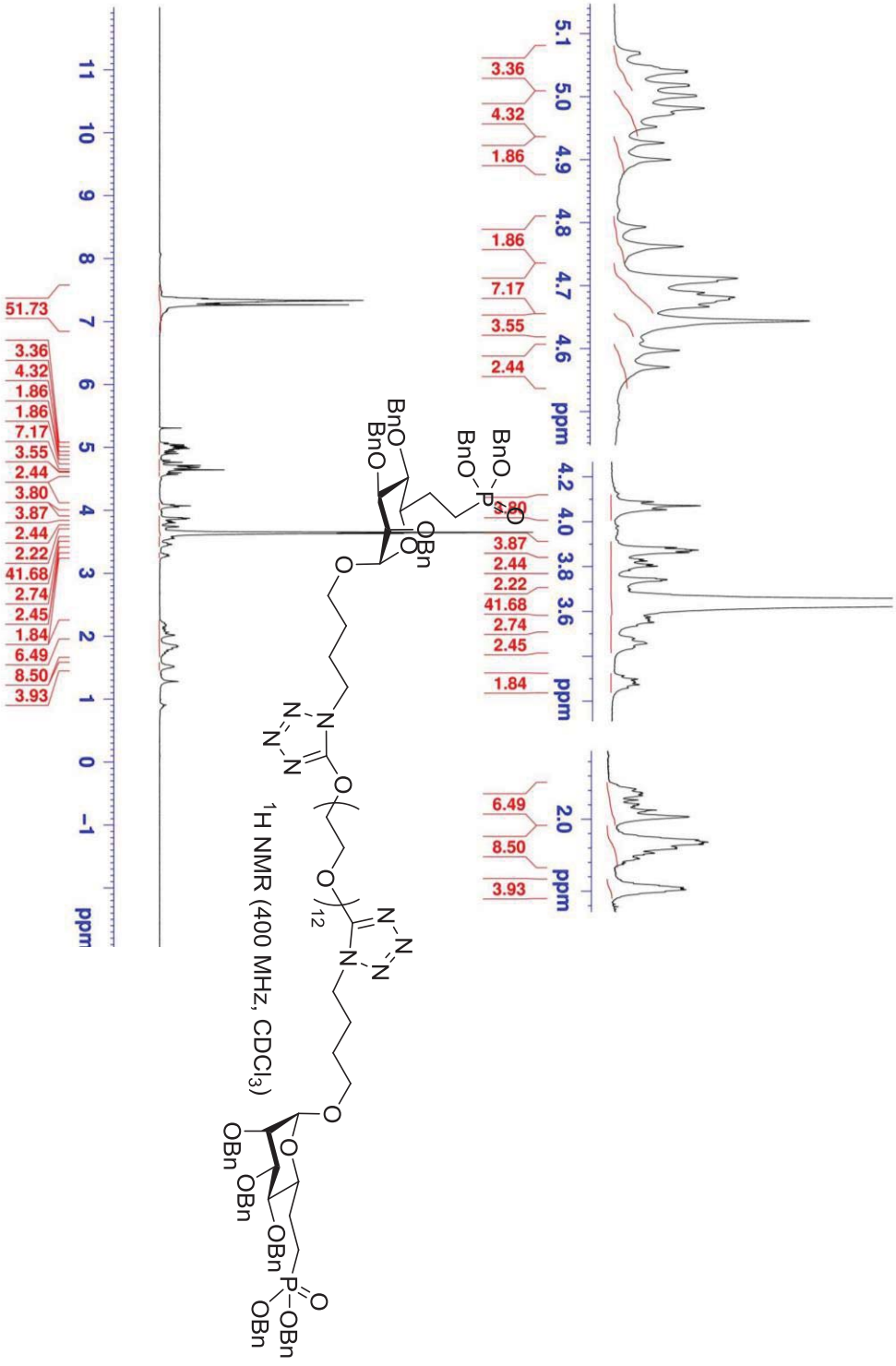
^{1}H NMR (400 MHz, CDCl$_3$)

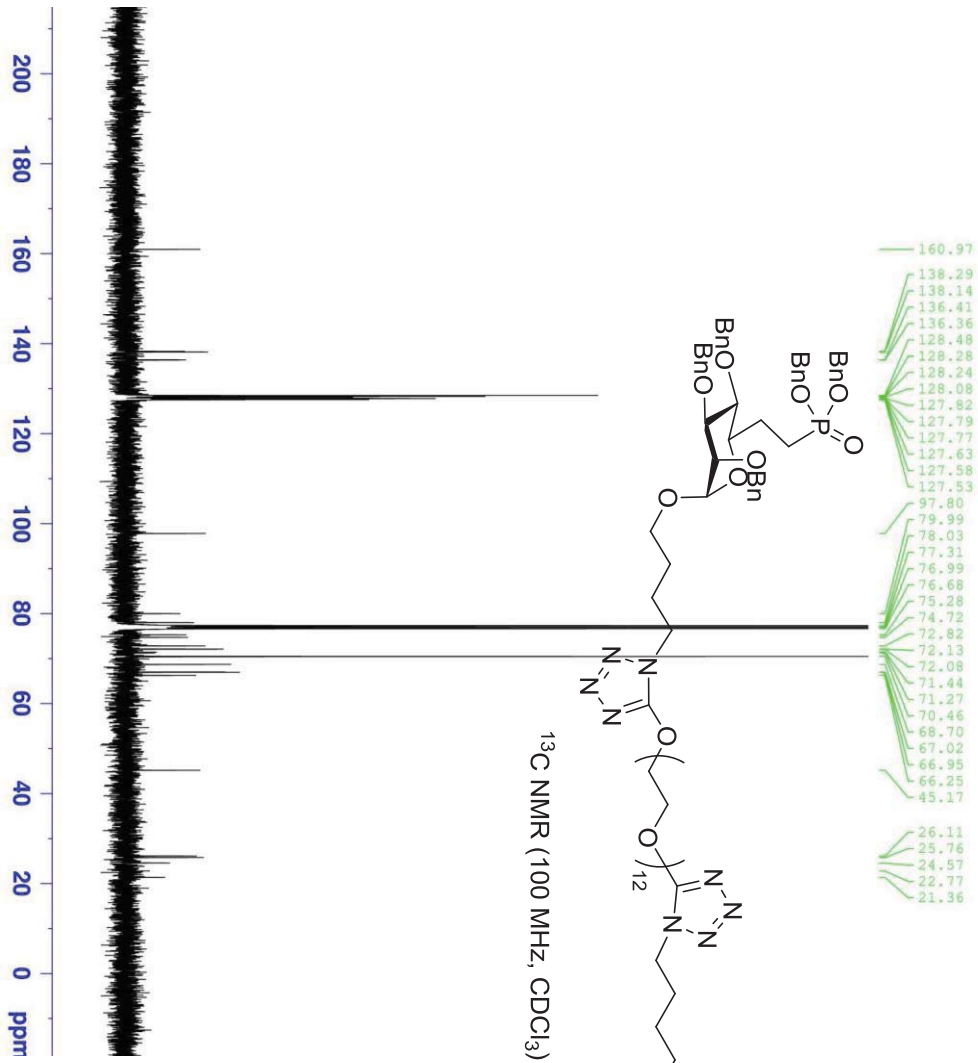
160.97
138.29
138.14
136.41
136.36
128.48
128.28
128.24
128.08
127.82
127.79
127.77
127.63
127.58
127.53
97.80
79.99
78.03
77.31
76.99
76.68
75.28
74.72
72.82
72.13
72.08
71.44
71.27
70.46
68.70
67.02
66.95
66.25
45.17
26.11
25.76
24.57
22.77
21.36
200
180
160
140
120
100
80
60
40
20
0
ppm
^{13}C NMR (100 MHz, CDCl$_3$)

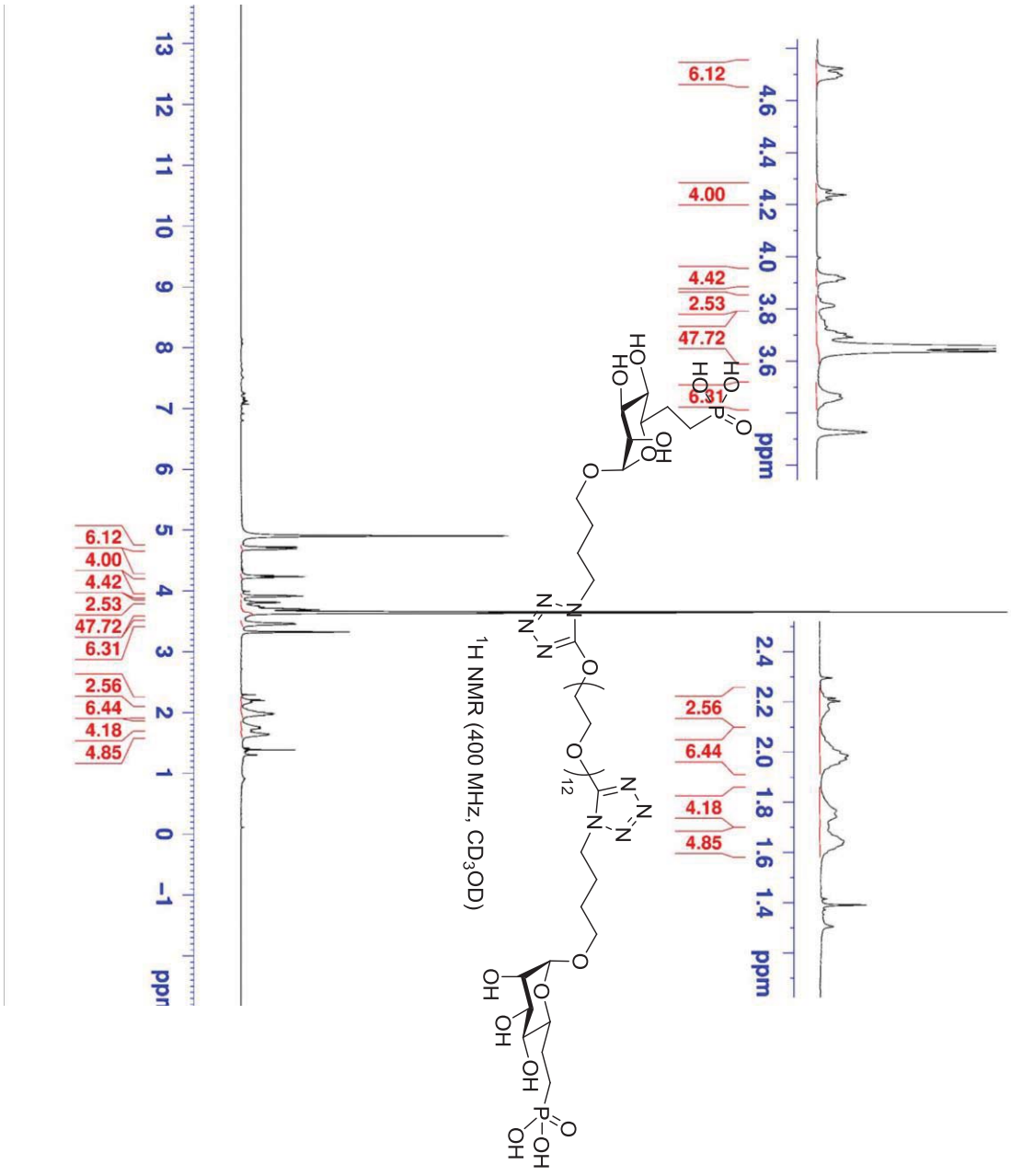
6.12
4.00
4.42
2.53
47.72
6.31
2.56
6.44
4.18
4.85
^{1}H NMR (400 MHz, CD_3OD)

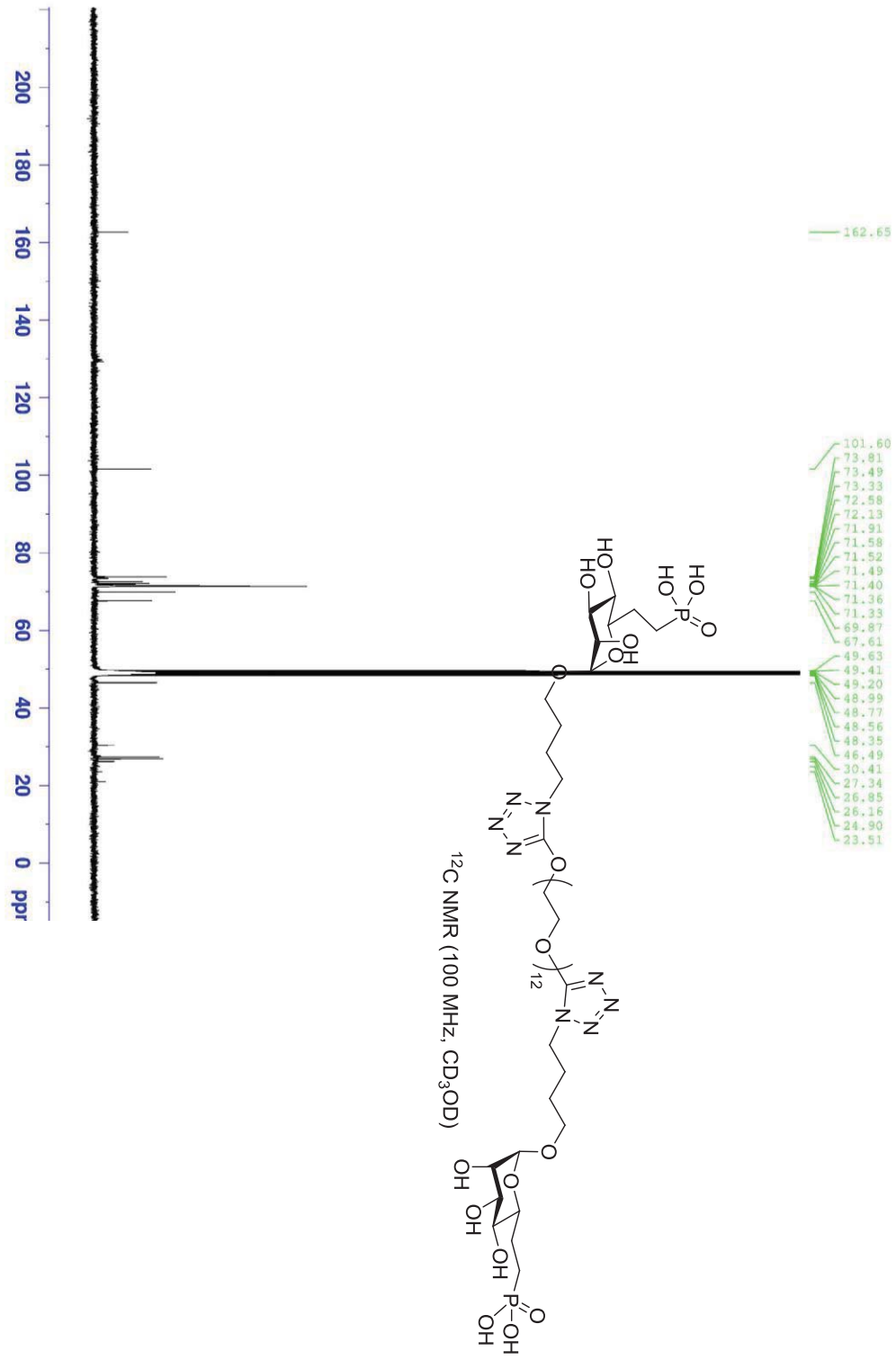
200
180
160
140
120
100
80
60
40
20
0
ppm
162.65
101.60
73.81
73.49
73.33
72.58
72.13
71.91
71.58
71.52
71.49
71.40
71.36
71.33
69.87
67.61
49.63
49.41
49.20
48.99
48.77
48.56
48.35
46.49
30.41
27.34
26.85
26.16
24.90
23.51
^{12}C NMR (100 MHz, CD$_3$OD)

Chapter 4

Carbafructopyranosyl 1,2-Diamines as New Chiral Scaffolds

I. Introduction

A. Chiral Pool in Asymmetric Catalysis

Naturally-occurring compounds, such as the natural phosphonates in Chapter one, have been great inspiration for medicinal chemists. On the other hand, natural products have also been magnificent resources for quite a different domain: asymmetric catalysis. Chiral pool-derived catalysts, ligands and auxiliaries have all contributed significantly to the development of numerous asymmetric transformations.[1] For instance, the cinchona alkaloid backbone, as classically presents itself in the natural product quinine, has made enormous impact as the stereo-differentiating element in the Sharpless asymmetric hydroxylation (ADH)[2], as well as the O' Donnell-Lygo-Corey chiral phase-transfer catalysts (PTCs)[3-5]. As marked cases in the terpenoid category, the α-pinene derived organoboron reagents, such as Alphine-borane™ and DIP-chloride, have been widely utilized in asymmetric reduction.[6] Furthermore, inspired by the efficiency of enzymes, chemists have extensively utilized amino acids in catalyst assembly.[7] Notably, amino acid derived phosphinooxazoline (PHOX) ligands have had a major impact on a range of transition metal (TM)-catalyzed reactions.[8] In a more biomimetic approach, Miller *et al* have developed a series of β-turn-based oligopeptides with the tetrapeptide catalytic core. These organocatalysts have shown remarkable selectivities in various transformations, including the Aldol reaction, conjugate additions, epoxidations, acylations, phosphorylations etc.[9-10]

Their abundance and variety in nature have made carbohydrates an amazing source of chirality.[11-20] The success of sugar based chiral catalysts can be epitomized by the historic tartaric acid derived ligands, such as diethyl tartrates (DET)[21], TADDOLs[22] and Chiraphos[23] (Fig. 4.1). Recent examples include Rajanbabu's diphosphinite ligands which was built upon the bicyclic 4,6-*O*-benzylidene-D-glucopyranose. The nickel-ligand complex catalyzes hydrocyanation reactions with a range of vinylarenes, with up to 91% ee.[24]

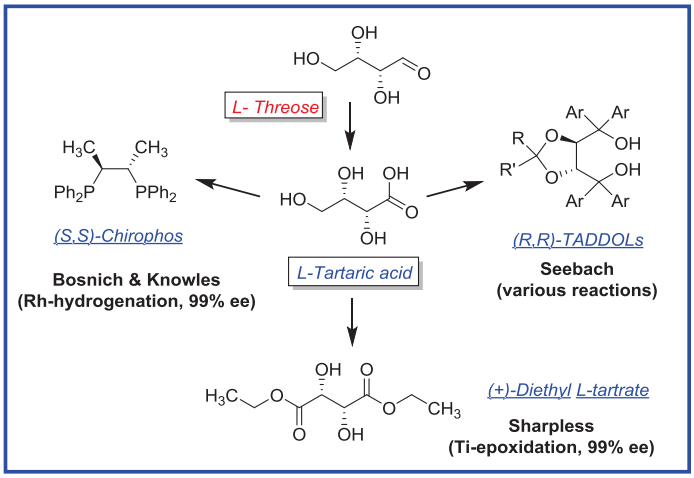

Figure 4.1: Classic ligands derived from L-threose

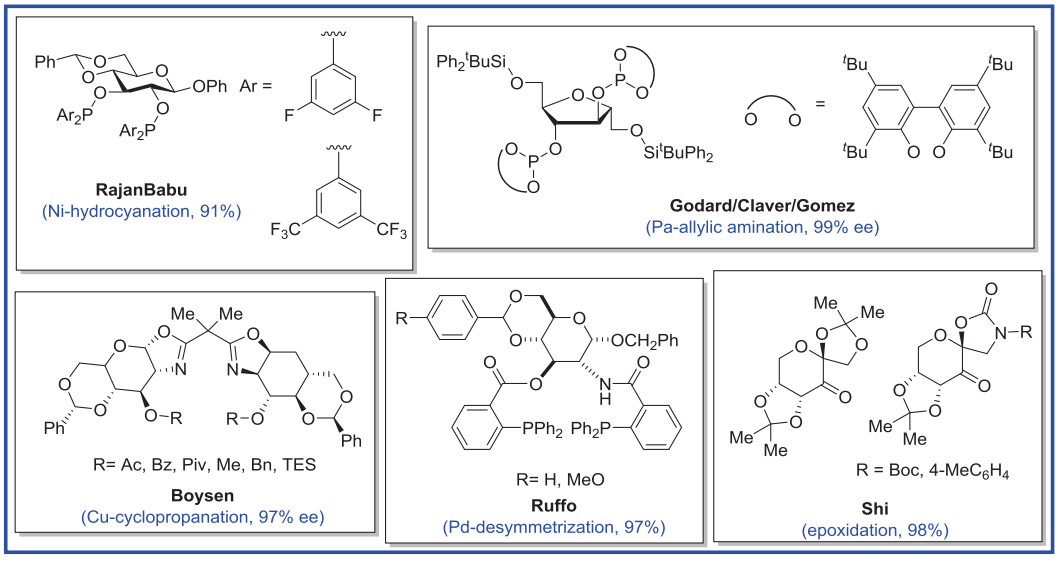

Figure 4.2: Some recent examples of carbohydrate derived ligands and catacatalysts

Moreover, Gomez, Claver and Godard reported a diphosphite ligand bearing a 2-deoxy-L-fructofuranose backbone which showed excellent enantioselectivities in the Pd-catalyzed allylic amination reactions.[24] Boysen group has developed a series of α-D-glucosamine based bis(oxazoline) (*gluco*Box) ligands. The 3-*O*-Ac *gluco*Box was utilized in the total synthesis of alkaloid (-)-desoxyeseroline via an enantioselective Cu-catalyzed cyclopropanantion of N-acyl indoles.[25] Adopting the same glucosamine motif, Ruffo and *et al* have synthesized a number of bis(phosphinoamide) ligands (Trost ligands).[26] They are exploited in the desymmetrization of *meso*-1,4-biscarbamate cyclopentene, via the Pd-promoted intramolecular allylic amination. In addition to these synthetically useful ligands, carbohydrate framework has also been successfully utilized in developing chiral organocatalysts. One of the most notable cases is Shi's seminal work on the ketone-mediated asymmetric epoxidation reactions.[27-29] The β-D-fructopyranose derived exocyclic ketones proved to be highly enantioselective (up to 97%), across a wide range of di- or tri-substituted alkenes (Fig. 4.2).[30-31]

B. A Chiral Pool Derived Salen Ligand Library

In 2005, our group reported a combinatorial approach to explore novel salen scaffolds. A 7×7 library was built on the diamines derived from chiral pool (Fig. 4.3). Particularly, terpenoid (β-pinene), amino acids (L-phenylalanine and L-phenylglycine) and carbohydrate (D-fructopyranose) are utilized to prepare the vicinal diamines. By coupling with various salicylaldehydes, a series of non-C_2-symmetric salen ligands were prepared. They were subsequently evaluated in the Co-(III)-mediated hydrolytic kinetic resolution (HKR) of terminal epoxides, as a platform to introduce the double-cuvette ISES.[32] Two hit salen scaffolds emerged from the screening. The β-pinene-diamine/α-

hydroxynaphthaldehyde combination showed high selectivity for the HKR of the matched epoxides. This salen ligand was recently utilized to set the stereochemistry, in a streamlined synthesis of pseudo-enantiomeric cores of linearifolin and zaluzanin A (Fig. 4.4).[33]

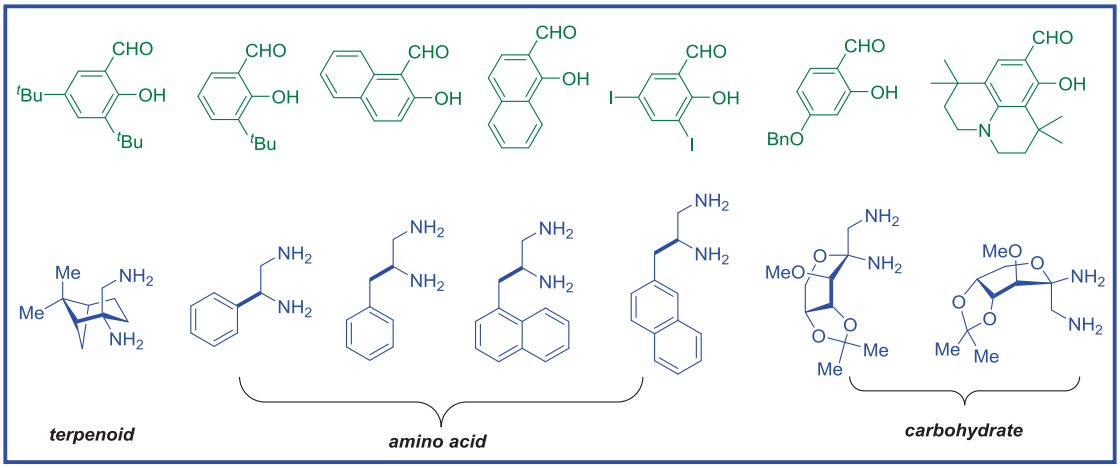

Figure 4.3: Salicylaldehydes and diamines used in the salen ligand assembly

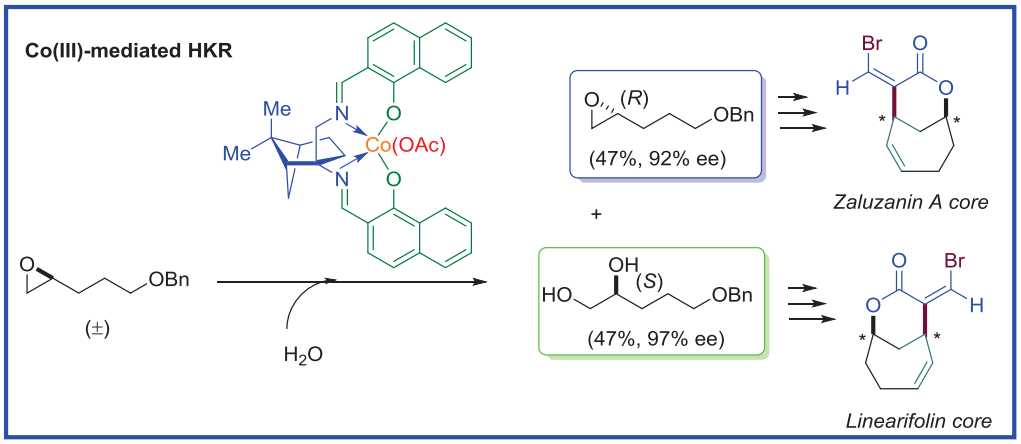

Figure 4.4: Applications of β-pinene derived Co(III)-salen catalyst

In addition, the β-D-fructopyranosyl-1,2-diamine showed great promise as a novel chiral motif. The salen ligand derived from this diamine and 3,5-diiodo-salicylaldehyde exhibited the highest E-value in the HKR of propylene oxide. Moreover,

this salen series showed an interesting enantioswitch, which seems to be only dependent on the salicylaldehyde counterpart. Namely, changing from 3,5-diiodo-salicylaldehyde to 3,5-di-*ter*-butyl-salicylaldehyde, the β-D-fructopyranosyl-diamine derived ligand manifested opposite enantio-preference in the HKR. It was postulated that an undetected anomerization might cause the change of the enantiopreferences. Given the excellent enantioselectivity of this novel salen scaffold, we set out to explore more about these ligands. Specifically, we set out to make the carbocyclic version of this carbohydrate based diamine to lock the anomeric center of the sugar.

C. Novel Screening Methods in Combinatorial Catalysis

After more than 200 years of research in organic synthesis, there is no doubt that the discovery of new reactivity gets more and more challenging. However, search for new types of reactions, particularly catalytic transformations, has become increasingly essential for many aspects of the society, such as energy and medicine. Despite some great successes in recent years[34], catalyst development is still a difficult process. The discovery of a highly efficient and selective catalyst often requires a combination of rational design, intuition and serendipity. In the last two decades, the combinatory chemistry has emerged as an approach to speed up the process. It has proved to be effective in catalyst discovery, via screening diverse catalytic elements including metals, chirality, etc.[35] Recently, taking this approach, MacMillan *et al* discovered a Ir(III)-mediated photoredox amine C-H arylation reaction.[36] By applying an automated workflow system, they screened a large number of potential reactions between various functional groups. Out of an array of identified reactions, the C-H arylation of tertiary amines presents the most interesting result, owing to the pharmaceutical values of the

produced benzylic amine motif. Moreover, in a more dynamic combinatorial approach, Hartwig *et al* screened a variety of catalysts with diverse mixture of substrates, and then utilized mass spectrometry to identify the products.[37] A Cu(I)-catalyzed alkyne hydroamination and two Ni(0)-promoted alkyne hydroarylation reactions were unveiled as new types of transformations (Fig. 4.5).

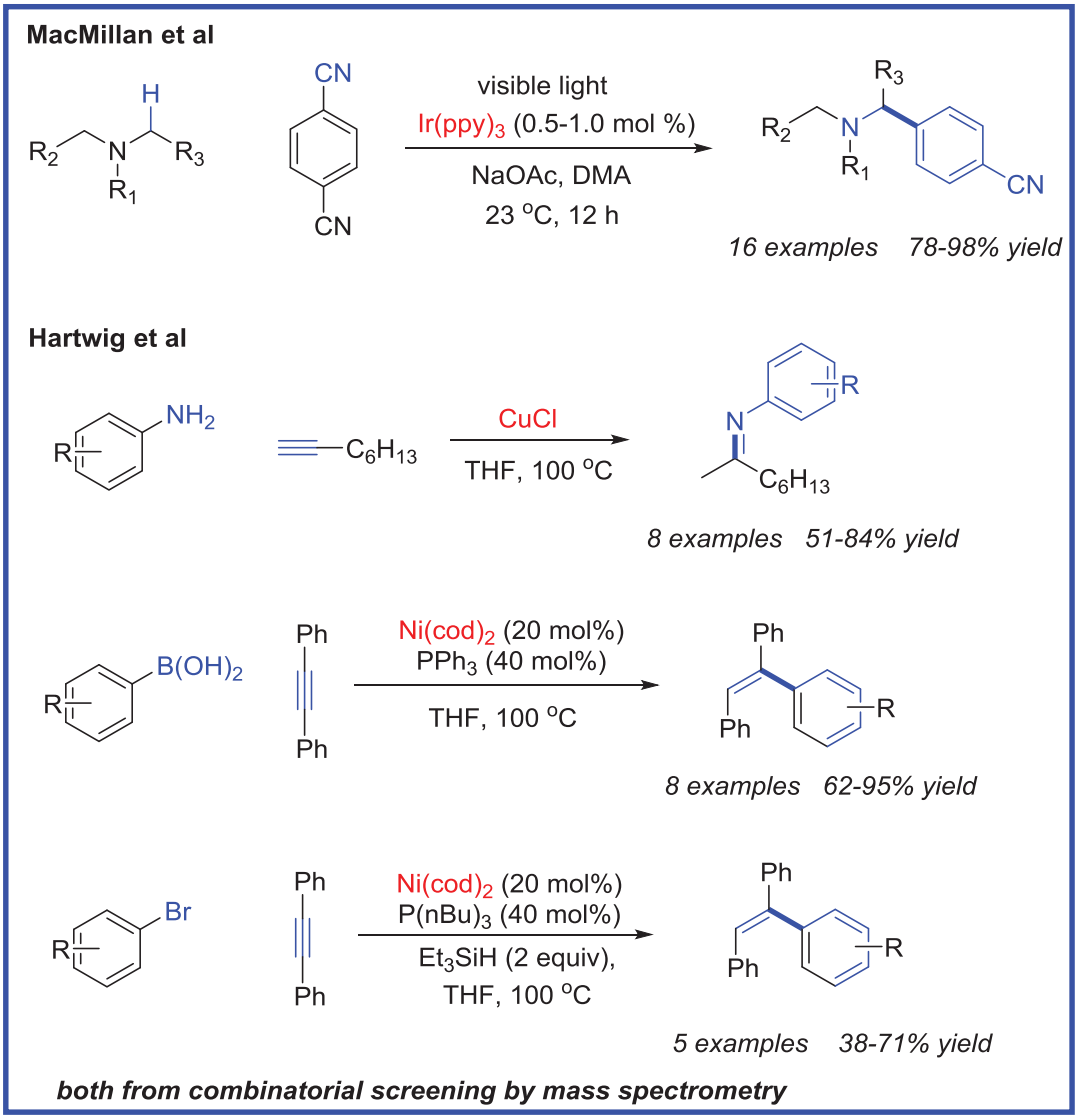

Figure 4.5: Novel reactivity discovered by combinatorial screening

Although great effort has been devoted to its development, the screening process is still arguably the "bottleneck" of the combinatorial catalysis.[38] Recently, Glorius *et al* nicely summarized some contemporary screening methods in combinatorial catalysis.[39] Notably, by tagging substrate with a pyrene, Kozmin *et al* were able to screen hundreds of reactions using laser desorption/ionization and time-of-flight mass spectrometry.[40] This label assisted LDI-TOF-MS technique eliminates the needs for an external matrix and also simplifies MS analysis. Through this novel screening method, they identified two interesting benzannulation reactions of siloxy alkyne; namely, the Au(III)-mediated annulation with 2-pyrone and Ag(I)-catalyzed cycloaddition with N-isoquinoline (Fig. 4.6).

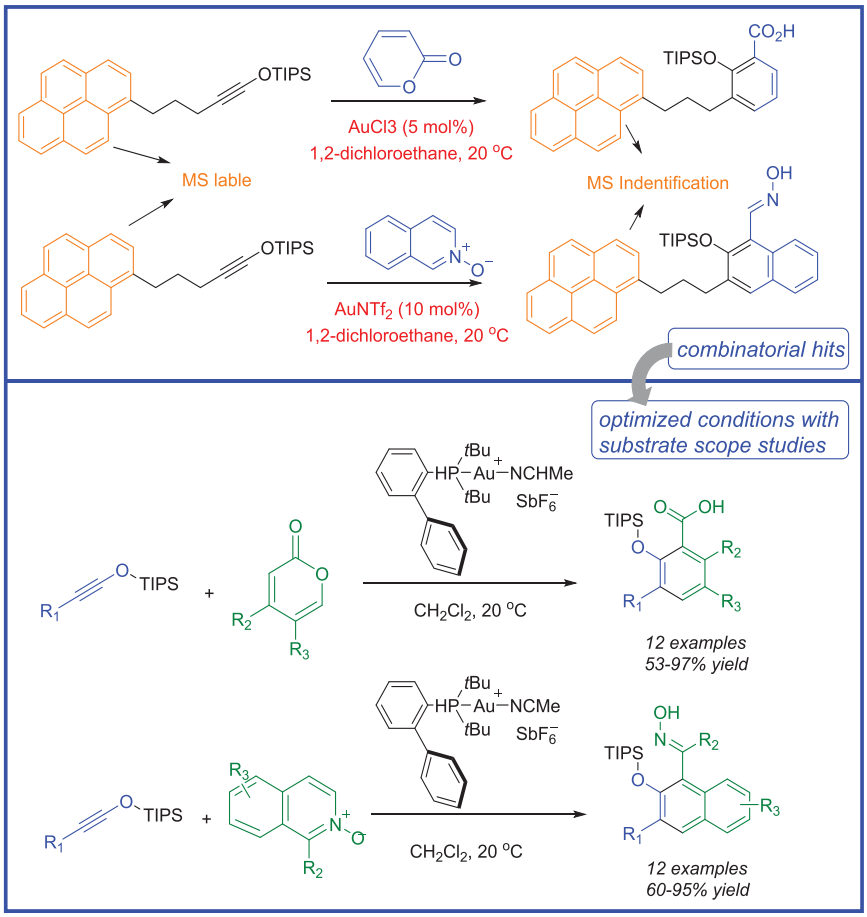

Figure 4.6: Label assisted mass spectrometry for novel reactivity

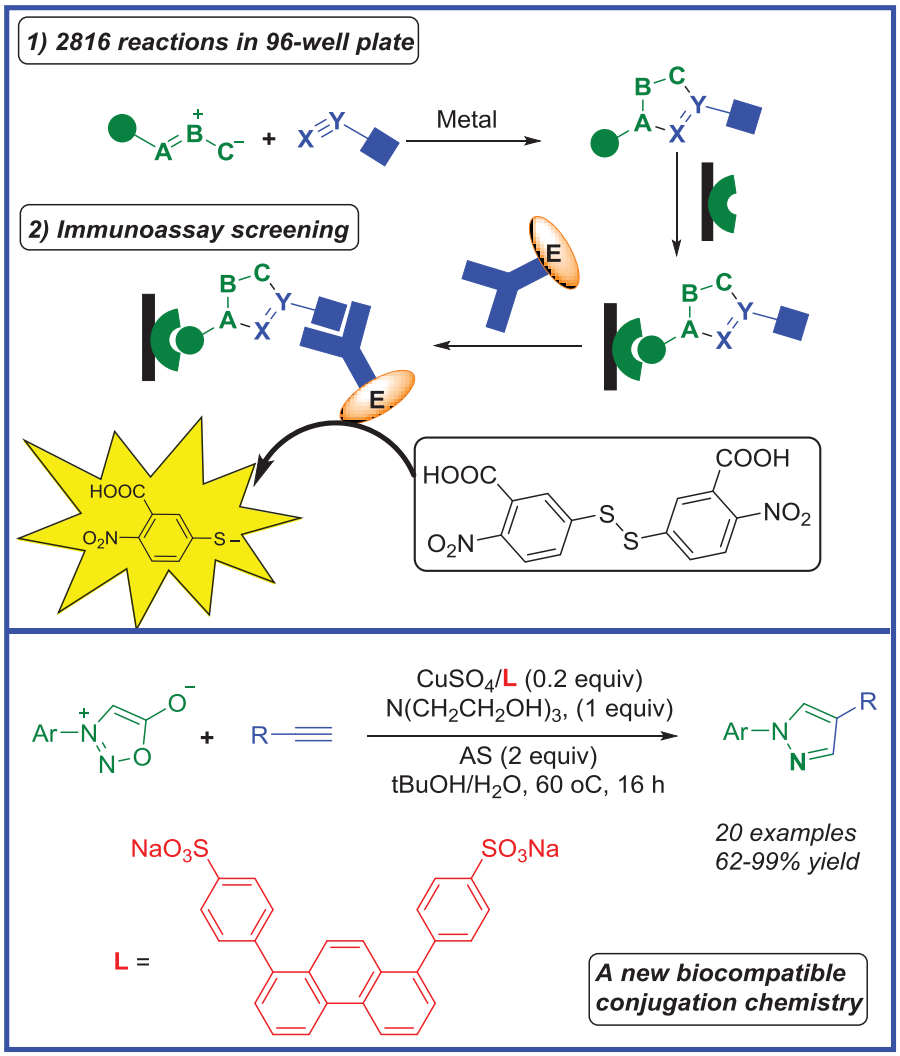

Figure 4.7: A new bioorthogonal chemistry disclosed by combinatorial immunoassay screening

Furthermore, enzyme immunoassays have shown their prowess in combinatorial catalysis.[41-42] Recently, Taran *et al* utilized the sandwich enzyme-linked immunosorbant assay (ELISA) to uncover a novel 1,3-dipolar cycloaddition reactions.[43] In this assay, one component was labeled with an epitope that can be recognized by a solid-supported monoclonal antibody (mAB), while the other component was labeled with a different epitope that binds to an acetylcholinesterase (AChE)-linked antibody. After the execution of 2816 reactions in 96-well plates, each reaction was treated with the solid-phase mAB, followed by the AChE-linked mAB. After several rounds of washing, the unreacted

components and the AChE-linked mAB were removed from the wells. Subsequent treatment with Ellman reagent (a colorimetric enzymatic substrate) lit up the wells that contain the hit reactions. Therefore, these cycloaddition reactions can be evaluated rapidly with visual screening (Fig. 4.7). After the initial screen and further optimization, Taran *et al* disclosed a new Cu-catalyzed sydnone-alkyne cycloaddition reaction which was shown to be biocompartible in the fluorescent labeling of BSA.

D. In Situ Enzymatic Screening

In 2002, our group unveiled a conceptually new screening method: In-Situ Enzymatic Screening (ISES).[44] By exploiting a bilayer system, we could monitor relative rates in real time for the allylic substitution reaction. The first Ni(0)-mediated allylic amination was revealed in this process (Fig. 4.8). Asymmetric version of this reaction was later developed, as an expeditious approach toward L-β,γ-unsaturated amino acids (Fig. 4.9).[45]

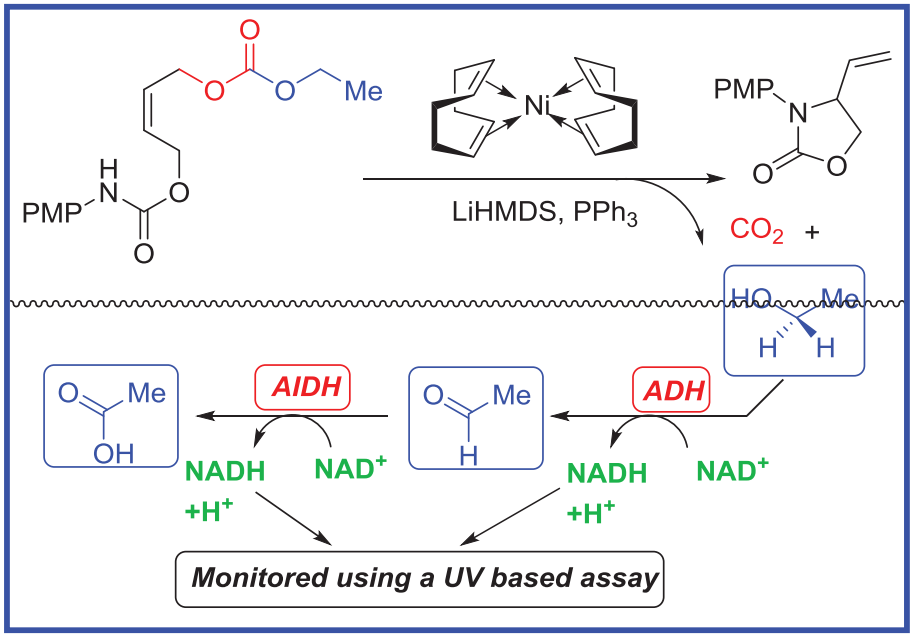

Figure 4.8: ISES for intramelecular allylic amination reactions

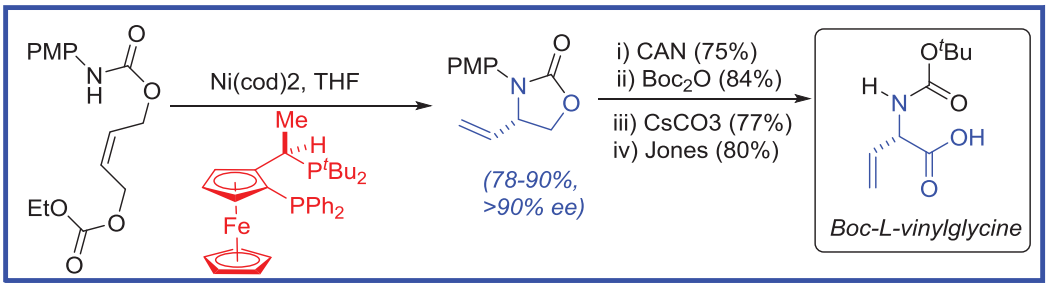

Figure 4.9: Asymmetric version of the Ni(0)-catalyzed allylic amination reaction

Recently, this first generation of ISES was adapted to a colorimetric method, utilizing the ABTS dye. The menthol byproduct from a (pseudo)halometalation/carbocyclization reaction diffused into the aqueous layer, where it was oxidized by an alcohol oxidase. The produced hydrogen peroxide was further oxidized to H_2O by two equivalent of ABTS dye under the catalysis of peroxidase. The generated $ABTS^{+\cdot}$ has a strong green color ($\varepsilon_{405\text{-}414}$ = ~ 70000 $M^{-1}cm^{-1}$), which allows for simple visual identification (Fig. 4.10). 1152 combinations of substrates and catalysts were rapidly screened using this colorimetric ISES. The electron-deficient rhodium catalyst was found to be an efficient catalyst for the bromination-carbocyclization reaction. Furthermore, a thiocyanation-carbocyclization reaction was identified as a new transformation under palladium catalysis. [46]

ISES has the advantage that the products do not need to be installed with a chromophore to be detected. This is particularly useful for evaluation of product ee's, as most of them are determined from HPLC traces. In 2005, our group revealed a "double cuvette" ISES, which not only measures the reaction rates, but also estimates the sense and magnitude of the enantioselection of the reaction.[32] In this second generation ISES, we utilized two reporting enzymes which have different enantiopreferences toward the products.

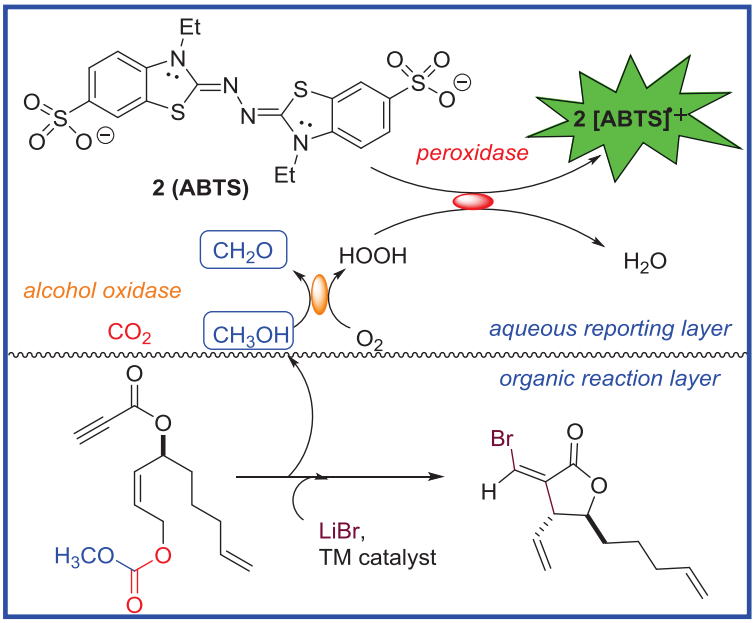

Figure 4.10: A colorimetric ISES for higher throughput screening

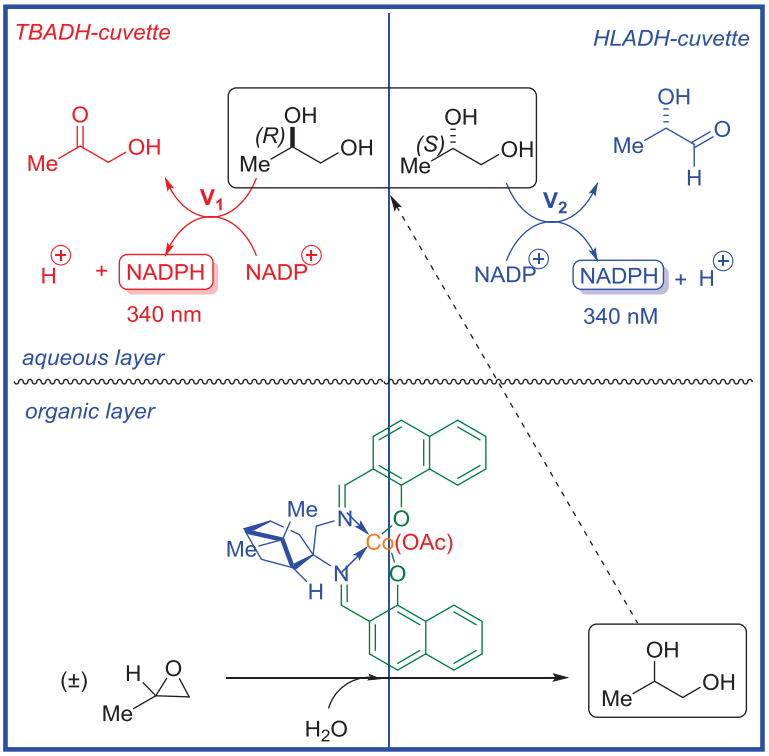

Figure 4.11: A schematic depiction of the Cassette-ISES

In this particular case, cobalt(III)-mediated HKR of propylene oxide was employed as a model reaction. Hydrolytica kinetic resolution of terminal epxoides,

particularly catalyzed by Co(III)-salen complexes developed by the Jacobsen group, proved to be a powerful synthetic tool in asymmetric synthesis and has been applied widely in natural product total synthesis. TBADH/HLADH pair was selected as the dual enzymatic screening system. For the oxidation of 1,2-propanediol by $NADP^+$, TBADH has an estimated enantioselectivity (Sel_{TBADH}) of 8.4 (v_R/v_S) at 40 mM concentration of the diol. On the other hand, HLADH oxidizes the diol with an estimated enantioselectivitiy (Sel_{HLADH}) of 0.34 (v_R/v_S), using NAD^+ as the cofactor. Thus, for each cobalt-salen catalyst, ISES was executed in two separated cuvettes, where the produced diol was oxidized in different rates (v_{TBADH} vs v_{HLADH}) (Fig. 4.11). To estimate the enantiomeric ratios from these reaction rates and enantioselectivities, equation (1) was derived and validated in multiple studies.[32, 47]

$$\frac{[R]}{[S]} = \frac{[\left(\frac{Sel_{E2}}{Sel_{E1}}\right)\times v_{E2} - v_{E1}]}{Sel_{E2}\times(v_{E1} - v_{E2})} \quad (1)$$

II. Results and Discussion

A. Synthesis of the Oxa- and Carbafructopyranose Derived Diamines

The α- and β-oxafructopyranosyl diamines were conveniently synthesized from D-fructose. Following the procedures in literature[48], 4- and 5-hydroxyl groups were selectively protected with acetonide in 75% yield. 3-hydroxyl group was then selectively methylated, with MeI and NaH, in 95% yield. A TMSOTf-mediated anomeric azidation led to a mixture (α : β = 1 : 4) of the α- and β-2-dexoy-2-azido-3-methyl-4,5-acetonide D-fructopyranose. Further triflation of 1-hydroxyl group, followed by $TMSN_3$ displacement provided the diazide **3** and **4** in excellent yields. The hydrogenation of the

diazides proved to be challenging. With 10 wt% of Pd/C or PtO_2, the reaction proceeded slowly and significant decomposition was occurred during this process. Consequently, the hydrogenation was attempted in much faster fashion. Pleasingly, with 50 mol% PtO_2 in THF, the diazides (potentially explosive) were efficiently converted to a mixture (α : β = 1 : 9) of α- and β-diamines (**5** and **6**) in quantitative yield (Fig. 4.12). The separation of these two diamines is particularly challenging, in part due to the instability of these diamino compounds. Therefore, the mixture of the α- and β-diamines was carried forward into the salen synthesis without further purification.

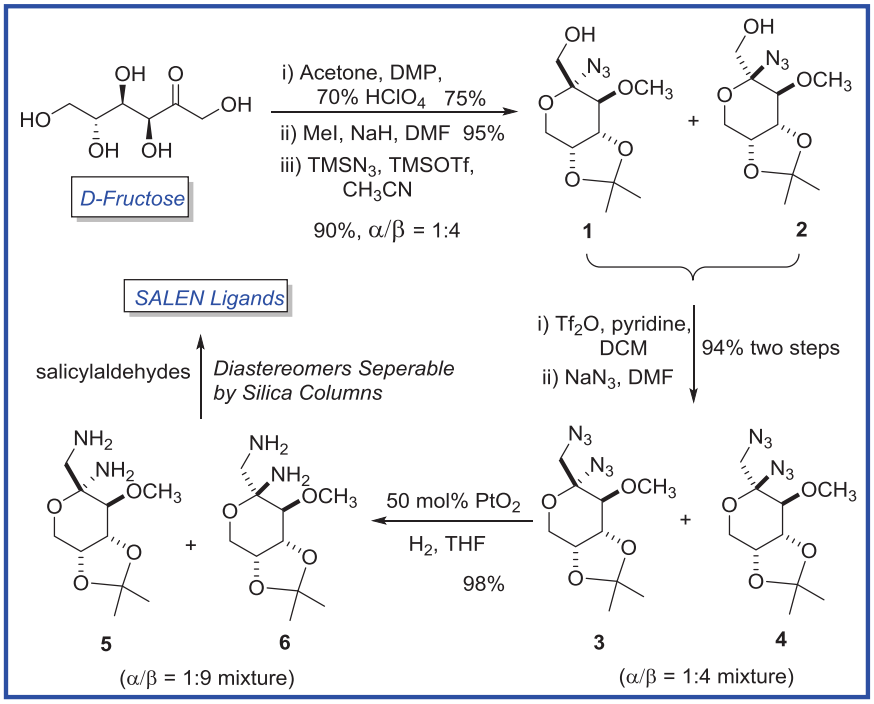

Figure 4.12: Synthesis of α- and β-D-oxafructopyranosyl 1,2-diamines

The synthesis of the D-carbafructose derived diamines was originally started from (-)-quinic acid (**7**).[49-51] **7** was treated with cyclohexanone under acidic conditions to afford the lactone **8**. Cleavage of the lactone, followed by PCC oxidation and

concomitant β-elimination gave compound **9**. After the reduction and treatment with acetone and acid, the more stable bicyclic compound **10** was generated. Barton deoxygenation, followed by Grignard addition and dihydroxylation provided **11**. The triol was selectively methylated and then cleaved using $Pb(OAc)_4$ to yield the cyclic ketone **12**. A standard Wittig-methylenation reaction converted the ketone to desired olefin **13** in 80% yield. The diazidation of the exocyclic alkene was realized adopting Snider's procedure.[52] The $Mn(OAc)_3$ mediated radical diazidation rendered diazide, as an "α/β" mixture (**14**:**15** = 75:25), in 80% yield. After chromatographic separation with silica column, these diastereomeric diazides were reduced by Pd/C catalyzed hydrogenation to give the respective diamines, **16** and **17**, in quantitative yield (Fig. 4.13).

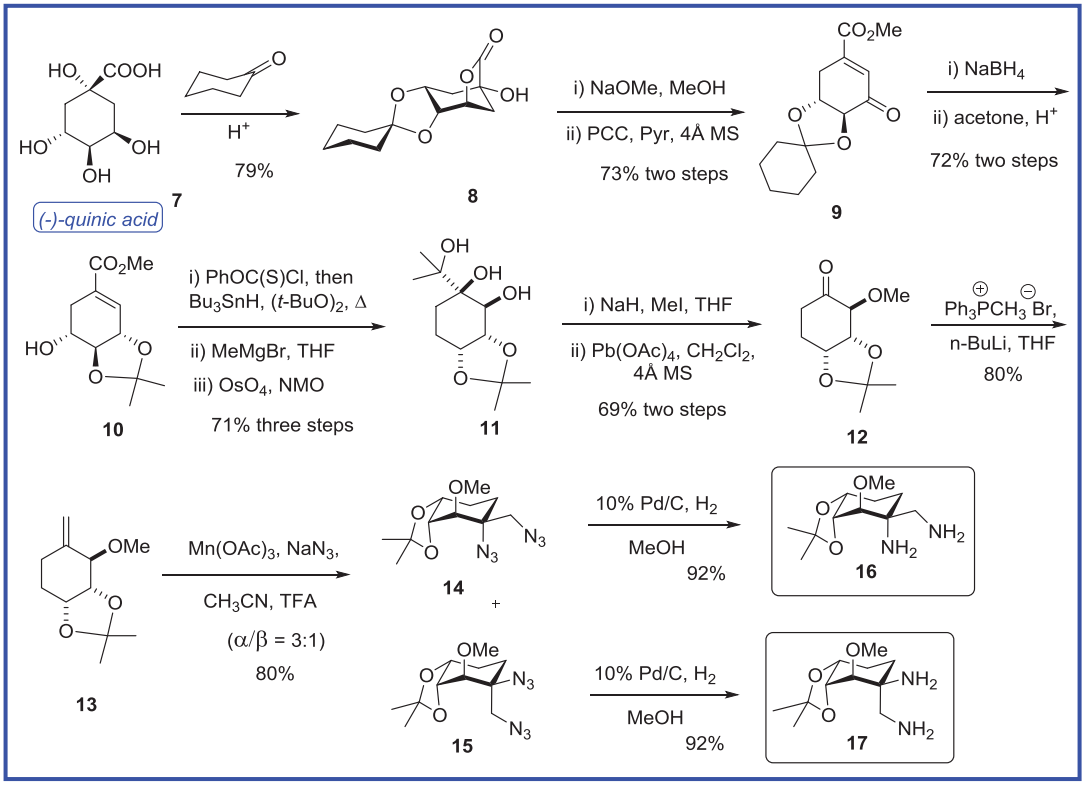

Figure 4.13: Synthesis of α- and β-D-carbafructopyranosyl 1,2-diamines

All the four diamines were subsequently utilized to build a focused 4×4 library of salen ligands. Coupling with four different salicylaldehydes, oxa- and carbafructopyranosyl-1,2-diamines yielded 15 out of 16 possible salen combinations. The

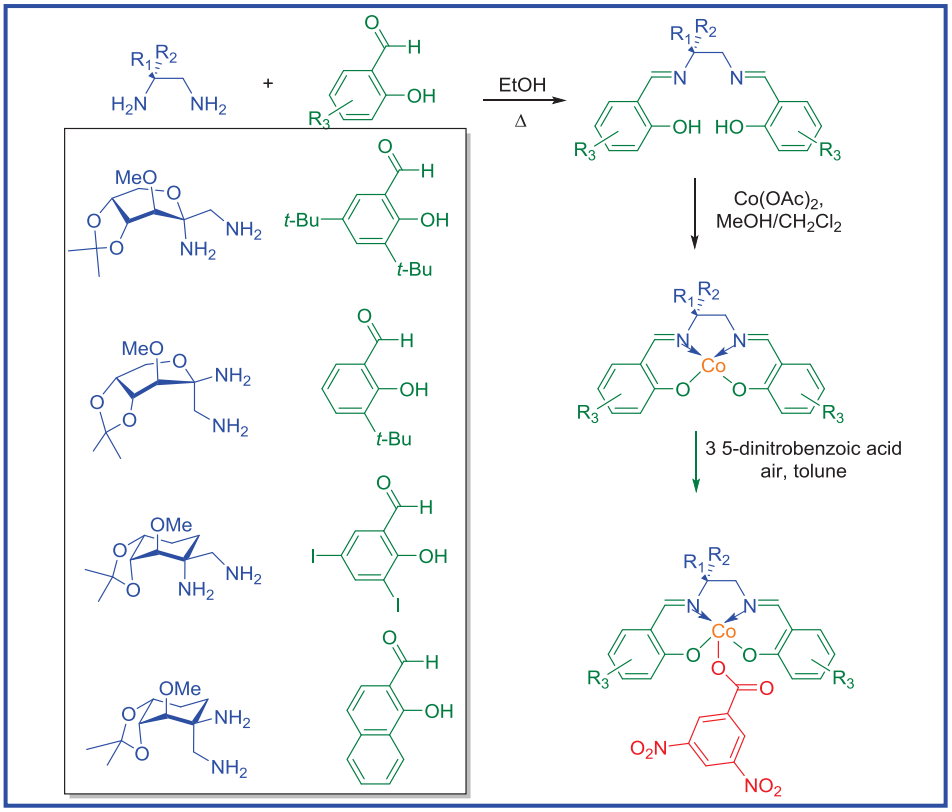

Figure 4.14: Synthesis of an oxa- and carbafructose based salen ligand library

active cobalt catalysts were then synthesized from the reactions between these salen ligands and $Co(OAc)_2$, followed by oxidation with air in the presence of 3,5-dinitrobenzoic acid (Fig. 4.14).

B. A New Miniaturized ISES

The "double cuvette" ISES was successfully introduced in 2005 to screen a 7×7 (42-membered) library. New reporting enzymes (LKADH, ketoreductases) were later recruited to expand the substrate scope.[33, 47] However, the scale of this "double cuvette"

ISES is not compatible with high through screen. For each cuvette, it normally requires 4 - 5 mg of the catalyst (0.25 mol% cat. loading) to give reliable reaction rates within a 30 min window. With varying conditions and substrates, this method requires a large quantity of each catalyst. This drawback hinders a broader screening of catalysts, particularly of the ones with limited access. Therefore, as a proof of principle for the high-through compatibility, we have developed a miniaturized ISES, and utilized it to evaluate the newly synthesized salen library.

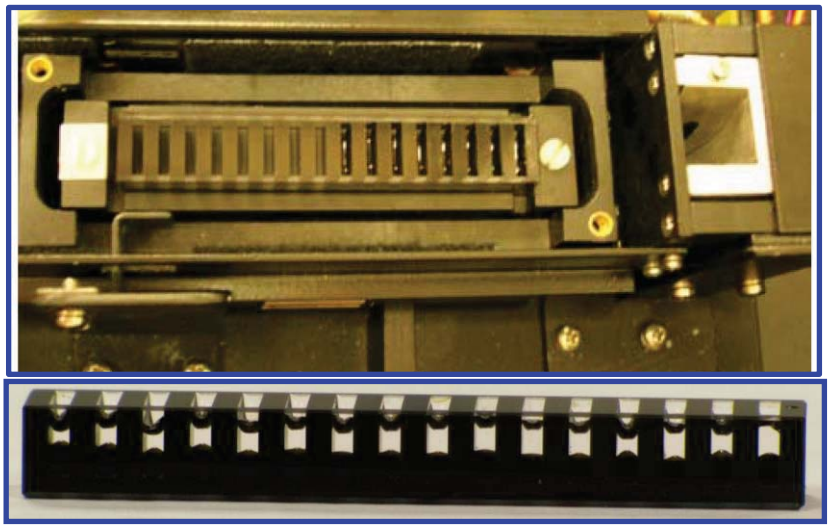

Fig 4.15: Schimadzu UV-2401 instrument with 16-well quartz micromulticell loaded with biphasic layers

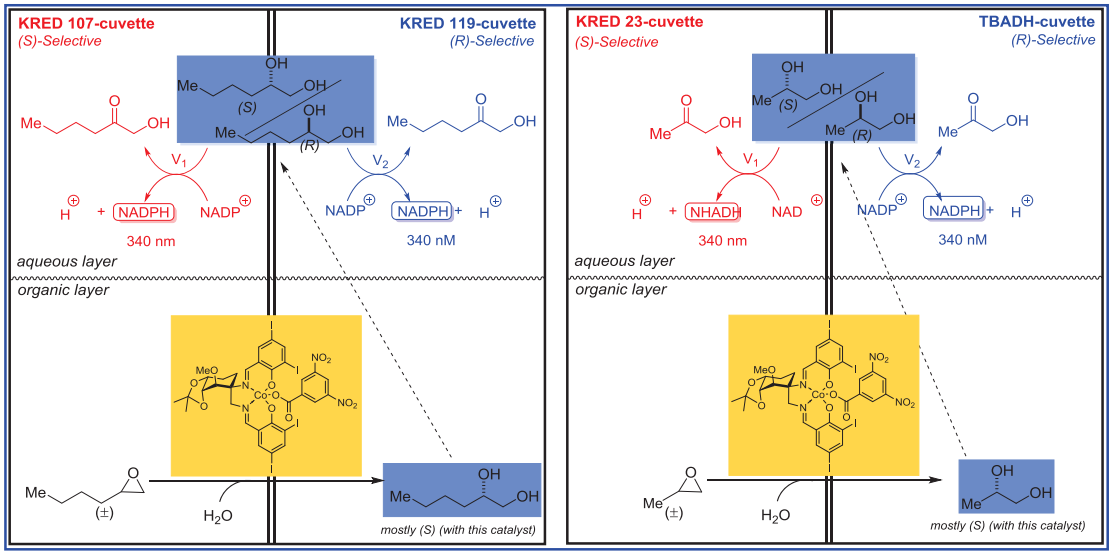

Figure 4.16: Schematic depictions of the new miniaturized multicellular

By exploiting a 16 multi-microcell array the total volume of the biphasic layer was scaled down to 110 μL from 1 mL. The "miniaturized" ISES requires 0.5 mol% catalyst loading to give readable rates within a short time (5 – 10 min) window. Consequently, the amount needed for each catalyst was reduced to < 1 mg per reaction. With same amount of catalysts, this newly developed platform allows ISES to evaluate five times more reactions than the "cuvette" setup. Furthermore, using the standard Shimadzu UV-2401 instrument, we were able to read up to 8 channels in one single experiment, representing a higher throughput screen (Fig. 4.15),.

Since previously-employed reporting enzyme HLADH is no longer commercially available, we set out to find easily-accessible alternatives. Hence, we have screened an array of Codexis KRED (ketoreductase) enzymes towards their activities with (*R*)- and (*S*)-1,2-hexane diol, as well as (*R*)- and (*S*)-1,2-propane diol. Based on the reaction rates and selectivity factors (k_S/k_R, see Fig. 4.24 in the experimental section for detailed kinetic analysis), KRED-107, and KRED-119 were picked as the reporting enzymes for the HKR of hexene oxide, while KRED-23 and TBADH were used to screen the HKR of propylene oxide (Fig. 4.16).

To examine the new ISES platform, the HKR reactions were also conducted under typical flask conditions. A comparison of the ISES estimated % ees and the HPLC determined % ees was compiled in Table 4.1. A three dimensional bar graph was also created to compare the two sets of data. The difference between ISES conditions and flask conditions should be noted. Under typical ISES conditions, reactions are carried out in a biphasic system. The produced diols diffuse into the aqueous layer and get read out

by the enzymes. However, under flask conditions, the reactions are usually conducted without extra solvent, and the products are isolated for ee determination. As seen in Table

Table 4.1: Screen of a 4 × 4 library of salen ligands for the Co(III)-

	a	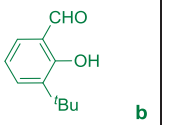 b	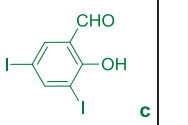 c	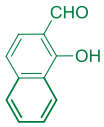 d
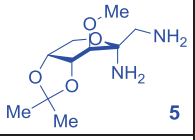 5	[77(+)] 69(+) *6.2(+)* [64(+)] 45(+) *4.0(+)*	[70(+)] 42(+) *2.6(+)* [67(+)] 40(+) *2.4(+)*	¶	§ # 25(+) *1.7(+)*
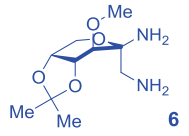 6	[33(-)] 64(-) *4.7(-)* # 52(-) *4.2(-)*	[28(-)] 40(-) *2.5(-)* [31(-)] 36(-) *2.4(-)*	[85(+)] 83(+) *13(+)* [77(+)] 85(+) *28(+)*	§ §
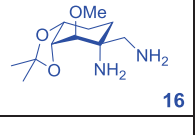 16	[53(-)] 37(-) *2.3(-)* [23(-)] 29(-) *2.0(-)*	[76(-)] 75(-) *8.2(-)* [40(-)] 45(-) *3.5(-)*	[91(-)] 85(-) *17(-)* [42(-)] 63(-) *5.0(-)*	[78(-)] 61(-) *4.3(-)* [59(-)] 55(-) *3.8(-)*
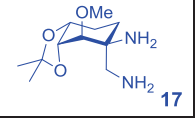 17	[39(-)] 28(-) *1.9(-)* # 30(-) *2.1(-)*	[67(-)] 48(-) *3.4(-)* [50(-)] 53(-) *3.4(-)*	[94(+)] 93(+) *56(+)* [77(+)] 92(+) *46(+)*	§ [13(-)] 34(-) *2.2(-)*

[a]Each box provides the HKR data of propylene oxide (black) and hexene oxide (blue). The ISES estimated % ees of the produced diols are presented in brackets, followed by the observed % ees (chiral HPLC) and calculated E-values. [¶]Difficulty was encountered in synthesizing appreciable quantities of this salen. [#]These catalysts gave ISES signals < 20 mAbs min-1 over 35 min. [§]These catalysts gave a conversion < 2% after 72 h.

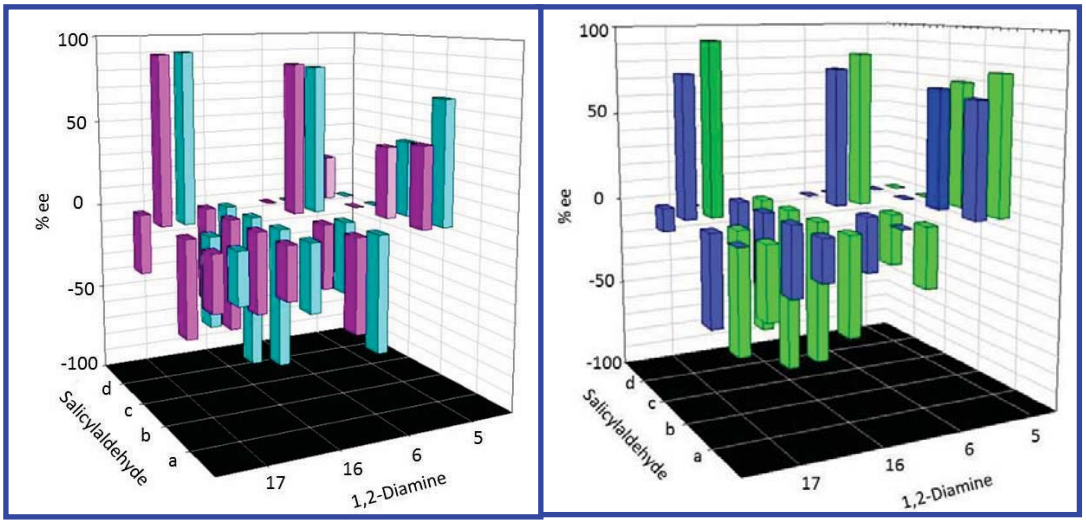

Figure 4.17: Three dimensional bar graph of ISES screening results

4.1 and Fig. 4.17, the estimated % ee's correlates well with the HPLC determined % ee's. Indeed, the "miniaturized" ISES decreases the reaction scale without sacrificing its accuracy, thereby providing a highly efficient screening tool.

C. Preserved Enantioswitch and Boosted Enantioselectivity

From this focused combinatorial screening, two interesting results have emerged. First, the salicylaldehyde-dependent enantioswitch was preserved in the carbafructopyranosyl series. Namely, the Co(III)-salen catalyst derived from β-D-carbafructopyranosyl diamine (**17**) and the sterically encumbering 3,5-di-*tert*-butylsalicylaldehyde (**a**) gives rise to (*R*)-diols, whereas the catalyst based on the same diamine and the electronically rich 3,5-diiodosalicylaldehyde (**c**) gives rise to the (*S*)-antipodes (Table 4.1). This observation disproves the suggestion that an "undetected anomerization" is the cause of the enantioswitch. In the carbafructose based ligands, the anomeric position is locked into α- or β-configuration, eliminating the possibility of anomerization. Therefore, this unusual enantioswitch is truly dependent on the choices of the pairing salicylaldehydes. This is quite interesting, considering the salicyladehyde is the achiral part of a salen ligand.

Perhaps, the more exciting result is the remarkable enantioselectivity enhancement from the oxafructopyranose-based ligand **6c** to its carbocyclic congener **17c**. Replacing the ring oxygen with CH_2 renders a much more (*S*)-selective Co(III)-salen complex, with an E-value[53] of 44 for the HKR of propylene oxide. Since salen ligand is considered as a "privileged" chiral scaffold and has been widely applied in many transformations[54-55], this novel combination of carbohydrate-based diamine and an unhindered salicylaldehyde clearly represents an important combinatorial hit.

Table 4.2: Substrates screening using Co(III)-DNB catalyst derived from salen 17c

entry	epoxides (±)	catalyst loading (mol%)	conditions[a]	conversion[b]	isolated epoxide[c]	isolated diol
1		0.14	neat, 0 °C, 15 h	45	50, -74, 44	46, 88, 34
2	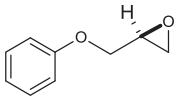	0.5	DCM, rt, 20 h	51	47, -96, 97	46, 92, 93
3	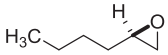	0.5	neat, 0 °C, 30 h	52	45, -99, 104	48, 91, 116
4	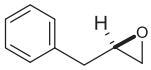	0.5	neat, 0 °C, 23 h	51	48, -97, 119	49, 92, 93
5	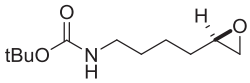	1.0	THF, rt, 35 h	44	55, -72, 49	40, 92, 52
6	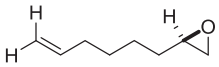	0.5	neat, rt, 30 h	54	40, -99, 61	48, 82, 40
7	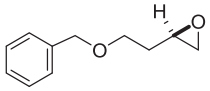	0.5	DCM, rt, 20 h	32	68, -39, 16	26, 86, 20
8	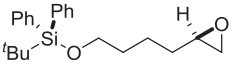	1.0	THF, rt, 50 h	28	63, -33, 17	28, 90, 27

[a]0.2-1 mol% of catalyst was added to a solution of epoxide in THF or DCM or neat condition. The mixture was cooled to 0 °C or kept at rt and 0.5 eq water was added to initiate the reaction. The reaction was stirred at 0 °C or rt until completion. [b]Conversion of the reaction was determined by ^{1}H NMR. [C]The purified yield, % ee and calculated E-value are listed consecutively.

The most promising Co(III)-salen(**17c**) catalyst was subsequently examined for HKR across a range of distinct epoxides, using standard flask conditions. Given the nature of kinetic resolution, the ee's of both remaining epoxide substrates and the formed diols were measured. Thus two independent selectivity factors were collected for each entry (Table 4.2), giving a fair judgment of the catalyst performance. Pleasingly, three substrates exhibited excellent resolution with E-values being around 50.[56] And near perfect resolution (E-value = ~ 100) was obtained for another three substrates, namely *O*-

phenylglycidol, hexene oxide and (2,3-epoxypropyl)benzene. We believe this salen ligand will find broad applications in various asymmetric transformations.

D. Comparison to A Directed Evolution Based Approach

Interestingly, the HKR result of *O*-phenylglycidol allows us to compare this small molecule-based combinatorial approach to Reetz's Combinatorial Active-site Saturation Test (CAST) strategy iteratively applying the CAST method, Reetz *et al* have evolved *A. niger* epoxide hydrolase for the HKR of *O*-phenylglycidol. They were able to improve the E-value from 14 to 115 over 5 cycles of directed evolution, after constructing ~ 20,000 mutants. Ultimately 9 individual residue were mutated from the wild type to afford the best evolved enzyme (Fig. 4.18).[57]

Reetz's approach starts from the native epoxide hydrolase. This is based on the knowledge that this enzyme catalyzes the HKR of epoxides. Likewise, we have selected the salen scaffold for our catalyst design. The evolution of the Co(III)-salen catalyst emanates from a 7×7 salen library that involves variation of diamine and salicylaldehyde components. The screening of the first generation catalysts rendered a similar starting point; namely, the Co(III)-salen(**6c**) catalyst showed an E-value of 13 for the HKR of (±)-propylene oxide. In the next round "catalyst evolution", the ring oxygen was substituted by a methylene group, initially as a method to support the salicylaldehyde-dependent enantioswitch. Nonetheless, this step boosted the selectivity to essentially the same value as Reetz's enzyme. Taken together, the combinatorial approach utilized in this work is highly complementary to other types of methods, such as the directed evolution strategy. On one hand, our combinatorial assembly of diverse salen structures provides unprecedented and valuable ligand motifs. One the other hand, the focused screening of

our fructose based salen array impoves the ligand, providng an efficient approach to ligand optimization.

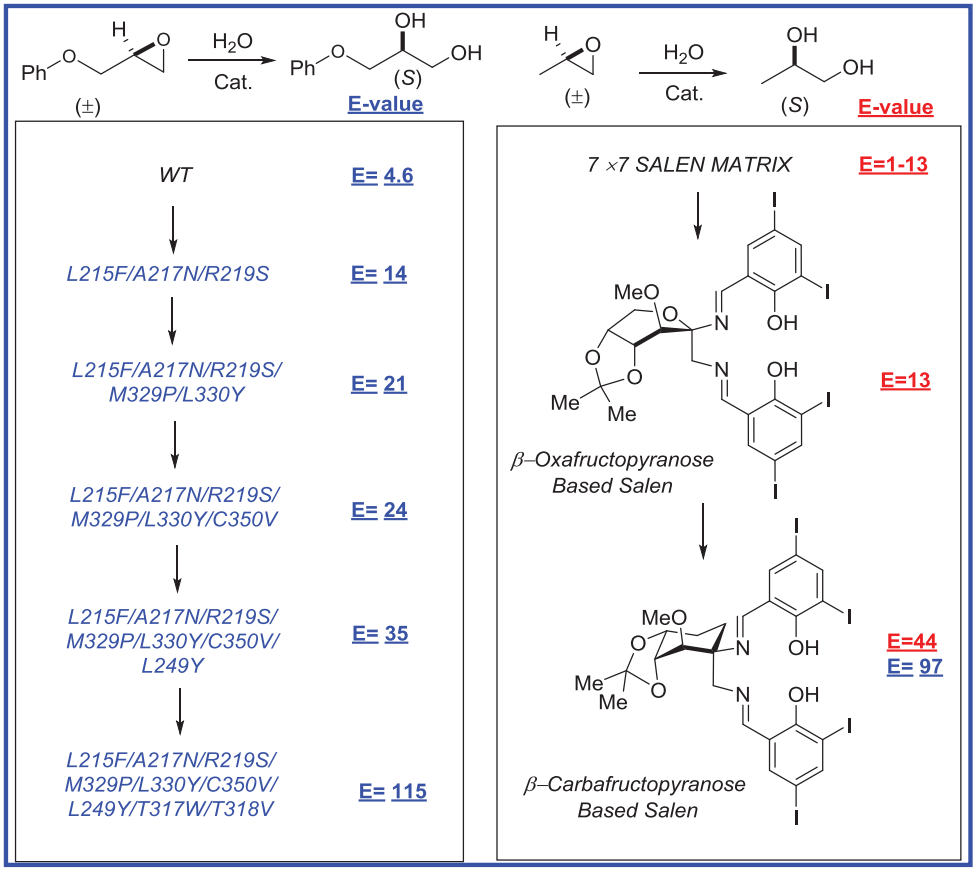

Figure 4.18: A comparison between directed evolution based approach and a combinatorial salen array based approach

E. X-Ray Structures and Transition State Model of HKR

To understand the difference between the oxa- and carbafructose derived catalysts, we set out to characterize some of the Co(II)-salen complexes by X-ray crystallography. The crystals of these complexes derived from **6a**, **6c**, and **17c** were successfully obtained. The x-ray crystallography studies gave very interesting results. Both oxacycles take a distorted boatlike conformation, whereas the corresponding carbacycle adopts a chairlike geometry (Fig. 4.19). It is possible this conformational

change of the fructose ring leads to the observed enantioselectivity improvement. And we believe that these oxafructopyranose rings twist to the boatlike structure to avoid the deleterious anomeric effect. Specifically, if the oxacycle was in the chairlike conformation, the C_2-N dipole would be aligned with the ring dipole, thereby reinforcing the molecular dipole moment. On the contrary, when taking the boatlike geometry, C_2-N dipole partially counteracts the ring dipole and stabilizes the molecule. However, to substantially support this theory and shed light on why chairlike geometry is more enantiodiscriminating, sophisticated density functional theory (DFT) calculations are inevitable in the future studies.

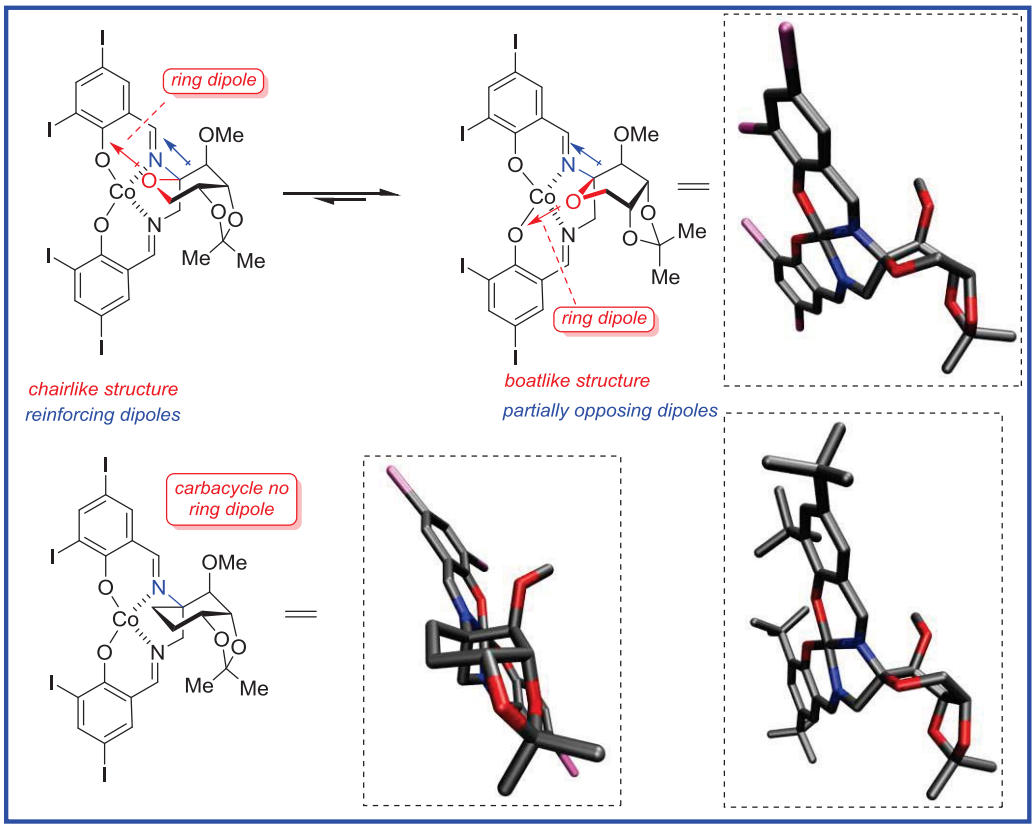

Figure 4.19: X-ray crystal structures of the Co(II)-salen complexes and a possible influence of dipole-dipole interactions on the ring conformation

Nonetheless, using the crystal structure of Co(II)-**17c** complex and some observations in literature, we were able to build a transition state model, attempting to interpret the origin of the enantiopreference. First, as Blackmond and Jacobsen suggested[58], we presumed the HKR studied here is a second-order reaction on the catalyst concentration. Thus, two molecules of the Co(III)-catalyst were incorporated into the transition state; one coordinates the epoxide oxygen, and the other delivers the nucleophile. Second, the 3D structure of Chin's aziridine-Co(III)-salen complex[59] was utilized as a guidance, to modulate the Co-O distances and the epoxide approaching angle to the cobalt-salen complex. Third, according to Jacobsen's recent DFT calculation, the O-Co-O-C dihedral angle (θ) has a major influence on the binding energy of a epoxide substrate, with an optimal range of $20 - 60^{\circ}$.[60]

Therefore, a bimolecular transition state model was constructed, using Accelrys View-Pro to avoid the unfavorable van der Waals interactions. As seen in Fig. 4.20, the epoxide binds strongly to the Co(III)-salen complex, through a 1.99 Å Co-O coordination bond, very close to the distance between Co and nitrogen in Chin's crystal structure (1.95 Å). In addition, the oxirane ring approaches the Co center at an angle (122° ± 18°) that is very similar to that from the binding aziridine (123° ± 3°). Furthermore, the O-Co-O-C dihedral angle in our model is shown to be around 24°. This is quite similar to the one observed in Chin's structure (33°), and very close to the global minimal on Jacobsen's chart. In the meantime, the nucleophilic hydroxyl group is well positioned to the attack the terminal carbon through a second molecule of catalyst. Consequently, we believe this model should serve well in the transition state prediction for the HKR reactions. Herein,

(*S*)-hexene oxide fits in nicely underneath the π-face of the OH-delivering Co-salen complex, elucidating the high enantio-preference of this catalyzed hydrolysis.

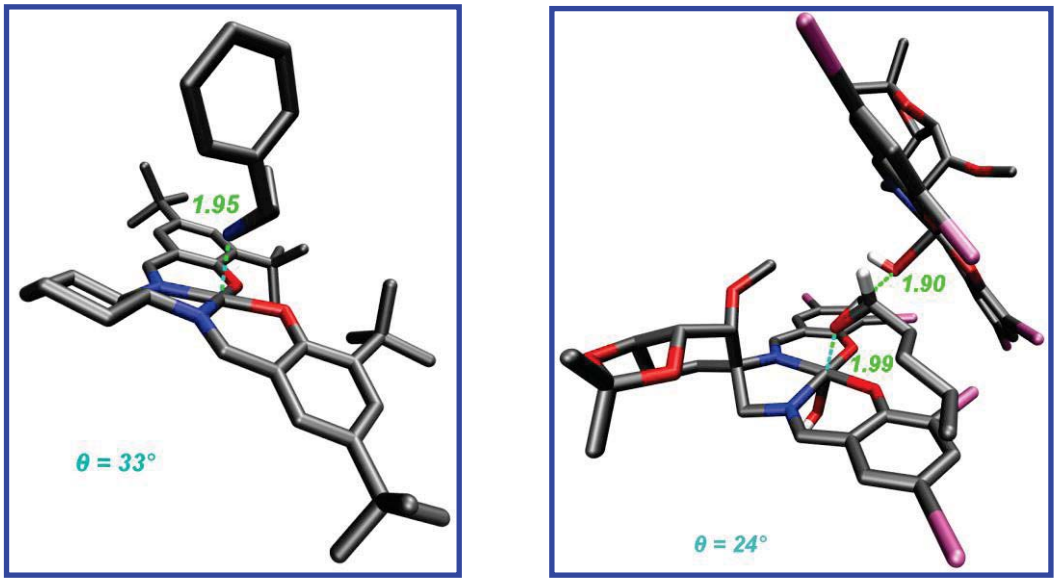

Figure 4.20. Transition-state model of Co(III)-catalyst derived from 17c in HKR of hexene oxide. The crystal structure of Chin's Co(III)-aziridine complex was shown on the left. Transition state model was for the Co(III)-mediated HKR was shown on the right. Co(II)-**17c** complex was first modified using *Spartan 2008*. Consulting the crystal structure of Jik Chin's Co(III)-aziridine complex, nucleophile hydroxyl group was added to the Co center. (*S*)-Hexene oxide (preferred enantiomer) was manually docked with the resulting model for the HO-Co(III)-12c complex, using Accelrys ViewerPro. The distance between the nucleophile oxygen and the electrophile carbon is ~1.90 Å. The Co-O coordination bond length is ~1.99 Å. The O-C0-O-C dihedral angle θ is 24°.

Finally, it was also noted that the stepped conformation of the salen complex could be important for the enantioselectivity. Therefore, we employed all the three crystal structures to estimate these step heights. As seen in Fig 4.21, two key parameters are measured for each complex: (i) the crystallographic rise angle and (ii) the $C_{2'}$-$C_{2''}$-distance (designated as "hypotenuse length"). Consequently, the step heights can be calculated from equation (2). Indeed, the largest step height (0.76 Å) is observed in the

Co(II)-17c complex (Fig. 4.22), which renders the best catalyst among this series. This is consistent with Jacobsen's theory and provides an additional criterion for the future catalyst design.

$$\text{step height} = sin(180^{o} - \text{rise angle}) \times \text{hypotenuse length} \quad (2)$$

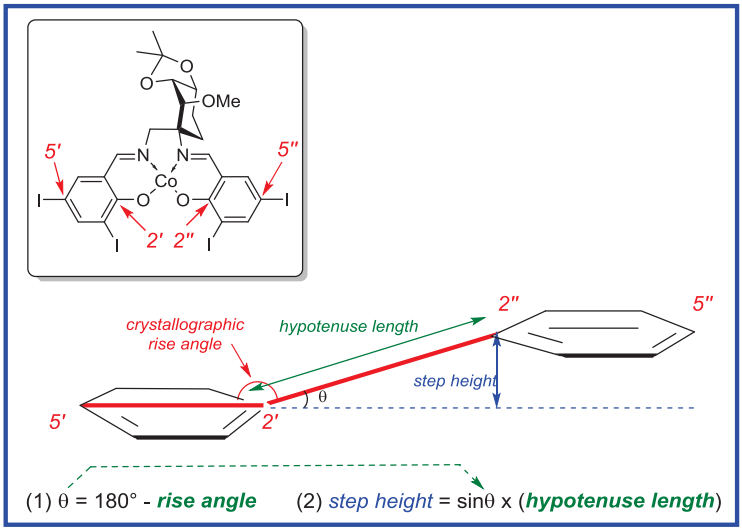

Figure 4.21: Measurment of step heigh for the Co(II)-17c complex

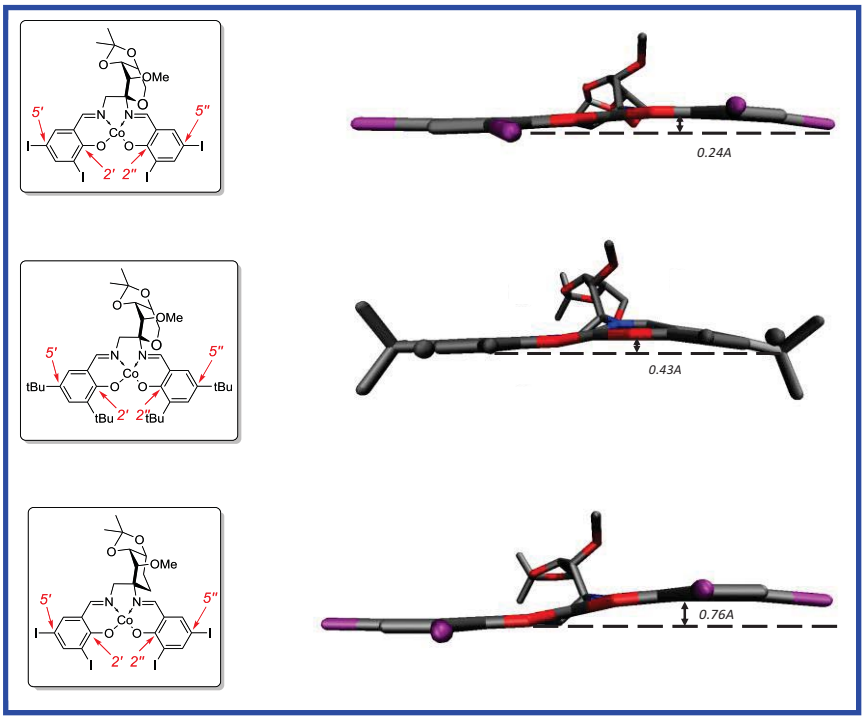

Figure 4.22 Step heights from the cystal structures of the Co(II)-salen complexes

F. Streamlined Synthesis of the α- and β-D-Carbafructopyranosyl-1,2-Diamines

To facilitate extensive studies of the valuable D-carbafructose derived diamines, we set out to develop a more streamlined synthesis, making these diamines more accessible. Specifically, we sought an expedient route to the key intermediate **12**. The new route started from α-methyl-D-mannopyranoside. Appel reaction could converted the 6-OH to the 6-iodide in excellent yield. The requisite acetonide was then selectively installed across the *cis*-configured 2,3-vicinal diol using a recipe of 2,2-dimethoxypropane/acetone with catalytic *p*-TsOH. Pleasingly, C-4-*O*-methylation and dehydrohalogenation were achieved in one pot in almost quantitative yield to give the enol ether intermediate **19**.

Several divalent, late transition metal catalysts ($HgCl_2$, $Pd(OAc)_2$ and $PdCl_2$) were examined, as well as variation of the solvent and temperature for the key type-II Ferrier rearrangement step. The optimal conditions employs 10 mol% $Pd(OAc)_2$ in a mixture of acetone, dioxane and water (40:40:20) at 0°C, providing rearranged product **20** in 85 % yield. The temperature proved to be critical, with warming the reaction to room temperature resulted in unwanted side products (Figure 4.23). To remove the extra hydroxyl group, Barton deoxygenation was first employed. However, the projected phenyl thionocarbonate ester proved to be unstable. It decomposes during the silica column purification to yield the corresponding α,β-unsaturated ketone in poor yield. Therefore, the route was modified and the acohol **20** was mesylated, followed by in situ β-elimination to the ketone intermediate in 80% yield. Hydrogenation then gave desired product **12** in quantitative yield. The newly developed synthesis saves 6 steps and raises the overall yield from 7% to 39%. The new route also starts from a cheaper commercial

source α-methyl-D-mannopyranoside ($109/100g-Aldrich) compared to (-)-quinic acid ($192/100g-Aldrich).

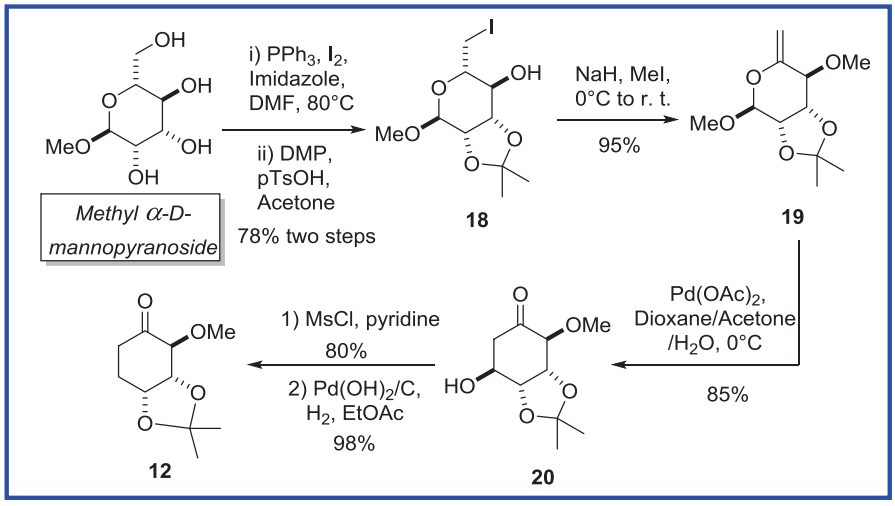

Figure 4.23: A streamlined synthesis of the key ketone intermediate

In conclusion, we have developed a miniaturized ISES manifold. This new ISES setup allows us to screen more reactions in a higher-throughput fashion. As a proof of principle, this screening method was utilized to examine a library of oxa- and carbafructopyranosyl 1,2-diamines derived salen ligands, towards the Co(III)-mediated HKR reactions. The β-D-carbafructopyranosyl 1,2-diamine/3,5-diiodosalicylaldehyde derived Co(III)-salen complex was shown to be a highly enantioselective catalyst, over 4 times more selective than the oxafructose derived catalyst. We believe that this novel chiral scaffold has the great potential to be applied in other types of asymmetric transformations, and this miniaturized ISES will be utilized to screen different reactions.

III. Experimental Section

A. Organic Synthesis

All reactions were conducted under nitrogen atmosphere using flame or oven-dried glassware, unless otherwise indicated. Methylene chloride was distilled from CaH_2. Toluene, THF and Et_2O were distilled from sodium benzophenone ketyl. Methanol was distilled from Mg, and ethanol from Na-diethyl phthalate. Alcohol dehydrogenase from *Thermoanaerobium brockii* (TBADH, EC 1.1.1.2), β-NAD^+ (sodium salt) and β-$NADP^+$ (sodium salt) were purchased from Sigma. KRED (ketoreductase) enzymes were purchased from Codexis. 3,5-Di-*tert*-butylsalicylaldehyde (a) was purchased from Alfa-Aesar, 3,5-diiodosalicylaldehyde (c) from Lancaster, 1-hydroxy-2-naphthaldehyde (d) from TCI America, 3-*tert*-salicylaldehyde (b), and cobalt(II)-acetate tetrahydrate from Aldrich. Flash chromatography was performed using Merck silica gel 60 (230-400 mesh). ^1H NMR spectra were recorded on Bruker-DRX-Avance-400 MHz, 500 MHz and 600 MHz instruments with chemical shifts reported relative to residual $CHCl_3$ (7.25 ppm) and CH_2Cl_2 (5.2 ppm). Proton-decoupled ^{13}C NMR spectra were acquired on Bruker-DRX-Avance-400 MHz, 500 MHz and 600 MHz instruments with chemical shifts reported relative to $CDCl_3$ (77.0 ppm). Optical rotations @589 nm were measured at 19 °C in an Autopol polarimeter. IR spectra were obtained using a Nicolet Avatar 360 FTIR spectrometer. Mass spectra were acquired at the Nebraska Center for Mass Spectrometry (University of Nebraska-Lincoln). Enzyme assays and ISES were performed on a Shimadzu 2401 spectrophotometer, equipped with a 16-microcell sample changer with temperature control. A Chiralcel OD (4.6 mm x 25 cm) chiral stationary phase was used for enantiomeric excess determinations by HPLC.

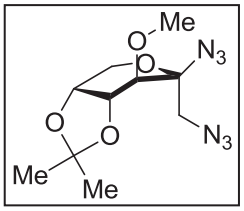

3-*O*-Methyl-4,5-*O*-isopropylidene-β-D-fructopyranosyl-1,2-diazide (4):

The starting material, 2-azido-2-deoxy-3-*O*-methyl-4,5-*O*-isopropylidene-β-*D*-fructopyranose was prepared following the known literature procedure.[52]

A flame dried flask was charged with the β-azido alcohol **2** (2.6 g, 10 mmol, 1 equiv) followed by pyridine (5 mL) and CH_2Cl_2 (15 mL). The flask was cooled to –20 °C and triflic anhydride (2.85 mL, 16.9 mmol, 1.7 equiv.) was added dropwise. The reaction was stirred at –20 °C for 20 min and then warmed up to rt and stirred till all the starting material was consumed. The reaction contents were diluted with ether and washed with 1N HCl followed by saturated $NaHCO_3$. The ethereal layer was treated with anhydrous Na_2SO_4 and vacuum dried. The triflate thus obtained was re-dissolved in DMF (10 mL), and sodium azide (2 g, 30.7 mmol, 3.1 equiv) was added to it. The contents were stirred overnight at 40-50 °C and diluted with ether, then washed with water and 1N HCl and then finally with saturated $NaHCO_3$. The ethereal layer was dried with anhydrous Na_2SO_4. Subsequent removal of ether and vacuum drying gave the diazide as a yellow oil (2.68 g, 94%, over two steps). ***Triflate:*** ^{1}H NMR (500 MHz, $CDCl_3$) 1.36 (s, 3H), 1.53 (s, 3H), 3.44 (d, *J* = 6 Hz, 1H), 3.56 (s, 3H), 4.11 (ddd, *J* = 2, 3, 13 Hz, 2H), 4.27-4.35 (m, 2H), 4.58 (d, *J* = 10 Hz, 1H), 4.69 (d, 10 Hz, 1H). ***Diazide:*** ^{1}H NMR (600 MHz, $CDCl_3$) 1.32 (s, 3H), 1.51 (s, 3H), 3.39 (d, *J* = 7 Hz, 1H), 3.51(s, 3H), 3.54 (app s, 2H), 4.03 (dd, *J* = 3, 13 Hz, 1H), 4.11 (app d, *J* = 13 Hz, 1H), 4.19-4.24 (unresolved, 2H); ^{13}C NMR (150 MHz, $CDCl_3$) 25.8, 27.8, 54.1, 59.8, 62.1, 72.9, 76.1, 78.8, 92.3,

109.3; FTIR (ATR) 2099 cm^{-1} (N_3 stretch); HRMS (FAB, 3-NOBA) calcd for $C_{10}H_{16}O_4N_6$ $(M+Li)^+$ 291.0643, obsd. 291.1398.

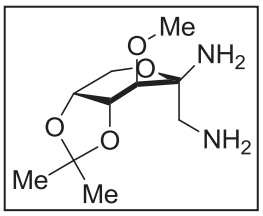

3-*O*-Methyl-4,5-*O*-isopropylidene-β-D-fructopyranosyl-1,2-diamine (6): Diazide (200 mg, 0.7 mmol) was dissolved in THF (2 mL) and platinum oxide (80 mg, 50 mol%) catalyst was added. The diazide was hydrogenated (52 psi) for 1 h and filtered through a pad of celite. The celite was washed several times with CH_2Cl_2 and the solvent was removed in *vacuo*. TLC indicated the complete reduction of diazide to a ninhydrin positive spot (R_f = 0.3, 95:4:1 CH_2Cl_2 : MeOH : NH_4OH). The diamine (mixture of anomers ~ 9:1; as seen from ^{13}C NMR) thereby obtained (160 mg, 98%) was of sufficient purity to be used directly for synthesis of salen ligands. The β-anomer: ^1H NMR (400 MHz, $CDCl_3$) 1.33 (s, 3H) 1.52 (s, 3H), 2.67 (d, J = 13 Hz, 1H), 2.84 (d, J = 13 Hz, 1H), 3.20 (d, J = 7 Hz, 1H), 3.5 (s, 3H), 3.83 (d, J = 13 Hz, 1H), 4.1- 4.28 (m, 3H); ^{13}C NMR (100 MHz, $CDCl_3$) 26.2, 28.1, 50.3, 58.8, 59.7, 74.0, 77.2, 80.4, 85.9, 108.6; HRMS (FAB, 3-NOBA) calcd for $C_{10}H_{20}O_4N_2$ $(M+H)^+$ 233.1503, obsd 233.1505.

This ~ 9:1 mixture of α- and β-diamine was used to prepare β-fructopyranose derived catalyst with 3,5-di-*tert*-butylsalicylaldehyde, 3-butylsalicylaldehyde 3,5-diiodosalicylaldehyde and 2-hydroxy-1-naphthaldehyde.[32]

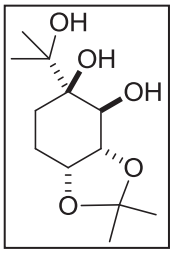

(3a*S*,4*S*,5*R*,7a*R*)-5-(2-hydroxypropan-2-yl)-2,2-dimethylhexahydrobenzo[*d*][1,3]-dioxole-4,5-diol (11): The starting material, alkene was prepared from the literature procedure.[49, 51] To a flask containing starting alkene (300 mg, 1.41 mmol, 1 equiv), *tert*-butanol (16 mL), N-methylmorpholine N-oxide (272 mg, 2.32 mmol, 1.63 equiv), water (0.153 mL, 8.5 mmol, 6 equiv), pyridine (0.82 mL, 10.1 mmol, 7.1 equiv), potassium osmate dihydrate (24 mg, 0.065 mmol, 0.045 equiv) was added. The contents were refluxed at 100 °C for 12 h. The TLC indicated completion of the reaction. The reaction was then quenched with satd $NaHSO_3$ and the volatiles were removed under reduced pressure. The contents were extracted with EtOAc after saturating the aqueous layer with NaCl. The organic layer was dried with sodium sulfate and passed through a pad of silica gel, concentrated and dried in *vacuo*. The crude reaction product (290 mg, crude yield 83%) was carried on to the next step. ^{1}H NMR (400 MHz, $CDCl_3$) 1.12 (s, 3H), 1.27 (s, 3H), 1.3 2 (s, 3H), 1.46 (s, 3H), 1.5 (m, 2H), 1.89 (br d, J = 14.4 Hz, 1H), 2.05 (m, 1H), 3.43 (s, 1H), 3.84 (d, J = 6 Hz, 1H), 4.07 (t, J = 7.3 Hz, 1H), 4.12 (s, 1H), 4.19 (s, 1H), 4.27 (m, 1H); ^{13}C NMR (100 MHz, $CHCl_3$) 21.9, 23.5, 25.4, 25.9, 26.1, 28.5, 73.9, 75.5, 75.8, 76.6, 80.6, 108.5.

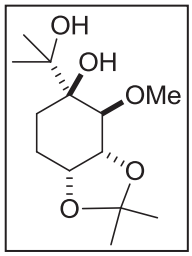

(3a*R*,4*S*,5*R*,7a*R*)-5-(2-hydroxypropan-2-yl)-4-methoxy-2,2-dimethylhexahydro-benzo[*d*][1,3]dioxol-5-ol (21): To a solution of triol **11** (290 mg, 1.18 mmol, 1 equiv) in THF (6 mL) at 0 °C, NaH (hexanes washed, 86 mg, 3.54 mmol, 3 equiv) was added in one portion and stirred for 10 min. The contents were cooled to –40 °C and iodomethane (74 μL, 1.18 mmol, 1 equiv) was added dropwise. The contents were stirred at –40 °C for 5 h

and then warmed to –20 °C (NaCl/ice mixture) and stirred for 8 h. The completion of the reaction was monitored by TLC. The reaction was quenched by added satd NH_4Cl and THF was removed under reduced pressure. The contents were extracted with EtOAc and the organic layer was washed with brine, dried over anhydrous Na_2SO_4, concentrated and dried under *vacuo*. The crude product was chromatographed (0→25% EtOAc-hexanes) to yield the title compound (265 mg, 72 %, over two steps). $[\alpha]_D$ –41.3 (*c* 5.05, $CHCl_3$); ^1H NMR (400 MHz, $CDCl_3$) 1.1 (s, 3H), 1.2 (s, 3H), 1.3 (s, 3H), 1.49 (s, 3H), 1.53 (m, 2H), 1.84 (ddd, *J* = 14.8, 7.9, 3.6 Hz, 1H), 2.06 (m, 1H), 3.18 (s, 1H), 3.48 (d, *J* = 7 Hz, 1H), 3.58 (s, 3H), 4.16 (s, 1H), 4.24 (app t, *J* = 5.6 Hz, 1H), 4.30 (m, 1H); ^{13}C NMR (100 MHz, $CDCl_3$) 22.3, 23.5, 25.6, 26.2, 26.4, 28.3, 58.7, 74.4, 76.0, 76.1, 80.8, 84.8, 108.0; HRMS (FAB) calcd for $C_{13}H_{24}O_5Li$ $(M+Li)^+$ 267.1784, obsd 267.1794.

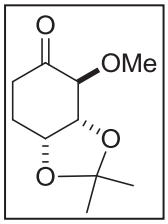

(3a*R*,4*S*,7a*R*)-4-methoxy-2,2-dimethyltetrahydrobenzo[*d*][1,3]dioxol-5(6*H*)-one (12): To a stirred suspension of the diol (100 mg, 0.384 mmol, 1 equiv) and dust of 3 Å molecular sieve in CH_2Cl_2 (8 mL) at rt, $Pb(OAc)_4$ (340 mg, 0.768 mmol, 2 equiv) was added. The contents were stirred for 10 min. TLC indicated complete conversion of the diol to the product, ketone. The reaction was quenched by adding satd. $NaHCO_3$ and extracted with ether. The organic layer was then washed with brine, dried over anhyd Na_2SO_4. Removal of solvent under reduced pressure yielded the title compound **S5** (77 mg, quantitative). $[\alpha]^{19}_D$ –69.6 (*c* 1.1, $CHCl_3$); ^1H NMR (400 MHz, $CDCl_3$) δ 1.33 (s, 3H), 1.43 (s, 3H), 2.09-2.14 (m, 1H), 2.21-2.30 (m, 2H), 2.46-2.55 (m, 1H), 3.41(s, 3H), 4.31 (dd, *J* = 6.8, 4.6 Hz, 1H), 4.41-

4.48 (m, 1H); ^{13}C NMR (100 MHz, $CDCl_3$) δ23,70, 24.38, 26.72, 32.68, 58.80, 72.29, 78.05, 84.23, 109.22, 207.53; HRMS (FAB) calcd for $C_{10}H_{17}O_4$ $(M+H)^+$ 201.1127, obsd 201.1119.

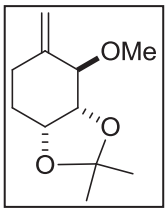

(3aR,4R,7aR)-4-methoxy-2,2-dimethyl-5-methylenehexahydrobenzo[d][1,3]dioxole (13): To a stirred ice-cold solution of Ph_3PCH_3Br (1.32 g, 2.14 mmol, 1.5 equiv), was added 1.3 M BuLi in hexanes (1.5 mL, 2.0 mmol, 1.4 equiv) slowly. The resulting yellow solution was stirred for 10 min at 0 °C, and the ethereal solution of the ketone (288 mg, 1.44 mmol, 1 equiv) was added slowly. Immediate precipitation appeared, the resulting suspension was stirred overnight, and quenched with 1 M NaOH. The product was extracted with ether, washed with brine and dried over Na_2SO_4. Removal of solvent under reduced pressure provided the crude product. The product was purified by column chromatography on silica gel to yield the terminal olefin **9** (228 mg, 80%) as a clear liquid. $[\alpha]^{19}_D$ –96.2 (*c* 1.0, $CHCl_3$); ^{1}H NMR (400 MHz, $CDCl_3$) δ 1.26 (d, *J* = 2.5 Hz, 3H), 1.41 (d, *J* = 2.6 Hz, 3H), 1.77-1.81 (m, 1H), 1.86-1.92 (m, 1H), 2.11-2.14 (m, 1H), 2.20-2.27 (m, 1H), 3.30 (d, *J* = 2.8 Hz, 3H), 3.61 (dt, *J* = 3.8, 1.1 Hz, 1H), 3.93-3.97 (m, 1H), 4.23-4.26 (m, 1H), 4.92 (d *J* = 1.08 Hz, 3H); ^{13}C NMR (100 MHz, $CDCl_3$) δ 25,32, 25.78, 26.15, 27.49, 57.25, 73.48, 79.43, 83.23, 108.18, 111.20, 142.53; HRMS (CI) calcd for $C_{11}H_{19}O_3$ $(M+H)^+$ 199.1334, obsd 199.1338.

(3aR,4R,5S,7aR)-5-azido-5-(azidomethyl)-4-methoxy-2,2-dimethylhexahydro-benzo[d][1,3]dioxole (β-diazide) (15):

A dry flask was charged with NaN_3 (442 mg, 6.8 mmol, 5 equiv), $Mn(OAc)_3.2H_2O$ (1.1 g, 4.1 mmol, 3 equiv) and CH_3CN (7 mL) and nitrogen gas was bubbled through the mixture. Then the mixture was cooled down to –20 °C and **13** (270 mg, 1.36 mmol, 1 equiv) was added to it dropwise. The reaction was initiated by the slow addition of TFA (0.21 mL). The reaction mixture was slowly warmed up to rt. After 3 h, aqueous $NaHSO_3$ solution was added and the reaction mixture was extracted with CH_2Cl_2. The organic layer was washed with satd Na_2CO_3 and dried. Column chromatography (10% Et_2O in hexanes) gave two fractions with very close R_f values, with 80% yield.

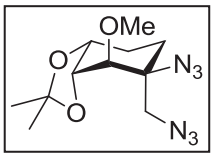

Fraction 1 yield the β-diazide **15** as a clear oil (84 mg, 22%); [ ]$^{19}_D$ – 84.2 (*c* 1.05, $CHCl_3$); ^{1}H NMR (400 MHz, $CDCl_3$) 1.32 (s, 3H), 1.48 (s, 3H), 1.59 (m, 1H), 1.71 (dt, *J* = 14, 5.5 Hz, 1H), 1.92 (m, 2H), 3.22 (d, *J* = 7.3 Hz, 1H), 3.53(s, 3H), 3.55 (d, *J* = 12.1 Hz, 1H), 3.62 (d, *J* = 12.1 Hz, 1H), 4.13 (dd, *J* = 7.2, 5.4 Hz 1H), 4.25 (m, 1H); ^{13}C NMR (100 MHz, $CDCl_3$) 21.8, 26.2, 26.3, 28.4, 55.3, 60.2, 65.8, 73.9, 79.7, 82.5, 108.5; HRMS (FAB) calcd for $C_{13}H_{19}N_6O_3$ $(M+H)^+$ 283.1519, obsd 283.1530.

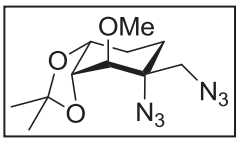

Fraction 2 yielded the α-diazide **14** as a clear oil (221 mg, 58%); [ ]$^{19}_D$ –110.3 (*c* 1.0, $CHCl_3$); ^{1}H NMR (400 MHz, $CDCl_3$) 1.31 (s, 3H), 1.49 (s, 3H), 1.64 (m, 2H), 1.83 (m, 1H), 2.03 (m, 1H), 3.18 (d, *J* = 13.4 Hz, 1H), 3.35 (d, *J* = 7.1 Hz, 1H), 3.55 (s, 3H), 3.68 (d, *J* = 13.4 Hz, 1H), 3.90 (app t, *J* = 6.8 Hz

1H), 4.21 (m, 1H); ^{13}C NMR (100 MHz, $CDCl_3$) 22.6, 25.4, 26.1, 28.2, 51.2, 60.4, 66.2, 73.3, 79.2, 85.2, 108.8; HRMS (FAB) calcd for $C_{11}H_{18}N_6O_3Li$ $(M+Li)^+$ 289.1600, obsd 289.1596.

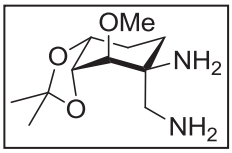

(3aR,4R,5S,7aR)-5-(aminomethyl)-4-methoxy-2,2-dimethylhexahydrobenzo-[d][1,3]dioxol-5-amine (β-diamine) (17): β-Diazide **15** (321 mg, 1.14 mmol) was dissolved in EtOH (10 mL) and 32 mg of 10% Pd/C was added. The resulting suspension was hydrogenated at 52 psi for 12 h, resulting total reduction to give the β-diamine **17** (262 mg, 100%). $[\alpha]^{19}_D$ –61.5 (*c* 0.76, $CHCl_3$); ^{1}H NMR (400 MHz, $CDCl_3$) 1.30 (br s, 4H), 1.33 (s, 3H), 1.5 (s, 3H), 1.54 (dt, *J* = 13.5, 4.6 Hz, 2H), 1.87 (br d, *J* = 13.2 Hz, 1H), 2.04 (tt, *J* = 13.3, 4.7Hz, 1H), 2.6 (d, *J* = 12.7 Hz, 1H), 2.63 (d, *J* = 12.7 Hz, 1H), 3.08 (d, *J* = 7.2, Hz, 1H), 3.51 (s, 3H), 4.16 (app t, *J* = 6.8 Hz, 1H), 4.26 (m, 1H); ^{13}C NMR (100 MHz, $CDCl_3$) 21.9, 26.4, 27.7, 28.4, 51.7, 56.0, 60.0, 74.4, 80.2, 84.1, 107.7; HRMS (FAB) calcd for $C_{13}H_{23}N_2O_3$ $(M+H)^+$ 231.1709, obsd 231.1700.

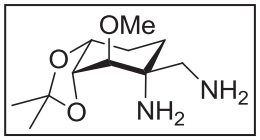

α-diamine (16): α-Diazide **14** (168 mg, 0.6 mmol) was dissolved in EtOH (5 mL) and 20 mg of 10% Pd/C was added. The resulting suspension was hydrogenated at 52 psi for 12 h, resulting total reduction to give α-diamine (135 mg, 100%). $[\alpha]^{19}_D$ –54.7 (*c* 0.35, $CHCl_3$); ^{1}H NMR (400 MHz, $CDCl_3$) 1.30 (br s, 3 H), 1.37-1.47 (m, 4 H), 1.48 (s, 3 H), 1.54 (dt, *J* = 13.6, 4 Hz, 1 H), 1.60-1.70 (m, 1 H), 1.92 (qt, *J* = 4, 15.6 Hz, 1 H), 2.42 (d, *J* = 13.2 Hz, 1 H), 2.67 (d, *J* = 13.2 Hz, 1 H),

3.14 (d, *J* = 7.2 Hz, 1 H), 3.51 (s, 3 H), 3.96 (dd, *J* = 5.6, 7.6 Hz, 1 H), 4.20-4.24 (m, 1 H); HRMS (ESI) calcd for $C_{13}H_{23}N_2O_3$ $(M+H)^+$ 231.1709, obsd 231.1706

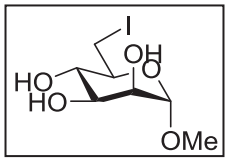

6-(iodomethyl)-4-methoxy-2,2-dimethyltetrahydro-3aH-[1,3]dioxolo[4,5-c]pyran-7-ol (22): Methyl-α-D-mannopyranose (9 g, 46.3 mmol) was suspended in 200 mL toluene at 80 °C, from that suspension was added triphenylphosphine (13.9 g, 53.3 mmol) and imidazole (10.88 g, 160 mmol) and kept stirring for 10 min at that temperature. Then iodine (17.2 g, 66.7 mmol) was added in portions over 0.5 h. The resulting suspension was vigorously stirred at 80 °C for 2 h and solution became dark brown. The solution was cooled and the product was extracted into H_2O (3×200 mL), the aqueous layer was washed with 200 mL of toluene and concentrated under vacuum. The crude was purified by column chromatography with pure ethyl acetate (R_f 0.45 in 50% ethylacetate in acetone) and pure product (11.3 g, 37.0 mmol, 80%) was obtained as white solid. $[\alpha]^{19}_D$ +64.3 (*c* 1.1, EtOH); ^{1}H NMR (400 MHz, D_2O) δ 3.37 (dd, *J* = 10.9, 7.1 Hz, 1H), 3.45 (ddd, *J* = 9.4, 7.1, 2.2 Hz, 1H), 3.57 (app t, *J* = 9.5, 9.4 Hz, 1H), 3.63 (dd, *J*= 10.9, 2.2 Hz, 1H), 3.76 (dd, = 9.5, 3.5 Hz, 1H), 3.93 (dd, *J*=3.4, 1.7 Hz, 1H), 4.73 (d, *J* = 1.4 Hz, 1H); ^{13}C NMR (100 MHz, D_2O) δ 6.1, 55, 69.8, 70.05, 70.6, 71.5, 101.1; HMRS (FAB) Calcd for $C_7H_{13}IO_5Li$ $(M+Li)^+$ 310.9968, obsd 310.9961.

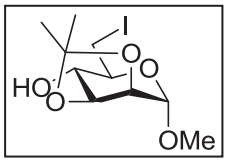

6-(Iodomethyl)-4-methoxy-2,2-dimethyltetrahydro-3aH-[1,3]dioxolo[4,5-c] pyran-7-ol (18): To a solution of **22** (7.5 g, 24.6 mmol, 1 equiv) in 120 mL acetone at 0 °C was added *p*-toluenesulfonic acid (936 mg, 4.92 mmol, 20%), followed by dropwise addition of dimethoxylpropane (9.1 mL, 73.8 mmol, 3 equiv) via syringe pump. The resulting solution was kept stirring for 3 h upon which time all the starting materials disappeared. The reaction was quenched by Et_3N (1.37 mL, 9.84 mmol, 40%) and organic solvent was evaporated under reduced pressure. The resulting residue were re-suspended in 60 mL water and extracted with EtOAc (3 × 60 mL). The organic layer was washed with brine and dried under Na_2SO_4, filtered and evaporated, resulted in pale yellowish liquid as clean product (8.5 g, 95%) without the need for further purification. $[\alpha]^{19}_{D}$ +33.4 (*c* 1.1, $CHCl_3$); ^{1}H NMR (400 MHz, $CDCl_3$) δ 1.34 (s, 3H), 1.51(s, 3H), 3.30 (dd, *J*=10.5, 7.1Hz, 1H), 3.4d (ddd, *J*=9.2, 7.1, 2.4Hz, 1H), 3,46 (s, 3H), 3.49 (ddd, *J*=9.4, 6.9, 3.4Hz 1H), 3.58(dd, *J*=10.6, 2.5Hz, 1H), 4.10-4.12 (m, 2H), 4.91 (s, 1H); ^{13}C NMR (100 MHz, $CDCl_3$) δ 6.81, 26.06, 27.97, 55,55, 68.95, 73.06, 75.69, 78.35, 98.33, 109.78; HMRS (FAB) Calcd for $C_{10}H_{18}IO_5$ $(M+H)^+$ 345.0121 obsd 345.0204.

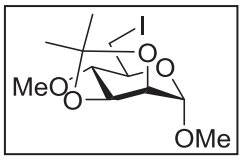

6-(iodomethyl)-4,7-dimethoxy-2,2-dimethyltetrahydro-3aH-[1,3]dioxolo[4,5-c] Pyran (23): To a solution of **18** (160 mg, 0.47 mmol) in 3 mL THF at 0 °C was added imidazole (6.8 mg, 0.1 mmol) and NaH (240 mg, 60% suspension in mineral oil, 6 mmol), followed by slow addition of MeI (62 μL, 1 mmol). The resulting solution was kept stirring at 0 °C for 3 h, upon which time TLC showed complete consumption of the starting material. The reaction is

quenched by saturated NH_4Cl and extracted with Et_2O. Organic phase was dried, filtered and evaporated. The crude product was purified by silica column chromatography to afford **23** as a clear oil (134 mg, 80%). ^{1}H NMR (400 MHz, $CDCl_3$) δ 1.31 (s, 3H), 1.51 (s, 3H), 3.07 (dd, *J* = 9.6, 6.9 Hz, 1H), 3.27 (dd, *J* = 10.3, 7.4 Hz, 1H), 3.35 (ddd, *J* = 9.6, 7.4, 2.2Hz, 1H), 3.43 (s, 3H), 3.50 (s, 3H), 4.06 (d, *J* = 5.7Hz, 1H), 4.14 (app t, 1H); ^{13}C NMR (100 MHz, $CDCl_3$) δ 7.15, 26.18, 27.93, 55.91, 59.25, 67.91, 75.76, 78.09, 81.65, 98.21, 109.29; HRMS ESI calcd for $C_{11}H_{19}O_5INa$ $(M+Na)^+$ 381.0175, obsd 381.0164.

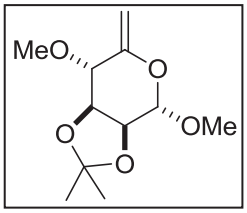

(3aR,4S,7S,7aR)-7-Hydroxy-4-methoxy-2,2-dimethyltetrahydrobenzo[d][1,3]dioxol-5(6H)-one (19): Two step procedure from **18**: To 150 mg **23** (0.42 mmol) in 5 mL DMF was added 0.7 mL DBU (0.46 mmol) at rt. The resulting mixture was stirred at 80 °C for overnight. The reaction mixture was cooled down and 60 mL EtOAc and 30 mL of saturated $NaHCO_3$ solution were added. The layers were separated and the organic layer was washed with water (3×60 mL), then with brine. The resulting organic phase was dried with Na_2SO_4 and evaporated under reduced pressure to give the product in 60% yield: $[\alpha]^{19}_D$ +49.1 (*c* 1.1, $CHCl_3$); ^{1}H NMR (400 MHz, $CDCl_3$) δ 1.33 (s, 3H), 1.48 (s, 3H), 3.46 (d, *J* = 0.7 Hz, 3H), 3.49 (d, *J* = 0.7Hz, 3H), 3.81 (dd, *J* = 0.8, 4.6 Hz, 1H), 4.16 (ddd, *J* = 7.2, 3.8, 0.5 Hz, 1H), 4.26 (dd, *J* = 7.1, 6.0 Hz, 1H), 4.43 (d, *J* = 0.8 Hz, 1H), 4.64 (d, *J* = 0.8 Hz, 1H), 4.86 (s, 1H); ^{13}C NMR (100 MHz, $CDCl_3$) δ 24.74, 26.89, 56.25, 57.91, 74.58, 75.86, 77.97, 93.22, 100.23, 109.80, 151.94; HMRS (FAB) Calcd for $C_{11}H_{18}O_5Li$ $(M+Li)^+$ 237.031, obsd 237.1316.

For the one-pot process: 1.3 g **18** (3.78 mmol) was dissolved in 40 mL DMF, cooled to 0°C and 0.47 mL MeI (7.56 mmol) was added, followed by 51 mg imidazole (0.76 mmol, 20%) and 272 mg NaH (11.3 mmol, washed with hexane to remove mineral oil). The reaction mixture was kept stirring at 0 °C for 3 h, TLC shows all SM converted to alkene product and iodide intermediate. The reaction mixture was left stirring at rt for overnight. TLC showed a single spot as the eliminated product. Work-up: The reaction mixture was added 60 mL EtOAc and 30 mL of saturated $NaHCO_3$ solution. The layers were separated and the organic layer was washed with water (3 × 60 mL), then with brine. The resulting organic phase was dried with Na_2SO_4 and evaporated under reduced pressure to give **19** as a colorless oil (0.85 g, 98%).

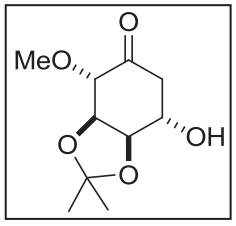

(3aR,4S,7S,7aR)-7-hydroxy-4-methoxy-2,2-dimethyltetrahydrobenzo[d][1,3]dioxol-5(6H)-one (20): 19 (5.21 g, 22.6 mmol) was dissolved in 120 mL solvent containing 2:2:1 volume ratio of acetone, dioxane and H_2O. The solution was cooled to 0 °C, $Pd(OAc)_2$ (10 mol %) was added in portions. Reaction mixture was kept at 0 °C for 12 h and the TLC showed complete consumption of the starting material. Reaction mixture was diluted with saturated NaCl and extracted with EtOAc (3 × 60 mL). The resulting organic phase was dried with Na_2SO_4, filtered and evaporated under reduced pressure. The residue was purified by column chromatography (R_f 0.25 at 50% EA in hexanes) and 4.15 g product were obtained (85% total yield, which contains about 8% of the 5-epimer). For the major

epimer: $[\alpha]^{19}_{D}$ -32.9 (*c* 1.0, $CHCl_3$); ^{1}H NMR (400 MHz, $CDCl_3$) δ 1.30 (s, 3H), 1.41 (s, 3H), 2.42 (dd, *J* = 18.3, 6.2 Hz, 1H), 2.75 (dd, *J* = 18.3, 5.0 Hz, 1H), 3.45 (s, 3H), 3.56-3.63 (m, 1H), 3.70 (d, *J* = 5.2 Hz, 1H), 4.27 (app. t, *J* = 6.9, 5.4Hz, 1H), 4.39 (dd, *J* = 7.0, 5.3Hz, 1H), 5.51-5.55 (m, 2H); ^{13}C NMR (100 MHz, $CDCl_3$) δ 24.26, 26.73, 41.86, 59.00, 67.50, 76.71, 77.04, 83.89, 109.77, 204.70; HRMS FAB calcd for $C_{10}H_{17}O_5$ $(M+H)^+$ 217.1076, obsd 217.1073.

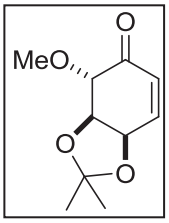

(3aR,4S,7aR)-4-methoxy-2,2-dimethyl-3a,4-dihydrobenzo[d][1,3]dioxol-5(7aH)-one (24): To a solution of **20** (692 mg, 3.2 mmol) in 10 mL of CH_2Cl_2 at 0 °C, were added diisopropyethyl amine (1.11 mL, 6.4 mmol) and 1 crystal of DMAP. Then MsCl (371 μL, 4.8 mmol) was added dropwise and the resulting solution was stirred at rt until SM disappeared. The reaction was quenched by addition of saturated NH_4Cl and extracted with CH_2Cl_2, column chromatography purification afforded **24** as a clear oil (480 mg, 76% yield). $[\alpha]^{19}_{D}$ –84.4 (*c* 0.65, $CHCl_3$); ^{1}H NMR (400 MHz, $CDCl_3$) δ 1.35 (d, *J* = 4.26 Hz, 3H), 1.40 (d, *J* = 4.38 Hz, 3H), 3.45 (d, *J* = 4.5 Hz, 3H), 3.82 (app.t, *J* = 4.4, 5.2 Hz, 1H), 4.47 (m, 1H), 4.73 (m, 1H), 5.99 (dd, *J* = 10.25, 4.53 Hz, 1H), 6.64-6.69 (m, 1H); ^{13}C NMR (100 MHz, $CDCl_3$) δ 26.29, 27.82, 59.17, 71.12, 76.68, 81.07, 110.96, 128.08, 143.32, 194.96; HRMS FAB calcd for $C_{10}H_{14}LiO_4$ $(M+Li)^+$ 205.1052, obsd 205.1046.

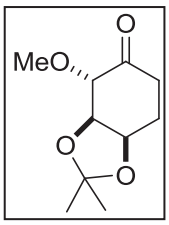

(3aR,4S,7aR)-4-methoxy-2,2-dimethyltetrahydrobenzo[d][1,3]dioxol-5(6H)-one (12): To a solution of **24** (200 mg, 1.0 mmol) in EtOAc (10 mL) was added 20% $Pd(OH)_2/C$ (20 wt%, 40 mg). The resulting mixture was hydrogenated at 20 psi for 1 h, the catalyst was then filtered off a pad of celite and washed with EtOAc. The filtrate was evaporated to give the ketone **8** as a colorless oil (202 mg, 100% yield). $[\alpha]^{19}_D$ –69.6 (*c* 1.1, $CHCl_3$); ^{1}H NMR (400 MHz, $CDCl_3$) δ 1.33 (s, 3H), 1.43 (s, 3H), 2.09-2.14 (m, 1H), 2.21-2.30 (m, 2H), 2.46-2.55 (m, 1H), 3.41(s, 3H), 4.31 (dd, *J* = 6.8, 4.6 Hz, 1H), 4.41-4.48 (m, 1H); ^{13}C NMR (100 MHz, $CDCl_3$) δ 23,70, 24.38, 26.72, 32.68, 58.80, 72.29, 78.05, 84.23, 109.22, 207.53; HRMS reported above.

General procedure for salen synthesis:

The oxa-fructopyranose diamine derived salens (**5a**-**5d**, **6a**-**6d**) were synthesized following previous procedures.[32] For the synthesis of the carba-fructopyranose diamine derived salens (**16a**-**16d**, **17a**-**17d**), a general procedure is described using **16a** as an example. To an oven-dried RB flask was added diamine **16** (388 mg, 1.68 mmol, 1 equiv), 3,5-di-*tert*-butylsalicylaldehyde (789 mg, 3.37 mmol, 2 equiv) and freshly distilled ethanol (5 mL). The reaction mixture was heated at 60 °C for 12 h. TLC indicated completion of the reaction. The reaction was concentrated in *vacuo*. The residue was purified by silica column chromatography (eluting with EtOAc/Hexanes: 0-30%) to afford salen **16a** as a yellow solid (729 mg, 63%). In some cases, the salen ligands

crystallized out during the reaction, therefore, the products were purified by simple trituration with cold ethanol.

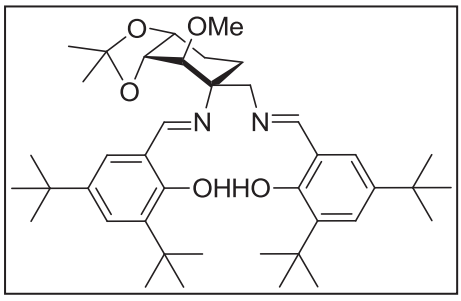

2,4-di-tert-butyl-6-((E)-((((3aR,4R,5R,7aR)-5-((E)-(3,5-di-tert-butyl-2-hydroxybenzylidene)amino)-4-methoxy-2,2-dimethylhexahydrobenzo[d][1,3]dioxol-5-yl)methyl)imino)methyl)phenol (16a): Following the general procedure for salen synthesis, a mixture of α-diamine (388 mg, 1.68 mmol) and 3,5-di-*tert*-butylsalicylaldehyde (789 mg, 3.37 mmol) in ethanol (5 mL) was heated at 60 °C for 12 h. The product **16a** (729 mg, 63%) was obtained as yellow solid after column chromatography purification. $[\alpha]^{19}_{D}$ +127.8 (*c* 0.7, CH_2Cl_2); ^{1}H NMR (400 MHz, CD_3Cl_3) 1.32 (s, 9H), 1.33 (s, 9H), 1.45 (s, 3H), 1.47 (s, 9H), 1.49 (s, 9H), 1.59 (s, 3H), 1.87-1.96 (m, 1 H), 1.97-2.10 (m, 2 H), 2.16-2.26 (m, 1 H), 3.52 (d, *J* = 7.2 Hz, 1 H), 3.66 (s, 3 H), 3.82 (d, *J* = 13.2 Hz, 1 H), 4.05 (d, *J* = 12.8 Hz, 1 H), 4.27 (dd, *J* = 4.4, 6.8 Hz, 1 H), 4.45 (dd, *J* = 2.8, 8.0 Hz, 1 H), 7.09 (d, *J* = 2.4 Hz, 1 H), 7.12 (d, *J* = 2.4 Hz, 1 H), 7.40 (d, *J* = 1.6 Hz, 2 H), 8.42 (s, 1 H), 8.54 (s, 1 H), 13.45 (s, 1 H), 14.25 (s, 1 H); ^{13}C NMR (100 MHz, CD_3Cl_3) 23.2, 26.1, 26.3, 28.3, 29.44, 29.45, 31.47, 31.51, 34.1, 35.1, 59.5, 61.4, 65.4, 73.8, 79.6, 86.4, 108.6, 117.8, 117.9, 126.1, 126.5, 127.0, 127.2, 136.66, 136.70, 139.8, 140.1, 158.0, 158.4, 163.9, 168.5; HMRS (ESI) Calcd for $C_{41}H_{62}N_2O_5Na$ $(M+Na)^+$ 685.4556 obsd 685.4531.

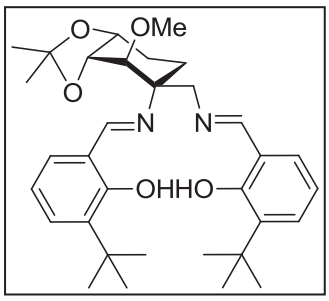

2-(tert-butyl)-6-((E)-((((3aR,4R,5R,7aR)-5-((E)-(3-(tert-butyl)-2-hydroxybenzylidene)amino)-4-methoxy-2,2-dimethylhexahydrobenzo[d][1,3]dioxol-5-yl)methyl)imino)methyl)phenol (16b): Following the general procedure for salen synthesis, a mixture of α-diamine (212 mg, 0.92 mmol) and 3-*tert*-butylsalicylaldehyde (328 mg, 1.84 mmol) in ethanol (5 mL) was heated at 60 °C for 12 h. The product (380 mg, 70%) was obtained as pale yellow solid after column chromatography purification. $[\alpha]^{19}_{D}$ +161.4 (*c* 2.5, CH_2Cl_2); ^{1}H NMR (400 MHz, CD_3Cl_3) 1.42 (s, 3 H), 1.44 (s, 9 H), 1.45 (s, 9 H), 1.56 (s, 3 H), 1.87- 1.94 (m, 1 H), 1.98 (dt, *J* = 14.8, 4 Hz, 1 H), 2.03-2.10 (m, 1 H), 2.15-2.23 (m, 1 H), 3.53 (d, *J* = 7.2 Hz, 1 H), 3.63 (s, 3 H), 3.81 (dd, *J* = 0.8, 13.2 Hz, 1 H), 4.02 (d, *J* = 13.2 Hz, 1 H), 4.25 (dd, *J* = 5.2, 6.4 Hz, 1 H), 4.43 (dd, *J* = 4.4, 9.2 Hz, 1 H), 6.80 (dt, *J* = 1.6, 7.6 Hz, 2 H), 7.08 (dd, *J* = 1.6, 7.6 Hz, 1 H), 7.11 (dd, *J* = 2.0, 8.0 Hz, 1 H), 7.32 (t, *J* = 0.8 Hz, 1 H), 7.34 (br s, 1 H), 8.38 (s, 1 H), 8.49 (s, 1 H), 13.59 (s, 1 H), 14.43 (s, 1 H); ^{13}C NMR (100 MHz, CD_3Cl_3) 22.7, 23.2, 26.2, 26.3, 28.3, 29.31, 29.33, 34.8, 59.4, 61.2, 65.4, 73.7, 73.7, 79.4, 85.9, 108.6, 117.6, 117.9, 118.5, 118.6, 129.4, 129.7, 129.9, 130.3, 137.4, 137.5, 160.2, 160.8, 163.6, 168.2; HMRS (ESI) Calcd for $C_{33}H_{46}N_2O_5Na$ $(M+Na)^+$ 573.3304 obsd 573.3302.

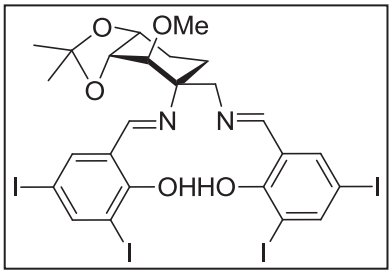

2-((E)-((((3aR,4R,5R,7aR)-5-((E)-(2-hydroxy-3,5-diiodobenzylidene)amino)-4-methoxy-2,2-dimethylhexahydrobenzo[d][1,3]dioxol-5-

yl)methyl)imino)methyl)-4,6-diiodophenol (16c): Following the general procedure for salen synthesis, a mixture of α-diamine (128 mg, 1.97 mmol) and 3,5-diiodosalicylaldehyde (1.46 g, 3.93 mmol) in ethanol (5 mL) was heated at 60 °C for 12 h. The product (1.01 g, 65%) was obtained as yellow solid after column chromatography purification. $[\alpha]^{19}_{D}$ +137.5 (*c* 0.8, CH_2Cl_2); ^{1}H NMR (400 MHz, CD_3Cl_3) 1.37 (s, 3 H), 1.49 (s, 3 H), 1.86-1.94 (m, 2 H), 1.98-2.04 (m, 1 H), 2.16-2.23 (m, 1 H), 3.37 (d, *J* = 7.2 Hz, 1 H), 3.56 (s, 3 H), 3.81 (d, *J* = 13.6 Hz, 1 H), 3.98 (d, *J* = 13.6 Hz, 1 H), 4.17 (dd, *J* = 5.2, 6.8 Hz, 1 H), 4.37 (dd, *J* = 3.2, 4.8 Hz, 1 H), 7.45 (d, *J* = 2 Hz, 1 H), 4.46 (d, *J* = 2 Hz, 1 H), 8.02 (s, 1 H), 8.03 (s, 1 H), 8.09 (s, 1 H), 8.11 (d, *J* = 2.4 Hz, 1 H), 13.99 (s, 1 H), 15.06 (d, *J* = 2.4 Hz, 1 H); ^{13}C NMR (100 MHz, CD_3Cl_3) 22.9, 25.7, 26.3, 28.2, 58.1, 61.0, 65.7, 73.4, 78.3, 79.4, 79.8, 85.3, 87.2, 89.2, 108.9, 119.2, 119.7, 140.1, 140.6, 149.1, 149.3, 160.3, 160.9, 162.6, 165.9; HMRS (ESI) Calcd for $C_{25}H_{26}N_2O_5I_4Na$ $(M+Na)^+$ 964.7918 obsd 964.7901.

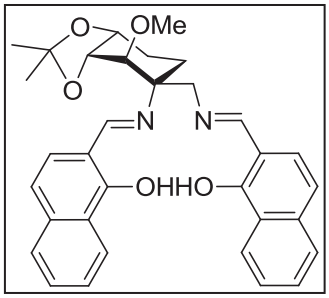

2-((E)-((((3aR,4R,5R,7aR)-5-((E)-((1-hydroxynaphthalen-2-yl)methylene)amino)-4-methoxy-2,2-dimethylhexahydrobenzo[d][1,3]dioxol-5-yl)methyl)imino)methyl)naphthalen-1-ol (16d): Following the general procedure for salen synthesis, a mixture of α-diamine **16** (122 mg, 1.87 mmol) and 2-hydroxy-1-naphthaldehyde (643 mg, 3.74 mmol) in ethanol (5 mL) was refluxed at 60 °C for 12 h. The product (488 mg, 64%) was obtained as yellow solid after column chromatography purification. [ ]$^{19}_{D}$ +1386 (*c* 1.0, CH_2Cl_2); ^{1}H NMR (400 MHz, CD_3Cl_3) 1.42 (s, 3 H), 1.55 (s, 3 H), 1.93-2.04 (m, 2 H), 2.18-2.27 (m, 1 H), 2.29-2.41

(m, 1 H), 3.53 (d, *J* = 7.6 Hz, 1 H), 3.73 (d, *J* = 13.6 Hz, 1 H), 3.79 (s, 3 H), 3.88 (d, *J* = 13.6 Hz, 1 H), 4.17 (dd, *J* = 5.2, 7.2 Hz, 1 H), 4.40 (dd, *J* = 3.2, 4.8 Hz, 1 H), 6.71 (d, *J* = 8.8 Hz, 1 H), 6.79 (d, *J* = 8.8 Hz, 1 H), 6.88 (dd, *J* = 8.8 Hz, 1 H), 6.92 (dd, *J* = 8.8 Hz, 1 H), 7.41- 7.47 (m, 1 H), 4.47-7.49 (m, 1 H), 7.52-7.59 (m, 3 H), 7.63 (d, *J* = 10.8 Hz, 1 H), 7.84 (d, *J* = 10.8 Hz,1 H), 7.96 (br s, 1 H), 8.40 (d, *J* = 8.0 Hz, 1 H), 8.49 (d, *J* = 8.0 Hz, 1 H), 13.97 (br s, 1 H), 13.03 (d, *J* = 10.8 Hz, 1 H); ^{13}C NMR (100 MHz, CD_3Cl_3) 22.7, 24.6, 26.3, 28.2, 55.1, 61.1, 62.9, 73.3, 79.2, 85.4,108.9, 110.2, 114.9, 116.6, 124.5, 125.0, 125.3, 125.5, 127.25, 127.29, 127.4, 127.6, 128.3, 129.8, 129.9, 130.4, 136.8, 137.7, 157.5, 165.3, 169.8, 177.3; HMRS (ESI) Calcd for $C_{33}H_{34}N_2O_5Na$ $(M+Na)^+$ 561.2365 obsd 561.2388.

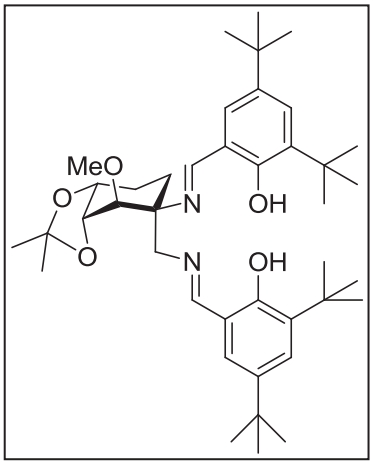

2,4-di-tert-butyl-6-((E)-(((3aR,4S,5S,7aR)-5-((E)-3,5-di-tert-butyl-2-hydroxybenzylideneamino)-4-methoxy-2,2-dimethylhexahydrobenzo[d][1,3]dioxol-5-yl)methylimino)methyl)phenol (17a): Following the general procedure for salen synthesis, a mixture of β-diamine **17** (207 mg, 0.9 mmol, 1 equiv) and 3,5-di-*tert*-butylsalicylaldehyde (380 mg, 1.62 mmol, 1.8 equiv) in ethanol (5 mL) was heated at 60 °C for 12 h. The product (429 mg, 80%) was obtained as pale yellow solid after addition of cold 10% water in EtOH. $[\alpha]^{19}_D$ -125.3 (*c* 1.6, CH_2Cl_2); ^{1}H NMR (400 MHz, CD_3Cl_3) 1.31 (s, 9H), 1.32 (s, 9H), 1.37 (s, 3H), 1.45 (s, 9H), 1.45 (s, 9H), 1.57 (s, 3H), 1.77-1.87 (m, 1H), 2.01-2.04 (m, 3H), 3.59 (d, *J* = 7.9 Hz, 1H), 3.63 (d, *J* = 12.1 Hz, 1H), 3.67 (s, 3H), 4.13 (d, *J* = 12.1 Hz, 1H), 4.22 (dd, *J* = 7.9, 5.2 Hz, 1H), 4.31 (t, *J* = 4.7 Hz, 1H), 7.11 (dd, *J* = 6.8, 2.4 Hz, 2H), 7.34 (d, *J* = 2.4

Hz, 1H), 7.39 (dd, *J* = 6.4, 2.4 Hz, 2H), 7.59 (d, *J* = 2.4 Hz, 1H), 8.41 (s, 1H), 8.70 (s, 1H), 13.56 (s, 1H), 13.95 (s, 1H); ^{13}C NMR (100 MHz, CD_3Cl_3) 14.11, 22.1, 22.6, 26.6, 28.4, 29.35, 29.43, 31.5, 31.6, 34.1, 35.1, 61, 64.5, 65.3, 74.4, 80.2, 83.2, 108.2, 117.8, 118.1, 126, 126.6, 127.2, 127.3, 136.8, 139.9, 140.2, 158.1, 158.4, 166.6, 167.9; HMRS (FAB) Calcd for $C_{41}H_{63}N_2O_5$ $(M+H)^+$ 663.4659 obsd 663.4727.

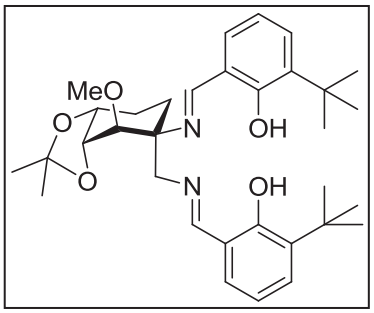

2-(tert-butyl)-6-((E)-((((3aR,4R,5S,7aR)-5-((E)-(3-(tert-butyl)-2-hydroxybenzylidene)amino)-4-methoxy-2,2-dimethylhexahydrobenzo[d][1,3]dioxol-5-yl)methyl)imino)methyl)phenol (17b): Following the general procedure for salen synthesis, a mixture of β-diamine (177 mg, 0.77 mmol, 1 equiv) and 3-*tert*-butylsalicylaldehyde (274 mg, 1.54 mmol, 2 equiv) in ethanol (5 mL) was heated at 60 °C for 12 h. The product (347 mg, 82%) was obtained as pale yellow solid after column chromatography purification. $[\alpha]^{19}_D$ -59.1 (*c* 0.7, CH_2Cl_2); ^{1}H NMR (400 MHz, $CDCl_3$) 1.38 (s, 3H), 1.45 (s, 9H), 1.49 (s, 9H), 1.58 (s, 3H), 1.74-1.85 (m, 1H), 2.01-2.12 (m, 3H), 3.59 (d, *J* = 8.0 Hz, 1H), 3.64 (d, *J* = 11.6 Hz, 1H), 3.66 (s, 3H), 4.14 (d, *J* = 12.0 Hz, 1H), 4.22 (dd, *J* = 5.2, 8.0 Hz, 1H), 4.34 (t, *J* = 2.4 Hz, 1H), 6.81 (d, *J* = 7.6, 1 H), 6.85 (d, *J* = 7.6, 1 H), 7.13 (dd, *J* = 1.6, 6.0 Hz, 1 H), 7.15 (dd, *J* = 1.6, 6.0 Hz, 1 H), 7.35 (dt, *J* = 1.6, 7.6 Hz, 2 H), 8.41 (s, 1 H), 8.71 (s, 1 H), 13.8 (s, 1 H), 14.16 (s, 1 H); ^{13}C NMR (100 MHz, CD_3Cl_3) 22.1, 26.6, 28.4, 28.6, 29.3, 29.4, 34.9, 60.9, 64.4, 65.3, 74.4, 80.2, 83.0, 117.8, 118.0, 118.6. 118.9, 129.7, 129.8, 129.9, 130.4, 137.56, 137.59, 160.4, 160.8, 166.3, 167.7; HMRS (ESI) Calcd for $C_{33}H_{46}N_2O_5Na$ $(M+Na)^+$ 573.3304 obsd 573.3301.

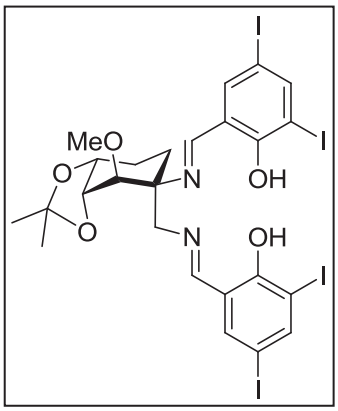

2-((E)-(((3aR,4S,5S,7aR)-5-((E)-2-hydroxy-3,5-diiodobenzylideneamino)-4-methoxy-2,2-dimethylhexahydrobenzo[d][1,3]dioxol-5-yl)methylimino)methyl)-4,6-diiodophenol (17c): Following the general procedure for salen preparation, a mixture of β-diamine **17** (65 mg, 0.28 mmol) and 3,5-diiodosalicylaldehyde (190 mg, 0.51 mmol, 1.8 equiv) in ethanol (3 mL) was heated at 50 °C overnight, the product (211 mg, 88%) was obtained as yellow solid after washing with cold Ethanol. $[\alpha]^{19}_{D}$ –138.4 (*c* 1.0, $CHCl_3$); ^{1}H NMR (400 MHz, CD_3Cl_3) 1.33 (s, 3H), 1.53 (s, 3H), 1.86-1.88 (m, 1H), 1.95-1.97 (m, 2H), 2.06-2.08 (m, 1H), 3.41 (d, *J* = 7.7 Hz, 3H), 3.59 (s, 3H), 3.98 (d, *J* = 12.5 Hz, 1H), 3.83 (d, *J* = 12.5 Hz, 1H), 4.8 (dd, *J* = 7.5, 5.4 Hz, 1H), 4.28 (br s, 1H), 7.48 (d, *J* = 1.9 Hz, 1H), 7.51 (d, *J* = 1.9 Hz, 1H), 8.04 (d, *J* = 1.9 Hz, 1H), 8.05 (d, *J* = 1.9 Hz, 1H), 8.12 (s, 1H), 8.37 (d, *J* = 1.73 Hz, 1H), 14.05 (s, 1H), 14.83 (s, 1H); ^{13}C NMR (100 MHz, CD_3Cl_3) 21.8, 26.3, 27.4, 28.4, 60.8, 63.9, 65.3, 73.7, 78.6, 79.3, 79.7, 83.9, 87.3, 88.9, 108.4, 119.4, 119.6, 139.9, 140.6, 149.0, 149.2, 160.3, 162.3, 163.8, 165.4; HMRS (FAB) Calcd for $C_{25}H_{27}N_2O_5I_4$ $(M+H)^+$ 942.8021 obsd 942.8115.

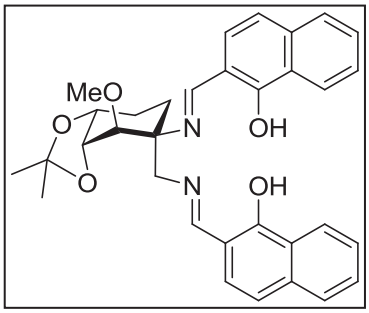

2-((E)-((((3aR,4R,5S,7aR)-5-((E)-((1-hydroxynaphthalen-2-yl)methylene)amino)-4-methoxy-2,2-dimethylhexahydrobenzo[d][1,3]dioxol-5-yl)methyl)imino)methyl)naphthalen-1-ol (17d): Following the general procedure for salen synthesis, a mixture of β-diamine (60 mg, 0.26 mmol) and 2-hydroxy-1-naphthaldehyde (89 mg,

0.52 mmol) in ethanol (2 mL) was heated at 60 °C for 12 h. The product (106 mg, 73%) was obtained as a brown solid after column chromatography purification. $[\alpha]^{19}_{D}$ +488 (*c* 1, CH_2Cl_2); ^{1}H NMR (400 MHz, $CDCl_3$) 1.36 (s, 3H), 1.56 (s, 3H), 1.89-2.01 (m, 1H), 2.03-2.22 (m, 3H), 3.47 (d, *J* = 6.8 Hz, 1H), 3.74 (d, *J* = 10.4 Hz, 1H), 3.76 (s, 3 H), 3.88 (d, *J* = 12.8 Hz , 1H), 4.26-4.32 (m, 2 H), 6.71 (d, *J* = 8.8 Hz, 1 H), 6.79 (d, *J* = 8.8 Hz, 1 H), 6.91 (d, *J* = 12.4 Hz, 1 H), 6.94 (d, *J* = 12.4 Hz, 1 H), 7.40-7.45 (m, 1 H), 7.46-7.51 (m, 1 H), 7.52- 7.61 (m, 3 H), 7.64 (d, *J* = 7.6 Hz, 1 H), 7.88 (s, 1 H), 7.92 (d, *J* = 10.4 Hz, 1 H), 8.46 (d, *J* = 8.0 Hz, 1 H), 8.50 (d, 8.0 Hz, 1 H), 13.68 (d, *J* = 10.4 Hz, 1 H), 13.95 (s, 1 H); ^{13}C NMR (100 MHz, CD_3Cl_3) 21.4, 25.5, 26.4, 28.4, 60.7, 61.5, 62.6, 73.7, 79.4, 82.5, 124.7, 125.2, 125.4, 125.6, 127.30, 127.31, 127.4, 127.9, 128.2, 129.9, 130.0, 130.6, 136.9, 137.7, 158.9, 164.7, 170.7, 178.0; HMRS (ESI) Calcd for $C_{33}H_{34}N_2O_5Na$ $(M+Na)^+$ 561.2365 obsd 561.2363.

General Procedure for Synthesis of Co(III)-Salen Catalysts (illustrated for 16a):

To a stirred solution of salen ligand **(16a)** (116 mg, 0.17 mmol, 1 equiv.) in 1 mL CH_2Cl_2, a methanolic (1 mL) solution of cobalt (II) acetate tetrahydrate (42 mg, 0.17 mmol, 1.0 equiv.), was added via cannula, under Ar. The Co(II)-salen complex precipitated out as a red solid. After filtration, the Co(II) complex was taken up in CH_2Cl_2 or toluene (2 mL) and stirred with 3,5-dinitrobenzoic acid (1 equiv.) open to the air. The oxidation could be followed by TLC [formation of a greenish-brown spot of lower Rf {Co-(III) complex} from the visibly red, higher Rf spot characteristic of the Co-(II) salen]. When TLC indicated the completion of the reaction (2-12 h), the solvent was evaporated, and the Co(III)-salen complex further dried *in vacuo*. The Co-(III)-salen complexes were

generally used directly for HKR experiments, under ISES (bilayer) conditions or under typical neat or one-phase flask conditions.

Table 4.3: HR-MS characterization of Co(III)-salen catalysts.

Catalyst	Molecular Formula	Calcd	obsd HR-MS (EI)
Co(III)-16a-3,5-DNB	$C_{41}H_{60}N_2O_5Co$	719.3834	719.3824
Co(III)-16b-3,5-DNB	$C_{33}H_{44}N_2O_5Co$	607.2582	607.2563
Co(III)-16c-3,5-DNB	$C_{25}H_{24}N_2O_5I_4Co$	998.7196	998.7170
Co(III)-16d-3,5-DNB	$C_{33}H_{32}N_2O_5Co$	595.1643	595.1635
Co(III)-17a-3,5-DNB	$C_{41}H_{60}N_2O_5Co$	719.3834	719.3833
Co(III)-17b-3,5-DNB	$C_{33}H_{44}N_2O_5Co$	607.2582	607.2604
Co(III)-17c-3,5-DNB	$C_{25}H_{24}N_2O_5I_4Co$	998.7196	998.7200
Co(III)-17d-3,5-DNB	$C_{33}H_{32}N_2O_5Co$	595.1643	595.1644

B. Miniaturized ISES (In Situ Enzymatic Screening) Experiments

A general procedure for the minituarized ISES to estimate both relative reaction rates and sense and magnitude of enantioselectivity is presented below. Cobalt-(III)-salen mediated HKR of (±)-propylene oxide and (±)-hexene oxide were chosen as model reactions. A new reporting system was developed in this work, so that more readily available enzymes might be used by chemists seeking to perform these ISES assays. To establish a new set of reporting enzymes for these model reactions, commercially available nicotinamide-dependent ketoreductases from Codexis (so-called KREDs) were screened for catalytic efficiency and enantioselectivity for the oxidation of the 1,2-diol products of these model HKR reactions (Note: One motivation here was the reduced

availability of the most utilized reporting enzyme heretofore; namely native HLADH = horse liver alcohol DH). As a result of these screening studies, TBADH (selective for *R*-1,2-propanediol) and KRED 23 (selective for *S*-1,2-propanediol) were selected as reporting enzymes for the HKR of (±)-propylene oxide. Correspondingly, KRED 107 and KRED 119 were selected as reporting enzymes for the HKR of (±)-hexene oxide. The details of the characterization of these new KRED reporting enzymes are provided herewith.

KRED Reporting Enzyme Characterization

1) KRED 107: The enantioselectivity of KRED 107 was estimated by comparing the initial velocities of (*R*)- vs. (*S*)-1,2-hexanediol oxidation at fixed initial concentrations between 1.25 and 100 mM at 25 °C. Each velocity measurement was performed in duplicate. The assay well contained the following: 2.2 mM NADP+ (3.5 μL from a 125 mM stock), 0.045 U of KRED 107, and various concentrations of either (*R*)- or (*S*)-1,2-hexanediol. In all cases, the final volume was adjusted to 0.2 mL using 50 mM sodium pyrophosphate buffer, pH 8.8. 2) KRED 119: The enantioselectivity of KRED 119 was estimated in the same manner as for KRED 107, as described above. 3). KRED 23: The enantioselectivity of KRED 23 was estimated by comparing the rates of (*R*)- vs. (*S*)-1,2-propanediol oxidation at fixed initial concentrations between 3 and 140 mM at 25 °C. Each velocity measurement was performed in duplicate. The assay well contained the following: 7.2 mM NAD^+ (5 μL from a 220 mM stock), 10 μL of a KRED 23 stock solution (2 mg in 250 μL buffer) and various concentrations of either (*R*)- or (*S*)-1,2-propanediol. In all cases, the final volume was adjusted to 150 μL using 50 mM sodium pyrophosphate buffer, pH 8.8.

Previously, we estimated during HKR-ISES experiments that the diol concentration is in the range of 2.5-70 mM. So, generally selectivity parameters appropriate for ISES screening are chosen based upon enantioselectivities observed in this concentration range. For KRED 119, a selectivity factor of 6.5 in favor of the (*R*)-1,2-hexanediol was used for ISES estimations. This corresponds to the selectivity observed in the standard assay cuvette at approximately 40 mM diol concentration. KRED 107 proved to be the most difficult reporting enzyme to parametrize, owing to its very high preference for the (*S*)-antipode of 1,2-hexanediol. In the end, iterative analysis of candidate fitting factors led us to assign a selectivity factor of 59 for this reporting enzyme (corresponds approximately to the selectivity of this reporting enzyme on the lower end of the aforementioned concentration window). Selectivity factors of 8.4 (v_S/v_R) for TBADH[2] and 6.5 (v_S/v_R) for KRED 23 were employed for 1,2-propanediol reporting. The complete set of enantiomeric diol screening data (rate vs. concentration) for each of the selected KRED screening enzymes is provided in Fig. 4.24.

Enzyme Standardization

Stock Solutions. The following stock solutions were made for enzyme standardization: 40 mM β-$NADP^+$, 130 mM β-NAD^+, 0.016mg/μL TBADH, 0.016 mg/μL KRED 23, 0.002 mg/μL KRED 107 and 0.002 mg/μL KRED 119 in 25 mM sodium phosphate buffer (pH 7.0), 2 M (*R*)-1,2-propanediol in water. Enzyme units were calculated by measuring the rate of formation of NADPH or NADH at 340 nm (*vide infra*). In each case, one S.I. unit is taken as the amount of enzyme catalyzing the formation of one μmol of NADPH per minute.

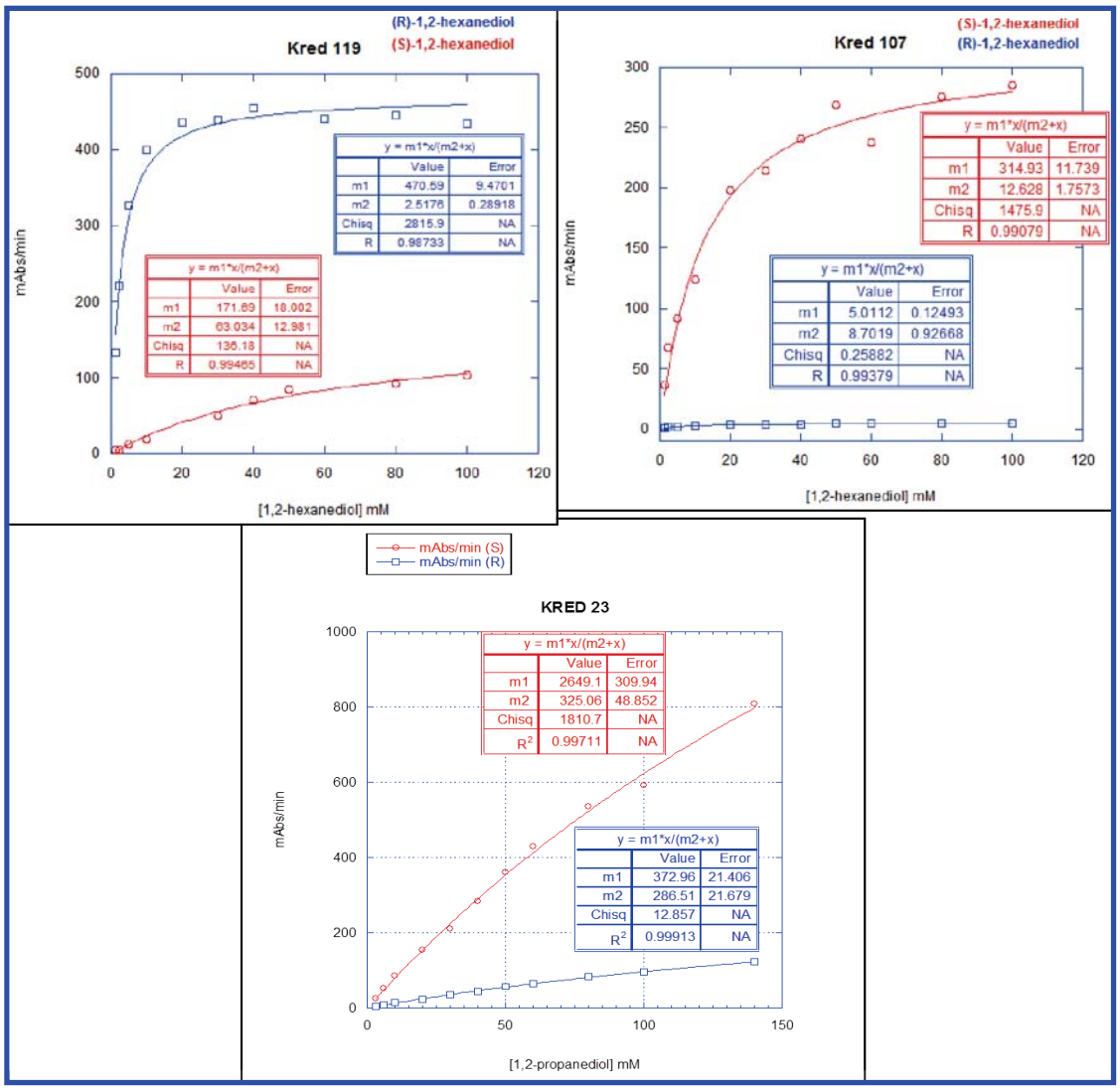

Figure 4.24: Enantioselectivities of the new reporting enzymes

Standardization of TBADH. The assay cuvette contained the following components: 2.2 mM (5 µL of 40 mM stock solution), β-$NADP^+$, 5 µL of TBADH stock solution, 71 µL of 50 mM sodium pyrophosphate buffer (pH 8.8), and 200 mM (9 µL of 2 M stock) of (*R*)-1,2-propanediol. The reaction was initiated by the addition of the (*R*)-1,2-propanediol, which typically gave a rate of 0.709 abs/min at 25°C at 340 nm

wavelength. This was indicative of 0.028 U/μL for the TBADH stock solution for the oxidation of (*R*)-1,2-propanediol.

Standardization of KRED 23. The assay cuvette contained the following components: 7.2 mM (5 μL of 130 mM stock solution) β-NAD^+, 5 μL of KRED 23 stock solution, 71 μL of 50 mM sodium pyrophosphate buffer (pH 8.8), and 200 mM (9 μL of 2 M stock) of (*R*)-1,2-propanediol. The reaction was initiated by the addition of the (*R*)-1,2-propanediol, which typically gave a rate of 0.540 abs/min at 25°C at 340 nm wavelength. This is indicative of 0.016 U/μL for the KRED 23 stock solution for the oxidation of (*R*)-1,2-propanediol.

Standardization of KRED 107. The assay cuvette contained the following components: 2.2 mM (5 μL of 40 mM stock solution), β-$NADP^+$, 5 μL of KRED 107 stock solution, 81 μL of 50 mM sodium pyrophosphate buffer (pH 8.8), and 200 mM (9 μL of 2 M stock) of (*R*)-1,2-hexanediol. The reaction was initiated by the addition of the (*R*)-1,2-hexanediol, which typically gave a rate of 0.124 abs/min at 25°C at 340 nm wavelength. This is indicative of 0.00398 U/μL for the KRED 107 stock solution for the oxidation of (*R*)-1,2-hexanediol.

Standardization of KRED 119. The assay cuvette contained the following components: 2.2 mM (5 μL of 40 mM stock solution) β-$NADP^+$, 5 μL of KRED 119 stock solution, 81 μL of 50 mM sodium pyrophosphate buffer (pH 8.8), and 200 mM (9 μL of 2 M stock) of (*R*)-1,2-hexanediol. The reaction was initiated by the addition of the (*R*)-1,2-hexanediol, which typically gave a rate of 0.291 abs/min at 25°C at 340 nm

wavelength. This was indicative of 0.00935 U/μL for the KRED 119 stock solution for the oxidation of (*R*)-1,2-hexanediol.

Layer Composition

Quartz cuvettes with nominal 1 mL volumes were used in all previous ISES experiments. Here, for the first time, we describe a general procedure utilizing a 16 multimicrocell array for "cassette" in situ enzymatic screening. For every catalyst, a four well "cassette screen" was performed over the two different substrates: propylene oxide and hexene oxide. For propylene oxide, well A contains TBADH and well B contains KRED 23. For hexene oxide, well C contains KRED 107 and well D contains KRED 119.

Organic Layer in Wells A and B. Both well A and B had the following composition: 10 μL propylene oxide (8.3 mg, 0.14 mmol), 10 μL of $CHCl_3$ and 0.25 mol% catalyst. The total organic layer volume was maintained to 20 μL. Organic Layer in Wells C and D. Both well C and D had the following composition: 10 μL hexene oxide (8.3 mg, 0.08 mmol), 10 μL of $CHCl_3$ and 0.25 mol% catalyst. The total organic layer volume was maintained to 20 μL.

Aqueous Layer in Well A. 0.1 U of TBADH (3.6 μL from a stock solution (0.028 U/μL)), 2.2 mM β-$NADP^+$ (5 μL from a 40 mM stock solution) and 81.4 μL of 50 mM sodium pyrophosphate buffer, pH 8.8. The total volume of the aqueous layer was maintained at 90 μL. Aqueous Layer in Well B. 0.1 U of KRED 23 (6.2 μL from a stock solution (0.016 u/μL)), 7.2 mM β-NAD^+ (5 μL of 130 mM stock solution) and 78.8 μL of 50 mM sodium pyrophosphate buffer (pH 8.8). The total volume of the aqueous layer

was maintained at 90 μL. Aqueous Layer in Well C. 0.0374 U of KRED 107 (9.4 μL from a stock solution (0.00398 U/μL)), 2.2 mM β-$NADP^+$ (5 μL from a 40 mM stock solution) and 75.6 μL of 50 mM sodium pyrophosphate buffer, pH 8.8. The total volume of the aqueous layer was maintained at 90 μL. Aqueous Layer in Well D. 0.0374 U of KRED 119 (4 μL from a stock solution (0.00935 U/μL)), 2.2 mM β-$NADP^+$ (5 μL from a 40 mM stock solution) and 81 μL of 50 mM sodium pyrophosphate buffer, pH 8.8. The total volume of the aqueous layer was maintained at 90 μL.

Step by Step Protocol

It was found practical to load the aqueous layers first. Routinely 90 μL aqueous layers were loaded into individuate wells of 16-well quartz multimicrocell either with a microsyringe or with a multichannel pipetter. The quartz cell was gently tapped to keep the layers evenly distributed in the solid quartz apparatus, then cooled on ice. Then the organic layers were prepared by briefly vortexing the catalyst stock in $CHCl_3$ with (±)-propylene oxide or (±)-hexene oxide in iced microcentrifuge tubes. The low volume (20 μL) organic layer was then loaded to each well, most easily by rapidly syringing below the aqueous layer. Catalyst screens were run at room temperature in duplicate, with ISES rates taken as the average of the two ΔOD_{340}/time values obtained, for the appropriate time window (*vide infra*).

C. HKR Reactions Under Flask Conditions

General Procedure for HKR of Epoxides: Two different general procedures were adapted based on the boiling points of the epoxides. In some cases, the epoxide was

opened with phenyl selenide anion. This latter protocol may be of advantage (i) to decrease the volatility of leftover epoxides, (ii) to introduce a UV chromophore (for UV detection – HPLC) and/or (iii) to improve enantiomeric peak resolution in chiral-HPLC.

Procedure for Epoxide Opening by Phenylselenide: Phenylselenide anion was prepared by slow addition of 3 equiv $NaBH_4$ into an ice-cold suspension of 1.5 equiv of diphenyl diselenide in ethanol (5-7 mL). The resulting mixture was heated at 40 °C for 20 – 40 min, until the solution became colorless. Then, either purified epoxide or the reaction mixture out of HKR was added to the ethanolic solution of phenyl selenide at 0 °C. The resulting reaction was slowly allowed to warm to rt and stirring was continued for 8 - 10 h at rt. The reaction was quenched with ~1 mL of NH_4Cl. The mixture was diluted with dichloromethane and dried over anhydrous Na_2SO_4. The crude product was obtained after filtration and the removal of the solvent. Silica gel column chromatography was used to isolate seleno-alcohol (and the diol, in cases, where the mixture of both epoxide and diol was added to phenyl selenide anion). **Mosher Ester Analysis:** For some seleno-alcohols, enantiomeric excess was estimated via a classical Mosher esterification procedure [CH_2Cl_2, NEt_3 (10 equiv), DMAP (cat.), *S*-Mosher acid chloride] followed by ^1H NMR analysis.

General Procedure A (Direct Treatment of the HKR Reaction Mixture with Phenyl Selenide): This procedure was adapted for propylene oxide, hexene oxide, 1, 2-epoxy-3-phenylpropane, butadiene monoxide and 1,2-epoxy-7-octene. Here, we describe a general procedure for propylene oxide.

Propylene oxide (Table 4.2, entry 1):

In this case catalyst **Co(III)-17c-3,5-DNB** (29.4 mg, 0.026 mmol, 1 mol%) was mixed with 1,2-epoxypropane (1.52 g, 26.1 mmol) and cooled to 0 °C. The reaction was initiated by 213 μL (0.5 equiv) of water and the stirring was continued for 12 h at 0 °C. For this substrate, the reaction mixture was added to the phenyl selenide solution at 0 °C. Workup and column chromatography provided selenoalcohol (2.06 g, 38%, 0→30% ether in pentane) and 1,2-propanediol (786 mg, 42%, 50→0% ether in EtOAc).

1-(Phenylseleno)-2-propanol: NMR data matched reported data.[7] The sign of the rotation was dependent on the solvent: in ethanol, $[\alpha]^{19}_{obsd}$ +4.5 (for 54% ee of *R*), $[\alpha]^{19}_{D}$ +8.3 (calcd); in CH_2Cl_2 $[\alpha]^{19}_{obsd}$ -28.1 (for 54% ee of *R*), $[\alpha]^{19}_{D}$ -52.1 (calcd). The enantiomeric excess of the 1-(phenylseleno)-2-propanol was estimated by derivatization as its *R*-Mosher ester - ^{1}H NMR, 3.02 (dd, 1H, *R*-enantiomer) & 2.93 (dd, 1H, *S*-enantiomer).

1,2-Propanediol: The diol was derivatized to its bis-(p-bromobenzoate) ester and the enantiomeric excess was measured in chiral HPLC (Chiralcel OD, hexanes:^{i}-PrOH 97:3, flow rate 1mL/min) t_R 9.9 min (*R*), 10.8 min (*S*).

1,2-Epoxyhexane (Table 4.2, entry 3):

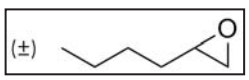

General Procedure A was followed, starting from 1,2-epoxyhexane (100 mg, 1.0 mmol), catalyst **Co(III)-17c-3,5-DNB** (5 mg, 0.005 mmol, 0.5 mol%) and 9 μL (0.5 equiv) of water at 0 °C for 30 h. ^{1}H NMR of a small aliquot of the reaction showed a 53% reaction conversion. Direct ring-opening with phenyl selenide anion was performed. Workup and column chromatography, provided

both the seleno-alcohol (116 mg, 45%, using 20% EtOAc in hexanes) and 1,2-hexanediol (57 mg, 48%, using 10% methanol in EtOAc).

1-(phenylseleno)-2-hexanol: ^{1}H NMR (400 MHz, $CDCl_3$) δ 0.87 (t, *J* = 6.4 Hz, 3H), 1.26-1.32 (m, 3H), 1.38-1.42 (m, 1H), 1.50-1.55 (m, 2H), 2.34 (br s, 1H), 2.85-2.90 (m, 1H), 3.12-3.16 (m, 1H), 3.63-3.67 (m, 1H), 7.24-7.26 (m, 3H), 7.51-7.53 (m, 2H); $[\alpha]^{19}_{obsd}$ -29.5 (for 99% ee of *R*), $[\alpha]^{19}_{D}$ -29.8, calcd (c = 1.1, $CHCl_3$). The enantiomers of the seleno alcohol were separable using Chiralcel OD column. For this alcohol (hexanes/*i*-PrOH 98:2, flow rate 1 mL/min), minor isomer, t_R = 10.5 min (*S*) and major isomer, t_R = 11.6 min (*R*).

1,2-Hexanediol: ^{1}H NMR (400 MHz, $CDCl_3$) δ 0.88 (t, *J* = 6.4 Hz, 3H), 1.23-1.41 (m, 6H), 2.69 (br s, 2H), 3.43-3.68 (m, 3H); $[\alpha]^{23}_{obsd}$ -33.93 (for 91% ee of *S*), $[\alpha]^{23}_{D}$ -37.28, calcd (c = 0.75, EtOH), [lit.[8] $[\alpha]_D$ = + 15.7 (c = 1.0, EtOH, for *R*-diol); lit.[9] $[\alpha]_D$ = – 22.1 (c = 1.0, EtOH, for *S*-diol), lit.[10] (*S*)-diol is -17.5° (c = 1.3, EtOH), lit.[11] (*S*)-diol is -17.0° (c = 1.09, EtOH), lit.[12] (*R*)-diol is +22.0 (c = 1.1, EtOH)]. The 1,2-diol was derivatized as its bis-*p*-bromobenzoate ester and the enantiomeric excess was determined using the same chiral column (hexanes/*i*-PrOH 97:3, flow rate 1 mL/min) for minor isomer, t_R = 6.9 min (*R*) and for major isomer, t_R = 8.0 min (*S*).

1,2-Epoxy-3-phenylpropane (Table 4.2, entry 4):

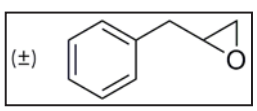

General Procedure A was followed, starting from epoxy-3-phenylpropane (315 mg, 2.3 mmol), catalyst **Co(III)-17c-3,5-DNB** (24.8 mg, 0.023 mmol, 1 mol%) and 22 μL (0.5 equiv) of water at 0 °C for 12 h. ^{1}H NMR of a small aliquot of the reaction showed a 49% reaction conversion. Direct ring-

opening with phenyl selenide anion ensued. After workup and column chromatography were obtained both the seleno-alcohol (329 mg, 48%, 0→50% ether in pentane) and 3-phenyl-1,2-propanediol (175 mg, 49%, 50→0% ether in EtOAc).

1-(Phenylseleno)-3-phenyl-2-propanol: ^{1}H NMR (400 MHz, $CDCl_3$) δ 2.36 (d, *J* = 3.6 Hz, 1H), 2.86-2.88 (m, 2H), 2.91-2.96 (m, 1H), 3.10-3.14 (m, 1H), 3.92-3.96 (m, 1H), 7.17-7.30 (m, 8H), 7.47-7.50 (m, 2H); $[\alpha]^{19}_{obsd}$ -24.6 (for 76% ee of *R*), $[\alpha]^{19}_{D}$ -32.4, calcd (c = 1.0, $CHCl_3$). The seleno-alcohol was resolved on Chiral column. For the seleno-alcohol (hexane/ i-PrOH 97:3, flow rate: 1 mL/min), major isomer, t_R = 17.1 min (*R*) and minor isomer, t_R = 19.3 min (*S*).

3-Phenylpropane-1,2-diol: ^{1}H NMR (400 MHz, $CDCl_3$) δ 2.68-2.78 (m, 2H), 3.44-3.48 (m, 2H), 3.63 (d, J = 10.8 Hz, 2H), 3.89 (d, J = 5.6 Hz, 1H), 7.18-7.31 (m, 5H); $[\alpha]^{19}_{obsd}$ -21.5 (for 92% ee of *S*), $[\alpha]^{19}_{D}$ -23.3, calcd (c = 1.0, $CHCl_3$), [lit.[12] $[\alpha]_D$ -18.6, (c = 1.3, $CHCl_3$) for *S*-diol), lit.[13] $[\alpha]^{20}_{D}$ +20.4, (c = 1.0, $CHCl_3$) for R-diol), lit.[14] $[\alpha]^{20}_{D}$ +15.0, (c = 1.0, $CHCl_3$) for *R*-diol), lit.[15] $[\alpha]_D$ -29.0, (c = 1.2, EtOH) for *S*-diol)]. 1,2-diol was resolved on Chiral column. For 1,2-diol (hexane/i-PrOH 92:8, flow rate: 1 mL/min), minor isomer, t_R = 12.1 min (*R*) and major isomer, t_R = 13.2 min (*S*).

1,2-Epoxy-7-octene (Table 4.2, entry 6):

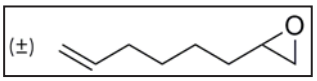

General Procedure A was followed, starting from 1,2-epoxy-7-octene (126 mg, 1.0 mmol), catalyst **Co(III)-17c-3,5-DNB** (5 mg, 0.005 mmol, 0.5 mol% loading) and 9 μL (0.5 equiv) of water at rt for 30 h. Direct ring-opening with phenyl selenide anion ensued. After workup and column

chromatography, were obtained both the seleno-alcohol (119 mg, 42%, using 20% EtOAc in hexanes) and oct-7-ene-1,2-diol (71 mg, 49%, using pure EtOAc).

1-(Phenylseleno)-oct-7-ene-2-ol: ^{1}H NMR (400 MHz, $CDCl_3$) δ 1.34-1.38 (m, 4H), 1.50-1.53 (m, 2H), 2.02 (d, J = 6.8 Hz, 2H), 2.38 (d, J = 4Hz, 1H), 2.84-2.90 (m, 1H), 3.11-3.15 (m, 1H), 3.65 (bs, 1H), 4.90-4.50 (m, 2H), 5.77-5.78 (m, 1H), 7.25-7.27 (m, 3H), 7.50-7.53 (m, 2H); $[\alpha]^{19}_{obsd}$ -36.4 (for 99% ee of *R*), $[\alpha]^{19}_{D}$ -36.7, calcd (c = 1.1, $CHCl_3$). The enantiomeric excess of this seleno alcohol was estimated by chiral HPLC (Chiralcel OD, hexanes/*i*-PrOH 97 :3, flow rate 1 mL/min, 254 nm), t_{Rmajor} = 11.6 min (*R*) and t_{Rminor} = 13.8 min (*S*).

Oct-7-ene-1,2-diol: ^{1}H NMR (400 MHz, $CDCl_3$) δ 1.29-1.46 (m, 6H), 2.01-2.06 (m, 2H), 3.05 (br s, 2H), 3.37-3.41 (m, 1H), 3.60-3.65 (m, 2H), 4.90-4.99 (m, 2H), 5.72-5.82 (m, 1H); $[\alpha]^{19}_{obsd}$ -2.6 (for 81% ee of *S*), $[\alpha]^{19}_{D}$ -3.2, calcd (c = 1.0, $CHCl_3$).

The enantiomeric excess of 7-octen-1,2-diol was determined by derivatization as its bis-(*p*-bromobenzoate) ester and chiral HPLC analysis (Chiralcel OD column, hexanes/*i*-PrOH, 97:3, flow rate 1 mL/min, 254 nm), t_{Rminor} = 15.0 min (*R*); t_{Rmajor} = 16.2 min (*S*).

General Procedure B (Separation of the Epoxide and Diol HKR Products):

(Illustrated for **3-phenoxy-1,2-epoxypropane**). This procedure is applicable to all remaining epoxides.

3-Phenoxy-1,2-epoxypropane (Table 4.2, entry 2):

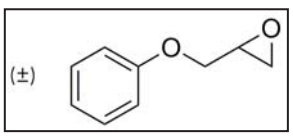

Catalyst **Co(III)-17c-3,5-DNB** (5 mg, 0.005 mmol, 0.5 mol%

loading) was mixed with 3-phenoxy-1,2-epoxypropane (150 mg, 1 mmol) and 300 μL of CH_2Cl_2. The mixture was cooled to 0 °C, and the reaction was initiated by adding 9 μL (0.5 equiv) of water and stirring was continued for 20 h at rt. After the reaction, silica gel column chromatography provided the unreacted 3-phenoxy-1,2-epoxypropanee (71 mg, 47%, using 50% ether in pentane) and 3-phenoxy-1,2-propanediol (77 mg, 46%, using 10% methanol in ether).

3-Phenoxy-1,2-epoxypropane: ^{1}H NMR (400 MHz, $CDCl_3$) δ 2.73-2.79 (m, 1H), 2.89-2.91 (t, J = 4.8 Hz, 1H), 3.33-3.37 (m, 1H), 3.94-4.04 (m, 1H), 4.19-4.25 (m, 1H), 6.88-7.00 (m, 3H), 7.23-7.33 (m, 2H); $[\alpha]^{19}_{obsd}$ +22.3 (for 97% ee of *S*), $[\alpha]^{19}_{D}$ +23.0, calcd (c = 1.4, $CHCl_3$). The enantiomers of this epoxide were separable using Chiralcel OD column. For the epoxide (hexanes:*i*-PrOH 87 :13, flow rate 1 mL/min), minor isomer, t_R = 8.2 min (*R*) and major isomer, t_R = 12.4 min (*S*).

3-Phenoxy-1,2-propanediol: ^{1}H NMR (400 MHz, $CDCl_3$) δ 2.54 (br s, 1H), 3.03 (br s, 1H), 3.71-3.84 (m, 2H), 4.01-4.11 (m, 3H), 6.88-6.98 (m, 3H), 7.23-7.30 (m, 2H); $[\alpha]^{19}_{obsd}$ -9.1 (for 92% ee of *R*), $[\alpha]^{19}_{D}$ -9.9, calcd (c = 1.4, $CHCl_3$), [lit.[16] $[\alpha]^{23}_{D}$ -10.0 (c = 1.9, EtOH)]. The enantiomers of the diol were also separable using Chiralcel OD column. For the diol (hexanes:*i*-PrOH 90:10, flow rate 1 mL/min), major isomer, t_R = 15.6 min (*R*) and minor isomer, t_R = 33.7 min (*S*).

6-[(*tert*-Butoxycarbonyl)-amino]-1,2-epoxyhexane (Table 4.2, entry 5):

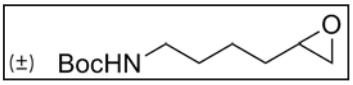

Following General Procedure B, catalyst **Co(III)-17c-3,5-DNB** (5 mg, 0.05 mmol, 1 mol% loading) with 6-[(*tert*-butoxycarbonyl)-amino]-1,2-epoxyhexane (107 mg, 0.5 mmol), 200 μL of THF and

water (4 μL, 0.2 mmol, 0.44 equiv) at rt for 35 h, provided the unreacted epoxide (59 mg, 55%, using pure ether) and the diol (47 mg, 40%, using 30% methanol in ether) after silica gel column chromatography.

6-[(*tert*-Butoxycarbonyl)-amino]-1,2-epoxyhexane: ^{1}H NMR (400 MHz, $CDCl_3$) δ 1.46 (s, 9H), 1.48-1.60 (m, 6H), 2.43-2.45 (m, 1H), 2.71-2.74 (m, 1H), 3.10-3.11 (m, 1H), 3.68 (m, 2H), 4.54 (br s, 1H); $[\alpha]^{19}_{obsd}$ +5.1 (for 72% ee of *R*), $[\alpha]^{19}_{D}$ +7.2, calcd (c = 1.1, $CHCl_3$). The enantiomeric excess of the epoxide was determined by converting the epoxide to 6-[(*tert*-butoxycarbonyl)-amino]-1-(phenylseleno)-2-hexanol.

6-[(tert-Butoxycarbonyl)-amino]-1-(phenylseleno)-2-hexanol: ^{1}H NMR (400 MHz, $CDCl_3$) δ 1.42 (s, 9H), 1.45-1.57 (m, 6H), 2.42 (br s, 1H), 2.84-2.89 (m, 1H), 3.08-3.13 (m, 3H), 3.64-3.66 (m, 1H), 4.50 (br s, 1H), 7.24-7.27 (m, 3H), 7.50-7.52 (m, 2H), $[\alpha]^{19}_{obsd}$ -10.5 (for 72% ee of R), $[\alpha]^{19}_{D}$ -14.6, calcd (c = 0.3, $CHCl_3$). The enantiomers of the seleno-alcohol were resolved on a Chiralcel OD column (92:8 hexanes:*i*-PrOH, flow rate: 1 mL/min), t_{Rmajor} = 16.0 min (*R*) and t_{Rminor} = 18.6 min (*S*).

6-[(*tert*-Butoxycarbonyl)-amino]-1,2-hexanediol: ^{1}H NMR (400 MHz, $CDCl_3$) δ 1.43 (s, 9H), 1.45-1.61 (m, 6H), 1.97 (br s, 1H), 2.16 (br s, 1H), 3.12-3.13 (m, 2H), 3.41-3.47 (m, 1H), 3.61-3.71 (m, 2H), 4.54 (br s, 1H); $[\alpha]^{19}_{obsd}$ -9.7 (for 92% ee of S), $[\alpha]^{19}_{D}$ -10.5, calcd (c = 1.0, $CHCl_3$). The diol was derivatized to its bis(p-bromobenzoate) and the enantiomers of the diol derivative were resolved using Chiralcel OD column (95:5 hexanes:*i*-PrOH, flow rate 1 mL/min), t_{Rminor} = 24.9 min (*R*) and t_{Rmajor} = 29.8 min (*S*).

4-Benzyloxy-1,2-epoxybutane (Table 4.2, entry 7):

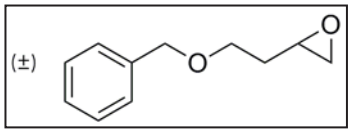

Following General Procedure B, catalyst **Co(III)-17c-3,5-DNB** (5 mg, 0.005 mmol, 0.5 mol% loading), 4-benzyloxy-1,2-epoxybutane[17] (178 mg, 1.0 mmol), 400 μL of CH_2Cl_2 and 9 μL of water at rt for 20 h provided the unreacted epoxide (121 mg, 68%, using 25% ether in pentane) and the product diol (51 mg, 26%, 0→100% EtOAc in ether), after silica gel column chromatography.

4-Benzyloxy-1,2-epoxybutane: ^{1}H NMR (400 MHz, $CDCl_3$) δ 1.77-1.84 (m, 1H), 1.89-1.95 (m, 1H), 2.54-2.56 (m, 1H), 2.79-2.82 (m, 1H), 3.07-3.12 (m, 1H), 3.63-3.67 (m, 2H), 4.56 (s, 2H), 7.28-7.38 (m, 5H); $[\alpha]^{23}_{obsd}$ +6.40 (for 39% ee of *R*), $[\alpha]^{23}_{D}$ +16.41, calcd (c = 1.0, $CHCl_3$), [lit.[18] $[\alpha]_D$ +16.6, (c = 3.0, $CHCl_3$) for *R*-epoxide and $[\alpha]_D$ -13.9, (c = 2.0, $CHCl_3$) for S-epoxide, lit.[19] $[\alpha]_D$ +16.9, (c = 2.51, $CHCl_3$) for *R*-epoxide and $[\alpha]_D$ -14.5, (c = 2.51, $CHCl_3$) for *S*-epoxide]. The enantiomeric excess of the epoxide was determined by converting the epoxide to 4-benzyloxy-1-phenylseleno-2-butanol with phenyl selenide.

4-Benzyloxy-1-phenylseleno-2-butanol: ^{1}H NMR (400 MHz, $CDCl_3$) δ 1.85-1.89 (m, 2H), 2.97-3.09 (m, 2H), 3.16 (br s, 1H), 3.62-3.68 (m, 2H), 3.93-3.96 (br s, 1H), 4.49 (s, 2H), 7.22-7.32 (m, 8H), 7.49-7.52 (m, 2H). The enantiomeric excess was determined from HPLC using Chiralcel OD column (95:5 hexanes:*i*-PrOH, flow rate 1 mL/min), t_{Rmajor} = 9.3 min (*R*) and t_{Rminor} = 13.9 min (*S*).

4-Benzyloxy-1,2-butanediol: ^{1}H NMR (400 MHz, $CDCl_3$) δ 1.71-1.82 (m, 2H), 2.59 (br s, 1H), 3.25 (br s, 1H), 3.46-3.50 (m, 1H), 3.59-3.69 (m, 3H), 3.70-3.91 (m, 1H), 4.50 (s, 2H), 7.25-7.36 (m, 5H); $[\alpha]^{23}_{obsd}$ -16.46 (for 86% ee of *S*), $[\alpha]^{23}_{D}$ -19.14, calcd (c = 0.65,

EtOH), [lit.[16] $[\alpha]^{23}_{D}$ -22.5, (c = 1.1, EtOH) for *S*-diol]. The enantiomers were resolved in chiral HPLC. (Chiralcel OD column, hexanes:*i*-PrOH 95:5, flow rate 1 mL/min), t_{Rminor} = 21.2 min (*R*) and t_{Rmajor} = 23.2 min (*S*).

5-[(*tert*-butyldiphenylsilyl)oxy]-1,2-epoxypentane (Table 4.2, entry 8):

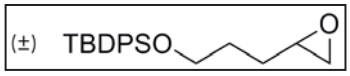

Following General Procedure B, the catalyst **Co(III)-17c-3,5-DNB** (10 mg, 0.01 mmol, 1 mol% loading) was mixed with 5-[(*t*-butyldiphenylsilyl)oxy]-1,2-epoxypentane[17] (343 mg, 1 mmol) and 500 μL of THF. The mixture was cooled to 0 °C, and the reaction initiated by adding 9 μL (0.5 equiv) of water and stirring continued for 50 h at rt. After the reaction, silica gel column chromatography provided the unreacted epoxide (214 mg, 63%, using ether) and 5-[(*tert*-butyldiphenylsilyl)oxy]-1,2-pentanediol (104 mg, 29%, using 10% methanol in ether).[20]

5-[(*tert*-Butyldiphenylsilyl)oxy]-1,2-epoxypentane: ^{1}H NMR (400 MHz, $CDCl_3$) δ 1.04 (s, 9H), 1.65-1.71 (m, 4H), 2.44-2.46 (m, 1H), 2.71-2.73 (m, 1H), 2.90-2.91 (m, 1H), 3.68-3.71 (m, 2H), 7.25-7.41 (m, 8H), 7.64-7.66 (m, 2H); $[\alpha]^{19}_{obsd}$ +1.0 (for 33 ee of *R*), $[\alpha]^{19}_{D}$ +3.15, calcd (c = 1.0, $CHCl_3$), [lit.[20] $[\alpha]_D$ -3.41, (c = 1.12, $CHCl_3$) for *S*-epoxide, lit.[21] $[\alpha]^{20}_{D}$ -2.71, (c = 1.1, $CHCl_3$) for *S*-epoxide]. The enantiomeric excess of the epoxide was determined by converting the epoxide to 5-[(*tert*-butyldiphenylsilyl)oxy]-1-(phenylseleno)-pentane-2-ol.

5-[(tert-Butyldiphenylsilyl)oxy]-1-(phenylseleno)-2-pentanol: ^{1}H NMR (400 MHz, $CDCl_3$) δ 1.01 (s, 9H), 1.57-1.71 (m, 4H), 2.75 (d, *J* = 3.6 Hz, 1H), 2.90-2.95 (m, 1H), 3.08-3.12 (m, 1H), 3.65 (t, *J* = 4.0 Hz, 2H), 3.68-3.74 (m, 1H), 7.23-7.26 (m, 3H), 7.34-

7.41 (m, 6H), 7.50-7.53 (m, 2H), 7.64 (dd, *J* = 1.6, 8.0 Hz, 4H). The enantiomeric excess was estimated using chiral HPLC (Chiralcel OD, hexanes:^{i}PrOH 98:2, flow rate: 1 mL/min), t_{Rminor} = 17.7 min (*S*) and t_{Rmajor} = 19.0 min (*R*).

5-(*tert*-Butyldiphenylsilyloxy)-pentane-l,2-diol: ^{1}H NMR (400 MHz, $CDCl_3$) δ1.01 (s, 9H), 1.58-1.73 (m, 4H), 2.16-2.19 (br s, 1H), 3.02 (br s, 1H), 3.42-3.47 (m, 1H), 3.63-3.87 (m, 4H), 7.25-7.41 (m, 8H), 7.64-7.66 (m, 2H); $[\alpha]^{19}_{obsd}$ -2.8 (for 90% ee of S), $[\alpha]^{19}_{D}$ -3.0, calcd (c = 1.2, $CHCl_3$); [lit[20]. $[\alpha]_D$ -1.27, c = 1.73, $CHCl_3$ for *S*-diol; lit.[21] $[\alpha]^{20}_{D}$ -1.0, (c = 1.03, CH_2Cl_2) for *S*-diol; lit.[22] $[\alpha]^{19}_{D}$ +1.0, (c = 0.39, $CHCl_3$) for *R*-diol]. The diol was derivatized as its bis(p-bromobenzoate) ester, and the enantiomers were resolved on a Chiralcel OD column (hexanes:*i*-PrOH 96:4, flow rate: 1 mL/min), t_{Rminor} = 7.3 min (*R*) and t_{Rmajor} = 8.8 min (*S*).

IV. References

1. Blaser, H. U., The chiral pool as a source of enantioselective catalysts and auxiliaries. *Chem. Rev.* **1992,** *92* (5), 935-52.
2. Kolb, H. C.; VanNieuwenhze, M. S.; Sharpless, K. B., Catalytic Asymmetric Dihydroxylation. *Chem. Rev. (Washington, D. C.)* **1994,** *94* (8), 2483-547.
3. Corey, E. J.; Xu, F.; Noe, M. C., A Rational Approach to Catalytic Enantioselective Enolate Alkylation Using a Structurally Rigidified and Defined Chiral Quaternary Ammonium Salt under Phase Transfer Conditions. *Journal of the American Chemical Society* **1997,** *119* (50), 12414-12415.
4. Lygo, B.; Andrews, B. I., Asymmetric Phase-Transfer Catalysis Utilizing Chiral Quaternary Ammonium Salts: Asymmetric Alkylation of Glycine Imines. *Acc. Chem. Res.* **2004,** *37* (8), 518-525.
5. O'Donnell, M. J., The Enantioselective Synthesis of α-Amino Acids by Phase-Transfer Catalysis with Achiral Schiff Base Esters. *Acc. Chem. Res.* **2004,** *37* (8), 506-517.
6. Brown, H. C.; Ramachandran, P. V., Versatile α-pinene-based borane reagents for asymmetric syntheses. *J. Organomet. Chem.* **1995,** *500* (1-2), 1-19.
7. Jarvo, E. R.; Miller, S. J., Amino acids and peptides as asymmetric organocatalysts. *Tetrahedron* **2002,** *58* (13), 2481-2495.
8. Helmchen, G.; Pfaltz, A., Phosphinooxazolines-A New Class of Versatile, Modular P,N-Ligands for Asymmetric Catalysis. *Acc. Chem. Res.* **2000,** *33* (6), 336-345.

9. Miller, S. J., In Search of Peptide-Based Catalysts for Asymmetric Organic Synthesis. *Acc. Chem. Res.* **2004,** *37* (8), 601-610.

10. Colby Davie, E. A.; Mennen, S. M.; Xu, Y.; Miller, S. J., Asymmetric Catalysis Mediated by Synthetic Peptides. *Chemical Reviews (Washington, DC, United States)* **2007,** *107* (12), 5759-5812.

11. Dieguez, M.; Pamies, O.; Claver, C., Ligands Derived from Carbohydrates for Asymmetric Catalysis. *Chemical Reviews (Washington, DC, United States)* **2004,** *104* (6), 3189-3215.

12. Dieguez, M.; Pamies, O.; Ruiz, A.; Diaz, Y.; Castillon, S.; Claver, C., Carbohydrate derivative ligands in asymmetric catalysis. *Coord. Chem. Rev.* **2004,** *248* (21-24), 2165-2192.

13. Pamies, O.; Dieguez, M.; Ruiz, A.; Claver, C., Sugar-based P-ligands for asymmetric hydrogenation. *Chim. Oggi* **2004,** *22* (10), 12-14, 16-17.

14. Castillon, S.; Claver, C.; Diaz, Y., C1 and C2-symmetric carbohydrate phosphorus ligands in asymmetric catalysis. *Chemical Society Reviews* **2005,** *34* (8), 702-713.

15. Jarosz, S., Sugars in the synthesis of natural products and their mimics. *Chim. Oggi* **2006,** *24* (3), 58-61.

16. Boysen, M. M. K., Carbohydrates as synthetic tools in organic chemistry. *Chem. - Eur. J.* **2007,** *13* (31), 8648-8659.

17. Dieguez, M.; Claver, C.; Pamies, O., Recent progress in asymmetric catalysis using chiral carbohydrate-based ligands. *Eur. J. Org. Chem.* **2007,** (28), 4621-4634.

18. Benessere, V.; Del Litto, R.; De Roma, A.; Ruffo, F., Carbohydrates as building blocks of privileged ligands. *Coord. Chem. Rev.* **2010,** *254* (5-6), 390-401.

19. Woodward, S.; Dieguez, M.; Pamies, O., Use of sugar-based ligands in selective catalysis: Recent developments. *Coord. Chem. Rev.* **2010,** *254* (17-18), 2007-2030.

20. Lehnert, T.; Ozuduru, G.; Grugel, H.; Albrecht, F.; Telligmann, S. M.; Boysen, M. M. K., More than just sweet. Sugar-derived stereodifferentiating agents for asymmetric synthesis. *Synthesis* **2011,** (17), 2685-2708.

21. Katsuki, T.; Sharpless, K. B., The first practical method for asymmetric epoxidation. *Journal of the American Chemical Society* **1980,** *102* (18), 5974-6.

22. Seebach, D.; Beck, A. K.; Heckel, A., TADDOLs, their derivatives, and TADDOL analogs: versatile chiral auxiliaries. *Angewandte Chemie, International Edition* **2001,** *40* (1), 92-138.

23. Fryzuk, M. D.; Bosnich, B., Asymmetric synthesis. Production of optically active amino acids by catalytic hydrogenation. *J Am Chem Soc* **1977,** *99* (19), 6262-7.

24. Balanta Castillo, A.; Favier, I.; Teuma, E.; Castillon, S.; Godard, C.; Aghmiz, A.; Claver, C.; Gomez, M., An outstanding palladium system containing a C2-symmetrical phosphite ligand for enantioselective allylic substitution processes. *Chem Commun (Camb)* **2008,** (46), 6197-9.

25. Oezueduru, G.; Schubach, T.; Boysen, M. M. K., Enantioselective Cyclopropanation of Indoles: Construction of All-Carbon Quaternary Stereocenters. *Org. Lett.* **2012,** *14* (19), 4990-4993.

26. Benessere, V.; De Roma, A.; Ruffo, F., Carbohydrates as building blocks of privileged ligands for multiphasic asymmetric catalysis. *ChemSusChem* **2008,** *1* (5), 425-430.

27. Shi, Y., Organocatalytic Asymmetric Epoxidation of Olefins by Chiral Ketones. *Acc. Chem. Res.* **2004,** *37* (8), 488-496.

28. Frohn, M.; Shi, Y., Chiral ketone-catalyzed asymmetric epoxidation of olefins. *Synthesis* **2000,** (14), 1979-2000.

29. Wong, O. A.; Shi, Y., Organocatalytic Oxidation. Asymmetric Epoxidation of Olefins Catalyzed by Chiral Ketones and Iminium Salts. *Chemical Reviews (Washington, DC, United States)* **2008,** *108* (9), 3958-3987.

30. Tu, Y.; Wang, Z.-X.; Shi, Y., An Efficient Asymmetric Epoxidation Method for trans-Olefins Mediated by a Fructose-Derived Ketone. *Journal of the American Chemical Society* **1996,** *118* (40), 9806-9807.

31. Wang, Z.-X.; Tu, Y.; Frohn, M.; Zhang, J.-R.; Shi, Y., An Efficient Catalytic Asymmetric Epoxidation Method. *Journal of the American Chemical Society* **1997,** *119* (46), 11224-11235.

32. Dey, S.; Karukurichi, K. R.; Shen, W.; Berkowitz, D. B., Double-Cuvette ISES: In Situ Estimation of Enantioselectivity and Relative Rate for Catalyst Screening. *Journal of the American Chemical Society* **2005,** *127* (24), 8610-8611.

33. Ginotra, S. K.; Friest, J. A.; Berkowitz, D. B., Halocarbocyclization Entry into the Oxabicyclo[4.3.1]decyl Exomethylene-δ-Lactone Cores of Linearifolin and Zaluzanin A: Exploiting Combinatorial Catalysis. *Org. Lett.* **2012,** *14* (4), 968-971.

34. http://www.nobelprize.org/nobel_prizes/chemistry/laureates/2010/.

35. Reetz, M. T., Combinatorial methods in catalysis by metal complexes. *Comprehensive Coordination Chemistry II* **2004,** *9*, 509-548.

36. Pirnot, M. T.; Rankic, D. A.; Martin, D. B. C.; MacMillan, D. W. C., Photoredox Activation for the Direct β-Arylation of Ketones and Aldehydes. *Science (Washington, DC, United States)* **2013,** *339* (6127), 1593-1596.

37. Robbins, D. W.; Hartwig, J. F., A Simple, Multidimensional Approach to High-Throughput Discovery of Catalytic Reactions. *Science (Washington, DC, United States)* **2011,** *333* (6048), 1423-1427.

38. Leung, D.; Kang, S. O.; Anslyn, E. V., Rapid determination of enantiomeric excess: a focus on optical approaches. *Chem Soc Rev* **2012,** *41* (1), 448-79.

39. Collins, K. D.; Gensch, T.; Glorius, F., Contemporary screening approaches to reaction discovery and development. *Nat Chem* **2014,** *6* (10), 859-871.

40. Cabrera-Pardo, J. R.; Chai, D. I.; Liu, S.; Mrksich, M.; Kozmin, S. A., Label-assisted mass spectrometry for the acceleration of reaction discovery and optimization. *Nat Chem* **2013,** *5* (5), 423-7.

41. Vicennati, P.; Bensel, N.; Wagner, A.; Creminon, C.; Taran, F., Sandwich immunoassay as a high-throughput screening method for cross-coupling reactions. *Angewandte Chemie, International Edition* **2005,** *44* (42), 6863-6866.

42. Quinton, J.; Kolodych, S.; Chaumonet, M.; Bevilacqua, V.; Nevers, M.-C.; Volland, H.; Gabillet, S.; Thuéry, P.; Créminon, C.; Taran, F., Reaction Discovery by Using a Sandwich Immunoassay. *Angewandte Chemie International Edition* **2012,** *51* (25), 6144-6148.

43. Kolodych, S.; Rasolofonjatovo, E.; Chaumontet, M.; Nevers, M.-C.; Créminon, C.; Taran, F., Discovery of Chemoselective and Biocompatible Reactions Using a High-Throughput Immunoassay Screening. *Angewandte Chemie International Edition* **2013,** *52* (46), 12056-12060.

44. Berkowitz, D. B.; Bose, M.; Choi, S., In situ enzymatic screening (ISES): a tool for catalyst discovery and reaction development. *Angewandte Chemie, International Edition* **2002,** *41* (9), 1603-1607.

45. Berkowitz, D. B.; Maiti, G., Following an ISES Lead: The First Examples of Asymmetric Ni(0)-Mediated Allylic Amination. *Org. Lett.* **2004,** *6* (16), 2661-2664.

46. Friest, J. A.; Broussy, S.; Chung, W. J.; Berkowitz, D. B., Combinatorial Catalysis Employing a Visible Enzymatic Beacon in Real Time: Synthetically Versatile (Pseudo)Halometalation/Carbocyclizations. *Angewandte Chemie, International Edition* **2011,** *50* (38), 8895-8899, S8895/1-S8895/97.

47. Dey, S.; Powell, D. R.; Hu, C.; Berkowitz, D. B., Cassette in situ enzymatic screening identifies complementary chiral scaffolds for hydrolytic kinetic resolution across a range of epoxides. *Angewandte Chemie, International Edition* **2007,** *46* (37), 7010-7014.

48. Mio, S.; Kumagawa, Y.; Sugai, S., Synthetic studies on (+)-hydantocidin. III. A new synthetic method for construction of the spiro-hydantoin ring at the anomeric position of D-ribofuranose. *Tetrahedron* **1991,** *47* (12-13), 2133-44.

49. Shing, T. K. M.; Tang, Y., A new approach to pseudo-sugars from (-)-quinic acid: facile syntheses of pseudo-β-D-mannopyranose and pseudo-β-D-fructopyranose. *J. Chem. Soc., Chem. Commun.* **1990,** (10), 748-9.

50. McComsey, D. F.; Maryanoff, B. E., Improved Synthesis of Pseudo-β-D-fructopyranose, a Carbocyclic Monosaccharide from (-)-Quinic Acid. *J. Org. Chem.* **1994,** *59* (9), 2652-4.

51. Shing, T. K. M.; Tang, Y., (-)-Quinic acid in organic synthesis. 2. Facile syntheses of pseudo-β-D-mannopyranose and pseudo-β-D-fructopyranose. *Tetrahedron* **1991,** *47* (26), 4571-8.

52. Snider, B. B.; Lin, H., An improved procedure for the conversion of alkenes and glycals to 1,2-diazides using Mn(OAc)3·2H2O in acetonitrile containing trifluoroacetic acid. *Synth. Commun.* **1998,** *28* (10), 1913-1922.

53. Chen, C. S.; Fujimoto, Y.; Girdaukas, G.; Sih, C. J., Quantitative analyses of biochemical kinetic resolutions of enantiomers. *Journal of the American Chemical Society* **1982,** *104* (25), 7294-7299.

54. Canali, L.; Sherrington, D. C., Utilization of homogeneous and supported chiral metal(salen) complexes in asymmetric catalysis. *Chemical Society Reviews* **1999,** *28* (2), 85-93.

55. Larrow, J. F.; Jacobsen, E. N., Asymmetric processes catalyzed by chiral (salen)metal complexes. *Topics in Organometallic Chemistry* **2004,** *6* (Organometallics in Process Chemistry), 123-152.

56. When E-vaule is over 50, either the remaining starting material or the product has a ee over 90%. Therefore, we consider it to be synthetically useful. .

57. Reetz, M. T.; Bocola, M.; Wang, L. W.; Sanchis, J.; Cronin, A.; Arand, M.; Zou, J.; Archelas, A.; Bottalla, A. L.; Naworyta, A.; Mowbray, S. L., Directed evolution of an enantioselective epoxide hydrolase: uncovering the source of enantioselectivity at each evolutionary stage. *J Am Chem Soc* **2009,** *131* (21), 7334-43.

58. Nielsen, L. P.; Stevenson, C. P.; Blackmond, D. G.; Jacobsen, E. N., Mechanistic investigation leads to a synthetic improvement in the hydrolytic kinetic resolution of terminal epoxides. *J Am Chem Soc* **2004,** *126* (5), 1360-2.

59. Kim, H. J.; Kim, W.; Lough, A. J.; Kim, B. M.; Chin, J., A cobalt(III)-salen complex with an axial substituent in the diamine backbone: stereoselective recognition of amino alcohols. *J Am Chem Soc* **2005,** *127* (48), 16776-7.

60. Ford, D. D.; Nielsen, L. P.; Zuend, S. J.; Musgrave, C. B.; Jacobsen, E. N., Mechanistic basis for high stereoselectivity and broad substrate scope in the (salen)Co(III)-catalyzed hydrolytic kinetic resolution. *J Am Chem Soc* **2013,** *135* (41), 15595-608.

V. NMR Spectra

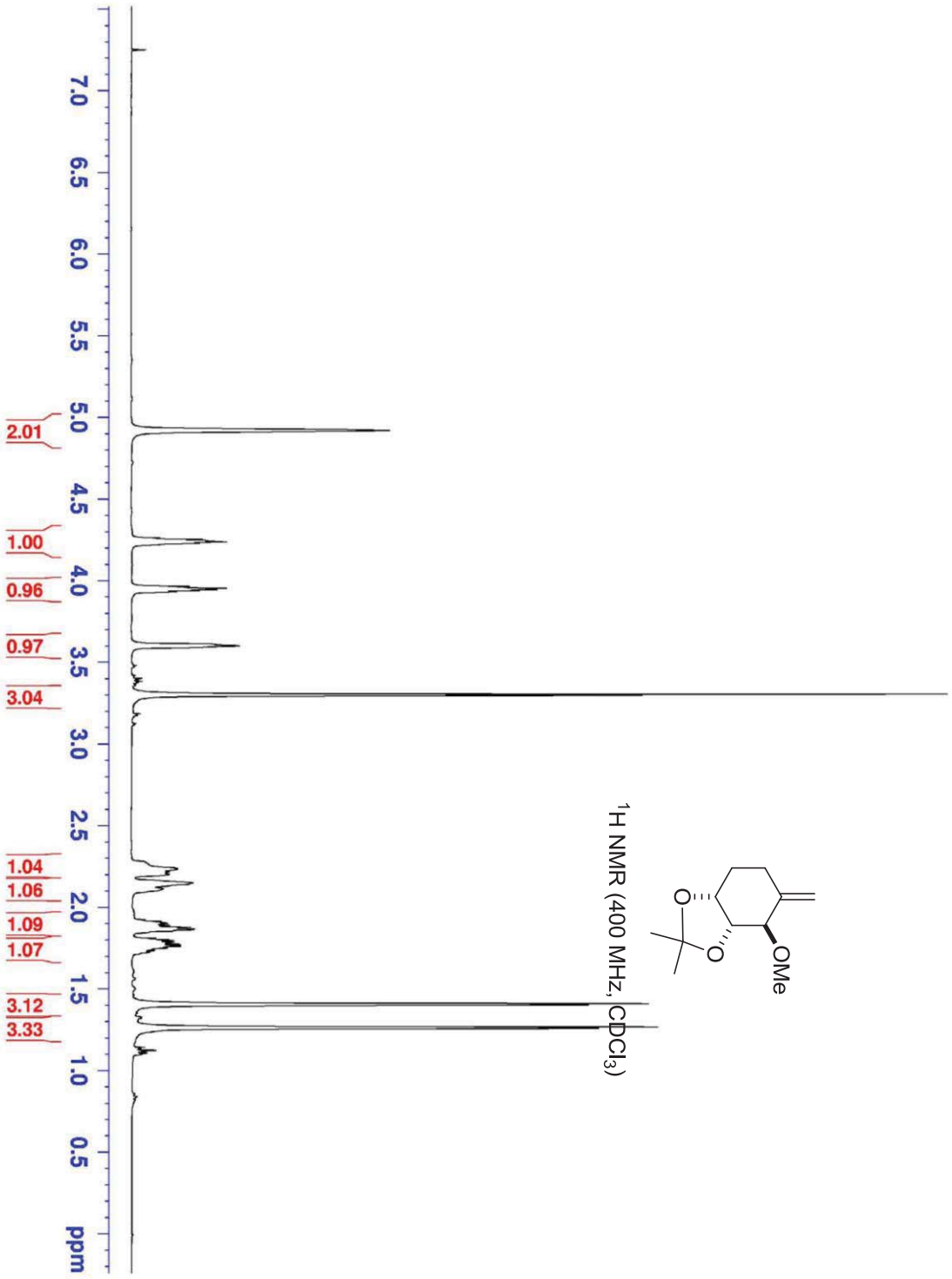

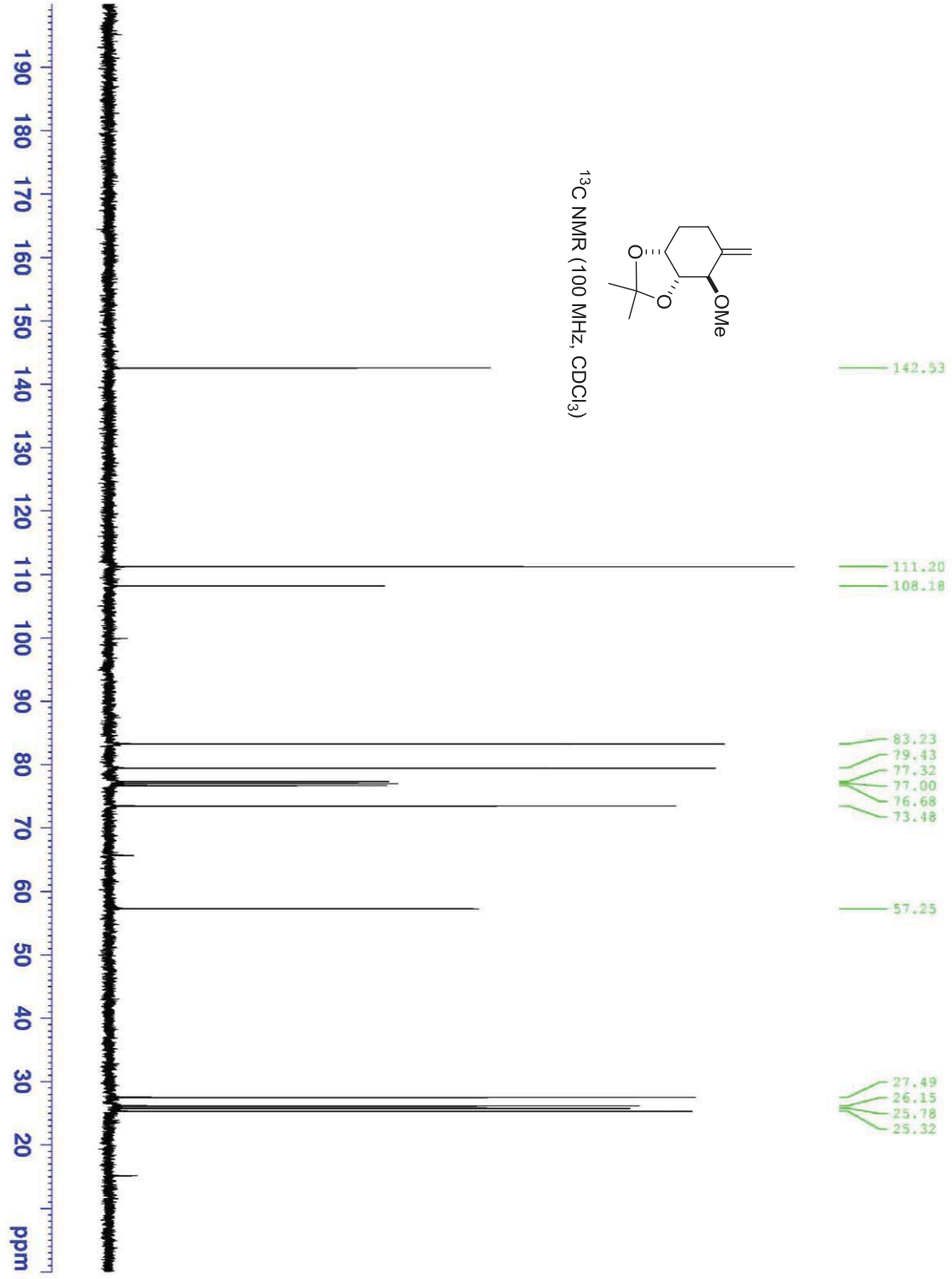
^{13}C NMR (100 MHz, $CDCl_3$)
OMe
142.53
111.20
108.18
83.23
79.43
77.32
77.00
76.68
73.48
57.25
27.49
26.15
25.78
25.32
190 180 170 160 150 140 130 120 110 100 90 80 70 60 50 40 30 20 ppm

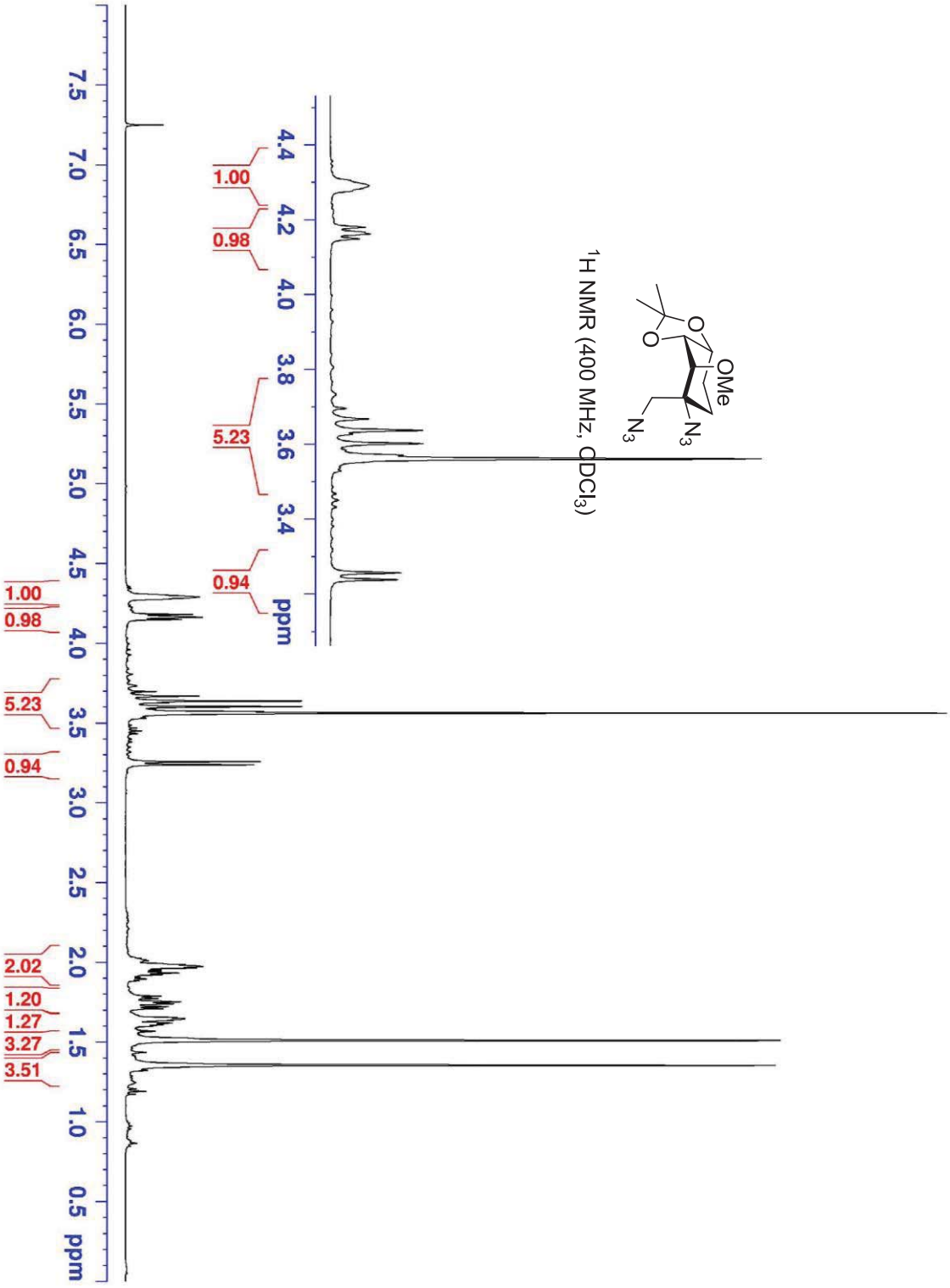
^{1}H NMR (400 MHz, CDCl$_3$)
OMe
N$_3$
N$_3$
O
O
1.00
0.98
5.23
0.94
2.02
1.20
1.27
3.27
3.51
ppm

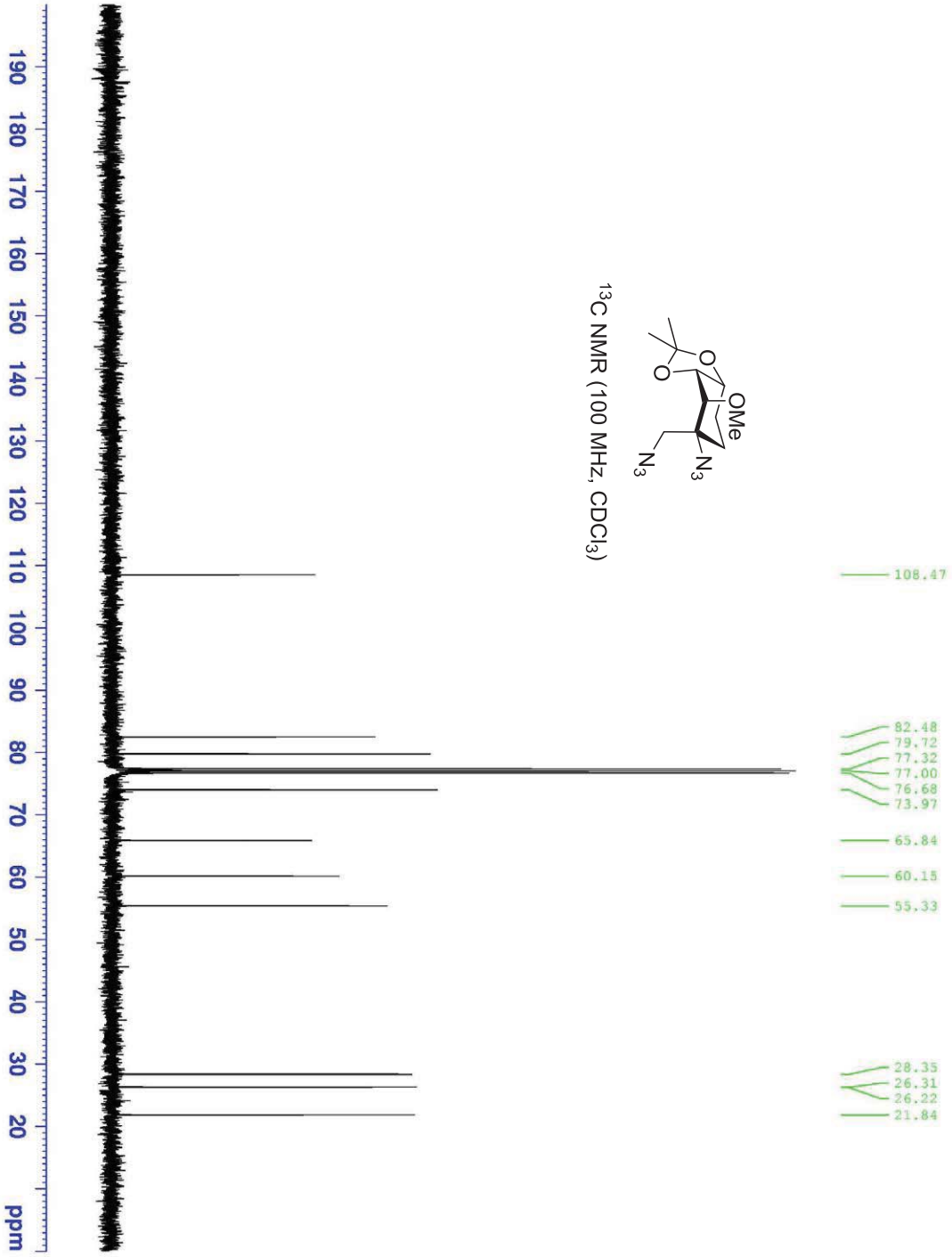
^{13}C NMR (100 MHz, $CDCl_3$)
OMe
N_3
N_3
O
O
108.47
82.48
79.72
77.32
77.00
76.68
73.97
65.84
60.15
55.33
28.35
26.31
26.22
21.84
190 180 170 160 150 140 130 120 110 100 90 80 70 60 50 40 30 20 ppm

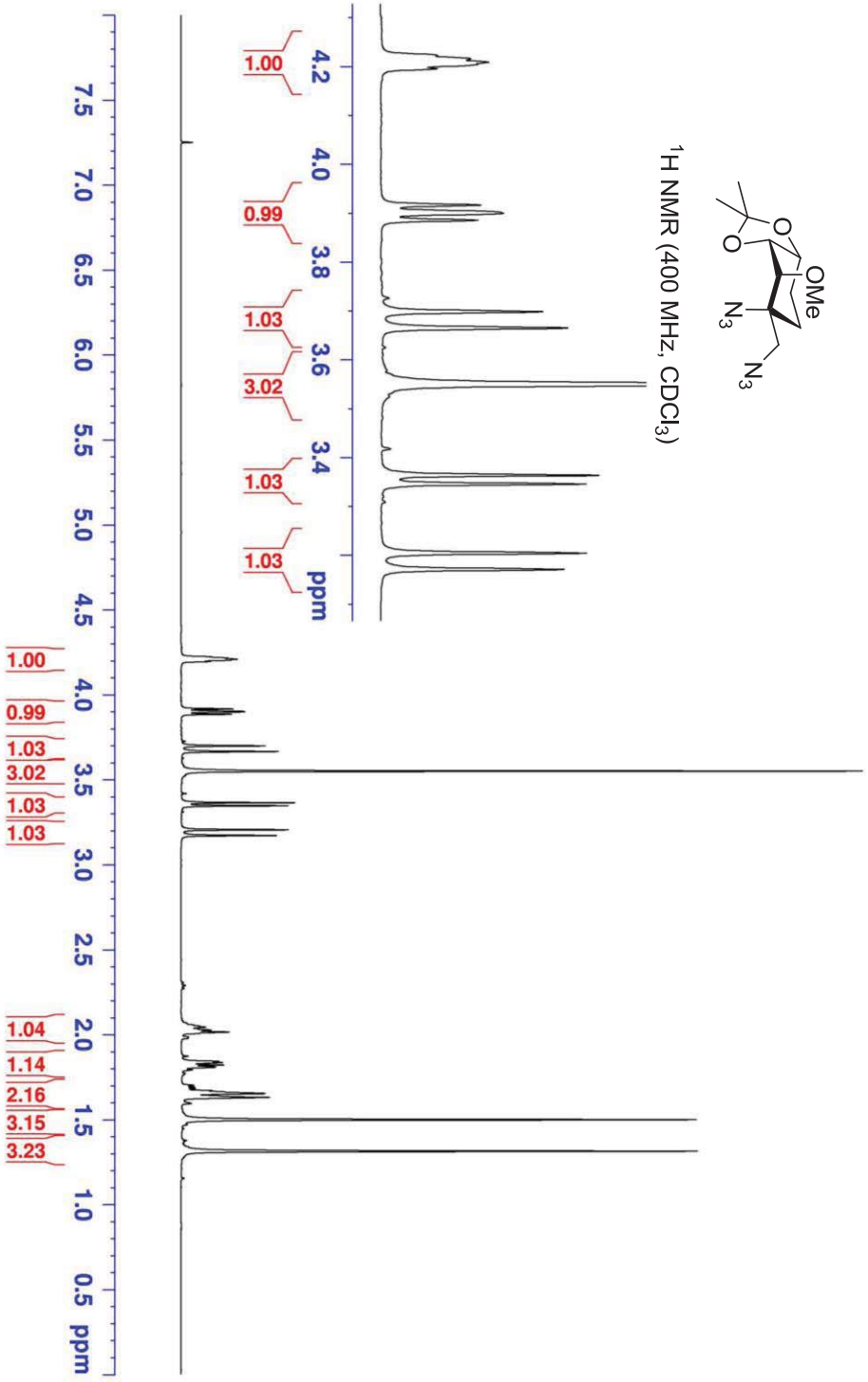
^{1}H NMR (400 MHz, $CDCl_3$)
OMe
N_3
N_3
1.00
0.99
1.03
3.02
1.03
1.03
1.04
1.14
2.16
3.15
3.23
ppm

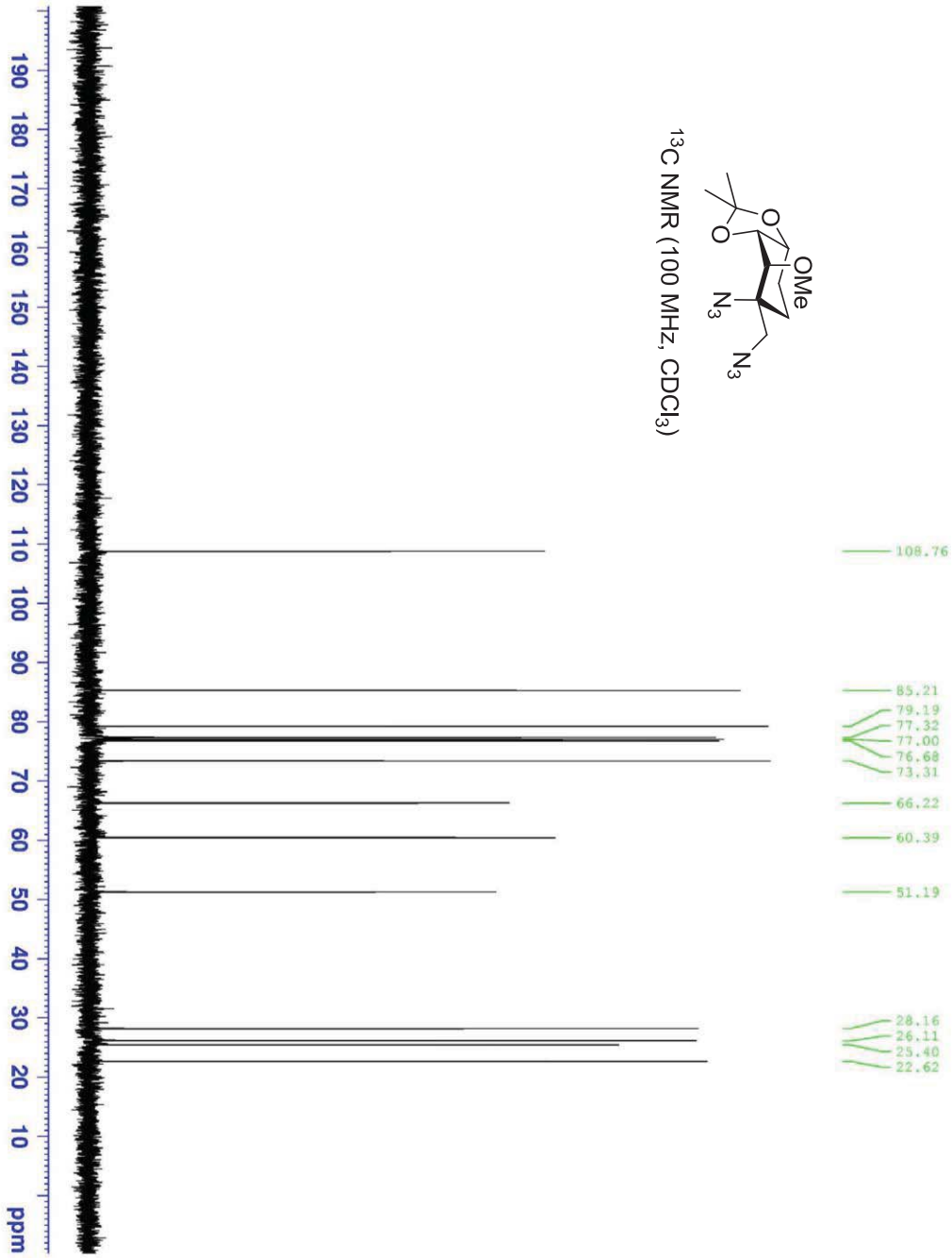
^{13}C NMR (100 MHz, CDCl$_3$)
OMe
N$_3$
N$_3$
108.76
85.21
79.19
77.32
77.00
76.68
73.31
66.22
60.39
51.19
28.16
26.11
25.40
22.62
190 180 170 160 150 140 130 120 110 100 90 80 70 60 50 40 30 20 10 ppm

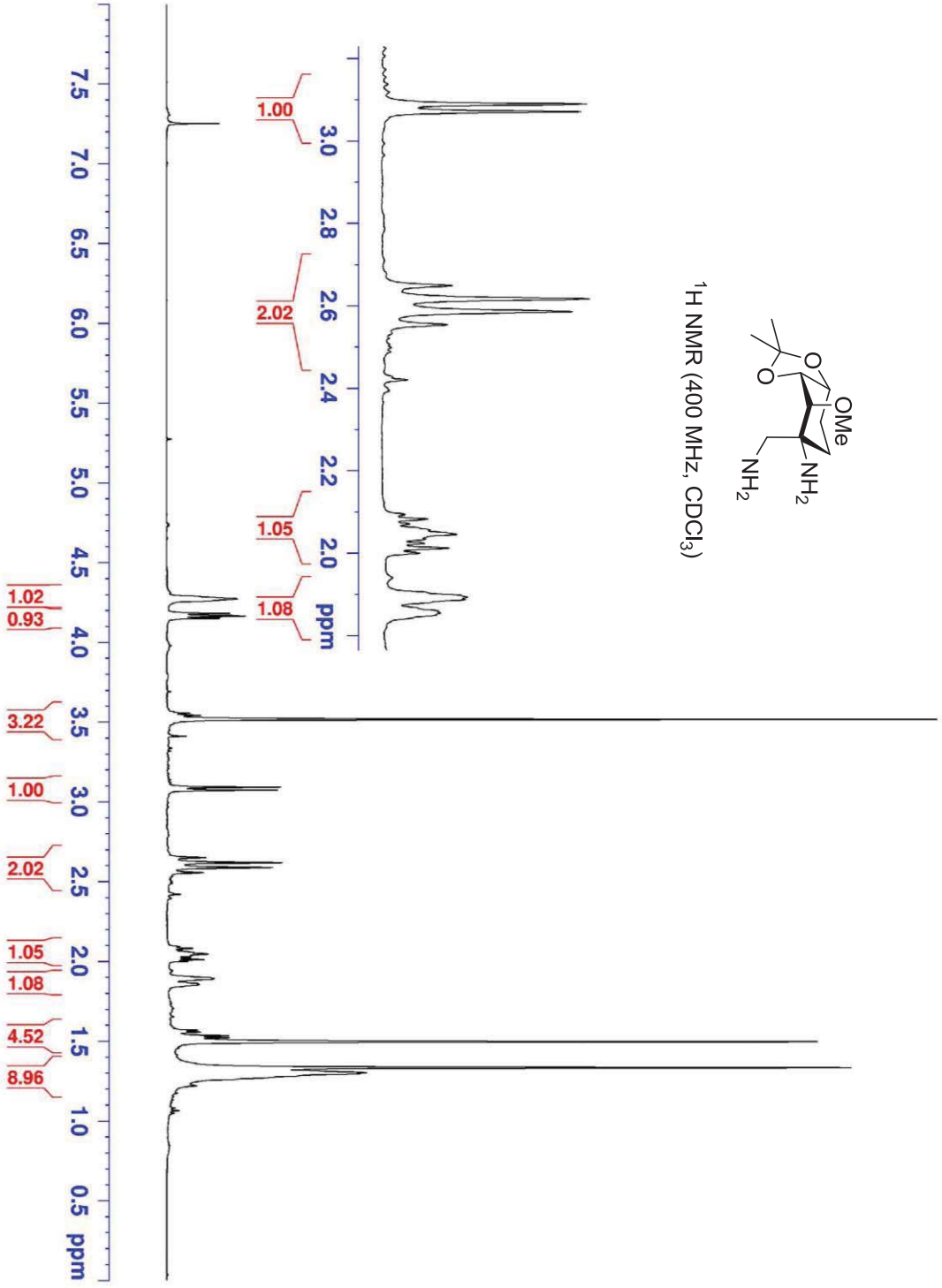
^{1}H NMR (400 MHz, $CDCl_3$)
OMe
NH_2
NH_2
O
O
1.00
2.02
1.05
1.08
1.02
0.93
3.22
1.00
2.02
1.05
1.08
4.52
8.96
ppm

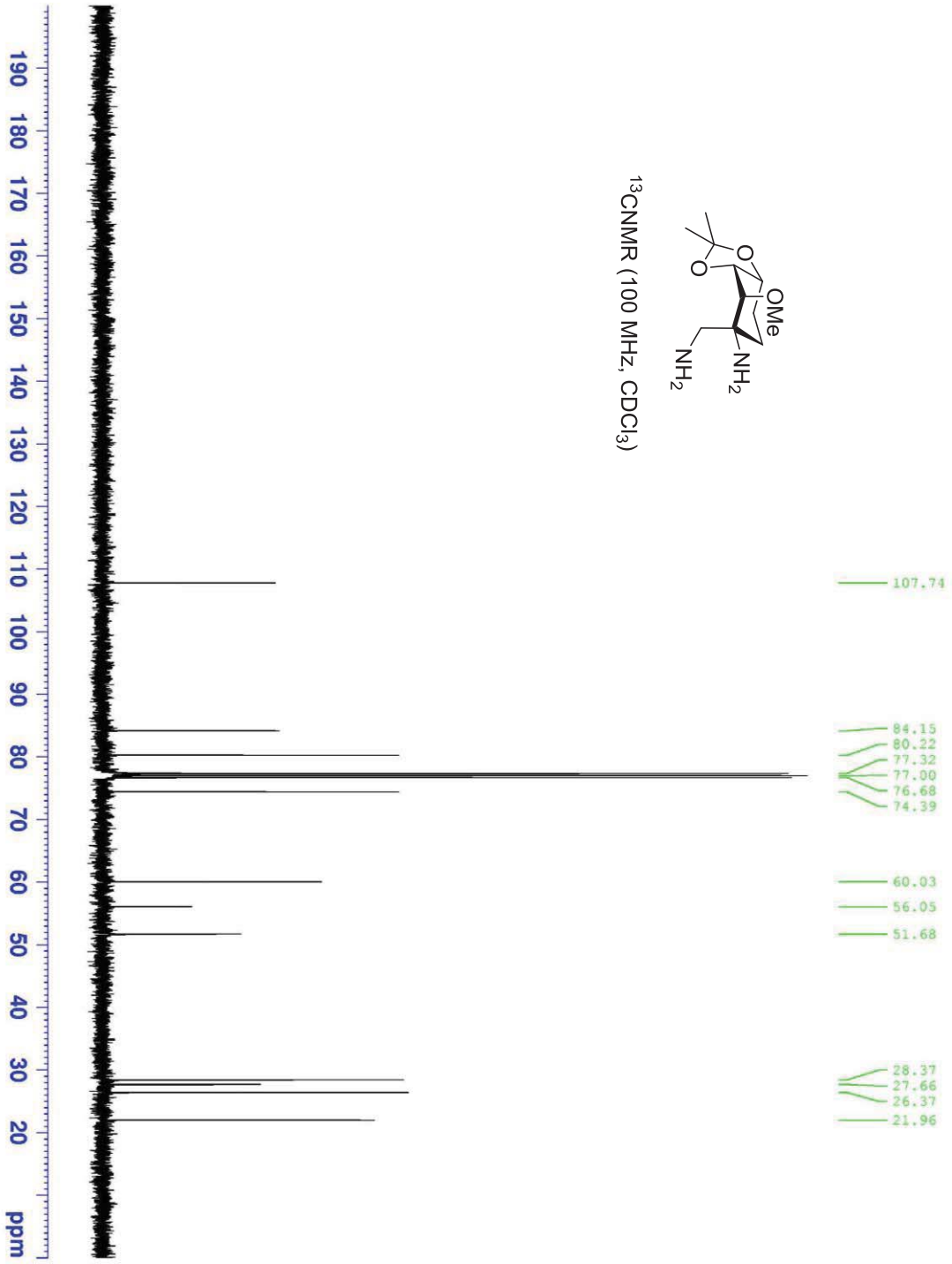
^{13}CNMR (100 MHz, $CDCl_3$)
OMe
NH_2
NH_2
107.74
84.15
80.22
77.32
77.00
76.68
74.39
60.03
56.05
51.68
28.37
27.66
26.37
21.96
190 180 170 160 150 140 130 120 110 100 90 80 70 60 50 40 30 20 ppm

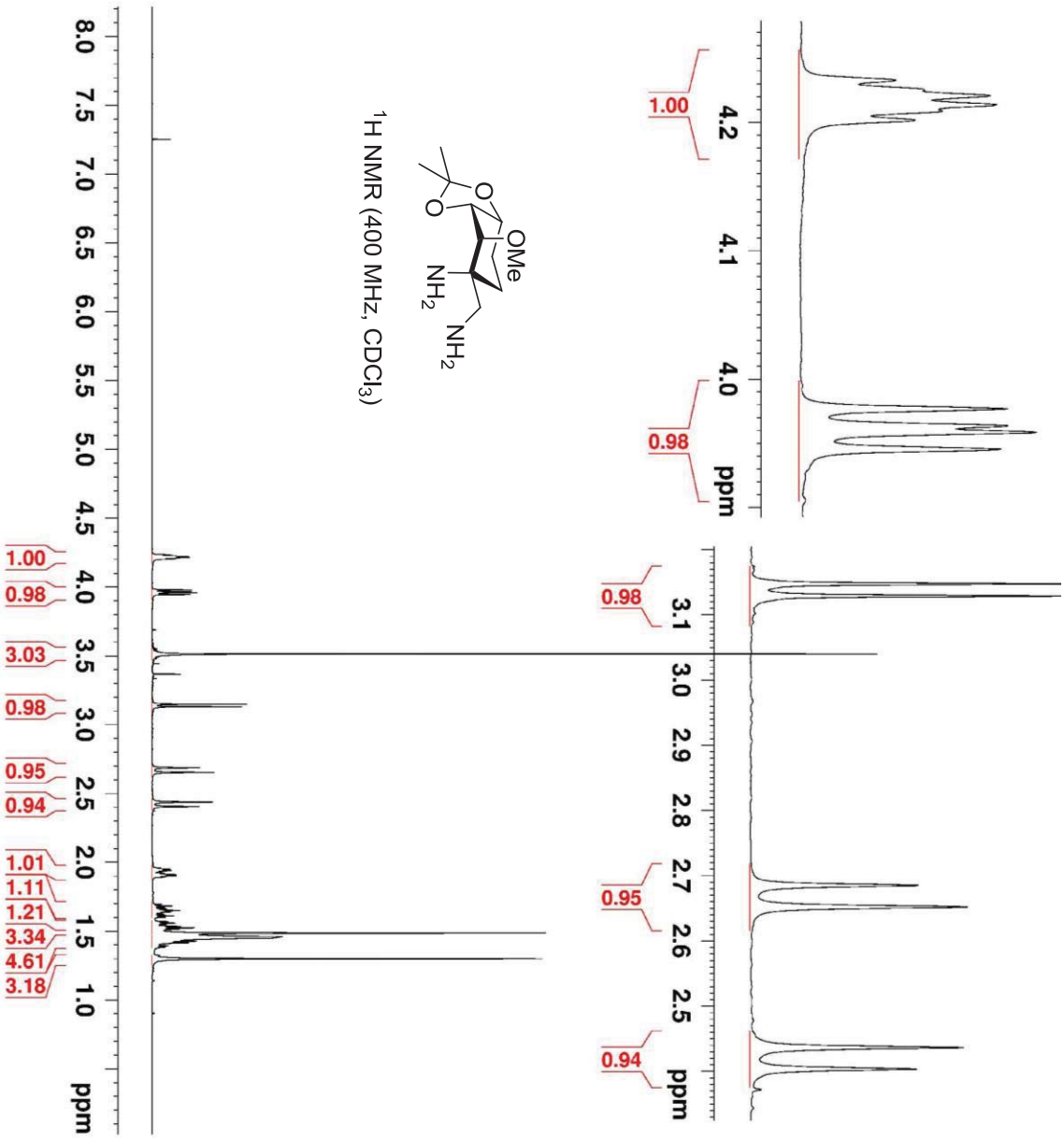
OMe
O
O
NH2
NH2
1H NMR (400 MHz, CDCl3)
1.00
0.98
3.03
0.98
0.95
0.94
1.01
1.11
1.21
3.34
4.61
3.18
8.0 7.5 7.0 6.5 6.0 5.5 5.0 4.5 4.0 3.5 3.0 2.5 2.0 1.5 1.0 ppm
1.00
0.98
4.2 4.1 4.0 ppm
0.98
0.95
0.94
3.1 3.0 2.9 2.8 2.7 2.6 2.5 ppm

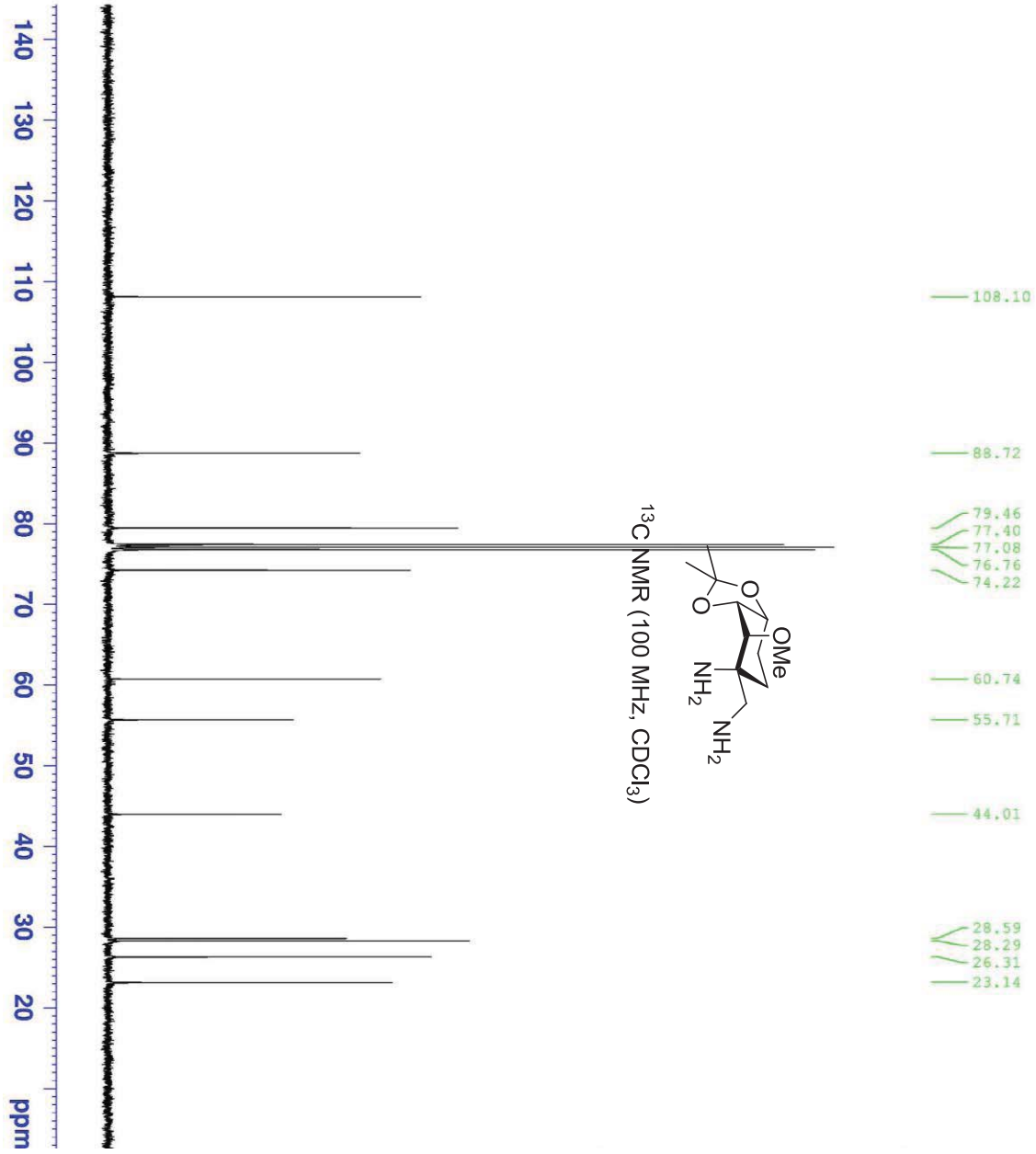
^{13}C NMR (100 MHz, $CDCl_3$)
OMe
NH_2
NH_2
108.10
88.72
79.46
77.40
77.08
76.76
74.22
60.74
55.71
44.01
28.59
28.29
26.31
23.14
140
130
120
110
100
90
80
70
60
50
40
30
20
ppm

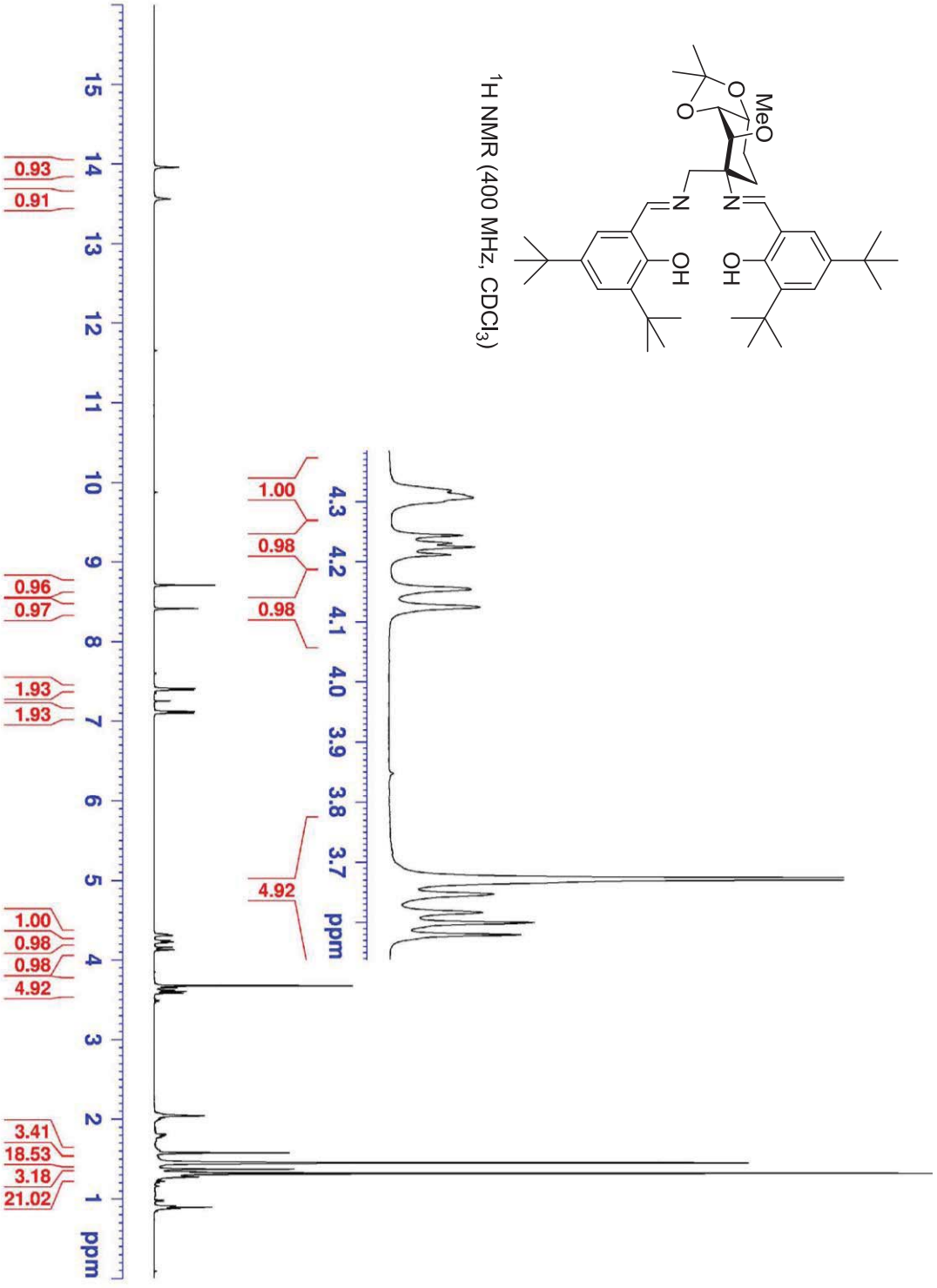
MeO
O
O
N
N
OH
OH
^{1}H NMR (400 MHz, CDCl$_3$)
0.93
0.91
0.96
0.97
1.93
1.93
1.00
0.98
0.98
4.92
3.41
18.53
3.18
21.02
ppm
1.00
0.98
0.98
4.92
ppm

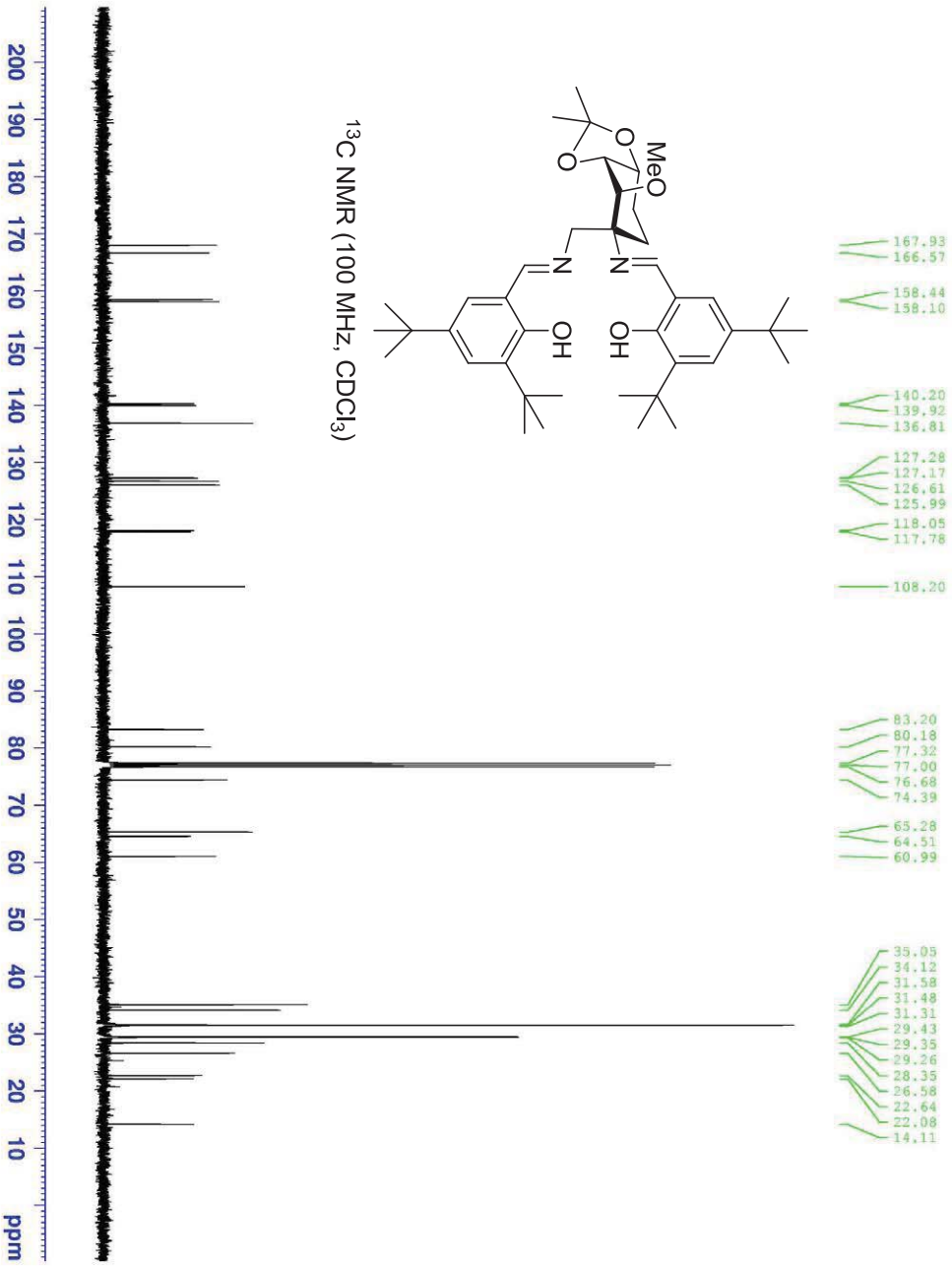
^{13}C NMR (100 MHz, $CDCl_3$)
MeO
O
O
N
N
OH
OH
167.93
166.57
158.44
158.10
140.20
139.92
136.81
127.28
127.17
126.61
125.99
118.05
117.78
108.20
83.20
80.18
77.32
77.00
76.68
74.39
65.28
64.51
60.99
35.05
34.12
31.58
31.48
31.31
29.43
29.35
29.26
28.35
26.58
22.64
22.08
14.11
200 190 180 170 160 150 140 130 120 110 100 90 80 70 60 50 40 30 20 10 ppm

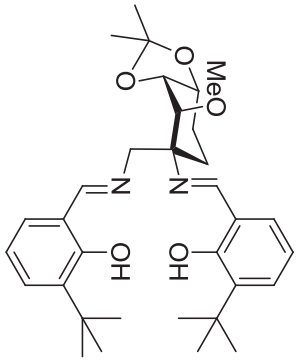

^{1}H NMR (400 MHz, $CDCl_3$)

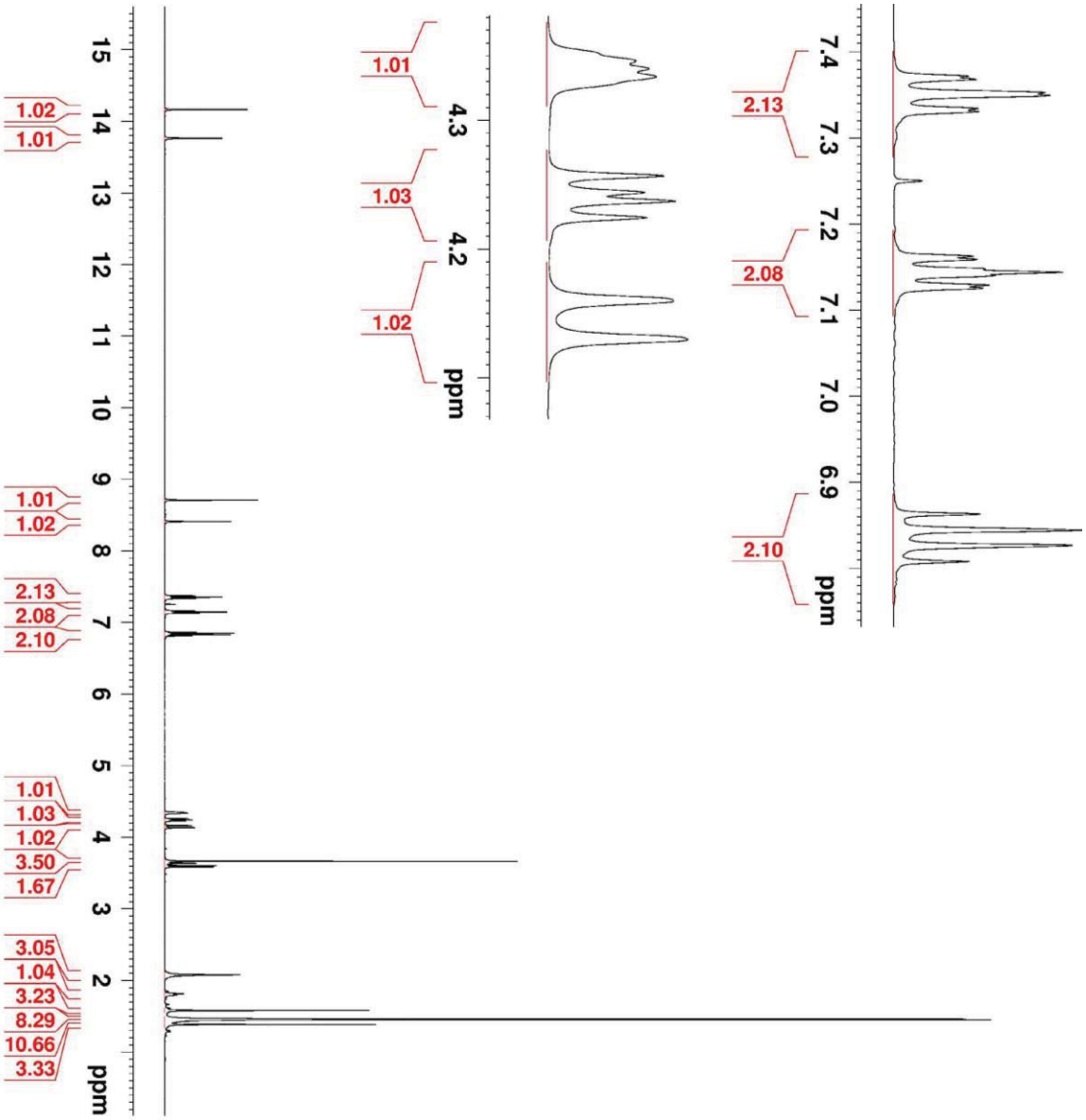

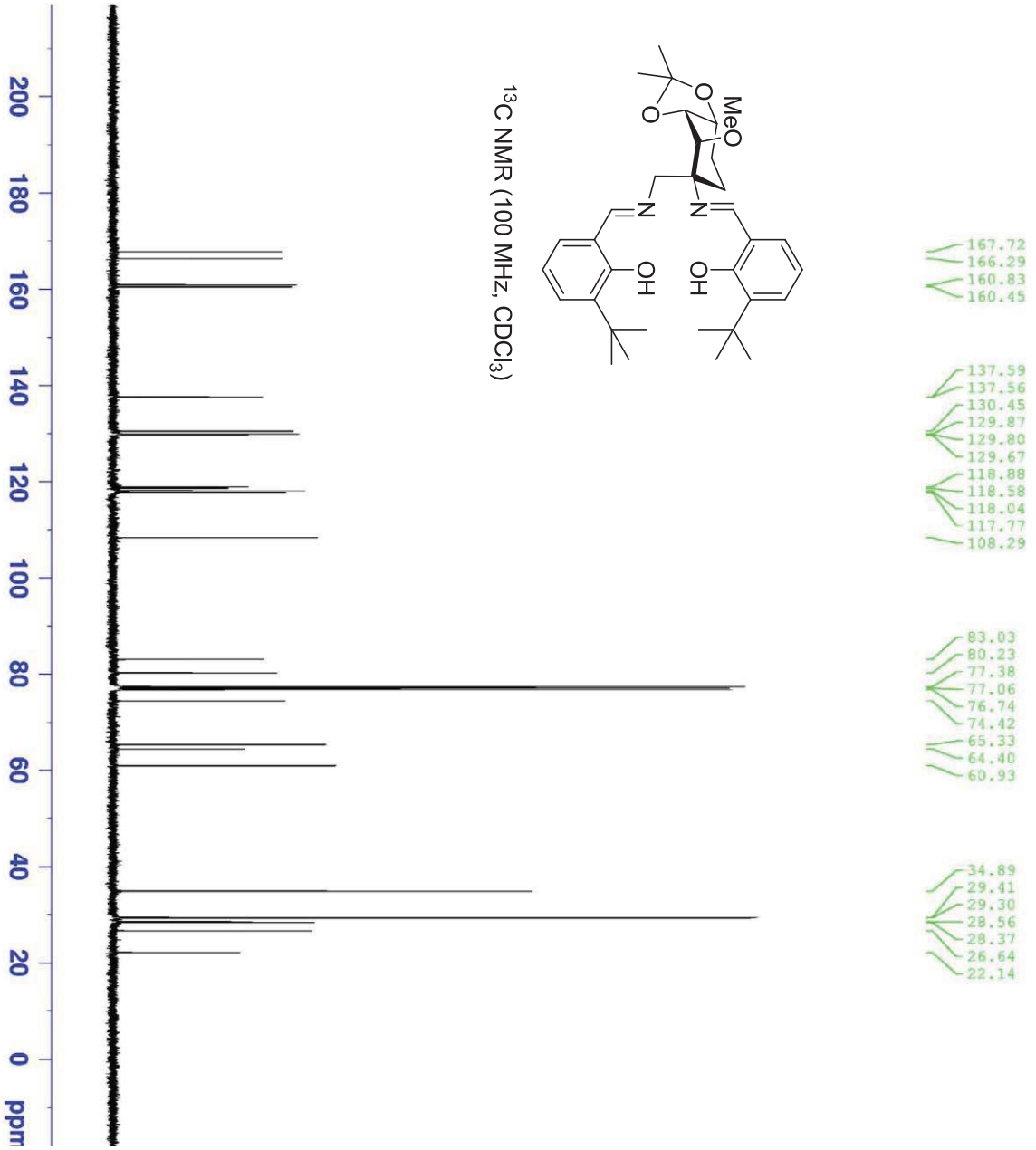
^{13}C NMR (100 MHz, CDCl$_3$)
MeO
O
O
N
N
OH
OH
167.72
166.29
160.83
160.45
137.59
137.56
130.45
129.87
129.80
129.67
118.88
118.58
118.04
117.77
108.29
83.03
80.23
77.38
77.06
76.74
74.42
65.33
64.40
60.93
34.89
29.41
29.30
28.56
28.37
26.64
22.14
200
180
160
140
120
100
80
60
40
20
0
ppm

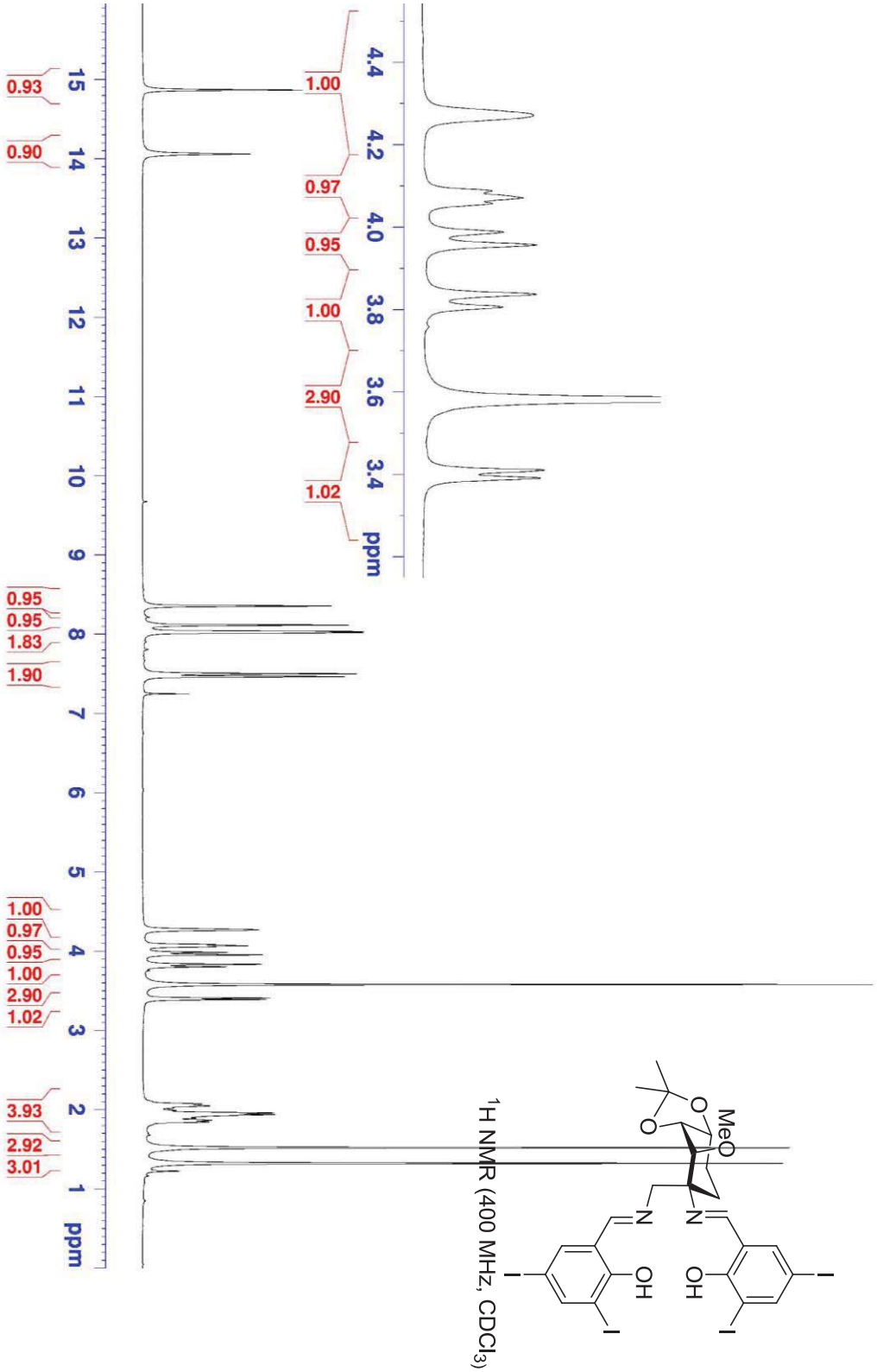
MeO
OH
OH
I
I
I
I
N
N
O
O
^{1}H NMR (400 MHz, CDCl$_3$)
ppm
0.93
0.90
0.95
0.95
1.83
1.90
1.00
0.97
0.95
1.00
2.90
1.02
3.93
2.92
3.01
1.00
0.97
0.95
1.00
2.90
1.02

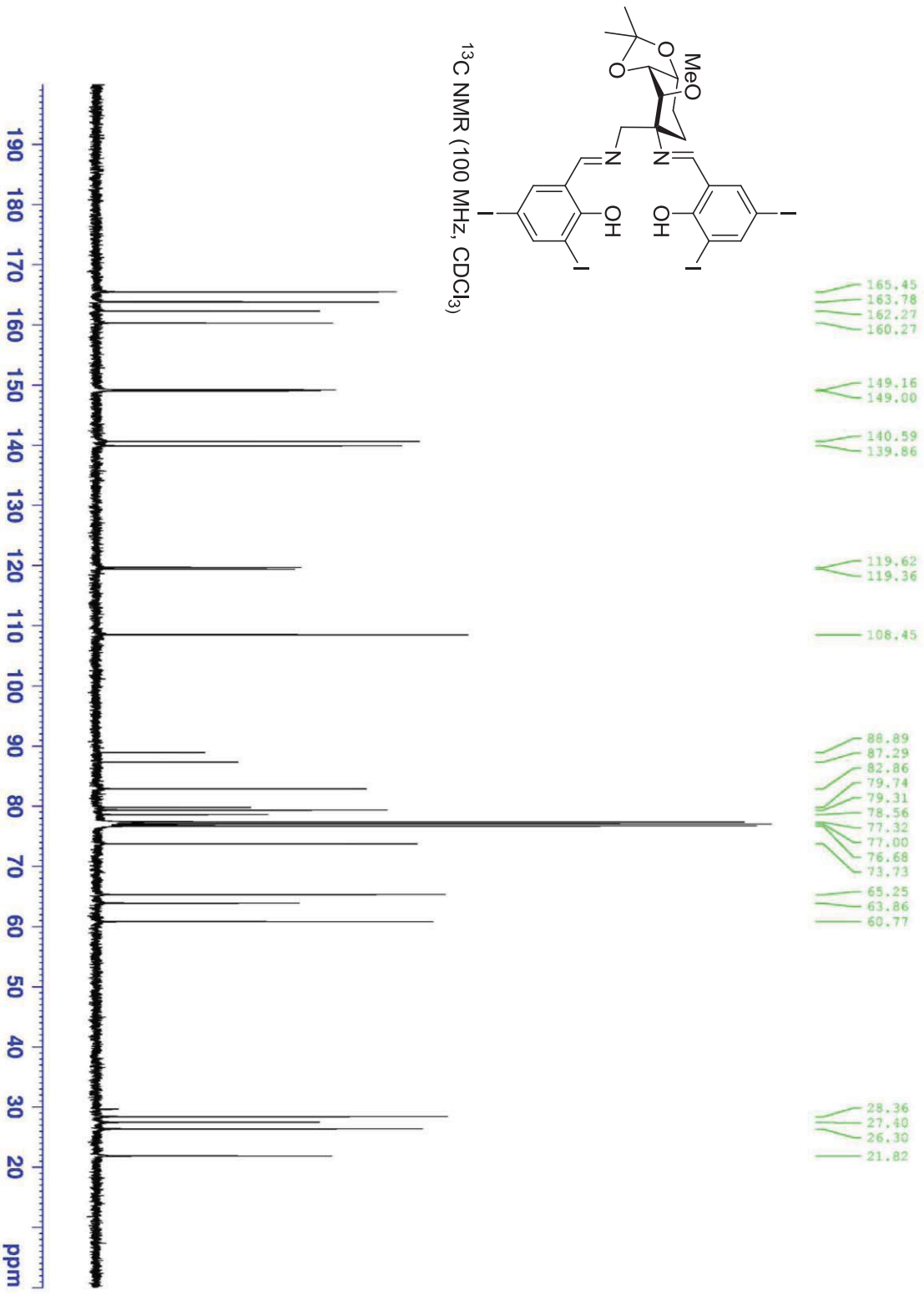
^{13}C NMR (100 MHz, $CDCl_3$)
MeO
O
O
N
N
OH
OH
I
I
I
I
165.45
163.78
162.27
160.27
149.16
149.00
140.59
139.86
119.62
119.36
108.45
88.89
87.29
82.86
79.74
79.31
78.56
77.32
77.00
76.68
73.73
65.25
63.86
60.77
28.36
27.40
26.30
21.82
190 180 170 160 150 140 130 120 110 100 90 80 70 60 50 40 30 20 ppm

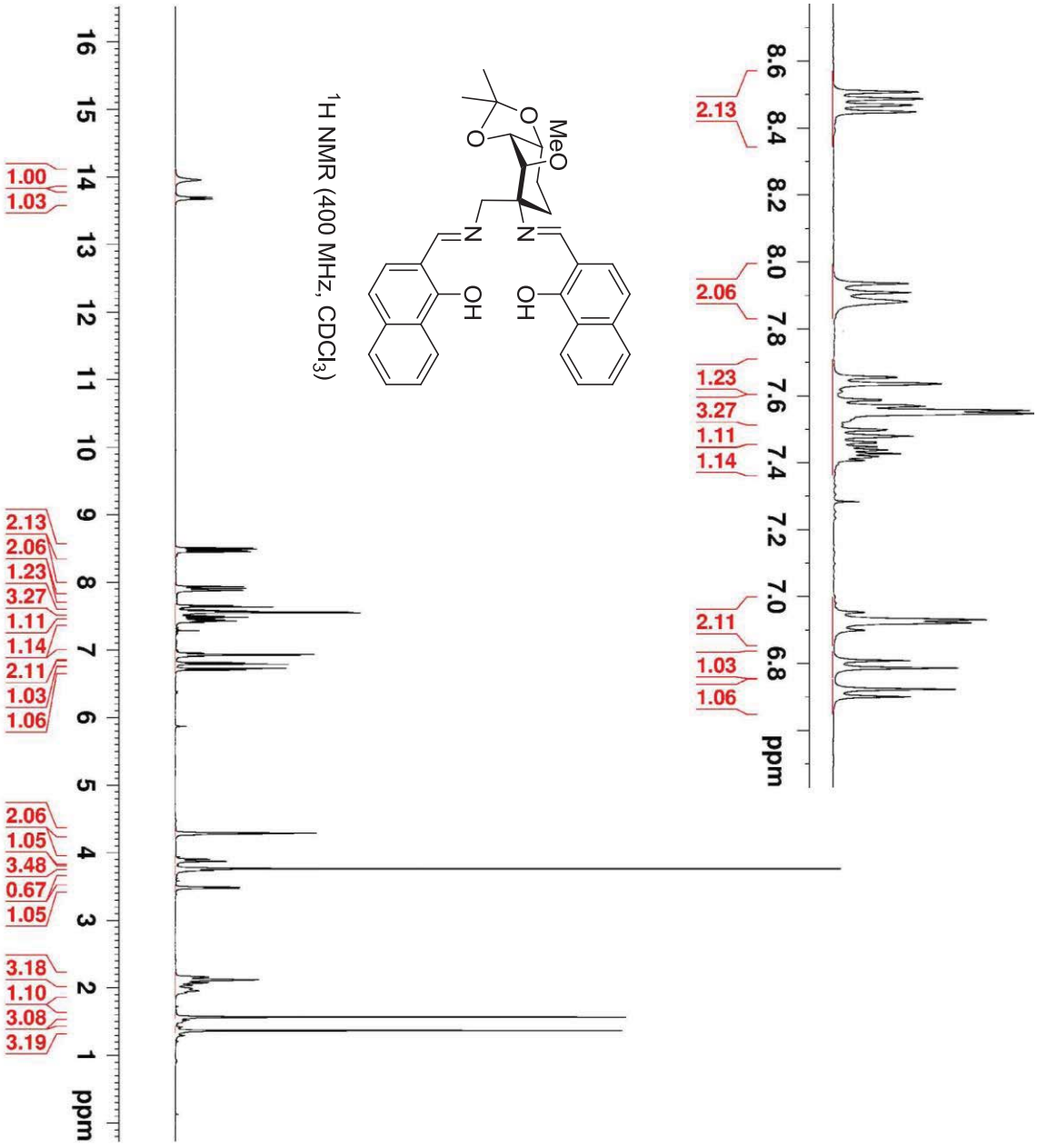
^{1}H NMR (400 MHz, $CDCl_3$)
MeO
O
O
O
N
N
OH
OH
ppm
1.00
1.03
2.13
2.06
1.23
3.27
1.11
1.14
2.11
1.03
1.06
2.06
1.05
3.48
0.67
1.05
3.18
1.10
3.08
3.19

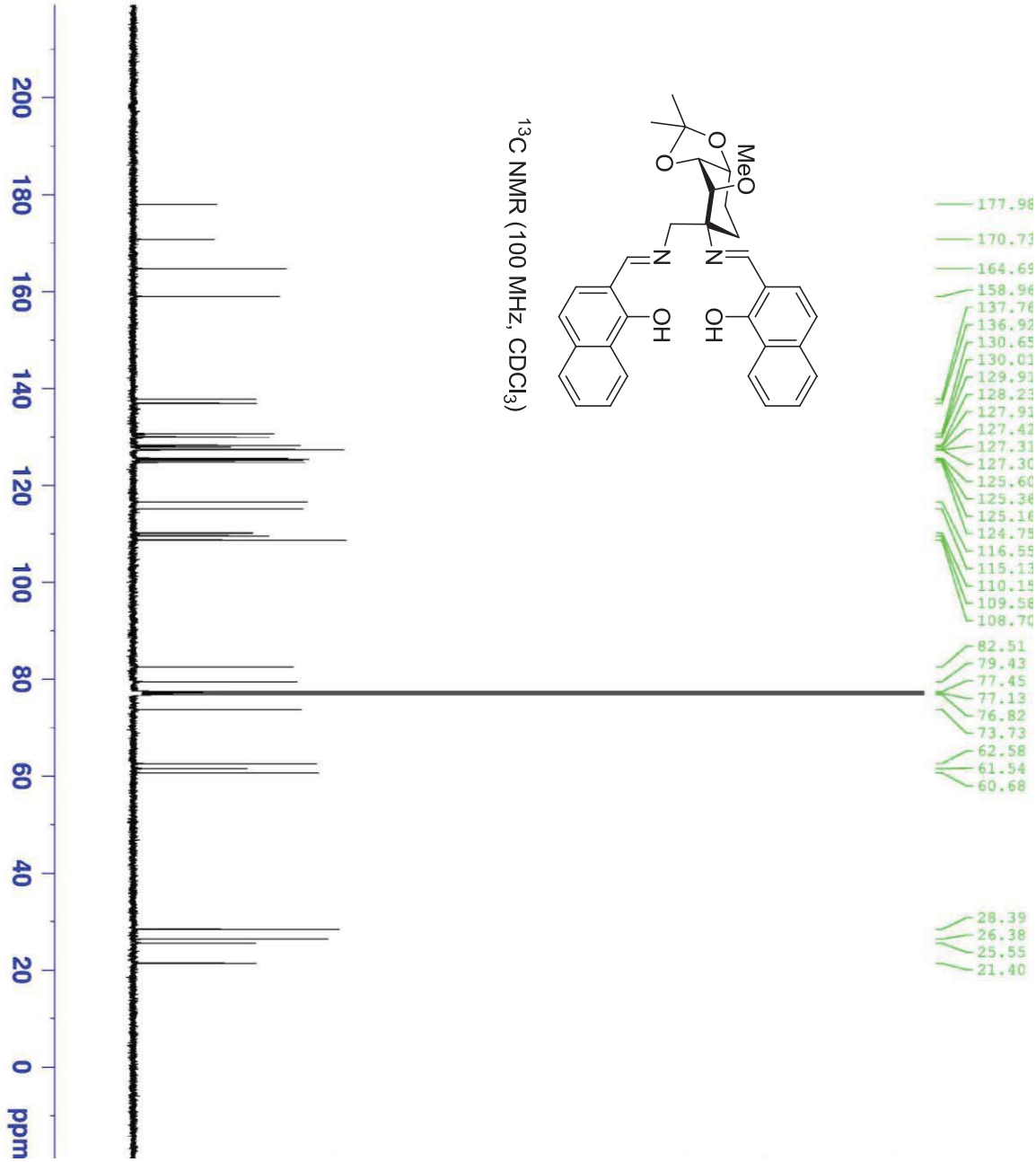
^{13}C NMR (100 MHz, $CDCl_3$)
MeO
O
O
N
N
OH
OH
177.98
170.73
164.69
158.96
137.76
136.92
130.65
130.01
129.91
128.23
127.91
127.42
127.31
127.30
125.60
125.36
125.16
124.75
116.55
115.13
110.15
109.58
108.70
82.51
79.43
77.45
77.13
76.82
73.73
62.58
61.54
60.68
28.39
26.38
25.55
21.40
200
180
160
140
120
100
80
60
40
20
0
ppm

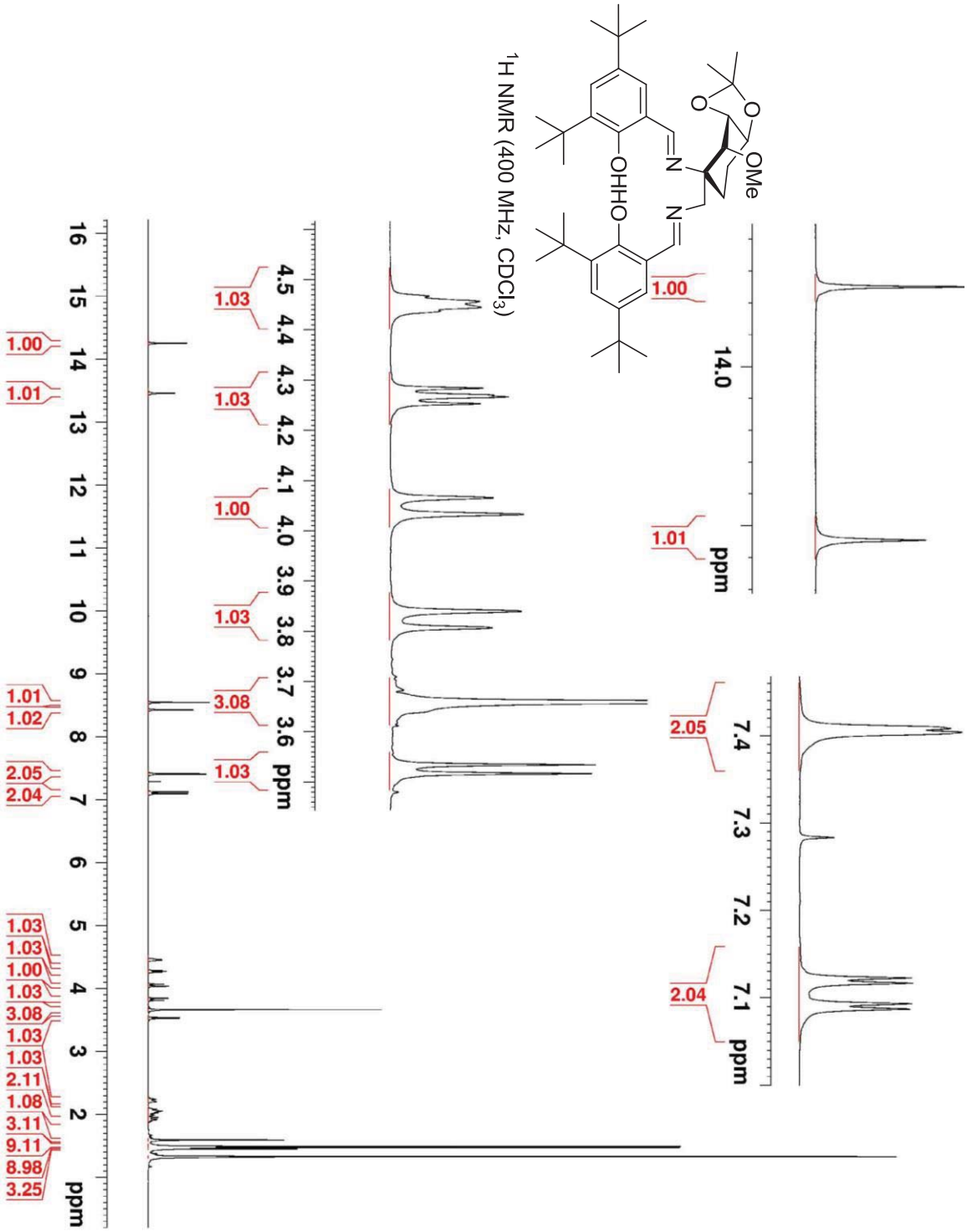
^{1}H NMR (400 MHz, CDCl$_3$)
OMe
OHHO
N
N
1.00
1.01
2.05
2.04
ppm

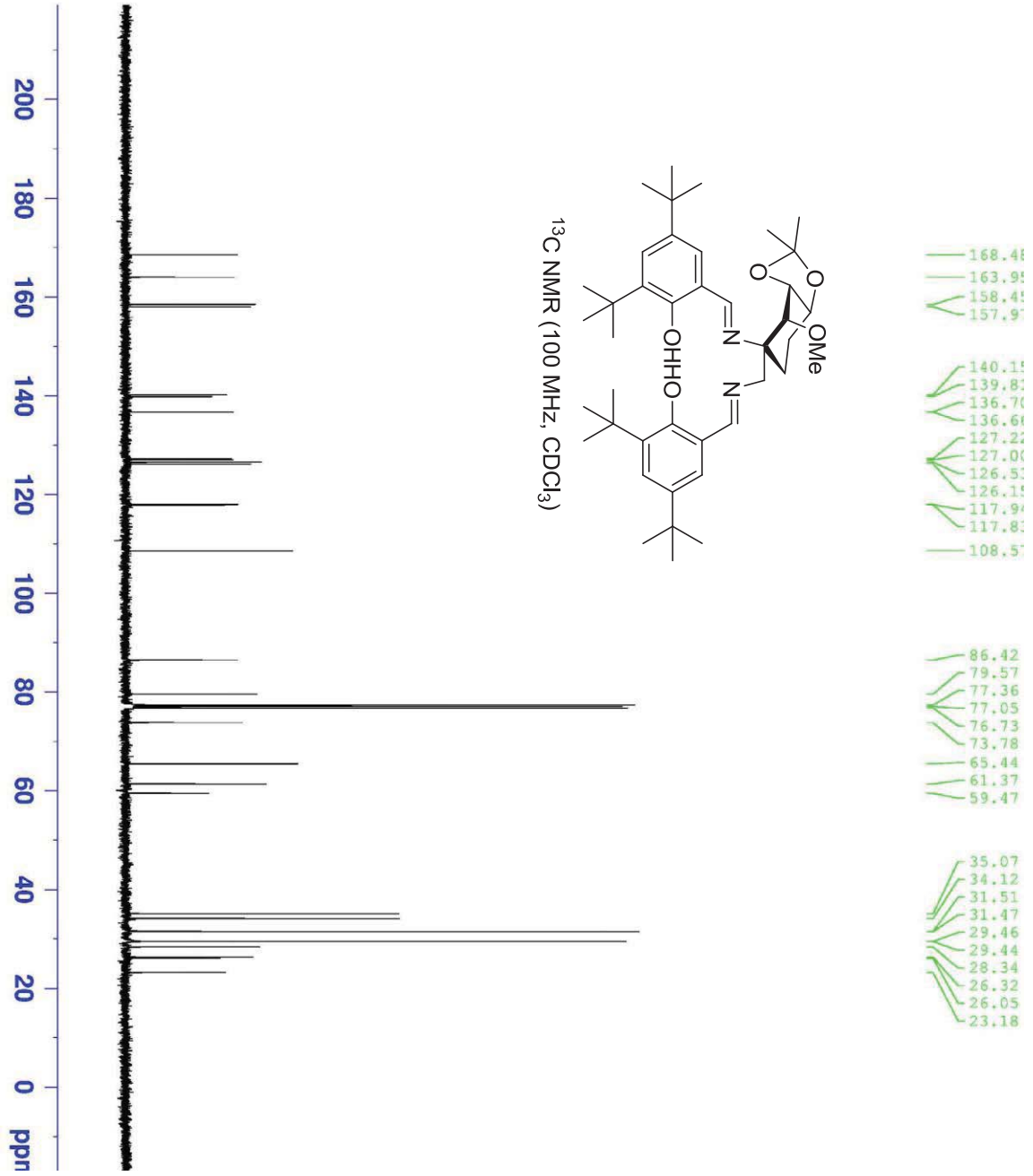
^{13}C NMR (100 MHz, $CDCl_3$)
OHHO
N
N
O
O
OMe
168.45
163.95
158.45
157.97
140.15
139.83
136.70
136.66
127.22
127.08
126.53
126.15
117.94
117.83
108.57
86.42
79.57
77.36
77.05
76.73
73.78
65.44
61.37
59.47
35.07
34.12
31.51
31.47
29.46
29.44
28.34
26.32
26.05
23.18
200
180
160
140
120
100
80
60
40
20
0
ppm

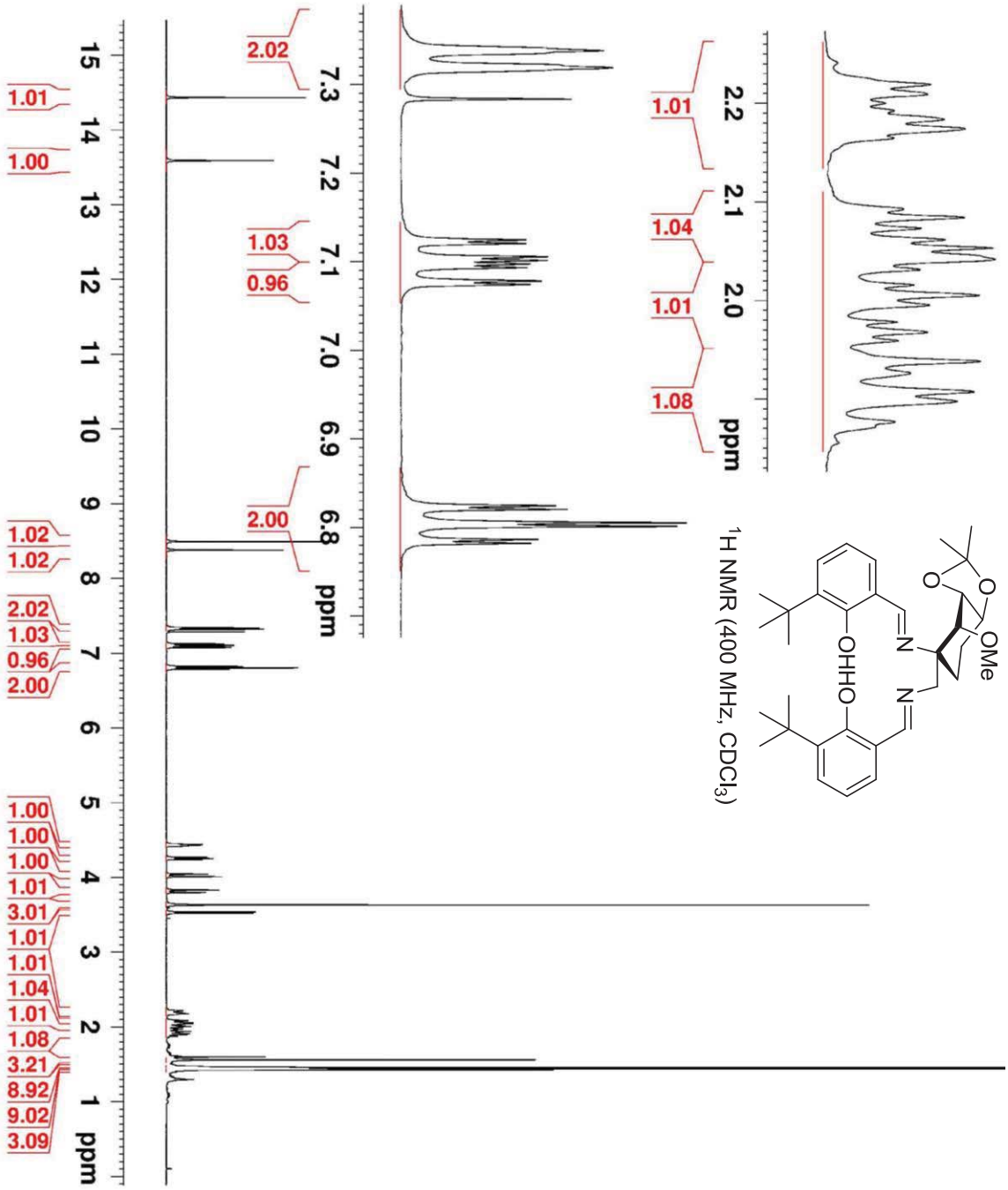
OMe
OHHO
N
N
^{1}H NMR (400 MHz, $CDCl_3$)
ppm
2.2
2.1
2.0
1.01
1.04
1.01
1.08
7.3
7.2
7.1
7.0
6.9
6.8
2.02
1.03
0.96
2.00
15
14
13
12
11
10
9
8
7
6
5
4
3
2
1
1.01
1.00
1.02
1.02
2.02
1.03
0.96
2.00
1.00
1.00
1.00
1.01
3.01
1.01
1.01
1.04
1.01
1.08
3.21
8.92
9.02
3.09

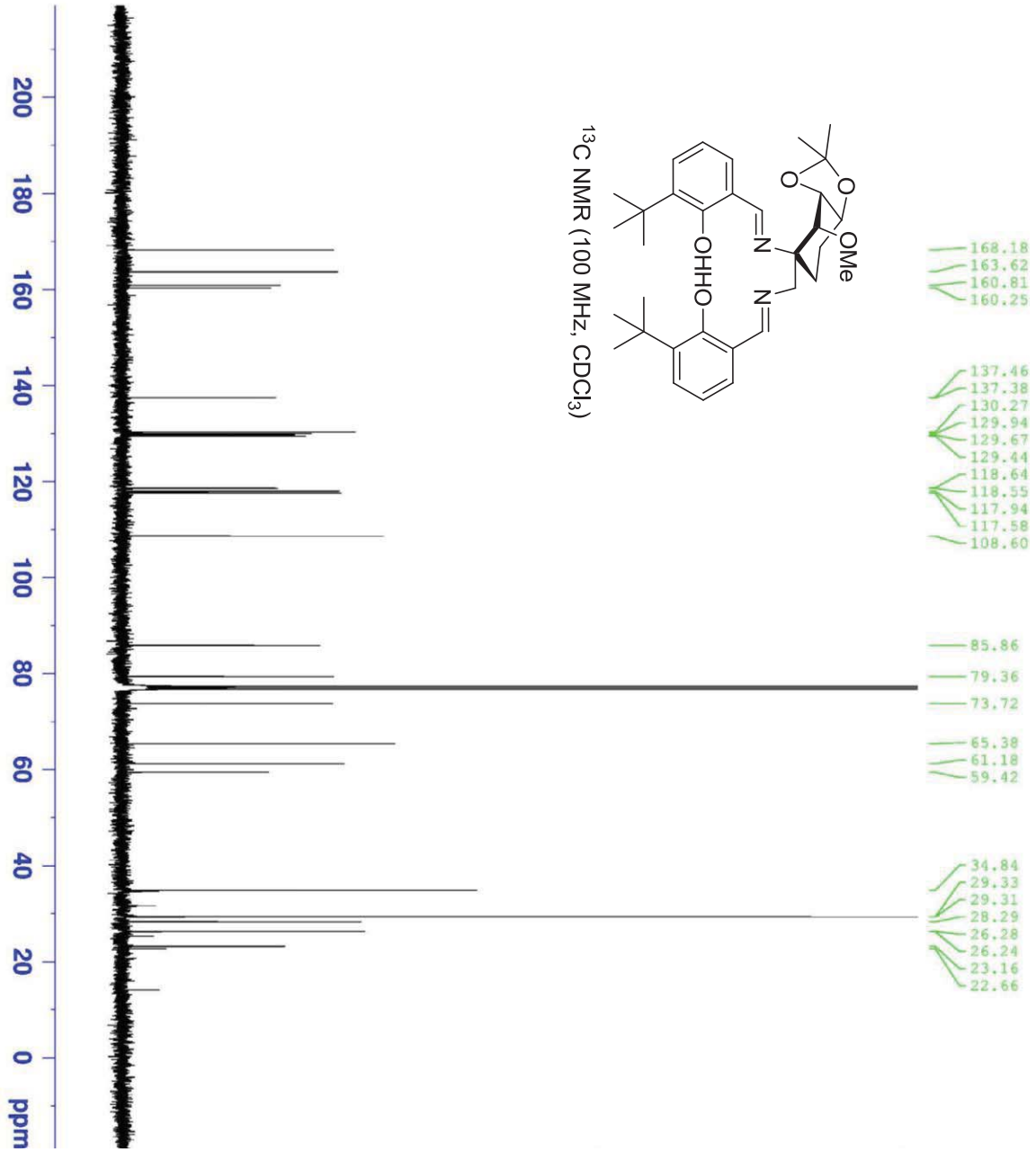
^{13}C NMR (100 MHz, $CDCl_3$)
OHHO
N
N
O
O
OMe
168.18
163.62
160.81
160.25
137.46
137.38
130.27
129.94
129.67
129.44
118.64
118.55
117.94
117.58
108.60
85.86
79.36
73.72
65.38
61.18
59.42
34.84
29.33
29.31
28.29
26.28
26.24
23.16
22.66
200
180
160
140
120
100
80
60
40
20
0
ppm

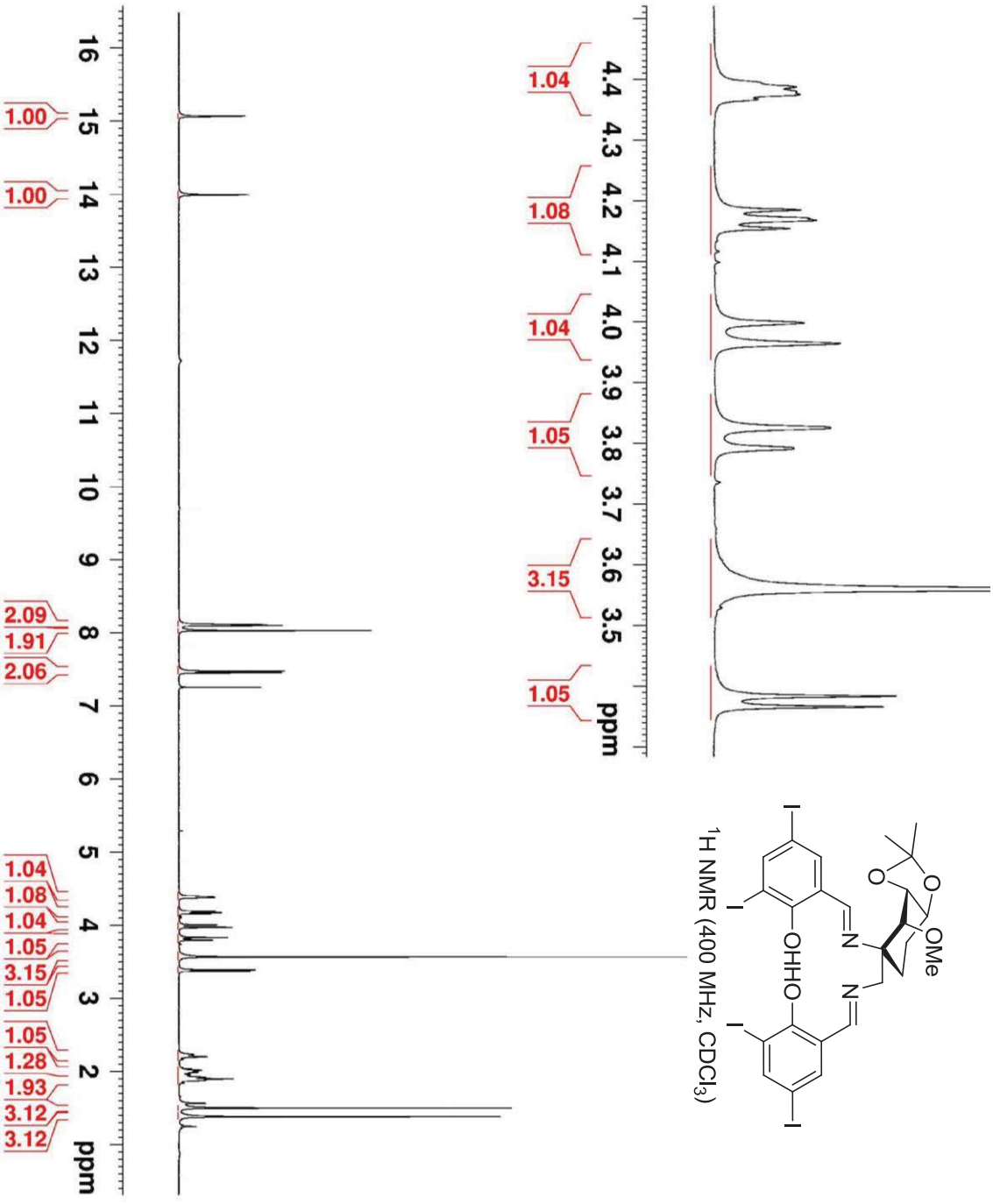
OMe
OHHO
N
N
I
I
I
I
^{1}H NMR (400 MHz, $CDCl_3$)
1.04
1.08
1.04
1.05
3.15
1.05
4.4 4.3 4.2 4.1 4.0 3.9 3.8 3.7 3.6 3.5 ppm
1.00
1.00
2.09
1.91
2.06
1.04
1.08
1.04
1.05
3.15
1.05
1.05
1.28
1.93
3.12
3.12
16 15 14 13 12 11 10 9 8 7 6 5 4 3 2 ppm

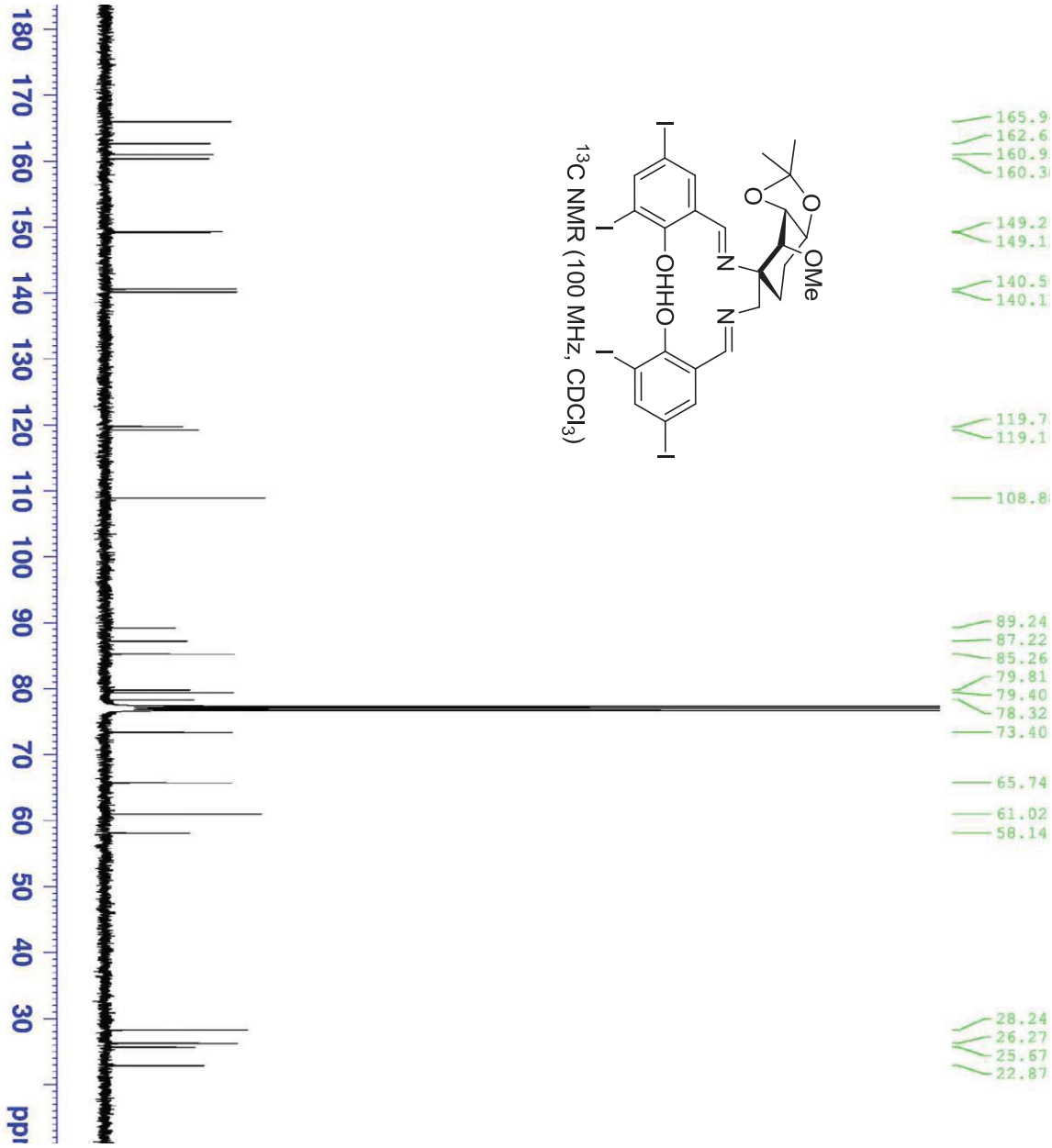
^{13}C NMR (100 MHz, $CDCl_3$)
OHHO
N
N
O
O
OMe
I
I
I
I
165.9
162.6
160.9
160.3
149.2
149.1
140.5
140.1
119.7
119.1
108.8
89.24
87.22
85.26
79.81
79.40
78.32
73.40
65.74
61.02
58.14
28.24
26.27
25.67
22.87
180 170 160 150 140 130 120 110 100 90 80 70 60 50 40 30
ppm

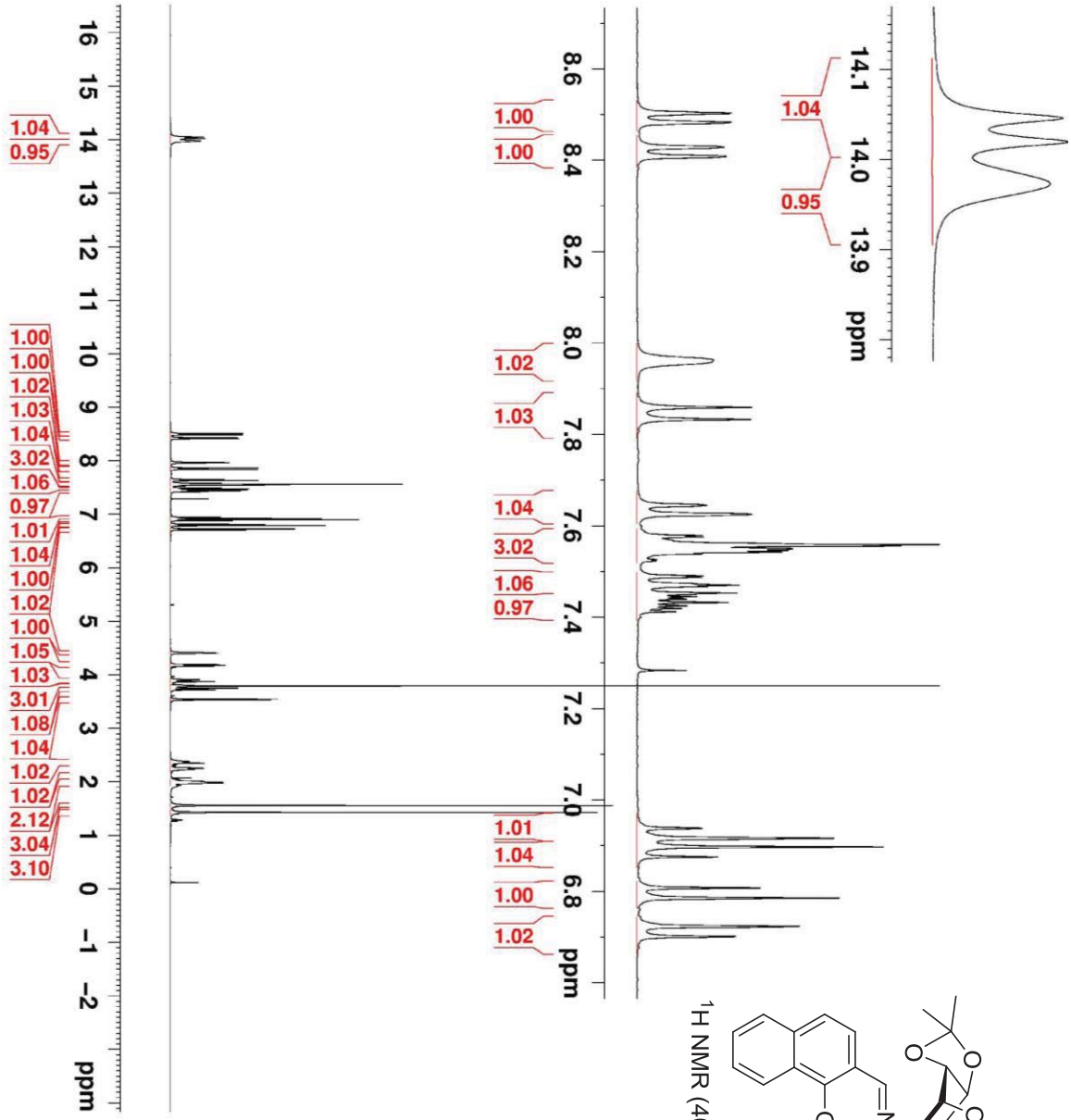

^{1}H NMR (400 MHz, $CDCl_3$)

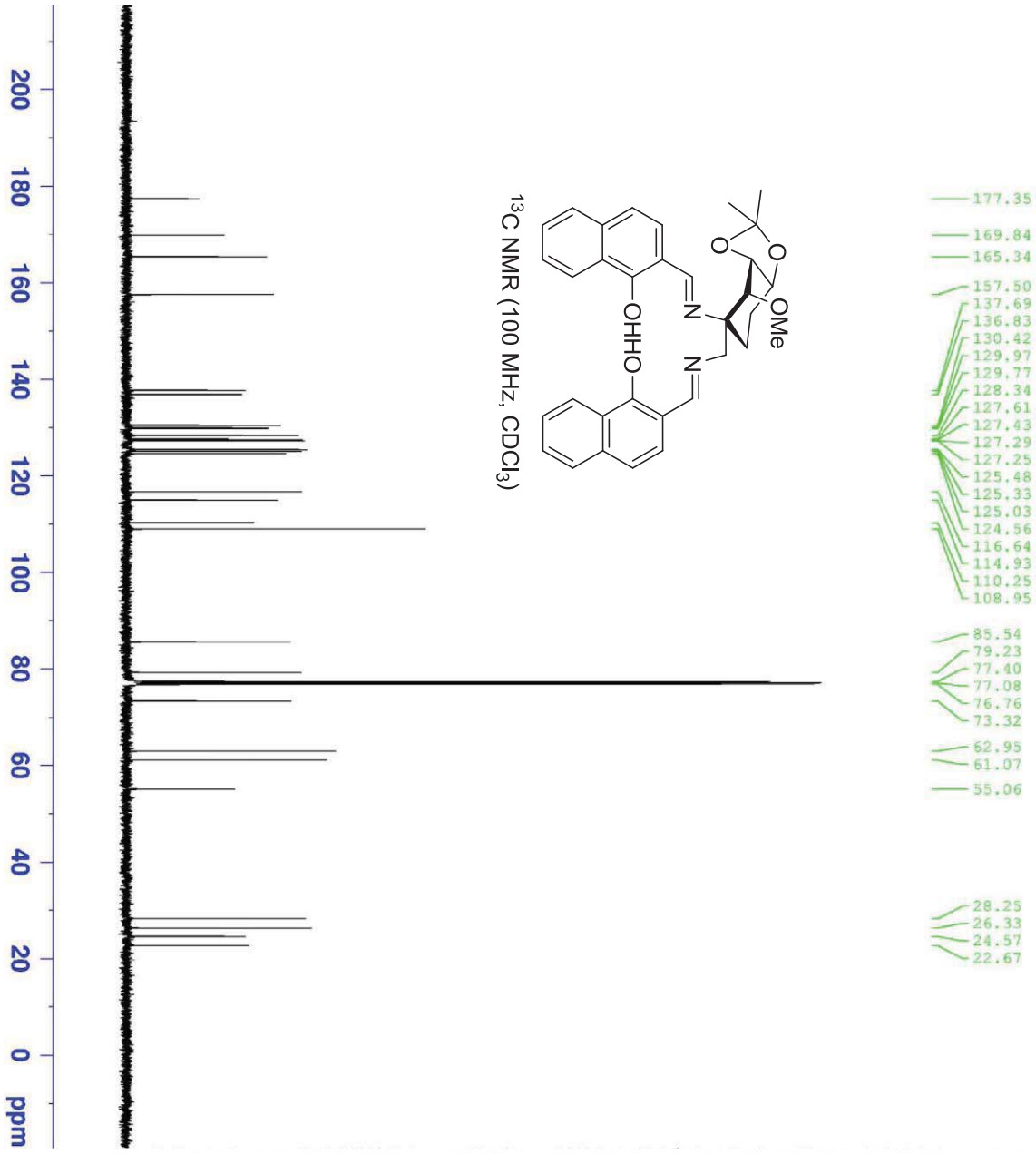
^{13}C NMR (100 MHz, $CDCl_3$)
OHHO
N
N
O
O
OMe
177.35
169.84
165.34
157.50
137.69
136.83
130.42
129.97
129.77
128.34
127.61
127.43
127.29
127.25
125.48
125.33
125.03
124.56
116.64
114.93
110.25
108.95
85.54
79.23
77.40
77.08
76.76
73.32
62.95
61.07
55.06
28.25
26.33
24.57
22.67
200
180
160
140
120
100
80
60
40
20
0
ppm